# The Separated Fringe Packet Survey: Updating Multiplicity of Solar-Type Stars within 22 Parsecs

by

CHRISTOPHER FARRINGTON

Under the Direction of Harold A. McAlister

# Abstract

Over the past half century, multiplicity studies have provided a foundation for the theories of stellar formation and evolution through understanding how likely it is that stars form alone or with companions. If spectroscopic orbits are combined with techniques that can determine visual orbits, we can access the most fundamental parameter of stellar evolution, stellar mass.

This dissertation is composed of two main sections. The first involves the investigation of the seminal multiplicity study of Duquennoy et al. (1991) which has been the "gold standard" for solar-type stars for nearly 20 years. Improvements in technology in the intervening years have improved the measurement accuracy for radial velocities and distances on which the study was based. Using Georgia State University's CHARA Array to search the systems in

Duquennoy & Mayor's multiplicity survey for overlooked companions along with a literature search covering regimes unreachable by the CHARA Array, we have found that more than 40% of the Duquennoy & Mayor's sample was further than originally believed and the uncorrected multiplicity percentages change from 57:38:4:1:0% (single:double:triple:quad:quint%) to 48:42.5:7.5:1:1% with the discoveries of multiple previously undiscovered companions.

The second part of this project describes the application of separated fringe packets for resolving the astrometric position of secondaries with small angular separations on long-baseline optical interferometers. The longest baselines of the CHARA Array allow access to a previously inaccessible range of separations compared with other techniques ($\leq$40 milliarcseconds) and the ability to very accurately angularly resolve a large number of single- and double-lined spectroscopic binaries. Combining astrometric and spectroscopic orbits provides assumption-free stellar masses and using the CHARA Array allows access to many previously unreachable systems available for high-accuracy mass determinations. We report the first angular separation measurements of seven spectroscopic binary systems, five additional separated fringe packet detections, ten systems with probably overlapping fringe packets, four systems with new data on pre-existing orbits, one completely new visual orbit for a SB2 system previously unresolved, and the detection of two previously unknown companions.

INDEX WORDS: Optical/infrared interferometry, Multiplicity studies, Solar-type stars, Stellar companions, Orbital parameters

# The Separated Fringe Packet Survey: Updating Multiplicity of Solar-Type Stars within 22 Parsecs

by

CHRISTOPHER FARRINGTON

A Dissertation Presented in Partial Fulfillment of Requirements for the Degree of

Doctor of Philosophy

in the College of Arts and Sciences

Georgia State University

2008

# The Separated Fringe Packet Survey: Updating Multiplicity of Solar-Type Stars within 22 Parsecs

by

CHRISTOPHER FARRINGTON

| | |
|---|---|
| Major Professor: | Harold A. McAlister |
| Committee: | Theo A. ten Brummelaar |
| | Douglas R. Gies |
| | Russel J. White |
| | Brian D. Mason |

Electronic Version Approved:

Office of Graduate Studies
College of Arts & Sciences
Georgia State University
December 2008

# Dedication

To my parents, Donald and Carol Farrington,

Without you, I never would have gotten this far –

# Acknowledgments

Most of all, I thank my parents and sister for always supporting me through the tough times I had and the transition to living in California. I would also like to thank all my friends outside of GSU who helped me immensely with affirmations and support through my grad school classes, Qualifying exams, and my move to Los Angeles; To all the grad students I worked with over the years; Dave Berger, Alvin Das, Ellyn Baines, Steve Williams, Wes Ryle, Jay Dunn, Erika Grundstrom, Angela Osterman, Kevin Marshall, John Subasavage, and all the rest, thank you for helping me survive the madness that is grad school; To Karloz and Shane, you two were a big part of the reason I came out to Los Angeles when the job was offered to me; And lastly, to Shauna Summers for sticking with me and caring for me during all the writing mish-mash I had to deal with, all the fun we had, dealing with how much stress I was inflicted with, and for making life in Los Angeles that much more wonderful.

Many, many thanks to the folks associated with CHARA and Mount Wilson: Theo ten Brummelaar, Nils Turner, Judit and Lazlo Sturmann, for keeping the Array in working order and putting up with my phone calls to them at home when something went wrong; P.J. Goldfinger for always being availble for questions when I didn't know how to do something when I was working late nights at the Array; The FLUOR, MIRC, PAVO, and VEGA crews important discussions while I was stuck while writing; Brian Mason and William Hartkopf for helping immensely with my orbits; and Gerard van Belle and Andy Boden for the use

of the space at the MSC and for helping with some ideas and dealing with living outside of Pasadena.

Special thanks to my committee, Hal McAlister for putting up with my constant questions and helping me get this wonderful job working at the Array on Mount Wilson; Theo ten Brummelaar for all the work with him on getting the software to work right, keeping me on track, and the all fun nights of observing full of Monty Python jokes and multiple stars; Brian Mason, you helped so much in getting the orbits correct and making sure that I got all the software from you to work properly with all those multitudes of emails; Russel White, for filling in when scheduling problems arose; and Doug Gies, your background support has been invaluable, teaching me how to make IDL work, and all the classes I learned a lot from.

Several people at GSU made the writing process so much easier to handle: Alvin Das, who wrote the general dissertation template; Ellyn Baines, whos constant help and support were priceless; Rajesh Deo, who kept the computers and network running, no small undertaking; and Todd Henry, for whose high expectations kept me constantly looking for the "science" around every corner.

This research has made extensive use of the *SIMBAD* database, operated at CDS, Strasbourg, France, the *VizieR Service* (Ochsenbein et al. 2000), and the Double Star Library, maintained by the U.S. Naval Observatory. This research also made use of data products from the Two Micron All Sky Survey, which is a joint project of the University of Massachusetts and the Infrared Processing and Analysis Center/California Institute of Technology, funded by the National Aeronautics and Space Administration and the National Science Foundation.

The CHARA Array, operated by Georgia State University, was built with funding provided by the National Science Foundation, Georgia State University, the W. M. Keck Foundation, and the David and Lucile Packard Foundation. This research is supported by the National Science Foundation under grant AST 0307562 and AST 0606958 as well as by funding from the offices of the Dean of the College of Arts and Science and the Vice President for Research at Georgia State University

# Contents

# Tables

# Figures

# Abbreviations and Acronyms

| | |
|---|---|
| **B** | baseline |
| **BSF** | Beam Synthesis Facility |
| **CHARA** | Center for High Angular Resolution Astronomy |
| **CPM** | Common Proper Motion |
| **CV** | Constant Velocity |
| **FOV** | field of view |
| **IR** | infrared |
| **mas** | milliarcseconds |
| **NIRO** | Near InfraRed Observer |
| **OPLE** | Optical Path Length Equalization |
| **PoP** | Pipes of Pan |
| **RV** | Radial Velocity |
| **SB** | Spectroscopic Binary |
| **SFP** | separated fringe packet |
| **S/N** | signal-to-noise ratio |
| **VB** | Visual Binary |
| **ZAMS** | Zero Age Main Sequence |

*If we look at the way cosmology has developed over the ages, we see the following trend. Copernicus, 500 years ago, told us that the Earth is not at the center of the solar system; the sun is.*

*Then Shapley, at the beginning of this century, showed us that the sun is not at the center of the galaxy, it's off in the boonies, out near the edge of the galaxy, 10 kiloparsecs away.*

*Then Hubble went on with his expanding universe and descripion of space to say, 'This question people worried about for 500 years was totally irrelevant. There is no center. So, why were you worrying about that, anyway? All points are equivalent. Everything is expanding uniformly, well-behaved. It is just space expanding.' So the whole question of a center was irrelevant.*

*If we have inflation with the bubble universes, we are not even the only universe. To worry about being the center of something that is not even the only one was really a silly thing.*

*Of course, now we realize too that we are not even made out of the right stuff. The bulk of the matter of the universe is something else. 90 percent of the universe is made out of something other than baryons.*

*Finally, when we study grand unified theories, theories of everything, we don't even seem to have the right number of dimensions.*

*—— Unknown*

# – 1 —

# Introduction

This dissertation describes the application of separated fringe packets to binary star studies and the updating of a seminal multiplicity survey of solar-type stars. Chapter 1 provides an introduction to the multiplicity studies and the gap between spectroscopic binary detection and speckle interferometry. Chapter 2 presents an overview of interferometry, the CHARA Array, and the currently active long baseline interferometers. Chapter 3 introduces the history, application, and limitations of separated fringe packets. Chapter 4 features the discussion of the selection of the observational sample and the comparison with the sample of Duquennoy et al. (1991) while Chapter 5 describes observations taken with the CHARA Array. Chapter 6 discusses the results of the observations and the implications of the changes in multiplicity. Chapter 7 presents interesting systems observed by this survey including new companions and orbits. Finally, Chapter 8 gives the conclusions reached from the changes in multiplicity and the overall effectiveness of separated fringe packet measurement of binary stars.

## 1.1 Multiplicity Studies (A&L vs. D&M)

In the search for better understanding of the processes of star formation and evolution, there is no more relevant knowledge than that of stellar multiplicity. Still, with millions of stars within reach of modern telescopes, it is hard to decide where to begin. If we start with stars like the Sun in the local stellar neighborhood, we can extend the results on the nature of solar-type stars to the Galaxy as a whole. We can better understand the scenarios of star formation (Halbwachs 1986; Trimble 1990), the constraints of how stars evolve with and without companions (Mayor & Mermilliod 1984), the Mass-Luminosity relation through precise masses (Gilmore & Roberts 1988), the search for very low mass companions (Kraus et al. 2005; Jao et al. 2003), planetary bodies and how they form (Eggenberger et al. 2008; Boss 2001), the history of star formation in our galaxy (Caballero 2007), and the stability of all such systems (Bahcall et al. 1985), all from a study of stellar multiplicity.

Over the past hundred years, studies of this type have been done on several occasions with variable results (15 to 55% multiplicity) over all stellar types. It is believed that the multiplicity of stars is not constant across stellar types, with B stars having quite a different multiplicity fraction than K stars. Abt & Levy (1976) (hereafter A&L) intended their survey to be an unbiased update to the many previous samples (Kuiper 1935, 1942; Jaschek & Jaschek 1957; Petrie 1960; Jaschek & Gómez 1970) that were plagued by selection effects which rarely included all types of star systems (spectroscopic binaries, visual doubles, and common proper motion pairs) by starting with solar-type stars (F3-G2 IV and V). Unfortunately, in the selection of their sample, it was later determined that it too was

biased in favor of a larger fraction of multiples.

Years later, Duquennoy et al. (1991) sought to rectify these mistakes with a survey of their own, this time without the bias that affected the previous surveys by using a distance rather than a brightness-limited sample. Their results have been the basis for formation and evolutionary models ever since. Duquennoy and Mayor (1991b, hereafter D&M) found that a significantly larger percentage of systems were single in comparison with A&L (percentages: 42:46:9:2 single:double:triple:quadruple for A&L and 57:38:4:1 for D&M), a smaller number of companions per system (0.70 for A&L and 0.49 for D&M), and that correction of A&L's results for the spurious binaries found in their sample by Morbey & Griffin (1987) gave nearly similar percentages. Additionally, D&M delved deep into the implications of the distribution and relations between the orbital elements and stellar masses as well as a very detailed discussion on the incompleteness of their survey.

### 1.1.1 Updating Solar-Type Multiplicities

Even when studies are believed to be free of bias, it is always useful to revisit them as technology advances in order to ensure the conclusions were valid. D&M's survey was published in 1991 and supposedly free of selection effects or bias. However, a satellite launched in 1989 would later show that the parallax-limited survey was not as limited as it would seem. Six years later, the HIPPARCOS and Tycho Catalogs (Perryman & ESA 1997) and the more recent update (van Leeuwen 2008) provided sub-milliarcsecond accuracy parallaxes for more than 100,000 stars, providing the SFP Survey a way to probe the D&M sample's major qualification.

In order to see how the changes in multiplicity have been affected by the determination of high quality parallaxes, precise radial velocity measurements, and many years of speckle interferometry observations, the D&M sample should be revisited. As surveys of this type generally require a large time commitment, we shall combine an active search for new companions with a literature search encompassing any observations of the targets since 1991. The consideration of companions will extend down to the theoretical brown dwarf-planetary boundary to include any new companions predicted by the original multiplicity and incompleteness study. For all the targets in the multiplicity sample, we shall examine not only the companions, but the known orbital elements and provide a comparison with D&M's analysis of the mass-ratio $q$, period distribution $\log P$, and the relationship between $\log P$ and the eccentricity $e$ to see how the changes in the percentages of the companions affects these distributions.

## 1.2 The Gap: Visual, Speckle, Spectroscopic, and Visibility Orbits

It is necessary to obtain both the spectroscopic and visual orbit to fully quantify the masses of the binary star components except for special cases like eclipsing binary systems. This presents a problem with many systems as the detection of the visual orbit of the secondary is strongly influenced by the distance, period and magnitude difference. Shorter periods bring the secondary closer to the primary, the distance shrinks the angular separation, and a magnitude difference larger than 3-4 magnitudes increases the likelihood that the secondary

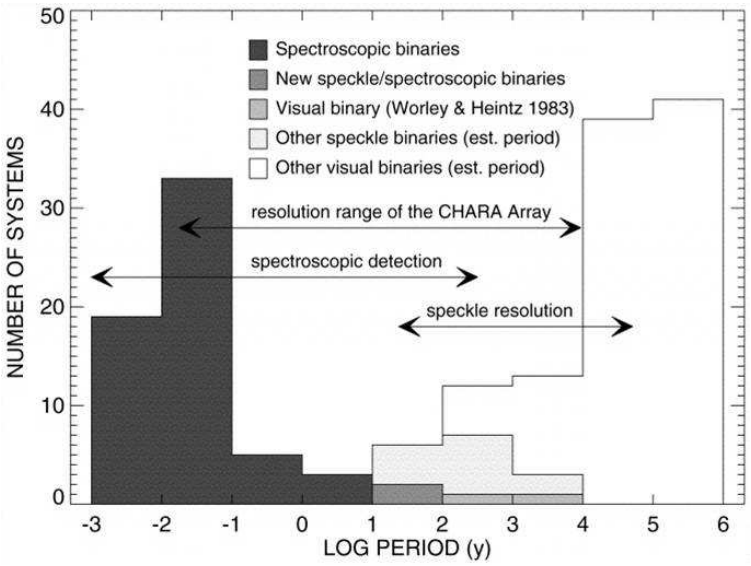


Figure. 1.1: O Star Period Distribution. The distribution of O stars has only a very small overlap between O stars with visual orbits, and those with spectroscopic orbits (from Mason et al. (1998b)). This can be shown not to be the general case when compared to Figure 1.2 which contains more than 6000 binaries of all spectral types and both methods.

will be overlooked. A different set of problems influences the detection of spectroscopic binaries. As the inclination of the orbit decreases to zero (face-on), the velocity variation goes to zero and falls below detection limits of the high resolution spectrographs. With long-term monitoring, it is possible but difficult to obtain estimates of spectroscopic orbits and mass ratios for double-lined binaries with long periods at almost any distance.

How big is the overlap between spectroscopic and visual binary detection? In a study of O stars, Mason et al. (1998b) shows very little overlap between the two methods (see Figure 1.1) from $\log P$ of -1 to 2 years. Is this gap prevalent for all spectral types or is it just a selection effect for O star binaries? Taking the entire Ninth Catalog of Spectroscopic Binary Orbits (Pourbaix et al. 2004) and the Sixth Catalog of Orbits of Visual Binary Stars (Hartkopf et al. 2001a) and plotting the number of stars in each case as a function of $\log P$,

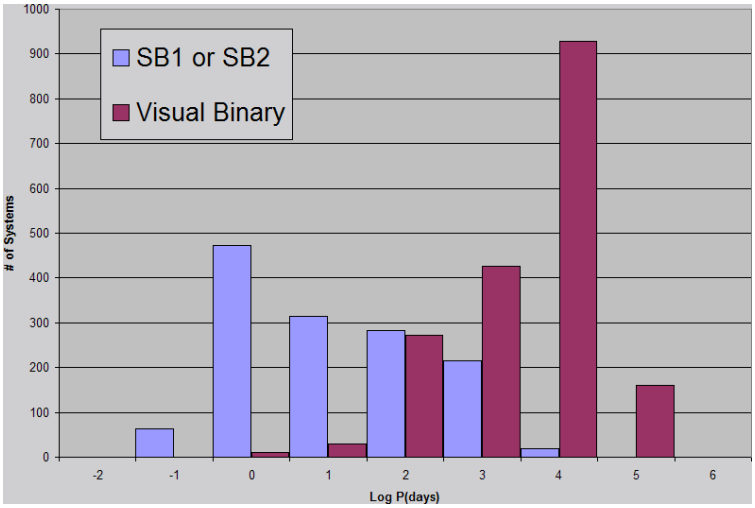


Figure. 1.2: Overall Binary Period Distribution. Shown here is the distribution of orbital periods for all binary stars in either the Ninth Catalog of Spectroscopic Binary Orbits (Pourbaix et al. 2004) and the Sixth Catalog of Orbits of Visual Binary Stars (Hartkopf et al. 2001a).

we can see in Figure 1.2 that there is much more overlap for all orbits than just for O stars. Why then are there relatively few simultaneous orbital solutions for stars with spectroscopic and visual orbits? The simple answer is that most of those systems have not been observed by both methods, the distances are so large that the angular separation is too small for conventional techniques, or those that have a detectable separation are sufficiently far away that the period is extremely long. One thing we can be sure of is that there are many spectroscopic binaries that are just waiting for visual observations when the right technique comes along.

So, we have radial velocity orbits of spectroscopic binaries of all periods, shapes, and sizes at almost every distance we can measure. Herein lies the problem. For those closest to the Sun, it is relatively easy to get visual orbits as these systems have quite large separations. As the distance increases however, we need access to much larger telescopes or different

techniques to angularly resolve the components. Large single telescopes can angularly separate the components of binaries to the limits of atmospheric seeing, sometimes down to sub-arcsecond separations. Speckle interferometry and adaptive optics on large telescopes can further increase this to the Rayleigh limit of the individual telescopes (35-40 milliarcseconds). It is at this point where we find a gap in coverage as advances in optical long-baseline interferometry (OLBI) can use visibility analysis to probe under 10-15 mas separations such as in the case of the orbit of HD 4676 (Boden et al. 1999b). The ability to fit visibility curves to binaries with OLBI is limited by the longest baselines available and is likely to produce unreliable results under 1 mas.

It would be beneficial to binary star studies to be able to bridge the angular separation gap with a new technique that would overlap with current methods to provide an unbroken resolution spectrum from visual to visibility binaries. How then can we probe this unexplored region of detection? The answer lies with a largely unexplored sub-field of long-baseline interferometry near the longest possible baselines.

## 1.3 The Separated Fringe Packet Method

The advent of OLBI's such as the CHARA Array allows us to probe the resolution gap between speckle interferometry and visibility analysis by utilizing the longest baselines in an interesting special case. If we consider a pair of stars separated by an angle between 10 and 100 mas that is observed with long baselines and with the correct orientation, then both stars will create separate fringe packets. Using the Infrared Optical Telescope Array (IOTA), Dyck

et al. (1995) showed that detecting separated fringe packets was possible on $\zeta$ Hercules with a separation of 1.466″. It was also shown that with two perpendicular baselines, complex multi-body systems could in theory be angularly resolved, though in practice, this is quite difficult. Lane & Muterspaugh (2004) and Bagnuolo et al. (2006) used the Palomar Testbed Interferometer (PTI) and the CHARA Array respectively to produce 20-40 microarcsecond ($\mu$as) astrometry for the position of the secondary of a binary star. Lane & Muterspaugh (2004) observed HR 6983 and obtained separated fringe packets, and using the rotation of the projected position angle of the single baseline due to the diurnal motion of the star, they measured a separation of 0.248″, which showed the overlap of angular resolution with speckle interferometry. Using larger baselines, Bagnuolo et al. (2006) also used the rotation of the baseline position angle on 12 Persei, obtaining separated fringe packets on a far smaller scale ($\sim$50 mas). It is this process that we have used extensively with interferometric observations of a large sample of solar-type systems. This kind of data allows us to search for companions that might have been missed in previous surveys and to measure separations of selected single- and double-lined spectroscopic binaries to obtain visual orbits and high-quality mass determinations.

*It is no good to try to stop knowledge from going forward. Ignorance is never better than knowledge.*

—— *Enrico Fermi*

– 2 —

# Long-Baseline Interferometry and the CHARA Array

This chapter aims to provide a basic understanding of long-baseline interferometry, reviews the definition of visibility, gives an overview of the CHARA Array and discusses current and future long-baseline interferometers.

When observing multiple stars, the ability to determine the angular separation of the components is of paramount importance. With contemporary speckle methods at single telescopes, resolving components with smaller separations requires observations with a larger diameter primary mirror. The prospect of building larger and larger telescopes becomes increasingly difficult and expensive. While speckle interferometry is able to separate individual components down to the diffraction limit of the telescope, even the largest telescopes fall short of being able to resolve a significant number of spectroscopic binaries. Long-baseline interferometry offers the potential for resolving many such systems.

## 2.1 Basic Interferometry

Traditional telescopes are limited to the inherent resolution modeled by the Rayleigh criterion, which is defined by $\theta = 1.22\lambda/B$ where $\lambda$ is the wavelength being observed, $B$ is the diameter of the telescope primary and $\theta$ is the resolution in radians. Interferometry has a clear advantage as $B$ is now the distance between the two telescopes (or Baseline) rather

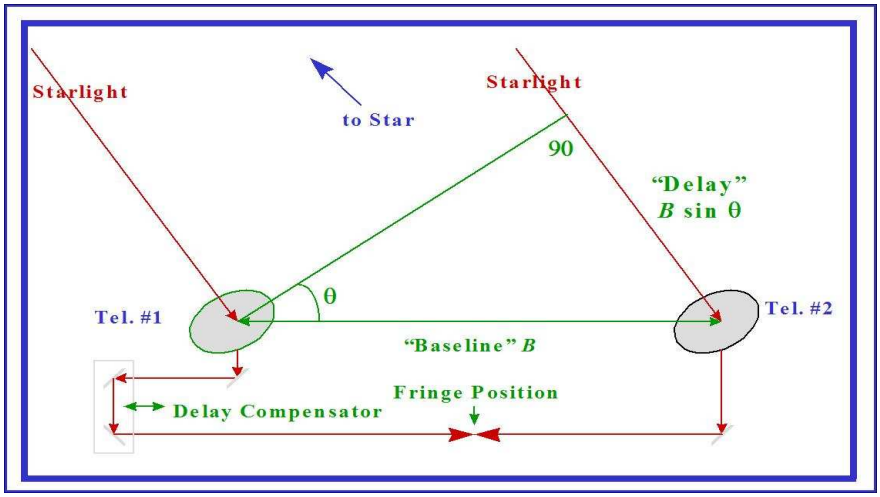


Figure. 2.1: Schematic of a basic interferometer (diagram by H. McAlister).

than the telescope diameter. The fringe production process leads to a modified criterion where the resolving limit is now $\theta = \lambda/2B$. With some of the longest baselines available, this can bring the limit of resolving two individual components from tens of milliarcseconds down to a fraction of a milliarcsecond (mas) at visible wavelengths.

There are several infrared and optical interferometers in use today, but all operate on the same basic principles. Light from an object is collected from each telescope and the individual beams are interfered with each other to produce a fringe pattern at the point of equal path length between the telescopes (see Figure 2.1). Interferometers measure the degree of complex coherence of an object, which leads to a powerful technique to measure stellar angular diameters, binary star separations, and/or the intensity distribution on the sky (Tango & Twiss 1980).

For IR and optical light, these paths need to be equalized to an accuracy of a few wavelengths. Additionally, as the object moves across the sky, the point at which the fringes

are created moves a significant amount, and thus the ability to find and keep fringes is a complex engineering challenge. The intricacy of such a system of beam transport and compensation requires multiple reflections that reduce the amount of light available for combination and hence signal-to-noise ratio (S/N), precise and steady alignment, and the ability to adjust to changing atmospheric conditions and instrumental drifts over the course of a night. The combination of these factors provides significantly better resolution at the cost of sensitivity and complexity.

## 2.2 Young's Double Slit Experiment

A simplified view of how interferometry works in practice can still best be described through Young's Double Slit experiment. As depicted in Figure 2.2, light passes through the slits (separated by distance $d$) onto a screen a distance $D$ away, the light from each slit will constructively and destructively interfere with itself and produce a pattern of light and dark areas referred to as a fringe pattern. The resulting intensity is given by:

$$I(x) = 4A^2 \cos^2 \left[ \frac{2\pi}{\lambda} \frac{xd}{D} \right], \tag{2.1}$$

where $A$ is the slit amplitude, $\lambda$ is the wavelength of the incoming light, and $x$ is the distance from the center of the two slits along the screen where $D \gg d$. Maxima of the resultant pattern occur at integer multiples of the wavelength ($xd/D = 0,\ \lambda,\ 2\lambda,\ ...\ m\lambda$) where 0 is the location of the central fringe and successive peaks are angularly separated by:

$$\alpha = \frac{x}{D} = \frac{\lambda}{d}. \tag{2.2}$$

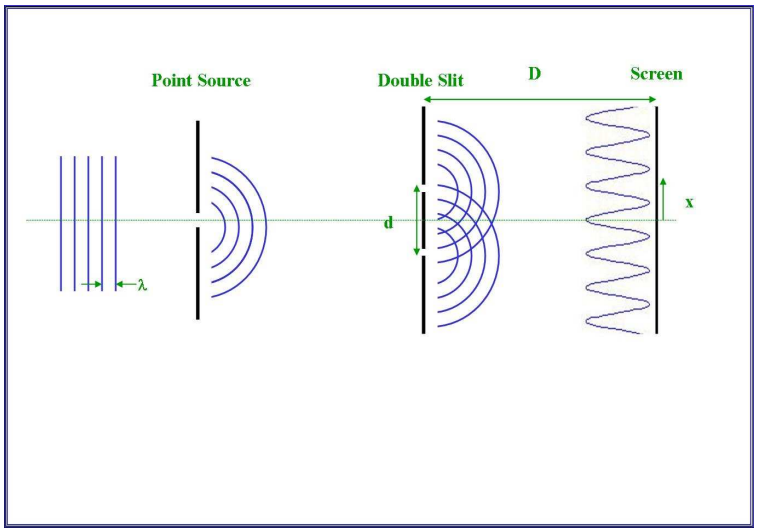


Figure. 2.2: Young's Double Slit Experiment Setup (diagram by H. McAlister). The light passing through the two pinholes constructively and destructively interfere, creating fringes of alternating dark and bright bands.

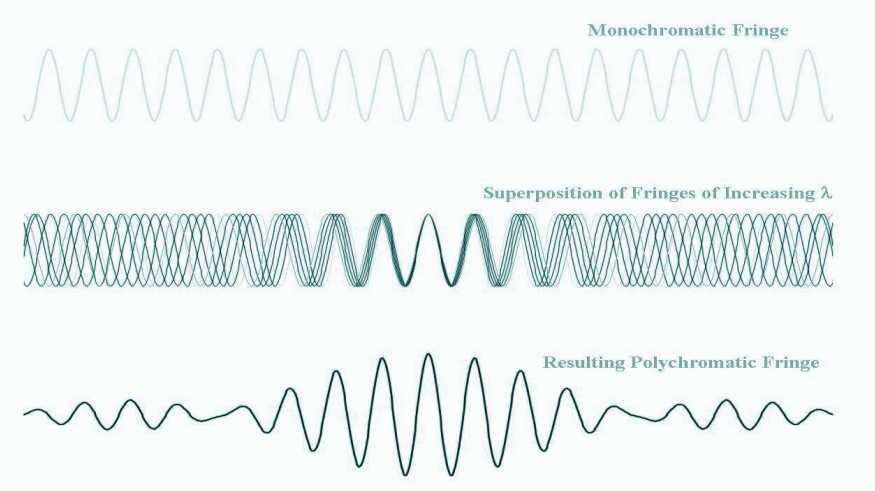


Figure. 2.3: Building an Interferometric Fringe (diagram by H. McAlister). Multiple wavelengths of light constructively and destructively interfere, creating the fringe pattern seen in the bottom panel centered on the point of zero path difference.

Figure 2.3 shows how changes from monochromatic to polychromatic light from a finite-filter bandwidth build an interference fringe for a realistic representation of data from an interferometer.

## 2.3 Fringe Visibility

Although this project does not involve visibility analysis, it is useful to describe the basis for producing the double fringes being observed. The van Cittert-Zernike theorem relates the complex coherence, $\mu(\vec{B})$, with the intensity distribution on the sky for a source, $I(\vec{\alpha})$, where $\vec{B}$ is the baseline vector between the two telescopes and $\vec{\alpha}$ is the two-dimensional sky coordinate (Thompson et al. 1986). In practice, the visibilities measured by an interferometer are the fourier transform of the intensity distribution at that spatial frequency. The Fourier transform terms of $\mu(\vec{B})$ and $I(\vec{\alpha})$ are related as follows:

$$\mu(\vec{B}) = \frac{\int I(\vec{\alpha}) e^{-ik\vec{B}\cdot\vec{\alpha}} d\vec{\alpha}}{\int I(\vec{\alpha}) d\vec{\alpha}}, \tag{2.3}$$

where $k = 2\pi/\lambda$.

The power of this relation lies in the fact that when $I(\vec{\alpha})$ cannot be imaged for a source, one can measure $\mu(\vec{B})$ and then infer $I(\vec{\alpha})$ for the ideal case or model alternate intensity distributions and fit the measurements to the model. For a two telescope interferometer, the phase component of $\mu(\vec{B})$ is lost through atmospheric turbulence (Tango & Twiss 1980) and all that remains is the amplitude.

Observationally, the contrast of a fringe pattern is a measure of the visibility amplitude, more simply known as "visibility". This is the basic observable of an interferometer, and was defined by Michelson (1920) as

$$V = \frac{I_{\max} - I_{\min}}{I_{\max} + I_{\min}}, \tag{2.4}$$

where $I_{\max}$ and $I_{\min}$ are the maximum and minimum intensities of the fringe respectively. Visibility ranges from $V = 0$, where fringes disappear, and the target is considered fully resolved, to $V = 1$, where the fringes are well-defined, and the target is a point source and considered unresolved.

The visibility equation is more complex in practice. Modeling a single star as a uniform disk (UD), the visibility equation is

$$V_{\mathrm{UD}} = \frac{2J_1(\pi B\theta_{\mathrm{UD}}/\lambda)}{\pi B\theta_{\mathrm{UD}}/\lambda}, \tag{2.5}$$

where $J_1$ is the first order Bessel function, $B$ is the baseline, $\theta_{\mathrm{UD}}$ is the UD diameter of the star in radians, and $\lambda$ is the wavelength used to observe (Lawson 2000).

The ability to measure visibility is as useful as it is powerful, enabling the interferometer to measure stellar diameters and close binaries, but there are two other observables we can use for information on binaries with angular separations between 10-100 mas. When the stars are sufficently separated, their fringe packets will no longer overlap. In the SFP survey, the most important measurements are the average separation between the maxima and the ratio of the amplitudes of the two separated fringe packets. These will be discussed in further detail in the following chapters.

## 2.4 The CHARA Array

This section is designed to give the reader a basic understanding of the CHARA Array. For a complete discussion of this instrument see ten Brummelaar et al. (2005).

Designed, constructed, and operated by Georgia State University's Center for High Angular Resolution Astronomy (CHARA), the CHARA Array sprawls across the Mount Wilson Observatory grounds in southern California along side groundbreaking historical telescopes such as the 100-inch Hooker telescope. The Array consists of six stationary 1-m alt-az telescopes situated in a Y-shaped pattern that produces 15 non-redundant baselines ranging from 34 to 330 meters. The telescopes are identified according to their orientation in relation to the cardinal directions as measured from the Beam Synthesis Facility (BSF) and designated by a 1 or 2, with the lower number being a larger distance from the center of the Array. Figure 2.4 displays the layout of the CHARA Array on Mount Wilson and its relation to the other major facilities based there. The telescopes are situated in non-redundant baseline in order to maximize coverage of the $u$,$v$ plane (the conjugate of $x$,$y$ cordinates). The $u$,$v$ coordinates are spatial frequencies that represent distances in the incident wavefront measured in wavelength units.

The light from these telescopes is transported as a 12.5-cm collimated beam through the 20-cm evacuated light pipes to the BSF for path equalization. These pipes are evacuated to about 0.1% of atmospheric pressure to eliminate turbulent distortion due differences in temperature and air path. The BSF consists of the Optical Path Length Equalization (OPLE)

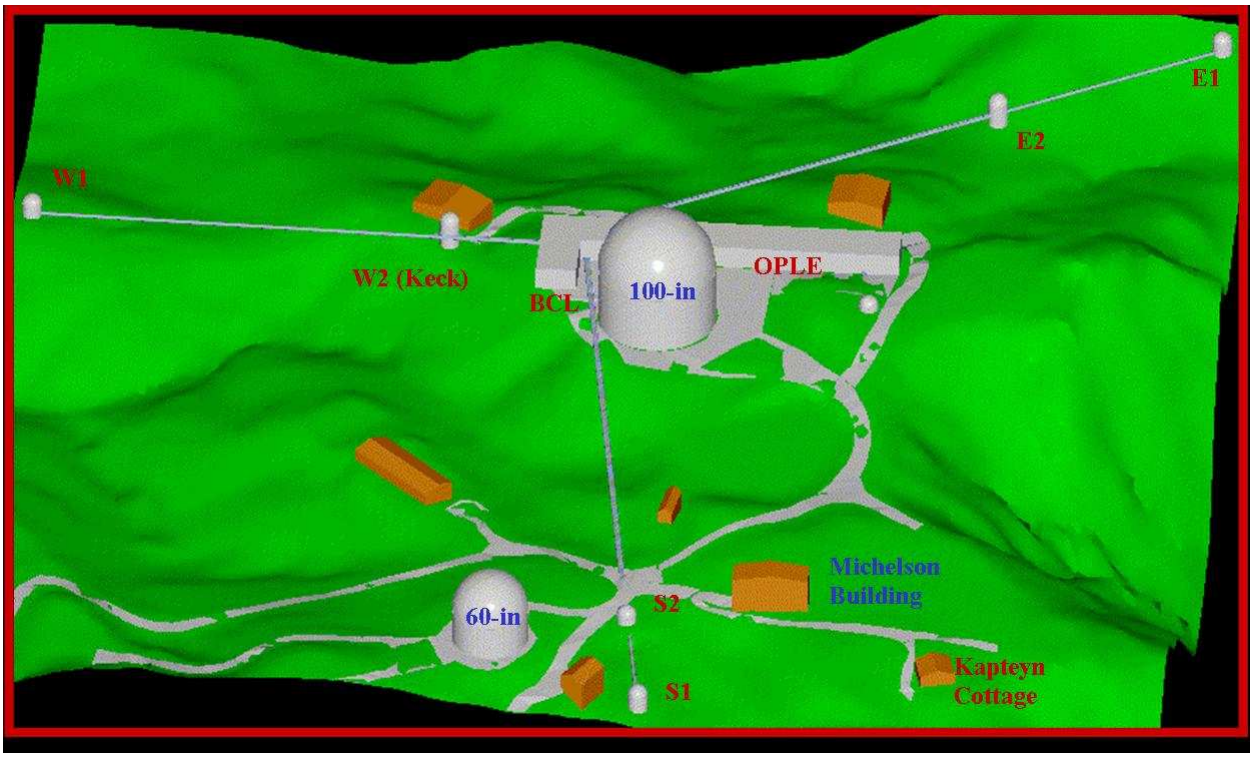


Figure. 2.4: The CHARA Array and Its Surroundings. North at the top (Diagram by T.A. ten Brummelaar)

facility and the Beam Combination Laboratory (BCL). Upon entering the facility, the beams are aligned parallel via "turning boxes" which send the light into the OPLE system. The path equalization is done in two stages, the first of which is done inside the evacuated light pipes through the "Pipes of Pan" (PoPs) which introduce fixed amounts of delay into the beam train (0, 36.6, 73.2, 109.7, and 143.1 meters).

These removable mirrors send the light back down the light pipe to a periscope which transports the beam out of the vacuum system and into the second stage of path equalization. Directly above the PoPs, the variable compensation of delay is achieved by six mobile carts on rails 45 m in length providing a maximum of ∼90 m of path compensation. These carts

remove the delay introduced by the sidereal motion of the object that changes the projected baseline length. The OPLE carts' positions are measured using a 1.3-$\mu$m laser metrology system which is accurate to $\pm$ 2 nm and provides control to under $\pm$ 10 nm RMS.

With the paths equalized, the beams are further reduced in size from 12.5 to 1.9 cm using a Beam Reducing Telescope (BRT) and split into separate visible and IR beams (at approximately 1 $\mu$m) with movable beam samplers consisting of a dichroic beam splitter and flat mirror. The visible light is directed to the active "tip/tilt" system for stellar tracking and the CLIMB (CLassic Interferometry with Multiple Baselines) visible beam combiner. The IR light is injected into "CHARA Classic," the standard instrument for the Array shown in Figure 2.5, which is a standard two-beam pupil-plane beam combiner whose outputs are focused onto the "Near IR Observer" (NIRO) detector through one of six filter positions now populated by the $H$ (1.67 $\mu$m), $K'$ (2.2 $\mu$m), $K$ continuum, and Bracket-$\gamma$ filters with future access to $J$ (1.22 $\mu$m) band. Fringes are found through a scanning modulation of the delay made possible by a "dithering mirror" attached to a piezoelectric stage driven in a saw-tooth pattern at a rate relating to the camera read-out rate at 5 samples per fringe (1000:200Hz, 750:150Hz, 500:100Hz and 250:50Hz). In order to obtain fringes at the CHARA Array, targets must meet two criteria: telescope tracking in the visible and sufficient IR photons to NIRO. At the inception of this project the limiting magnitudes for the CHARA Array were $K \leq +6.0$ and $V \leq 8.0$. Subsequently, upgrades to the Array have improved the limiting magnitudes to $K \leq +8.0$ and $V \leq +10.5$. All data taken for this project were recorded at 750 or 500 Hz and using the $K'$ filter (2.13 $\mu$m) unless otherwise noted.

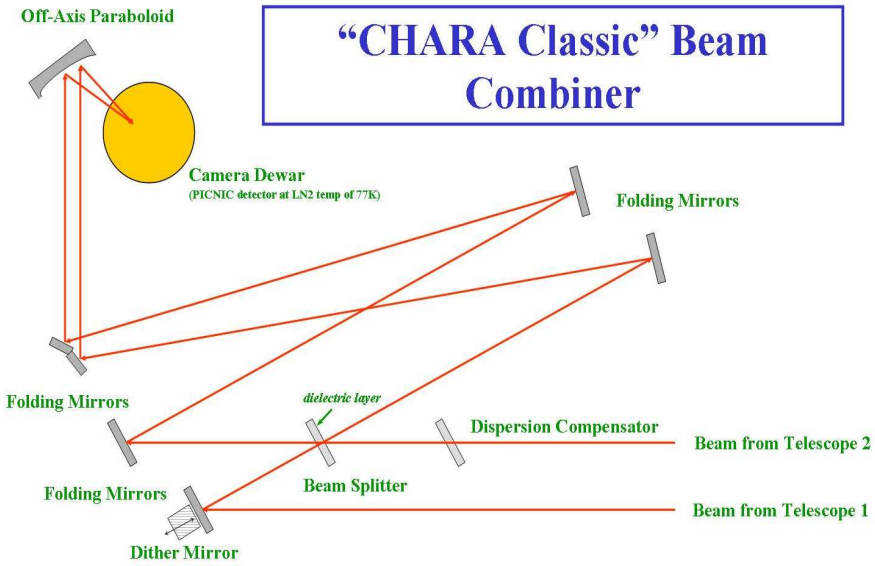


Figure. 2.5: Schematic of the "CHARA Classic" Beam Combiner (diagram by H. McAlister).

## 2.5 Early and Current Interferometry

### 2.5.1 Interferometry Beginnings

In 1868, Armand Fizeau was the first to discover a remarkable relation between the dimensions of the fringes and the source of light that would later lead to the idea that the diameter of an extended disk could be measured interferometrically by measuring the length of the baseline where the contrast of the fringes reaches its first null (Fizeau 1868). Using two adjustable slits on the 36-inch refractor at Lick Observatory, Michelson (1891) was able to use the interference pattern of the moons of Jupiter to determine their angular diameters. Following the successful double star observations of Schwarzschild (1896) and Anderson (1920) using movable slits along the optical path, Michelson (1920) used masks on the 60- and 100-inch reflectors on Mount Wilson to measure the separation of Capella. The first

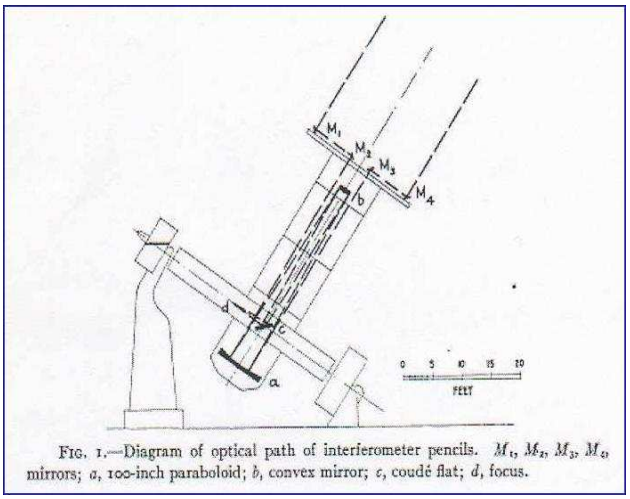


FIG. 1.—Diagram of optical path of interferometer pencils. $M_1$, $M_2$, $M_3$, $M_4$, mirrors; *a*, 100-inch paraboloid; *b*, convex mirror; *c*, coudé flat; *d*, focus.

Figure. 2.6: Schematic of Michelson's Interferometer (from Michelson & Pease (1921). Reproduced by permission of the AAS.).

practical application of long baseline interferometry to determine the diameters of individual stars was completed by Michelson & Pease (1921) with the 20-foot interferometer consisting of two fixed and two moveable flat mirrors on a steel beam installed on the Cassegrain cage of the 100-inch Hooker telescope on Mount Wilson (see Figure 2.6). With this, Michelson was able to make the first measurement of the angular size of the supergiant Betelgeuse ($\alpha$ Orionis).

With the success of the 20-ft beam on the Hooker telescope, Francis Pease began planning a larger stand-alone instrument to measure the diameters of stars with smaller diameters (Lawson 2006). Designed and built by Pease in 1931, the 50-ft interferometer was housed in what is now the Mount Wilson Institute Office and Shop building on Mount Wilson, near the 100-inch telescope dome. Though the concepts were sound, the project was ahead of its time and plagued with problems. In the same style of the 20-ft, the Pease interferometer

consisted of a inverted *A*-frame trestle on a rotating guide that would tilt the instrument to follow a star across the sky. Unfortunately, the frame was so large, that it suffered from flexure which introduced variation in path length of the beams. That, combined with the speckled images produced by the 38 cm mirrors on each end of the beam, excessive vibration, and polarization mismatch between the arms of the interferometer only allowed results with an accuracy of 10-20%. At longer baselines, the fringe motion rapidly increased, keeping this instrument from producing much of value. Still, the attempt provided valuable insight into the necessary requirements for optical interferometry eventually to be built upon by Labeyrie.

With the development of long baseline interferometry on hold, small and medium single aperture telescopes remained productive through the efforts of slit, eyepiece, and micrometer measurements of double stars by Wilson (1936) and van den Bos (1959). Thousands of double star measurements had been accumulated for hundreds of systems over several decades and further improved upon by Finsen (1951) with the invention of the single piece eyepiece interferometer which significantly improved the ability to adjust the aperture settings and reduce the number of false detections.

Following the development of radio interferometry after World War II, (Hanbury Brown & Twiss 1956) developed the principles behind the "intensity interferometer", how the correlations in measured intensity rather than electric fields can be used to measure stellar diameters. The results of these experiments on Sirius led to the development of the Narrabri Intensity Interferometer (NII). With a 188-m baseline and blue sensitivity, the NII produced

diameters for dozens of hot stars Hanbury Brown et al. (1967), but was limited by bandwidth to only the brightest systems. This project spurred development in "direct detection" interferometry, where the electric fields are combined before photon detection, and those involved would later go on to develop the Sydney University Stellar Interferometer (SUSI).

In one decade, Antoine Labeyrie provided the astronomical world with two distinct interferometric techniques that would push the boundaries of stellar astronomy. As a graduate student in Meudon, Labeyrie first proposed the technique of speckle interferometry (the fourier analysis of speckle patterns of instantaneous star images) (Labeyrie 1970). Five years later, Labeyrie built a long-baseline optical Michelson interferometer at Nice Observatory, and obtained fringes by directly interfering light from Vega ($\alpha$ Lyrae) from two separate telescopes 12 m apart (Labeyrie 1975). While unable to measure any astrophysical quantities from the fringes he detected from Vega, the proof that the technique was possible blazed the path for future long baseline interferometers.

### 2.5.2 Past and Present Interferometers

As technology has improved, interferometers have gotten significantly more complex and numerous. The scientific output of modern interferometers covers many astronomical interests: measurements of stellar diameters (e.g., Ciardi et al. 2001; Berger et al. 2006; Baines et al. 2008), determining binary star orbits (e.g., Bagnuolo et al. 2006; Boden et al. 2006; Raghavan et al. 2008), observing rapidly rotating stars (e.g., McAlister et al. 2005; Aufdenberg et al. 2006), probing the circumstellar regions of Be and T Tauri stars (e.g., Tycner et al. 2005; Eisner et al. 2006; Gies et al. 2007), and even imaging binary stars and stellar surfaces

(e.g., Monnier et al. 2007; Zhao et al. 2008). As of this writing, there are seven operational long baseline interferometers operating in the visible and infrared with two more (Large Binocular Telescope (LBT) and Magdalena Ridge Observatory (MRO)) under construction and several more space and ground-based projects under design study. Table 2.1 provides information for each of these and their operational statistics.

#### 2.5.2.1 Infrared Spatial Interferometer

The Infrared Spatial Interferometer (ISI) is a heterodyne interferometer operating in the mid-infrared ($\sim 10\mu$m) consisting of three relocatable 1.65-m aperture siderostats at Mount Wilson Observatory. Unlike most optical interferometers, ISI uses the heterodyne technique of mixing the IR stellar radiation with a laser and detecting the resulting microwave "beating" of these two signals. Thus, ISI does not require a series of mirrors to transport light to an optical lab, and the instrument achieves delay compensation electronically. ISI still measures many of the same parameters of stellar phenomena but in a manner more closely related to radio interferometry. This type of interferometer still can collect data on stellar diameters (Weiner et al. 2000), limb-darkening coefficents, dimensions of dust shells (Hale et al. 1997), and high spatial resolution infrared spectroscopy of stars and planetary atmospheres (Monnier et al. 2000).

#### 2.5.2.2 Keck Interferometer

Using the two ten-meter telescopes on Mauna Kea, the Keck Interferometer (KI) is comprised of the largest apertures of any interferometer. Separated by 85 m and operating in the infrared at 2.2 $\mu$m and 10 $\mu$m, the KI is a superlative instrument for detecting fainter objects, dust surrounding young stars (Millan-Gabet et al. 2006), galaxy cores (Swain et al. 2003), and the search for extra solar planets (Eisner 2007). The Keck Interferometer also features a nulling mode which suppresses the light from the primary source in order to detect very faint companions or dust in the surrounding environment Barry et al. (2008)

#### 2.5.2.3 Navy Prototype Optical Interferometer

Located on Anderson Mesa, Arizona, the Navy Prototype Optical Interferometer (NPOI) consists of two arrays of 50-cm siderostats with four fixed elements for astrometric measurements and six movable elements for interferometric imaging. With baselines of 2 to 437 m, NPOI has produced a large body of observations and scientific papers since its first light in 1996. Projects conducted to date include rapid rotators (Peterson et al. 2006), multiple star systems (Hummel et al. 2003), and Be star disks (Tycner et al. 2005).

#### 2.5.2.4 Palomar Testbed Interferometer

Though originally developed as a testbed for the Keck Interferometer, the Palomar Testbed Interferometer (PTI) stands on its own as a quality instrument that has led to many scientific publications. In addition to its publicly available database of observations and calibrator catalog, PTI remains the only interferometer capable of simultaneous fringe tracking on the

object and its calibrator star. Operating in the infrared (1.4 $\mu$m to 2.5 $\mu$m) with a maximum 110-m baseline, PTI can probe the inner dust regions of Herbig Ae/Be stars (Eisner et al. 2007) and has produced many interferometric orbits of close ($\lesssim$5 mas) binary stars (Boden et al. 1999a,b)

#### 2.5.2.5 Sydney University Stellar Interferometer

A six-element purely north-south oriented interferometer located near Narrabri, New South Wales, Australia, the Sydney University Stellar Interferometer (SUSI) was developed to provide long-baseline observations of stellar diameters and effective temperatures (Davis et al. 2007), multiple star systems (North et al. 2007), and pulsating stars (Ireland et al. 2005) with high accuracy in visible light (400-900 nm). The recent development of the Precision Astronomical Visible Observer (PAVO) and collaboration with CHARA scientists will permit simultaneous observations of an object from two hemispheres with 1% precision.

#### 2.5.2.6 Very Large Telescope Interferometer

In a similar arrangement as the Keck Interferometer, the Very Large Telescope Interferometer (VLTI) consists of the four main fixed 8-m "Unit Telescopes" of the VLT and four moveable 1.8-m "Auxiliary Telescopes" that can produce baselines of up to 200-m. The placement of Auxiliary Telescopes provides superb u,v coverage while also yeilding an excellent magnitude limit. The combination of the long baselines and multiple large aperture telescopes allows for unique observations of the galactic center (Pott et al. 2008), dust surrounding AGN (Beckert et al. 2008), and probing the inner disk around Be stars (Kraus et al. 2008)

#### 2.5.2.7 The CHARA Array

While we have discussed how the CHARA Array works in a previous section, we did not include how the Array compares to currently operating interferometers. With baselines of 30 to 330 meters over six fixed 1-m apertures, the CHARA Array may not have the longest single baseline, the most telescopes (both belonging to SUSI), or the largest aperatures (KI) but can combine the best aspects of all of these. Currently, the six telescopes are able to provide light to five different instruments: CHARA Classic (ten Brummelaar et al. 2005), Fiber-Linked Unit for Optical Recombination (FLUOR) (Coude du Foresto et al. 2003), Michigan InfraRed Combiner (MIRC) (Monnier et al. 2007), Visible spEctroGraph and polArimeter (VEGA) (Mourard et al. 2008), and Precision Astronomical Visible Observation (PAVO) (Ireland et al. 2008). Classic, FLUOR, and MIRC operate in the IR, and VEGA and PAVO in the visible spectral domains. Another two instruments are in the final stages of design and implementation: the CHARA multiple beam combiner (CLIMB - CLassic Interferometry with Multiple Baselines), which will allow closure phase measurements and simultaneous multiple baselines for instant separated fringe packet solutions, and the CHAMP fringe tracker for phase locking of the fringes on all six baselines. The Array also has the ability to operate two programs simultaneously on two to four telescopes at a time and the capability for one or both programs to be controlled remotely via secure virtual private networks from the remote operations centers in Atlanta, Paris, Ann Arbor, Grasse, and Sydney.

Table. 2.1: Currently Operational Long-Baseline Interferometers

| **Facility Acronym** | **Site Location** | **Collecting Elements and Aperature(cm)** | **Baseline Range (m)** | **Operating Wavelength ($\mu$m)** |
|---|---|---|---|---|
| ISI | Mt. Wilson, USA | 3 x 165 | 4-70 | 11 |
| KI | Muana Kea, USA | 2 x 1,000 | 85 | 1.5-5 & 10 |
| NPOI | Anderson Mesa, USA | 10 x 50 | 2-437 | 0.45-0.85 |
| PTI | Mt. Palomar, USA | 3 x 40 | 86-110 | 1.5-2.4 |
| SUSI | Narrabri, AUS | 11 x 14 | 5-640 | 0.4-0.90 |
| VLTI | Cerro Paranal, CHL | 4(4)[§] x 820(180)[§] | 8-200 | 1-2.5 & 10-20 |
| CHARA | Mt. Wilson, USA | 6 x 100 | 30-331 | 0.5-2.13 |

*Notes.*

[§]Includes four 8.2-m telescopes and four auxilliary 1.8-m telescopes.

ISI: Infrared Spatial Interferometer (Hale et al. 2000); SUSI: Sydney University Stellar Interferometer (Davis et al. 1999); NPOI: Navy Prototype Optical Interferometer (Armstrong et al. 1998); PTI: Palomar Testbed Interferometer (Colavita et al. 1999); CHARA: Center for High Angular Resolution Astronomy Array (ten Brummelaar et al. 2005); KI: Keck Interferometer (Colavita et al. 2004); VLTI: Very Large Telescope Interferometer (Richichi 2007);

*We are all in the gutter, but some of us are looking at the stars.*

*—— -Oscar Wilde*

# – 3 —

# Separated Fringe Packets

This chapter aims to give a background on the concept of Separated Fringe Packets, how they are formed and utilized, determining the primary fringe packet, how separate baselines and baseline rotation allow determination of the location of the secondary, and the factors that introduce error into the calculations.

## 3.1 Theory and History of Separated Fringe Packets

In order to determine the correct orientation for a secondary source with an interferometer, there is a potential ambiguity of 180° in position that needs to be overcome. Previous methods for removing this ambiguity when using an interferometer include using closure phase requiring three or more telescopes (Shao & Colavita 1992), or via the dispersed fringe technique with two telescopes by spectrally dispersing fringes within their bandpass (Schloerb 1990). The technique applied here uses only two telescopes at a time in different orientations to extract the location of the secondary of a binary star with simple geometric techniques bypassing visibility measurements completely. With the advent of long baseline optical interferometers, this theory that was proposed, discussed, and seemingly unused since its inception can now be fully tested and applied to current and future multiple star studies.

In order to validate the transfer scan mode on the Fine Guidance Sensors on the Hubble Space Telescope in the early part of the 1990's, Franz et al. (1992) conducted a series of tests

on binary stars in the Hyades cluster using the transfer functions (plots of the visibility of the interference pattern) of the two beams of linearly polarized light. As the polarizations of these beams are orthogonal, the transfer functions represent sensitivities in the $x$ and $y$ directions. At the time, the program did not have a suitable list of calibrators with which to determine the absolute directions of $x$ and $y$ with respect to known sources, and so it was impossible to completely determine with high accuracy the absolute locations of the possible companions.

Dyck et al. (1995) conducted similar experiments using the Infrared Optical Telescope Array (IOTA) on a well-studied, widely-separated binary, $\zeta$ Hercules, in an attempt to revive the notion of using a two-telescope interferometer to bypass the position angle ambiguity associated with interferometry. The practical usage and theory on the application of this process provides the basis for Separated Fringe Packet (SFP) investigations as applied in this project. Nearly a decade had passed after Dyck et al. (1995) published this groundwork before another example of SFP study was put into practice. Lane & Muterspaugh (2004) used a fringe tracker on the Palomar Testbed Interferometer (PTI) to allow for delay scanning on a larger angular scale while keeping the phase information for differential astrometry of a binary system. During the scientific commissioning of the CHARA Array, Bagnuolo et al. (2006) completed a similar study on separated fringes using a slightly different technique on 12 Persei, a less widely separated binary with a previous speckle orbit.

### 3.1.1 Separated Fringe Packets with IOTA

As noted by Dyck et al. (1995), that in the case of a binary star for which both components are within the field of view of the interferometer, it is possible with the correct orientation, that the interferometer will produce non-overlapping fringes for each star at widely-separated delay positions. The observed double interference pattern can be seen as a linear combination of the individual fringes and scaled by the relative brightness of each source. The difference in delay or path between the two fringe packets is based upon the orientation of the binary system (separation and position angle) and the orientation of the baseline in use at the time of the observation and modified by atmosphere seeing variations - mostly due to the movement of fringes during measurement due to differing air path lengths referred to as "piston error." In the case of binaries with small separations or through orientation where the baseline is nearly orthogonal to the separation of the system, the fringe patterns will overlap and the standard visibility analysis is applicable. For wider binaries, each fringe will produce a distinct interference fringe of its own with relative amplitudes proportional to the brightness of the individual sources.

For IOTA, it was possible to drive the delay line at a high enough rate to record the delay referenced positions of each fringe packet and "freeze" the phase-perturbing effects of the atmosphere and obtain a snapshot of the one-dimensional cross section of the system. This technique, called "delay referencing" by Dyck et al. (1995), allows for the referencing of different source components to a common fiducial and preserves the relative positional information of the system. This was then tested on $\zeta$ Her using the north-south IOTA baseline on

multiple occasions, alternating between $\zeta$ Her and a single unresolved calibrator star to show that the formation of the secondary fringe packet was not due to instrumental artifacts. Additionally, modeling with synthetic data was done to determine how well these "snapshots" could handle multiple components. Using a system comprised of four components, the theoretical response of IOTA on both baselines was calculated with varying separations and brightness ratios, and it was determined that the best course for observing systems with multiple components would be to observe the source over a wide range of times and allowing the rotation of the projected baseline to help sample the $UV$ plane. Through the information that had been gathered from IOTA, Dyck et al. (1995) have shown conclusively that this technique was able to locate and measure the relative position of the secondary with reasonable accuracy on separations available to IOTA, and their work provides the foundation for the SFP survey at the CHARA Array.

### 3.1.2 Previous Separated Fringe Packets with PTI and the CHARA Array

Nearly a decade later, two efforts (Lane & Muterspaugh 2004; Bagnuolo et al. 2006) used similar approaches to obtain approximately the same information. Through the use of a fringe tracker on PTI on a "wide" binary, Lane & Muterspaugh (2004) were able to obtain separation errors of $\approx$16 $\mu$as for the binary HD 171779. As each 150$\mu$m delay modulated scan was typically 1.5 seconds and the fringe separation nearly one-third of the scan, the phase locking fringe tracker was absolutely necessary to keep the positional and temporal coherence of the individual fringes intact. Using a different, yet complementary approach

of "side-lobe verniering" (the modulation of the separation as the secondary's fringe packet rides over the side-lobes of the primary), Bagnuolo et al. (2006) produced separation errors of $\sim$25 $\mu$as for 12 Per with a significantly smaller separation ($\sim$50 mas from CHARA vs $\sim$250 mas from PTI). The "free" phase reference from the modulation of separation from the side-lobes provided the CHARA Array a method to obtain excellent accuracy for smaller angular separations without using a fringe tracker. Moreover, the accuracy of the side-lobe verniering provided a refinement of an existing visual and spectroscopic orbit and yielded the fundamental parameters of the system to an accuracy of $\sim$1%. Both of these determinations show the limiting accuracy of single baseline measurements with phase referencing on their respective instruments but require significant observing time dedicated to a single object.

## 3.2 Utilizing Separated Fringe Packets

With the basics of fringes and the CHARA Array established, the combination of the two leads to an interesting special case. But, first it is necessary to define the limits of the Array's resolution. The limiting resolution of the CHARA Array can be defined by the location of the first null in the fringe visibility, and is computed to be 1.6 mas, with the $K'$ filter on the longest baseline available (S1/E1 $\sim$330m). Higher resolutions are available by measuring the visibility higher up the visibility curve but for the purposes of this project we shall be examining a different regime that does not require visibility calibrations.

A more important value for this discussion is the coherence length of the fringes, defined as

$$\Lambda_{\rm coh} = \frac{\lambda_0^2}{\Delta\lambda}, \tag{3.1}$$

where $\lambda_0$ is the central wavelength of the filter used, $\Delta\lambda$ is the effective filter width and $\Lambda_{coh}$ is a measure of the width of the fringe packet. This quantity is solely defined by the filter in use and is calculated to be 18.15 $\mu$m for all observations in this project. Expanding outwards, another important quantity to discuss is the extent of the dither throw. As was mentioned in the previous section, the dither mirror is powered through a saw-tooth pattern for scanning through the delay region in where the fringe is supposed to lie. The piezoelectric stage upon which the mirror is mounted has a scan length of 86.9 $\mu$m, which due to the reflection of the mirror, means when run to its limit, we are scanning through 173.8 $\mu$m of delay. More recently (though it does not affect calculations before January 2008), the dither has been upgraded for higher precision yielding a delay scanning maximum of 142.43 $\mu$m. The coherence length and the length of the dither scan along with the projected baseline given by

$$\vec{B} = \sqrt{u^2 + v^2} \tag{3.2}$$

where $u$ and $v$, the snapshot projection of the baseline in spatial frequency units (cycles/arcsec) as laid out by H.M. Dyck in the Principles of Long Baseline Stellar Interferometry Lawson (2000) are defined by

$$u = B_E \cos h - B_N \sin b \sin h + B_L \cos b \sin h / 206265\lambda \tag{3.3}$$

and

$$\begin{aligned} v = B_E \sin\delta \sin h \quad &+ \quad B_N(\sin b \sin\delta \cos h + \cos b \cos\delta) \\ &- \quad B_L(\cos b \sin\delta \cos h - \sin b \cos\delta)/206265\lambda \end{aligned} \tag{3.4}$$

where $h$ and $\delta$ are the hour angle and declination of the object, $b$ is the latitude of the observatory, $B_E$, $B_N$, and $B_L$ are the position vectors of each telescope with respect to the reference telescope S2, and $\vec{B}$ is the instantaneous projected baseline length. This relation allows us to determine the one-dimensional "Field Of View" of the instrument for searching outside of the primary fringe packet using

$$\vec{\rho}_{\rm mas} = \frac{206.265\vec{\rho}_{\mu\rm m}}{B(m)}. \tag{3.5}$$

There are two limits to consider when searching for secondary fringes. When determining the inner limit for close fringes, one can set a generous bound for estimation by using the location of the first null calculated by the fringe coherence length. As shown in the example fringe envelope plot in Figure 3.1, by limiting the separation at the point where the secondary fringe maxima occurs at the location of the first null of the primary fringe we have a reasonable limit for the smallest separation detectable. For the opposite case of the limit of wide fringes, the separations available are purely based on the length of the dither scan.

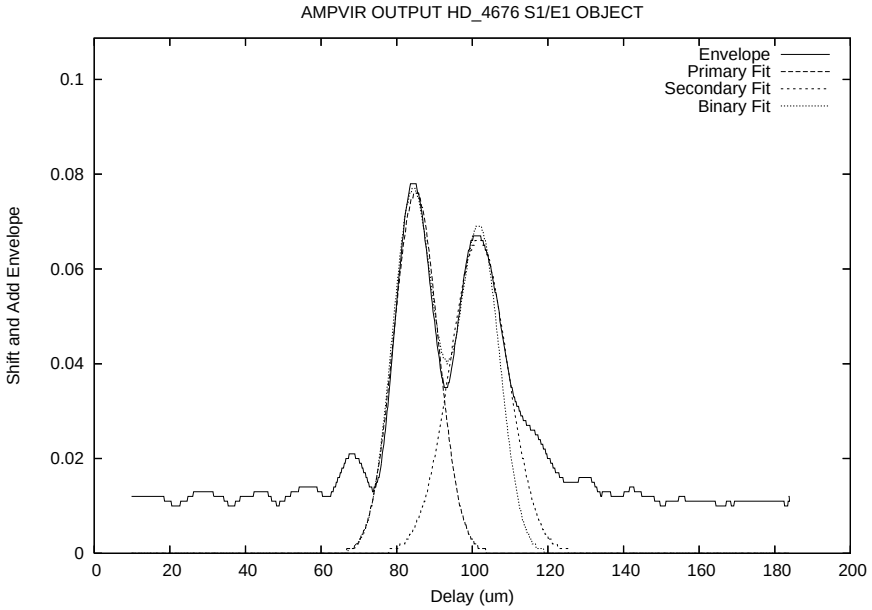


Figure. 3.1: Closest SFP for this Project. An example of the closest separated fringe packet system (HD 4676) recorded by this project. This envelope trace of the two fringes was taken on the longest baseline (S1/E1). As this orbit was at maximum elongation with the baseline nearly parallel to the separation at the time, fringes on the secondary baseline were not found. Calculated projected separation for the secondary fringe was slightly inside the coherence length at 17 $\mu$m.

The on-sky separation related to these limits is also a function of the projected baseline. For each baseline and pop combination, there is a limit on the projected length of the baseline that is determined by the area of the sky and the fixed delay increments being used. With the close/wide secondary fringe estimated separation and the limits of the projected baselines, we can give estimates for each baseline of the search space available. These values have been tabulated and are compiled in Table 3.1 that shows the min/max separation for the largest and smallest projected baselines for each combination. It is conceivably possible to measure secondary fringes within the coherence length limit provided that the secondary is of sufficient brightness and is completely unresolved in angular diameter, but this requires very good seeing to avoid blending the fringes together.

## 3.3 Determining the Primary Packet

As discussed previously, when observing a binary star system with baselines of proper orientation and length, each component creates a separate fringe packet if the angular separation is sufficiently wide. This allows the observer to measure a component of separation along the projected baseline and not the true angular separation and position angle. The first thing to be considered when dealing with double packets is which one truly represents the primary. For components that are within the range we are considering (10-100 mas), generally we need to use the longest baselines available in order to record both packets within the scanning range of the Array. This creates a difficulty for larger diameter objects that have companions as these same baselines will at least partially resolve these stars' photospheres which lowers the visibility for their respective packets. If the system is composed of two stars at the same distance and of approximately the same diameter, both packets will be resolved to the same extent, and the brighter of the two will be represented by the larger packet. Conversely, if the stars are different in size, such as a giant primary and a dwarf secondary, and the system has a large parallax, the fringe packet relating to the primary could appear to be smaller than the secondary due to the array partially or fully resolving the disk of that star. For an example of this, see Chapter 6.2.13 on HD 170153.

Table. 3.1: Configurations of the CHARA Array

| **Baseline** | $\Theta$ | **Max B (m)** | **Min B (m)** | **Min $\vec{\rho}$ Min B (mas)** | **Max $\vec{\rho}$ Min B (mas)** | **Min $\vec{\rho}$ Max B (mas)** | **Max $\vec{\rho}$ Max B (mas)** |
|---|---|---|---|---|---|---|---|
| S1-S2 | -9.72 | 34.08 | 19.23 | 194.64 | 1394.13 | 109.86 | 786.90 |
| E2-E1 | 57.15 | 65.89 | 29.21 | 128.18 | 918.10 | 56.82 | 406.98 |
| W2-W1 | -81.03 | 107.93 | 37.44 | 100.00 | 716.23 | 34.69 | 248.45 |
| W2-E2 | 63.04 | 156.28 | 65.40 | 57.25 | 410.03 | 23.96 | 171.58 |
| W2-S2 | -42.99 | 173.63 | 112.09 | 33.40 | 239.23 | 21.56 | 154.44 |
| W2-S1 | -19.28 | 210.96 | 131.31 | 28.51 | 204.20 | 17.75 | 127.10 |
| W2-E1 | 61.29 | 221.84 | 93.88 | 39.88 | 285.63 | 16.88 | 120.87 |
| E2-S2 | 17.69 | 248.13 | 155.56 | 24.07 | 172.37 | 15.09 | 108.06 |
| W1-S2 | -42.99 | 249.39 | 144.66 | 25.88 | 185.37 | 15.01 | 107.52 |
| W1-E2 | 77.56 | 251.34 | 113.45 | 33.00 | 236.34 | 14.90 | 106.69 |
| W1-S1 | -39.14 | 278.50 | 172.80 | 21.67 | 155.18 | 13.44 | 96.28 |
| E2-S1 | 14.46 | 278.77 | 169.33 | 22.11 | 158.36 | 13.43 | 96.19 |
| E1-S2 | 25.70 | 302.34 | 202.89 | 18.45 | 132.16 | 12.38 | 88.69 |
| W1-E1 | 73.34 | 313.54 | 134.27 | 27.88 | 199.71 | 11.94 | 85.52 |
| E1-S1 | 22.27 | 330.67 | 215.92 | 17.34 | 124.19 | 11.32 | 81.09 |

*Notes.* The first four columns are the absolutes for each baseline: 1. Which telescopes are used. 2. The position angle of that baseline with respect to north. 3&4. The max and min projected baseline lengths. The final four columns are calculated observables. Columns 5&6 are the max and min separations on sky in mas using the minimum projected baseline. Columns 6&7 represent the same on the maximum projected baseline. These represent the limits in 1-D sky coverage that are attainable with each baseline. The lower limit is calculated rather conservatively based on the coherence length for the filter in use and is not a hard limit. The upper limit, however, is based on the widest set of complete fringes that will fit within the dither mirror scan.

## 3.4 Rotation and Orthogonal Baselines

If prior spectroscopic information for the system exists, estimates for each of the component's angular diameter and magnitude difference can be used to determine which fringe packet represents the primary, then determination of the companion's true position can be investigated. In the absence of this information, it is customary to select the fringe with the largest average amplitude as the primary as the difference in amplitudes is influenced to a higher degree by the magnitude difference if compared to differential resolution of the components except in specfic cases. Since the location of the second packet only supplies a vector separation, other methods must be used in conjunction with the observations to get complete results. Two similar methods provide observers with the necessary information to determine where the secondary truly lies.

The simplest course is to use multiple telescopes when available during the course of the night, and this is the method that was most used over the course of this project. With the addition of a second baseline (most times at $60-90^{\circ}$ offset) with a suitable orientation of the companion and the telescopes, the observer can switch between the two baselines over the course of the night and produce SFPs on both. The diagram in Figure 3.2 shows a simplified example of the ideal case where we have two perfectly perpendicular baselines that can be used to determine the true separation and position angle of the secondary for systems where the period is much greater than one day.

If only one baseline is available, then an alternate method should be employed. Over the course of the night, from the perspective of the object, the orientation of the baseline being

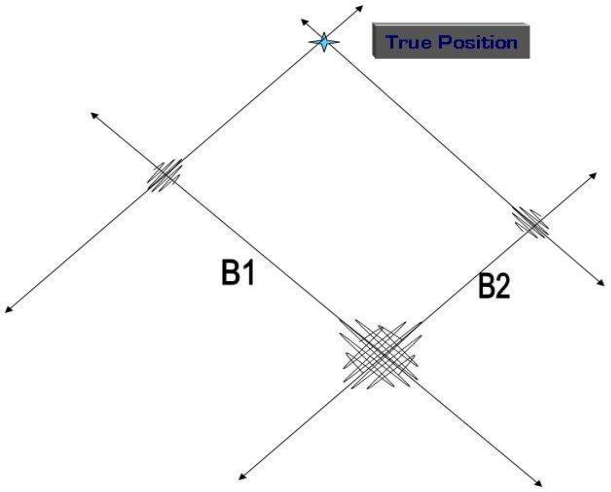


Figure. 3.2: Location of the Secondary Using Ideal Orthogonal Baselines. While this is almost never achieved due to telescope placement and projection effects, this diagram provides the configuration sought after by the observer.

used appears to change length and position angle depending on the star's location in the sky. This change in position angle is generally referred to as baseline rotation and is identical to "earth rotation aperture synthesis." Figure 3.3 shows a diagram giving a general idea on how baseline rotation can be used to determine the location of the secondary. By either taking multiple observations one after another or by switching stars and observing the same object at regular intervals, the observer can use the rotation of the baselines to build up a string of data over which the extension lines from the secondary packet will cross at the true location of the secondary. Combinations of rotation and orthogonal baselines can be used for better accuracy and quadrant determination.

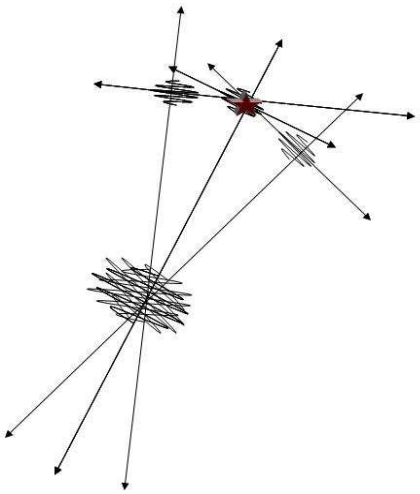

Figure. 3.3: Locating the Secondary with Rotation. A more realistic case when only one baseline is available. Realistically, this is how most SFPs are recorded and supplemented with secondary baselines to get the secondary's location.

## 3.5 Calculating Fringe Separation

Now that the process of how separated fringes can be used is established, quantification of the separation must be determined. The reduction program, written by Theo ten Brummelaar, begins by attempting to locate the fringes within the scans. It takes the Fourier transform of the scan for each side of the detector and searches the area around the frequency where the fringes are expected and and at sufficient distance away in the frequency domain to get measures of the fringe and noise power. The program will select a scan as having a fringe if the $S/N \geq 1$ and if the fringe is observed on both detector channels. Poor scans can be automatically removed or can be done manually depending on the settings of the program.

Once the scans with fringes have been determined, a bandpass filter around the fringe frequency is used to eliminate the noise frequencies leaving only the fringe signal. In order to easily determine the fringe separation, it is best to obtain the envelopes of the fringes to

measure the distance between the maxima. The fringe signal is Hilbert transformed using

$$\mathcal{F}(H(u))(w) = (-i\mathrm{sgn(w)}) \cdot \mathcal{F}(\mathrm{u})(\mathrm{w}) \tag{3.6}$$

where the $\mathcal{F}$ denotes the fourier transform and has the effect of shifting the phase of the negative frequencies 180° resulting in their negation, leaving only the positive frequencies. This signal is retransformed into the real domain where the absolute value is taken, and the result is the fringe envelope.

The envelopes of all the scans are then combined through a "shift-and-add" procedure to get a value for the separation of the secondary. This can be done in two methods depending on the data quality. On nights of good seeing where the data have a high signal-to-noise ratio, it is beneficial to use the "Correlation" method which will correlate the locations of the two fringes with subsequent scans to retain the orientation of the secondary. If the amplitudes of the fringes are nearly the same, the maxima have small separation, or the data quality is low, the "Max" method takes the maximum of the envelope (the primary fringe), and shifts all subsequent scans so that the maxima overlap which can build up signal in at the location of the secondary for easier measurement. This is most needed where fringe amplitudes are nearly the same and the seeing causes fluctuation of the amplitudes leading to the secondary fringe maximum being larger than the primary and hence an orientation opposite of the true one may result.

After the "shift-and-add" procedure, the software will fit a Gaussian to the primary fringe envelope and search the remainder of the scan for a second maximum. If one is found, the

program will fit a second Gaussian to that location and finally attempt to fit both simultaneously. The location of the primary is subtracted from the secondary giving the vector separation based on Equation 3.5 and the direction along the baseline for that observation. The separation of the fringes in microns as calculated by the program is comprised of the instantaneous projected baseline length at the time of observation and depends on the absolute calibration of the position of the dither mirror, calibrated by laser metrology and accurate to $\leq 1\mu$m.

Using a line perpendicular to the position angle of the baseline at the point of the maximum for the secondary fringe from each data set on both baselines, the observer can extend these lines to the point where they all intersect at the actual position of the secondary. An IDL routine written by Theo ten Brummelaar takes the vector separations and creates these perpendicular lines and calculates the intersection point for each pair of lines if the angle between them is larger than the selected minimum. In the general area of the intersection points, the program calculates the sum of the squares of the distance to each line and finds the minimum which is determined to be the location of the secondary. The final obtained values for each triangulation provide a measure of the error in the determination of this location. From this point, the distances to all lines are calculated. Two values are determined from the distances: the mean and maximum distance. Using these values as radii, error circles are plotted along with the lines and the locations of the primary and secondary as shown in Figures 3.4 and 3.5.

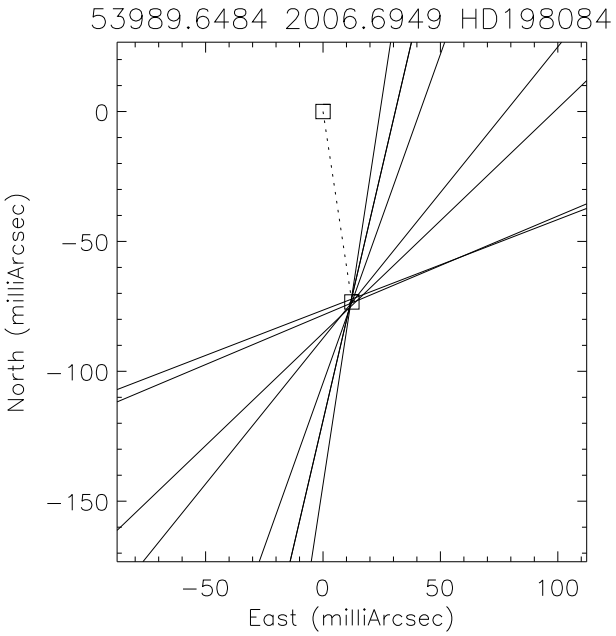


Figure. 3.4: Example Triangulation Plot for HD 198084. An example triangulation plot for 7 data files from 2006 September 10 to September 12. The two □ symbols represent the locations of the two stars at that time with the dashed line between them as the direction vector to the secondary. Each individual solid line represents one data file and is a ⊥ line from the peak of the secondary fringe. Where these lines meet can be considered the true location of the secondary.

## 3.6 Limiting Accuracy

As with all methods, there are limits to the range of objects and companions that can be detected. In addition to the limitations of the telescopes and instrument in use, errors due to atmospheric distortion, camera noise, and fringe movement need to be examined. The four factors in the following sections discuss estimates of errors and the limitations on the object parameters being considered when the data are quantified. Estimations for the errors for atmospheric distortion, photon noise, and temporal coherence are based on Lane & Muterspaugh (2004) and adapted for the CHARA Array's parameters.

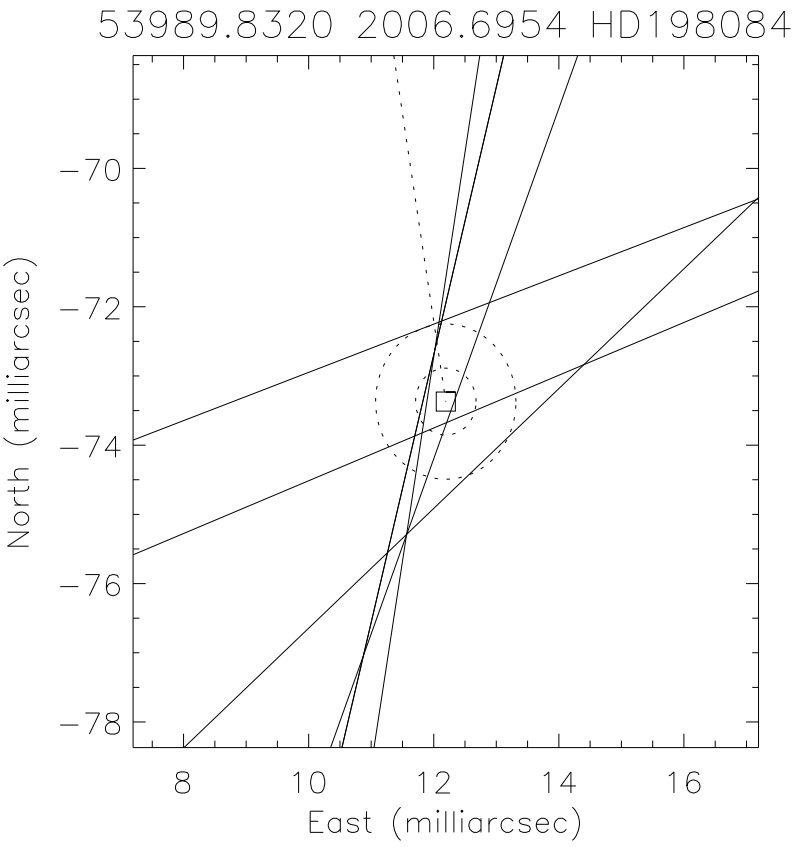


Figure. 3.5: Example Triangulation with Error. Shown here is the region around the area of the secondary to show the calculated location and error circles. Each solid line is a perpendicular from the secondary fringe with the square as the determined true secondary star location. The large circle has a radius of the distance from the secondary to the furthest line whereas the smaller circle is the average distance to all lines.

### 3.6.1 Magnitude and $\Delta$ Magnitude Limitations

Since no telescope or camera is infinitely sensitive, there are magnitude limits imposed upon otherwise available targets. Two conditions must be met before observations of a system are made. The first, telescope tracking on the object using the CHARA tracking servo, has the greatest sensitivity and is the least important limit for this project. Tracking on an object is accomplished in the $V$ band by a CCD after the $K'$ band light from the telescopes is routed

to the beam combination table. The limitations on the magnitude of the star being tracked are currently not a hard limit and as of this writing, systems down to $V = +10.5$ are able to be locked onto for tracking.

In order to transport the light to the CHARA Beam Combination Laboratory, a non-trivial number of reflections is needed, and through the 19 reflections from the telescope to injection into the "Classic" beam combiner, a significant amount of light is lost. This, combined with the camera sensitivity in the slowest read mode (250 Hz), limits the magnitudes available in the science bands ($K$, $H$ and $J$). A reasonable approximation of the observational limit for the CHARA Array is +7.5 using the $K'$ filter ($\lambda_0$=2.1329 $\mu$m, $\Delta\lambda$=0.6222 $\mu$m).

With the sensitivity limitations on the instrument established, we can turn our attention to the detection of the secondary fringe. Two factors influence this. As mentioned previously in this chapter, it becomes increasingly difficult to quantify the location of the secondary fringe as the separation decreases. The first three rows of Figure 3.6 show the effects of decreasing delay separation of a pair of ideal fringes with $\Delta$m=1 from 100 $\mu$m to 20 $\mu$m. As these are the ideal noiseless case, it is obvious that atmospheric and detection noise would obscure merging fringes. The bottom three rows of Figure 3.6 show the effect of increasing $\Delta$m with a fixed separation. The difference changes the contrast of the fringes from clearly visible with $\Delta$m=0.5 at the top, $\Delta$m=1.5 in the middle, to barely discernable at a $\Delta$m=2.5 at the bottom. As these fringes are also without noise, they are relatively easy to see. For realistic cases, the detection of the secondary can be practically unseen for individual scans, but discernable as the scans are integrated in a shift-and-add process. For systems where

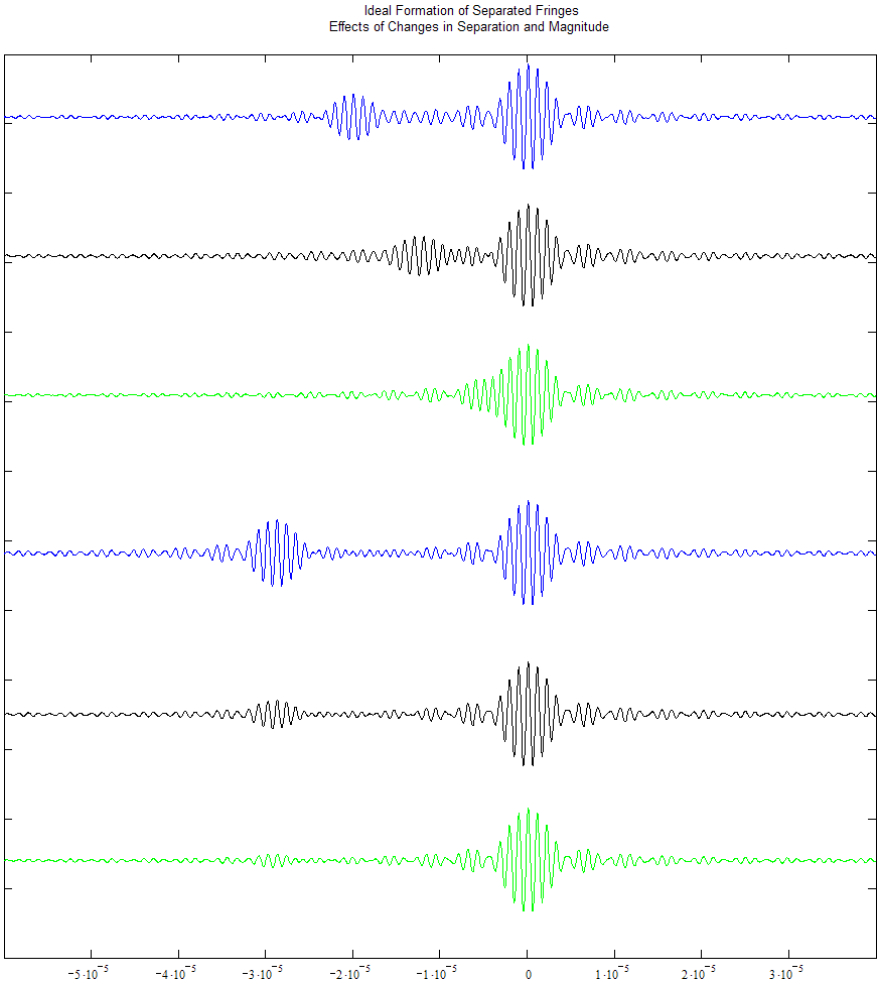


Figure. 3.6: Effects of $\Delta$m and Separation on Separated Fringe Packets. The top three scans show the effects of decreasing separation on a $\Delta$m=1.0 set of fringes. It is easy to see how as the separation decreases the discernability of the location of the secondary becomes increasingly more difficult. The bottom three scans show increasing $\Delta$m from 0.5 to 2.5 magnitudes with a constant separation. Below $\Delta$m=2.0 it becomes a non-trivial matter to locate the secondary even under ideal (no noise) conditions which can be corrected for to some extent by the summation of multiple scans to increase the signal-to-noise ratio.

the companion is faint, increasing the number of scans for each data set can increase the chances of detecting a companion with a large magnitude difference. An estimate of the maximum $\Delta$m we can reasonably obtain from the CHARA Array in the described modes is approximately $\Delta$m=2.5.

### 3.6.2 Anisoplanatism

In order to quantify the astrometric performance of the interferometer, we must account for the three major sources of error affecting the measurement of separated fringes. Originally analyzed by Shao & Colavita (1992) and restated by Lane & Muterspaugh (2004), the perturbation of a simultaneous astrometric measurement of two sources is defined as the error in path length of the light from the two sources as it passes through differing amounts of atmosphere. The primary result of astrometric error $\sigma_a$ due to anisoplanatism is given in arcseconds by

$$\sigma_a = 540 B^{-2/3} \theta t^{-1/2} \tag{3.7}$$

where $\theta$ is the angular separation between stars in radians, $B$ is the baseline in meters, $t$ is the integration time in seconds. This calculation assumes a standard atmospheric turbulence profile (Lindegren 1980). Using estimates of $B$=300 m, $t$=0.25 seconds, and $\theta$=60 mas we obtain $\sigma_a$=7.01 $\mu$as.

### 3.6.3 Photon Noise

The error in projected separation due to read/photon noise ($\sigma_p$) from the detector in arcseconds can be quantified as

$$\sigma_p = \frac{\lambda}{2\pi B} \frac{1}{\sqrt{N}} \frac{1}{S/N} \tag{3.8}$$

where $B$ is the baseline, $\lambda$ is the wavelength of the recorded light, $N$ is the number of scans, and $S/N$ is the signal-to-noise ratio of the individual fringes. Using the same baseline estimate as the previous approximation ($B$=300 m) with $N$=220 scans, $\lambda$=2.15 $\mu$m, and $S/N$=20 for an average fringe signal-to-noise obtainable with the CHARA Array, we obtain an estimate of $\sigma_p$=0.79 $\mu$as.

### 3.6.4 Temporal Coherence

The last and largest source of error for the determination of the separation between separated fringe packets, the temporal coherence encompasses the fringe movement during the scan. Also called "piston error," quantifying this is considerably more difficult. Using Equation 6 from Lane & Muterspaugh (2004) with some modifications based on the different instrument and recording times and eliminating the term relating to the phase tracker available at the Palomar Testbed Interferometer (PTI), the expression is then given by

$$\sigma_{tc}^2(mas) = \left(\frac{\lambda}{2\pi B}\right)^2 \frac{1}{N} \int_0^\infty A(f)S(f)\,df \tag{3.9}$$

where $A(f)$ is a measure of the power spectral density of fringe phase observed through the atmosphere and is approximated by

$$A(f) \propto f^{-\alpha}. \tag{3.10}$$

The $\alpha$ parameter is within the range 2.5 to 2.7. $S(f)$ is the sampling function representing the phase sampling while scanning across one fringe and the time taken to move between

fringes given by

$$S(f) = \sin^2(2\pi f \tau_p)\mathrm{sinc}^2(\pi f \tau_\Lambda). \tag{3.11}$$

Here, $\tau_p$ is the time delay between recording of individual fringes (fringe separation ($\Delta d$) / scan velocity ($v_s$)), and $\tau_\Lambda$ is the time required to scan the individual fringes (coherence length ($\Lambda$) / scan velocity ). Using the previous parameters in the other error sources ($B$, $\lambda$, $N$) combined with $v_s$=569.7 $\mu$m/s, $\Delta d$=60 $\mu$m, and $\Lambda$=36.3 $\mu$m, we obtain a value for $\sigma_{tc}$ on order with the estimate given by Lane & Muterspaugh (2004) for a system without a fringe tracker (0.491 mas vs 0.016 mas) and by far the most dominant error term for the measurement of separated fringes.

### 3.6.5 Additional Error Sources

Other instrumental factors can influence the calculations for determining accurate separations between fringes, but are mostly neglected as they are orders of magnitude smaller than the the largest error source. For the calibration of the separation of the fringes, it is necessary to know the location of the dithering mirror attached to the piezoelectric stage to a high precision. Fortunately, the calibration of the piezo position is known to 0.01-0.1 microns, which is less than 0.1 mas on the longest baselines when all other quantities are known.

In order to actually observe a star's fringes, the length of the baseline must be know to very high precision, which in turn implies high precision measurements of the locations of the telescopes. An accurate "baseline solution" is necessary to find fringes and the location

of each telescope is known to many decimal places, so when converting the separation of fringes from microns in the lab to separation on the sky, the uncertainty of the baseline values produces errors many magnitudes smaller than all other sources of error discussed here.

*Ah, there's nothing more exciting than science. You get all the fun of... sitting still, being quiet, writing down numbers, paying attention... Science has it all.*

*—— Seymour Skinner, Principal*

# – 4 —

# The Multiplicity Sample

## 4.1 The Duquennoy & Mayor Sample

The Duquennoy and Mayor survey (Duquennoy et al. 1991) (hereafter D&M) was devoted to a spectroscopic study of stellar multiplicity in the solar neighborhood using a similar method to Abt & Levy (1976). Drawing from their original sample of 291 objects observed with the COrelation RAdial VELocities (CORAVEL) spectrometer at the Haute-Provence Observatory, D&M selected limiting criteria for which stars would be eliminated to produce an unbiased sample. For their "nearby G-dwarf star complete sample" they selected all the primary stars in the Gliese (1969) catalogue of spectral type F7-G9 north of declination $-15°$, of IV-V, V, or VI luminosity class, and closer than 22 pc ($\geq$45 mas parallax). Of the original 291 objects in their extended sample only 164 primaries and 30 common proper motion secondaries (of which only 17 were observable with CORAVEL) fit these criteria. It is these 181 D&M objects that will be referred to herein unless otherwise noted.

The D&M survey was intended to be an update of the effort by Abt & Levy (1976) (hereafter A&L) with better constraints and completeness. It was noticed that the A&L survey was heavily biased by double-lined spectroscopic binaries and was magnitude limited rather than distance limited (Branch 1976). Additionally, when the A&L spectroscopic binaries were re-examined, most of the new discoveries were rejected as spurious (Morbey

& Griffin 1987). The misinterpereted binaries included a large portion of the short period binaries in the A&L sample and heavily biased the overall multiplicity of their G-dwarf sample.

D&M discuss in detail why the selection of their sample is superior to the previous G-dwarf survey. Their sample included nearby stars north of declination $-15°$ accessible from Haute-Province. The greatest advantage they claim is that their survey is distance limited rather than magnitude limited. The possibility that by the selection of the parallaxes there still remained a selection bias was not lost on D&M, but they were reasonably sure that this selection method was far superior to that of A&L. Additionally, it was discussed that the use of $\pi_{\rm trig}$ rather than $\pi_{\rm phot}$ prevented the inclusion of bias toward SB2's when the comparison was made on similar search volumes. Interestingly, the very parameter they counted on to be unbiased for the selection of the sample will be shown to have a large effect when we compare the original trigonometric parallaxes then available to those later produced by HIPPARCOS. The possible bias of the trigonometric parallaxes from systems with periods of less than a year concerned D&M though we will see later in this discussion that systems of all periods in fact were farther away than calculated and introduced a far larger correction than expected.

A further limitation was placed on the D&M sample from CORAVEL having difficulty distinguishing the spectral lines of stars earlier than F6V from the lack of discernable metallic lines and the increasing number of rapid rotators with the earlier spectral types. Also from this stage, known and suspected giants were removed from the sample to the best of their

ability though it appears that due to parallax errors and misclassifications that some slipped through the selection process. In order to detect long-period and low-amplitude binaries, along with the attempt to sample a range in orbital periods, the survey was done over a much longer time interval than the A&L survey. As with all updates, the technology supporting the newer survey allowed for far better precision in velocity measurement (0.3 km/s vs. 1.2 km/s) and the detection of less inclined orbits with smaller velocity amplitudes. All of these factors, combined with the selection of the systems from one of the most studied catalogs (Gliese 1969) providing the most complete supporting data for each system, and nearly double the average observations per system, provide convincing evidence of the superior quality of the selection process for the D&M survey.

## 4.2 Selection of Target Stars

In order to be as complete as possible, this project's starting sample included the complete extended sample of D&M's 291 observed stars. The criteria selected for acceptance into the final sample was that the objects must not be known giants, and must be readily observable with the CHARA Array. In order to be classified "observable," stars needed to be north of $-5°$, and brighter than magnitude $K = +5.5$ and $V = +7.0$. Subsequent upgrades to the CHARA Array since the beginning of this project have increased the sensitivity of the camera and tracking, allowing easy observing down to magnitude $K = +7.0$ and tracking on stars to $V = +10.5$. For consistency, however, the brighter limits were maintained.

From the original 291 stars in the extended sample, 145 were accessible with the CHARA

Array. In order to have an adequate number of possible spectroscopic binaries to test the SFP method, an additional 28 single- and double-lined spectroscopic binaries were selected from the CHARA Catalog of Orbital Elements of Spectroscopic Binary Stars (Taylor et al. 2003) that fit the ideal range of separations for double fringe packet discovery using the selected baselines. However, 13 of the selected SB's were already included in the sample. The resulting list of 160 objects thus became the sample for the SFP survey.

## 4.3 Initial Comparison

Even though the sample sizes of the D&M and SFP survey are quite similar, the overlap is less than what was expected. Primarily due to the magnitude limits at that time for the CHARA Array, only 88 systems are contained in both samples. Of those 88 objects, a little more than half (46) were originally classified as single, 37 as double, 3 as triple, and the remaining two as quadruple. Many stars of the original sample were unable to be observed due to instrumental limitations of the Array at the onset of the project, but it should be noted that after tailoring the list to the capabilities of the Array, the proportions of single vs. multiple stars (52:48% single:multiple) and average number of known companions (0.56 companions per system) were similar to D&M's determination. Even in the wider view of the 160 stars of the complete SFP survey, the proportions remained close to D&M's values (57:43% single:multiple).

## 4.4 Other Multiplicity Samples since D&M

In the years since the completion of the D&M survey, a few efforts have sought to expand upon the multiplicity of many different types of stellar systems. As these types of surveys take a considerable amount of time, many are ongoing and contain far more systems than D&M or A&L but cover the same general format. Other surveys, such as that of Mason et al. (1998a) concentrated on the multiplicity of O-stars using speckle interferometry and radial velocity measurements. If we look at other radial velocity surveys such as Abt & Willmarth (2006), Nidever et al. (2002), Halbwachs et al. (2003) and Nordström et al. (2004), it can be seen that though they look at the same types of systems, each tended to look at the implications of the multiplicity (distributions in mass ratio $q$, period, eccentricity, etc.) rather than the multiplicity as a whole and generally focus on only one type of instrument.

The studies of Abt & Willmarth (2006) and Nidever et al. (2002) focused primarily on the orbits of spectroscopic binaries and obtaining high precision radial velocities while only barely expanding on the multiplicity fraction. Halbwachs et al. (2003) concentrated their effort on a sample similar to D&M's but dealt mainly with binaries with periods of $\leq$10 years and the comparison with spectroscopic binaries in open clusters. Closest in scope is the very large "Big G" survey of Nordström et al. (2004) which collected Strömgren *ubvy* photometry and radial velocities of more than 16,000 F, G, and K stars over a shorter timescale for most systems (1-3 years). The "Big G" survey was mostly focused on ages and metallicities and their distribution but did discuss multiplicity. They found similar percentages of binaries to the D&M survey though their sample was magnitude limited and when restrcted to the

systems inside 40 parsecs the percentages remain the same. What is not mentioned in their discussion is the occurance of higher order multiples and a slight discrepancy in their "single" star definition. Of the 16,682 stars in their list, they mention that 11,060 are "stars that are not known to be double" and of those 7,817 have radial velocities consistant with being true single stars. This leads to only 46% of the sample being proven to be single not including possible face-on binaries.

It is quite beneficial to include data from speckle interferometry and radial velocity studies with the optical long-baseline interferometry (OLBI) as each discipline has selection effects in detection. The reality is that while it is difficult to obtain long term monitoring of stellar systems using multiple types of instruments, each kind of observation can detect companions where the others would miss them entirely. While radial velocity monitoring allows the detection of fast, very close companions or longer period orbits with secondaries with discernable moving spectral lines at almost any distance, it becomes increasingly difficult as the orbits become face on, have larger separations with longer periods, or exhibit with very small velocity amplitudes. Conversely, speckle and long baseline interferometry excel on stars with wide separations, face-on orbits, or very long periods but are less effective as the systems become more distant (smaller separations). All detection methods have problems detecting the secondary when $\Delta$m or the mass ratio is large. These techniques are quite complementary and yet most surveys naturally cannot employ the capablities of all approaches. Thus, the SFP survey is only able to obtain one type of observation and we must consider information from other sources in order to visualize the complete picture.

While the major data collection phase of this survey will be comprised of IR interferometry in the 10 to 100 mas separation range, a complimentary literature search will help establish multiplicity data from other sources in order to discern fully if the stars have companions in any detection regime.

*The most exciting phrase to hear in science,*
*the one that heralds new discoveries,*
*is not 'Eureka!' but 'That's funny...'*

—— *Isaac Asimov*

# – 5 —

# Observing Method and Log

## 5.1 Observational Planning

With such a large number of targets in this survey, attempts were made to observe every object on the list as many times as possible with two nearly-orthogonal baselines. However, as with all survey work, there was never enough time to observe everything with consistency. Over the course of the project, the ability to switch baselines during the night became easier and was adopted into the observing program to shorten the time between observations. Initially, the Array was configured for one PoP combination and all stars available on that baseline were to be observed before switching to another PoP. This proved too inefficient, as it led to as many as seven days between observing the same stars on the other baseline. After the first observing run, all subsequent runs either switched baselines every day or during the same night.

Due to the all-sky nature of these objects, only about half are observable at any given time. Furthermore, each PoP combination allowed only a third of those available to be observed at any one given time. For the thirty-month data acquisition phase of this project, seven large blocks of time were scheduled on the CHARA Array ranging from 5 to 18 days each as well as several small 2- to 3-day allotments. Approximately 50% of every run was lost due to weather, smoke from forest fires, or mechanical difficulties.

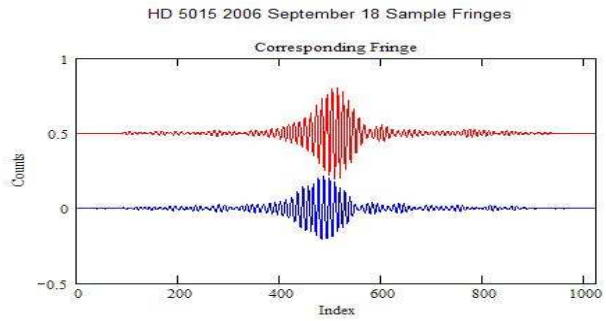


Figure. 5.1: Example Non-Detection of Secondary Fringes. Data from HD 5015 on 2006 September 18.

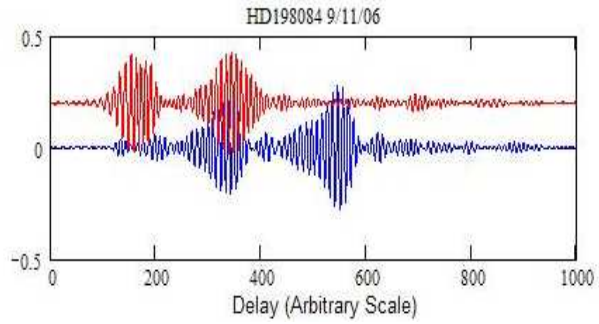


Figure. 5.2: Example Detection of Separated Fringes. Data from HD 198084 on 2006 September 11.

## 5.2 Examples of Detection and Non-Detection

Envelope plots and notes for each star are given in Appendix A in the same format as the examples below. For each system if available, Appendix A will contain at least one envelope plot for single stars and two or more envelope plots plus triangulation plots for all secondary locations. Figures 5.1 and 5.3 show example fringes and an envelope plot made up of the combined scans from one data set as an example of a non-detection (i.e., a single star). Figures 5.2 and 5.4 give examples of SFP detection with the same type of example fringes and envelope plots.

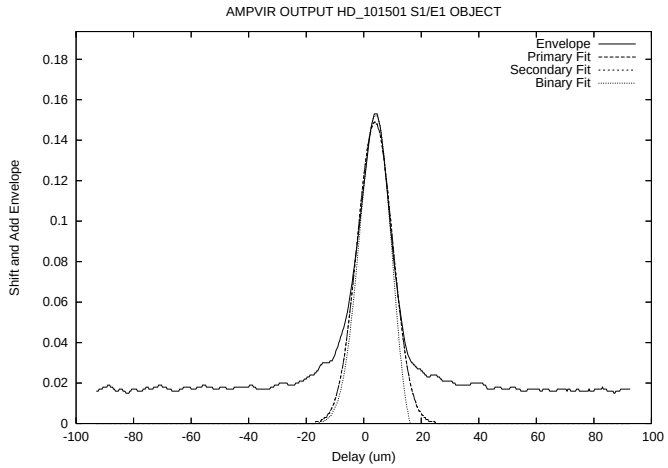


Figure. 5.3: HD 101501 Non-Detection Example Envelope. An example of a single star envelope plot with only one fringe. The grey line represents the shifted and summed fringe envelope for one data file on 2007 Feburary 3 on the E1/S1 baseline. The dashed and dotted lines are the fitted Gaussians to the primary fringe and where the reduction program believes the secondary packet should be.

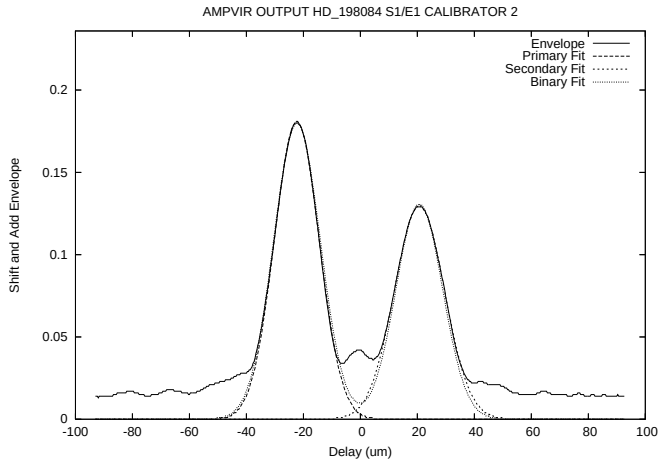


Figure. 5.4: Example SFP Detection Envelope for HD 198084. Example fringe envelope fit summed over all scans from a single data file on 2007 July 26 on the E1/S1 baseline. The grey line is the actual shifted and summed envelope for ∼200 scans, the dashed and dotted lines are the Gaussian fits to the primary and secondary fringe envelopes, and the tiny dotted line is the combined fit.

## 5.3 Observing Log

Between 2005 September and 2007 December, data were obtained on the CHARA Array using multiple baselines and configurations. Table 5.1 lists the observed systems, the type of system (known single, double, triple, etc), the total number of observations of that system, UT date of the observations, the baselines used, number of observations on that baseline, and whether or not an SFP was found for that system. Designations for the Status column are as follows:

VB - Visual Binary,

SB1/2/O - Single-lined / Double-lined Spectroscopic Binary /with orbit,

SB? - Possible Spectroscopic Binary,

CV - Constant Velocity,

CPM - Common Proper Motion Binary (generally listed with the companion if included in the target list),

VAR? - Uncertain Variable radial velocity (probably not due to binarity)

LWSB - Line-Width Spectroscopic Binary,

NEW SFP - Previously unknown companion discovered via SFP, and

CHARA SB1/2 - Single- and Double-Lined Spectroscopic Binaries from the CHARA Catalog of Orbital Elements of Spectroscopic Binary Stars.

Table. 5.1: Observing Log

| Object HD | Status | Total | SFP? | UT Dates | Baseline | #/date |
|---|---|---|---|---|---|---|
| 123 | VB | 9 | No | 2005/10/05 | W1/S1 | 3 |
| | | | | 2005/10/11 | S1/E1 | 3 |
| | | | | 2006/09/10 | W1/S1 | 1 |
| | | | | 2006/09/18 | S1/E1 | 2 |
| 4614 | VB | 18 | No | 2005/10/04 | W1/S1 | 3 |
| | | | | 2005/10/11 | S1/E1 | 3 |
| | | | | 2006/09/10 | W1/S1 | 1 |
| | | | | 2006/09/11 | W1/S1 | 1 |
| | | | | 2006/09/18 | S1/E1 | 1 |
| | | | | 2007/09/02 | S2/W1 | 1 |
| | | | | 2007/11/15 | S1/E1 | 4 |
| | | | | 2007/11/16 | S1/E1 | 4 |
| 4676 | SB2 | 10 | Yes | 2005/10/02 | W1/S1 | 3 |
| | | | | 2005/10/07 | S1/E1 | 3 |
| | | | | 2006/09/11 | W1/S1 | 1 |
| | | | | 2006/09/13 | S1/E1 | 1 |
| | | | | 2006/09/19 | W1/S1 | 1 |
| | | | | 2007/10/02 | S1/E1 | 1 |
| 5015 | CV | 36 | No | 2005/10/04 | W1/S1 | 3 |
| | | | | 2005/10/11 | S1/E1 | 3 |
| | | | | 2006/09/10 | W1/S1 | 1 |
| | | | | 2006/09/18 | S1/E1 | 1 |
| | | | | 2007/09/02 | S2/W1 | 1 |
| | | | | 2007/10/10 | E1/W1 | 10 |
| | | | | 2007/11/03 | E1/W1 | 9 |
| | | | | 2007/11/17 | S1/E1 | 8 |
| 5857 | SB? | 5 | No | 2007/08/03 | S1/E1 | 1 |
| | | | | 2007/10/19 | W1/S1 | 2 |
| | | | | 2007/10/19 | S1/E1 | 2 |
| 6582 | SB1O | 27 | No | 2005/10/04 | W1/S1 | 3 |
| | | | | 2005/10/11 | S1/E1 | 3 |
| | | | | 2006/09/11 | W1/S1 | 1 |
| | | | | 2006/09/18 | S1/E1 | 1 |
| | | | | 2007/07/01 | E1/W1 | 4 |
| | | | | 2007/07/18 | S1/E1 | 6 |
| | | | | 2007/07/19 | S1/E1 | 8 |
| | | | | 2007/09/02 | S2/W1 | 1 |
| 6920 | CV | 13 | No | 2005/10/04 | W1/S1 | 3 |
| | | | | 2005/10/06 | S1/E1 | 3 |
| | | | | 2007/09/13 | S1/E1 | 5 |
| | | | | 2007/10/20 | W1/S1 | 1 |
| | | | | 2007/10/20 | S1/E1 | 1 |
| 9021 | CHARA SB1 | 29 | Yes | 2005/10/04 | W1/S1 | 3 |
| | | | | 2005/10/11 | S1/E1 | 3 |
| | | | | 2006/09/11 | W1/S1 | 2 |

Continued on Next Page...

Table. 5.1 - Continued

| Object HD | Status | Total | SFP? | UT Dates | Baseline | #/date |
|---|---|---|---|---|---|---|
| | | | | 2006/09/12 | W1/S1 | 2 |
| | | | | 2006/09/17 | W1/S1 | 3 |
| | | | | 2006/09/18 | S1/E1 | 2 |
| | | | | 2007/07/26 | S1/E1 | 1 |
| | | | | 2007/08/02 | S1/E1 | 1 |
| | | | | 2007/08/03 | S1/E1 | 2 |
| | | | | 2007/09/02 | S2/W1 | 2 |
| | | | | 2007/09/15 | S1/E1 | 2 |
| | | | | 2007/09/17 | S2/W1 | 1 |
| | | | | 2007/10/03 | W1/S1 | 2 |
| | | | | 2007/11/19 | E2/S2 | 1 |
| | | | | 2007/11/20 | E2/S2 | 1 |
| | | | | 2007/11/22 | E2/S2 | 1 |
| 9407 | CV | 9 | No | 2005/10/04 | W1/S1 | 3 |
| | | | | 2005/10/11 | S1/E1 | 3 |
| | | | | 2006/09/11 | W1/S1 | 1 |
| | | | | 2006/09/18 | S1/E1 | 1 |
| | | | | 2007/09/02 | S2/W1 | 1 |
| 9826 | CV | 33 | No | 2006/09/18 | S1/E1 | 1 |
| | | | | 2007/02/08 | S1/E1 | 2 |
| | | | | 2007/08/02 | S1/E1 | 2 |
| | | | | 2007/09/05 | S2/W1 | 6 |
| | | | | 2007/09/06 | S2/W1 | 10 |
| | | | | 2007/09/12 | S1/E1 | 8 |
| | | | | 2007/09/13 | S1/E1 | 4 |
| 10307 | SB1O | 9 | No | 2005/09/29 | W1/S1 | 2 |
| | | | | 2005/10/06 | S1/E1 | 3 |
| | | | | 2007/09/17 | W1/S1 | 1 |
| | | | | 2007/09/18 | S1/E1 | 1 |
| | | | | 2007/10/20 | W1/S1 | 1 |
| | | | | 2007/10/20 | S1/E1 | 1 |
| 10697 | CV | 14 | No | 2006/09/19 | W1/S1 | 2 |
| | | | | 2007/09/13 | S1/E1 | 3 |
| | | | | 2007/09/14 | S1/E1 | 4 |
| | | | | 2007/10/02 | S1/E1 | 1 |
| | | | | 2007/10/19 | W1/S1 | 1 |
| | | | | 2007/10/19 | S1/E1 | 1 |
| | | | | 2007/10/20 | W1/S1 | 1 |
| | | | | 2007/10/20 | S1/E1 | 1 |
| 11909 | CHARA SB1 | 7 | Yes | 2005/10/02 | W1/S1 | 3 |
| | | | | 2005/10/07 | S1/E1 | 3 |
| | | | | 2006/09/11 | W1/S1 | 1 |
| 12235 | CV | 6 | No | 2005/10/02 | W1/S1 | 3 |
| | | | | 2005/10/07 | S1/E1 | 3 |
| 12923 | CHARA SB1 | 7 | No | 2005/10/02 | W1/S1 | 3 |
| | | | | 2005/10/07 | S1/E1 | 3 |

Continued on Next Page...

Table. 5.1 - Continued

| Object HD | Status | Total | SFP? | UT Dates | Baseline | #/date |
|---|---|---|---|---|---|---|
| | | | | 2007/12/17 | S1/E1 | 1 |
| 13480 | CHARA SB2 | 10 | No | 2005/09/29 | W1/S1 | 3 |
| | | | | 2005/10/06 | S1/E1 | 3 |
| | | | | 2006/09/11 | W1/S1 | 1 |
| | | | | 2007/08/03 | S1/E1 | 1 |
| | | | | 2007/10/20 | W1/S1 | 1 |
| | | | | 2007/10/20 | S1/E1 | 1 |
| 13974 | SB2O | 8 | Yes | 2005/09/28 | W1/S1 | 3 |
| | | | | 2005/10/06 | S1/E1 | 3 |
| | | | | 2007/10/20 | W1/S1 | 1 |
| | | | | 2007/10/20 | S1/E1 | 1 |
| 14214 | CHARA SB1 | 6 | No | 2005/10/02 | W1/S1 | 3 |
| | | | | 2005/10/07 | S1/E1 | 3 |
| 15335 | CV | 9 | No | 2005/09/27 | W1/S1 | 3 |
| | | | | 2005/10/06 | S1/E1 | 3 |
| | | | | 2006/09/10 | W1/S1 | 1 |
| | | | | 2007/10/20 | W1/S1 | 1 |
| | | | | 2007/10/20 | S1/E1 | 1 |
| 16739 | SB2O | 11 | Yes | 2006/09/10 | W1/S1 | 1 |
| | | | | 2006/09/17 | W1/S1 | 2 |
| | | | | 2006/09/18 | S1/E1 | 1 |
| | | | | 2006/10/05 | S1/E1 | 6 |
| | | | | 2006/12/01 | S1/E1 | 1 |
| 16895 | VB | 13 | No | 2005/09/29 | W1/S1 | 3 |
| | | | | 2006/09/10 | W1/S1 | 1 |
| | | | | 2006/09/18 | S1/E1 | 1 |
| | | | | 2007/11/03 | E1/W1 | 8 |
| | | | | 2007/12/24 | S1/E1 | 6 |
| 17433 | SB1O | 7 | No | 2005/09/28 | W1/S1 | 3 |
| | | | | 2005/10/06 | S1/E1 | 3 |
| | | | | 2007/10/20 | S1/E1 | 1 |
| 19373 | CV | 23 | No | 2005/09/29 | W1/S1 | 2 |
| | | | | 2006/09/18 | S1/E1 | 1 |
| | | | | 2006/09/19 | W1/S1 | 2 |
| | | | | 2007/01/25 | S1/E1 | 1 |
| | | | | 2007/08/28 | W1/S1 | 2 |
| | | | | 2007/09/08 | S1/E1 | 9 |
| | | | | 2007/11/04 | E1/W1 | 6 |
| 20630 | SB? | 25 | No | 2005/10/02 | W1/S1 | 3 |
| | | | | 2006/09/19 | W1/S1 | 1 |
| | | | | 2007/09/09 | S1/E1 | 9 |
| | | | | 2007/09/10 | S1/E1 | 5 |
| | | | | 2007/10/19 | W1/S1 | 1 |
| | | | | 2007/10/19 | S1/E1 | 1 |
| | | | | 2007/12/23 | S1/E1 | 5 |
| 21242 | SB2O | 10 | No | 2005/09/28 | W1/S1 | 3 |
| | | | | 2005/10/06 | S1/E1 | 3 |

Continued on Next Page...

Table. 5.1 - Continued

| Object HD | Status | Total | SFP? | UT Dates | Baseline | #/date |
|---|---|---|---|---|---|---|
| | | | | 2006/09/19 | W1/S1 | 1 |
| | | | | 2007/02/04 | S1/E1 | 3 |
| 22484 | SB? | 18 | No | 2005/10/02 | W1/S1 | 3 |
| | | | | 2007/02/25 | S1/E1 | 1 |
| | | | | 2007/09/09 | S1/E1 | 8 |
| | | | | 2007/10/19 | W1/S1 | 1 |
| | | | | 2007/10/19 | S1/E1 | 1 |
| | | | | 2007/12/23 | S1/E1 | 4 |
| 24546 | CHARA SB2 | 29 | Yes | 2005/09/29 | W1/S1 | 3 |
| | | | | 2005/10/11 | S1/E1 | 3 |
| | | | | 2006/09/11 | W1/S1 | 1 |
| | | | | 2006/09/17 | W1/S1 | 1 |
| | | | | 2006/09/18 | S1/E1 | 2 |
| | | | | 2006/09/19 | W1/S1 | 3 |
| | | | | 2006/12/01 | S1/E1 | 6 |
| | | | | 2007/01/17 | S1/E1 | 1 |
| | | | | 2007/01/26 | S1/E1 | 1 |
| | | | | 2007/02/04 | S1/E1 | 3 |
| | | | | 2007/02/05 | S1/E1 | 1 |
| | | | | 2007/08/03 | S1/E1 | 2 |
| | | | | 2007/09/15 | S1/E1 | 2 |
| 25680 | CV | 7 | No | 2005/10/02 | W1/S1 | 3 |
| | | | | 2005/10/06 | S1/E1 | 3 |
| | | | | 2007/02/04 | S1/E1 | 1 |
| 25893 | CV | 4 | No | 2006/09/18 | S1/E1 | 1 |
| | | | | 2006/09/19 | W1/S1 | 1 |
| | | | | 2007/01/26 | S1/E1 | 1 |
| | | | | 2007/09/15 | S1/E1 | 1 |
| 25998 | CV | 9 | No | 2005/09/28 | W1/S1 | 3 |
| | | | | 2005/10/06 | S1/E1 | 3 |
| | | | | 2006/09/18 | S1/E1 | 1 |
| | | | | 2006/09/19 | W1/S1 | 1 |
| | | | | 2007/01/26 | S1/E1 | 1 |
| 29203 | CV | 9 | No | 2005/09/29 | W1/S1 | 3 |
| | | | | 2005/10/11 | S1/E1 | 3 |
| | | | | 2006/09/17 | W1/S1 | 1 |
| | | | | 2006/09/18 | S1/E1 | 1 |
| | | | | 2007/01/26 | S1/E1 | 1 |
| 30282 | CHARA SB1 | 10 | No | 2005/09/29 | W1/S1 | 3 |
| | | | | 2005/10/06 | S1/E1 | 3 |
| | | | | 2006/09/18 | S1/E1 | 1 |
| | | | | 2006/09/19 | W1/S1 | 1 |
| | | | | 2007/01/26 | S1/E1 | 1 |
| | | | | 2007/09/15 | S1/E1 | 1 |
| 30652 | CV | 21 | No | 2005/10/02 | W1/S1 | 3 |
| | | | | 2007/03/12 | S1/E1 | 1 |
| | | | | 2007/10/19 | W1/S1 | 1 |

Continued on Next Page...

Table. 5.1 - Continued

| Object HD | Status | Total | SFP? | UT Dates | Baseline | #/date |
|---|---|---|---|---|---|---|
| | | | | 2007/10/19 | S1/E1 | 1 |
| | | | | 2007/11/05 | S1/E1 | 15 |
| 32537 | SB1O | 8 | No | 2005/09/29 | W1/S1 | 3 |
| | | | | 2005/10/11 | S1/E1 | 3 |
| | | | | 2006/09/18 | S1/E1 | 1 |
| | | | | 2007/09/15 | S1/E1 | 1 |
| 33564 | CV | 19 | No | 2005/10/11 | S1/E1 | 3 |
| | | | | 2006/09/10 | W1/S1 | 1 |
| | | | | 2006/09/11 | W1/S1 | 1 |
| | | | | 2007/11/18 | E2/S2 | 8 |
| | | | | 2007/11/19 | E2/S2 | 6 |
| 34411 | CV | 34 | No | 2005/09/27 | W1/S1 | 3 |
| | | | | 2005/10/11 | S1/E1 | 3 |
| | | | | 2006/09/19 | W1/S1 | 1 |
| | | | | 2007/01/26 | S1/E1 | 5 |
| | | | | 2007/11/03 | E1/W1 | 8 |
| | | | | 2007/11/15 | S1/E1 | 6 |
| | | | | 2007/11/17 | S1/E1 | 7 |
| 35296 | CPM w/35171 | 6 | No | 2005/10/02 | W1/S1 | 3 |
| | | | | 2007/02/25 | S1/E1 | 2 |
| | | | | 2007/09/15 | S1/E1 | 1 |
| 39587 | SB1O | 8 | No | 2005/10/02 | W1/S1 | 3 |
| | | | | 2005/10/06 | S1/E1 | 3 |
| | | | | 2007/02/25 | S1/E1 | 2 |
| 41330 | CV | 7 | No | 2005/09/29 | W1/S1 | 3 |
| | | | | 2005/10/11 | S1/E1 | 3 |
| | | | | 2007/01/25 | S1/E1 | 1 |
| 42807 | SB? | 1 | No | 2007/03/20 | S1/E1 | 1 |
| 43587 | CPM | 2 | No | 2007/02/25 | S1/E1 | 2 |
| 43821 | CHARA SB1 | 1 | No | 2007/03/20 | S1/E1 | 1 |
| 45088 | CHARA SB2 | 1 | No | 2007/03/20 | S1/E1 | 1 |
| 48682 | CV | 10 | No | 2007/02/03 | S1/E1 | 1 |
| | | | | 2007/12/24 | S1/E1 | 9 |
| 50692 | CV | 0 | No | | | |
| 52711 | CV | 2 | No | 2007/01/17 | S1/E1 | 1 |
| | | | | 2007/01/25 | S1/E1 | 1 |
| 58946 | SB? | 22 | No | 2007/01/17 | S1/E1 | 1 |
| | | | | 2007/01/25 | S1/E1 | 6 |
| | | | | 2007/02/03 | S1/E1 | 1 |
| | | | | 2007/11/16 | S1/E1 | 7 |
| | | | | 2007/11/17 | S1/E1 | 7 |
| 61859 | CHARA SB2 | 2 | No | 2007/01/17 | S1/E1 | 1 |
| | | | | 2007/02/03 | S1/E1 | 1 |
| 62613 | CV | 4 | No | 2007/04/03 | S1/E1 | 3 |
| | | | | 2007/04/14 | S1/E1 | 1 |
| 69897 | SB? | 2 | No | 2007/01/17 | S1/E1 | 1 |

Continued on Next Page...

Table. 5.1 - Continued

| Object HD | Status | Total | SFP? | UT Dates | Baseline | #/date |
|---|---|---|---|---|---|---|
| | | | | 2007/02/04 | S1/E1 | 1 |
| 71148 | CV | 3 | No | 2007/11/14 | S1/E1 | 1 |
| | | | | 2007/11/19 | E2/S2 | 2 |
| 72905 | CV | 6 | No | 2007/04/03 | S1/E1 | 3 |
| | | | | 2007/04/14 | S1/E1 | 1 |
| | | | | 2007/04/17 | W1/S1 | 2 |
| 72945 | SB1O | 1 | No | 2007/02/25 | S1/E1 | 1 |
| 75732 | CPM | 21 | No | 2007/01/17 | S1/E1 | 1 |
| | | | | 2007/02/03 | S1/E1 | 1 |
| | | | | 2007/02/06 | S1/E1 | 3 |
| | | | | 2007/03/09 | S1/E1 | 3 |
| | | | | 2007/03/20 | S1/E1 | 1 |
| | | | | 2007/03/26 | S1/E1 | 6 |
| | | | | 2007/03/30 | S1/E1 | 6 |
| 76943 | SB1O | 1 | No | 2007/02/03 | S1/E1 | 1 |
| 78154 | VB | 2 | No | 2007/04/03 | S1/E1 | 2 |
| 78366 | CV | 0 | No | | | |
| 79028 | SB? | 7 | No | 2007/04/14 | S1/E1 | 2 |
| | | | | 2007/04/17 | W1/S1 | 2 |
| | | | | 2007/11/14 | S1/E1 | 1 |
| | | | | 2007/11/19 | E2/S2 | 2 |
| 82328 | VAR? | 12 | No | 2007/11/02 | E2/W2 | 9 |
| | | | | 2007/11/14 | S1/E1 | 1 |
| | | | | 2007/11/19 | E2/S2 | 2 |
| 84737 | CV | 1 | No | 2007/05/28 | W1/S1 | 1 |
| 86728 | CV | 20 | No | 2007/01/26 | S1/E1 | 1 |
| | | | | 2007/11/15 | S1/E1 | 10 |
| | | | | 2007/11/16 | S1/E1 | 3 |
| | | | | 2007/12/24 | S1/E1 | 6 |
| 89125 | CV | 1 | No | 2007/06/01 | W1/S1 | 1 |
| 90089 | CV | 3 | No | 2007/04/11 | S1/E1 | 2 |
| | | | | 2007/05/28 | W1/S1 | 1 |
| 90508 | CPM | 4 | No | 2007/04/14 | S1/E1 | 1 |
| | | | | 2007/04/17 | W1/S1 | 2 |
| | | | | 2007/05/28 | W1/S1 | 1 |
| 90839 | SB?/CV | 17 | No | 2007/04/03 | S1/E1 | 4 |
| | | | | 2007/04/11 | S1/E1 | 2 |
| | | | | 2007/05/28 | W1/S1 | 1 |
| | | | | 2007/11/16 | S1/E1 | 10 |
| 95128 | CV | 3 | No | 2007/01/23 | S1/E1 | 2 |
| | | | | 2007/05/28 | W1/S1 | 1 |
| 98231 | Quad | 2 | No | 2006/06/09 | S1/E1 | 1 |
| | | | | 2007/02/06 | S1/E1 | 1 |
| 99028 | CV | 5 | No | 2007/02/06 | S1/E1 | 1 |
| | | | | 2007/02/16 | S1/E1 | 1 |
| | | | | 2007/02/25 | S1/E1 | 2 |

Continued on Next Page...

Table. 5.1 - Continued

| Object HD | Status | Total | SFP? | UT Dates | Baseline | #/date |
|---|---|---|---|---|---|---|
| | | | | 2007/03/12 | S1/E1 | 1 |
| 100203 | CV | 4 | No | 2007/04/03 | S1/E1 | 2 |
| | | | | 2007/04/11 | S1/E1 | 2 |
| 101501 | CV | 13 | No | 2007/02/03 | S1/E1 | 1 |
| | | | | 2007/02/06 | S1/E1 | 1 |
| | | | | 2007/11/15 | S1/E1 | 7 |
| | | | | 2007/12/24 | S1/E1 | 4 |
| 101606 | CHARA SB1 | 10 | Yes | 2006/06/08 | S1/E1 | 2 |
| | | | | 2007/02/06 | S1/E1 | 2 |
| | | | | 2007/02/16 | S1/E1 | 1 |
| | | | | 2007/03/09 | S2/E2 | 1 |
| | | | | 2007/03/10 | S1/E1 | 1 |
| | | | | 2007/03/11 | S1/E1 | 1 |
| | | | | 2007/05/27 | S1/E2 | 1 |
| | | | | 2007/06/01 | W1/S1 | 1 |
| 102870 | SB? | 12 | No | 2007/03/09 | S1/E1 | 6 |
| | | | | 2007/03/12 | S1/E1 | 1 |
| | | | | 2007/05/30 | W1/S1 | 1 |
| | | | | 2007/12/23 | S1/E1 | 4 |
| 103095 | CPM | 23 | No | 2007/05/27 | E2/S1 | 1 |
| | | | | 2007/05/28 | W1/S1 | 1 |
| | | | | 2007/11/16 | S1/E1 | 8 |
| | | | | 2007/11/17 | S1/E1 | 3 |
| | | | | 2007/12/24 | S1/E1 | 10 |
| 107700 | CHARA SB1 | 9 | Yes | 2006/06/08 | S1/E1 | 2 |
| | | | | 2007/02/16 | S1/E1 | 1 |
| | | | | 2007/02/25 | S1/E1 | 2 |
| | | | | 2007/03/09 | S2/E2 | 1 |
| | | | | 2007/03/10 | S1/E1 | 1 |
| | | | | 2007/03/11 | S1/E1 | 1 |
| | | | | 2007/06/01 | W1/S1 | 1 |
| 109358 | CV | 6 | No | 2007/05/26 | E2/S1 | 4 |
| | | | | 2007/05/27 | E2/S1 | 1 |
| | | | | 2007/05/28 | W1/S1 | 1 |
| 110897 | CV | 7 | No | 2007/05/26 | E2/S1 | 4 |
| | | | | 2007/05/27 | E2/S1 | 1 |
| | | | | 2007/05/28 | W1/S1 | 2 |
| 111395 | CV | 2 | No | 2007/05/28 | W1/S1 | 2 |
| 114379 | LWSB | 1 | No | 2007/05/28 | W1/S1 | 1 |
| 114710 | CV | 1 | No | 2007/02/06 | S1/E1 | 1 |
| 115383 | CPM | 0 | No | | | |
| 117043 | CV | 7 | No | 2006/06/03 | S1/E1 | 2 |
| | | | | 2006/06/05 | W1/S1 | 1 |
| | | | | 2006/06/06 | S1/E1 | 2 |
| | | | | 2007/04/11 | S1/E1 | 2 |
| 117176 | CV | 11 | No | 2007/02/06 | S1/E1 | 1 |
| | | | | 2007/03/30 | S1/E1 | 1 |

Continued on Next Page...

Table. 5.1 - Continued

| Object HD | Status | Total | SFP? | UT Dates | Baseline | #/date |
|---|---|---|---|---|---|---|
| | | | | 2007/04/02 | S1/E1 | 8 |
| | | | | 2007/05/07 | E1/W2 | 1 |
| 120136 | SB? | 26 | No | 2007/02/05 | S1/E1 | 10 |
| | | | | 2007/03/27 | S1/E1 | 1 |
| | | | | 2007/03/25 | S1/E1 | 2 |
| | | | | 2007/03/26 | S1/E1 | 5 |
| | | | | 2007/03/30 | S1/E1 | 8 |
| 120787 | SB | 4 | No | 2007/04/11 | S1/E1 | 2 |
| | | | | 2007/05/27 | E2/S1 | 1 |
| | | | | 2007/06/01 | W1/S1 | 1 |
| 121370 | SB1O | 2 | No | 2007/02/05 | S1/E1 | 1 |
| | | | | 2007/02/25 | S1/E1 | 1 |
| 122742 | SB1O | 3 | No | 2007/02/05 | S1/E1 | 1 |
| | | | | 2007/03/12 | S1/E1 | 1 |
| | | | | 2007/03/30 | S1/E1 | 1 |
| 126053 | CV | 2 | No | 2007/03/12 | S1/E1 | 1 |
| | | | | 2007/03/30 | S1/E1 | 1 |
| 126660 | Triple | 16 | No | 2006/06/03 | S1/E1 | 1 |
| | | | | 2006/06/05 | W1/S1 | 1 |
| | | | | 2006/06/06 | S1/E1 | 1 |
| | | | | 2007/04/11 | S1/E1 | 2 |
| | | | | 2007/05/24 | W1/S1 | 5 |
| | | | | 2007/07/16 | S1/E1 | 6 |
| 128167 | VAR? | 4 | No | 2007/05/30 | W1/S1 | 1 |
| | | | | 2007/06/01 | W1/S1 | 2 |
| | | | | 2008/06/04 | W2/S2 | 1 |
| 130948 | CV | 2 | No | 2007/02/04 | S1/E1 | 1 |
| | | | | 2007/06/23 | W1/S1 | 1 |
| 131156 | VB | 7 | No | 2007/03/12 | S1/E1 | 5 |
| | | | | 2007/05/28 | W1/S1 | 1 |
| | | | | 2007/06/01 | W1/S1 | 1 |
| 131511 | CHARA SB1 | 2 | No | 2006/06/08 | S1/E1 | 2 |
| | | | | 2007/06/23 | W1/S1 | 1 |
| 133640 | Triple | 4 | No | 2006/06/05 | W1/S1 | 2 |
| | | | | 2006/06/06 | S1/E1 | 1 |
| | | | | 2007/04/11 | S1/E1 | 1 |
| 134083 | CV | 2 | No | 2006/06/09 | S1/E1 | 1 |
| | | | | 2007/06/23 | W1/S1 | 1 |
| 134323 | SB1O | 2 | No | 2007/05/30 | W1/S1 | 1 |
| | | | | 2007/06/01 | E2/S1 | 1 |
| 136064 | CV | 4 | No | 2006/06/03 | S1/E1 | 3 |
| | | | | 2006/06/05 | W1/S1 | 1 |
| 137107 | VB w/137108 | 2 | No | 2007/05/27 | E2/S1 | 1 |
| | | | | 2007/05/30 | W1/S1 | 1 |
| 137108 | VB w/137107 | 3 | No | 2007/05/27 | E2/S1 | 1 |
| | | | | 2007/05/30 | W1/S1 | 2 |

Continued on Next Page...

Table. 5.1 - Continued

| Object HD | Status | Total | SFP? | UT Dates | Baseline | #/date |
|---|---|---|---|---|---|---|
| 140538 | CPM | 3 | No | 2007/04/02 | S1/E1 | 1 |
| | | | | 2007/05/30 | W1/S1 | 1 |
| | | | | 2007/06/01 | W1/S1 | 1 |
| 141004 | CV | 3 | No | 2007/04/02 | S1/E1 | 1 |
| | | | | 2007/05/30 | W1/S1 | 1 |
| | | | | 2007/05/31 | W1/S1 | 1 |
| 142373 | CV | 4 | No | 2006/06/05 | W1/S1 | 2 |
| | | | | 2006/06/06 | S1/E1 | 2 |
| 142860 | CV | 12 | No | 2007/04/02 | S1/E1 | 1 |
| | | | | 2007/05/30 | W1/S1 | 1 |
| | | | | 2007/06/23 | W1/S1 | 1 |
| | | | | 2007/07/20 | S1/E1 | 3 |
| | | | | 2007/07/21 | S1/E1 | 6 |
| 143761 | CV | 5 | No | 2006/06/04 | W1/S1 | 2 |
| | | | | 2006/06/05 | W1/S1 | 1 |
| | | | | 2006/06/06 | S1/E1 | 2 |
| 144284 | SB1O | 6 | No | 2006/06/03 | S1/E1 | 2 |
| | | | | 2006/06/05 | W1/S1 | 2 |
| | | | | 2006/06/06 | S1/E1 | 2 |
| 144579 | CPM | 15 | No | 2006/06/09 | S1/E1 | 3 |
| | | | | 2007/06/23 | W1/S1 | 1 |
| | | | | 2007/07/07 | S2/E2 | 6 |
| | | | | 2007/07/08 | S2/E2 | 2 |
| | | | | 2007/07/25 | S1/E1 | 1 |
| | | | | 2007/08/03 | S1/E1 | 1 |
| | | | | 2007/08/04 | S1/E1 | 1 |
| 146362 | CV | 1 | No | 2007/05/16 | S1/E1 | 1 |
| 147266 | CV | 3 | No | 2007/04/02 | S1/E1 | 1 |
| | | | | 2007/05/30 | W1/S1 | 1 |
| | | | | 2007/06/23 | W1/S1 | 1 |
| 150680 | SB1 | 4 | No | 2006/06/04 | W1/S1 | 2 |
| | | | | 2006/06/06 | S1/E1 | 2 |
| 151613 | CHARA SB1 | 7 | No | 2006/06/05 | W1/S1 | 2 |
| | | | | 2006/06/06 | S1/E1 | 1 |
| | | | | 2007/06/21 | S1/E1 | 1 |
| | | | | 2007/06/22 | W1/S1 | 1 |
| | | | | 2007/08/02 | S1/E1 | 1 |
| | | | | 2007/08/03 | S1/E1 | 1 |
| 151623 | CV | 1 | No | 2007/05/28 | W1/S1 | 1 |
| 152391 | CV | 4 | No | 2007/04/02 | S1/E1 | 1 |
| | | | | 2007/05/30 | W1/S1 | 1 |
| | | | | 2007/06/23 | W1/S1 | 1 |
| | | | | 2007/07/22 | W1/S1 | 1 |
| 153597 | SB1O | 6 | No | 2006/06/03 | S1/E1 | 2 |
| | | | | 2006/06/05 | W1/S1 | 2 |
| | | | | 2007/06/21 | S1/E1 | 1 |

Continued on Next Page...

Table. 5.1 - Continued

| Object HD | Status | Total | SFP? | UT Dates | Baseline | #/date |
|---|---|---|---|---|---|---|
| | | | | 2007/06/22 | W1/S1 | 1 |
| 154417 | CV | 4 | No | 2007/04/02 | S1/E1 | 2 |
| | | | | 2007/06/01 | S1/E2 | 1 |
| | | | | 2007/07/22 | W1/S1 | 1 |
| 154633 | CV | 6 | No | 2006/09/18 | S1/E1 | 4 |
| | | | | 2007/06/21 | S1/E1 | 1 |
| | | | | 2007/06/22 | W1/S1 | 1 |
| 157214 | CV | 8 | No | 2006/06/04 | W1/S1 | 2 |
| | | | | 2006/06/06 | S1/E1 | 2 |
| | | | | 2006/09/09 | S1/E1 | 2 |
| | | | | 2006/09/10 | S1/E1 | 1 |
| | | | | 2006/09/11 | W1/S1 | 1 |
| 160269 | Triple | 4 | No | 2006/09/18 | S1/E1 | 2 |
| | | | | 2007/06/21 | S1/E1 | 1 |
| | | | | 2007/06/22 | W1/S1 | 1 |
| 161797 | CV | 2 | No | 2006/09/13 | S1/E1 | 1 |
| | | | | 2007/06/23 | W1/S1 | 1 |
| 162003 | CV | 25 | No | 2006/09/18 | S1/E1 | 1 |
| | | | | 2007/06/21 | S1/E1 | 1 |
| | | | | 2007/06/22 | W1/S1 | 1 |
| | | | | 2007/07/16 | S1/E1 | 8 |
| | | | | 2007/07/17 | S1/E1 | 2 |
| | | | | 2007/10/10 | E1/W1 | 8 |
| | | | | 2007/11/17 | S1/E1 | 4 |
| 162004 | CV | 36 | No | 2006/09/18 | S1/E1 | 1 |
| | | | | 2007/06/21 | S1/E1 | 1 |
| | | | | 2007/06/22 | W1/S1 | 1 |
| | | | | 2007/07/16 | S1/E1 | 10 |
| | | | | 2007/07/17 | S1/E1 | 4 |
| | | | | 2007/10/10 | E1/W1 | 10 |
| | | | | 2007/11/17 | S1/E1 | 9 |
| 165341 | CHARA SB2 | 3 | No | 2006/09/19 | W1/S1 | 1 |
| | | | | 2007/07/22 | S1/E1 | 1 |
| | | | | 2007/07/22 | W1/S1 | 1 |
| 165908 | VB | 2 | No | 2006/09/09 | S1/E1 | 1 |
| | | | | 2007/10/02 | W1/S1 | 1 |
| 166285 | CHARA SB1 | 1 | No | 2006/09/19 | W1/S1 | 1 |
| 168009 | CV | 2 | No | 2006/09/09 | S1/E1 | 1 |
| | | | | 2006/09/11 | W1/S1 | 1 |
| 168151 | CV | 7 | No | 2006/06/03 | S1/E1 | 2 |
| | | | | 2006/06/05 | W1/S1 | 1 |
| | | | | 2006/09/18 | S1/E1 | 2 |
| | | | | 2007/06/21 | S1/E1 | 1 |
| | | | | 2007/06/22 | W1/S1 | 1 |
| 170153 | SB2O | 25 | Yes | 2006/06/03 | S1/E1 | 2 |
| | | | | 2006/06/05 | W1/S1 | 3 |
| | | | | 2006/06/06 | S1/E1 | 1 |

Continued on Next Page...

Table. 5.1 - Continued

| Object HD | Status | Total | SFP? | UT Dates | Baseline | #/date |
|---|---|---|---|---|---|---|
| | | | | 2006/09/18 | S1/E1 | 2 |
| | | | | 2007/04/14 | S1/E1 | 1 |
| | | | | 2007/04/24 | W1/S1 | 1 |
| | | | | 2007/05/28 | W1/S1 | 1 |
| | | | | 2007/07/26 | S1/E1 | 1 |
| | | | | 2007/08/02 | S1/E1 | 3 |
| | | | | 2007/08/03 | S1/E1 | 2 |
| | | | | 2007/09/16 | W1/S1 | 1 |
| | | | | 2007/10/03 | W1/S1 | 2 |
| | | | | 2007/10/20 | W1/S1 | 1 |
| | | | | 2007/11/19 | E2/S2 | 2 |
| | | | | 2007/01/22 | E2/S2 | 2 |
| 173093 | NEW SFP | 12 | Yes | 2006/05/14 | W1/W2 | 10 |
| | | | | 2006/09/19 | W1/S1 | 2 |
| 173667 | CV | 25 | No | 2006/09/19 | W1/S1 | 1 |
| | | | | 2007/07/20 | S1/E1 | 3 |
| | | | | 2007/07/21 | S1/E1 | 9 |
| | | | | 2007/08/04 | S1/E1 | 1 |
| | | | | 2007/09/10 | S1/E1 | 11 |
| 175225 | SB? | 4 | No | 2006/09/09 | S1/E1 | 1 |
| | | | | 2006/09/11 | W1/S1 | 1 |
| | | | | 2007/06/21 | S1/E1 | 1 |
| | | | | 2007/06/22 | W1/S1 | 1 |
| 176051 | VB | 4 | No | 2006/09/09 | S1/E1 | 1 |
| | | | | 2006/09/10 | S1/E1 | 1 |
| | | | | 2007/10/02 | W1/S1 | 1 |
| | | | | 2007/10/20 | W1/S1 | 1 |
| 180777 | SB? | 8 | No | 2005/10/04 | W1/S1 | 3 |
| | | | | 2006/06/03 | S1/E1 | 2 |
| | | | | 2006/06/05 | W1/S1 | 1 |
| | | | | 2007/06/21 | S1/E1 | 1 |
| | | | | 2007/06/22 | W1/S1 | 1 |
| 181655 | NEW SFP | 51 | Yes | 2005/10/05 | W1/S1 | 3 |
| | | | | 2005/10/06 | S1/E1 | 3 |
| | | | | 2006/06/04 | W1/S1 | 1 |
| | | | | 2006/06/05 | W1/S1 | 1 |
| | | | | 2006/06/06 | S1/E1 | 3 |
| | | | | 2006/09/09 | S1/E1 | 1 |
| | | | | 2006/09/10 | S1/E1 | 2 |
| | | | | 2006/09/11 | W1/S1 | 2 |
| | | | | 2006/09/12 | W1/S1 | 1 |
| | | | | 2006/09/13 | S1/E1 | 2 |
| | | | | 2007/04/14 | S1/E1 | 1 |
| | | | | 2007/05/07 | S2/E2 | 1 |
| | | | | 2007/05/27 | E2/S1 | 3 |
| | | | | 2007/05/28 | W1/S1 | 1 |
| | | | | 2007/05/29 | S1/E2 | 2 |

Continued on Next Page...

Table. 5.1 - Continued

| Object HD | Status | Total | SFP? | UT Dates | Baseline | #/date |
|---|---|---|---|---|---|---|
| | | | | 2007/05/30 | W1/S1 | 1 |
| | | | | 2007/06/03 | S2/W2 | 2 |
| | | | | 2007/06/04 | W1/W2 | 1 |
| | | | | 2007/07/09 | S2/E2 | 1 |
| | | | | 2007/07/23 | S1/E1 | 1 |
| | | | | 2007/07/25 | S1/E1 | 1 |
| | | | | 2007/07/29 | S1/E1 | 1 |
| | | | | 2007/08/03 | S1/E1 | 1 |
| | | | | 2007/08/11 | S2/E2 | 1 |
| | | | | 2007/08/12 | S2/E2 | 1 |
| | | | | 2007/08/17 | W1/S1 | 2 |
| | | | | 2007/09/01 | W1/S1 | 1 |
| | | | | 2007/09/15 | S1/E1 | 2 |
| | | | | 2007/10/02 | S1/E1 | 1 |
| | | | | 2007/10/02 | W1/S1 | 1 |
| | | | | 2007/10/20 | S1/E1 | 2 |
| | | | | 2007/10/20 | W1/S1 | 2 |
| | | | | 2007/11/19 | E2/S2 | 1 |
| | | | | 2007/11/22 | E2/S2 | 1 |
| 182572 | SB? | 10 | No | 2006/09/19 | W1/S1 | 1 |
| | | | | 2007/09/09 | S1/E1 | 9 |
| 184467 | CHARA SB2 | 46 | Yes | 2005/10/04 | W1/S1 | 3 |
| | | | | 2005/10/11 | S1/E1 | 3 |
| | | | | 2006/06/03 | S1/E1 | 3 |
| | | | | 2006/06/04 | W1/S1 | 1 |
| | | | | 2006/06/05 | W1/S1 | 3 |
| | | | | 2006/06/06 | S1/E1 | 1 |
| | | | | 2006/09/12 | W1/S1 | 2 |
| | | | | 2006/09/18 | S1/E1 | 2 |
| | | | | 2007/04/14 | S1/E1 | 1 |
| | | | | 2007/04/24 | W1/S1 | 1 |
| | | | | 2007/05/27 | S1/E2 | 2 |
| | | | | 2007/05/28 | W1/S1 | 1 |
| | | | | 2007/05/29 | S1/E2 | 4 |
| | | | | 2007/06/04 | W1/W2 | 1 |
| | | | | 2007/06/21 | S1/E1 | 3 |
| | | | | 2007/06/22 | W1/S1 | 1 |
| | | | | 2007/07/27 | S1/E1 | 2 |
| | | | | 2007/07/27 | W1/S1 | 1 |
| | | | | 2007/08/02 | S1/E1 | 2 |
| | | | | 2007/08/03 | S1/E1 | 3 |
| | | | | 2007/09/16 | W1/S1 | 1 |
| | | | | 2007/10/02 | W1/S1 | 2 |
| | | | | 2007/10/03 | W1/S1 | 2 |
| | | | | 2007/11/22 | E2/S2 | 1 |
| 185395 | CV | 1 5 | No | 2005/10/05 | W1/S1 | 3 |
| | | | | 2006/09/11 | W1/S1 | 1 |

Continued on Next Page...

Table. 5.1 - Continued

| Object HD | Status | Total | SFP? | UT Dates | Baseline | #/date |
|---|---|---|---|---|---|---|
| | | | | 2006/09/13 | S1/E1 | 4 |
| | | | | 2007/08/02 | S1/E1 | 1 |
| | | | | 2007/08/03 | S1/E1 | 1 |
| | | | | 2007/11/02 | E2/W1 | 5 |
| 186408 | CV | 7 | No | 2005/10/04 | W1/S1 | 3 |
| | | | | 2006/06/03 | S1/E1 | 2 |
| | | | | 2006/09/11 | W1/S1 | 1 |
| | | | | 2006/09/13 | S1/E1 | 1 |
| 186427 | CV | 10 | No | 2005/10/05 | W1/S1 | 3 |
| | | | | 2006/09/11 | W1/S1 | 1 |
| | | | | 2006/09/13 | S1/E1 | 1 |
| | | | | 2007/09/12 | S1/E1 | 5 |
| 186760 | CV | 12 | No | 2005/10/05 | W1/S1 | 3 |
| | | | | 2006/09/18 | S1/E1 | 1 |
| | | | | 2007/06/21 | S1/E1 | 1 |
| | | | | 2007/06/22 | W1/S1 | 1 |
| | | | | 2007/07/31 | S1/E1 | 6 |
| 187013 | CV | 10 | No | 2005/10/05 | W1/S1 | 3 |
| | | | | 2005/10/06 | S1/E1 | 3 |
| | | | | 2006/09/10 | S1/E1 | 1 |
| | | | | 2006/09/11 | W1/S1 | 1 |
| | | | | 2007/05/31 | E2/S1 | 1 |
| | | | | 2007/05/31 | W1/S1 | 1 |
| 187691 | CPM | 13 | No | 2006/09/19 | W1/S1 | 1 |
| | | | | 2007/09/09 | S1/E1 | 8 |
| | | | | 2007/07/22 | W1/S1 | 1 |
| | | | | 2007/07/22 | E1/S1 | 1 |
| | | | | 2007/07/24 | S1/E1 | 1 |
| | | | | 2007/07/24 | W1/S1 | 1 |
| 188512 | CV | 4 | No | 2007/06/01 | E2/S1 | 1 |
| | | | | 2007/07/22 | S1/E1 | 1 |
| | | | | 2007/07/24 | S1/E1 | 1 |
| | | | | 2007/08/04 | S1/E1 | 1 |
| 190360 | CPM | 5 | No | 2006/09/11 | W1/S1 | 1 |
| | | | | 2007/05/31 | W1/S1 | 1 |
| | | | | 2007/06/23 | W1/S1 | 1 |
| | | | | 2007/10/19 | W1/S1 | 1 |
| | | | | 2007/10/19 | S1/E1 | 1 |
| 190406 | CV | 3 | No | 2006/09/19 | W1/S1 | 1 |
| | | | | 2007/07/22 | S1/E1 | 1 |
| | | | | 2007/07/22 | W1/S1 | 1 |
| 193664 | CV | 27 | No | 2005/10/05 | W1/S1 | 3 |
| | | | | 2005/10/11 | S1/E1 | 3 |
| | | | | 2006/09/18 | S1/E1 | 1 |
| | | | | 2007/05/24 | W1/S1 | 4 |
| | | | | 2007/05/25 | W1/S1 | 5 |
| | | | | 2007/06/21 | S1/E1 | 1 |

Continued on Next Page...

Table. 5.1 - Continued

| Object HD | Status | Total | SFP? | UT Dates | Baseline | #/date |
|---|---|---|---|---|---|---|
| | | | | 2007/06/22 | W1/S1 | 1 |
| | | | | 2007/06/28 | E1/W1 | 2 |
| | | | | 2007/07/31 | S1/E1 | 7 |
| 194012 | CV | 4 | No | 2006/09/19 | W1/S1 | 1 |
| | | | | 2007/07/22 | W1/S1 | 1 |
| | | | | 2007/07/22 | S1/E1 | 1 |
| | | | | 2007/07/24 | S1/E1 | 1 |
| 195987 | SB2 | 6 | Yes | 2006/06/04 | W1/S1 | 1 |
| | | | | 2006/06/06 | S1/E1 | 1 |
| | | | | 2006/09/11 | W1/S1 | 1 |
| | | | | 2006/09/13 | S1/E1 | 1 |
| | | | | 2007/10/03 | W1/S1 | 1 |
| | | | | 2007/10/20 | W1/S1 | 1 |
| 196795 | CHARA SB1 | 7 | Yes | 2007/06/01 | E2/S1 | 1 |
| | | | | 2007/06/16 | W1/S2 | 1 |
| | | | | 2007/07/22 | S1/E1 | 1 |
| | | | | 2007/07/24 | S1/E1 | 1 |
| | | | | 2007/07/24 | W1/S1 | 1 |
| | | | | 2007/09/09 | S1/E1 | 1 |
| | | | | 2007/10/19 | S1/E1 | 1 |
| 198084 | CHARA SB1 | 66 | Yes | 2005/10/05 | W1/S1 | 3 |
| | | | | 2005/10/11 | S1/E1 | 4 |
| | | | | 2006/06/03 | S1/E1 | 2 |
| | | | | 2006/06/04 | W1/S1 | 1 |
| | | | | 2006/06/05 | W1/S1 | 3 |
| | | | | 2006/06/06 | S1/E1 | 2 |
| | | | | 2006/09/10 | W1/S1 | 1 |
| | | | | 2006/09/11 | W1/S1 | 3 |
| | | | | 2006/09/12 | W1/S1 | 4 |
| | | | | 2006/09/13 | S1/E1 | 1 |
| | | | | 2006/09/17 | W1/S1 | 1 |
| | | | | 2007/04/14 | S1/E1 | 1 |
| | | | | 2007/05/27 | S1/E2 | 2 |
| | | | | 2007/05/28 | W1/S1 | 1 |
| | | | | 2007/05/29 | S1/E2 | 4 |
| | | | | 2007/05/30 | W1/S1 | 2 |
| | | | | 2007/06/03 | S2/W2 | 2 |
| | | | | 2007/06/04 | W1/W2 | 3 |
| | | | | 2007/06/17 | W1/S2 | 1 |
| | | | | 2007/06/18 | S1/E1 | 1 |
| | | | | 2007/06/21 | S1/E1 | 1 |
| | | | | 2007/06/22 | W1/S1 | 1 |
| | | | | 2007/07/25 | S1/E1 | 1 |
| | | | | 2007/07/26 | S1/E1 | 1 |
| | | | | 2007/07/26 | W1/S1 | 2 |
| | | | | 2007/08/02 | S1/E1 | 2 |
| | | | | 2007/08/03 | S1/E1 | 4 |

Continued on Next Page...

Table. 5.1 - Continued

| Object HD | Status | Total | SFP? | UT Dates | Baseline | #/date |
|---|---|---|---|---|---|---|
| | | | | 2007/09/16 | W1/S1 | 2 |
| | | | | 2007/10/02 | W1/S1 | 1 |
| | | | | 2007/10/03 | W1/S1 | 4 |
| | | | | 2007/11/19 | E2/S2 | 2 |
| | | | | 2007/11/20 | E2/S2 | 1 |
| | | | | 2007/11/22 | E2/S2 | 2 |
| 202275 | VBO | 23 | Yes | 2006/07/28 | S1/E1 | 4 |
| | | | | 2006/09/19 | W1/S1 | 2 |
| | | | | 2007/06/16 | S2/W1 | 2 |
| | | | | 2007/07/24 | S1/E1 | 3 |
| | | | | 2007/10/15 | S2/W1 | 4 |
| | | | | 2007/10/16 | S2/W1 | 8 |
| 202444 | VAR? | 9 | No | 2005/10/05 | W1/S1 | 3 |
| | | | | 2005/10/06 | S1/E1 | 3 |
| | | | | 2006/09/11 | W1/S1 | 1 |
| | | | | 2006/09/13 | S1/E1 | 1 |
| | | | | 2007/10/20 | S1/E1 | 1 |
| 202573 | CV | 8 | No | 2005/10/05 | W1/S1 | 3 |
| | | | | 2005/10/07 | S1/E1 | 3 |
| | | | | 2006/09/19 | W1/S1 | 1 |
| | | | | 2007/10/20 | S1/E1 | 1 |
| 206826 | SB? | 4 | No | 2007/10/02 | S1/E1 | 1 |
| | | | | 2007/10/19 | W1/S1 | 1 |
| | | | | 2007/10/19 | S1/E1 | 1 |
| | | | | 2007/12/16 | S1/E1 | 1 |
| 206860 | CV | 6 | No | 2007/07/22 | S1/E1 | 2 |
| | | | | 2007/07/24 | S1/E1 | 2 |
| | | | | 2007/07/24 | W1/S1 | 2 |
| 210027 | SB1O | 8 | No | 2005/10/07 | S1/E1 | 3 |
| | | | | 2006/09/10 | W1/S1 | 1 |
| | | | | 2006/09/19 | W1/S1 | 1 |
| | | | | 2007/06/16 | S2/W1 | 1 |
| | | | | 2007/10/19 | W1/S1 | 1 |
| | | | | 2007/10/19 | S1/E1 | 1 |
| 215648 | CV | 20 | No | 2006/09/10 | W1/S1 | 1 |
| | | | | 2007/06/16 | S2/W1 | 1 |
| | | | | 2007/07/16 | S1/E1 | 4 |
| | | | | 2007/07/21 | S1/E1 | 14 |
| 217014 | CV | 3 | No | 2006/09/10 | W1/S1 | 1 |
| | | | | 2006/09/19 | W1/S1 | 1 |
| | | | | 2007/07/24 | W1/S1 | 1 |
| 219080 | CV | 6 | No | 2005/10/05 | W1/S1 | 3 |
| | | | | 2006/09/10 | W1/S1 | 1 |
| | | | | 2006/09/11 | W1/S1 | 1 |
| | | | | 2007/10/02 | S1/E1 | 1 |
| 221950 | CHARA SB2 | 8 | Yes | 2005/10/02 | W1/S1 | 3 |
| | | | | 2005/10/07 | S1/E1 | 3 |

Continued on Next Page...

Table. 5.1 - Continued

| Object HD | Status | Total | SFP? | UT Dates | Baseline | #/date |
|---|---|---|---|---|---|---|
| | | | | 2007/08/03 | S1/E1 | 2 |
| 222368 | SB? | 33 | No | 2005/10/02 | W1/S1 | 3 |
| | | | | 2005/10/07 | S1/E1 | 3 |
| | | | | 2006/12/07 | S1/E1 | 6 |
| | | | | 2007/07/20 | S1/E1 | 11 |
| | | | | 2007/09/09 | S1/E1 | 5 |
| | | | | 2007/09/10 | S1/E1 | 5 |
| 223778 | CHARA SB2 | 9 | No | 2005/10/05 | W1/S1 | 3 |
| | | | | 2005/10/11 | S1/E1 | 3 |
| | | | | 2006/09/10 | W1/S1 | 1 |
| | | | | 2006/09/11 | W1/S1 | 1 |
| | | | | 2007/09/02 | S2/W1 | 1 |
| 224930 | VBO | 3 | No | 2007/10/02 | S1/E1 | 1 |
| | | | | 2007/10/19 | W1/S1 | 1 |
| | | | | 2007/10/19 | S1/E1 | 1 |

## 5.4 Completeness

Though a significant number of stars in this survey were observed over the course of this project, a minority of objects were inadequately or not at all observed. A truly complete survey would extend this effort by many years. As time was limited, we shall look at how complete the survey was in the time allotted. A star was not considered completed until it had been observed on both baselines with less than a week between observations. Even this bare minimum is a rather daunting task for a survey of this size within two years. An alternative and more practical definition of completeness would be observing the same system several times with both baselines over the course of the project. An additional criterion can be added as multiple observations on a single baseline with plenty of rotation can also be

considered as completing a star. It is difficult to quantify the overall survey completeness as the observations were erratically spaced, do not include every star in each observing period, and so many systems were observed only once. While it is probable that we have missed shorter period/small-angular separation systems, those systems with periods longer than 50 days at the distances restricted by the survey should have been detected provided that more than one baseline was used or significant rotation occured.

If we consider the geometry of a single one-dimensional scan, we can estimate how much area around the central fringe has been observed with a single scan. With recent upgrades to CHARA Classic, the new fold-back dither has a shorter movement but better accuracy so we will use the limits of this configuration for this example. After compiling data on the length of the scans, it was determined that the most common dither throw is 142.43 $\mu$m, and is quite consistent. This combined with the basic geometry of how vector separations project the secondary packet onto the scan give us a simple area over which one observation measures (see Section 1.3 and 3.4). The diagrams in Figure 5.5 and 5.6 display a simple yet effective way to describe how one or more scans can give us a measure of completeness.

So for a single observation, when operating with the same filter (herein, the $K'$ filter with $\lambda_0$=2.1329 $\mu$m, $\Delta\lambda$=0.6222 $\mu$m) gives us a constant width for a "forbidden" zone where fringes of the secondary would be undetected for all scans. For a single scan then we can say that 75% of the area around the primary fringe has been scanned for objects within the detection limits. This area searched does depend on the length of the baseline projection at the time of acquisition. Stars with more than the minimum distance but lying within the

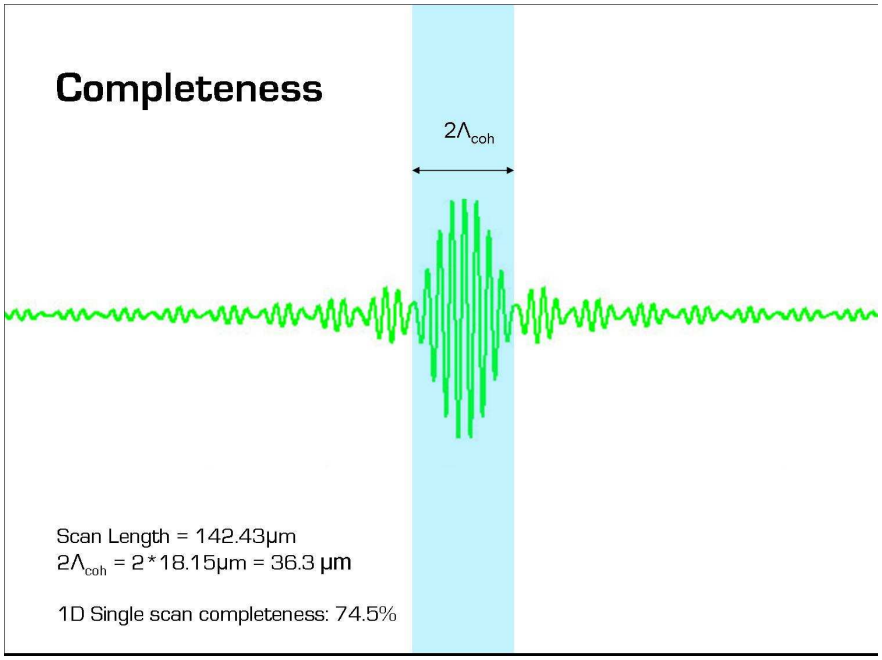


Figure. 5.5: Completeness for One Scan. This simple schematic shows effectively the percentage of area around the central fringe is being scanned. Since a second object within the brightness limit for detection could be anywhere vertically in this schematic and still be projected back onto the scan, the percentage of area scanned remains the same as we miss anything directly perpendicular within the coherence length of the fringe $2\Lambda_{coh}$ which is constant from scan to scan.

perpendicular region of the scan are undiscovered but can be acquired through taking more than one scan on the same baseline with significant rotation or by the use of a secondary baseline. The only area that is unable to be searched is the segment within the fringe packet itself and for that we would need to use the classical technique of calibrated visibilites.

The area scanned is not the only place fringes can form. For a star such as HD 202275 with separations of $\gtrsim$150 mas, the longest baselines were producing secondary fringe packets up to 200 microns of delay away from the primary. While practically impossible to record such a distance on the longest baselines, switching to a more compact baseline could place the two packets within easy recording range. Theoretically, it is possible for a second fringe

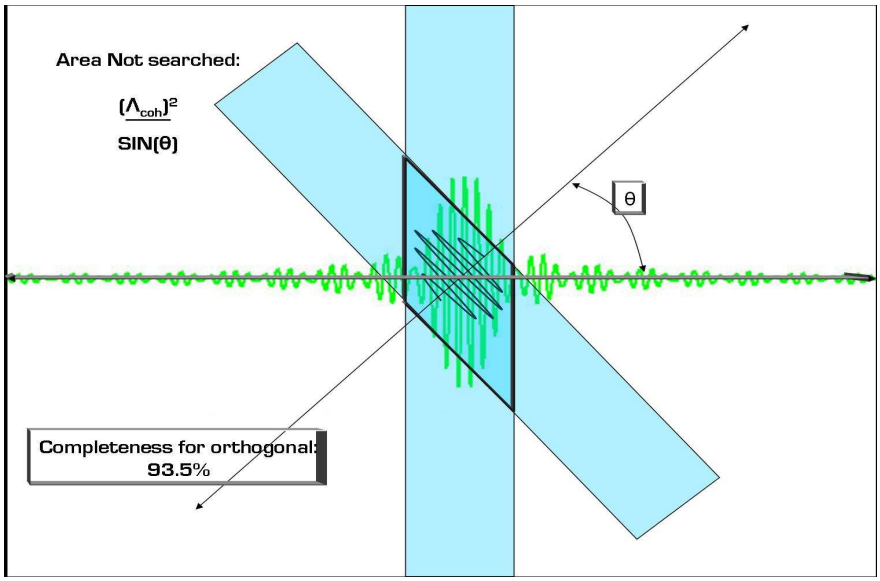


Figure. 5.6: Effect of Rotation on Completeness. With the application of a secondary baseline in conjuction with the primary, more area is available to be searched. With the extra baseline the area that is unexplored becomes an elongated parallelogram (defined as $\frac{\Lambda_{coh}}{\sin\theta}$) which as we approach the orthogonal approaches 94% completeness.

to be nearly as far away as allowed by the baseline within the blur spot of the star based on seeing conditions.

For the sake of this discussion, we will consider all three definitions of completeness. Using this, of the 160 stars on the observing list, 109 targets were observed at least three times on each of the primary baselines within a week of the previous baseline. An additional 48 systems were observed at least once on only one baseline without being observed on a complementary baseline during the same run. Three stars from the entire list of objects (HD 50692, HD 78366, and HD 115383) were unable to be observed due to time constraints. If we look at the distribution of the time of year when the stars are available and which stars are incomplete, most of the objects that were not completed are winter objects. A large portion of the time that was allotted to this project that was lost due to weather was during

this time as traditionally November through April is fraught with inclement weather. Even with these losses, almost 1300 observations were made over the thirty months of the project and include twelve definite SFP detections, at least ten systems with a probable secondary fringe packet significantly overlapping that of the primary, enough data to add to or revise two orbits, a completely new visual orbit for a system never before resolved visually, and a detection of a previously unknown companion.

## 5.5 Data Reduction

The raw data from the CHARA Array form a single long sequence of dither mirror positions and photon counts with a shutter sequence at the beginning and end. Two separate reduction programs were available for use and adapted to fit the needs of this project. Both programs different but similar reductions but are written for different platforms and programming languages, and always provided the same answer. For all results in this discussion, the program "VisUVCalc" written in MathCAD by H.A. McAlister and A. Jerkstrand and based on Benson et al. (1995) directly fits the fringes and was used to produce many of the graphical representations of the example fringes while the programs written by T. ten Brummelaar in C and IDL which Fourier fits the fringes were primarily used for the shift-and-add secondary fringe search, separation calculations, and locating of the true position of the secondary as these codes could queue up many files simultaneously.

After an observing run was completed, objects that obviously displayed SFPs were given reduction priority. Through the reduction process, each file was broken up into its individ-

ual scans, had noise removed through bandpass filtering around the fringe frequency, and processed through a sub-program that locates the fringes in the each scan. Fringes are then Hilbert transformed keeping only the positive frequencies into a fringe envelope. As the program does not know which fringe is the primary, it selects the location of the maximimum of the envelope (or you can designate which maximum) and shifts all subsequent scans to that position and then sums all scans. When observing in bad seeing conditions, the separation of the two fringes can vary by a significant amount which causes the peaks of the envelope to broaden as they are being added together. Generally this does not deter the observer from getting a good location for the secondary fringe, though it does increase the error of the measurement on the order of a few percent.

After this shift-and-add process is complete, the program will write the configuration of the array and the separation determined for the SFPs along with the calculated error into a file for processing by a separate IDL routine. Once all files for that star are completed, the IDL program will take the position angle of the baseline used and the separation and create perpendicular lines for each secondary fringe to the baseline at the maxima of the secondary fringe envelope and compute the intersection points. From this final step, we get a position angle on the sky and a separation with errors relating to the distance between the intersection points of the vector lines.

For the cases where multiple orbital points are created, the individual points along with their epochs averaged over the time between the observations are input into a grid search FORTRAN program from the U.S. Naval Observatory (Hartkopf et al. 1989) along with best

estimates for period, eccentricity, and epoch of periastron passage. The grid search program searches parameter space for the best estimates for all seven orbital elements and plots the orbit with the lowest $\chi^2$ along with the observed and calculated values for each epoch. For several examples of this, see Chapter 7.1 - 7.3 on HD 181655, HD 184467, and HD 198084.

*For those who want some proof that physicists are human,*
*the proof is in the idiocy of all the different units*
*which they use for measuring energy.*

*—— Richard Feynman*

# – 6 —

# Observational Results

For this chapter, we shall discuss the detections of secondary fringes for objects in the survey, non-detections and possible reasons for not detecting a secondary fringe, and the detection of previously missed companions through the survey and literature search.

## 6.1 Non-Detections

Since this survey was composed of a significant number of presumed solitary stars, there is a majority of non-detections. For most of the systems on both lists, this was to be expected. However, the other fifteen stars from the CHARA Catalog were predicted to display a second packet for which one was not observed. There are several possible independent factors which could contribute to the non-detection. It was believed when this project started that it was conceivable to detect a secondary packet closer than was actually possible. Initially we were seeking to explore the region between spectroscopic, calibrated visibility and speckle interferometry binary detections but estimations of how close we could detect a secondary fringe were untested and several binaries were added to the list with predicted separations that were too small. We predicted the separations of both single- and double-lined spectroscopic binaries with estimates of their parallax and calculated $a \sin i$ and selected those that fell within the overly generous range of 5-50 mas. Most of those that were missed fell within the range of 5-10 mas and were nearly all nearby short-period (less than 100 day)

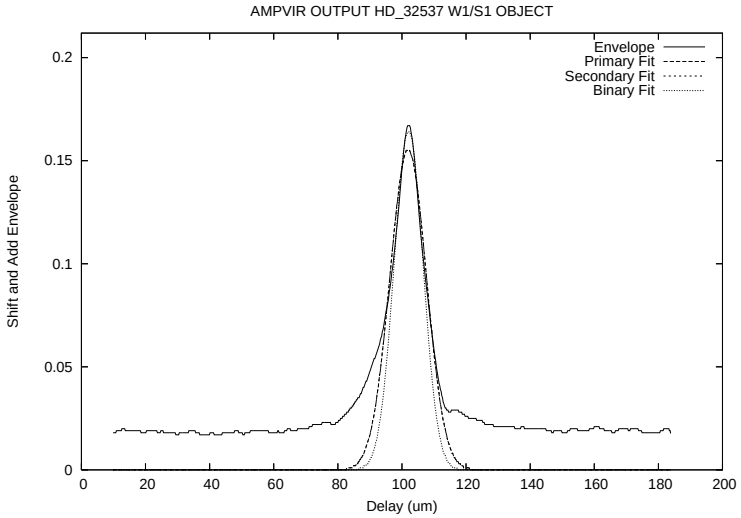


Figure. 6.1: HD 32537 Fringe Envelope Elongation. Example fringe envelope fit summed over all scans from a single data file on 2005 September 29 on the W1/S1 baseline. The grey line is the actual shifted envelope and the dotted line is the gaussian fit to the primary fringe. Consistant elongation on one side of the primary fringe could be an effect of the secondary. With the mass function from the spectroscopic orbit, it is likely that the companion is relatively faint and may only barely register.

spectroscopic binaries that would otherwise be measured through visibility analysis. Sample fringe envelopes for all data from the CHARA SFP survey that did not detect a companion are compiled in Appendix A.

Several of these systems showed hints of a blended secondary fringe packet in the envelope calculations. An example is shown in Figure 6.1 of HD 32537 where consistently one side of the primary fringe packet is elongated for all scans regardless of scanning direction. Since the predicted average separation for this system was less than 9 mas, it is to be expected that the secondary would not fully separate from the main fringe. It is possible that with either prolonged observational effort or the addition of a calibrator that we could extract orbital information but these are beyond the scope of this work.

In general, even with systems with wider separations, it is possible to miss the companion. It was discussed in a previous chapter on detection limits that companions with a magnitude

difference of two or more may be lost in the detector noise. Other detection biases primarily involve implications of the geometry of the system and the interferometer. If the orientation of the system is such that the instantaneous projected baseline happens to be perpendicular to that of the separation of the system only one fringe would be seen as the projected location of the secondary would lie within the primary. Additionally, if the hour angle of the star is such that the baseline is near its minimum, closer secondaries would not be sufficiently separated as projection effects can shorten the longest baselines by more than 100 meters.

## 6.2 Stars with Separated Fringe Packets

The objects from the CHARA Catalog (Taylor et al. 2003) were selected for the express purpose of exhibiting separated fringe packets. Additionally we were anticipating at least one target from D&M's list to display a previously unknown companion. Although not all of the targets that we expected SFPs from were confirmed, we did collect data on 17 objects that displayed a second packet. Of these, fifteen were listed in the CHARA Catalog, and five of those were also in the D&M survey. The final two had previously unknown companions. One was in the original D&M list but was not included in the multiplicity statistics due to its parallax, and the remaining system was added to the list after the survey had begun as it was the correct spectral type and had displayed a secondary packet when used as a calibrator for a separate project.

Table. 6.1: Updated Multiplicity for the D&M Survey

| Name HD | D&M Status | D&M Mult | New Mult | New Mult w/$\pi$ | MK Type | D&M $\pi$ (mas) | Hipparcos $\pi$ (mas) |
|---|---|---|---|---|---|---|---|
| 123 | VB | Double | Triple | Triple | G5V + (G8V + early M) | 45 | 49.3 |
| 1461 | CV | Single | Single | x | G0V | 52 | 42.67 |
| 1835 | CV | Single | Single | Single | G5VH-05 | 49 | 49.05 |
| 3196AB | VB/SB1 | Triple | Triple | Triple | F8V + (G0V + M) | 63 | 47.51 |
| 4614AB | VB | Double | Double | Double | G0V + K7V | 170 | 167.99 |
| 4676ab | SB2 | Double | Double | x | F8V + F8V | 46 | 41.8 |
| 4813 | SB? | Single | Single | Single | F7IV-V | 64 | 64.69 |
| 5015 | CV | Single | Single | Single | F8V | 64 | 53.85 |
| 5294 | CV | Single | Single | x | G5 | 49 | 33.92 |
| 5857 | SB? | Single | Double | x | G5 + M? | 50 | 6.54 |
| 6582AB | SB10 | Double | Double | Double | G5Vb + sdM | 130 | 132.42 |
| 6920 | CV | Single | Single | x | F8V | 50 | 18.98 |
| 9562 | CV | Single | Single | x | G1V | 68 | 33.71 |
| 9826 | CV | Single | Double | Double | F8V + M4.5 | 62 | 74.25 |
| 10086 | CV | Single | Single | Single | G5IV | 51 | 46.73 |
| 10307 | SB10 | Double | Double | Double | G1.5V + | 87 | 79.09 |
| 10697 | CV | Single | Single | x | G5IV | 61 | 30.71 |
| 11964AB | CPM | Double | Double | x | G9VCN+1 | 50 | 29.43 |
| 12051 | CV | Single | Single | x | G5 | 48 | 40.74 |
| 13974ab | SB20 | Double | Double | Double | G0.5V + M? | 97 | 92.2 |
| 16620AB | VB | Double | Double | x | F5V + F5V | 69 | 36.99 |
| 16739ab | SB20 | Double | Double | x | F8V + G1.5V | 46 | 40.52 |
| 16895AB | VB | Double | Double | Double | F7V + M1.5 | 79 | 89.03 |
| 17433 | SB10 | Double | Double | x | K0 + ? | 47 | 22.73 |
| 18803 | CV | Single | Single | Single | G8V | 55 | 47.25 |
| 19034 | CV | Single | Single | x | G5 | 46 | 28.33 |
| 19373 | CV | Single | Single | Single | G0V | 86 | 94.93 |
| 19994AB | CPM | Double | Double | Double | F8V + M? | 49 | 44.69 |
| 20619 | CV | Single | Single | x | G1.5V | 65 | 40.52 |
| 20630 | SB? | Single | Single | Single | G5Vv | 107 | 109.18 |
| 22484 | SB? | Single | Double | Double | F9IV-V + M | 61 | 72.89 |
| 22879 | CV | Single | Single | x | F9V | 47 | 41.07 |

Continued on Next Page...

Table. 6.1 – Continued

| Name HD | D&M Status | D&M Mult | New Mult | New Mult w/$\pi$ | MK Type | D&M $\pi$ (mas) | Hipparcos $\pi$ (mas) |
|---|---|---|---|---|---|---|---|
| 25680 | CV | Single | Single | Single | G5V | 69 | 59.79 |
| 25893 | CV | Double | Double | Double | G5 + K2 | 37 | 48.59 |
| 29203 | CV | Single | Single | x | G8V | 53 | 5.68 |
| 31966 | CV | Single | Single | x | G5V | 48 | 28.49 |
| 32923AB | CV | Single | Single | Single | G4V | 59 | 63.02 |
| 33093 | CV | Single | Single | x | G0IV | 49 | 27.6 |
| 34411 | CV | Single | Single | Single | G1.5IV-V | 67 | 79.08 |
| 35171 | CPM v | Single | Single | Single | K2 | 63 | 69.76 |
| 35296 | CPM | Double | Double | Double | F8V + K0 | 63 | 68.19 |
| 37124 | CV | Single | Single | x | G4IV-V | 55 | 30.08 |
| 39587 | SB10 | Double | Double | Double | G0VH-03 + M | 101 | 115.43 |
| 39881 | CV | Single | Single | x | G5IV | 47 | 35.72 |
| 41330 | CV | Single | Single | x | G0V | 46 | 37.9 |
| 42807 | SB? | Single | Single | Single | G2V | 57 | 55.2 |
| 43587AB | CPM | Double | Triple | Triple | G0V + M3.5 | 50 | 51.76 |
| 46588 | SB? | Single | Single | Single | F8V | 47 | 56.02 |
| 48682 | CV | Single | Single | Single | G0V | 68 | 60.56 |
| 50692 | CV | Single | Single | Single | G0V | 52 | 57.89 |
| 52711 | CV | Single | Single | Single | G4V | 58 | 52.37 |
| 61994ab | SB20 | Double | Double | x | G5V + K? | 45 | 35.13 |
| 62613 | CV | Single | Single | Single | G8V | 70 | 58.67 |
| 64096AB | VB | Double | Double | Double | F9V + G4V | 69 | 59.98 |
| 64606 | SB1 | Double | Double | Double | G8V + M? | 52 | 52.01 |
| 65583 | CV | Single | Single | Single | G8V | 58 | 59.52 |
| 68146AB | SB | Double | Double | Double | F6.5V + M2 | 50 | 44.47 |
| 69830 | CV | Single | Single | Single | G8+v | 79 | 79.48 |
| 71148 | CV | Single | Single | Single | G5V | 47 | 45.89 |
| 72905 | CV | Single | Single | Single | G1.5Vb | 64 | 70.07 |
| 75732AB | CPM | Double | Double | Double | G8V + M4 | 74 | 79.8 |
| 76151 | CV | Single | Single | Single | G3V | 85 | 58.5 |
| 78154AB | VB | Double | Double | Double | F6IV + K2V | 54 | 48.87 |
| 78366 | CV | Single | Single | Single | F9V | 46 | 52.25 |
| 79028 | SB? | Double | Double | Double | F9V + M? | 46 | 51.12 |
| 81809AB | SB20 | Double | Double | x | G2V + G9V | 50 | 32.01 |

Continued on Next Page...

Table. 6.1 – Continued

| Name HD | D&M Status | D&M Mult | New Mult | New Mult w/$\pi$ | MK Type | D&M $\pi$ (mas) | Hipparcos $\pi$ (mas) |
|---|---|---|---|---|---|---|---|
| 82443 | CV | Single | Double | Double | K1vk + M5.5 | 54 | 56.35 |
| 82885AB | VB | Double | Double | Double | G8IIIv + M5V | 109 | 89.45 |
| 84737 | CV | Single | Single | Single | G0.5Va | 66 | 54.26 |
| 86728 | CV | Single | Triple | Triple | G3Va + (M6.5 + M8) | 54 | 67.14 |
| 90508AB | CPM | Double | Double | x | F9V + M? | 52 | 42.45 |
| 90839 | CPM-SB? | Double | Double | Double | F8V + K7V | 82 | 77.82 |
| 91889AB | CPM-CV | Double | Single | x | F8V | 45 | 40.67 |
| 95128 | CV | Single | Single | Single | G1V | 74 | 71.04 |
| 97334 | CV | Single | Double | Double | G0V + L4.5 | 52 | 46.04 |
| 98231AB | Quad | Quad | Quad | Quad | (G0V+M3V)+(F8.5V+K2V) | 127 | 127 |
| 98281 | CV | Single | Single | Single | G8V | 54 | 45.48 |
| 101177AB | VB/SB1 | Triple | Triple | x | G2V + (K2V + M?) | 49 | 42.94 |
| 101501 | CV | Single | Single | Single | G8V | 110 | 104.81 |
| 102870 | SB? | Single | Single | Single | F9V | 100 | 91.74 |
| 103095AB | CPM | Double | Double | Double | G8Vp | 113 | 109.22 |
| 103431/2 | CPM | Double | Double | x | G5 + G0 | 53 | 27.01 |
| 106116 | CV | Single | Double | x | G4V + ? | 46 | 29.5 |
| 108754 | SB10 | Double | Triple | x | G7V + ?? | 51 | 19.2 |
| 108799A | VB | Double | Double | x | G1/G2V | 48 | 40.03 |
| 109358 | CV | Single | Single | Single | G0V | 109 | 119.46 |
| 110010 | SB1 | Double | Double | x | G0 + M | 51 | 27.94 |
| 110897 | CV | Single | Single | Single | G0V | 65 | 57.57 |
| 114710 | CV | Single | Single | Single | G0V | 120 | 109.23 |
| 115043 | CV | Single | Single | x | G1Va + | 50 | 38.92 |
| 115383 | CPM | Double | Double | Double | G0Vs + M/L? | 77 | 55.71 |
| 116459 | CV | Single | Single | x | G0 | 49 | 18.64 |
| 118576AB | CPM | Double | Double | x | G8V + K1 | 48 | 18.4 |
| 119124AB | CPM | Double | Double | x | F7.7V + K7 | 50 | 39.64 |
| 120136A | CPM/SB? | Double | Double | Double | F6IV + M2 | 57 | 64.12 |
| 120787 | pSB | Double | Single | x | G3V xxx | 64 | 8.3 |
| 122742 | SB10 | Double | Double | Double | G8V + M? | 61 | 60.24 |
| 125184 | SB? | Single | Single | x | G5IV | 62 | 30.47 |
| 126053 | CV | Single | Single | Single | G1V | 61 | 56.82 |
| 126660AB | Triple | Triple | Triple | Triple | (F7V + M3.5V) + M? | 68 | 68.63 |

Continued on Next Page...

Table. 6.1 – Continued

| Name HD | D&M Status | D&M Mult | New Mult | New Mult w/$\pi$ | MK Type | D&M $\pi$ (mas) | Hipparcos $\pi$ (mas) |
|---|---|---|---|---|---|---|---|
| 129333 | SB10 | Double | Double | x | G0V + (0.5Msun) | 48 | 29.46 |
| 130948 | CV | Single | Triple | Triple | G2V + (L2 + L2) | 70 | 55.73 |
| 131156AB | VB | Double | Double | Double | G8V + K4V | 148 | 149.26 |
| 133640AB | Triple | Triple | Triple | Triple | G1V + (G2V + K4V?) | 84 | 78.39 |
| 134319 | CV | Single | Triple | x | G5V + 2BD | 53 | 22.59 |
| 136064 | CV | Single | Single | x | F9IV | 47 | 39.51 |
| 137107/8 | VB | Double | Double | Double | G0V + G3V | 60 | 54.9 |
| 140538AB | CPM | Double | Double | Double | G2V + M? | 46 | 68.16 |
| 141004 | CV | Single | Single | Single | G0V | 94 | 85.08 |
| 142373 | CV | Single | Single | Single | F8Ve | 56 | 63.08 |
| 144284 | SB10 | Double | Double | Double | F8IV + K? | 46 | 47.79 |
| 144287 | SB10 | Double | Double | Double | G8V + M? | 53 | 46.56 |
| 144579 | CPM | Double | Double | Double | G8V | 80 | 69.61 |
| 146233 | CV | Single | Single | Single | G2Va | 61 | 71.3 |
| 146361Aab | Quad | Quad | Quint | Quint | ((G0Ve+G1V)+G2V)+(M2.5+MV) | 45 | 46.11 |
| 147266 | CV | Single | Single | x | G8IIIb | 99 | 9.46 |
| 149414AB | Triple | Triple | Triple | x | (F8 + K?) + M | 51 | 20.71 |
| 150433 | CV | Single | Single | x | G0 | 45 | 33.84 |
| 150706 | CV | Single | Single | x | G0 | 56 | 36.73 |
| 152391 | CV | Single | Single | Single | G8.5Vk | 67 | 59.04 |
| 153631 | SB10 | Double | Double | x | G0V + M? | 59 | 38.21 |
| 154345 | CV | Single | Single | Single | G8V | 62 | 55.37 |
| 154417 | CV | Single | Single | Single | F8.5IV-V | 49 | 49.06 |
| 156826 | CV | Single | Single | x | G9V | 81 | 18.74 |
| 157214 | CV | Single | Single | Single | G0V | 73 | 69.48 |
| 158614AB | VB | Double | Double | Double | G9IV-V + K? | 52 | 61 |
| 159222 | CV | Single | Single | x | G8V | 51 | 42.2 |
| 160269AB | Triple | Triple | Triple | Triple | (F9V + K3V) + M1V | 67 | 70.98 |
| 165401 | CV | Single | Single | x | G0V | 45 | 41 |
| GJ703 | CV | Single | Single | x | G0 | 72 | 16.73 |
| 165908AB | VB | Double | Double | Double | F6V + K4V | 61 | 63.88 |
| 168009 | CV | Single | Single | Single | G2V | 46 | 44.08 |
| 170153ab | SB20 | Double | Double | Double | K0V+K7V Or F7V+late G | 125 | 124.11 |
| 175225 | SB? | Single | Double | x | G9Va + M2 | 49 | 38.32 |

Continued on Next Page...

Table. 6.1 – Continued

| Name HD | D&M Status | D&M Mult | New Mult | New Mult w/$\pi$ | MK Type | D&M $\pi$ (mas) | Hipparcos $\pi$ (mas) |
|---|---|---|---|---|---|---|---|
| 176051AB | VB | Double | Double | Double | F9V + K1V | 54 | 66.76 |
| 176982 | CV | Single | Single | x | G5 | 54 | 10.52 |
| 177745 | CV | Single | Single | x | K0 | 57 | 30.16 |
| 178428 | SB10 | Double | Double | Double | G4VCN+05 + M | 59 | 47.72 |
| 183650 | CV | Single | Single | x | G5 | 49 | 27.47 |
| 184385 | SB? | Single | Single | Single | G5V | 46 | 49.61 |
| 186760 | CV | Single | Single | x | G0V | 45 | 22.23 |
| 187691AC | CPM | Double | Double | Double | F8V + M4.5 | 47 | 51.57 |
| 190067 | CV | Single | Single | Single | G7V | 49 | 51.71 |
| 190360AB | CPM | Double | Double | Double | G7IV-V + M4.5 | 56 | 62.92 |
| 190406 | CV | Single | Double | Double | G0V + L6 | 58 | 56.6 |
| 191854AB | VB | Double | Double | x | G4V + G8V | 46 | 19.45 |
| 193664 | CV | Single | Single | Single | G3V | 67 | 56.92 |
| 195987 | SB2 | Double | Double | Double | G9V + K? | 51 | 46.08 |
| 196850 | CV | Single | Single | x | G0 | 48 | 37.12 |
| 197076AB | CPM | Double | Double | Double | G5V | 49 | 47.65 |
| 198802 | CV | Single | Single | x | G1V | 46 | 22.17 |
| 199803 | CV | Single | Single | x | K0 | 54 | 20.98 |
| 202275AB | VBO | Double | Double | Double | F5V + F7V | 55 | 54.11 |
| 202573 | CV | Single | Single | x | G5V | 55 | 5.5 |
| GJ823 | CV | Single | Single | x | G5 | 66 | 14.51 |
| 206860 | CV | Single | Double | Double | G0VH + T2.5? | 66 | 54.37 |
| 207966 | CPM | Double | Double | x | G5 + M0 | 46 | 33.93 |
| 210277 | CV | Single | Single | Single | G0V | 47 | 46.97 |
| 213429ab | SB2 | Double | Double | x | F7V + K? | 46 | 39.18 |
| 214615AB | Triple | Triple | Triple | x | (G9V + K0V) + M3 | 47 | 25.42 |
| 216777A | CPM | Double | Double | x | G6V + WD | 48 | 28.72 |
| 217014 | CV | Single | Single | Single | G2V+ | 73 | 65.1 |
| 222368 | SB? | Single | Single | Single | F7V | 71 | 72.51 |
| 224930AB | VBO | Double | Double | Double | G5Vb + K7V | 84 | 80.63 |
| 9407 | CV | Removed | Removed | Single | G6V | 38 | 47.65 |
| 111395 | CV | Removed | Removed | Single | G5V | 34 | 58.23 |
| 117043 | CV | Removed | Removed | Single | G6V | 27 | 46.86 |
| 117176 | CV | Removed | Removed | Single | G5V | 41 | 55.22 |

Continued on Next Page...

Table. 6.1 – Continued

| Name HD | D&M Status | D&M Mult | New Mult | New Mult w/$\pi$ | MK Type | D&M $\pi$ (mas) | Hipparcos $\pi$ (mas) |
|---|---|---|---|---|---|---|---|
| 143761 | CV | Removed | Removed | Single | G0Va | 42 | 57.38 |
| 186408/27 | CV | Removed | Removed | Double | G1.5Vb + G3V | 36 | 46.25 |

*Notes.*

Column 2 lists the type of system as determined by the previous D&M survey. Columns 3, 4, and 5 give the multiplicity status in three different stages: D&M's original classification, updated with new companions, and the updated list with systems removed due to changes in parallax or discovered giants. Those that were removed are shown with an 'x' and are not considered in the multiplicity statistics (notes on individual systems that were changed or removed are listed in Chapter 6.3.1). The changes in parallax are shown in the last two columns. At the end of the table are the 6 systems that were previously removed from the sample but which should have been included based on their parallax.

### 6.2.1 SFP Systems

Most of these systems displayed a second packet on at least one baseline but due to scheduling conflicts, weather, and other limits to observing time, we were unable to follow up with extra observations. Each object is discussed below beginning with the systems for which we were unable to get complete observations. Example envelope and triangulation plots, when available, are shown in Appendix B. Virtually all of these objects will benefit from follow-on observations to determine their full set of visual orbital elements.

#### 6.2.1.1 HD 4676

64 Pisces: SB2 w/orbit, P = 13.82 days, i = 73°.92 (Konacki 2005). A well-observed double-lined spectroscopic binary consisting of two nearly identical F8V stars that has had a calibrated visibility interferometric orbit calculated by Boden et al. (1999b) with PTI. For this system, the separations on the sky are quite small (5-10 mas) at maximum elongation and with such an inclined orbit the secondary's SFP would only be seen near the two orbital maxima. With such a short period it was difficult to time the observations with the period and area of the sky which would allow the longest possible baseline, but we were able to observe the system at least once and see a separate fringe packet for the secondary (See Appendix §B.1).

#### 6.2.1.2 HD 11909

$\iota$ Aries: SB1, P = 1567.66 days. Classified in 1946 as a K1Vp, it has since been reclassified as a G5 with unspecified luminosity class but with its miniscule parallax and bright apparent

magnitude it is suspected to be a pair of giants. In Figures B.10 and B.11 in Appendix § B.3, we can see that during the 2005 observing season, we detected a second packet on both W1/S1 on Oct 2, and S1/E1 on Oct 7. During this time in the orbit, the secondary was approaching periastron (0.833 phase) but due to the long period of the orbit, we can still assume that the secondary was moving slow enough to allow both points to be used as a single point to get a reasonable estimate for the position of the companion. For that single point we calculate an actual separation and position angle ($\rho$=23.17±0.371 mas, $\theta$=218.29±0.92) as well as an estimated magnitude difference ($\Delta m_K$=1.33±0.39). The companion will be near apastron for the next year, and it would be beneficial to observe this system for eventual visual orbit determination .

#### 6.2.1.3 HD 24546

43 Persei: SB2, P = 30.44 days, $e = 0.63$ (Abt & Levy 1976). Another pair of nearly identical F5 stars though the luminosity class is listed as either IV or V depending on the author. The Fourth Interferometric Catalog (Hartkopf et al. 2001b) only lists two measurements and various radial velocity surveys report very few observations of this system since the orbit by Wallerstein (1973). It is listed by Tokovinin (1997) as having a tertiary visual companion. Figures B.17 and B.18 in Appendix § B.5 show two separate occasions of the detection of the secondary, but multiple observations were unable to be taken for this object. The two survey observations taken here were in January and February of 2007 nearly half an orbit apart (phases 0.43 and 0.72 respectively), and it would be useful to devote more concentrated time to get more observations of this system. Radii and orbital data would be most beneficial

to the nature of this system as it is classified as overluminious by Griffin & Suchkov (2003). It is also listed with a possible visual companion at 60″ that may be physical.

#### 6.2.1.4 HD 101606

62 Ursae Majoris: SB1/2, P = 267.508 days, e = 0.853, i $\sim$ 90°. This pair of metal-poor late F stars is discussed very thoroughly by Griffin et al. (1999). Recent speckle observations point to a near edge-on orbit. After a lengthy discussion and an updated spectroscopic orbit, Griffin settled on F7IV-V and F9V for the spectral types of the components together with 14 speckle observations, more observations could serve to pin down the precise inclination and determine the fundamental parameters for the possible subgiant. During a short observing run in the summer of 2006, this system displayed a second packet flagging it for repeat observations. Figures B.19 and B.20 in Appendix § B.6 were taken from S1/E1 in 2007 March, a little more than one full orbit later (0.54 phase in 2006 June and 0.58 in 2007 March).

#### 6.2.1.5 HD 107700

12 Comae Berenices: SB1 w/orbit, P = 396.49 days, e = 0.60. There have been two spectroscopic efforts for determining the orbit for this system, the first being Vinter Hansen (1940) and a follow up by Abt & Willmarth (1999) for which the orbital elements were unchanged. Both sets of authors agree on the spectral classifications of the components (primary G0 III-IV and A3 secondary). Although there have been eleven speckle observations since the orbit was first published, none have yet detected the secondary. HD 107700 displayed a

secondary fringe in 2006 June, and Figures B.21 and B.22 in Appendix § B.7 show the two envelopes from 2007 March 10 and 11, , which clearly show a second packet. However, insufficent rotation was available to get a proper location for the secondary. As the secondary was only about half way to apastron, it is clear that with further observations most of the orbit should be available to resolution with the CHARA Array's longest baselines.

#### 6.2.1.6 HD131511

DE Boötis: SB1 w/orbit, P = 125.4 days. High spectral resolution data with 3 m/s velocity precision were taken by Nidever et al. (2002) from the Keck and Lick observatories and produced a very high quality spectroscopic orbit. Three years later, Jancart et al. (2005) used astrometric data from HIPPARCOS to determine the visual orbital elements of the system which show another nearly edge-on orbit. This system was one of the lesser observed targets, accumulating only three observations between 2005 and 2007. Although undetected in 2006 June, the secondary did appear in a single observation in 2007 June and is displayed in Figure B.24 in Appendix § B.8.

#### 6.2.1.7 HD 166285

BU 637AB: SB1, P = 199.55 days. Another nearly equal pair of mid-F dwarfs (F5V and F6V) as suggested by Griffin (1999b) taken from the CHARA Spectroscopic Catalog as a SFP candidate for observation. Like HD 24546, this system shows an absolute magnitude anomaly between the Strömgren *ubvy* photometry and the calculated magnitude from the trigonometric parallax that indicate it is overluminious. Figure B.25 in Appendix § B.9

shows the envelope calculated from the only observation in 2006 September at 0.34 phase.

#### 6.2.1.8 HD 196795

BAG 14Aa,Ab: Triple (SB1 + Visual w/ orbits), P = 2.51 and 39.4 years. An interesting hierarchical triple system with a large difference in orbital plane inclinations ($i_{inner}$ = 18°.3, $i_{outer}$=86°.9) determined by Malogolovets et al. (2007). The initial spectroscopic orbit was determined by Duquennoy & Mayor (1988) and hints at a much lower mass than determined by the visual solution presented by Malogolovets et al. who stated that a combined solution presented large errors due to the combined effects of small radial velocities of the inner system, the small inclination and systematic errors of the radial velocity measurements from the influence of the outer component. Figures B.36 and B.37 in Appendix § B.12 show the detection of the secondary packet in 2007 July and October and adds another candidate for study in future programs.

#### 6.2.1.9 HD 202275

$\delta$ Equulei: SB2 w/orbit, P = 2083.1 days. A very well observed pair of mid-F dwarfs that have more than 100 RV and almost 200 speckle observations as well as combined visual and spectroscopic solutions presented by Pourbaix (2000), Arenou et al. (2000) and Muterspaugh et al. (2008). Although extra data are always welcomed for existing orbits and would have provided additional SFP confirmation, it was often unfeasible to collect data for this system. With the average separation at 232 mas, the use of the longest CHARA baselines precluded getting both fringes in the scanning window and as shorter baselines were often unavailable,

considerable time would have been lost for the acquisition of data of this particular system. On a few occasions we were able to obtain both fringes such as those shown in Figures B.38 and B.39 in Appendix § B.13 from the S2/W1 baseline in 2007 June.

#### 6.2.1.10 HD 221950

16 Pisces: SB2, P = 45.4585 days. A high-precision spectroscopic orbit recently determined for this system (Tomkin & Fekel 2008) gives ≤1% accuracy for the orbital dimensions and masses. A visual orbit for this system would yield very precise masses and as such this object remains a high priority target for the project. Unfortunately, two-baseline coverage was obtained with too large a time interval between observations to have any meaning for such a short orbit, and the observations of 2005 October 2 and 7 are shown in Figures B.40 and B.41 in Appendix § B.14 with the secondary component only visible for the S1/E1 baseline.

### 6.2.2 SFP Systems with Triangulation

Four systems were given more thorough observational scrutiny to yield new companions, new orbits, or additional points on existing orbits. These results are discussed below.

#### 6.2.2.1 HD 9021

38 Casseopia: SB1 w/orbit, P = 134.1 days. It seems the first and only full spectroscopic orbit was published more than 50 years ago (Wright & Pugh 1954), and the system has only subsequently been lightly studied by both speckle and spectroscopic means. Two other

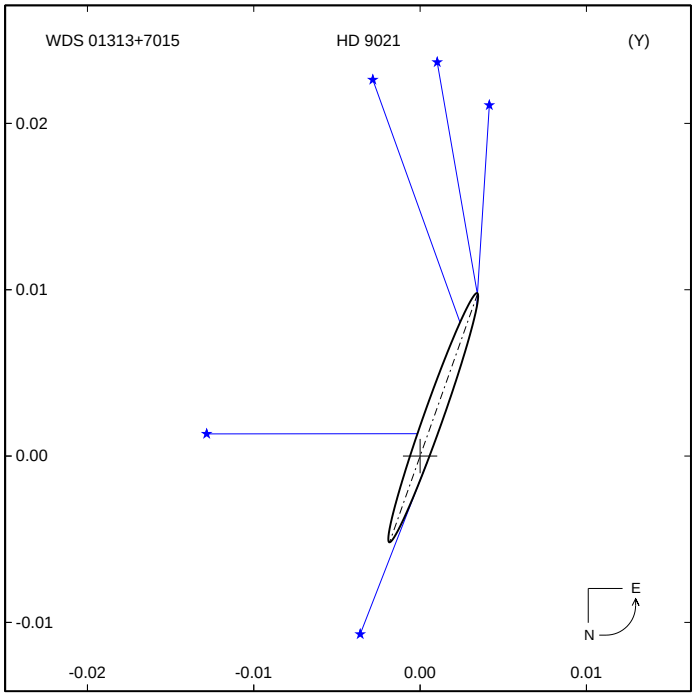


Figure. 6.2: Orbit for HD 9021, 2006-2008. Plot of the previously calculated astrometric orbit from Jancart et al. (2005) with the points calculated from the SFP survey. The stars represent the 5 observed positions that are connected by doted lines to the predicted positions. Halbwachs (1981) predicted that the semi-major axis would be approximately 26 mas from the previous spectroscopic orbit which is consistant with the points taken by the CHARA Array rather than the astrometric orbit seen here.

mentions of this system are useful to pry into the history of this unequal pair of mid-F stars. The most recent, presented by Jancart et al. (2005), is a photocentric orbit from HIPPARCOS data for which the computed value for the semi-major axis was determined to be a miniscule 7.95 mas. The semi-major axis measurement does not match well with the data collected here which is implied by the photocentric orbit. The prediction of Halbwachs (1981) for the estimated angular separation for the secondary (26 mas) agrees with the data points collected by the SFP survey ($\rho$ of 21.5, 23.7, 12.9, 11.9 and 22.8 mas). Figures B.3 and B.4 show two sample double fringe envelopes from 5 observations on back to back nights in September 2006. As there are only five points from which to calculate a visual

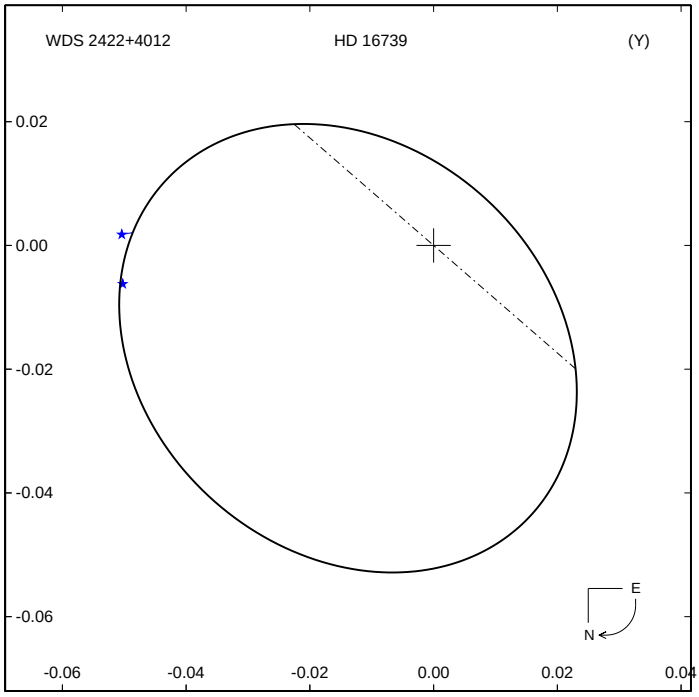


Figure. 6.3: Orbit for HD 16739, 2006-2007. Plot of the orbit of HD 16739 with orbital elements taken from Bagnuolo et al. (2006). The stars on the orbit represent observations taken from 2006 containing three vector separations each. The point with the largest error ($\geq$1 mas) was from two separate days (September 17-18) while the other with far greater accuracy from three points on the same night on October 5.

orbit, large errors make orbital determination for this system meaningless at this time. For now, we can see that the accepted orbit for this system fits the general shape of the photocentric orbit as shown in Figure 6.2. Interestingly, if we take the values published by Jancart and attempt to calculate the masses through Kepler's Laws with the 7.95 mas separation, we obtain $M_P$=0.059$M_\odot$ and $M_S$=0.034$M_\odot$. However, if instead we use an estimate closer to the approximate semi-major axis we see from the SFP determination, we obtain $M_P$=1.25$M_\odot$ and $M_S$=0.77$M_\odot$, which are rather close to the masses calculated by Jancart. Other envelopes and triangulations taken at the CHARA Array are included in Appendix B.2.

#### 6.2.2.2 HD 16739

12 Persei: SB2 w/orbit, P = 330.982 days. As this well-studied system appeared in the original D&M study, the CHARA Spectroscopic Binary Catalog, and the first CHARA SFP Binary (Bagnuolo et al. 2006), this provided another excellent test of using multiple baselines to obtain secondary locations on predetermined orbits. Unfortunately, what little data were obtained for this system were plagued by bad seeing, high noise, and large errors. Nevertheless, enough was obtained to produce two points rather close together along the west side of the orbit seen in Figure 6.3. The solution for the orbit was not re-calculated, but the points were used to test how well the locations would fit with the currently established orbit. Although only two points in one quadrant were able to be obtained for this test, the results are satisfactory. Other envelopes and triangulations taken at the CHARA Array are included in Appendix B.4.

#### 6.2.2.3 HD 170153

$\chi$ Draconis: SB2 w/orbit, P = 280.517 days. Another member of both the D&M sample and the CHARA catalogs with a very wide 127 mas semi-major axis that produces double fringe packets. As this system is very close (8 parsecs), the primary is sufficiently large in diameter to be resolved at the longest baseline, and the lower amplitide fringe packet was determined to be that of the primary star. Thus, vector separations were measured in the opposite direction. With that in mind, the data were reduced and fit remarkably well to the previous spectroscopic orbit from Pourbaix (2000). If one compares Figure 6.4 and 6.5, it can be seen

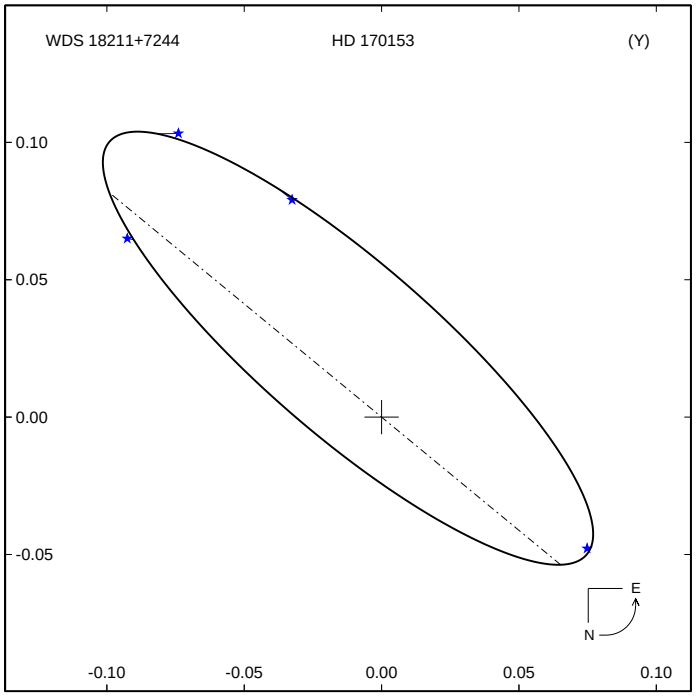


Figure. 6.4: Orbit for HD 170153, 2006-2007. Plot of the orbit of HD 170153 with orbital elements taken from Pourbaix (2000). The four points obtained by the CHARA SFP survey are designated by the stars and represent two to five vector separations each. All points agree well with the previous orbit with far better accuracy than the speckle points seen in Figure 6.5.

that the accuracy of the secondary locations is superior to the speckle measurements but require much more effort to obtain. Extra observations were attempted at the unsampled phases in Figure 6.5 in order to observe the secondary near closest visual approach to obtain a more complete solution. However, these attepts were unsuccessful due to adverse weather. Other envelopes and triangulations taken at the CHARA Array are included in Appendix B.10.

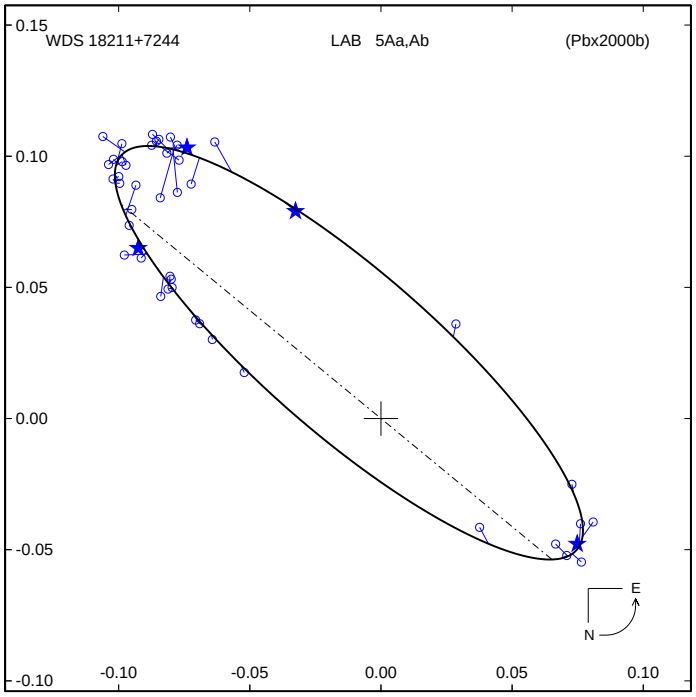


Figure. 6.5: Speckle Orbit Plot for HD 170153, 1973-1994. Orbit taken from the Sixth Catalog of Orbits of Visual Binary Stars (open circles) for comparison to the accuracy of the SFP secondary locations (stars) plotted in Figure 6.4.

#### 6.2.2.4 HD 173093

HR 7304: Single? F7V - During an observing run for another project in 2006, this supposed single star was intended to be used as a calibrator for visibility analysis and was discovered to have a secondary fringe packet by Nils Turner. As this project was interested in SFP systems, it was passed along for further study. While this star is solar type (F7V), it falls well outside the range of the parallax-limited multiplicity survey. A search determined that Nordström et al. (2004) measured variablilty and flagged this system as a probable binary star with five radial velocity measurements. Unfortunately, there was insufficient time to observe this object on more than one occasion. Figures 6.6 and 6.7 show the envelope

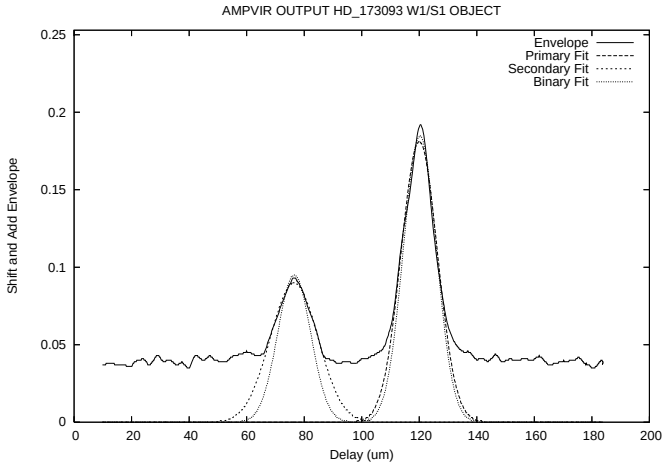


Figure. 6.6: HD 173093 on 2006 September 19 using the W1/S1 baseline.

obtained for one file in 2006 September when an attempt was made to get the secondary location with multiple baselines, and the triangulation of the secondary through minimal baseline rotation when it was erroneously being used as a calibrator in 2006 May. As this is another new visible companion, effort will be made to add observations of this system to future observing plans to combine with a future spectroscopic orbit and determine the masses. Envelopes and triangulations taken at the CHARA Array are included in Appendix B.11.

## 6.3 Multiplicity Revisited

Even with all the observations obtained by this project, no new companions were found for the objects that were used in the multiplicity sample of D&M. This does not mean that the multiplicity for the original sample has not changed since its original publication. Since 1991, advances have been made in the accuracy of radial velocity measurements that have allowed detections of variations down to several meters per second. Additionally, the HIPPARCOS

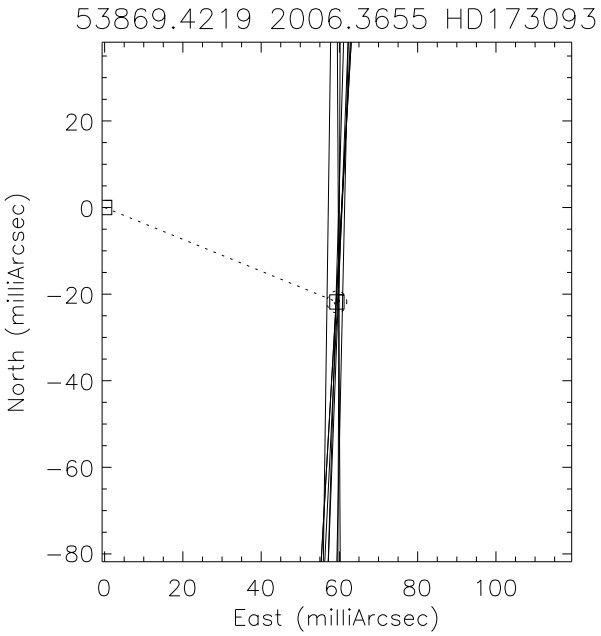


Figure. 6.7: Triangulation Plot for HD 173093. Although this system shows separated fringe packets, reduction of the data obtained during this run is mostly inconclusive. The baseline used did not provide much rotation and is not to be included in any future orbit.

satellite has greatly improved the quality of parallaxes for most of the stars in both surveys. In this section we will discuss the new companions detected after the D&M survey as well as the implications of the improved parallaxes on the multiplicity of local solar-type stars.

For the formation of the original multiplicity sample, D&M selected a distance of 22 pc ($\pi$=0.045 arcsec) as one of the criteria for a star to be included in the statistics. If we go back to the multitude of parallaxes used for the multiplicity sample and compare them to the most recent HIPPARCOS update (van Leeuwen 2008), we can see that nearly 40% of the systems had parallaxes that were significantly different from pre-HIPPARCOS values. This could be explained by misclassification of giants, unknown companions, or just outright errors in calculation for the techniques that were available at the time.

In the following section we will look at the stars for the multiplicity sample that have had a status change either from newly discovered companions, parallax changes, or giant misclassification. For this approach, companions are included up to the demarcation mass where the companion would be considered a planet. This covers both brown and white dwarf secondaries which will be considered for multiplicity as well as planetary companions which will not be included in the statistics. Table 6.1 displays three columns based on the stages of the multiplicity changes to be discussed here, beginning with D&M's original classification, the classification based on inclusion of newly discovered companions, and finally the retention or removal of the system based on the new parallaxes and the recognition of stars with a giant luminosity class being applied to the original criteria.

Table. 6.2: Stars Originally Removed for Discrepant Parallax

| **Stars Removed for Discrepant $\pi$ Only** | | | |
|---|---|---|---|
| HD1461 | HD22879 | HD110010 | HD177745 |
| HD4676 | HD29203 | HD115043 | HD183650 |
| HD5294 | HD31966 | HD118576 | HD186760 |
| HD6920 | HD33093 | HD119124 | HD191854 |
| HD9562 | HD37124 | HD125184 | HD196850 |
| HD10697 | HD39881 | HD129333 | HD198802 |
| HD11964 | HD41330 | HD136064 | HD199803 |
| HD12051 | HD61994 | HD149414 | GJ823 |
| HD16620 | HD81809 | HD150433 | HD207966 |
| HD16739 | HD90508 | HD150706 | HD213429 |
| HD17433 | HD101177 | HD153631 | HD214615 |
| HD19034 | HD103432 | HD159222 | HD216777 |
| HD20619 | HD108799 | HD165401 | |

### 6.3.1 Individual System Notes

The following sections include notes for individual systems that were changed or removed from the updated sample and the reasons behind each change. Additionally, there were many stars that only were removed from the D&M sample due to the change in parallax. Such systems are listed here in Table 6.2. The previous and current parallaxes for these objects are also listed in Table 6.1 along with the all other stars in the multiplicity sample. Envelope traces for those systems observed by the CHARA SFP Survey are included in Appendix A.

#### 6.3.1.1 HD 123

HR 5, STF3062AB: A known visual double dating back to the early 1800's, D&M noted that there was a possible unseen companion for component B with either a period of 6.9 years or 1.08 days depending on the source. As the $\Delta$m and separation made the object unfavorable for interpretation by D&M, the system was left as a multiplicity of two. In 1999, Griffin (1999a) observed the system with CORAVEL in order to discern the truth of the variations of component B and discovered a spectroscopic orbit of approximately 47 days. With the outer orbit (P$\sim$107 years) rather well established from over 100 years of observing, the fractional mass of component B having been previously determined as $M_{\rm B}$=0.546, and the mass sum from the visual orbit, the derived mass for component B is a bit over one solar mass which is too large for its spectral type. With the spectroscopic orbit quite well determined, it was estimated that with the $\Delta$m of the Bb system being nearly 5 magnitudes, the companion was likely to be a $\sim$0.3 solar mass object, probably an early M dwarf. With the discovery of

this companion, the system's multiplicity was revised from double to triple for this survey.

#### 6.3.1.2 HD 5857

GJ 46.1: Listed as SB? by D&M, yet still classified as single for the purposes of the multiplicity study since the measure was so uncertain. A companion was confirmed later in the second version of the HIPPARCOS Input Catalog (Turon et al. 1993) and the HST Guide Star Catalog (Lasker et al. 1996) with the secondary at 4.2″ and 249°. Even though this would change the multiplicity, when the updated parallax is compared to the previous, this system is removed from the list because it is more than 100 parsecs further than it was originally thought to be. With $V - K$=-4, $m_{/rmK}$=4.8 and a 6.54 mas HIPPARCOS parallax, it is reasonable to assume that one or both of the components is a giant as they are far too bright in the infrared to be dwarfs. No luminosity class has been assigned in the existing literature on the star.

#### 6.3.1.3 HD 9826

$\upsilon$ Andromeda: Originally designated CV (constant velocity) for the multiplicity study, D&M could not have known that this system would later become one of the most interesting objects in recent years. In addition to having at least three and possibly four Jupiter-sized planets, it is one of the relatively few planetary systems with a stellar companion. Discovered by Lowrance et al. (2002) and since confirmed in multiple papers, the F8V primary has a M4.5V companion at about 55″ with an orbital distance of 750 AU. This indeed qualifies the system's promotion from single to double.

#### 6.3.1.4 HD 22484

10 Taurus: As this was listed as a SB? with no extraneous notes, the change in status is probably shaky at best. A rather close star at only 13.7 pc, a search of the literature and surrounding stars shows the star LHS 5074 has a similar proper motion (same general direction with nearly 0.5″/yr proper motion) and it is suggestive that these stars are a common proper motion (CPM) pair. Even though no parallax for this $V = +14$ M star exists, this is definitely a new companion.

#### 6.3.1.5 HD 43587

CAT 1Aa,Ab: CPM (G0V + M3.5V). In addition to the faint ($V$=+13.4) common proper motion companion at 95″, recent work has identified a secondary star within 1″. Adaptive optics observations from the Canada-France-Hawaii Telescope (CFHT) were presented by Catala et al. (2006) as a follow up to the RV detection of a stellar mass companion whose amplitude should have been just above the errors with CORAVEL. With the addition of this stellar companion ($M_{\odot} \sim 0.5$ and $\Delta$m $\sim$ 2.5-3.0) to this CPM system, HD 43587 is considered to be triple instead of double for the multiplicity statistics.

#### 6.3.1.6 HD 82443

LDS3903A: CV (dG9). A rather unremarkable star from the D&M survey with no additional information other than its basic data, it appears to have a CPM companion at 65″ detected with a combination of the 2MASS and NLTT catalogs (Reid & Cruz 2002) which place the M5.5 companion at the same parallax.

#### 6.3.1.7 HD 86728

20 Leonis Minoris, GJ 376A: Measurements from D&M, HIPPARCOS, and ground-based astrometry (Heintz 1988) indicate no companion. Analysis by Gizis et al. (1999) show that there is not only one, but probably two late M dwarf companions that were indicated in the LHS and 2MASS catalogs with identical proper motion. Further discussion reveals that Gl 376B has the spectrum of a late M dwarf but is far too bright to be a single star. The conclusions reached by Gizis et al. indicate that this object is a pair of nearly equal luminosity M6.5-8 dwarfs, so the Gl 376 system is elevated to triple star status (G3V, M6.5, M8).

#### 6.3.1.8 HD 91889

GJ 398.1AB: Listed by D&M as a CPM with the secondary as a possible SB at 14″. Subsequent searches around this system have yet to confirm this secondary in the DSS, 2MASS or any other survey. The only other possibility is that the secondary is an object at twice D&M's original estimate of separation (BD-11 2918B) with a proper motion only 1/10th the size of the primary's. The possibility that the companion has been missed is not unlikely, but for the purposes of this project, this system will be considered single. Regardless of the multiplicity, subsequent measurements of the parallax of the system place the primary outside the range of the multiplicity sample ($\pi$=40.67), and it will not be considered in the statistics.

#### 6.3.1.9 HD 97334

STTA108AB, GJ 417AB: CPM (G0V). A faint companion designated L4.5 (12-13 $M_J$) was recently discovered by Kirkpatrick et al. (2000), and more completely studied by Cruz et al. (2003). D&M's predictions on undiscovered Brown Dwarf (BD) companions for their sample mention a possible 3-25 very low mass companion (VLMC) and include this in their incompleteness study. With the discovery of the BD companion, this system will be considered double.

#### 6.3.1.10 HD 106116

LPM 416AB, GJ458.1: CV (G4V). The Catalogue of the Components of Double and Multiple stars (CCDM) (Dommanget & Nys 2000) and Tycho double star catalog (Fabricius et al. 2002) list a companion for this primary at $2''$ and $5^\circ$ with no magnitude or any other information. Even with component B included, we shall not include this system as the parallax has changed from 46 mas to 29.5 mas putting it well out of range for this study.

#### 6.3.1.11 HD 108754

TOK 27, GJ 469.1: SB1O (G8V). Possible new companion discovered as a tertiary component of this system by Tokovinin et al. (2006). At $5''$, it is listed as tentative, and no companion is indicated in the 2MASS all-sky survey. Inclusion of this would change the multiplicity to triple, but the parallax for the system has changed rather drastically since the original survey ($\pi$=51 mas has dropped to 19.2 mas). Thus, the system has been removed from the present sample.

#### 6.3.1.12 HD 120787

GJ 529.1: SB (G8V). Selected as a possible SB from D&M, this system is probably not a dwarf, and yet in the D&M survey and almost every mention of the star since then, it remains classified as one. Even now after 2MASS has posted magnitudes of $m_{\rm K}$=+3.9 and an 8.3 mas parallax, it remains classified as a dwarf when it is far more likely to be a giant with its brightness at that distance. HD 120787 is no longer included in the multiplicity sample.

#### 6.3.1.13 HD 130948

POT 1Abc, GJ 564: CV (dG2). Classified by D&M as single and by Gliese (1969) as SB, it was not long until Potter et al. (2002) discovered that this system has two BD companions. Using adaptive optics on the Subaru Telescope, they were able to separate the two companions, 8 magnitudes fainter, from the primary 2.63″ away and the BDs individually (separated by 134 mas) over 7 months to ensure that the companions were not background objects. Predicted spectral types are listed as L4±1. For the purposes of multiplicity for this project, we shall consider this object triple.

#### 6.3.1.14 HD 134319

MCT 7A, GJ 577: CV (dG5e). Although the change in distance determinations puts this system too far out to be included in the statistics (D&M = 53 mas vs HIPPARCOS = 22.6 mas), it is interesting to note that this system has two newly discovered BD companions (Lowrance et al. 2003; Mugrauer et al. 2004). The BDs for a 82 mas pair of similar brightness

that is 4″.3 distant from the primary.

#### 6.3.1.15 HD 146361

$\sigma$ CrB: Quad (((G0Ve+G1V)+G2V)+M2.5V). A hierarchical quadruple system thought before this year to have two double systems orbiting each other (HD 146361 & HD 146362) with a 900 year period. A recent CHARA visibility study (Raghavan et al. 2008) has discovered that one of the components of one of these doubles has a companion of its own, rendering this system a quintuple. As the original multiplicity survey contained no multiplicity higher than four, a new classification has been included for the multiplicity statistics.

#### 6.3.1.16 HD 147266

GJ 618.3: CV (dG7). With an unknown source for the very large listed parallax (99 mas photometric and/or trigonometric) in D&M, this single star has since been corrected from a G dwarf to a G8IIIb with a very small HIPPARCOS parallax (9.5 mas). This star now fails two of the initial criteria and is eliminated from the sample.

#### 6.3.1.17 HD 156826

GJ 668.1: CV (G9V). This system saw a large reduction in parallax from D&M to HIPPARCOS (81 mas to 18.7 mas) with a large $K$ magnitude ($m_K$=4.25) leading us to believe that it is in fact not a dwarf and should not be included in the statistics.

#### 6.3.1.18 GJ 703

GJ 703: CV (G6). Another probable giant with large parallax change (72 mas to 16.7 mas) that is not kept for the statistical analysis.

#### 6.3.1.19 HD 175225

TRN 3, GJ 732.1: SB? (dG8). D&M suggested that the RV variations were possibly from a long-period companion but as it was unverified, it was not used for their multiplicity study. An AO collaborative effort of CHARA contributors working on the Mount Wilson 100-inch telescope discovered the companion classified as a probable M2V approximately $1''$ from the primary Turner et al. (2001). Unfortunately, the HIPPARCOS parallax is too small for this target to remain within the sample limits.

#### 6.3.1.20 HD 176982

STF2434AB, GJ 740.1: CV (dG5). A large $V - K$ and discrepant parallax (10.5 mas) compared to previous values indicates another probable giant, and therefore, this target was removed from the sample.

#### 6.3.1.21 HD 190406

15 Sagitta, GJ 779AB: CV (G1V). AO observations of this system by Liu et al. (2002) detected a faint CPM BD of L3-L6 spectral type at 790 mas. As the parallax did not change much from previous values, we reclassify this system as double and retain it for the sample.

#### 6.3.1.22 HD 197076

GJ 797: CPM (dG2+M). The companion is listed as a marginally variable M star at 94−125″. At this point confirmation is difficult as no new observations of the companion are mentioned and SIMBAD lists component B explicitly as not a companion. However, component C is not listed as a companion yet still has nearly the same proper motion and is the proper brightness and spectral type. Thus, the system is retained in its present multiplicity.

#### 6.3.1.23 HD 202573

GJ 822.2: CV (G5V). As with several previous stars, GJ 822.2 has a bright $K$ magnitude and a very small parallax ($m_K$=4.73, $\pi$=5.50) and is still listed everywhere as a G5V, an obvious misclassification. With a previous parallax of 55 mas, it might be that a misprint allowed this system to remain in the sample, however, as a probable giant, it is removed from the following multiplicity recalculation.

#### 6.3.1.24 HD 206826

LUH 4, HN Pegasi: CV (dG0Ve). A constant velocity star as listed by D&M with no extra information. Although the newer parallax does change the distance to the system, it remains within the sample. Recent work by Luhman et al. (2007) has yielded a companion as a candidate T-dwarf (T2.5), one of the few known of this type. With this discovery, the status of this system changes from single to double.

### 6.3.2 Stars Removed from D&M

Additionally, all the stars originally removed from the sample were investigated, to determine the reason they were not included and checked against recent data to decide if they were correctly removed. Included in Table 6.3 are six stellar systems that were removed based on the data available at the time but in fact are within the sample limits. All the systems in this table meet all the other criteria for inclusion except for the distance.

Table. 6.3: Stars Removed from D&M Erroneously

| **HD** | **Multiplicity & Spectral Type** | $\pi_{D\&M}$ **(mas)** | $\pi_{Hip}$ **(mas)** |
|---|---|---|---|
| 9407 | CV G6V | 38 | 47.6 |
| 111395 | CV G5V | 34 | 58.2 |
| 117043 | CV G6V | 27 | 46.9 |
| 117176 | CV G5V | 41 | 55.2 |
| 143761 | CV G0Va | 42 | 57.4 |
| 186408/27 | CPM G1.5V+G3V | 36 | 46.3 |

*Note.* Each of these systems was removed from the multiplicity sample by D&M only due to the limit on the parallax. As HIPPARCOS has updated the distances to these objects to bring them within the imposed limit, these six have been included into the current multiplicity sample.

*These instruments have play'd me so many tricks that I have'at last found them out in many of their humours.*

—— *William Herschel*

# – 7 —

# Case Studies

In this chapter we will discuss three systems of note from this survey that provide new or updated results from data collected at the CHARA Array. Included here are several orbital points for a system with a new companion (HD 181655), extra observations for a system with revised orbital elements (HD 184467), and a completely new astrometric orbit for a well-known spectroscopic orbit which had not previously been visually separated (HD 198084). Table 7.1 includes the individual observations of each system as measured vector separations and true calculated secondary locations for each observational grouping.

Table. 7.1: Secondary Locations for SFP systems HD 181655, 184467, and 198084

| **System** | **MJD** | **B(m)** | $\vec{\theta}$**(deg)** | $\vec{\rho}$**(mas)** | $BY_{calc}$ | $\theta$ | $\rho$**(mas)** |
|---|---|---|---|---|---|---|---|
| HD181655-1 | 53648.204 | 254.62 | 121.03 | 67.40 | | | |
| | 53648.208 | 252.39 | 120.35 | 65.72 | | | |
| | 53648.213 | 249.98 | 119.65 | 67.27 | | | |
| | 53649.153 | 330.25 | 8.64 | 0.00 | 2005.7600 | 98.6 | 58.8 |
| -2 | 53890.267 | 270.10 | 4.98 | 73.57 | | | |
| | 53891.469 | 275.73 | 132.82 | 73.15 | | | |
| | 53892.251 | 279.31 | 230.15 | 30.50 | | | |
| | 53892.280 | 297.19 | 226.82 | 37.11 | | | |
| | 53892.384 | 328.03 | 210.66 | 65.04 | 2006.4268 | 341.4 | 62.0 |
| -3 | 53987.253 | 330.01 | 182.58 | 134.97 | | | |
| | 53988.221 | 330.29 | 189.42 | 141.28 | | | |
| | 53989.225 | 271.08 | 128.46 | 84.45 | | | |
| | 53989.314 | 227.63 | 114.65 | 52.25 | | | |
| | 53990.242 | 265.28 | 125.13 | 76.99 | | | |
| | 53991.178 | 330.65 | 197.32 | 136.70 | 2006.6949 | 354.2 | 92.3 |
| -4 | 54247.362 | 271.77 | 31.73 | 70.99 | | | |
| | 54247.449 | 278.43 | 15.67 | 90.65 | | | |
| | 54247.503 | 278.76 | 4.09 | 98.65 | | | |
| | 54248.485 | 276.51 | 133.96 | 91.32 | | | |
| | 54249.400 | 276.69 | 24.10 | 82.65 | | | |
| | 54249.407 | 277.11 | 22.84 | 81.99 | | | |
| | 54250.375 | 274.20 | 158.14 | 103.31 | 2007.4042 | 164.5 | 78.6 |
| -5 | 54393.117 | 271.57 | 128.82 | 70.81 | | | |
| | 54393.186 | 242.88 | 117.83 | 49.46 | | | |
| | 54393.231 | 330.65 | 161.94 | 127.88 | | | |
| | 54393.241 | 330.62 | 159.77 | 125.50 | 2007.8007 | 177.6 | 82.5 |
| -6 | 54697.261 | 248.12 | 9.66 | 101.52 | | | |
| | 54697.349 | 248.12 | 170.19 | 102.96 | | | |
| | 54699.316 | 248.06 | 176.10 | 103.06 | | | |
| | 54699.321 | 248.07 | 174.99 | 103.91 | | | |
| | 54699.394 | 247.63 | 159.01 | 98.79 | 2008.6354 | 356.9 | 86.3 |
| HD184467-1 | 53647.169 | 251.09 | 122.31 | 46.42 | | | |
| | 53647.173 | 249.95 | 121.44 | 47.20 | | | |
| | 53647.176 | 248.57 | 120.42 | 44.88 | | | |
| | 53654.159 | 314.73 | 186.15 | 46.11 | | | |
| | 53654.162 | 314.84 | 185.36 | 45.66 | | | |
| | 53654.166 | 314.93 | 184.59 | 46.84 | 2005.7662 | 153.5 | 54.4 |
| -2 | 53889.388 | 295.80 | 36.77 | 99.48 | | | |
| | 53889.461 | 310.54 | 19.37 | 90.15 | | | |
| | 53890.280 | 276.43 | 3.28 | 74.79 | | | |
| | 53891.324 | 276.11 | 349.98 | 56.23 | | | |
| | 53891.507 | 248.82 | 120.60 | 23.01 | | | |
| | 53892.458 | 311.19 | 18.05 | 90.32 | 2006.4236 | 45.9 | 101.3 |

Continued on Next Page...

Table. 7.1 - Continued

| System | MJD | B(m) | $\vec{\theta}$(deg) | $\vec{\rho}$(mas) | $BY_{calc}$ | $\theta$ | $\rho$(mas) |
|---|---|---|---|---|---|---|---|
| -3 | 53990.155 | 268.78 | 322.09 | 50.25 | | | |
| | 53990.229 | 251.45 | 302.60 | 38.01 | | | |
| | 53996.212 | 314.25 | 8.87 | 61.17 | | | |
| | 53996.292 | 313.72 | 348.91 | 63.65 | 2006.7048 | 352.8 | 63.4 |
| -4 | 54247.376 | 241.68 | 35.25 | 61.48 | | | |
| | 54247.480 | 258.23 | 11.65 | 22.09 | | | |
| | 54248.436 | 270.22 | 144.93 | 59.52 | | | |
| | 54249.437 | 254.45 | 20.45 | 39.71 | | | |
| | 54249.440 | 254.92 | 19.61 | 37.75 | | | |
| | 54249.486 | 258.91 | 9.09 | 20.16 | | | |
| | 54249.493 | 259.27 | 7.31 | 19.01 | 2007.4049 | 88.5 | 105.5 |
| -5 | 54272.409 | 310.09 | 20.24 | 56.47 | | | |
| | 54272.413 | 310.54 | 19.38 | 53.12 | | | |
| | 54272.481 | 315.09 | 2.64 | 23.56 | | | |
| | 54273.314 | 274.89 | 160.01 | 21.26 | 2007.4703 | 80.6 | 112.5 |
| HD198084-1 | 53648.272 | 229.32 | 108.68 | 40.23 | | | |
| | 53648.277 | 227.14 | 107.57 | 40.56 | | | |
| | 53648.279 | 225.88 | 106.93 | 41.83 | | | |
| | 53654.134 | 309.07 | 24.80 | 117.93 | | | |
| | 53654.138 | 309.71 | 23.86 | 123.05 | | | |
| | 53654.142 | 310.30 | 22.94 | 123.16 | | | |
| | 53654.149 | 311.35 | 21.19 | 123.19 | 2005.7676 | 222.9 | 87.2 |
| -2 | 53889.412 | 288.97 | 222.65 | 29.80 | | | |
| | 53889.472 | 305.81 | 208.95 | 22.02 | | | |
| | 53890.436 | 289.91 | 274.22 | 20.52 | 2006.4213 | 89.1 | 32.4 |
| -3 | 53892.397 | 286.09 | 224.36 | 31.25 | | | |
| | 53892.436 | 299.27 | 215.32 | 25.69 | | | |
| | 53892.481 | 308.97 | 204.94 | 18.15 | 2006.4280 | 95.1 | 34.1 |
| -4 | 53988.375 | 210.31 | 279.53 | 25.03 | | | |
| | 53989.249 | 262.20 | 311.72 | 73.83 | | | |
| | 53989.328 | 234.71 | 291.56 | 43.73 | | | |
| | 53989.372 | 210.46 | 279.60 | 24.45 | | | |
| | 53990.138 | 275.71 | 340.78 | 96.47 | | | |
| | 53990.144 | 275.43 | 339.13 | 97.73 | | | |
| | 53990.218 | 267.92 | 319.12 | 83.77 | | | |
| | 53990.352 | 220.94 | 284.50 | 31.94 | 2006.6949 | 170.3 | 75.0 |
| -5 | 54249.418 | 242.69 | 35.70 | 80.90 | | | |
| | 54249.422 | 243.76 | 34.83 | 81.01 | | | |
| | 54249.474 | 254.28 | 23.52 | 72.01 | | | |
| | 54249.481 | 255.33 | 21.91 | 71.99 | 2007.4062 | 248.1 | 78.8 |
| -6 | 54254.388 | 168.62 | 2.79 | 23.22 | | | |
| | 54254.425 | 168.42 | 173.90 | 12.66 | | | |
| | 54255.388 | 101.78 | 134.14 | 18.33 | | | |
| | 54255.436 | 105.56 | 118.12 | 28.66 | | | |
| | 54255.485 | 107.76 | 102.73 | 33.33 | 2007.4219 | 250.1 | 77.7 |
| -7 | 54268.458 | 241.22 | 134.86 | 43.33 | | | |

Continued on Next Page...

Table. 7.1 - Continued

| **System** | **MJD** | **B(m)** | $\vec{\theta}$**(deg)** | $\vec{\rho}$**(mas)** | $BY_{calc}$ | $\theta$ | $\rho$**(mas)** |
|---|---|---|---|---|---|---|---|
| | 54269.498 | 314.87 | 13.12 | 56.23 | 2007.5654 | 255.4 | 74.5 |
| -8 | 54314.397 | 316.20 | 7.74 | 18.47 | | | |
| | 54314.481 | 314.92 | 167.02 | 31.33 | | | |
| | 54315.347 | 312.39 | 19.24 | 15.47 | | | |
| | 54315.430 | 316.87 | 178.88 | 19.92 | | | |
| | 54315.474 | 315.22 | 168.04 | 31.81 | | | |
| | 54315.514 | 311.13 | 158.41 | 45.75 | 2007.5876 | 277.8 | 60.6 |
| -9 | 54359.261 | 255.37 | 125.24 | 50.11 | | | |
| | 54359.407 | 308.98 | 335.07 | 59.99 | 2007.7078 | 316.1 | 40.5 |
| -10 | 54375.119 | 273.53 | 331.24 | 40.66 | | | |
| | 54376.145 | 270.37 | 143.42 | 39.22 | | | |
| | 54376.194 | 261.26 | 310.71 | 32.33 | | | |
| | 54376.291 | 223.03 | 105.52 | 19.00 | | | |
| | 54376.313 | 210.45 | 99.60 | 16.75 | 2007.7535 | 345.7 | 31.3 |
| -11 | 54423.155 | 233.97 | 350.10 | 19.63 | | | |
| | 54423.179 | 232.44 | 344.40 | 27.12 | | | |
| | 54424.184 | 231.80 | 342.61 | 28.99 | 2007.8833 | 107.3 | 38.2 |
| -12 | 54426.154 | 233.60 | 348.45 | 24.66 | | | |
| | 54426.172 | 232.35 | 164.11 | 29.99 | 2007.8919 | 111.6 | 40.0 |
| -13 | 54693.343 | 256.52 | 143.78 | 16.75 | | | |
| | 54693.382 | 242.62 | 153.83 | 29.11 | | | |
| | 54693.463 | 313.15 | 287.64 | 67.80 | | | |
| | 54693.499 | 307.82 | 296.49 | 46.69 | 2008.6215 | 222.4 | 88.3 |

*Note.* All CHARA Array observations for HD 181655, HD 184467, and HD 198084. Each set of vector observations (along with the projected baseline length and epoch of observation) in columns two through five were combined to create the true location of the secondary and average time of all the data points defined in the last three columns. Errors associated with each observation for HD 181655 and HD 184467 are $\leq$1 mas or for HD 198084 are mostly less than one mas except for 2, 3, 7, 9, and 12 which errors are no more than 4 mas.

## 7.1 HD 181655

HR 7345: Out of all the systems observed in the SFP survey, this one has proved the most difficult. Designated as spectral type G8V, this star has been observed on multiple occasions with a variety of techniques and instruments. Never once has any one detected a companion. Both Nidever et al. (2002) and Nordström et al. (2004) observed this system multiple times over the course of the last two decades and found it to be a stable radial velocity source down to 100 m/s with no hint of a spectroscopic companion. Additionally HD 181655 was observed interferometrically with the CHARA speckle camera on the Canada-France-Hawaii Telescope (CFHT) (McAlister et al. 1987) and on 46 separate nights with all three baselines of PTI (van Belle et al. 2008) for their calibrator catalog. On the CFHT program, no companion was detected down to 38 mas and while the system was rejected from the catalog of calibrators, it was not due to binarity.

At the beginning of the survey, there were thus no expectations of finding new companions for this star but for completeness the system was kept in the selection of stars to be observed at the Array. The selection process for the SFP sample included many systems that were outside the parallax range for the D&M multiplicity selection and with a parallax of $\pi_{\rm Hip}$=39.64 mas, HD 181655 fit the criteria to be observed with the CHARA Array and so was retained. During the first observational season, this object was observed on both available baselines on two sequential days and only exhibited a secondary fringe packet on one of the two baselines (W1/S1) used during the observing run. It is unknown if the other baseline (S1/E1) was perpendicular to the secondary at that time or if the secondary packet

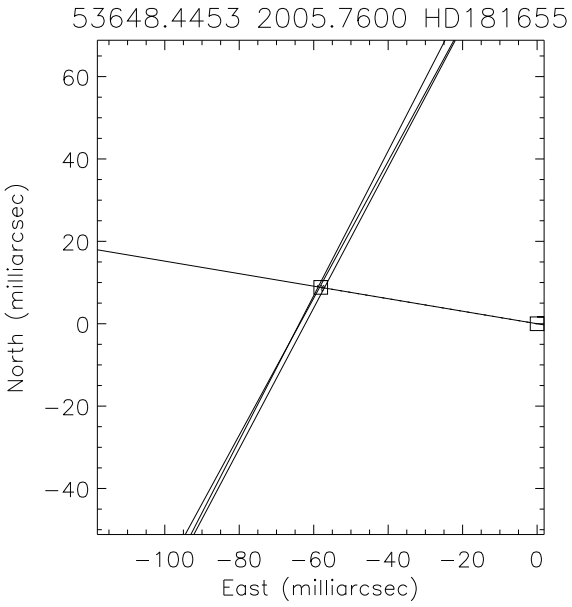


Figure. 7.1: Triangulation Plot for HD 181655, 2005.7600. As no second fringe packet was located on S1/E1 (the nearly horizontal line), it is assumed that the secondary was perpendicular to the baseline. This may not necessarily be the case and this point may be disregarded in the future.

was just outside the range of scanning, so this observation shows at least that a companion exists. We will assume that the secondary's position was perpendicular to this baseline and is shown as such in Figure 7.1.

Although it was assumed to be the discovery of a companion, it was desirable to obtain a confirmation. When acquiring the star in the 1-m CHARA telescopes, it was noticed that there was another star in the finder telescope (FOV = ∼30 arcmin) which was determined to be HD 181470, an A0III spectroscopic binary of approximately the same brightness. The pointing of the telescope was checked every time the system was observed by initializing the telescopes on a known bright star. Moreover, the known spectroscopic binary exhibits a period of only 10 days at a estimated HIPPARCOS distance of ∼250 parsecs making the

possible separation far under the limits available to the CHARA Array. With the confirmation that we were observing the correct system, it was decided that there was in fact a new companion to HD 181655, and the system was selected for high priority observations.

In the nearly three years of observing this system, more than 50 observations have been made when time was available. Unfortunately, very few instances permitted multiple observations of the system to be made on one night or on more than one baseline. During the allotted observational windows, many times this system was only available for short periods of time, the target was unable to be observed more than once due to weather, or more recently, the secondary was just too wide for the available baselines to be observed. As of 2008 August, enough observations were made in a short time period for six secondary triangulations to be determined. This includes the possible perpendicular detection of the first observation and the orientation of the rest of the points raises an interesting orbital quandary.

Over the past year, the CHARA data have been checked and re-reduced with both reduction programs which have always given the identical position angles and separations and was done at the same time as the other systems in this survey to ensure that the reduction was done consistently. When this was completed, the calculations for the other systems placed their secondaries correctly on their respective orbits and allows the assumption that the values for this object's secondary are in the correct quadrant. Appendix C.1 contains all six plots for the triangulation of the secondary and Table 7.1 shows the calculated locations for each observaton epoch. One thing to notice is that with the exception of the first observation,

all locations of the secondary have been calculated to be along the north-south axis. The times between the observations vary from between 97 to 305 days rather erratically with the times between the points in the same general quadrant on the order of 90 to 150 days and the opposite quadrant being larger than 250 days.

It is unlikely that this is a quadrant flip due to selection of the wrong fringe packet as primary. For all observations, the secondary fringe was always smaller than the primary and unlike the case of HD 170153 where the primary star was large enough to be resolved by the baselines in use, if the primary star is actually a G8V at the HIPPARCOS distance, the approximate angular size for the primary would be $\sim$0.32 mas and practically unresolved at even the largest of the CHARA baselines. Even without an orbit there are a few things we can determine about the stars comprising this system from the data we have. Using the HIPPARCOS updated parallax, the Two Micron All Sky Survey (2MASS) $K$ magnitudes (Skrutskie et al. 2006), and the ratio of the amplitudes of the individual fringe packets, we can determine the individual visual and absolute $K$ magnitudes ($m_{K_P}$=5.76$\pm$0.10, $M_{K_P}$=3.73$\pm$0.11, $m_{K_S}$=6.29$\pm$0.10, $M_{K_S}$=4.26$\pm$0.11) in addition to the $K$ magnitude difference for the system ($\Delta m_K$=0.532$\pm$0.053).

## 7.2 HD 184467

MCA 56A, HIP 95995: The 494-day system now known to comprise HD 184467, which is a nearby, high proper motion star, was an International Astronomical Union (IAU) velocity standard star until McClure (1983) found radial velocity variations with the Dominion Astro-

physical Observatory (DAO) 1.2 m telescope and determined the star to be a spectroscopic binary that was double-lined for less than 20% of its orbit. Two separate efforts (Arenou et al. 2000; Pourbaix 2000) combined the spectroscopy with speckle observations from the Fourth Catalogue of Interferometric Measurements of Binary Stars (Hartkopf et al. 2001b) and determined the complete set of orbital elements. The data collected at the CHARA Array provide six new points to be incorporated with the 22 existing speckle observations in a revised orbital solution.

To determine the geometric elements of the orbit, we have used the dynamical elements from the Ninth Catalog of Spectroscopic Binary Orbits (Pourbaix et al. 2004) as initial values in our solution. In addition to our new SFP astrometry, we have included speckle observations cataloged by the Fourth Catalog with weights assigned by the catalog. Typical weighting of the data involves a number of factors based on the closeness to the Rayleigh limit for the aperture, observer skill, number of observations, and technique used to obtain the measurements (Hartkopf et al. 2001a). The weighting of the CHARA SFP data is based on factors such as angle between projected baseline measurements, number of observations comprising a single measurement, time delay between first and last measurement, and closeness of the secondary fringe to the limit at which it is detectable. With the inclusion of our points, the parameters of the orbit agree within a few percent to the previous determinations of Arenou and Pourbaix including the calculation of the masses of $M_P = 0.824 \pm 0.095 M_\odot$ and $M_S = 0.768 \pm 0.094 M_\odot$ from Kepler's Law and $M_P = 0.83 \pm 0.12 M_\odot$ and $M_S = 0.77 \pm 0.11 M_\odot$ from $M \sin^3 i$. For comparison, results of our new orbital solution are

shown with the previous determinations of Arenou and Pourbaix in Table 7.2.

Additionally, we calculate the orbital parallax from the relation

$$\pi_{\rm orb} = \frac{a'' \sin i}{13751\sqrt{1-e^2}(K_P + K_S)P} \tag{7.1}$$

from (Heintz 1978) using the values from Table 7.2 which gives $\pi_{\rm orb}$=59.16±2.04 mas. All three calculated orbital parallaxes agree with HIPPARCOS value of $\pi_{\rm Hip}$=58.94±0.64 mas.

Table. 7.2: Comparison of Orbital Elements For HD 184467

| | **Pourbaix(2000)** | | **Arenou et al. (2000)** | | **CHARA(2008)** | |
|---|---|---|---|---|---|---|
| **Elements** | **Values** | **Errors** | **Values** | **Errors** | **Values** | **Errors** |
| $P$ (days) | 494.091 | 0.26 | 494.75 | 0.48 | 494.16 | 0.58 |
| $T$ (MJD) | 46164.9 | 1.66 | 48641.21 | 3.1 | 46671.43 | 8.52 |
| $a$ (mas) | 86 | 1.4 | 84 | 3 | 84.2 | 0.84 |
| $e$ | 0.360 | 0.0078 | 0.34 | 0.013 | 0.371 | 0.006 |
| $\omega$ (deg ) | 356 | 2.1 | 177.8 | 2.1 | 16.57 | 4.1 |
| $i$ (deg) | 144 | 2.4 | 144.6 | 1.7 | 144.0 | 1.29 |
| $\Omega$ (deg) | 243 | 1.5 | 74.6 | 6.8 | 256.9 | 2.66 |
| $\pi$ (mas) | 59 | 4.1 | 57.99 | 0.57 | 59.16 | 2.04 |
| $M_{\rm P}$ ($M_\odot$) | 0.8 | 0.15 | 0.83 | 0.09 | 0.82 | 0.09 |
| $M_{\rm S}$ ($M_\odot$) | 0.8 | 0.14 | 0.79 | 0.09 | 0.77 | 0.09 |

*Note.* Comparison of two previous visual and spectroscopic orbital solutions for HD184467 with the new calculation from CHARA data. Columns P(2000) and A(2000) contain the elements taken from Pourbaix (2000) and Arenou et al. (2000).

It is apparent from Figure 7.2, that the results from the CHARA Array agree well with the speckle data. The points for the first orbital solution were completed before the SFP

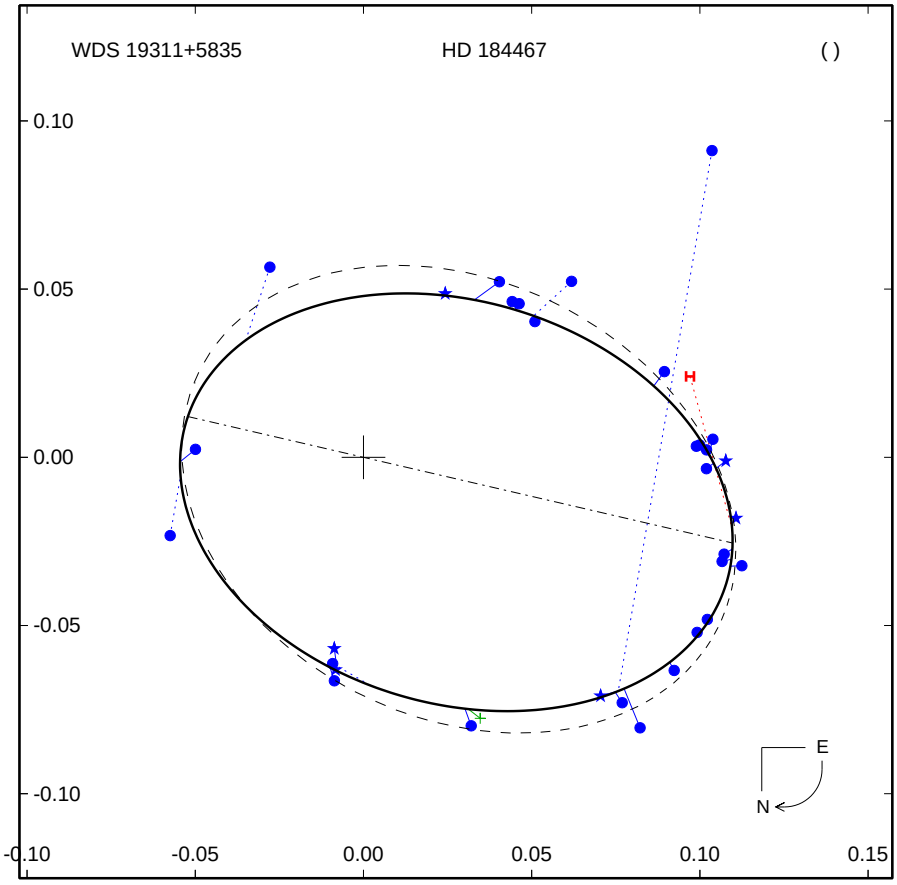


Figure. 7.2: Orbit Plot for HD 184467, 1980-2008. Included in this solution are all speckle interferometry measurements from the Fourth Catalog of Interferometric Measurements of Binary Stars (Hartkopf et al. 2001b) in addition to the CHARA SFP Survey data. The filled circles represent the speckle measurements from the Fourth Catalog, the HIPPARCOS measurement is denoted by the H, and the CHARA measurements are represented by the stars. The orbit calculated with the inclusion of the CHARA points is the solid black line which is similar to the orbit of Pourbaix shown by the dashed oval.

solution program from T. A. ten Brummelaar was complete and as such were done with little precision. Nevertheless, the solution fit well with the previous orbital solution of Pourbaix (2000), and when the same positons were re-calculated with the new software, the same orbital elements were obtained with smaller errors. The calculated final orbit including both speckle points and the re-reduced CHARA SFP secondaries is shown without the speckle information in Figure 7.3.

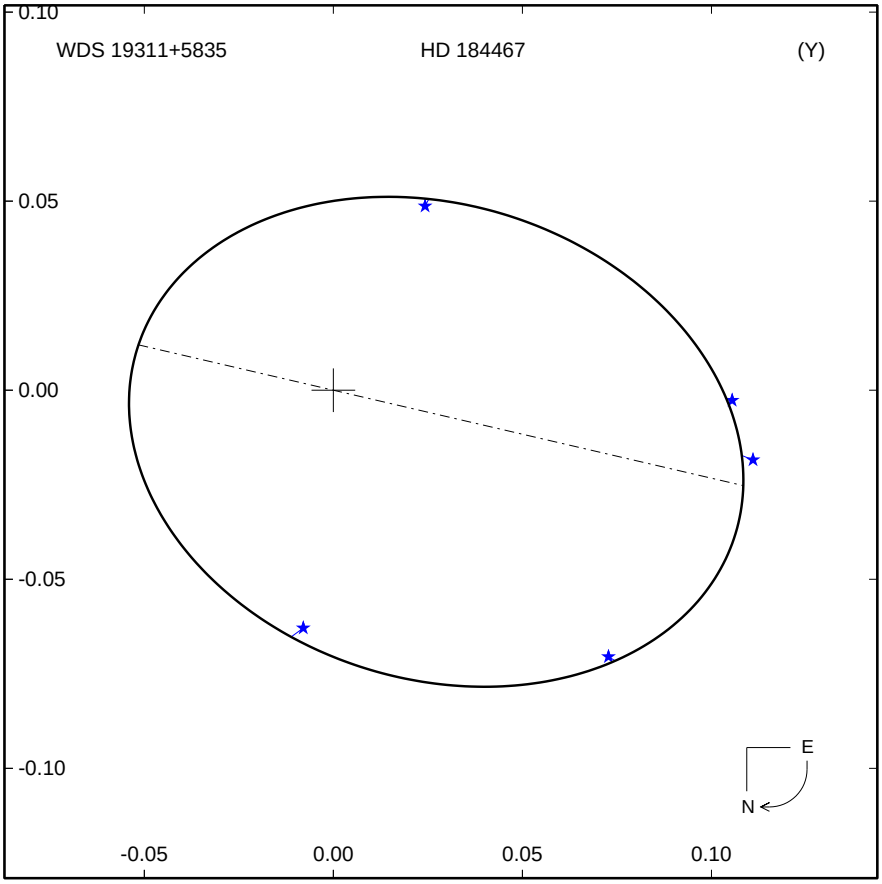


Figure. 7.3: Orbit Plot for HD 184467, 2005-2008. To show how well the orbit in Figure 7.2 fits with the CHARA SFP data, the SFP orbit points are plotted alone and fit quite well. On the lower left, what once was two points very close in epoch were rereduced and combined to give a single location with far smaller errors while the re-reduction of all other points with the software from T. A. ten Brummelaar remained the same.

With three similar orbital solutions all approximately determining the same masses, we can be reasonably sure of the calculated values. From the relative amplitudes of the fringe packets, a $\Delta m_K$ is easily obtainable but can be contaminated by data sets with taken in bad seeing. In seeing conditions that are less than ideal, the fringe amplitude can fluctuate many times during a single data set, and with separated fringe packets, the variations can affect one fringe, both fringes, or neither. In order to minimize the effect this has on the

magnitude difference calculation, the calculated ratio from each of the 27 files was averaged after removing data from nights with particularly bad seeing. The ratio of the amplitudes provides a brightness ratio which can be converted to magnitudes by

$$\Delta m_K = 2.5 \log \left( \frac{b_2}{b_1} \right) \tag{7.2}$$

and with a brightness ratio of $b_2/b_1$=0.80±0.06, we obtain $\Delta m_K$=0.24±0.05. From these values, individual apparent and absolute magnitudes can be determined from the combined apparent magnitude ($m_K$=4.46±0.02) from 2MASS (Skrutskie et al. 2006) and the new distance from HIPPARCOS via

$$m_S = m + 2.5 \log \left( 1 + \left( 10^{0.4 \Delta m} \right) \right) \tag{7.3}$$

which gives the individual $K$ magnitudes of $m_{K_P}$=5.32±0.09 and $m_{K_S}$=5.55±0.09. Using the standard absolute magnitude formula

$$M_{V,K} = m_{V,K} + 5 \log(\pi) + 5 \tag{7.4}$$

individual absolute $K$ magnitudes of $M_{K_P}$=4.17±0.09 and $M_{K_S}$=4.40±0.09 are calculated. The same can be done for the $V$ magnitudes provided we can locate valid $\Delta m_V$. From Arenou et al. (2000), a $\Delta m_V$=0.34±0.04 was determined from HIPPARCOS measurements. Also provided are visual magnitude differences from various speckle measurements from 2000 to 2006 which can be averaged into another estimate of $\Delta m_V$=0.26±0.05. The above

calculations can be performed using a combined apparent $V$ of $m_V$=6.599±0.015 (Mermilliod 1994), giving values of $m_{V_P}$=7.20±0.03 and $m_{V_S}$=7.54±0.03 for the HIPPARCOS $\Delta m_V$ and $m_{V_P}$=7.23±0.03 and $m_{V_S}$=7.49±0.03 from the speckle $\Delta m_V$.

In order to calculate the bolometric magnitudes, a proper correction is needed and so we adopt $BC$= -0.42 (Cox 2000) as the spectral typing (K2V) is quite consistent among nearly all previous measurements. Calculating the luminosities from these magnitudes is trivial by using a rearrangement of

$$M_{\rm bol} = -2.5 \log \left( \frac{L}{L_\odot} \right) + 4.74 \tag{7.5}$$

giving us two values for each component ($L_P$=0.44±0.02 $L_\odot$ and $L_S$=0.32±0.01 $L_\odot$ from HIPPARCOS, and $L_P$=0.43±0.02 $L_\odot$ and $L_S$=0.34±0.01 $L_\odot$ from speckle). These four luminosities, masses and the Mass-Luminosity relation from (Aller et al. 1982)

$$\log \left( \frac{L}{L_\odot} \right) = 3.8 \log \left( \frac{M}{M_\odot} \right) + 0.08, \tag{7.6}$$

valid for $M > 0.2 M_\odot$, are plotted in Figure 7.4 where the $X$ and box values are from the speckle $\Delta$m, and the circle and diamond represent the HIPPARCOS $\Delta$m. Even though the mass errors are large, it can be said that since three separate orbital calculations produced similar masses, it is likely that the luminosities calculated here represent reality. If we accept this, it would mean the components are under-luminous and possibly subdwarfs. Supporting this is the measurement of system metallicity ($[Fe/H]$=-0.22); Nordström et al. (2004), but

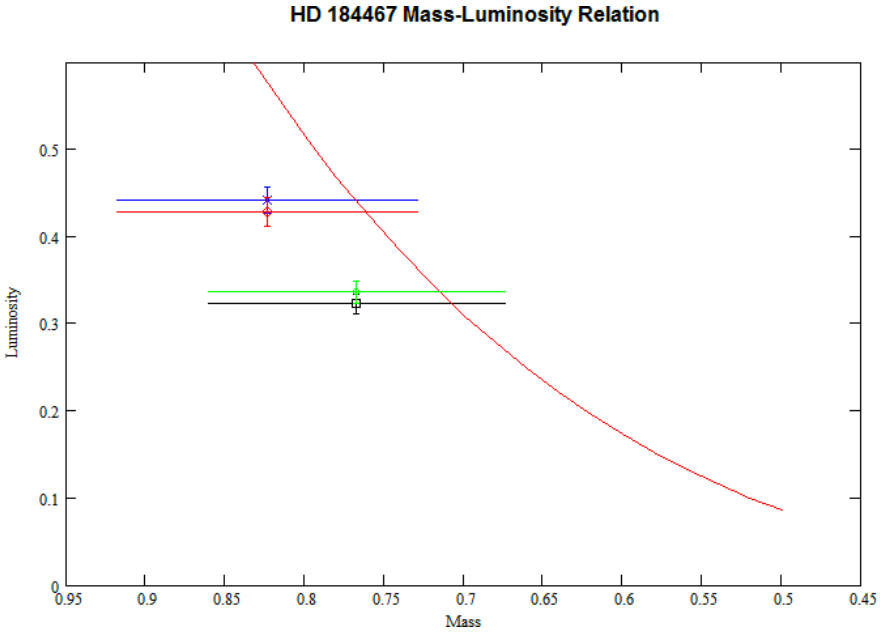


Figure. 7.4: Mass-Luminosity Plot for HD 184467. Shown here are the two sets of luminosities (in units of $L_{\odot}$) calculated for the individual masses (in units of $M_{\odot}$) based on the differing $\Delta m_V$'s between speckle interferometry and HIPPARCOS measurements. The $X$ and box values show the calculated luminosities from speckle while the circle and diamond represent the HIPPARCOS $\Delta m_V$. Low metallicity measurements for the system suggest possible early K subdwarf components.

with only one supporting bit of evidence this classification is not clear. Future observations of this system are planned to determine the stellar radii in order to support this hypothesis (Boyajian et al. 2008).

## 7.3 HD 198084

HR 7955 has a long history of radial velocity coverage culminating with R.F Griffin's detection of a 523-day radial velocity variation (Griffin 1999c). Griffin noted that earlier investigators Abt & Levy (1976); Beavers & Eitter (1986) had not detected the companion's spectrum even at favorable phases. Griffin's effort was more successful, catching a conspic-

uous double lined phase in 1996. Over the course of five years, Griffin saw double lines at 24 out of 38 epochs. Using all previous data available to him, Griffin determined an orbit with residuals of $\pm 0.4$ km/s and inferred from the commonly accepted spectral typing that an inclination of approximately $23^\circ \pm 1^\circ$ would be necessary for the masses to fall within the appropriate range for stars of this type. Furthermore, he pointed out that the star is a good target for speckle interferometry due to its brightness and a separation likely larger than 50 mas. Nevertheless, it appears that no speckle measurements of HD 198084 have been taken.

Separated fringe packets for this star were detected on both baselines early-on in this program, and because it was previously unresolved, HD 198084 was observed as frequently as possible. Hence, a total of 60 observations were made over seven separate observing runs to produce 12 individual astrometric points for this orbit. The system was observed within 15 days of periastron on two separate occasions, and, due to the eccentric nature of this orbit and the rapid movement of the secondary, the observations during those two observing runs produced three points for the orbit. An example of the triangulation of the secondary for this system can be seen in Figure 7.5 with the the complete compilation of plots shown in Appendix C.3.

Our new astrometric measurements were combined with the spectroscopic elements of Griffin (1999c) in a grid search to determine the previously unknown visual elements of the system. We have sampled approximately two orbital periods to date, and, while the phase coverage is limited, Figure 7.6 shows that it provides a reasonably good distribution of observed phases, including observations before and after periastron. Calculated orbital

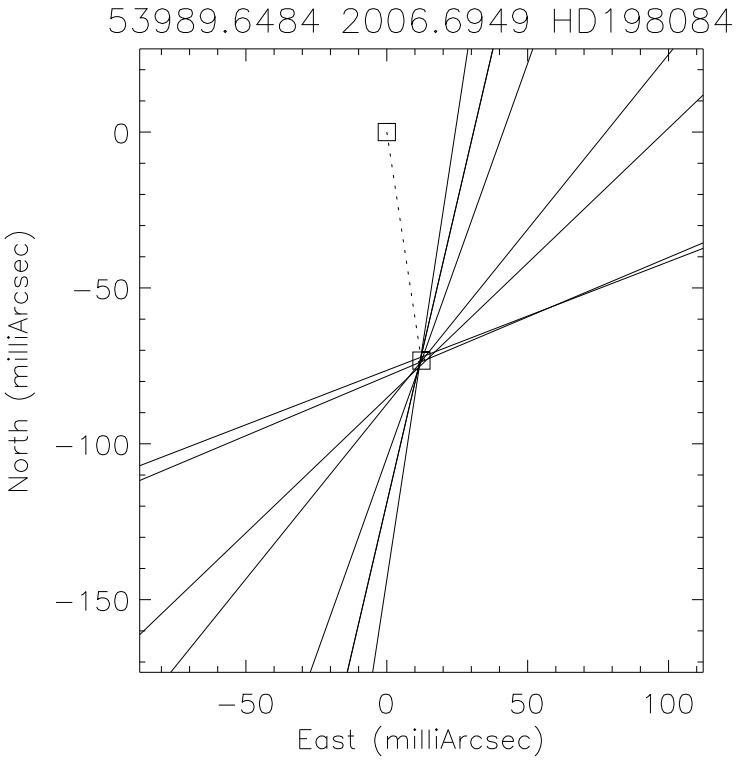


Figure. 7.5: Triangulation Plot for HD 198084, 2006.6949. Sample triangulation from 4 data files from 2006 September 11 to September 12.

elements with errors are listed in Table 7.3. The masses obtained from the orbit determined here via Kepler's Laws ($M_P = 1.54 \pm 0.16 M_\odot$ and $M_S = 1.50 \pm 0.16 M_\odot$) and the $M \sin^3 i$ calculation ($M_P = 0.677 \pm 0.19 M_\odot$ and $M_S = 0.636 \pm 0.19 M_\odot$) are significantly different and atypical for stars of late-F classification. The masses determined from Kepler's Laws are not unreasonable but the large mass discrepancy from the $M \sin^3 i$ can possibly be explained by the significant deviation from the predicted inclination. Masses of 1.1 to 1.3 $M_\odot$ would be more reasonable and with more observations to decrease the error in inclination, a more accurate answer would be probable.

Table. 7.3: HD 198084 Calculated Orbital Elements

| **Method** | **P** **days** | $T_0$ **MJD** | **a** **mas** | $e$ | $\omega$ **deg** | $i$ **deg** | $\Omega$ **deg** | $\pi$ **(mas)** | $M_P$ $M_\odot$ | $M_S$ $M_\odot$ |
|---|---|---|---|---|---|---|---|---|---|---|
| Orbgrid(WH) | 523.36 | 50205.84 | 66.8 | 0.553 | 81.7 | 29.5 | 311.3 | 48.6 | 1.54 | 1.50 |
| | ±1.25 | ±9.63 | ±1.1 | ±0.007 | ±4.0 | ±2.1 | ±4.4 | ±3.3 | ±0.16 | ±0.16 |
| M-C(JDM) | 523.87 | 50205.20 | 64.5 | 0.547 | 68.4 | 22.7 | 325.3 | 35.5 | 1.37 | 1.28 |
| | ±1.53 | ±7.45 | ±1.2 | ±0.007 | ±3.0 | ±0.1 | ±5.6 | ±1.2 | ±0.10 | ±0.09 |

*Note* Prelimiary orbital elements for HD198084. While the orbit from Orbgrid (Hartkopf et al. 1989) in the first row fits with the previous spectroscopic elements, the inclination is higher than the value of 23°±1° predicted by Griffin (1999c). The second calculation comes from a Monte-Carlo solution program provided by J.D. Monnier while constraining the $a \sin i$ to match the updated HIPPARCOS parallax and $\omega$ set to the value listed for the Griffin orbit (suggested by G. Torres in reference to an incomplete and unpublished spectroscopic orbit that matches the Griffin orbit.)

This significant error in inclination also affects the calculated orbital parallax determined from this orbit. Previous determinations from HIPPARCOS give the parallax as 36.87±0.46 mas and more recently updated in 2008 as 36.64±0.46 mas. Guillermo Torres was gracious enough to recalculate the HIPPARCOS parallax with the CHARA visible orbit and determined the revised distance of 36.26±0.36 mas. Griffin postulated that the parallax was not entirely reliable as it does not take into account the orbit, but the orbital parallax calculated here seems to change far more than expected. From the inclination of 29.5±2.1 calculated from the preliminary orbit, the orbital parallax is determined to be 48.5±3.3 mas.

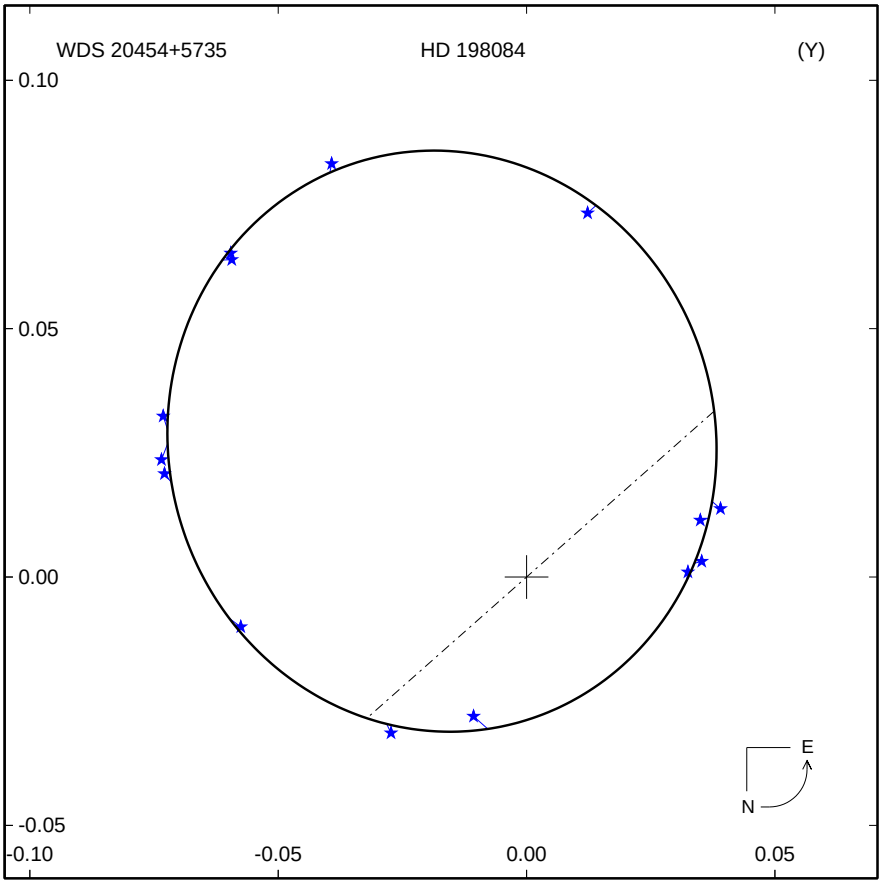


Figure. 7.6: Orbit Plot for HD 198084, 2005-2008 (ORBGRID). The point for 2008 August was added to the plot after the orbit was calculated to see how precise the calculation of the location of the secondary would fit onto the determined orbit. Overlapping points in the upper left near apastron are almost exactly two orbital periods apart (2005.7676 and 2008.6215) and provide confirmation that the points taken do in fact represent actual locations on the orbit.

The errors for this are nearly 4 times as large as the HIPPARCOS errors and dominated by the large uncertainty in inclination.

It is likely that there is more than one solution for this orbit with enough variation to allow a smaller inclination. Using a completely different fitting program provided by J.D Monnier to test this, the $a \sin i$ values were constrained to match the new HIPPARCOS parallax, $\omega$ was set to the value from the previous spectroscopic orbits (as suggested by G. Torres in

reference to an incomplete and unpublished spectroscopic orbit whose $\omega$ matches the Griffin orbit), and all other elements remaining the same. The resulting orbit shown in Figure 7.7 shows a quite similar orbit encompassing most of the selected orbit points except those during mid-2007 which were quite noisy and taken in bad seeing. The errors for these points (3-4 mas) make significantly larger error circles. The second orbital fit (shown in the last two rows of Table 7.3) allows a much better fit for most elements including the masses now calculated from $M \sin^3 i$ to be $M_P = 1.366 \pm 0.101 M_\odot$ and $M_S = 1.279 \pm 0.089 M_\odot$ and $M_P = 1.412 \pm 0.092 M_\odot$ and $M_S = 1.322 \pm 0.087 M_\odot$ from Kepler's Laws. Also improved is the orbital parallax, which in the previous calculation was wildly different than new orbitally weighted HIPPARCOS distance. The new orbital parallax is quite close to the accepted distance to the system at $\pi_{\rm SFP} = 35.45 \pm 1.24$ mas.

To progress further, we need $\Delta m_V$ from another instrument or we can make an assumption. From the relative amplitudes of the fringe packets (assuming the seeing was good and the components are unresolved, which is most likely the case due to the distance and assumed spectral types), a $\Delta m_K$ is easily obtainable. The ratio of the amplitudes provides a brightness ratio which can be converted to magnitudes by Equation 7.2 for which a brightness ratio of $b_2/b_1 = 0.72 \pm 0.05$ leads to $\Delta m_K = 0.36 \pm 0.04$. From these values, individual apparent and absolute magnitudes can be determined from the combined apparent magnitude ($m_K = 3.27 \pm 0.24$) from 2MASS (Skrutskie et al. 2006) and the new distance from HIPPARCOS. Using Equation 7.4 and the individual $K$ magnitudes of $m_{K_P} = 3.86 \pm 0.25$ and $m_{K_S} = 4.21 \pm 0.25$, individual absolute $K$ magnitudes of

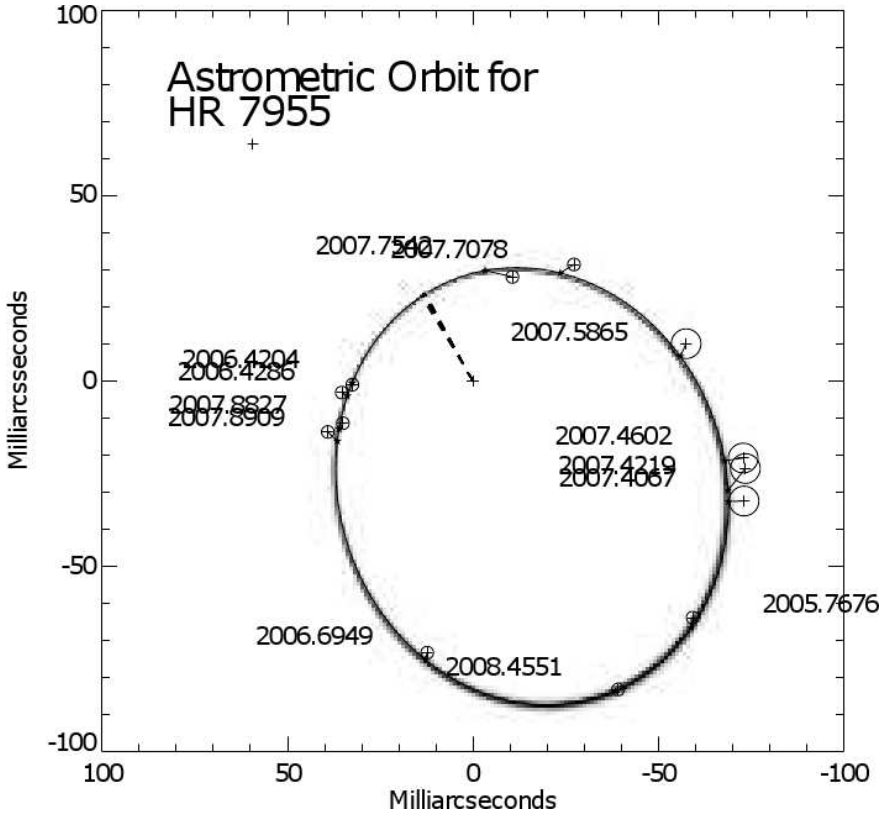


Figure. 7.7: Orbit Plot for HD 198084, 2005-2008, from J.D Monnier. Orbital solution done by Monte Carlo orbital element search program provided by from J.D. Monnier. The orbital elements obtained from this solution are similar to the previous determination and required a fixed $a \sin i$ to match the HIPPARCOS parallax and a set $\omega$ from the spectroscopic orbit.

$M_{K_P} = 1.65 \pm 0.25$ and $M_{K_S} = 2.01 \pm 0.26$ are calculated. In order to get luminosities for these stars, we would need to follow the same procedure for $V$ to get the individual, absolute, and bolometric magnitudes from the system magnitude ($m_V = 4.52 \pm 0.01$, Mermilliod (1994)), but the CHARA Array is incapable of determining these $V$-band quantities and no other relevant measurements exist.

As previous authors have assumed the components are made up of similar spectral types and the calculated masses differ by approximately the mass errors, we could assume $\Delta m_K \propto \Delta m_V$. Using the $m_V$ and the method used for the individual $m_K$ relation,

$m_{V_P} = 5.11 \pm 0.07$ and $m_{V_S} = 5.46 \pm 0.07$. This agrees with the estimate of Griffin (1999c) of between 0.2 and 0.4 magnitudes from the ratio of the line depths. It should be noted that from the system magnitudes, we calculate $V - K$=1.249 which along with the calculated masses implies a spectral type closer to F6V than F8V. In order to calculate the bolometric magnitudes, a proper correction is needed and so we adopt $BC$= -0.15 (Cox 2000) for stars slightly larger than the predicted F8V spectral type. With this we obtain $M_{V_P} = 2.91 \pm 0.08$ and $M_{V_S} = 3.25 \pm 0.08$ for the absolute magnitudes, and $M_{\mathrm{bol_P}} = 2.79 \pm 0.08$ and $M_{\mathrm{bol_S}} = 3.06 \pm 0.08$.

Calculating luminosities from the bolometric magnitudes is permitted by Equation 7.5. Much like the $V-K$ and masses, the luminosities ($L_P = 6.22 \pm 0.41\ L_\odot$ and $L_S = 4.51 \pm 0.30\ L_\odot$) are far too large for stars of this spectral type or even main-sequence stars of this mass. Based on this information where all calculated values suggest late F stars with brighter than normal magnitudes and luminosity, we must decide wether or not the assumption that was made here, $\Delta m_K = \Delta m_V$ is correct. If the assumption is valid, then it is quite likely that both of these stars are probably evolved but have yet to become giants as suggested by Griffin. On the other hand, if we believe that the assumption may be the cause of this discrepancy, we can "cheat" and calculate the $\Delta m_V$ in a different manner.

This other assumption also can be problematic as it is based on estimating the $\Delta m_V$ through a Zero-Age Main-Sequence (ZAMS) relation between mass and bolometric magnitude. This relation from Cox (2000) comes in two slightly different forms that give approximately the same value where

$$\log\left(\frac{M}{M_\odot}\right) = 0.48 - 0.105 M_{\rm bol} \tag{7.7}$$

is valid for $-8 \leq M_{\rm bol} \leq 10.5$ (Aller et al. 1982) and the very similar

$$\log\left(\frac{M}{M_\odot}\right) = 0.46 - 0.10 M_{\rm bol} \tag{7.8}$$

valid for $M_{\rm bol} < 7.5$ (Harris et al. 1968) for which the values and errors associated with the transition from apparent magnitudes to luminosities only vary in the third digit after the decimal. For the calculation of the $\Delta m_V$ in this case, we obtain $\Delta m_V = 0.29 \pm 0.12$ which contains a significant error term due to the 6-7% errors of the masses. Even with this large error term, the calculation of the luminosities through the same process as above yields $L_P = 6.05 \pm 0.42\ L_\odot$ and $L_S = 4.68 \pm 0.32\ L_\odot$ which is consistent and brings the values only slightly closer together. Through this assumption, we can also calculate what the luminosities should be if these stars were on the main sequence with the masses they are calculated to have.

Instead of only using the above relations for getting an estimate of $\Delta m_V$, we could instead take the bolometric magnitudes we calculated and insert them into the luminosity formula. Plotted in Figure 7.8, the two sets of determined masses have been used with the two Mass-$M_{\rm bol}$ relations to calculate where the stars would reside if they are unevolved. Along with these values, the luminosities calculated from just the magnitudes and distances appear far above the ZAMS predicted positions.

From all these calculations, the conclusion can be reached that these are late F subgiants.

Work is being planned to test this conculsion as one possibility remains that could change the nature of the calculations. One quantity that the CHARA Array can derive with appropriate planning is the angular diameters for the components. As the result we obtained was not assumed at the beginning, one unmentioned assumption passes through all these calculations which is that both components were unresolved. If these truly are the subgiants that they appear to be, it is possible that the diameters are such that the components are each partially resolved, which would bias any $\Delta$m calculation made here. This should be resolved in the coming months when observing time becomes available.

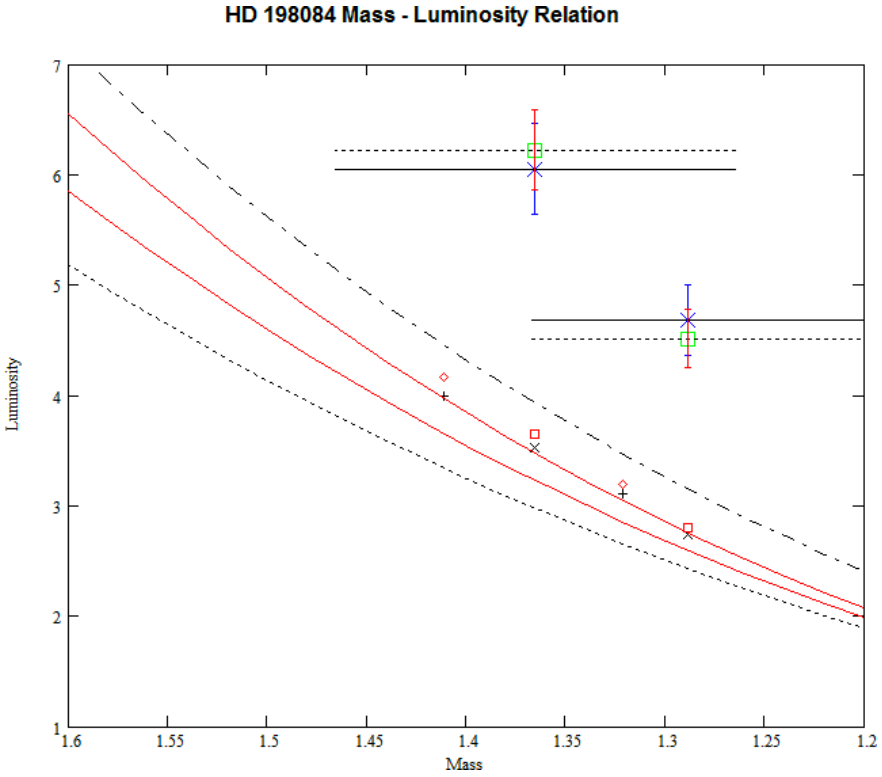


Figure. 7.8: Mass-Luminosity Plot for HD 198084. Calculated luminosities for the primary and secondary for the assumption 1 ($\Delta m_V$=$\Delta m_K$) are represented by the box and assumption 2 ($\Delta m_V$= 0.286) represented by the X. These are far above the lines plotted that show the varying ZAMS M-L relation of $L \propto M^{\alpha}$. The $\alpha$'s shown here are $\alpha$=3.5, 3.75, 3.8 and 4.0. Along the ZAMS are the calculated values where the stars should reside if they were zero-age. Using the two Mass-$M_{bol}$ relations, and both of the mass calculations, we obtain the four primary and four secondary points along the M-L relation with the $M \sin^3 i$ values plotted as the X and box, and the Kepler's Law mass plotted as plus and diamond.

*The most incomprehensible thing about the world is that it is comprehensible.*

—— *Albert Einstein*

# – 8 —

# Discussion

## 8.1 Updated Multiplicity Statistics for Solar-Type Stars Within 22 Parsecs

Now that it has been determined that there are changes to the multiplicity of the original sample, we can take a look at the sample as a whole and see how its composition has changed. The original D&M sample, consisted of 164 systems and fractional numbers of 57:38:4:1:0% (single:double:triple:quadruple:quintuple%). If you add in all the new companions from the research done for this survey neglecting any removal of systems that no longer fit the selection criteria, the percentages change to 51:40:8:0.5:0.5% for those same 164 systems. To be truly consistent, we must apply the same selection criteria to the list again to remove any systems that no longer fall in the distance-limited sample as a result of HIPPARCOS, and recheck the objects removed previously to ensure they were not removed erroneously. For the 291 systems in the wide sample, it was determined that 6 systems, including the common proper-motion pair HD 186408/186427, should be added to the main sample since HIPPARCOS found that they are nearer than previously thought. Of the 164 stars in the multiplicity sample, only 100 retained membership based upon a distance closer than the limit, 22.5 pc. Table 6.1 shows which stars were removed in column 5 (represented with an $x$), with their old and new parallax in columns 7 and 8, and with the systems erroneously

removed at the end of the table. With these considerations, we again look at the multiplicity of the remaining 106 systems, and with that significant decrease in sample size we are left with a multiplicity percentages of 48:42.5:7.5:1:1%. A short summary of these numbers can be seen in Table 8.1 along with the number of companions per system. Ironically, this rather substantial change to the number of companions per system puts the overall G-dwarf multiplicity fraction closer to what Abt & Levy determined, even though their sample was heavily biased by false detections.

Table. 8.1: Overall Multiplicity

| **Multiplicity** | **A&L** | | **D&M** | | **Current** | | **Corrected** | |
|---|---|---|---|---|---|---|---|---|
| | # | % | # | % | # | % | # | % |
| Single | 52 | 42 | 93 | 56.7 | 83 | 50.6 | 51 | 48.1 |
| Double | 57 | 46 | 62 | 37.8 | 66 | 40.9 | 45 | 42.5 |
| Triple | 11 | 9 | 7 | 4.3 | 13 | 7.3 | 8 | 7.5 |
| Quadruple | 3 | 2 | 2 | 1.2 | 1 | 0.6 | 1 | 0.95 |
| Quintuple | 0 | 0 | 0 | 0.0 | 1 | 0.6 | 1 | 0.95 |
| Systems | 123 | 100 | 164 | 100 | 164 | 100 | 106 | 100 |
| Companions | 85 | | 82 | | 99 | | 68 | |
| Comp/system | 0.69 | | 0.50 | | 0.60 | | 0.64 | |

*Note.* Included here are the number of systems of each multiplicity type and the percentages associated with them for the original D& M sample, the sample with updated companions, and the final list corrected to remove those stars that no longer fall within the parallax limited range. The last three rows detail the total number of systems contained in each multiplicity level, the number of companions, and the number of companions per system respectively.

It is seen that solar-type stars are more likely to have at least one companion than indicated by previous surveys. This invites a re-examination of several other discussion topics of D&M. How does this affect the distribution of $q$ (mass fraction: $q = M_2/M_1$), $\log P$, and the overall scatter of $\log P$ vs. $e$? In fact, there is very little change. Looking at Figures 8.1, 8.2, and 8.3, we can see very little difference in the overall distributions. The maxima for $q$ and $\log P$ remain very much the same and the scatter of $\log\ P$ vs. $e$ also is not altered to a large degree, leaving the conclusions made by D&M valid for this sample. It is interesting to see a large number of the eccentric young binaries (a major binary formation tracer) have been removed due to their parallax change. This implies that the spatial density of these systems is less than previously believed. A rather large number (10) of the doubles that were eliminated from the sample in this effort have been discovered to be almost twice as far away as they were originally calculated along with at least five mis-identified giants whose classifications have still not been corrected. One such star, HD 5857, has been classified on multiple occasions as recently as 2007 as a G5 without a luminosity class, has a glaring $V - K$=+4.0 and a tiny 9 mas parallax which seem to have gone unnoticed by most. It also seems strange that a few of these same stars had parallaxes that were almost 10 times larger than currently measured (ex. HD 147266 with $\pi_{\rm old}$=99 mas and $\pi_{\rm Hip}$=9.45 mas) where it leads to the question of whether or not a misplaced decimal point allowed some of these systems to be included accidentally!

The most significant revision resulting from this effort was the change in multiplicity and through that, the number of companions per system. Though many of the additional com-

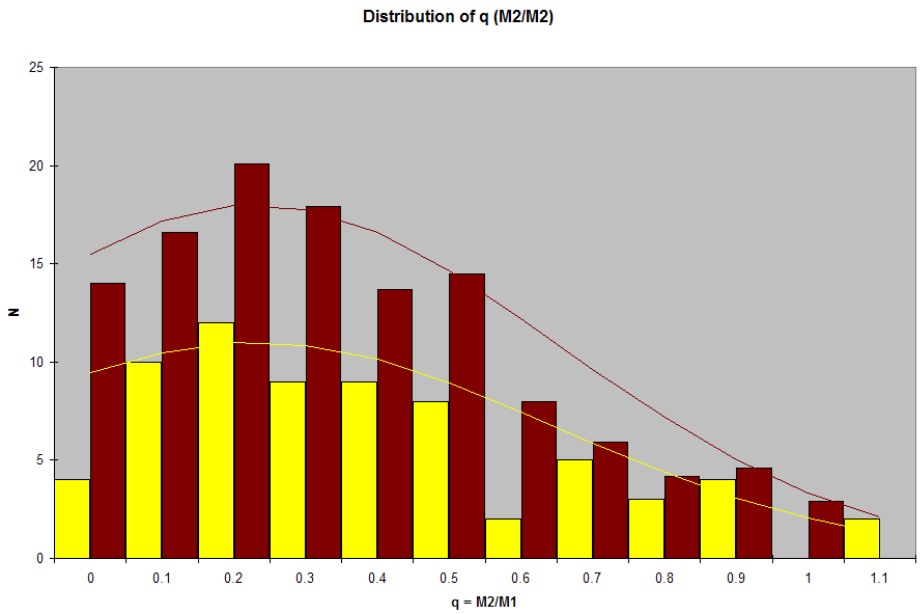


Figure. 8.1: Distribution of Mass Ratio from the D&M and SFP Samples. The larger darker bars on the right of each bin show the distribution of the secondary mass compared with the primary for the sample before being corrected for parallax. The bars to the left show how the distribution in general remains much the same with the removal of 64 and the addition of 6 systems. Although the same in general distribution, a significant number of systems in the 0-0.1 and 0.6-0.7 bins were eliminated with respect to the others. The similarly colored lines mimic the distribution fits for each subset.

panions that have since been discovered were covered through the predicted missing multiples (most of the new companions were low mass M, L and T dwarfs), the sheer number of systems eliminated from this project through the changes in parallax was surprising. Also, nearly a sixth of those stars removed were within 5 mas of the cut-off 45 mas limit for both D&M's and this sample. A more significant change would have been the altering of the maxima in either $q$ or $\log P$, neither of which occurred. Thus, it is reasonable to accept the conclusions of the most likely companion mass being small compared to the primary and the peak of the unimodal distribution of periods remains at approximately 180 years as determined by D&M.

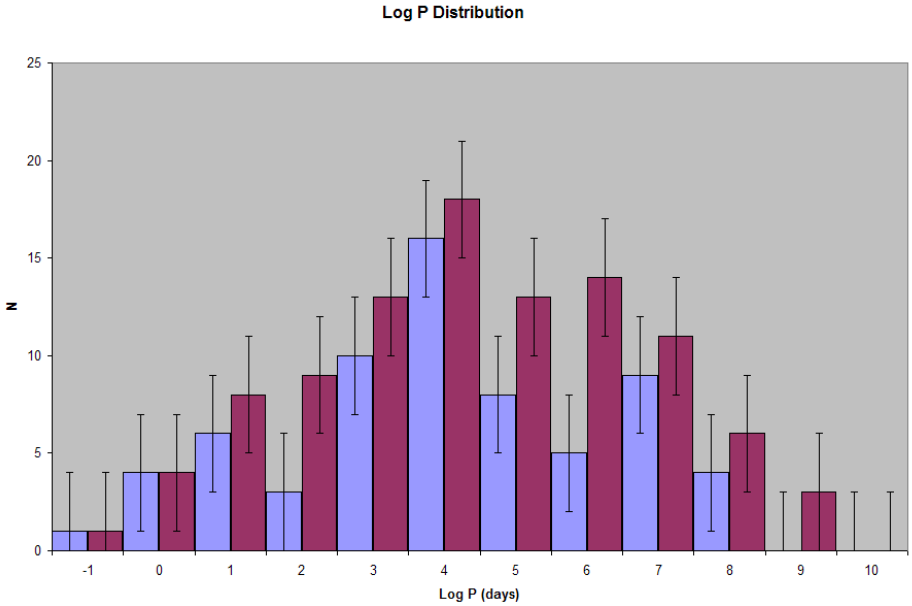


Figure. 8.2: Distribution of $logP$. The distribution of orbits, in the same format as Figure 8.1, show that the samples of the SFP Survey and D&M are quite similar. The lighter bars show dips in bins 2, 5 and 6, due mostly to the removal of systems with misrepresented parallaxes. Many of the systems removed in the 250 to 25,000 year zone were common-proper motion binaries whose parallaxes had been overestimated where the period was based mostly on the separation.

## 8.2 Separated Fringe Packet Orbit Determination

The use of separated fringe packets to resolve very close (15-100 mas) binary systems provides an excellent bridge between speckle interferometry and visibility orbital analysis. There are at least 300 systems in the Ninth Catalog of Spectroscopic Binary Orbits (Pourbaix et al. 2004) that would easily fall within this range, many under the speckle interferometry resolution limit, whose visual orbits could be determined through the use of separated fringe packet analysis. Many more partially completed orbits such as those for HR 266 and 9 Cygnus, where undersampled orbital phases occur where separations fall under 40 mas, could potentially be completed with separated fringe packets. While more time consuming and complex

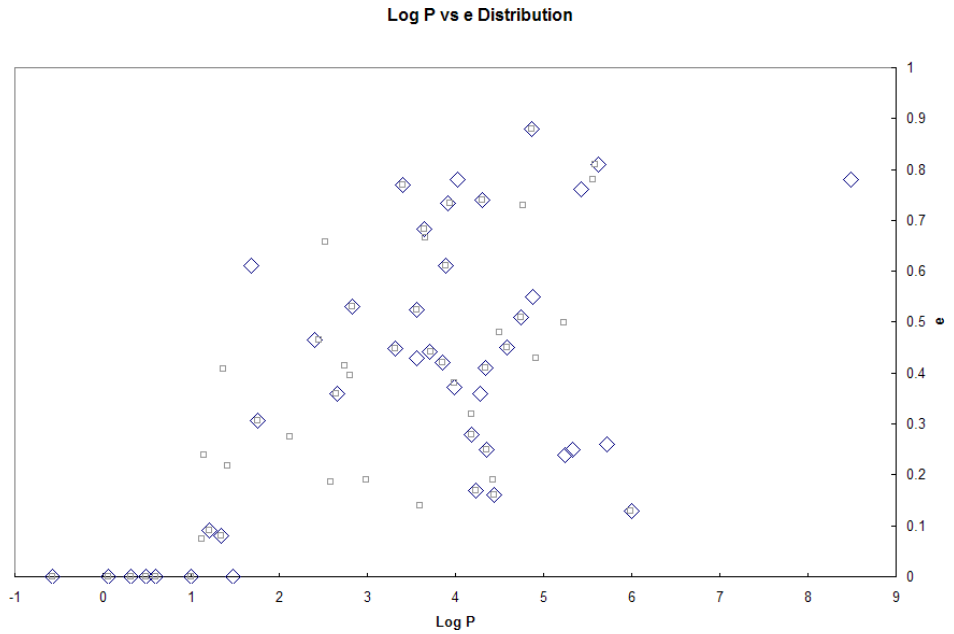


Figure. 8.3: The Period (d) and Eccentricity Distribution for Solar-Type Stars in Binaries. The removal of nearly one third of the systems in the sample did not significantly change the overall distribution of the relation of the eccentricity with respect to the period. The small squares (D&M) and the larger diamonds (SFP survey) still show quite a bit of overlap with the same general scatter. One thing to be noticed is that a significant number of the short period young binaries considered a tracer of binary formation have been removed through parallax changes reducing the concentration of such objects in the local neighborhood.

than speckle interferometry, SFP observations provide smaller errors and probe a separation regime that is beyond the limits of speckle interferometry, and with proper planning it is possible to characterize fully the location of a companion for more than 25 systems in a single night. The upcoming three telescope beam combiner (CLassic Interferometry on Multiple Baselines (CLIMB)) for the CHARA Array will allow simultaneous triangulation of the secondary in only a few minutes. This approach will avoid the need to alter the baseline configuration and the tracking of the secondary in short-period widely-separated binaries and fast-moving companions near periastron for eccentric orbits, with which the current SFP method has some difficulty.

## 8.3 General Conclusions and Future Work

I observed 157 of the 160 stellar systems within a carefully detailed sample available to the CHARA Array in an attempt to locate possible missing companions from the extended D&M sample. I was able to acquire a significant number of observations on 109 of the primary stars with an additional 49 systems which received marginal coverage. Two new companions (HD 173093 and 181655) have been discovered through all the observations obtained through the separated fringe packet survey, though due to the parallax of those systems, they are not included in the overall multiplicity statistics. Additionally, seven systems have been angularly separated for the first time (HD 9021, 11909, 24546, 107700, 131511, 166285, and 198084). Nearly 40% of the systems observed by the Array have never been observed with speckle interferometry, so we have contributed to the observational completeness of these systems through our observations. We can also reasonably say that those systems which did not exhibit separated fringe packets are devoid of companions with $\Delta m \leq 2.0$ in the range of 15-100 mas.

Significant changes have been found for the multiplicity of solar-type stars in the neighborhood through this project. The survey of D&M was shown to be biased from erroneous parallax measurements, and this resulted in the removal of far away systems that comprise nearly 40% of the systems from the multiplicity sample. This also changed the raw percentages from 57:43% to 48:52% (single:multiple%) before incompleteness adjustments, and it shifted the overall number of companions per system toward the values determined by A&L. There are three refinements made by D&M that we should investigate. The most

minor refinement, the inclusion of the stars without orbits but which have a low probability of variations being attributed to instrumental noise ($P(\chi^2) < 0.01$), is mentioned only once and does not appear to affect the final percentages presented. As D&M ignore this group of potential spectroscopic binaries, we shall likewise ignore these in consideration of the SFP sample. Actual changes applied to the multiplicity are derived from the incompleteness study and are broken into two sections. An evaluation of the mass ratio distribution indicated approximately 22 systems (13.4%) with $q > 0.1$ remain undetected. Modifying D&M's multiplicity fraction with these missed systems, the percentages change to 43:57%. Finally, the probability that the remaining single systems of having a very low mass companion (VLMC) between 0.01-0.10$M_{\odot}$ is determined to be as high as 20% (14 systems), and this factor adjusts the overall multiplicity to 35:65%.

Application of these same incompleteness parameters to the SFP sample is somewhat complicated. Do we just blindly apply the same percentages to the smaller sample, or do the detections of companions from more accurate techniques and technology subtract from the estimates of missed systems? The most likely answer is that the new companions can modify the incompleteness estimates as they were previously accounted for. Regardless, we shall apply both postulates to the SFP sample and see how they compare with D&M. Modifying the SFP sample with the exact percentages used by D&M promotes or transforms 14 systems from single to binary via the mass ratio distribution, and 7 systems with possible VLMCs leaving the multiplicity as 28:72% (single:multiple%). If we instead consider the 5 new M-dwarf companions (HD 123, 9826, 43587, 82443, and 86728) and the 4 VLMC systems

(HD 97334, 130948, 190406, and 206860) as included in the incompleteness measurements, the resulting multiplicity of 37:63 then becomes quite similar to D&M's calculated values.

However, the removal of so many systems from an already small sample allows the inclusion or exclusion of a single system to be statistically significant. The addition of systems in the southern sky could radically change the percentages of solar-type stars with companions closer than 22 parsecs. Combining the results from this study with the observations from Nordström et al. (2004) and any southern hemisphere speckle surveys that occur in the coming years would solidify the conclusions drawn here.

In addition to the multiplicity changes presented here, 17 systems exhibited separated fringe packets when observed with the long baselines of the CHARA Array. Eleven of these had confirmed secondary packets but did not receive enough observations to allow computation of the true on-sky positions. The other six, however, provided excellent test cases for multi-baseline commissioning of a large-scale separated fringe packet effort. Using previous spectroscopic and visual orbits for 12 Persei, $\chi$ Draconis, and HD 184467, it was shown that the determination of the secondary location matches the predicted values. Comparing the previous photcentric orbit from HIPPARCOS for HD 9021 by Jancart et al. (2005) where the semi-major axis of the orbit was calculated to be 7.95 mas, and the data from the SFP survey with a angular semi-major axis of 22 mas as predicted by Halbwachs (1981), we can see that the orbit is rather similar. Furthermore, the masses calculated by Jancart et al. actually only make sense when the orbit is larger than 20 mas. The consistent acquisition of separated fringe packets for HD 181655 confirms that we have discovered a companion of

similar magnitude with a long period. With the inclusion of many years of radial velocity measurements showing no variation above 100 m/s, we can conclude that the inclination of the system is likely to be small. Finally, the long-term monitoring of the double-lined spectroscopic binary HD 198084 provides an excellent visual orbit to complement the spectroscopic orbit of Griffin (1999c) which, when combined, delivers reasonably accurate masses ($\leq$7% errors) for a pair of probable subgiants.

Further orbital monitoring of these and other spectroscopic systems is planned along with calibrated visibility measurements to determine the radii of HD 184467 and 198084 to confirm the conclusions that the primaries are evolved. Application of SFP analysis for other single- and double-lined spectroscopic binaries on a larger scale will be attempted in the following year. This hopefully will provide another efficient method for determining orbits, obtaining accurate masses, and completing the chain of resolution from wide visual to sub-milliarcsecond visibility orbits.

# References

Abt, H. A., & Levy, S. G. 1976, ApJS, 30, 273

Abt, H. A., & Willmarth, D. 2006, ApJS, 162, 207

Abt, H. A., & Willmarth, D. W. 1999, ApJ, 521, 682

Aller, L. H. et al. 1982, Landolt-Börnstein: Numerical Data and Functional Relationships in Science and Technology - New Series " Gruppe/Group 6 Astronomy and Astrophysics " Volume 2 Schaifers/Voigt: Astronomy and Astrophysics / Astronomie und Astrophysik " Stars and Star Clusters / Sterne und Sternhaufen (Landolt-Bornstein: Numerical Data and Functional Relationships in Science and Technology)

Anderson, J. A. 1920, ApJ, 51, 263

Arenou, F., Halbwachs, J.-L., Mayor, M., Palasi, J., & Udry, S. 2000, in IAU Symposium, Vol. 200, IAU Symposium on the Formation of Binary Stars, ed. B. Reipurth & H. Zinnecker, 135P–+

Armstrong, J. T. et al. 1998, ApJ, 496, 550

Aufdenberg, J. P. et al. 2006, ApJ, 645, 664

Bagnuolo, Jr., W. G. et al. 2006, AJ, 131, 2695

Bahcall, J. N., Hut, P., & Tremaine, S. 1985, ApJ, 290, 15

Baines, E. K., McAlister, H. A., ten Brummelaar, T. A., Turner, N. H., Sturmann, J., Sturmann, L., Goldfinger, P. J., & Ridgway, S. T. 2008, ApJ, 680, 728

Barry, R. K. et al. 2008, The Astrophysical Journal, 677, 1253

Beavers, W. I., & Eitter, J. J. 1986, ApJS, 62, 147

Beckert, T., Driebe, T., Hönig, S. F., & Weigelt, G. 2008, A&A, 486, L17

Benson, J. A., Dyck, H. M., & Howell, R. R. 1995, Appl. Opt., 34, 51

Berger, D. H. et al. 2006, ApJ, 644, 475

Boden, A. F. et al. 1999a, ApJ, 515, 356

——. 1999b, ApJ, 527, 360

Boden, A. F., Torres, G., & Latham, D. W. 2006, ApJ, 644, 1193

Boss, A. P. 2001, ApJ, 551, L167

Boyajian, T. S. et al. 2008, ApJ, 683, 424

Branch, D. 1976, ApJ, 210, 392

Caballero, J. A. 2007, ApJ, 667, 520

Catala, C., Forveille, T., & Lai, O. 2006, AJ, 132, 2318

Ciardi, D. R., van Belle, G. T., Akeson, R. L., Thompson, R. R., Lada, E. A., & Howell, S. B. 2001, ApJ, 559, 1147

Colavita, M. M. et al. 1999, ApJ, 510, 505

Colavita, M. M., Wizinowich, P. L., & Akeson, R. L. 2004, in New Frontiers in Stellar Interferometry, Proceedings of the SPIE, ed. W. A. Traub, Vol. 5491, 454

Coude du Foresto, V. et al. 2003, in Presented at the Society of Photo-Optical Instrumentation Engineers (SPIE) Conference, Vol. 4838, Interferometry for Optical Astronomy II., ed. W. A. Traub, 280–285

Cox, A. N. 2000, Allen's astrophysical quantities, 4th ed., Edited by A. N. Cox (New York: AIP Press; Springer)

Cruz, K. L., Reid, I. N., Liebert, J., Kirkpatrick, J. D., & Lowrance, P. J. 2003, AJ, 126, 2421

Davis, J. et al. 2007, Publications of the Astronomical Society of Australia, 24, 151

Davis, J., Tango, W. J., Booth, A. J., ten Brummelaar, T. A., Minard, R. A., & Owens, S. M. 1999, MNRAS, 303, 773

Dommanget, J., & Nys, O. 2000, A&A, 363, 991

Duquennoy, A., & Mayor, M. 1988, A&A, 195, 129

Duquennoy, A., Mayor, M., & Halbwachs, J.-L. 1991, A&AS, 88, 281

Dyck, H. M., Benson, J. A., & Schloerb, F. P. 1995, AJ, 110, 1433

Eggenberger, A. et al. 2008, in Multiple Stars Across the H-R Diagram, ed. S. Hubrig, M. Petr-Gotzens, & A. Tokovinin (Springer-Verlag Berlin Heidelberg), 169–+

Eisner, J. A. 2007, Nature, 447, 562

Eisner, J. A., Chiang, E. I., & Hillenbrand, L. A. 2006, ApJ, 637, L133

Eisner, J. A., Chiang, E. I., Lane, B. F., & Akeson, R. L. 2007, ApJ, 657, 347

Fabricius, C., Høg, E., Makarov, V. V., Mason, B. D., Wycoff, G. L., & Urban, S. E. 2002, A&A, 384, 180

Finsen, W. S. 1951, MNRAS, 111, 387

Fizeau, A. H. 1868, C. R. Acad. Sci., 66, 934

Franz, O. G., Wasserman, L. H., Nelan, E., Lattanzi, M. G., Bucciarelli, B., & Taff, L. G. 1992, AJ, 103, 190

Gies, D. R. et al. 2007, ApJ, 654, 527

Gilmore, G., & Roberts, M. S. 1988, Comments on Astrophysics, 12, 123

Gizis, J. E., Monet, D. G., Reid, I. N., Kirkpatrick, J. D., & Burgasser, A. J. 1999, ArXiv Astrophysics e-prints

Gliese, W. 1969, Veroeffentlichungen des Astronomischen Rechen-Instituts Heidelberg, 22, 1

Griffin, R. F. 1999a, The Observatory, 119, 27

——. 1999b, The Observatory, 119, 81

——. 1999c, The Observatory, 119, 272

Griffin, R. F., Mayor, M., Udry, S., & Tomkin, J. 1999, The Observatory, 119, 213

Griffin, R. F., & Suchkov, A. A. 2003, ApJS, 147, 103

Halbwachs, J. L. 1981, A&AS, 44, 47

——. 1986, A&A, 168, 161

Halbwachs, J. L., Mayor, M., Udry, S., & Arenou, F. 2003, A&A, 397, 159

Hale, D. D. S. et al. 2000, ApJ, 537, 998

——. 1997, ApJ, 490, 407

Hanbury Brown, R., & Twiss, R. Q. 1956, Nature, 178, 1046

Hanbury Brown, R. H., Davis, J., Allen, L. R., & Rome, J. M. 1967, MNRAS, 137, 393

Harris, III, D. L., Strand, K. A., & Worley, C. E. 1968, Empirical Data on Stellar Masses, Luminosities, and Radii (Basic Astronomical Data: Stars and stellar systems,

by K. A. Strand. (Chicago: University of Chicago Press)), 273

Hartkopf, W. I., Mason, B. D., & Worley, C. E. 2001a, AJ, 122, 3472

Hartkopf, W. I., McAlister, H. A., & Franz, O. G. 1989, AJ, 98, 1014

Hartkopf, W. I., McAlister, H. A., & Mason, B. D. 2001b, AJ, 122, 3480

Heintz, W. D. 1978, Geophysics and Astrophysics Monographs, 15

——. 1988, AJ, 96, 1072

Hummel, C. A. et al. 2003, AJ, 125, 2630

Ireland, M. J. et al. 2008, in Optical and Infrared Interferometry, Proceedings of the SPIE, ed. M. Schller, W. C. Danchi, & F. Delplancke, Vol. 7013, 10

Ireland, M. J., Tuthill, P. G., Davis, J., & Tango, W. 2005, MNRAS, 361, 337

Jancart, S., Jorissen, A., Babusiaux, C., & Pourbaix, D. 2005, A&A, 442, 365

Jao, W.-C., Henry, T. J., Subasavage, J. P., Bean, J. L., Costa, E., Ianna, P. A., & Méndez, R. A. 2003, AJ, 125, 332

Jaschek, C., & Gómez, A. E. 1970, PASP, 82, 809

Jaschek, C., & Jaschek, M. 1957, PASP, 69, 546

Kirkpatrick, J. D. et al. 2000, AJ, 120, 447

Konacki, M. 2005, ApJ, 626, 431

Kraus, A. L., White, R. J., & Hillenbrand, L. A. 2005, ApJ, 633, 452

Kraus, S., Preibisch, T., & Ohnaka, K. 2008, ApJ, 676, 490

Kuiper, G. P. 1935, PASP, 47, 15

——. 1942, ApJ, 95, 201

Labeyrie, A. 1970, A&A, 6, 85

——. 1975, ApJ, 196, L71

Lane, B. F., & Muterspaugh, M. W. 2004, ApJ, 601, 1129

Lasker, B. M. et al. 1996, VizieR Online Data Catalog, 2143, 0

Lawson, P. R., ed. 2000, Principles of Long Baseline Stellar Interferometry (Pasadena: JPL PUB 00-009, 2000)

Lawson, P. R. 2006

Lindegren, L. 1980, A&A, 89, 41

Liu, M. C., Fischer, D. A., Graham, J. R., Lloyd, J. P., Marcy, G. W., & Butler, R. P. 2002, ApJ, 571, 519

Lowrance, P. J., Kirkpatrick, J. D., & Beichman, C. A. 2002, ApJ, 572, L79

Lowrance, P. J., The Nicmos Environments Of Nearby Stars Team, & STIS 8176 Team. 2003, in IAU Symposium, Vol. 211, Brown Dwarfs, ed. E. Martín (San Francisco: Astronomical Society of the Pacific), 295

Luhman, K. L. et al. 2007, ApJ, 654, 570

Malogolovets, E. V., Balega, Y. Y., & Rastegaev, D. A. 2007, Astrophysical Bulletin, 62, 111

Mason, B. D., Gies, D. R., Hartkopf, W. I., Bagnuolo, Jr., W. G., ten Brummelaar, T., & McAlister, H. A. 1998a, AJ, 115, 821

Mason, B. D., Henry, T. J., Hartkopf, W. I., Ten Brummelaar, T., & Soderblom, D. R. 1998b, AJ, 116, 2975

Mayor, M., & Mermilliod, J. C. 1984, in IAU Symposium, Vol. 105, Observational Tests of the Stellar Evolution Theory, ed. A. Maeder & A. Renzini (Reidel Publishing Company, Dordrecht, The Netherlands, Boston, MA, Hingham, MA), 411–+

McAlister, H. A., Hartkopf, W. I., Hutter, D. J., Shara, M. M., & Franz, O. G. 1987, AJ, 93, 183

McAlister, H. A. et al. 2005, ApJ, 628, 439

McClure, R. D. 1983, PASP, 95, 201

Mermilliod, J.-C. 1994, Bulletin d'Information du Centre de Donnees Stellaires, 45, 3

Michelson, A. A. 1891, PASP, 3, 274

——. 1920, ApJ, 51, 257

Michelson, A. A., & Pease, F. G. 1921, ApJ, 53, 249

Millan-Gabet, R. et al. 2006, ApJ, 641, 547

Monnier, J. D., Danchi, W. C., Hale, D. S., Tuthill, P. G., & Townes, C. H. 2000, ApJ, 543, 868

Monnier, J. D. et al. 2007, Science, 317, 342

Morbey, C. L., & Griffin, R. F. 1987, ApJ, 317, 343

Mourard, D. et al. 2008, in Optical and Infrared Interferometry, Proceedings of the SPIE, ed. M. Schller, W. C. Danchi, & F. Delplancke, Vol. 7013, 12

Mugrauer, M. et al. 2004, A&A, 417, 1031

Muterspaugh, M. W. et al. 2008, AJ, 135, 766

Nidever, D. L., Marcy, G. W., Butler, R. P., Fischer, D. A., & Vogt, S. S. 2002, ApJS, 141, 503

Nordström, B. et al. 2004, A&A, 418, 989

North, J. R., Davis, J., Tuthill, P. G., Tango, W. J., & Robertson, J. G. 2007, MNRAS, 380, 1276

Ochsenbein, F., Bauer, P., & Marcout, J. 2000, A&AS, 143, 23

Perryman, M. A. C., & ESA. 1997, The HIPPARCOS and TYCHO catalogues (Noordwijk, Netherlands: ESA Publications Division, Series: ESA SP Series vol no: 1200)

Peterson, D. M. et al. 2006, Nature, 440, 896

Petrie, R. M. 1960, Annales d'Astrophysique, 23, 744

Pott, J.-U., Eckart, A., Glindemann, A., Kraus, S., Schödel, R., Ghez, A. M., Woillez, J., & Weigelt, G. 2008, A&A, 487, 413

Potter, D., Martín, E. L., Cushing, M. C., Baudoz, P., Brandner, W., Guyon, O., & Neuhäuser, R. 2002, ApJ, 567, L133

Pourbaix, D. 2000, A&AS, 145, 215

Pourbaix, D. et al. 2004, A&A, 424, 727

Raghavan, D. et al. 2008, ApJ, 900, 109

Reid, I. N., & Cruz, K. L. 2002, AJ, 123, 2806

Richichi, A. 2007, in Astronomical Society of the Pacific Conference Series, Vol. 378, Why Galaxies Care About AGB Stars: Their Importance as Actors and Probes, ed. F. Kerschbaum, C. Charbonnel, & R. F. Wing (San Francisco: Astronomical Society of the

Pacific), 193

Schloerb, F. P. 1990, in Society of Photo-Optical Instrumentation Engineers (SPIE) Conference Series, Vol. 1237, Society of Photo-Optical Instrumentation Engineers (SPIE) Conference Series, ed. J. B. Breckinridge, 154

Schwarzschild, K. 1896, Astronomische Nachrichten, 139, 353

Shao, M., & Colavita, M. M. 1992, A&A, 262, 353

Skrutskie, M. F. et al. 2006, AJ, 131, 1163

Swain, M. et al. 2003, ApJ, 596, L163

Tango, W. J., & Twiss, R. Q. 1980, in Progress in optics. Volume 17. (Amsterdam: North-Holland Publishing Co.), 241

Taylor, S. F., Harvin, J. A., & McAlister, H. A. 2003, PASP, 115, 609

ten Brummelaar, T. A. et al. 2005, ApJ, 628, 453

Thompson, A. R., Moran, J. M., & Swenson, G. W. 1986, Interferometry and synthesis in radio astronomy (New York, Wiley-Interscience, 1986, 554 p.)

Tokovinin, A., Thomas, S., Sterzik, M., & Udry, S. 2006, A&A, 450, 681

Tokovinin, A. A. 1997, A&AS, 124, 75

Tomkin, J., & Fekel, F. C. 2008, AJ, 135, 555

Trimble, V. 1990, MNRAS, 242, 79

Turner, N. H., ten Brummelaar, T. A., McAlister, H. A., Mason, B. D., Hartkopf, W. I., & Roberts, Jr., L. C. 2001, AJ, 121, 3254

Turon, C. et al. 1993, Bulletin d'Information du Centre de Donnees Stellaires, 43, 5

Tycner, C. et al. 2005, ApJ, 624, 359

van Belle, G. T. et al. 2008, ApJS, 176, 276

van den Bos, W. H. 1959, ApJS, 4, 45

van Leeuwen, F. 2008, VizieR Online Data Catalog, 1311, 0

Vinter Hansen, J. M. 1940, PASP, 52, 399

Wallerstein, G. 1973, PASP, 85, 115

Weiner, J., Danchi, W. C., Hale, D. D. S., McMahon, J., Townes, C. H., Monnier, J. D., & Tuthill, P. G. 2000, ApJ, 544, 1097

Wilson, Jr., R. H. 1936, PASP, 48, 195

Wright, K. O., & Pugh, R. E. 1954, Publications of the Dominion Astrophysical Observatory Victoria, 9, 407

Zhao, M. et al. 2008, ApJ, 684, 195

# Appendices

# – A —

# Non-Detection of Separated Fringe Packets

This appendix includes example fringe envelope fits from all non-detections of separated fringe packets for the observed systems in this dissertation. Each plot contains a solid grey line depicting the actual summed envelope from a single file on the date listed for the object, a dashed line showing the Gaussian fit for the primary fringe, and dotted lines where the program attempted to fit a secondary if applicable. All data files were reduced with identical parameters where it would attempt to fit a secondary fringe with a Gaussian if one existed. Two plots are included if the system has more than one observation on either seperate baselines, the same baseline on two different days, or multiple observations of the system on the same day. Full details of the observations are given in §6.3.1 and Table. 5.1.

# A.1 Observed Stars Right Ascension 00-06 Hours

## A.1.1 HD 123

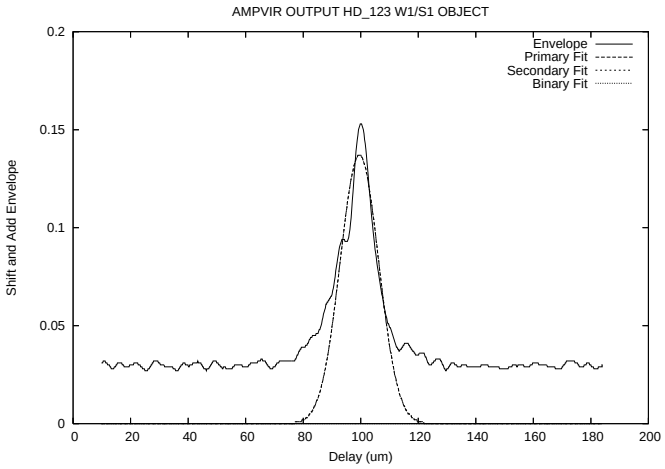


Figure. A.1: HD 123 Fringe Envelope on 2005 October 5 on the W1/S1 Baseline.

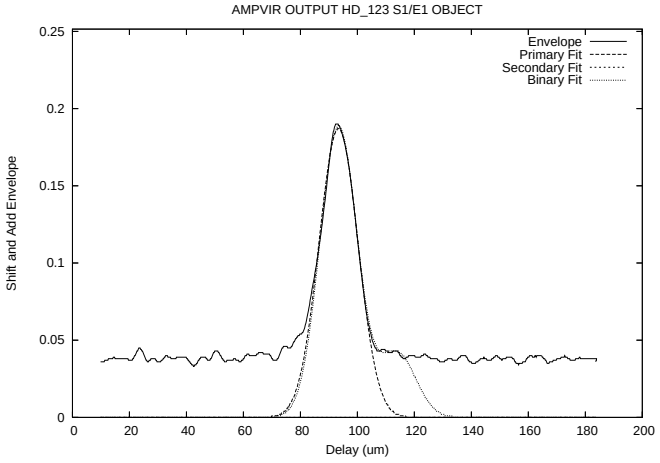


Figure. A.2: HD 123 Fringe Envelope on 2005 October 11 on the E1/S1 Baseline.

### A.1.2 HD 4614

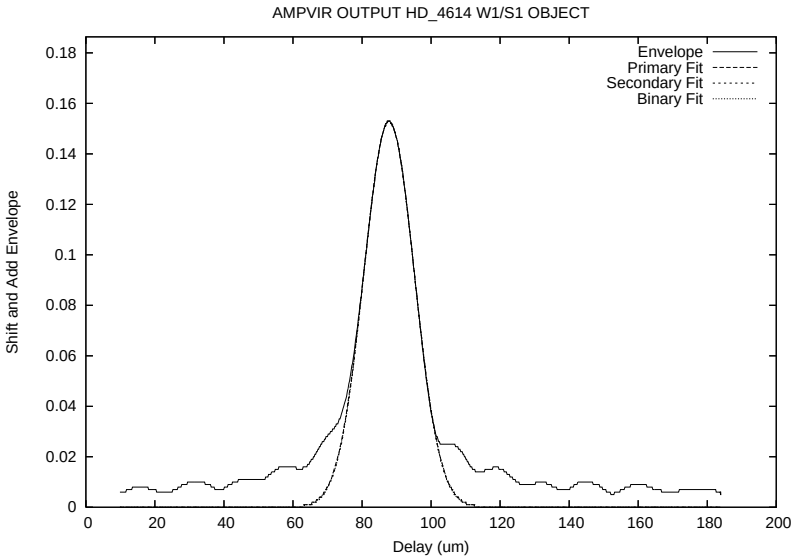


Figure. A.3: HD 4614 Fringe Envelope on 2006 September 11 on the W1/S1 Baseline.

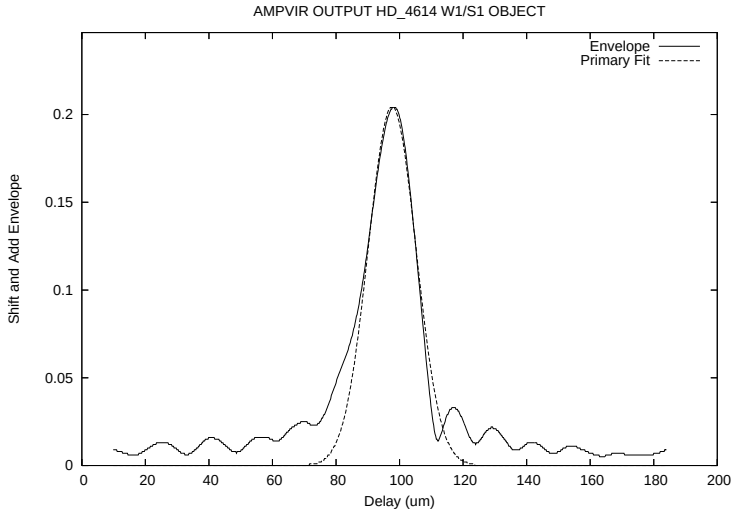


Figure. A.4: HD 4614 Fringe Envelope on 2006 September 10 on the W1/S1 Baseline.

### A.1.3 HD 5015

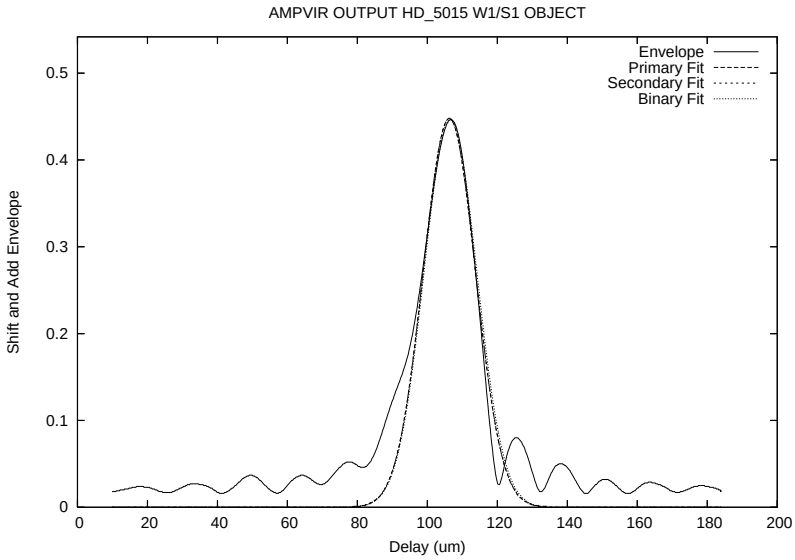


Figure. A.5: HD 5015 Fringe Envelope on 2006 September 10 on the W1/S1 Baseline.

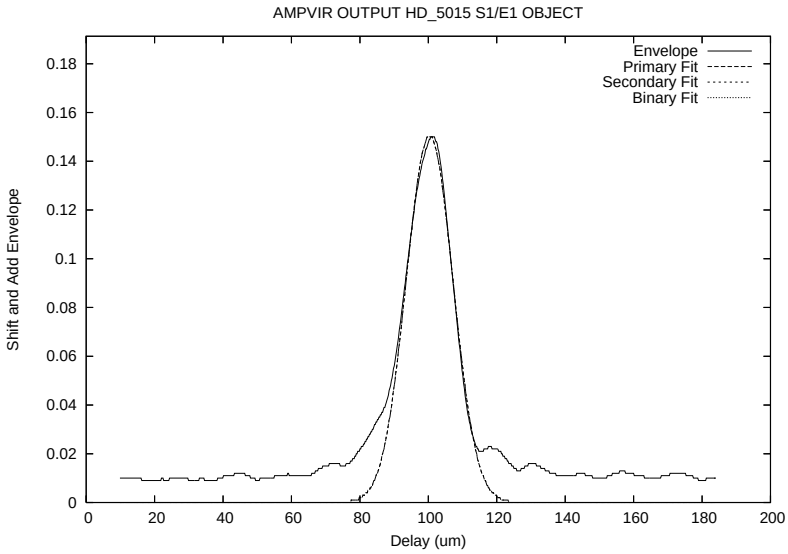


Figure. A.6: HD 5015 Fringe Envelope on 2006 September 18 on the E1/S1 Baseline.

### A.1.4 HD 5857

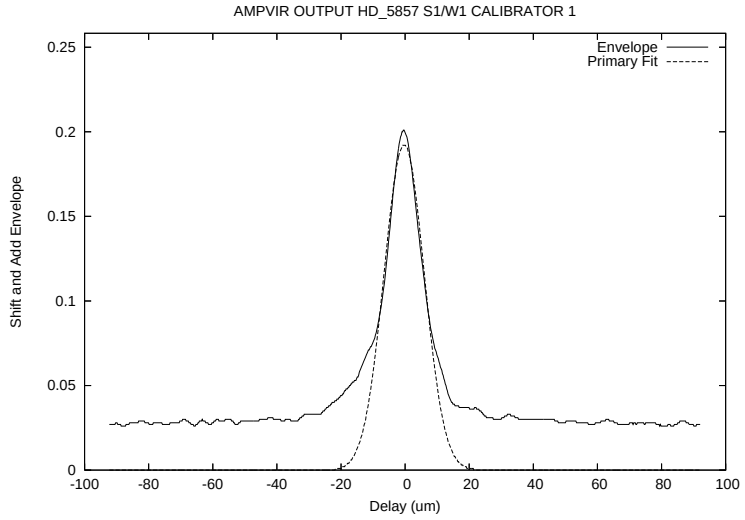


Figure. A.7: HD 5857 Fringe Envelope on 2007 October 19 on the W1/S1 Baseline.

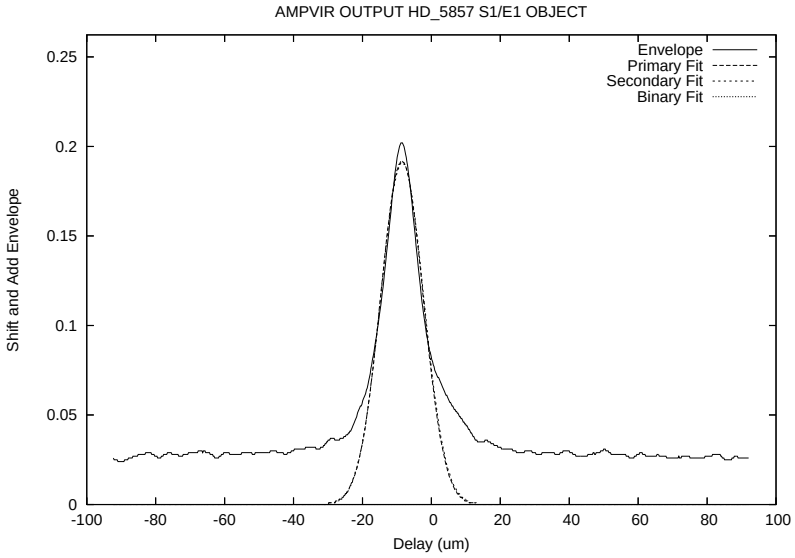


Figure. A.8: HD 5857 Fringe Envelope on 2007 October 19 on the E1/S1 Baseline.

### A.1.5 HD 6582

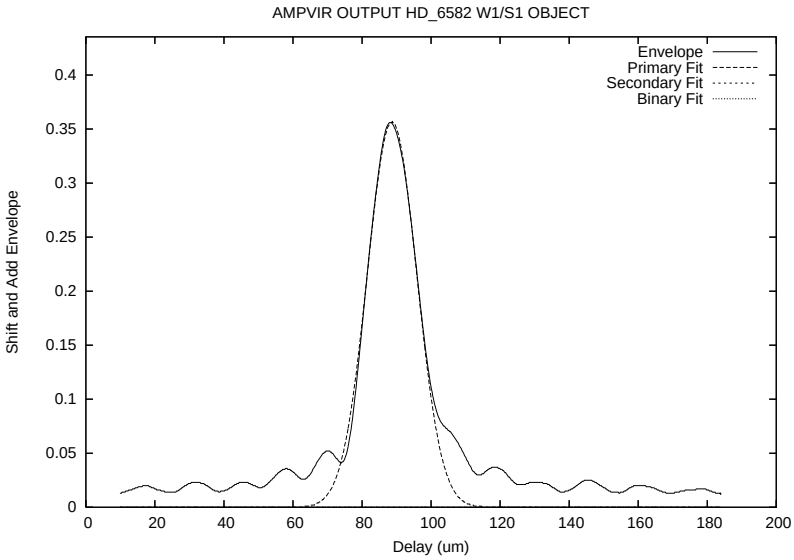


Figure. A.9: HD 6582 Fringe Envelope on 2006 September 11 on the W1/S1 Baseline.

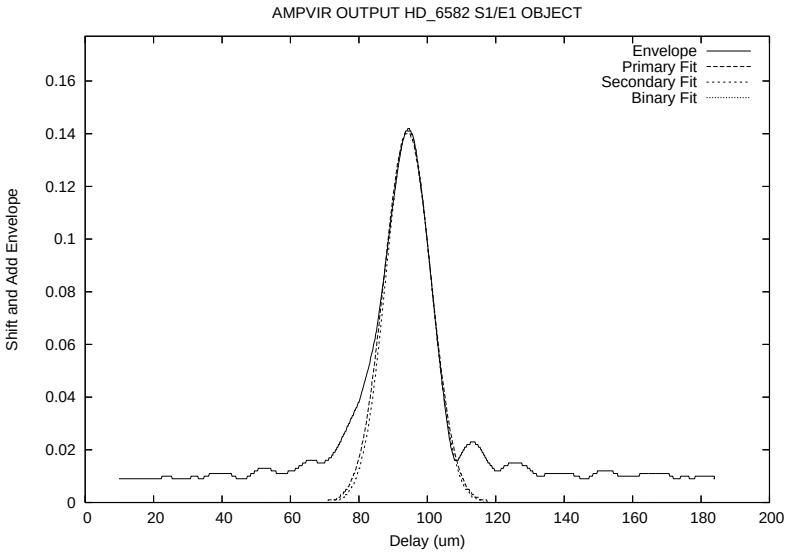


Figure. A.10: HD 6582 Fringe Envelope on 2006 September 18 on the E1/S1 Baseline.

### A.1.6 HD 6920

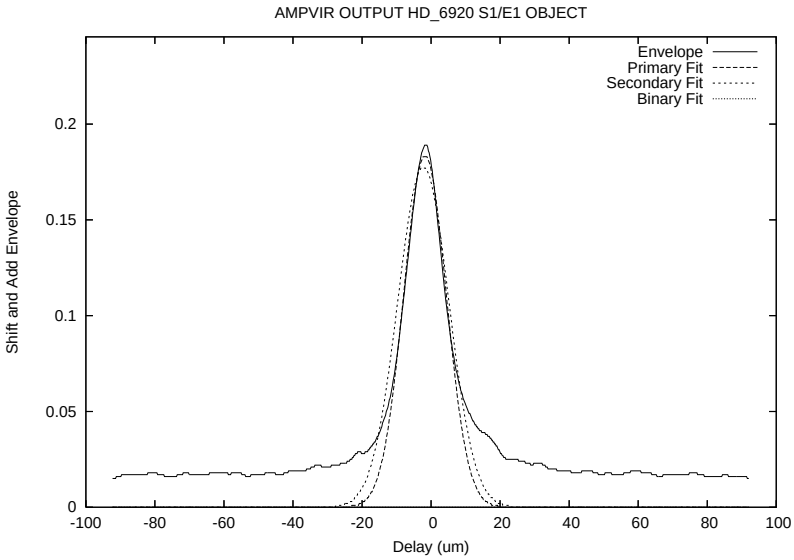


Figure. A.11: HD 6920 Fringe Envelope on 2007 October 20 on the E1/S1 Baseline.

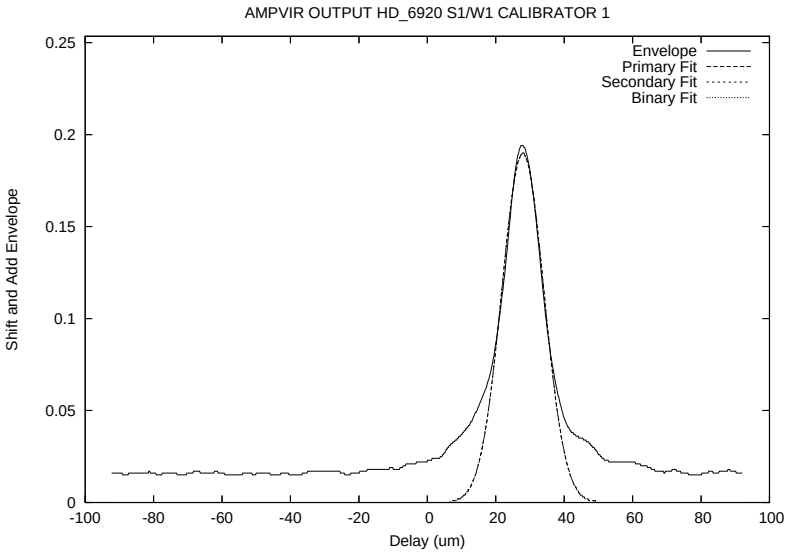


Figure. A.12: HD 6920 Fringe Envelope on 2007 October 20 on the W1/S1 Baseline.

### A.1.7 HD 9407

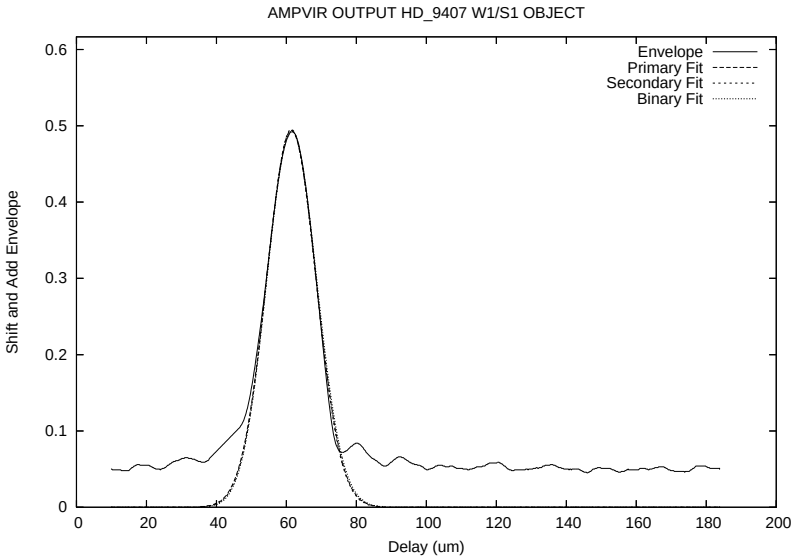


Figure. A.13: HD 9407 Fringe Envelope on 2006 September 11 on the W1/S1 Baseline.

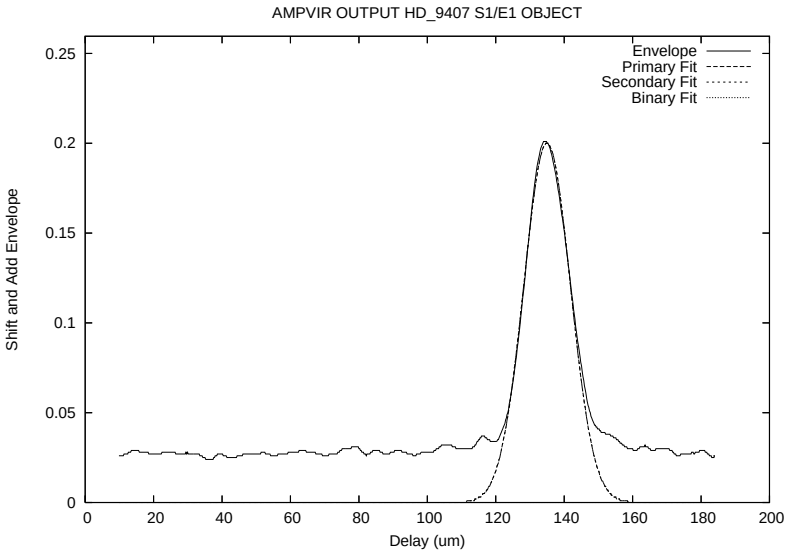


Figure. A.14: HD 9407 Fringe Envelope on 2006 September 18 on the E1/S1 Baseline.

### A.1.8 HD 9826

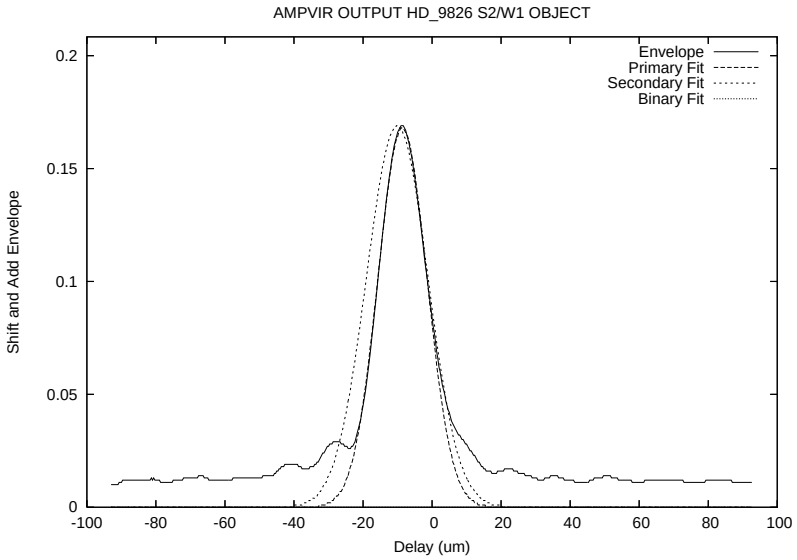


Figure. A.15: HD 9826 Fringe Envelope on 2007 September 5 on the W1/S2 Baseline.

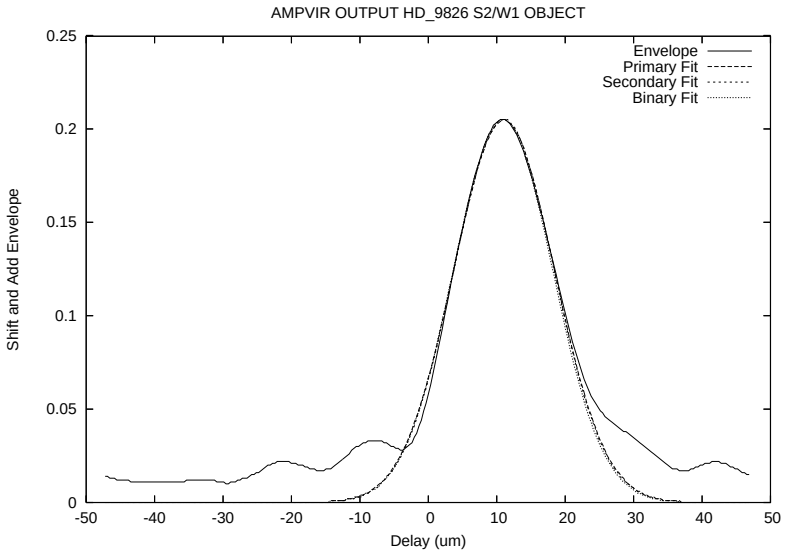


Figure. A.16: HD 9826 Fringe Envelope on 2007 September 6 on the W1/S2 Baseline.

### A.1.9 HD 10307

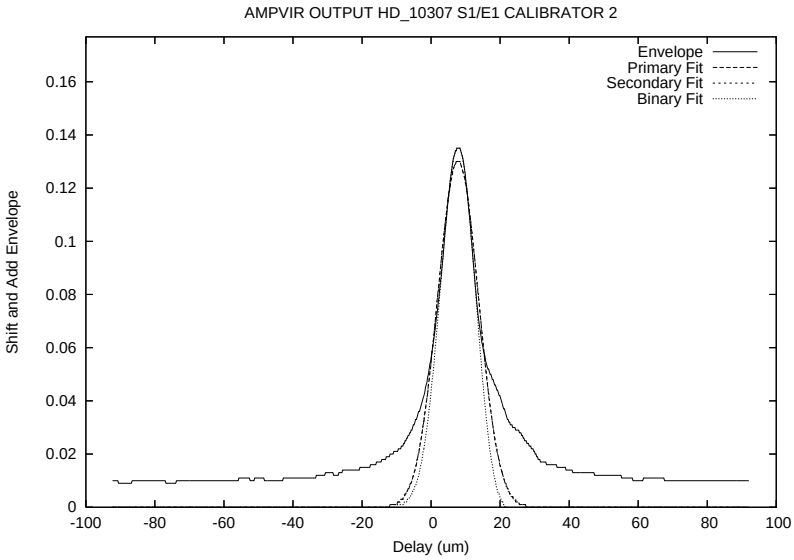


Figure. A.17: HD 10307 Fringe Envelope on 2007 October 20 on the E1/S1 Baseline.

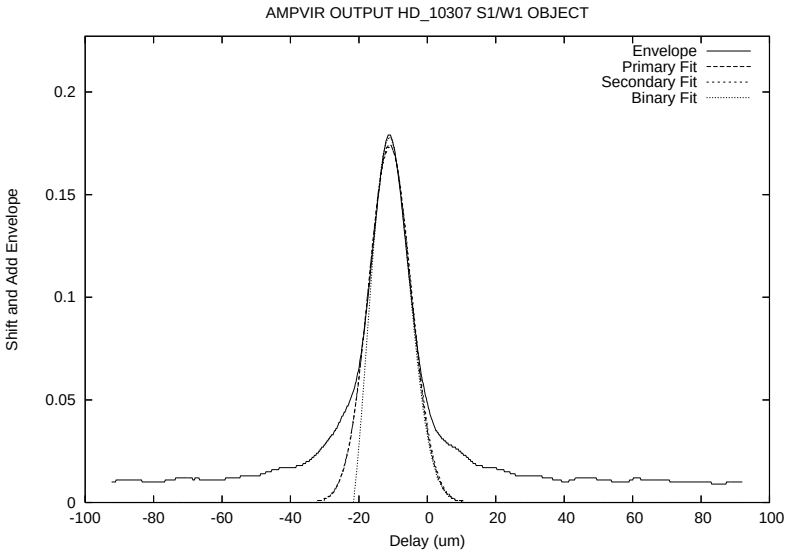


Figure. A.18: HD 10307 Fringe Envelope on 2007 October 20 on the W1/S1 Baseline.

### A.1.10 HD 10697

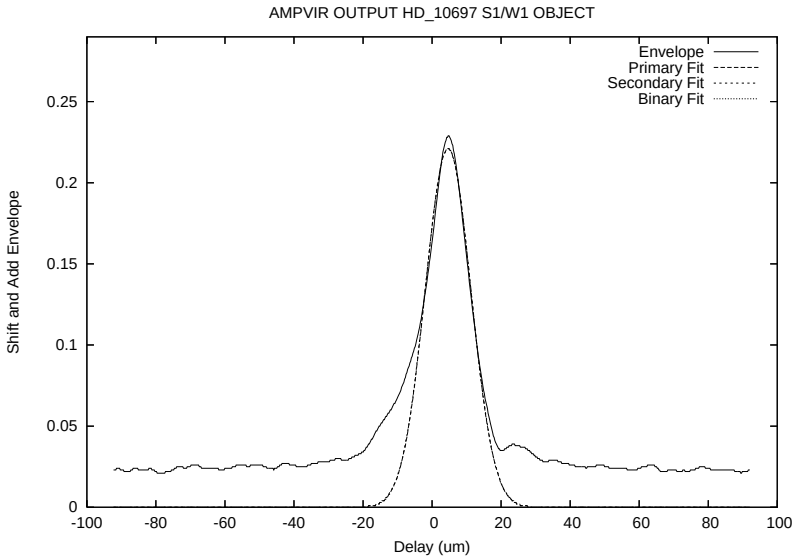


Figure. A.19: HD 10697 Fringe Envelope on 2007 October 20 on the W1/S1 Baseline.

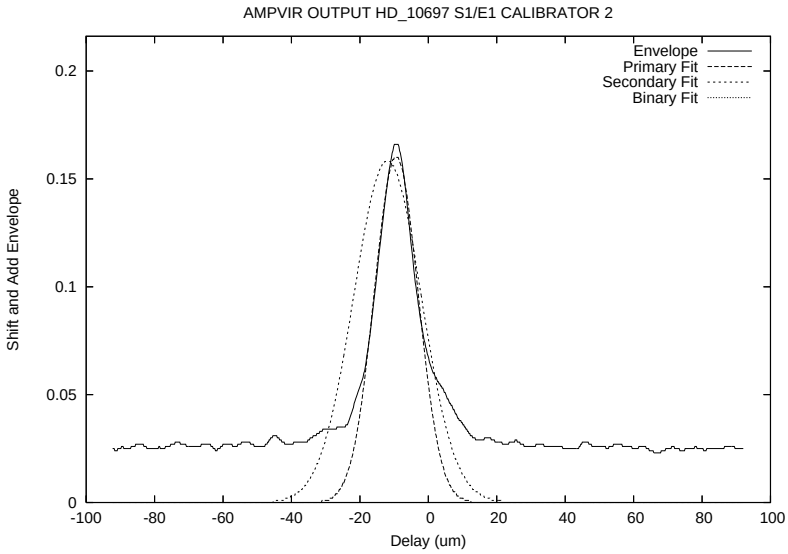


Figure. A.20: HD 10697 Fringe Envelope on 2007 October 20 on the E1/S1 Baseline.

### A.1.11 HD 12235

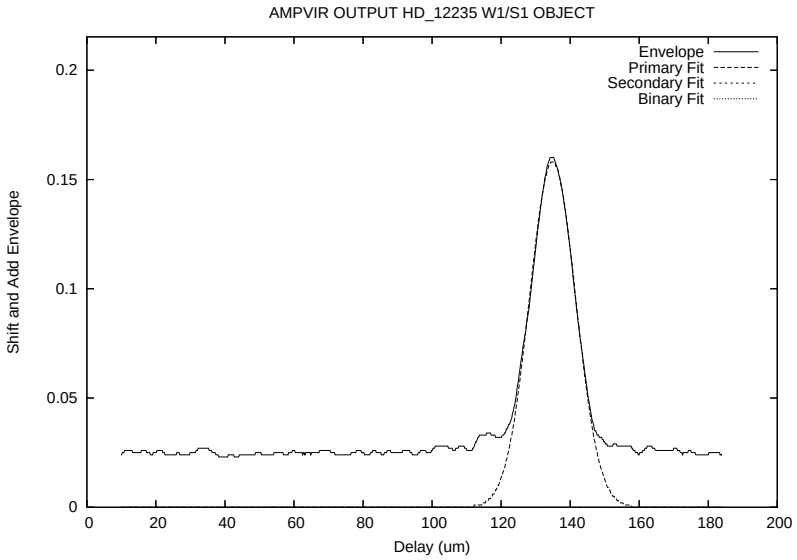


Figure. A.21: HD 12235 Fringe Envelope on 2005 October 2 on the W1/S1 Baseline.

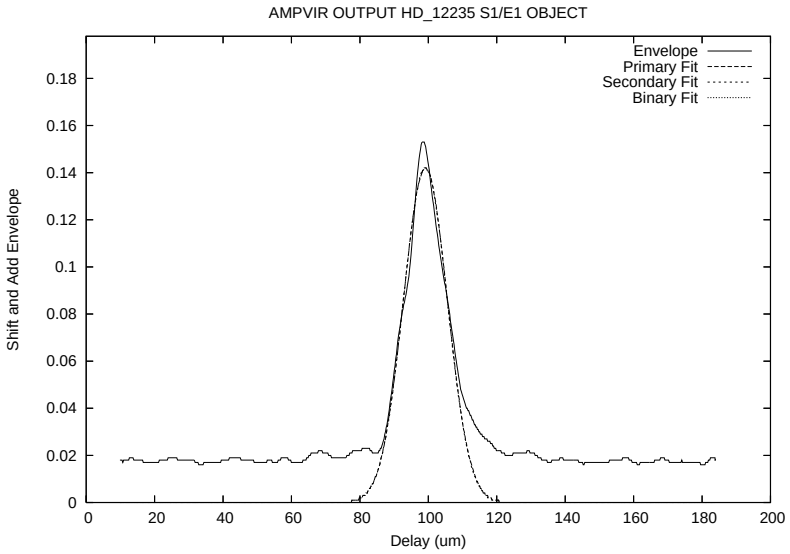


Figure. A.22: HD 12235 Fringe Envelope on 2005 October 7 on the E1/S1 Baseline.

### A.1.12 HD 12923

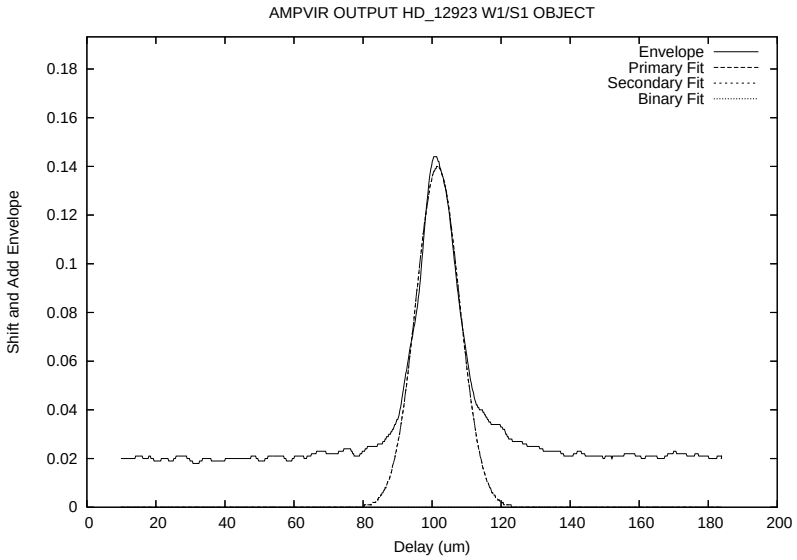


Figure. A.23: HD 12923 Fringe Envelope on 2005 October 2 on the W1/S1 Baseline.

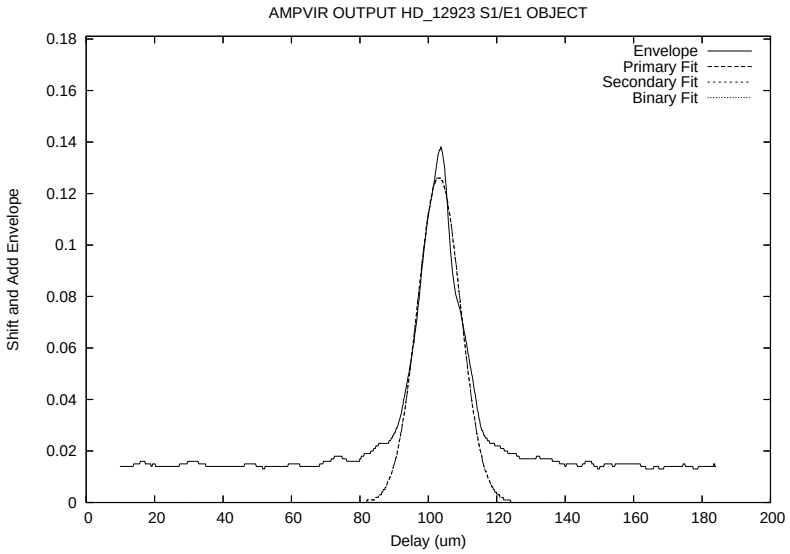


Figure. A.24: HD 12923 Fringe Envelope on 2005 October 7 on the E1/S1 Baseline.

### A.1.13 HD 13480

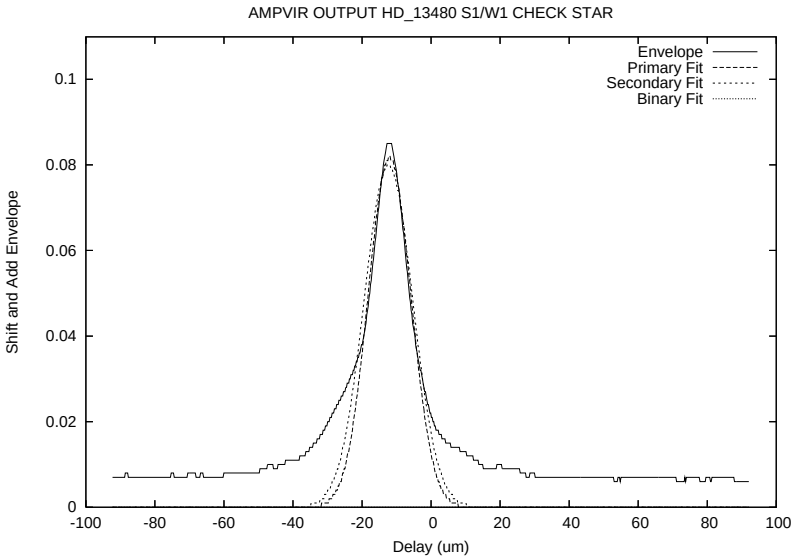


Figure. A.25: HD 13480 Fringe Envelope on 2005 September 29 on the W1/S1 Baseline.

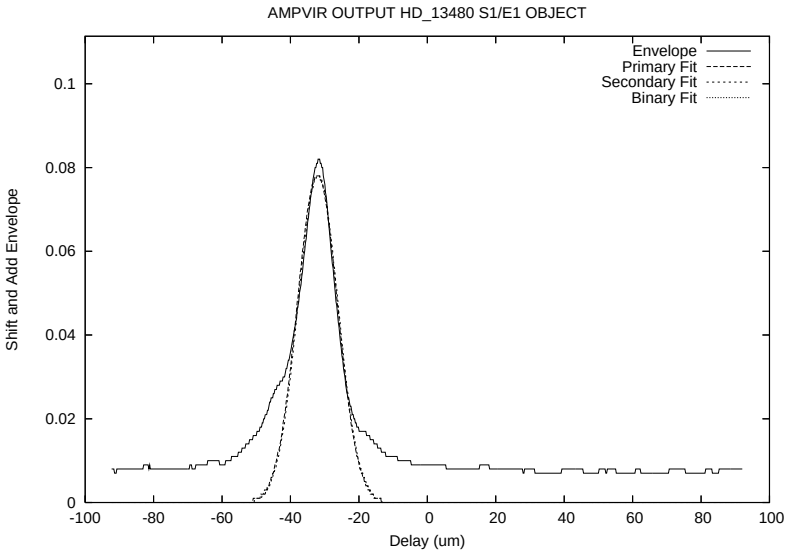


Figure. A.26: HD 13480 Fringe Envelope on 2005 October 6 on the E1/S1 Baseline.

### A.1.14 HD 13974

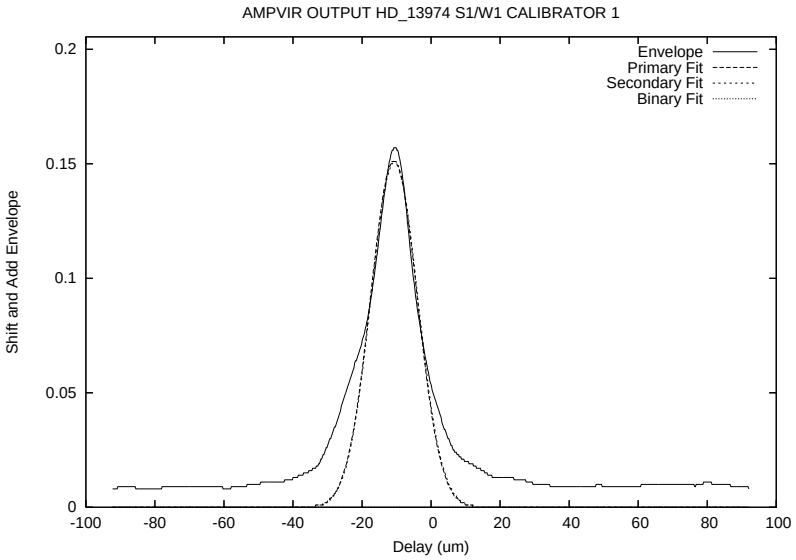


Figure. A.27: HD 13974 Fringe Envelope on 2007 October 20 on the W1/S1 Baseline.

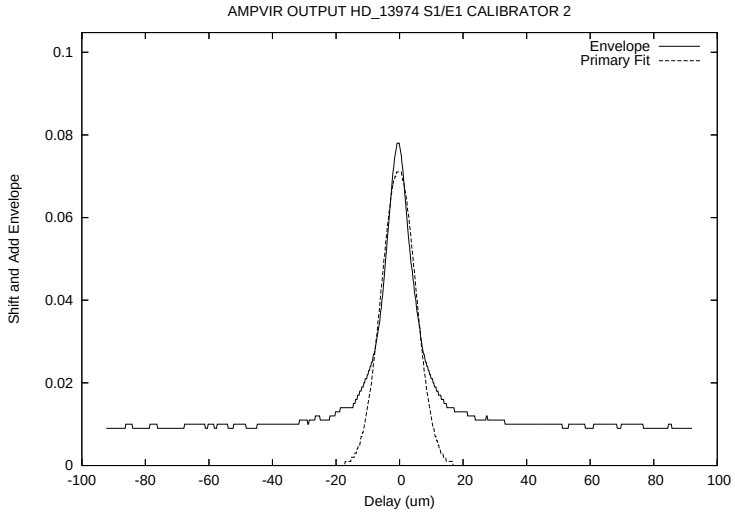


Figure. A.28: HD 13974 Fringe Envelope on 2007 October 20 on the E1/S1 Baseline.

### A.1.15 HD 14214

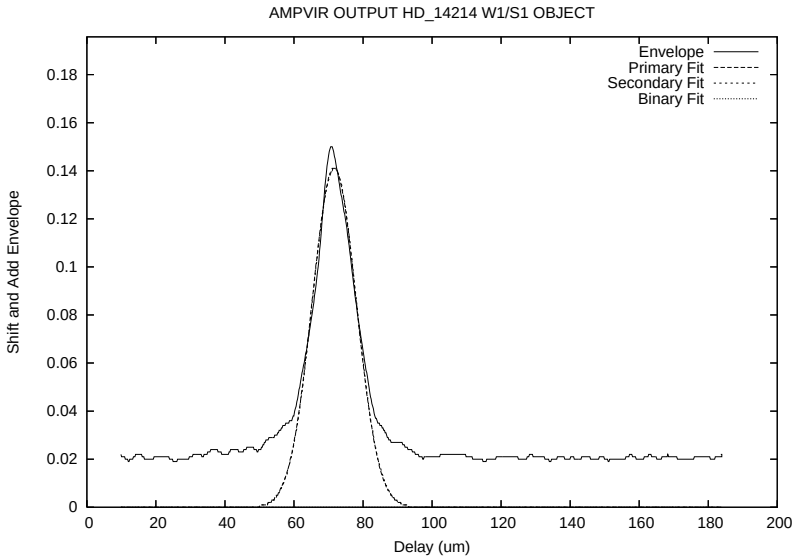


Figure. A.29: HD 14214 Fringe Envelope on 2005 October 2 on the W1/S1 Baseline.

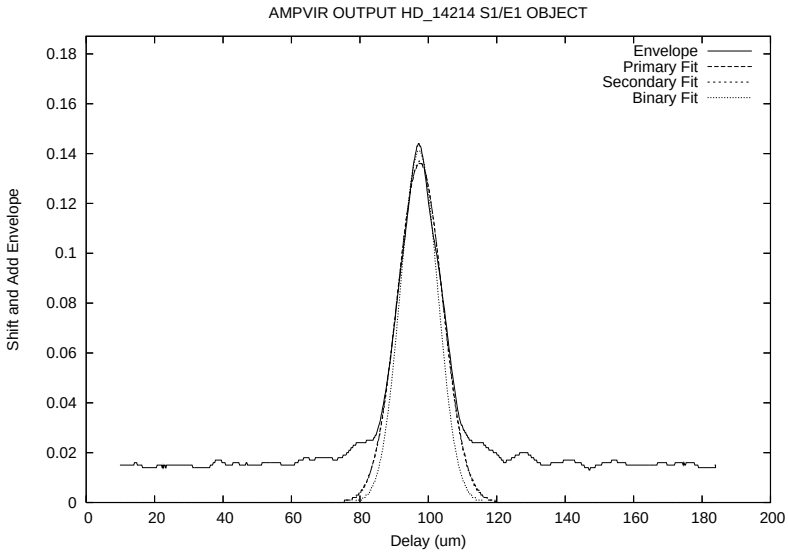


Figure. A.30: HD 14214 Fringe Envelope on 2005 October 7 on the E1/S1 Baseline.

### A.1.16 HD 15335

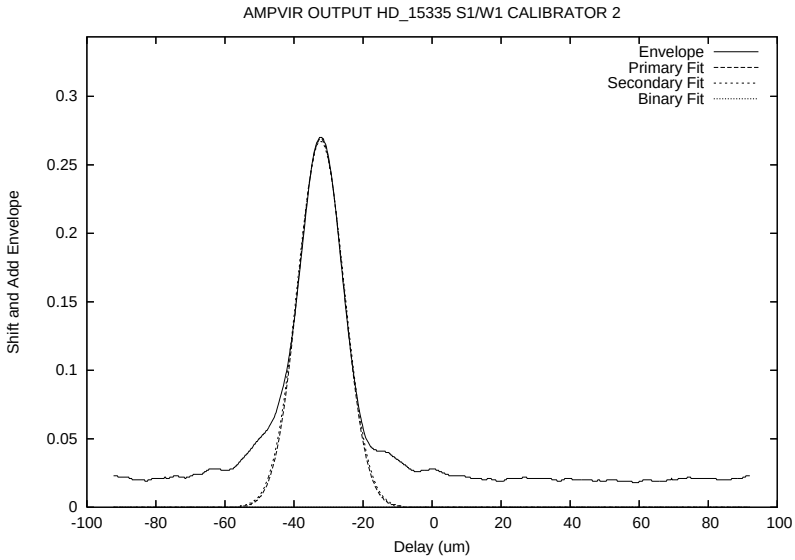


Figure. A.31: HD 15335 Fringe Envelope on 2007 October 20 on the W1/S1 Baseline.

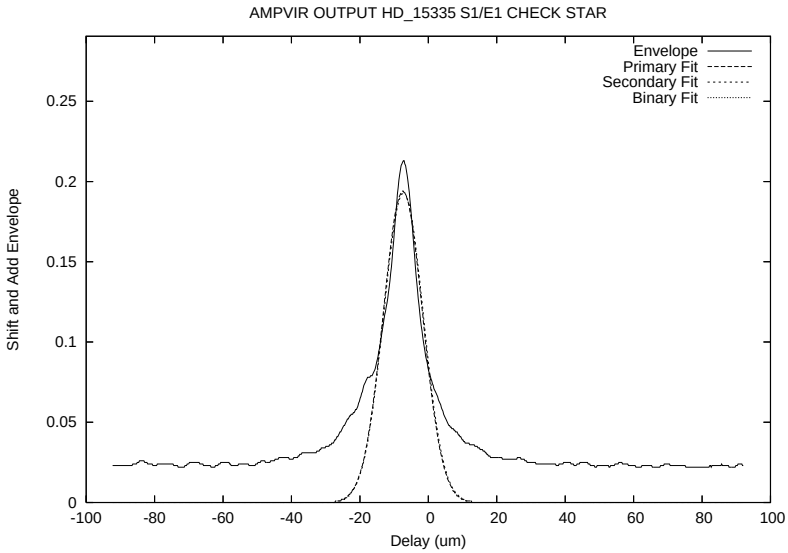


Figure. A.32: HD 15335 Fringe Envelope on 2007 October 20 on the E1/S1 Baseline.

### A.1.17 HD 16895

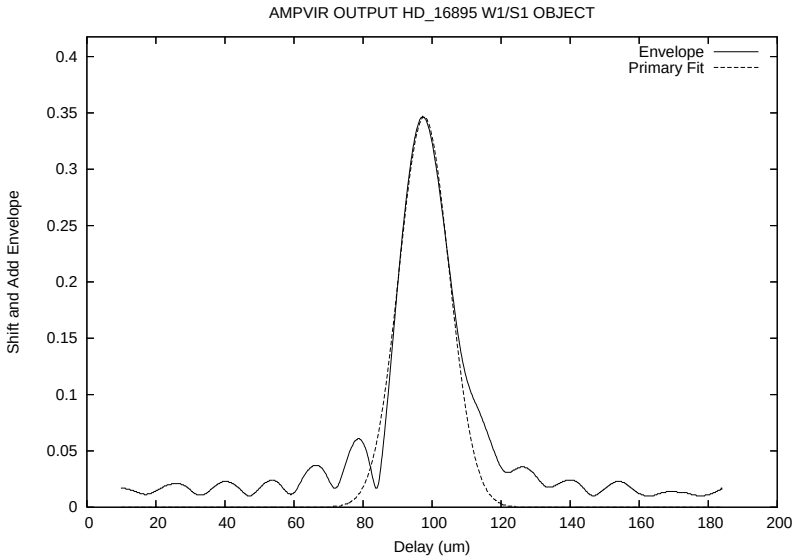


Figure. A.33: HD 16895 Fringe Envelope on 2006 September 10 on the E1/S1 Baseline.

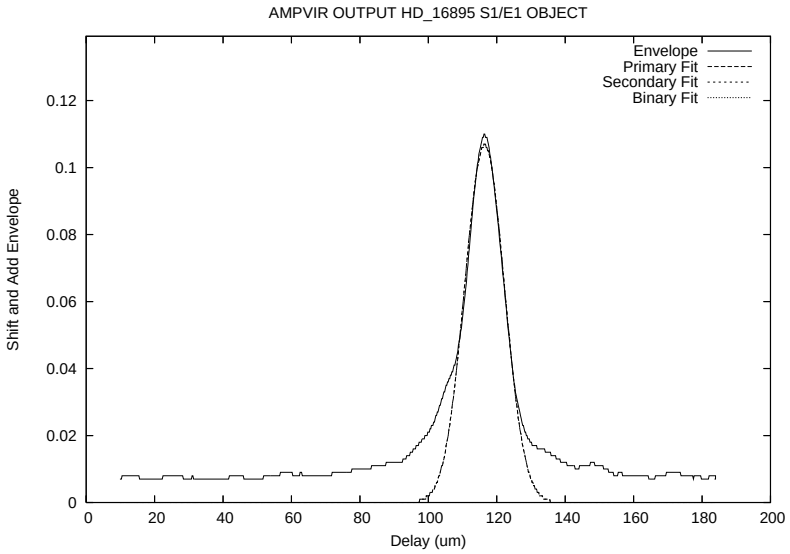


Figure. A.34: HD 16895 Fringe Envelope on 2006 September 18 on the E1/S1 Baseline.

### A.1.18 HD 17433

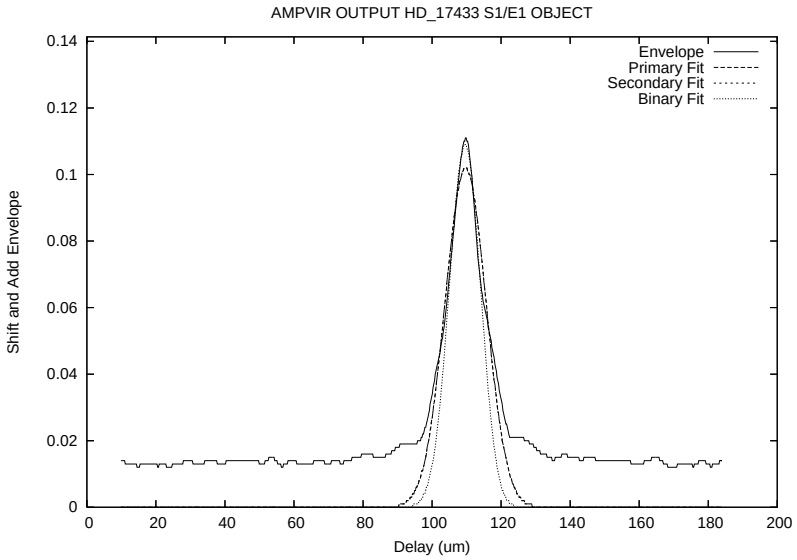


Figure. A.35: HD 17433 Fringe Envelope on 2005 September 19 on the W1/S1 Baseline.

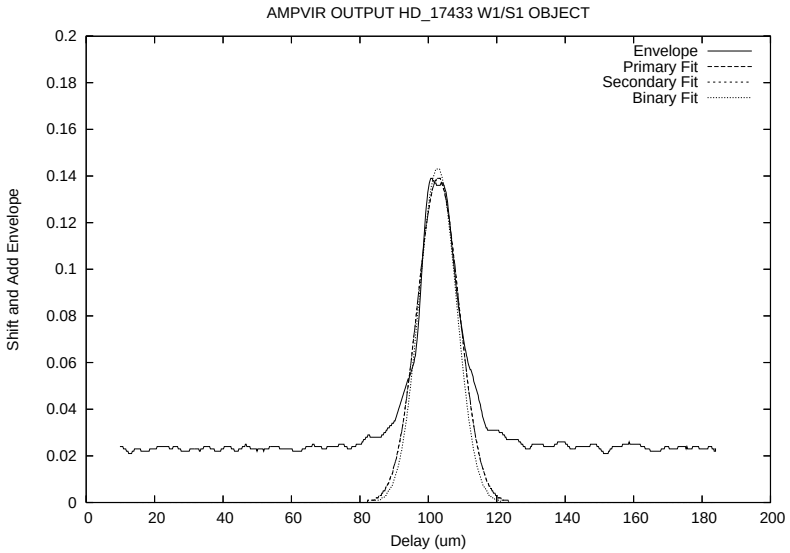


Figure. A.36: HD 17433 Fringe Envelope on 2005 October 6 on the E1/S1 Baseline.

### A.1.19 HD 19373

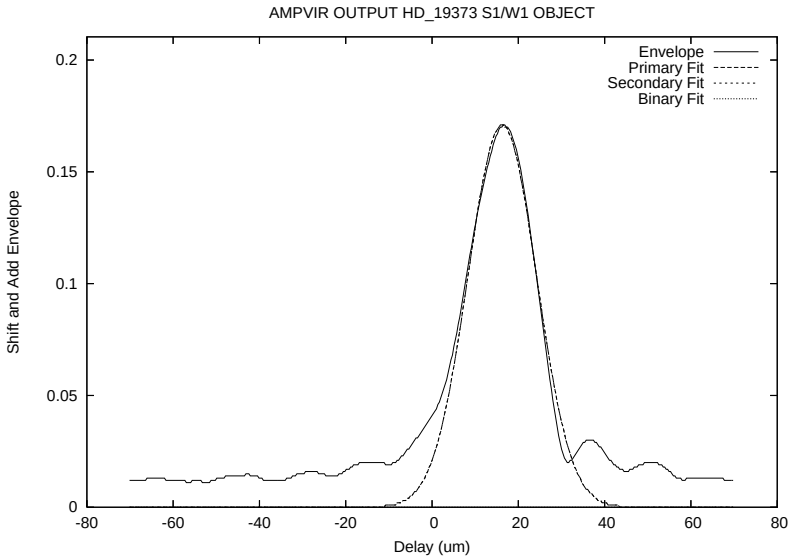


Figure. A.37: HD 19373 Fringe Envelope on 2007 August 28 on the W1/S1 Baseline.

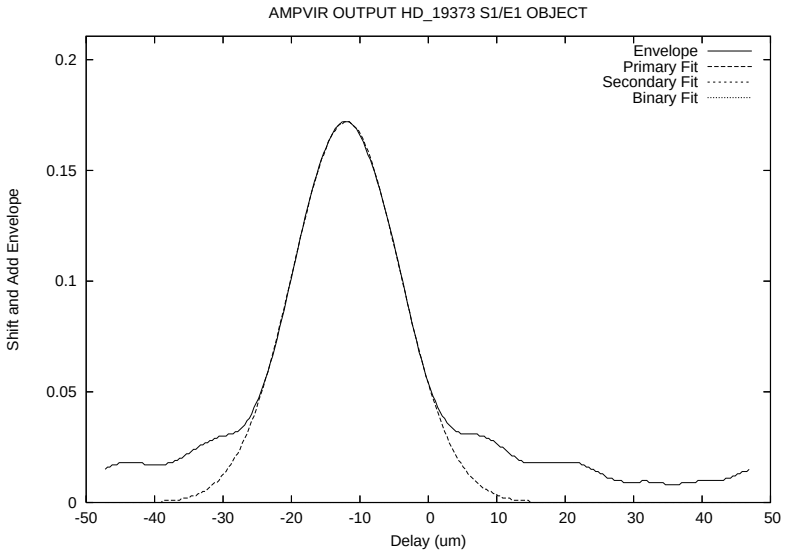


Figure. A.38: HD 19373 Fringe Envelope on 2007 September 8 on the E1/S1 Baseline.

## A.1.20 HD 20630

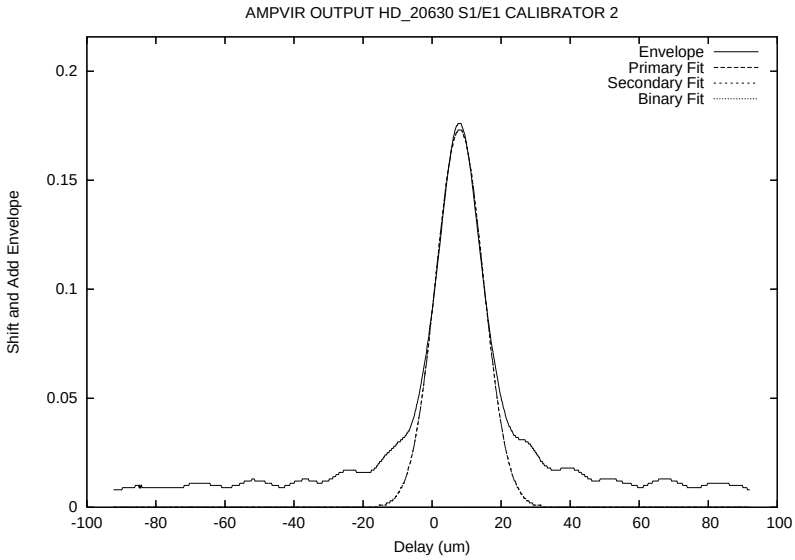


Figure. A.39: HD 20630 Fringe Envelope on 2007 October 19 on the E1/S1 Baseline.

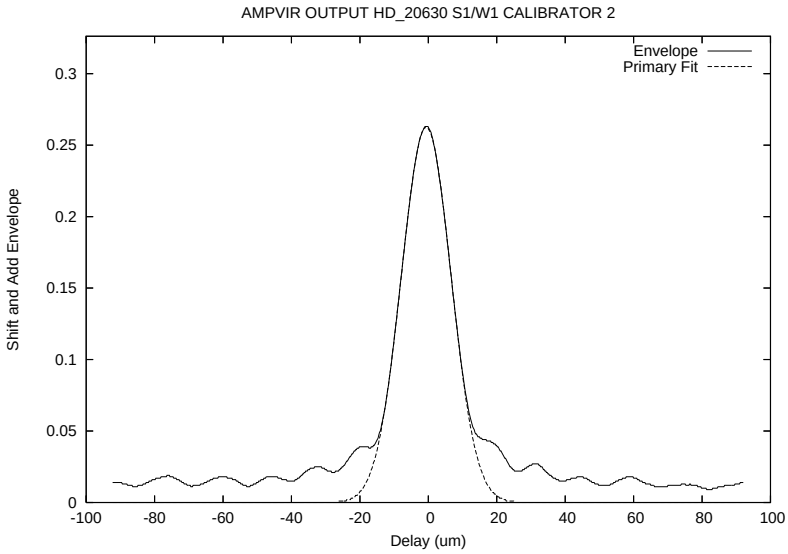


Figure. A.40: HD 20630 Fringe Envelope on 2007 October 19 on the W1/S1 Baseline.

### A.1.21 HD 21242

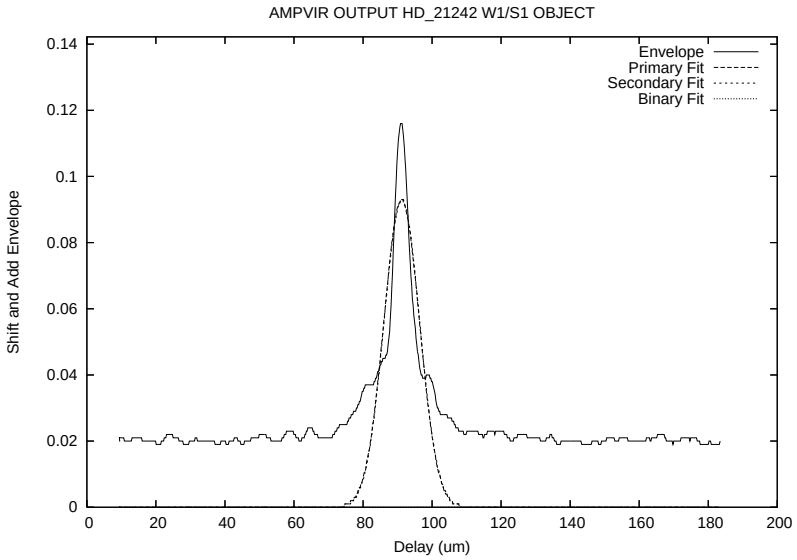


Figure. A.41: HD 21242 Fringe Envelope on 2005 September 28 on the W1/S1 Baseline.

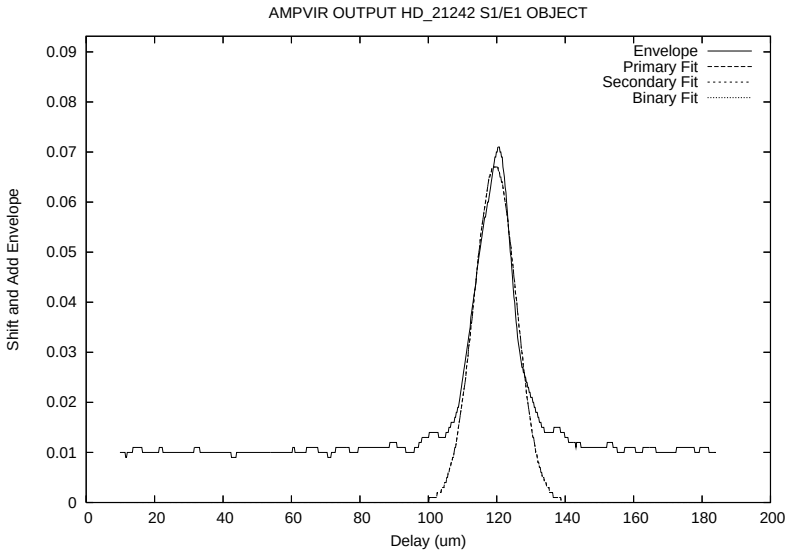


Figure. A.42: HD 21242 Fringe Envelope on 2005 October 6 on the E1/S1 Baseline.

## A.1.22 HD 22484

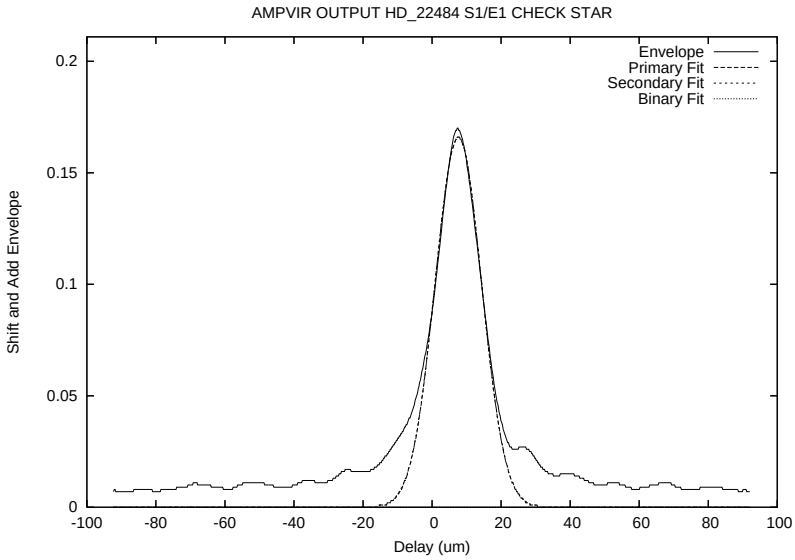


Figure. A.43: HD 22484 Fringe Envelope on 2007 October 19 on the E1/S1 Baseline.

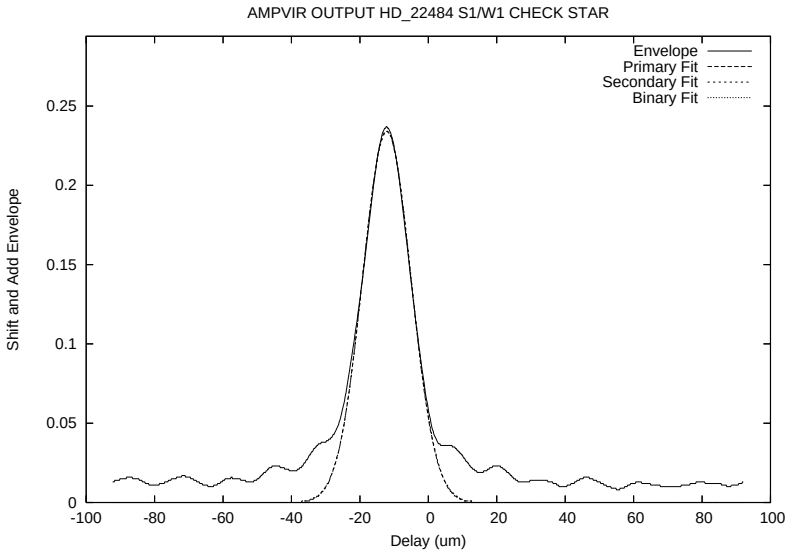


Figure. A.44: HD 22484 Fringe Envelope on 2007 October 19 on the W1/S1 Baseline.

## A.1.23 HD 25680

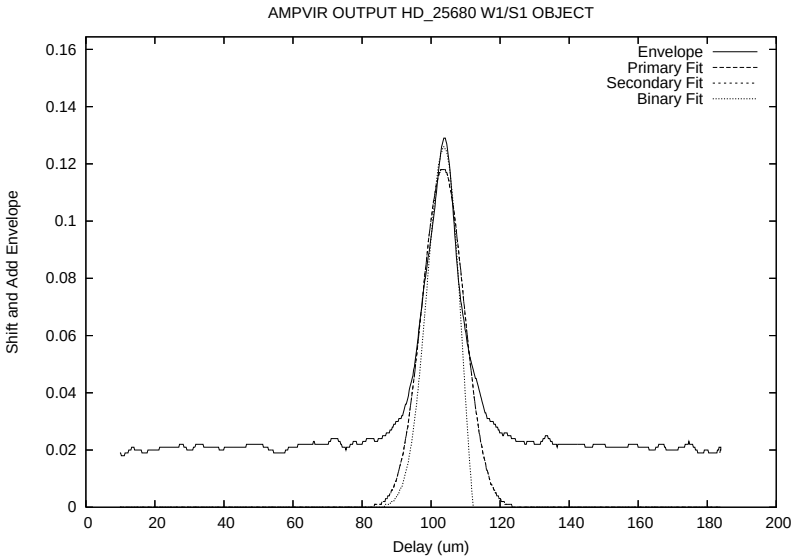


Figure. A.45: HD 25680 Fringe Envelope on 2005 October 2 on the W1/S1 Baseline.

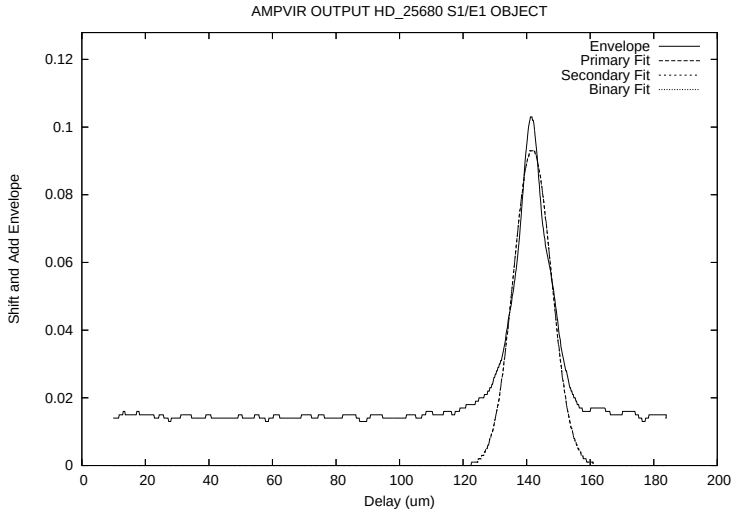


Figure. A.46: HD 25680 Fringe Envelope on 2005 October 6 on the E1/S1 Baseline.

### A.1.24 HD 25893

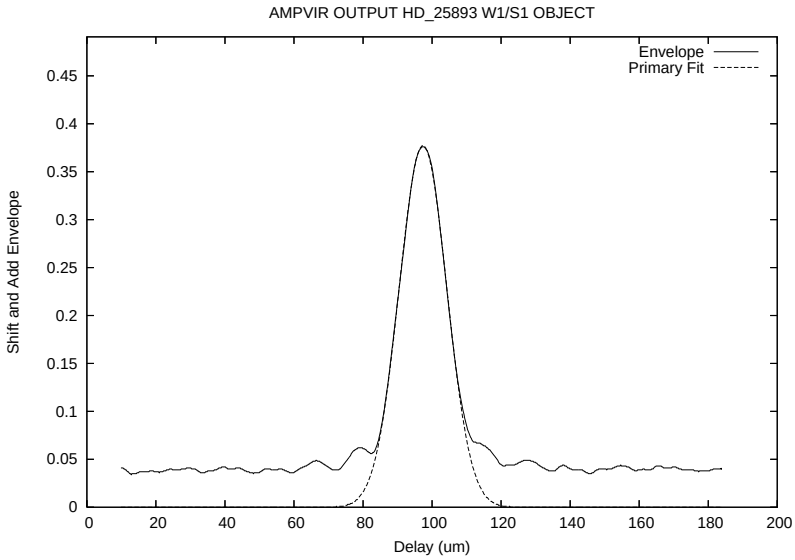


Figure. A.47: HD 25893 Fringe Envelope on 2005 September 18 on the W1/S1 Baseline.

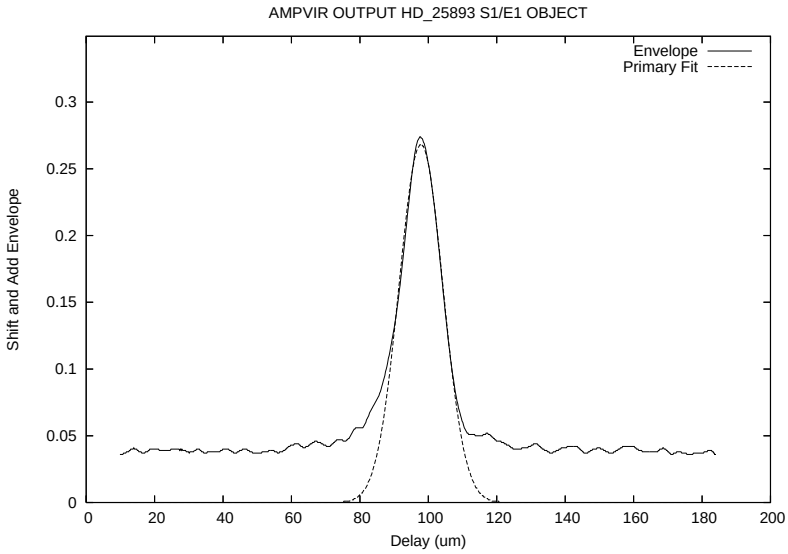


Figure. A.48: HD 25893 Fringe Envelope on 2006 September 19 on the E1/S1 Baseline.

## A.1.25 HD 25998

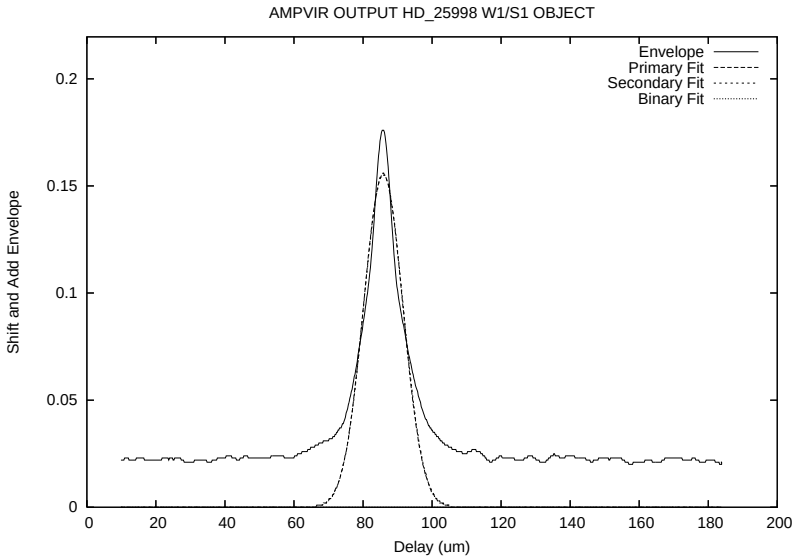


Figure. A.49: HD 25998 Fringe Envelope on 2005 September 29 on the W1/S1 Baseline.

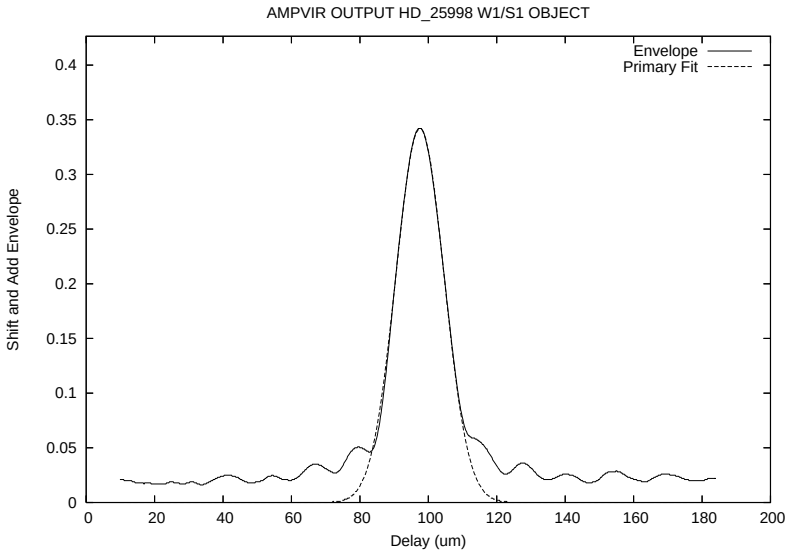


Figure. A.50: HD 25998 Fringe Envelope on 2006 September 19 on the W1/S1 Baseline.

### A.1.26 HD 29203

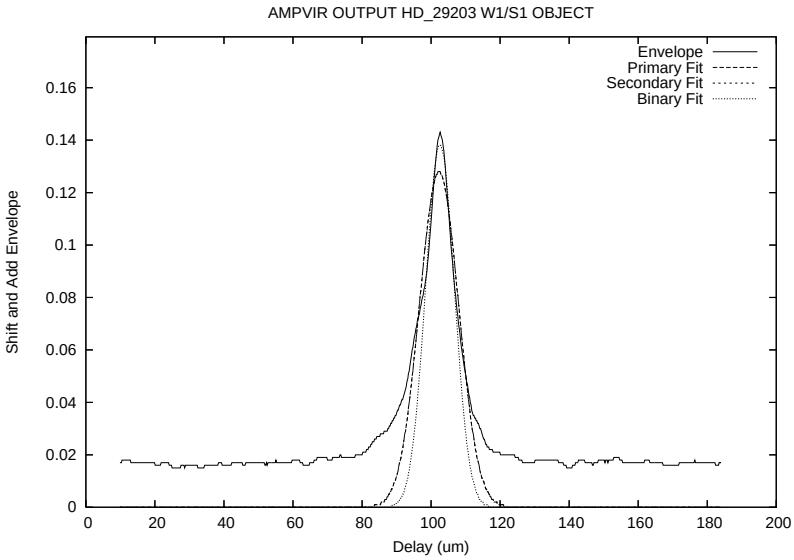


Figure. A.51: HD 29203 Fringe Envelope on 2005 September 29 on the W1/S1 Baseline.

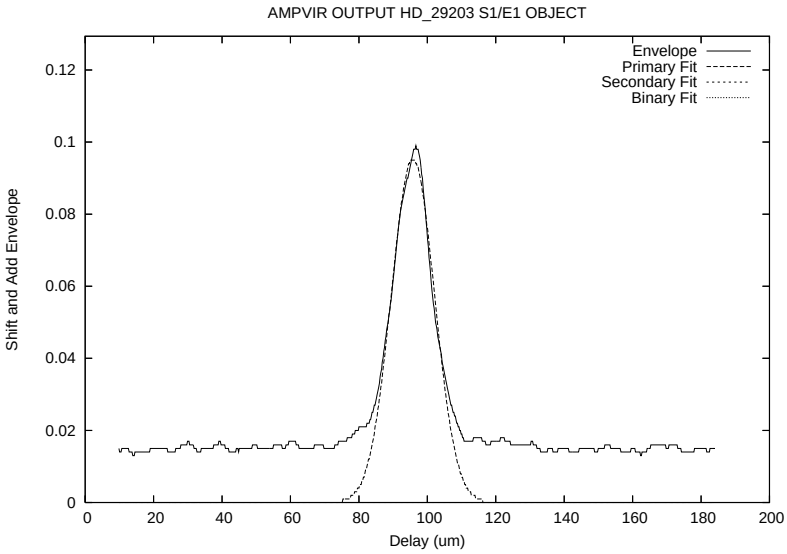


Figure. A.52: HD 29203 Fringe Envelope on 2005 October 11 on the E1/S1 Baseline.

## A.1.27 HD 30282

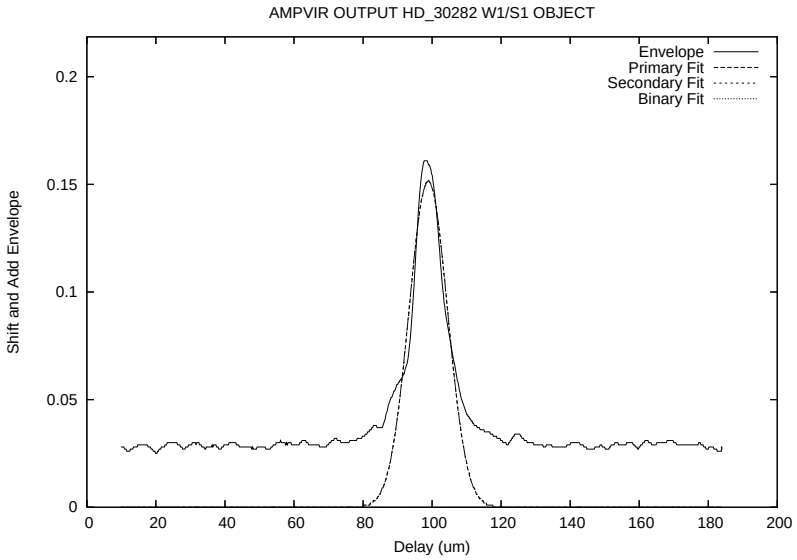


Figure. A.53: HD 30282 Fringe Envelope on 2005 September 29 on the W1/S1 Baseline.

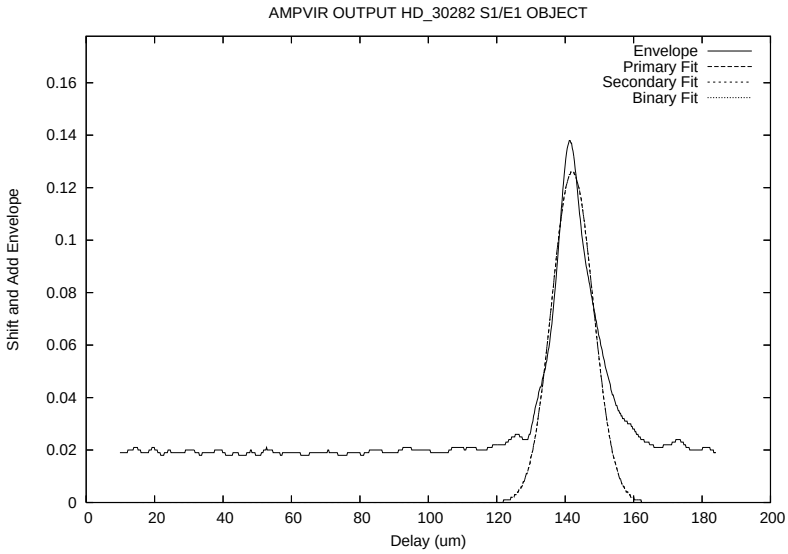


Figure. A.54: HD 30282 Fringe Envelope on 2005 October 6 on the E1/S1 Baseline.

## A.1.28 HD 30652

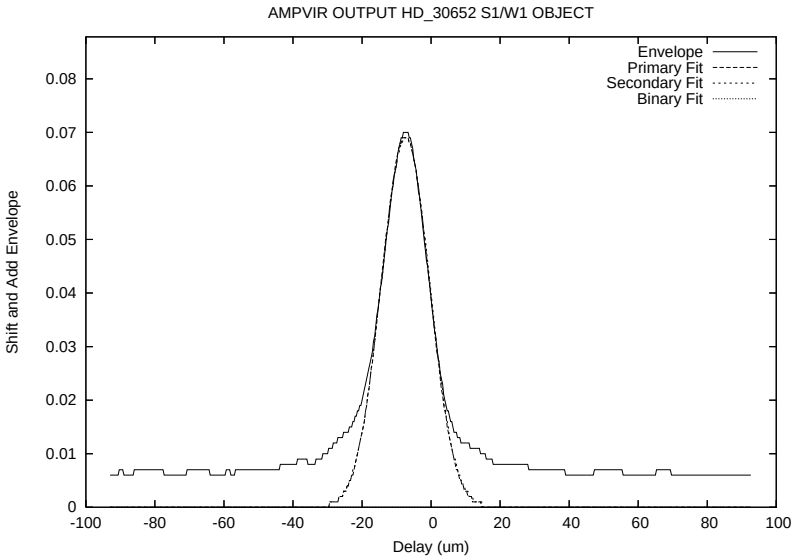


Figure. A.55: HD 30652 Fringe Envelope on 2007 October 19 on the W1/S1 Baseline.

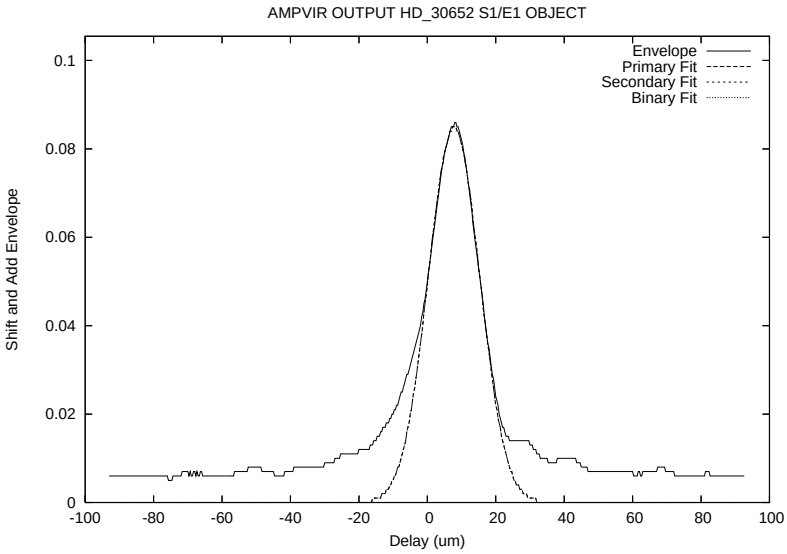


Figure. A.56: HD 30652 Fringe Envelope on 2007 October 19 on the E1/S1 Baseline.

## A.1.29 HD 32537

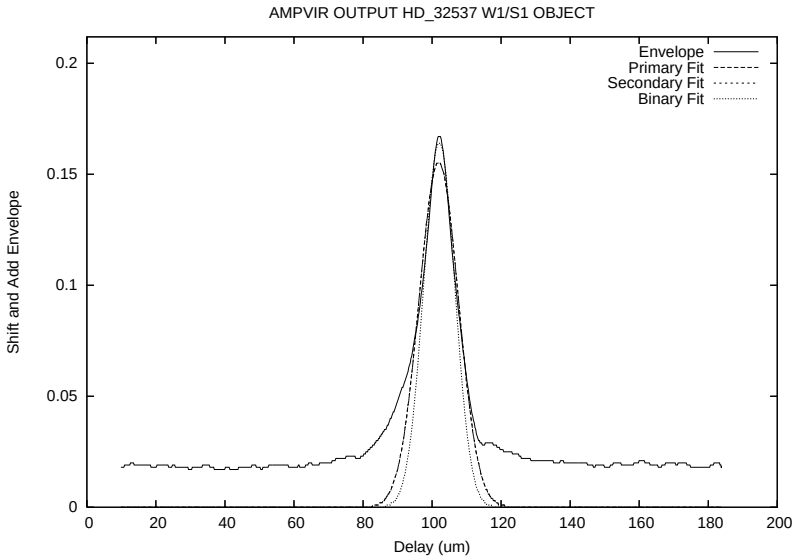


Figure. A.57: HD 32537 Fringe Envelope on 2005 September 29 on the W1/S1 Baseline.

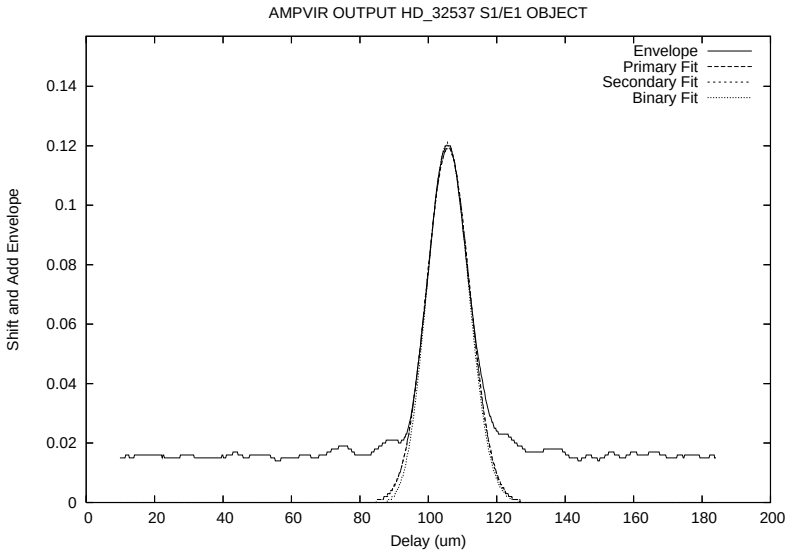


Figure. A.58: HD 32537 Fringe Envelope on 2005 October 11 on the E1/S1 Baseline.

### A.1.30 HD 33564

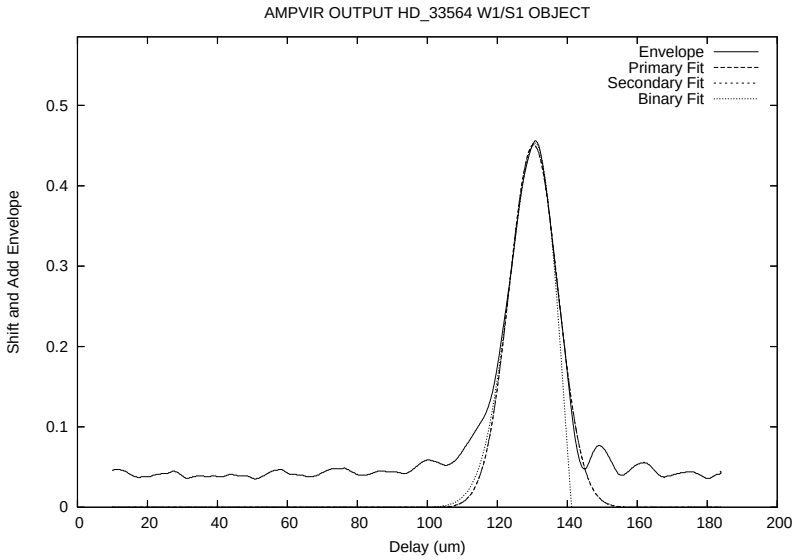


Figure. A.59: HD 33564 Fringe Envelope on 2006 September 10 on the W1/S1 Baseline.

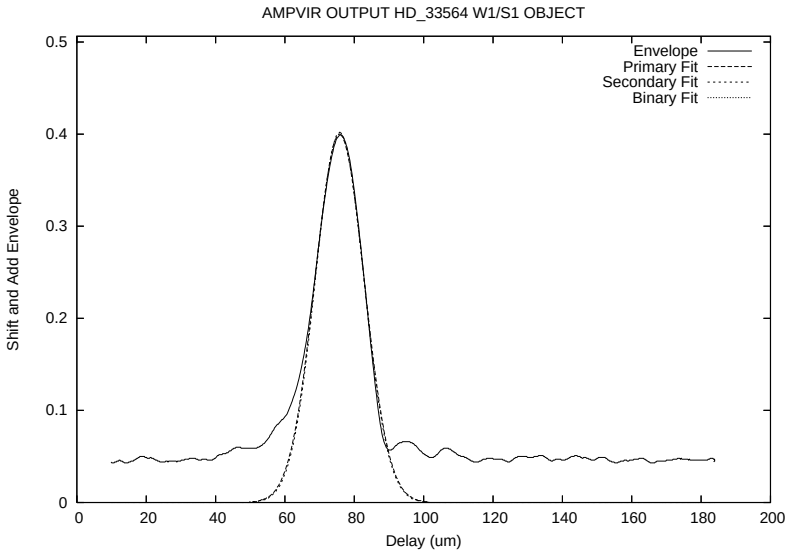


Figure. A.60: HD 33564 Fringe Envelope on 2006 September 11 on the W1/S1 Baseline.

### A.1.31 HD 34411

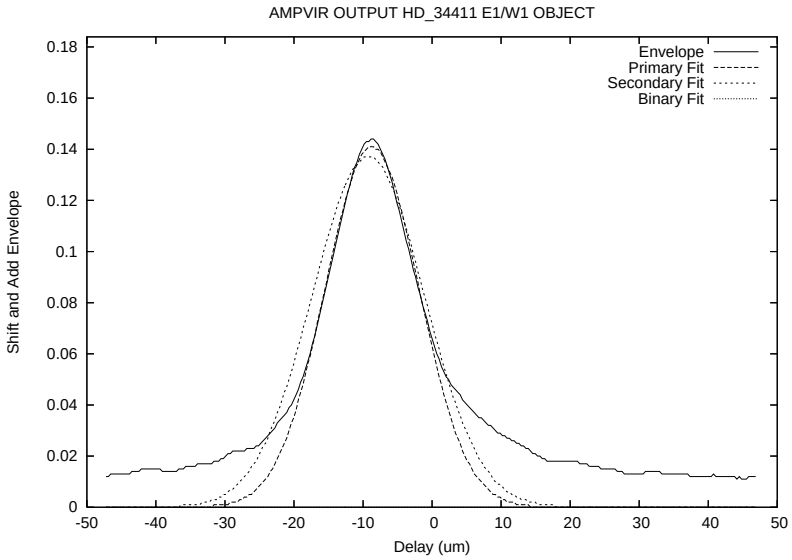


Figure. A.61: HD 34411 Fringe Envelope on 2007 November 3 on the E1/S1 Baseline.

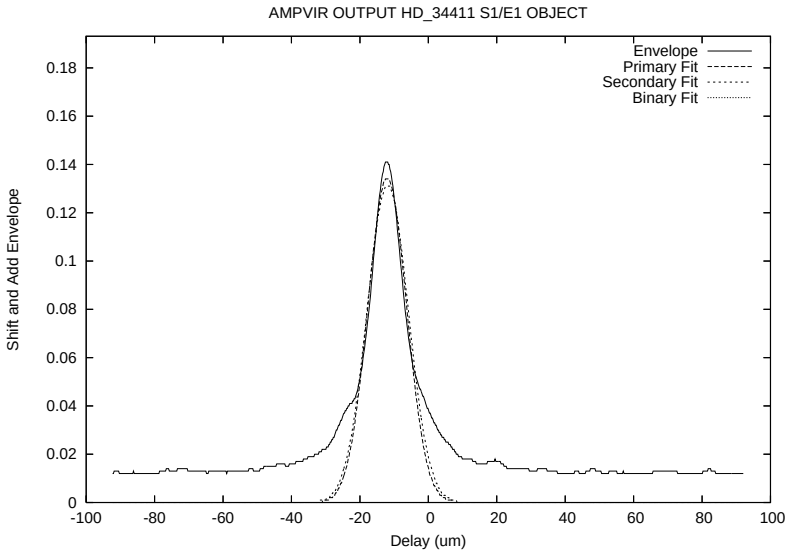


Figure. A.62: HD 34411 Fringe Envelope on 2007 November 11 on the E1/S1 Baseline.

## A.1.32 HD 35296

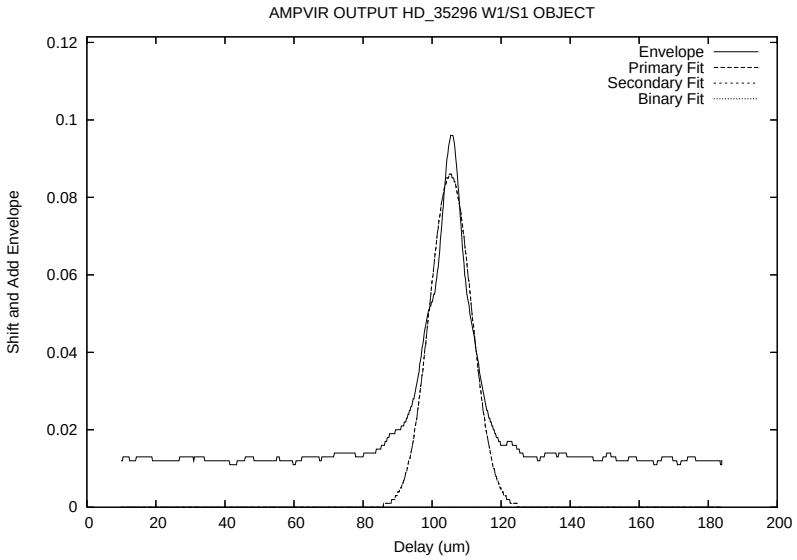


Figure. A.63: HD 35296 Fringe Envelope on 2005 October 2 on the W1/S1 Baseline.

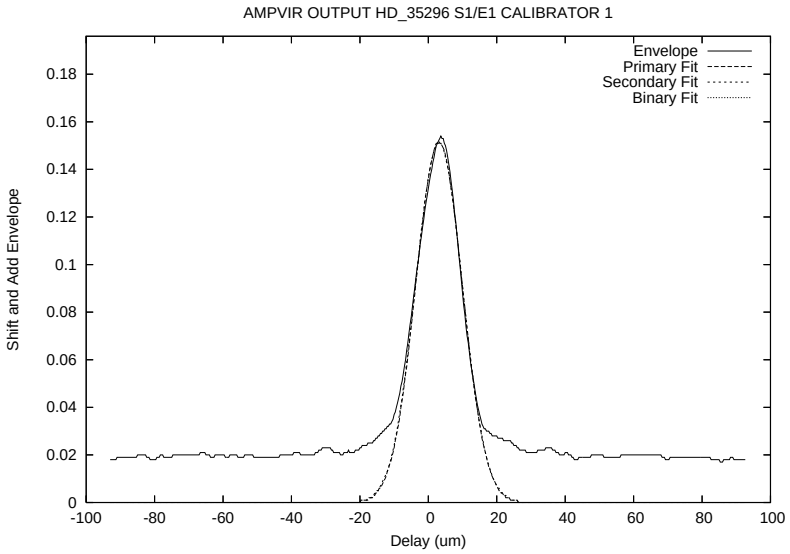


Figure. A.64: HD 35296 Fringe Envelope on 2007 September 15 on the E1/S1 Baseline.

### A.1.33 HD 39587

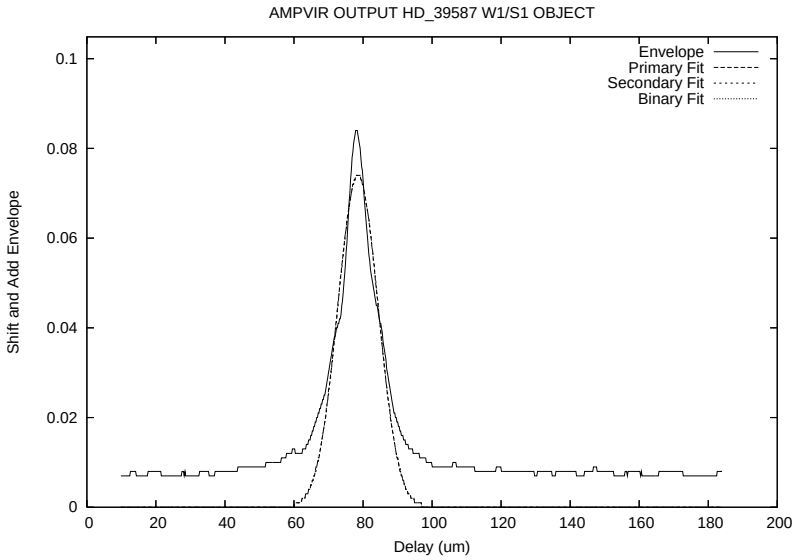


Figure. A.65: HD 39587 Fringe Envelope on 2005 October 2 on the W1/S1 Baseline.

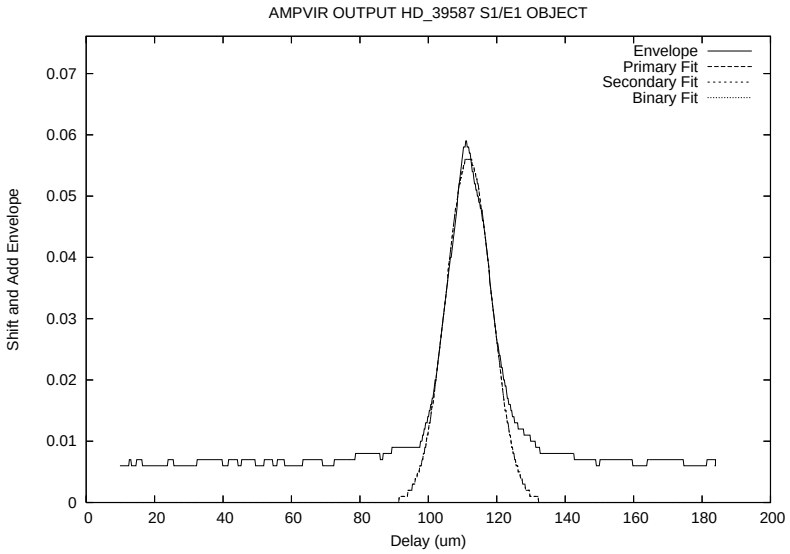


Figure. A.66: HD 39587 Fringe Envelope on 2005 October 6 on the E1/S1 Baseline.

### A.1.34 HD 41330

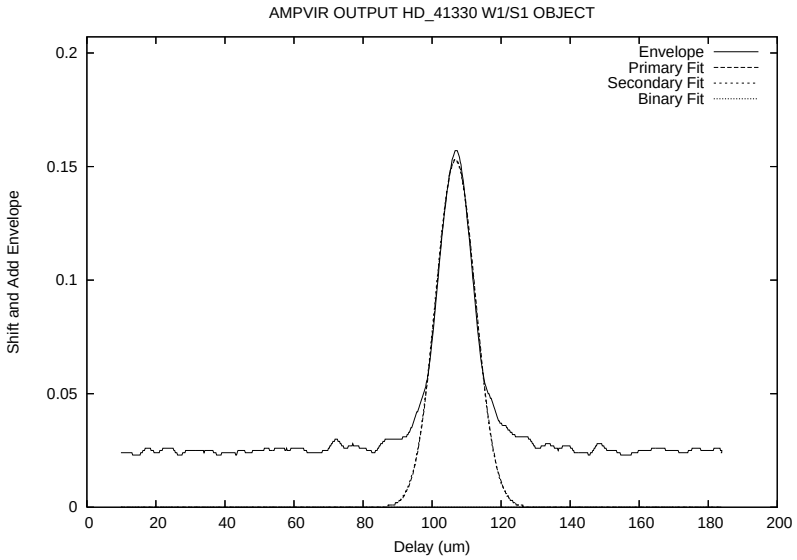


Figure. A.67: HD 41330 Fringe Envelope on 2005 September 29 on the W1/S1 Baseline.

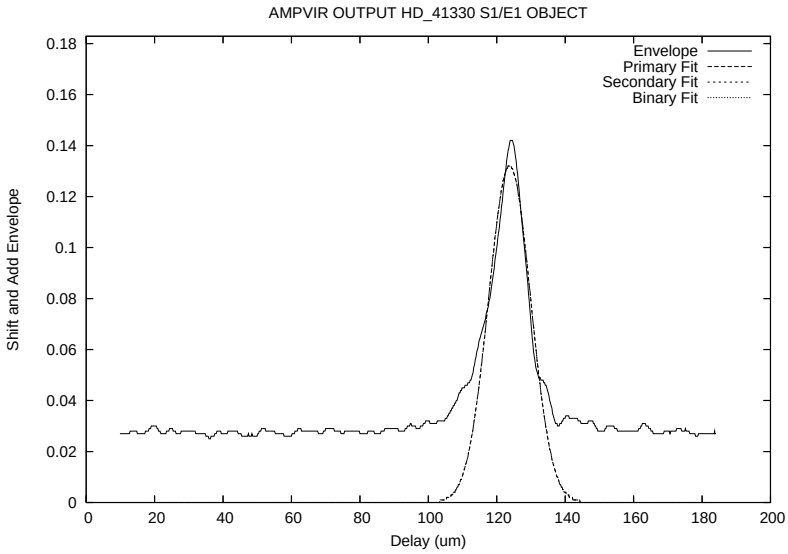


Figure. A.68: HD 41330 Fringe Envelope on 2005 October 11 on the E1/S1 Baseline.

## A.1.35 HD 42807

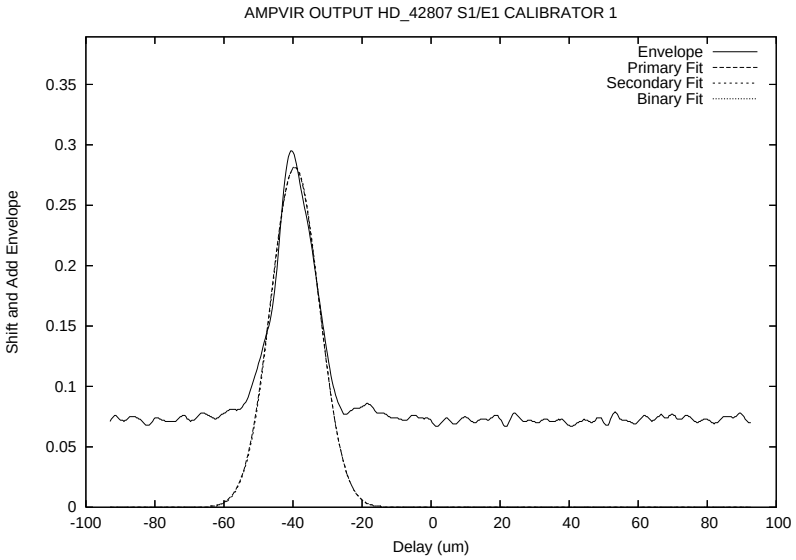


Figure. A.69: HD 42807 Fringe Envelope on 2007 March 20 on the E1/S1 Baseline.

## A.1.36 HD 43821

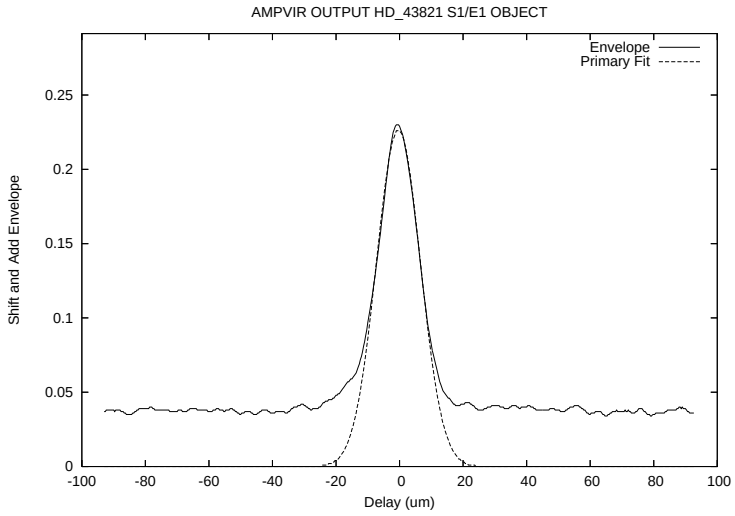


Figure. A.70: HD 43821 Fringe Envelope on 2007 March 20 on the E1/S1 Baseline.

## A.1.37 HD 43587

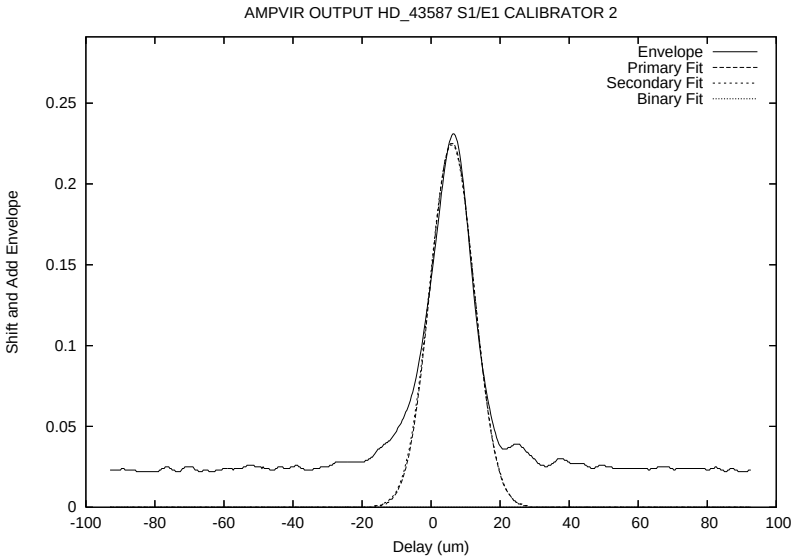


Figure. A.71: HD 43587 Fringe Envelope on 2007 Feburary 25 on the E1/S1 Baseline.

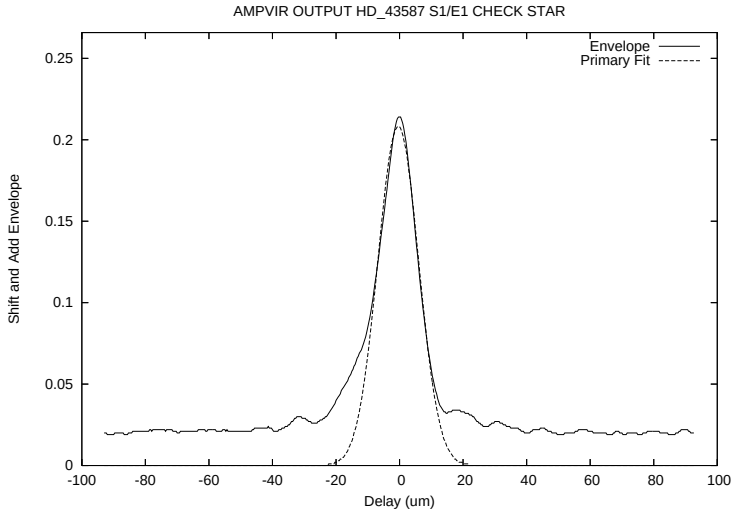


Figure. A.72: HD 43587 Fringe Envelope on 2007 Feburary 25 on the E1/S1 Baseline.

### A.1.38 HD 45088

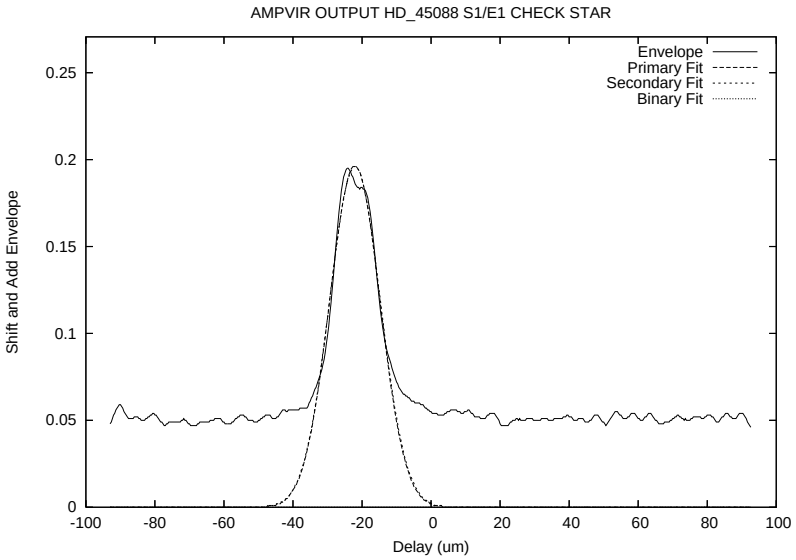


Figure. A.73: HD 45088 Fringe Envelope on 2007 March 20 on the E1/S1 Baseline.

### A.1.39 HD 48682

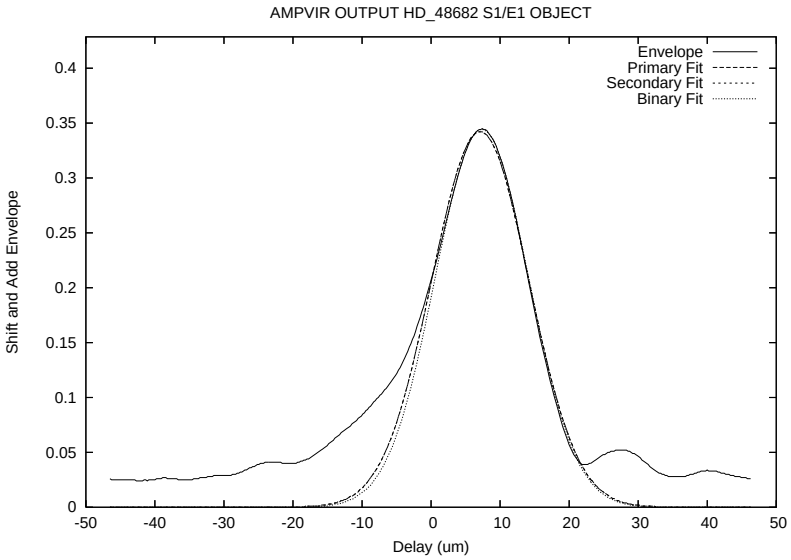


Figure. A.74: HD 48682 Fringe Envelope on 2007 December 24 on the E1/S1 Baseline.

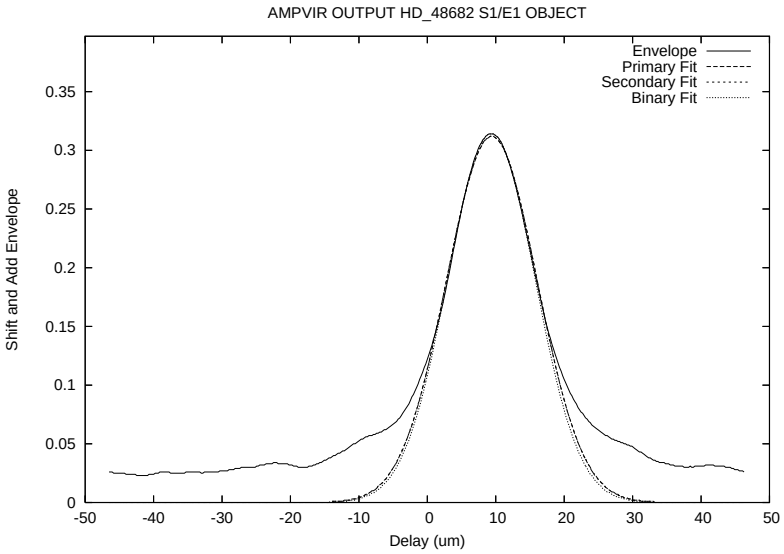


Figure. A.75: HD 48682 Fringe Envelope on 2007 December 24 on the E1/S1 Baseline.

# A.2 Observed Stars Right Ascension 07-12 Hours

## A.2.1 HD 52711

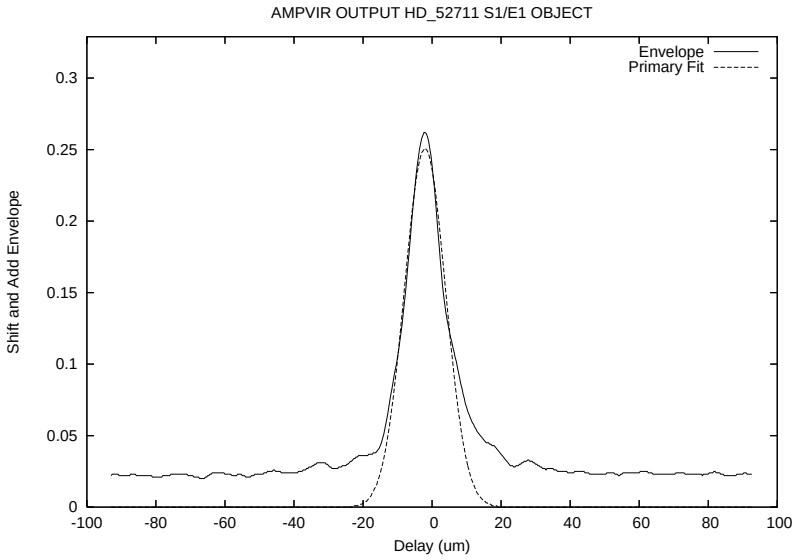


Figure. A.76: HD 52711 Fringe Envelope on 2007 January 17 on the E1/S1 Baseline.

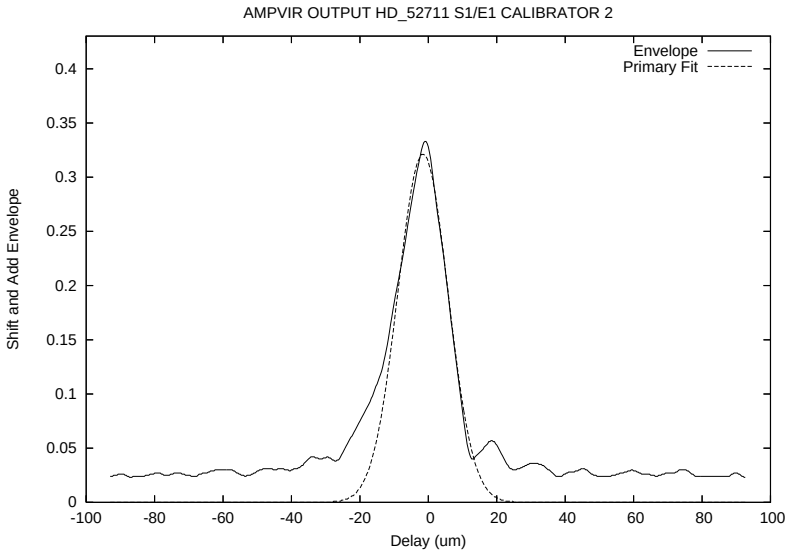


Figure. A.77: HD 52711 Fringe Envelope on 2007 January 25 on the E1/S1 Baseline.

## A.2.2 HD 58946

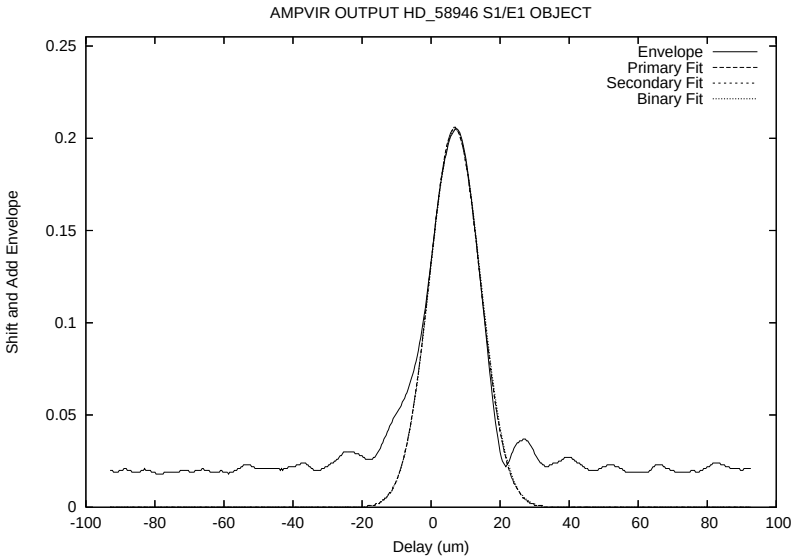


Figure. A.78: HD 58946 Fringe Envelope on 2007 January 17 on the E1/S1 Baseline.

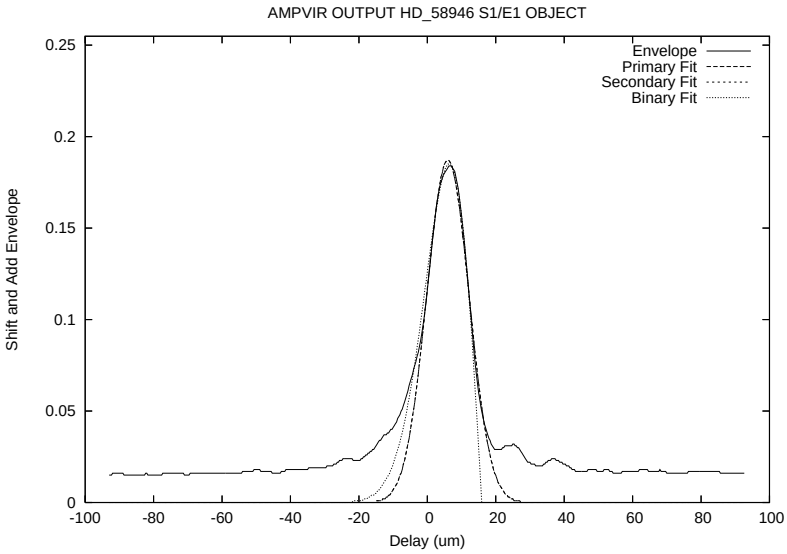


Figure. A.79: HD 58946 Fringe Envelope on 2007 Feburary 3 on the E1/S1 Baseline.

### A.2.3 HD 61859

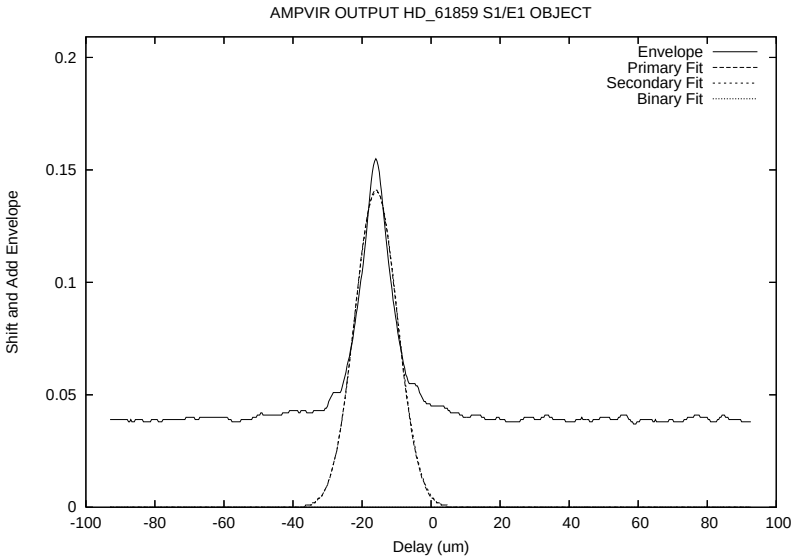


Figure. A.80: HD 61859 Fringe Envelope on 2007 January 17 on the E1/S1 Baseline.

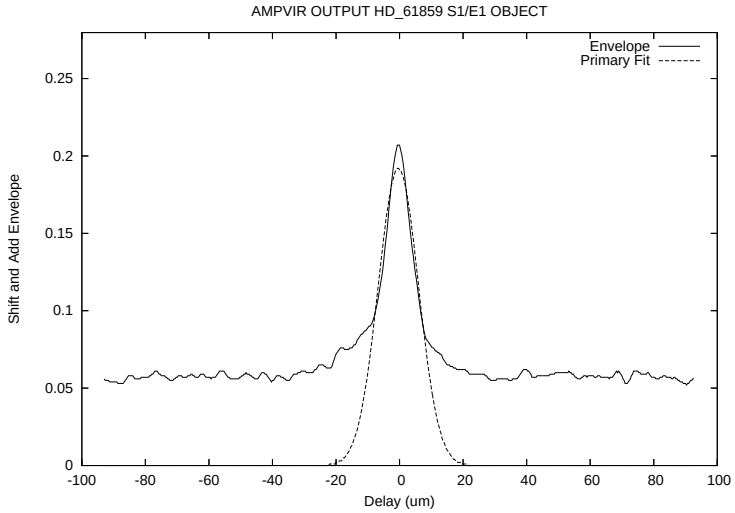


Figure. A.81: HD 61859 Fringe Envelope on 2007 Feburary 3 on the E1/S1 Baseline.

## A.2.4 HD 62613

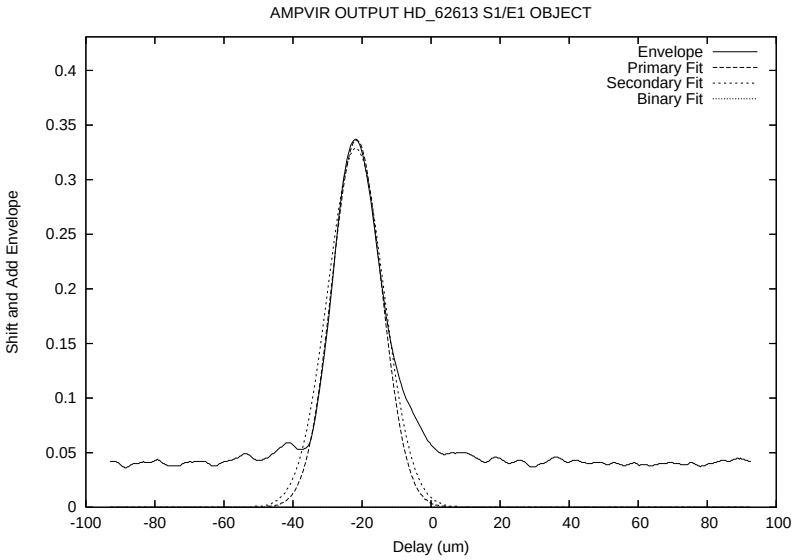


Figure. A.82: HD 62613 Fringe Envelope on 2007 April 3 on the E1/S1 Baseline.

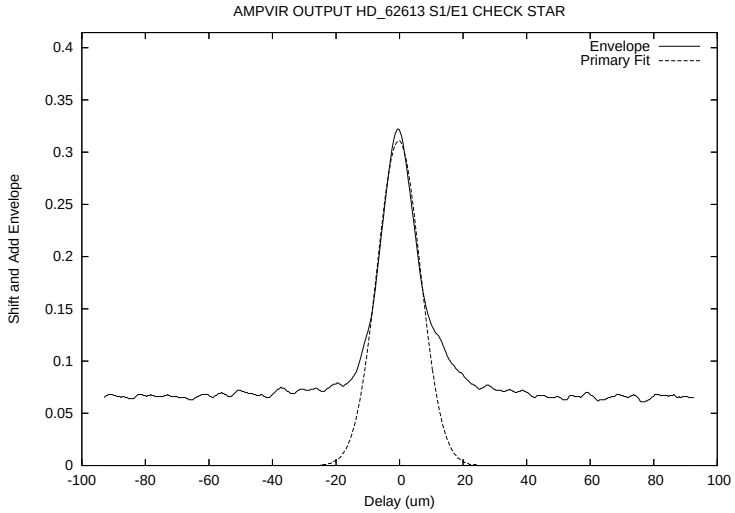


Figure. A.83: HD 62613 Fringe Envelope on 2007 April 14 on the E1/S1 Baseline.

## A.2.5 HD 69897

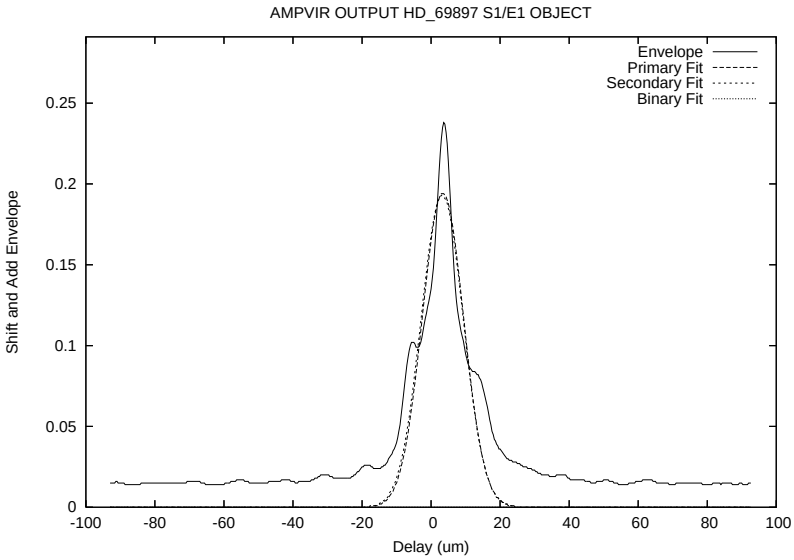


Figure. A.84: HD 69897 Fringe Envelope on 2007 January 17 on the E1/S1 Baseline.

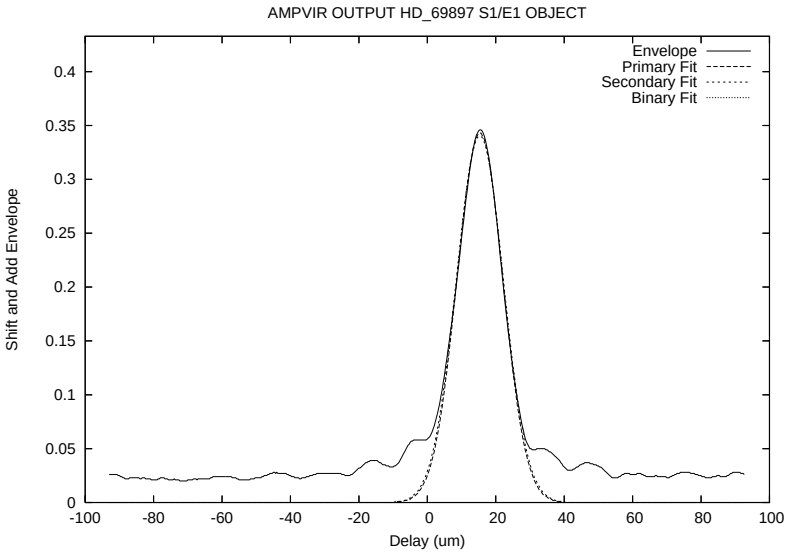


Figure. A.85: HD 69897 Fringe Envelope on 2007 Feburary 4 on the E1/S1 Baseline.

### A.2.6 HD 71148

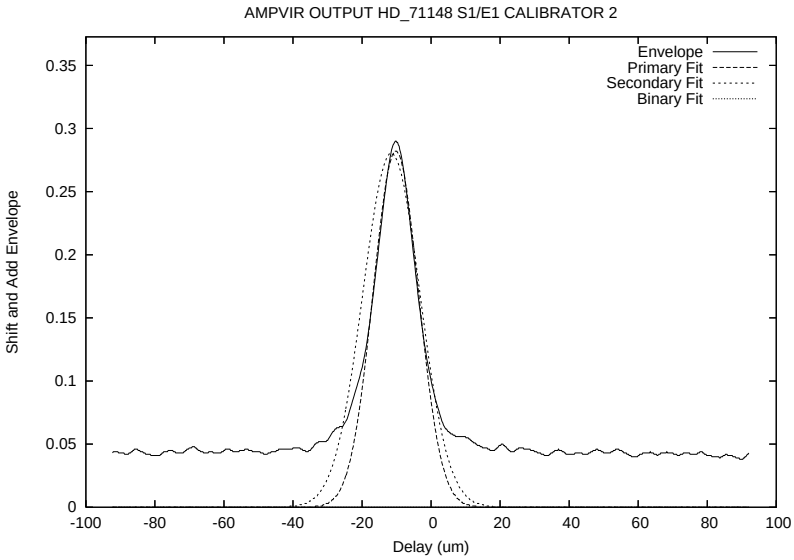


Figure. A.86: HD 71148 on 2007 November 14 on the E1/S1 Baseline.

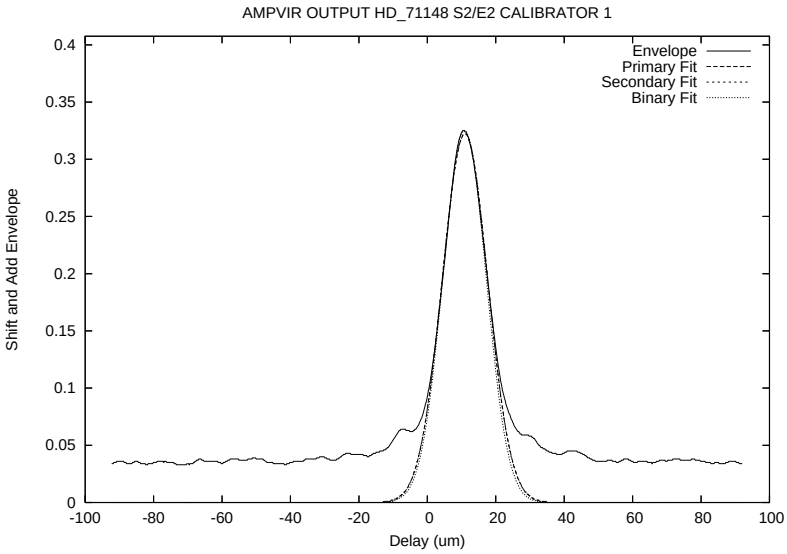


Figure. A.87: HD 71148 Fringe Envelope on 2007 November 19 on the E2/S2 Baseline.

## A.2.7 HD 72905

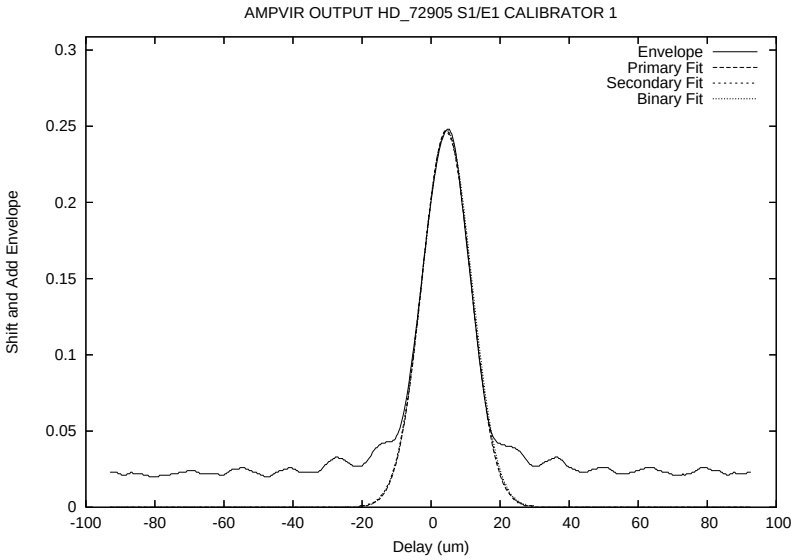


Figure. A.88: HD 72905 Fringe Envelope on 2007 April 14 on the E1/S1 Baseline.

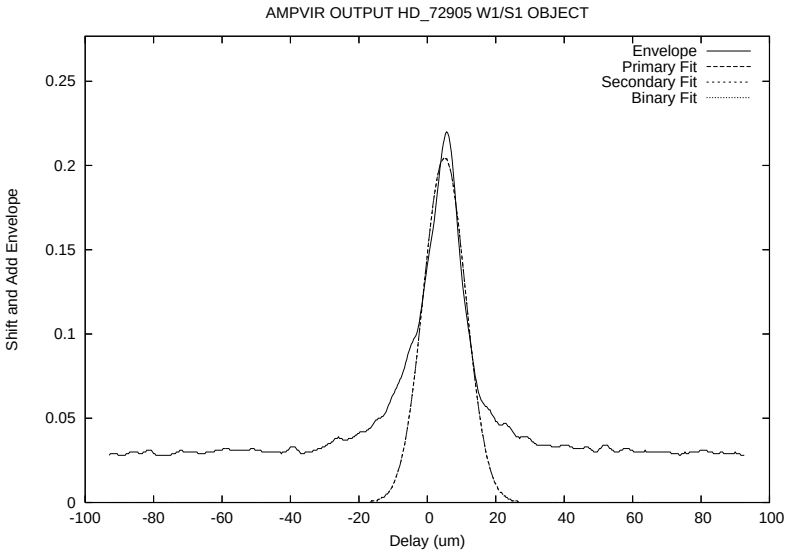


Figure. A.89: HD 72905 Fringe Envelope on 2007 April 17 on the W1/S1 Baseline.

## A.2.8 HD 72945

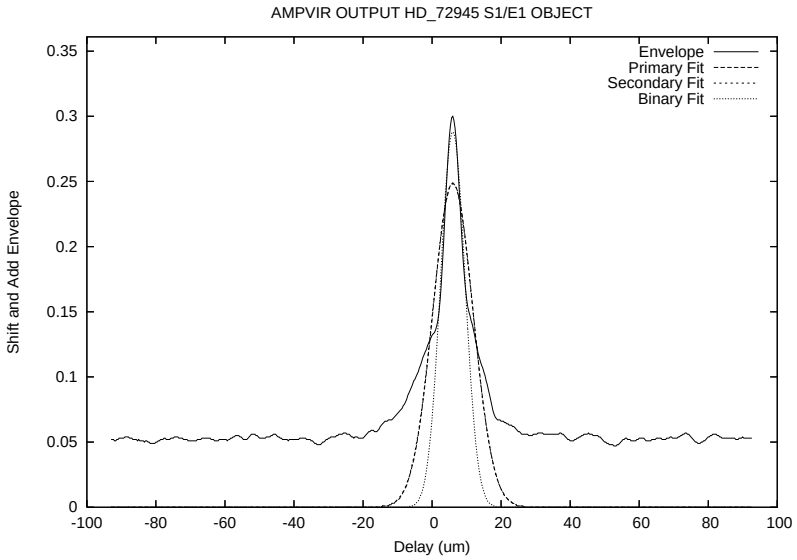


Figure. A.90: HD 72945 Fringe Envelope on 2007 Feburary 25 on the E1/S1 Baseline.

## A.2.9 HD 76943

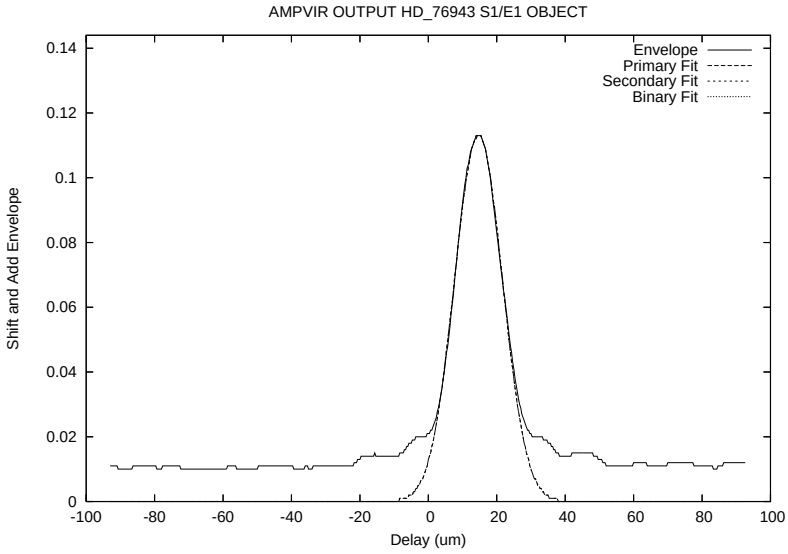


Figure. A.91: HD 76943 Fringe Envelope on 2007 Feburary 3 on the E1/S1 Baseline.

### A.2.10 HD 75732

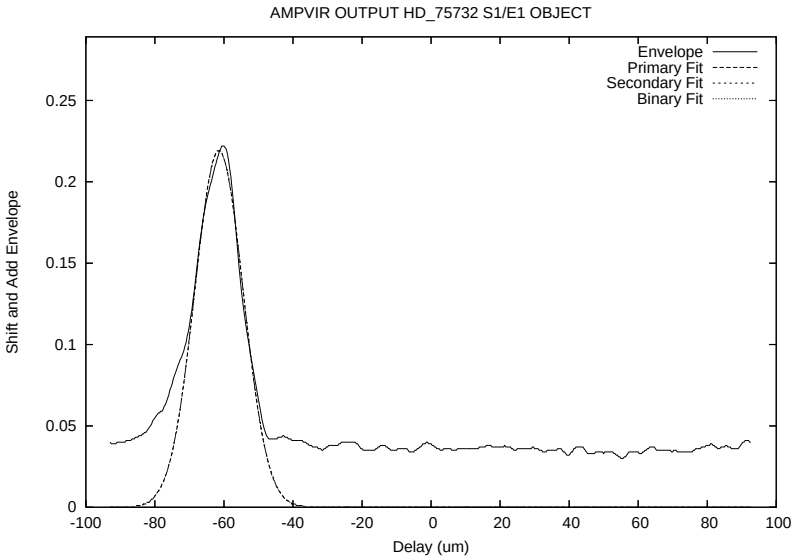


Figure. A.92: HD 75732 Fringe Envelope on 2007 Feburary 3 on the E1/S1 Baseline.

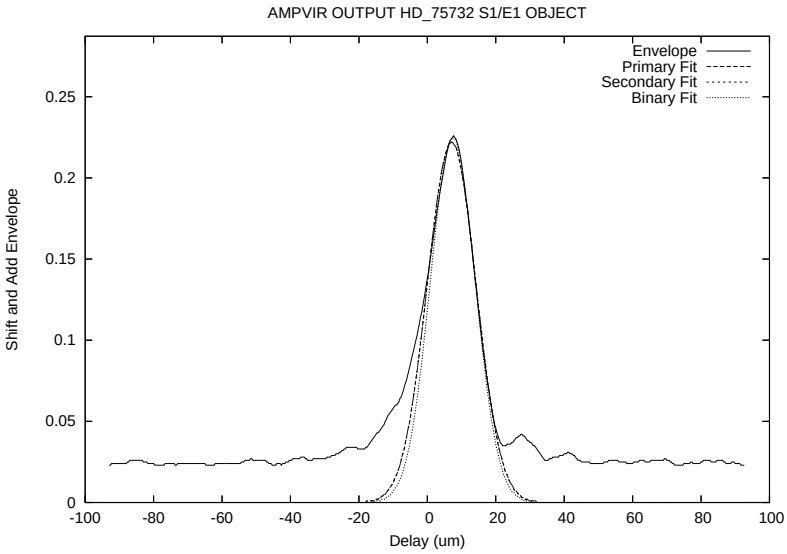


Figure. A.93: HD 75732 Fringe Envelope on 2007 Feburary 6 on the E1/S1 Baseline.

## A.2.11 HD 78154

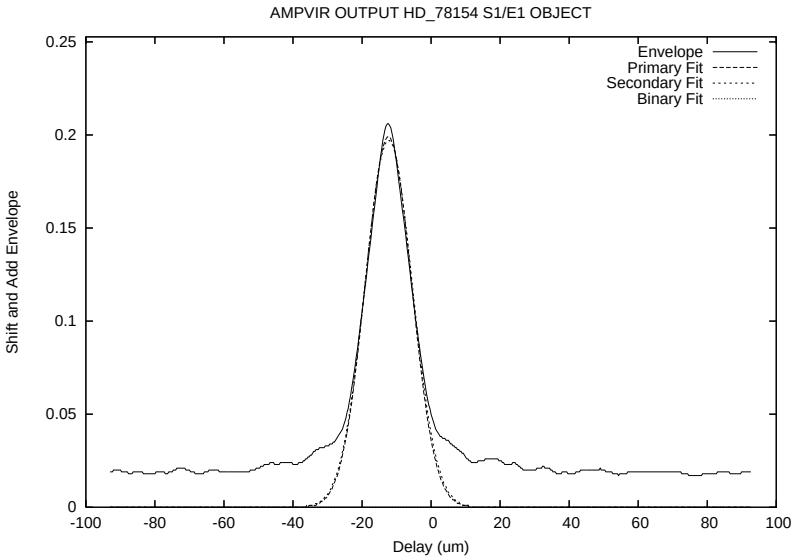


Figure. A.94: HD 78154 Fringe Envelope on 2007 April 3 on the E1/S1 Baseline.

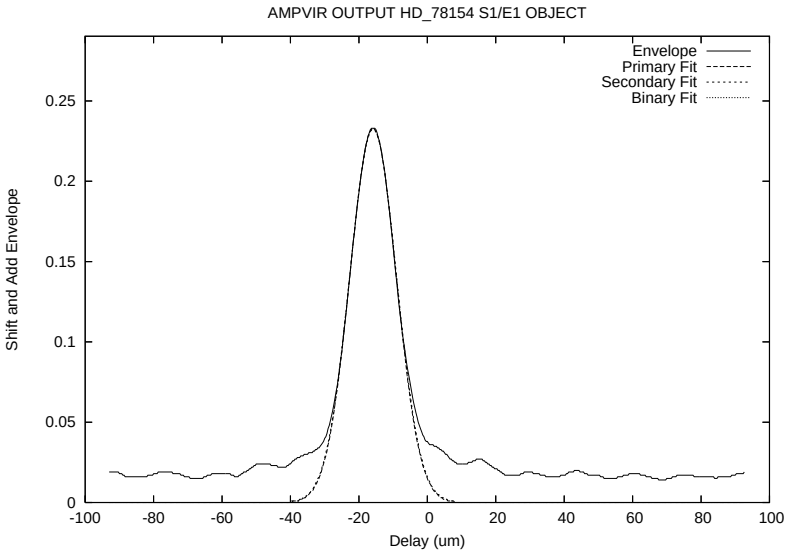


Figure. A.95: HD 78154 Fringe Envelope on 2007 April 3 on the E1/S1 Baseline.

## A.2.12 HD 79028

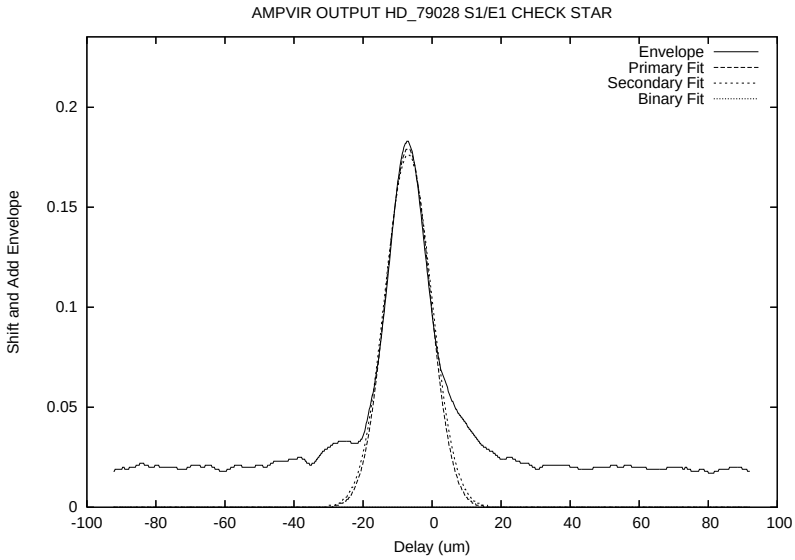


Figure. A.96: HD 79028 Fringe Envelope on 2007 November 14 on the E1/S1 Baseline.

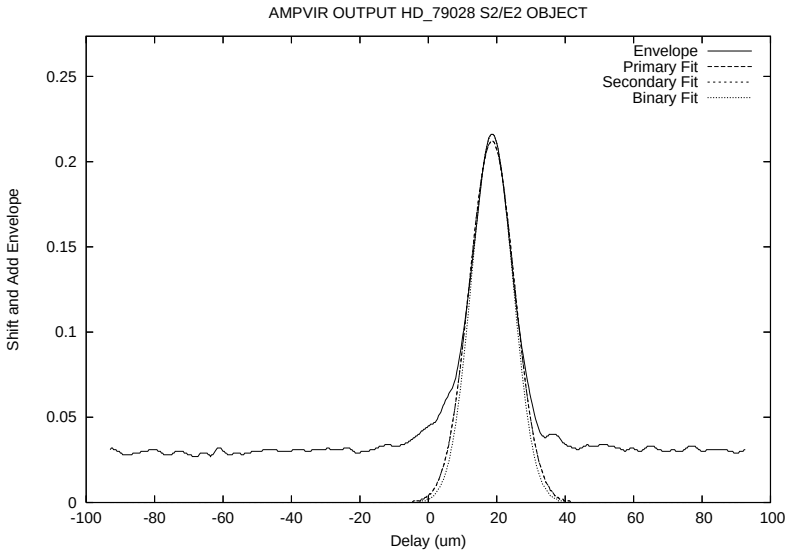


Figure. A.97: HD 79028 Fringe Envelope on 2007 November 19 on the E2/S2 Baseline.

## A.2.13 HD 82328

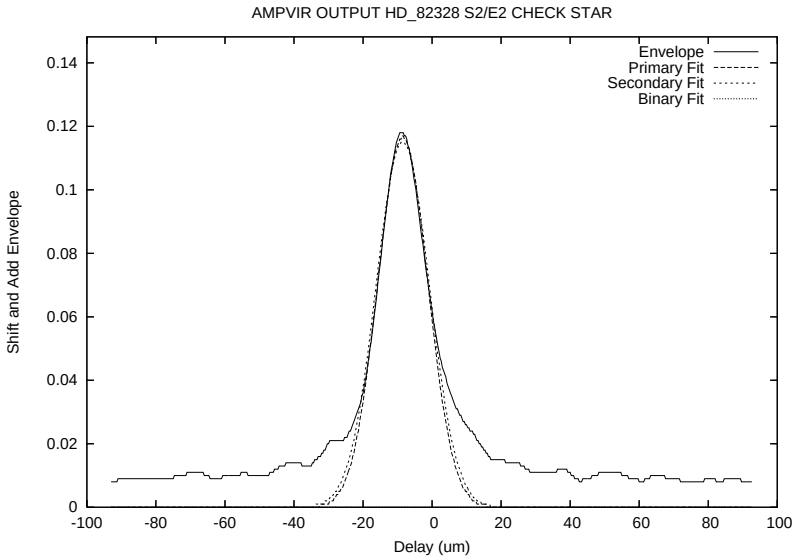


Figure. A.98: HD 82328 Fringe Envelope on 2007 November 14 on the E1/S1 Baseline.

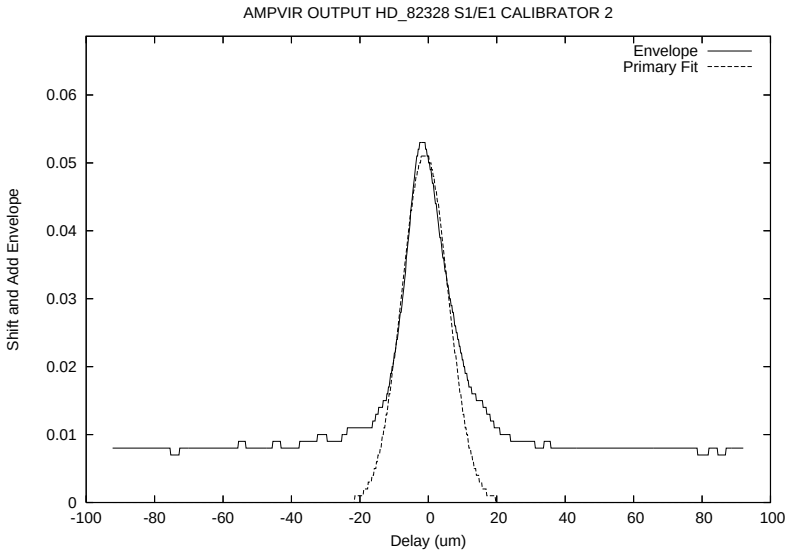


Figure. A.99: HD 82328 Fringe Envelope on 2007 November 19 on the E2/S2 Baseline.

## A.2.14 HD 84737

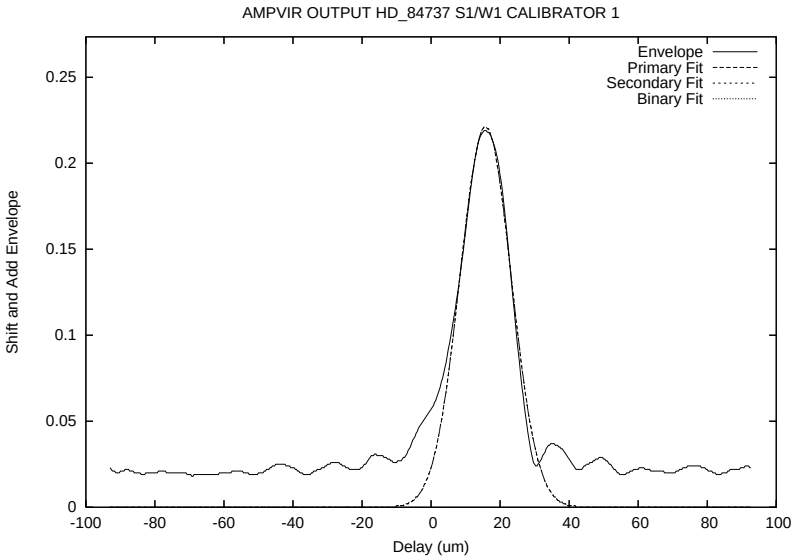


Figure. A.100: HD 84737 Fringe Envelope on 2007 May 28 on the W1/S1 Baseline.

## A.2.15 HD 89125

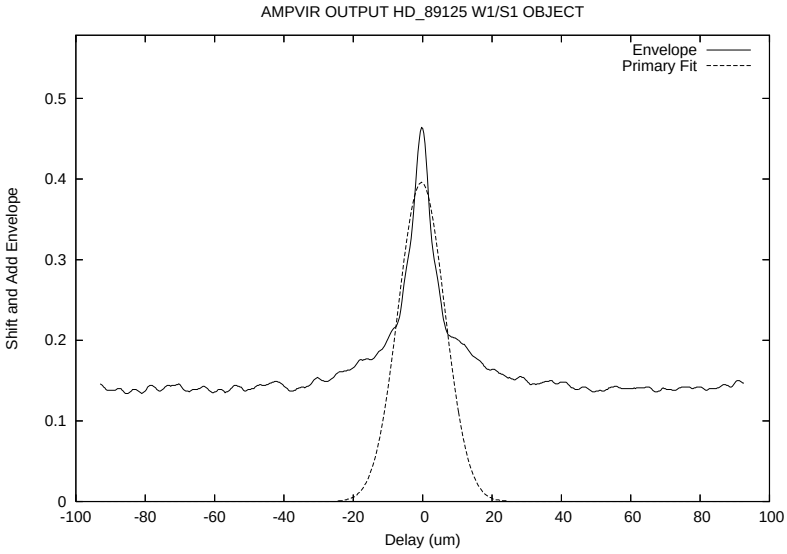


Figure. A.101: HD 89125 Fringe Envelope on 2007 June 1 on the W1/S1 Baseline.

## A.2.16 HD 86728

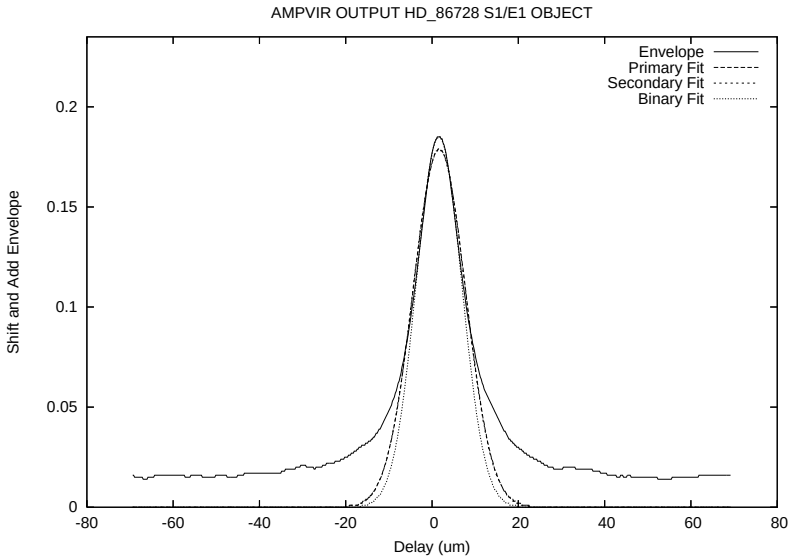


Figure. A.102: HD 86728 Fringe Envelope on 2007 November 15 on the E1/S1 Baseline.

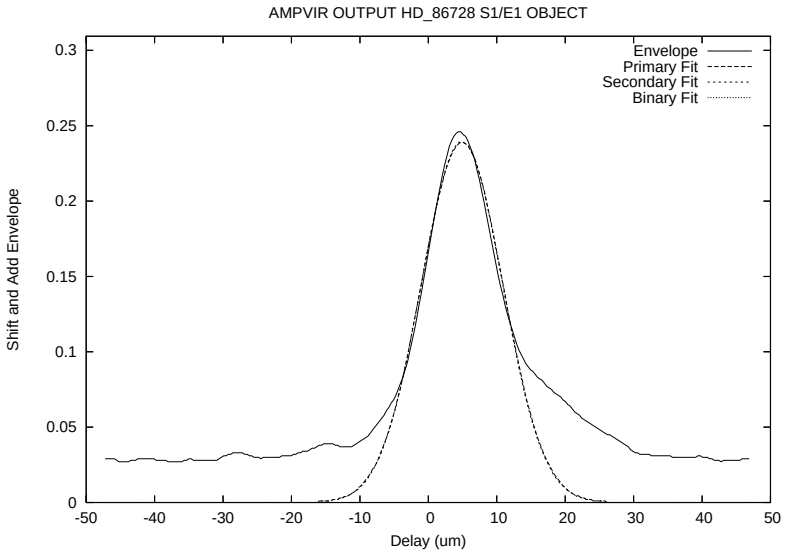


Figure. A.103: HD 86728 Fringe Envelope on 2007 November 16 on the E1/S1 Baseline.

## A.2.17 HD 90089

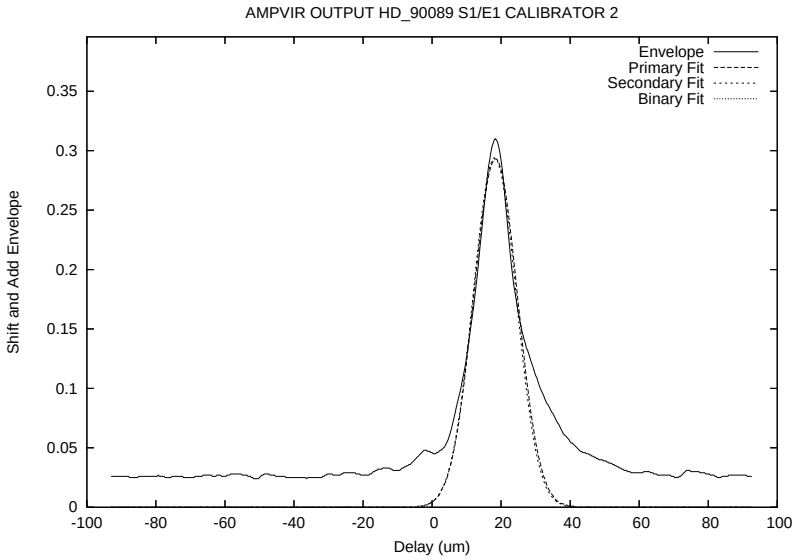


Figure. A.104: HD 90089 Fringe Envelope on 2007 April 11 on the E1/S1 Baseline.

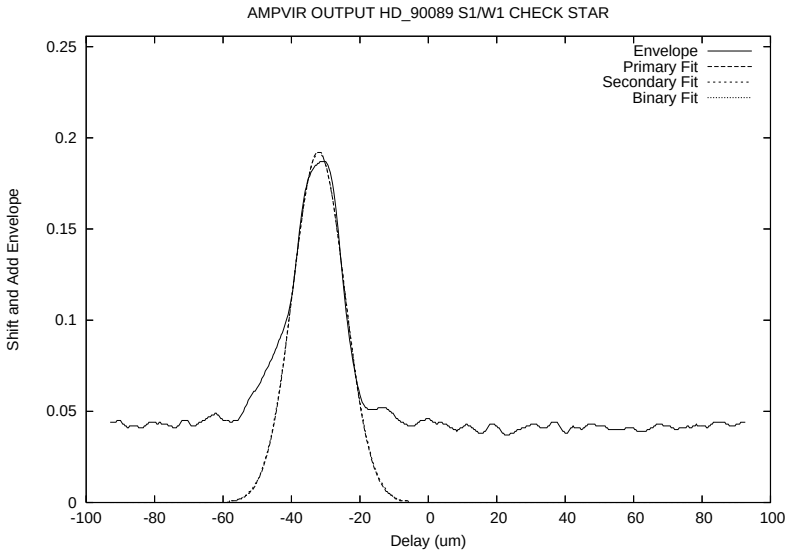


Figure. A.105: HD 90089 Fringe Envelope on 2007 May 28 on the W1/S1 Baseline.

## A.2.18 HD 90508

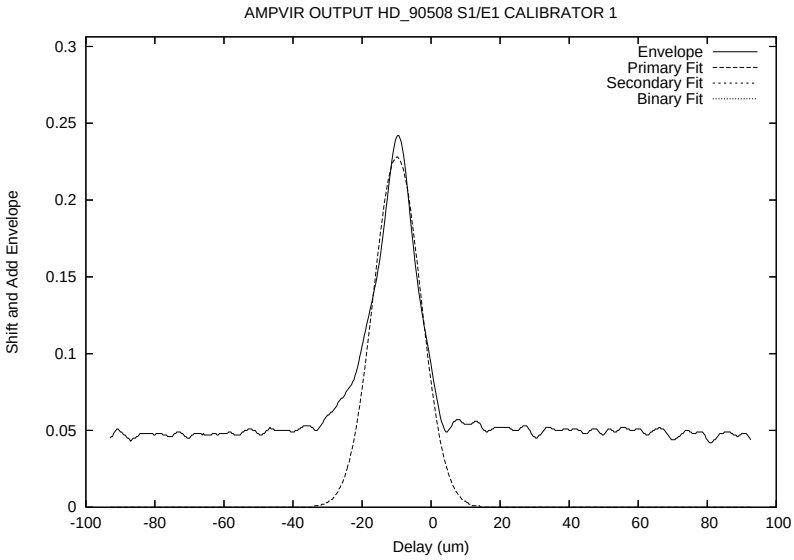


Figure. A.106: HD 90508 Fringe Envelope on 2007 April 14 on the E1/S1 Baseline.

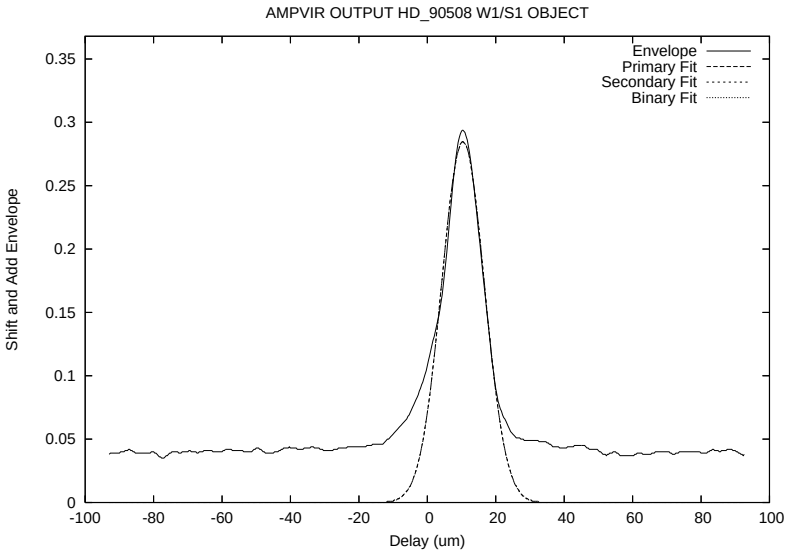


Figure. A.107: HD 90508 Fringe Envelope on 2007 April 17 on the W1/S1 Baseline.

## A.2.19 HD 90839

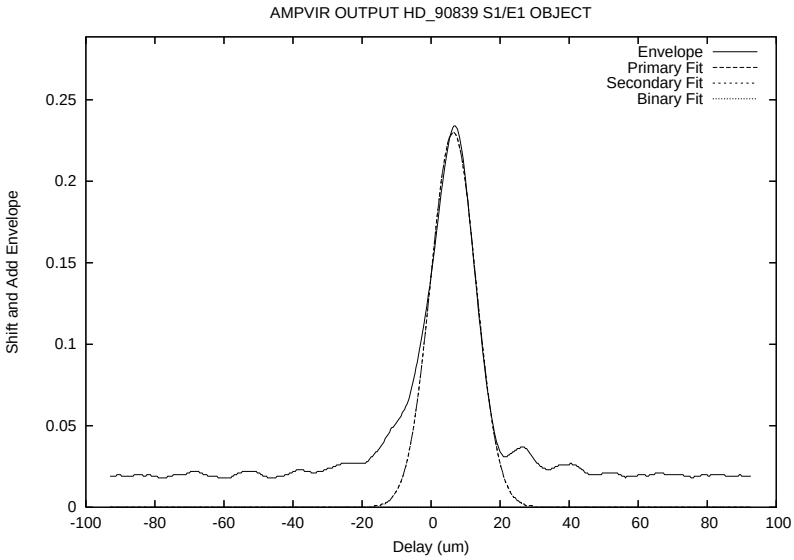


Figure. A.108: HD 90839on 2007 April 3 on the E1/S1 Baseline.

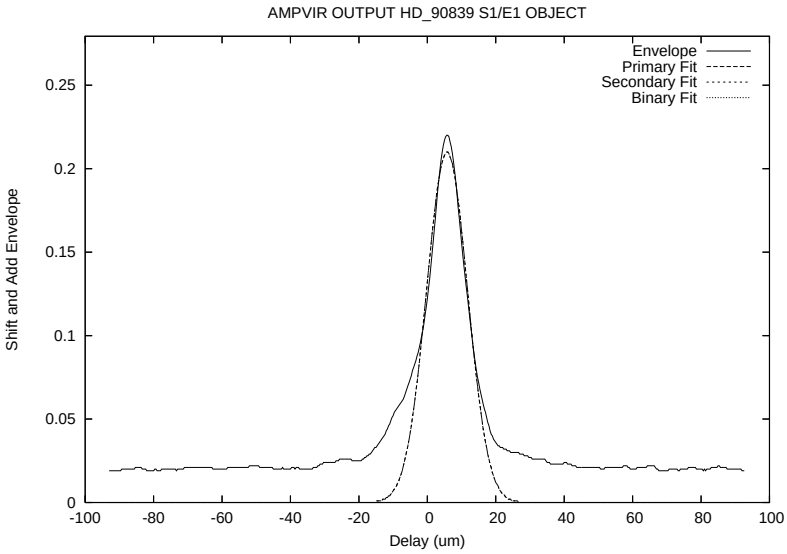


Figure. A.109: HD 90839 Fringe Envelope on 2007 April 11 on the E1/S1 Baseline.

## A.2.20 HD 95128

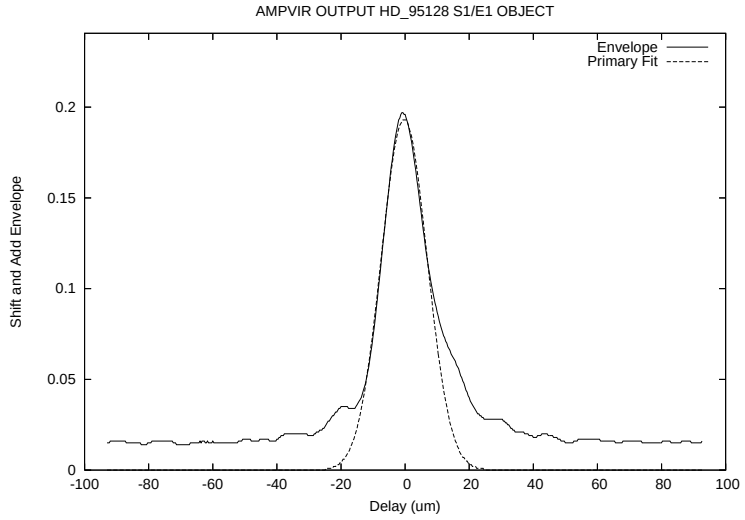


Figure. A.110: HD 95128 Fringe Envelope on 2007 January 19 on the E1/S1 Baseline.

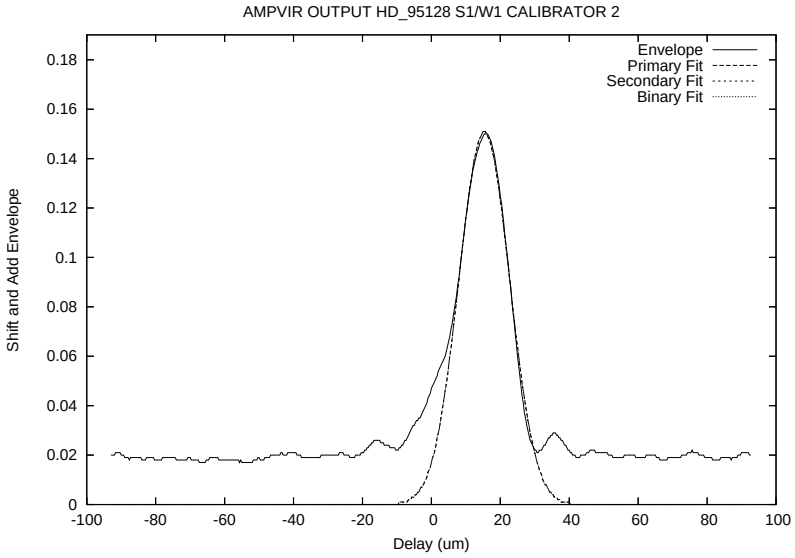


Figure. A.111: HD 95128 Fringe Envelope on 2007 May 28 on the W1/S1 Baseline.

## A.2.21 HD 98231

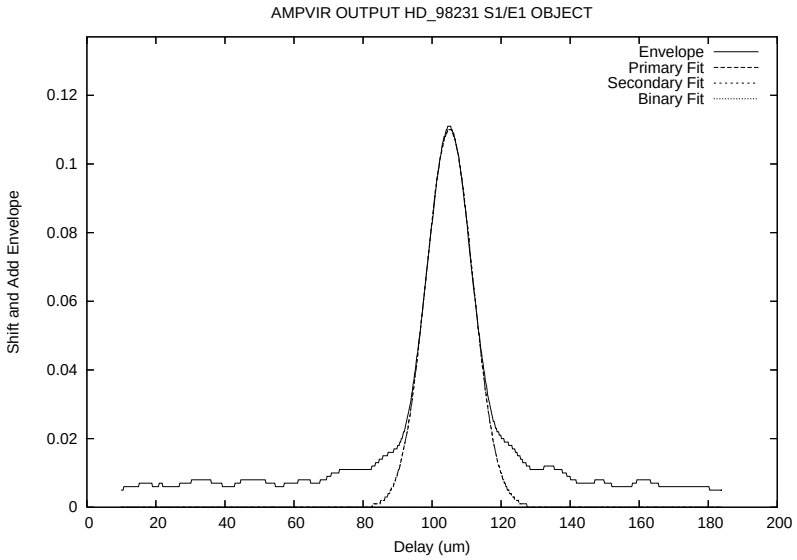


Figure. A.112: HD 98231 Fringe Envelope on 2006 June 9 on the E1/S1 Baseline.

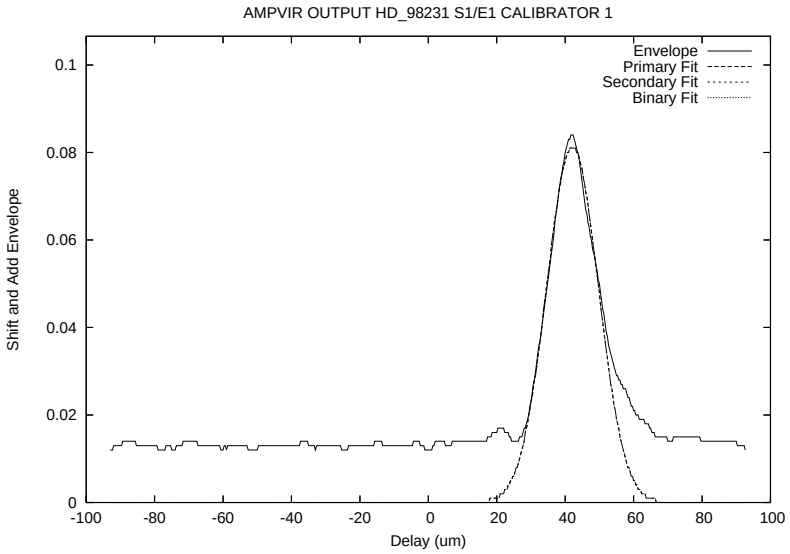


Figure. A.113: HD 98231 Fringe Envelope on 2007 October 6 on the E1/S1 Baseline.

## A.2.22 HD 99028

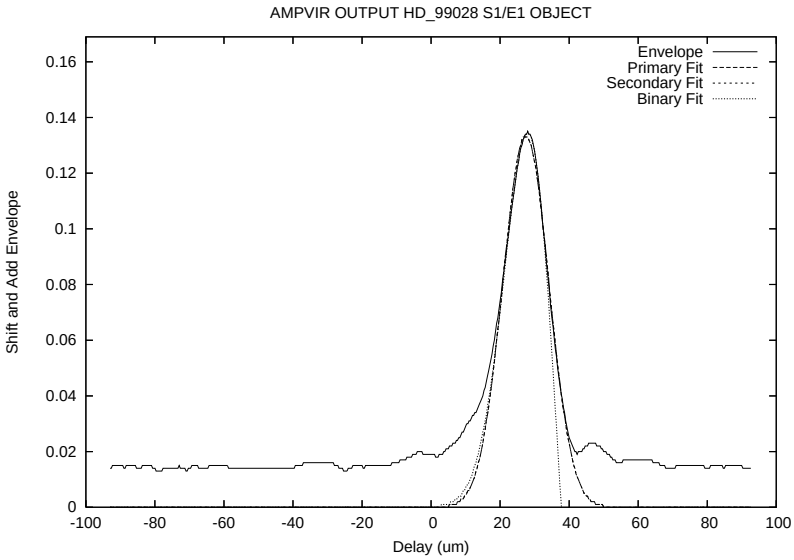


Figure. A.114: HD 99028 Fringe Envelope on 2007 Feburary 6 on the E1/S1 Baseline.

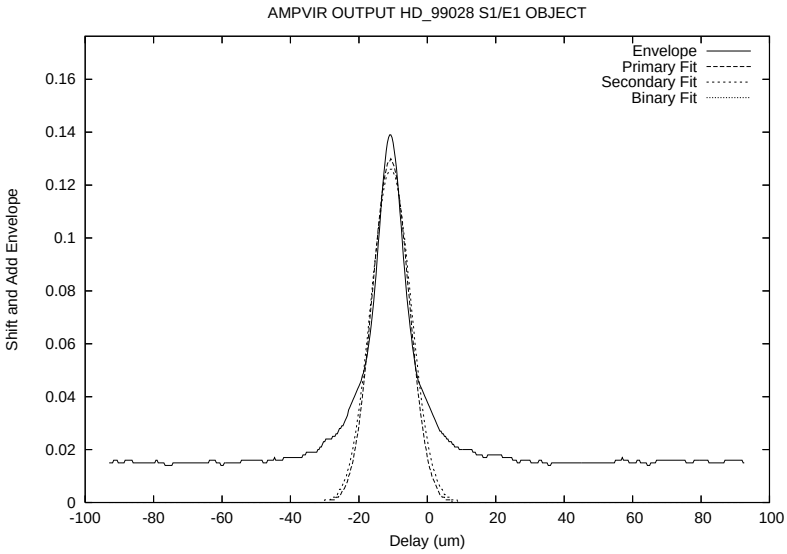


Figure. A.115: HD 99028 Fringe Envelope on 2007 Feburary 16 on the E1/S1 Baseline.

## A.2.23 HD 100203

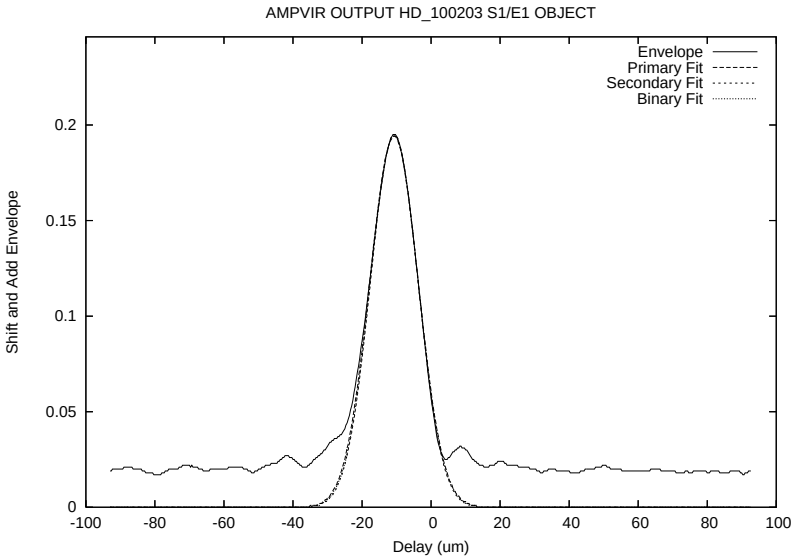


Figure. A.116: HD 100203 Fringe Envelope on 2007 April 3 on the E1/S1 Baseline.

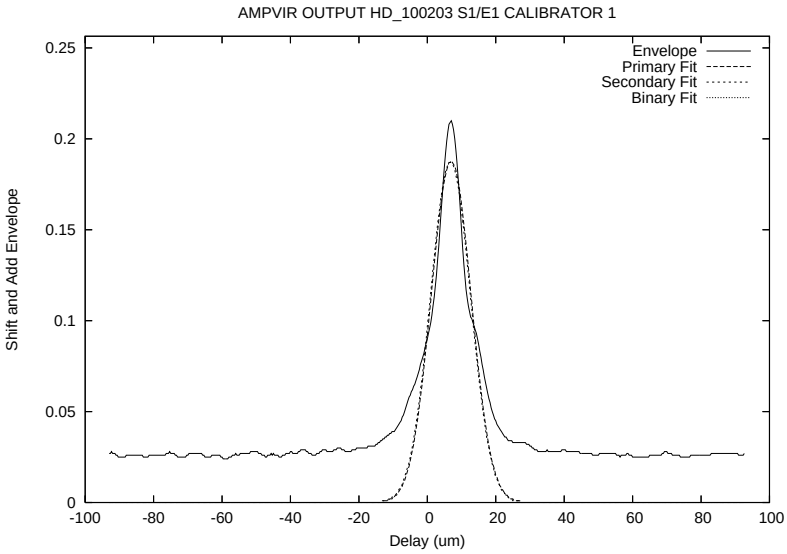


Figure. A.117: HD 100203 Fringe Envelope on 2007 April 11 on the E1/S1 Baseline.

## A.2.24 HD 101501

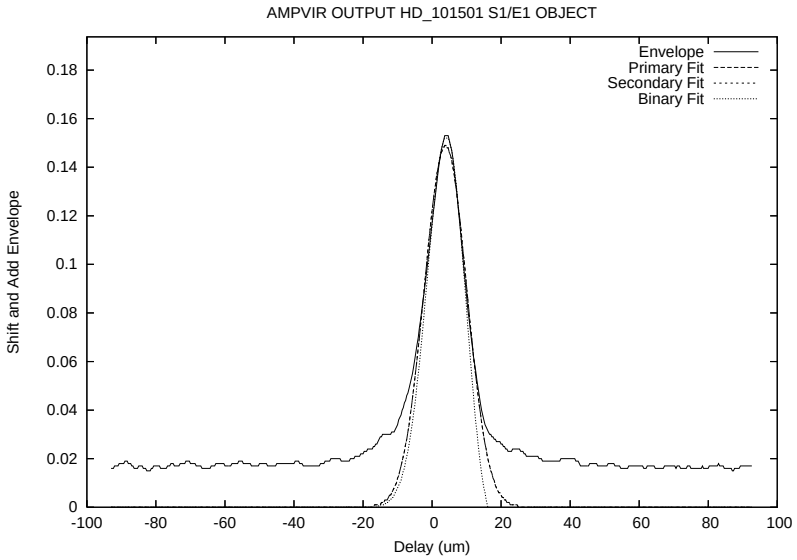


Figure. A.118: HD 101501on 2007 Feburary 3 on the E1/S1 Baseline.

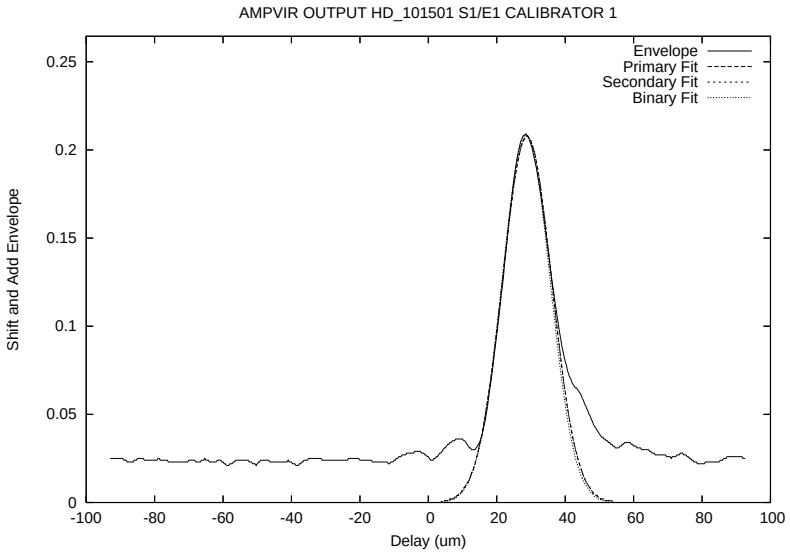


Figure. A.119: HD 101501 Fringe Envelope on 2007 Feburary 6 on the E1/S1 Baseline.

## A.2.25 HD 102870

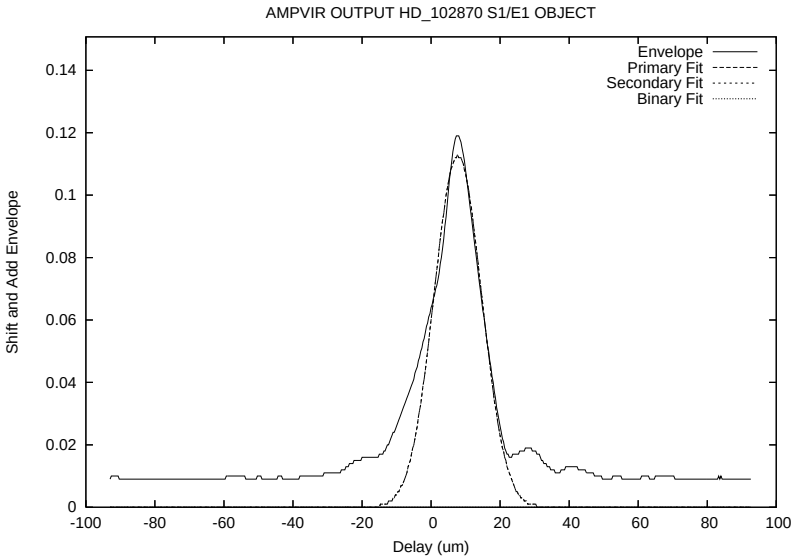


Figure. A.120: HD 102870 Fringe Envelope on 2007 March 9 on the E1/S1 Baseline.

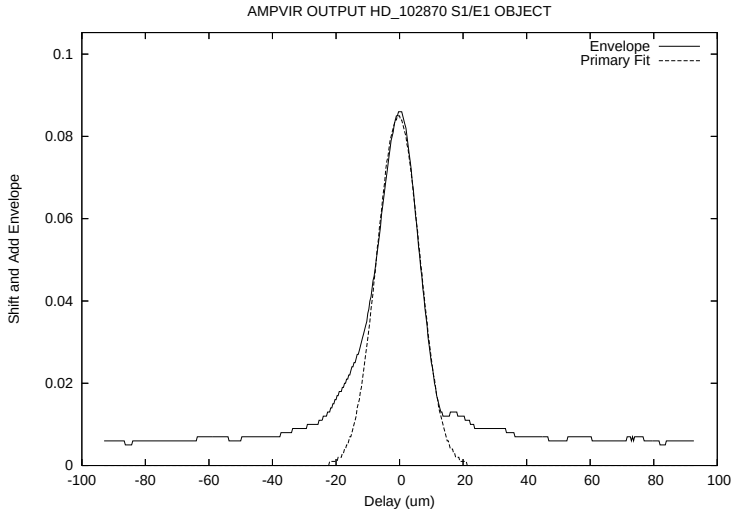


Figure. A.121: HD 102870 Fringe Envelope on 2007 March 12 on the E1/S1 Baseline.

## A.2.26 HD 103095

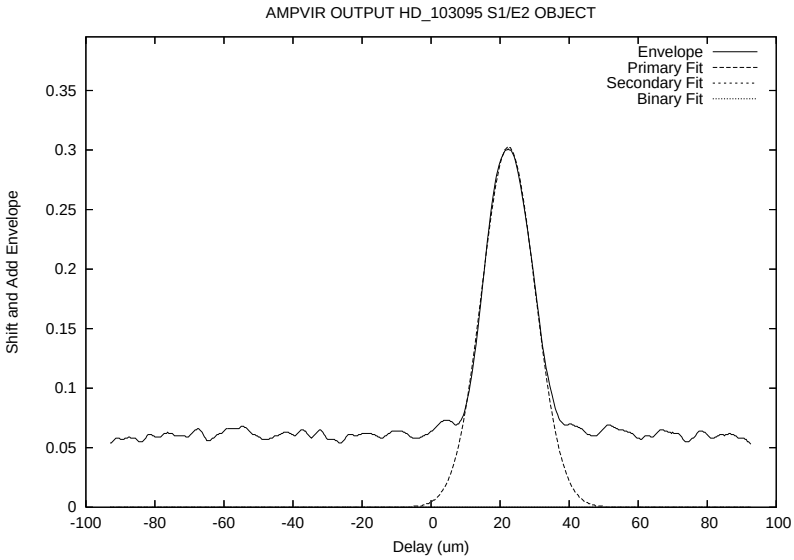


Figure. A.122: HD 103095 Fringe Envelope on 2007 May 27 on the E2/S1 Baseline.

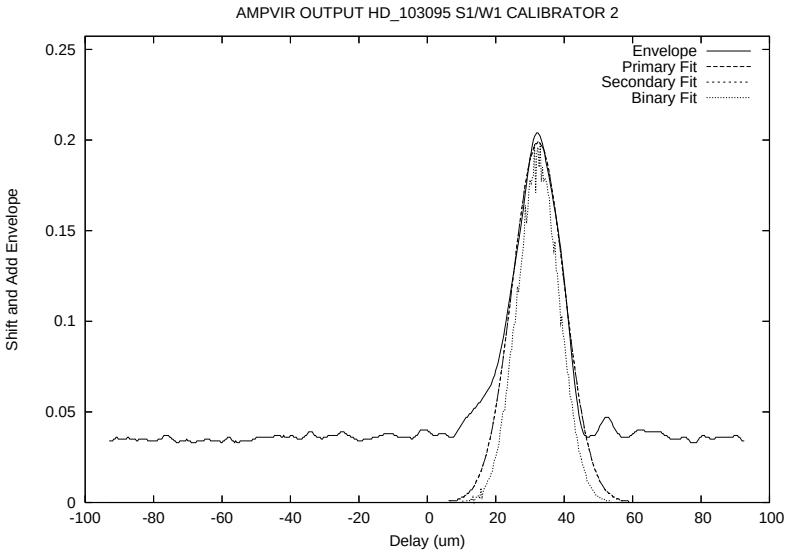


Figure. A.123: HD 103095 Fringe Envelope on 2007 May 28 on the W1/S1 Baseline.

## A.2.27 HD 109358

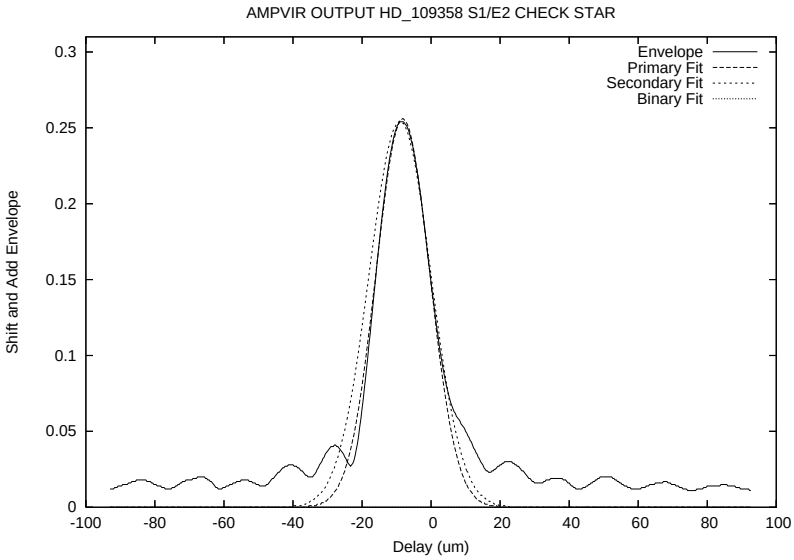


Figure. A.124: HD 109358 Fringe Envelope on 2007 May 27 on the E2/S1 Baseline.

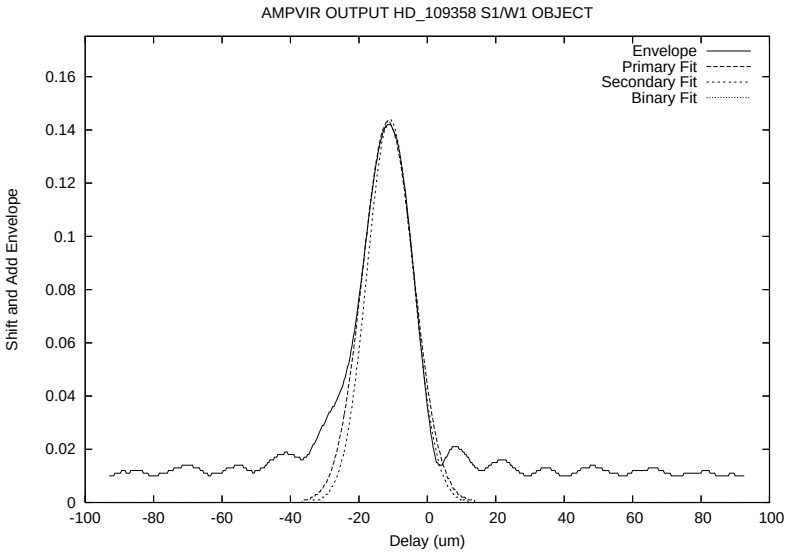


Figure. A.125: HD 109358 Fringe Envelope on 2007 May 28 on the W1/S1 Baseline.

## A.2.28 HD 110897

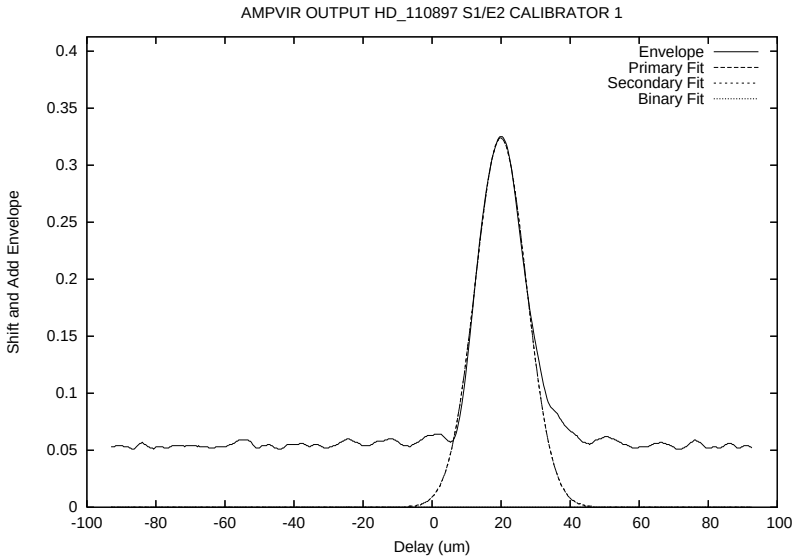


Figure. A.126: HD 110897 Fringe Envelope on 2007 May 27 on the E2/S1 Baseline.

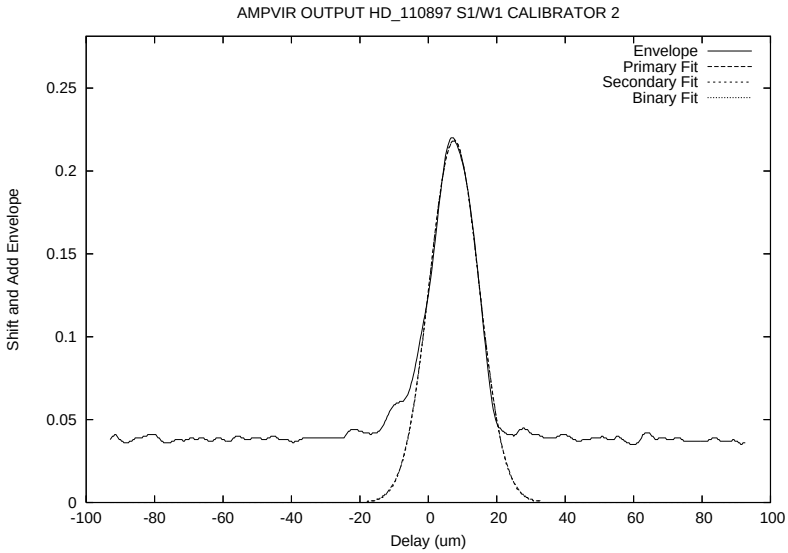


Figure. A.127: HD 110897 Fringe Envelope on 2007 May 28 on the W1/S1 Baseline.

## A.2.29 HD 111395

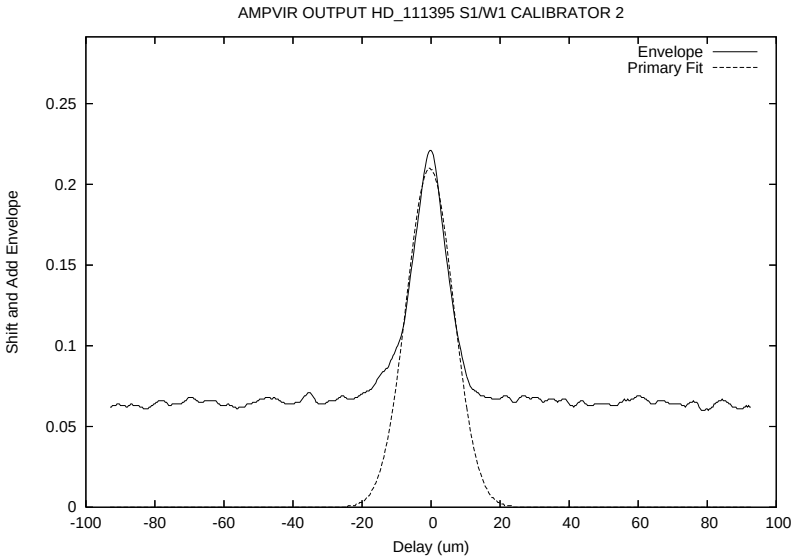


Figure. A.128: HD 111395 Fringe Envelope on 2007 May 28 on the W1/S1 Baseline.

# A.3 Observed Stars Right Ascension 13-18 Hours

## A.3.1 HD 114379

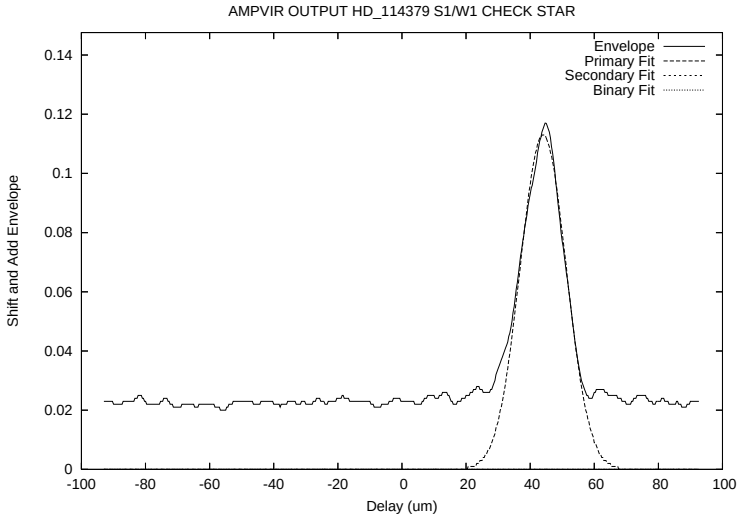


Figure. A.129: HD 114379 Fringe Envelope on 2007 May 28 on the W1/S1 Baseline.

## A.3.2 HD 114710

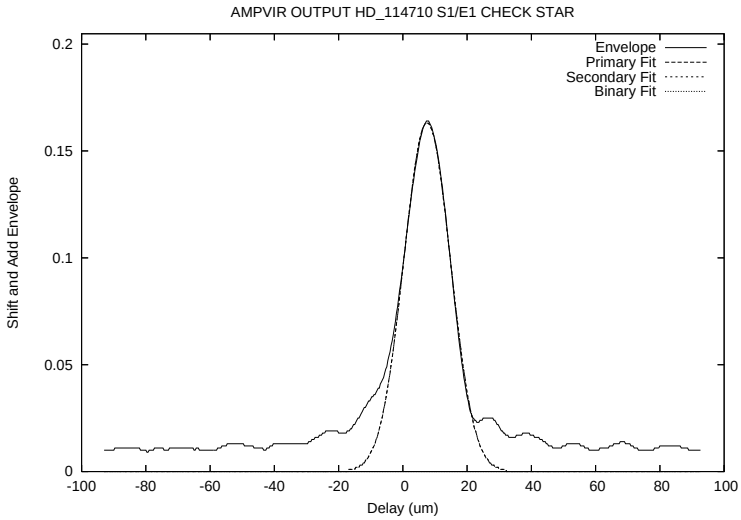


Figure. A.130: HD 114710 Fringe Envelope on 2007 Feburary 6 on the E1/S1 Baseline.

### A.3.3 HD 117043

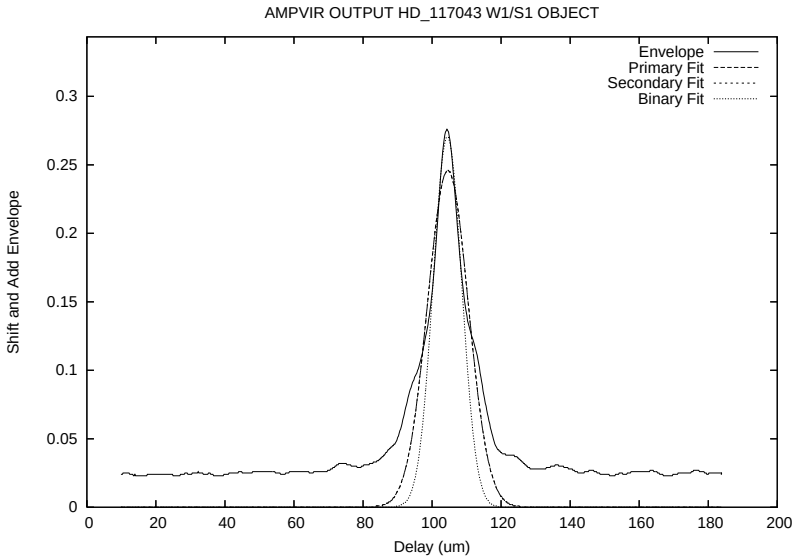


Figure. A.131: HD 117043 Fringe Envelope on 2006 June 5 on the W1/S1 Baseline.

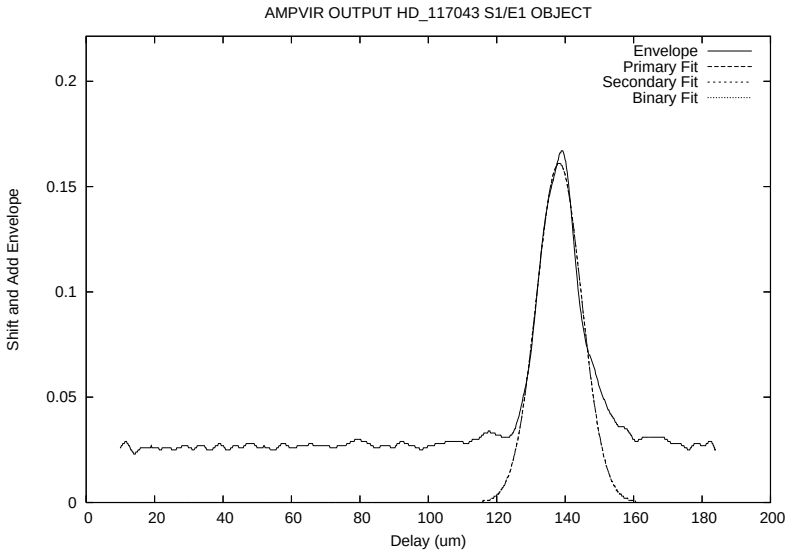


Figure. A.132: HD 117043 Fringe Envelope on 2006 June 6 on the E1/S1 Baseline.

### A.3.4 HD 117176

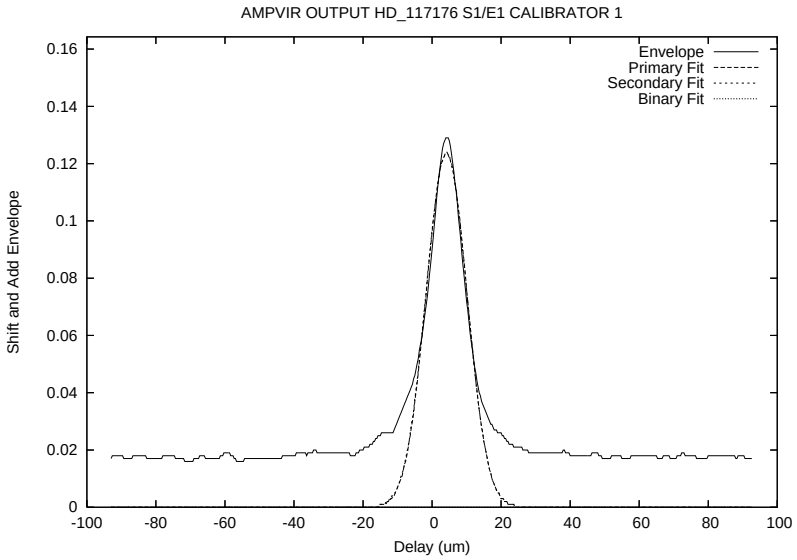


Figure. A.133: HD 117176 Fringe Envelope on 2007 March 30 on the E1/S1 Baseline.

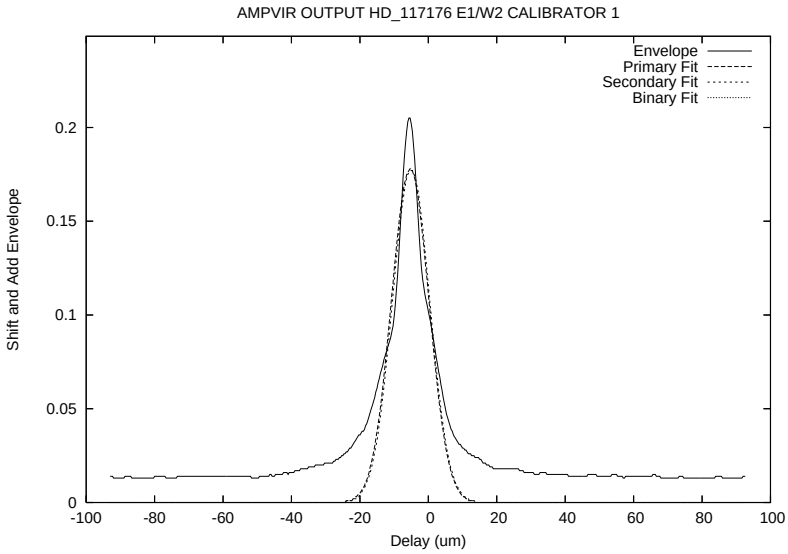


Figure. A.134: HD 117176 Fringe Envelope on 2007 May 7 on the E1/W2 Baseline.

### A.3.5 HD 120136

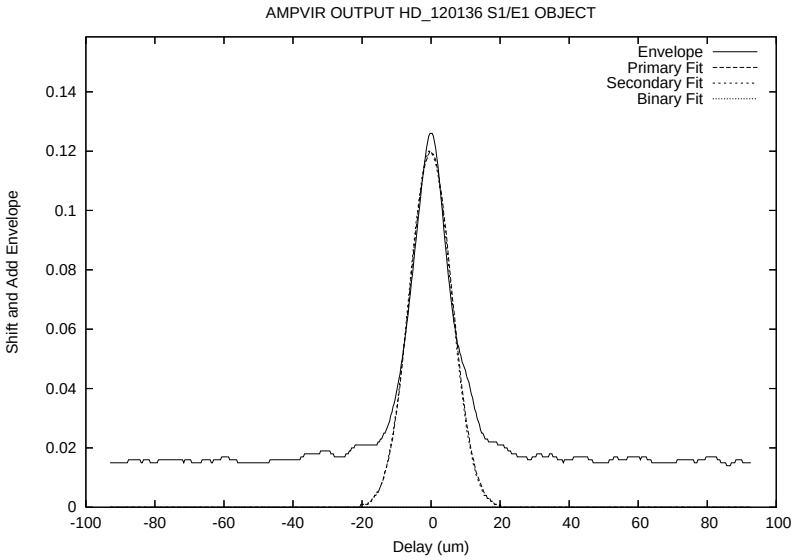


Figure. A.135: HD 120136 Fringe Envelope on 2007 March 25 on the E1/S1 Baseline.

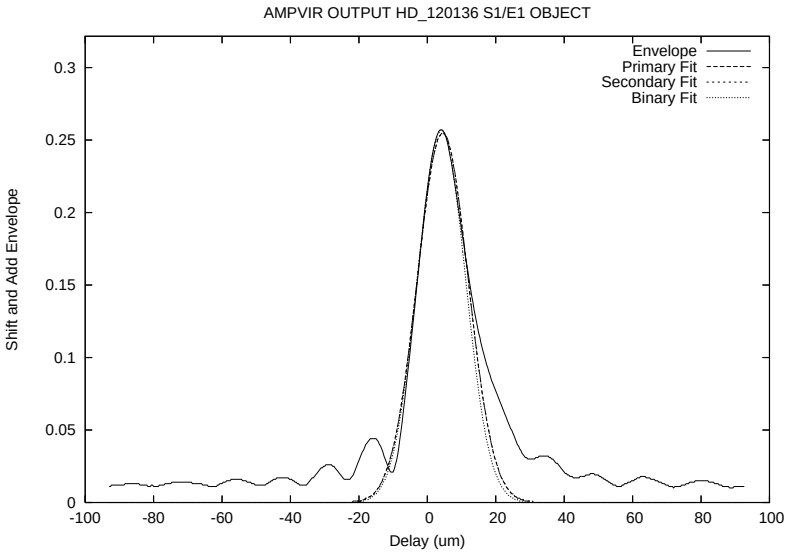


Figure. A.136: HD 120136 Fringe Envelope on 2007 March 26 on the E1/S1 Baseline.

### A.3.6 HD 120787

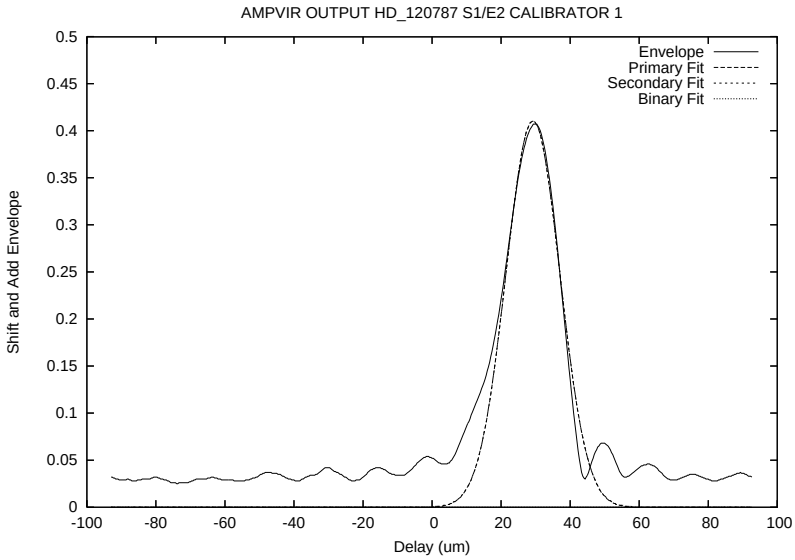


Figure. A.137: HD 120787 Fringe Envelope on 2007 May 27 on the E2/S1 Baseline.

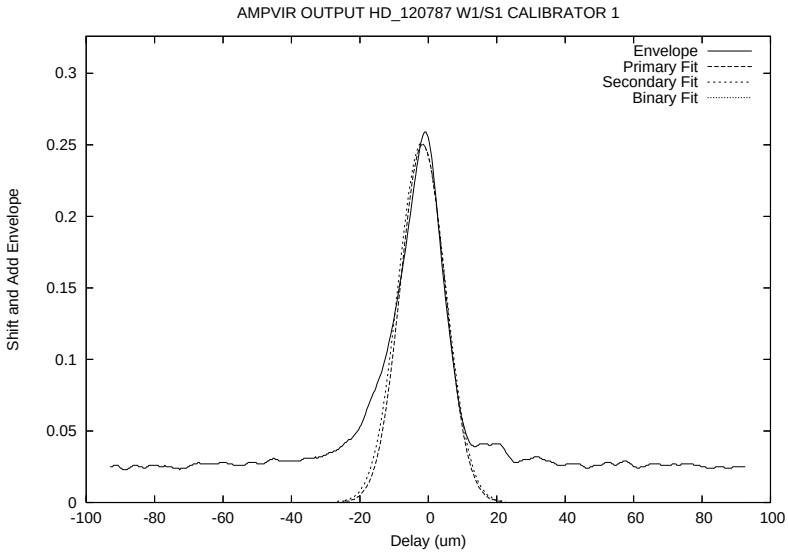


Figure. A.138: HD 120787 Fringe Envelope on 2007 June 1 on the W1/S1 Baseline.

## A.3.7 HD 121370

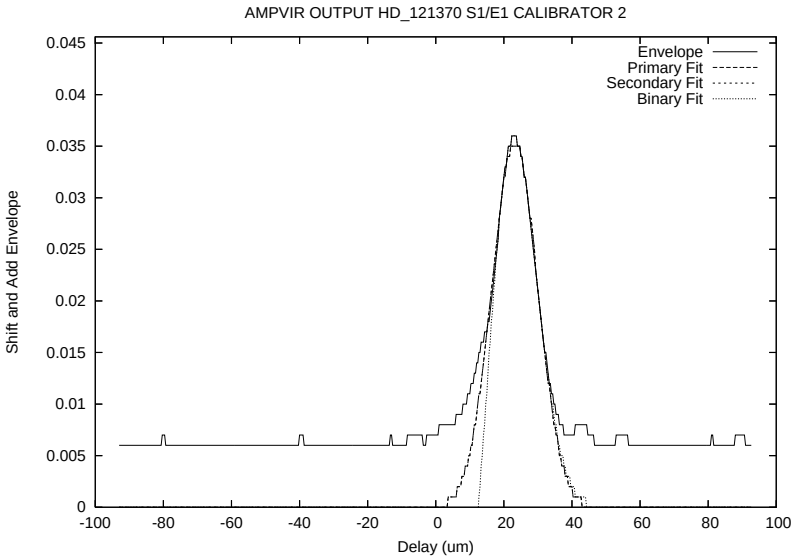


Figure. A.139: HD 121370 Fringe Envelope on 2007 Feburary 5 on the E1/S1 Baseline.

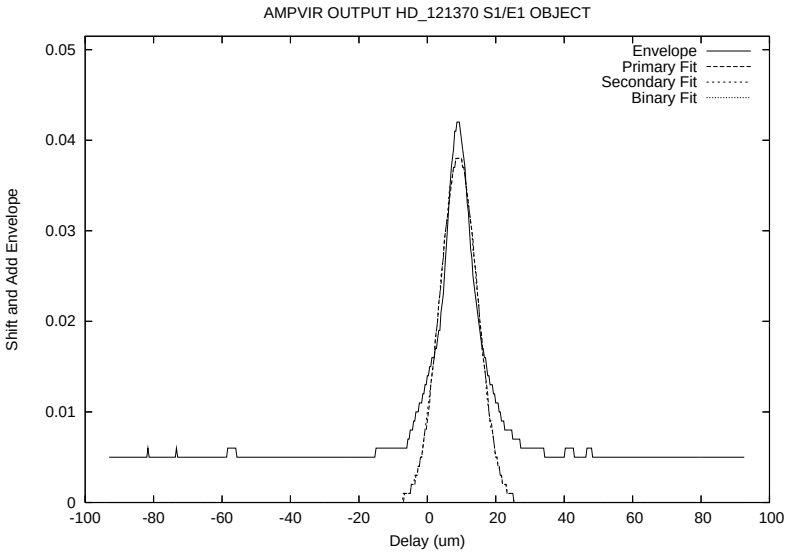


Figure. A.140: HD 121370 Fringe Envelope on 2007 Feburary 25 on the E1/S1 Baseline.

## A.3.8 HD 122742

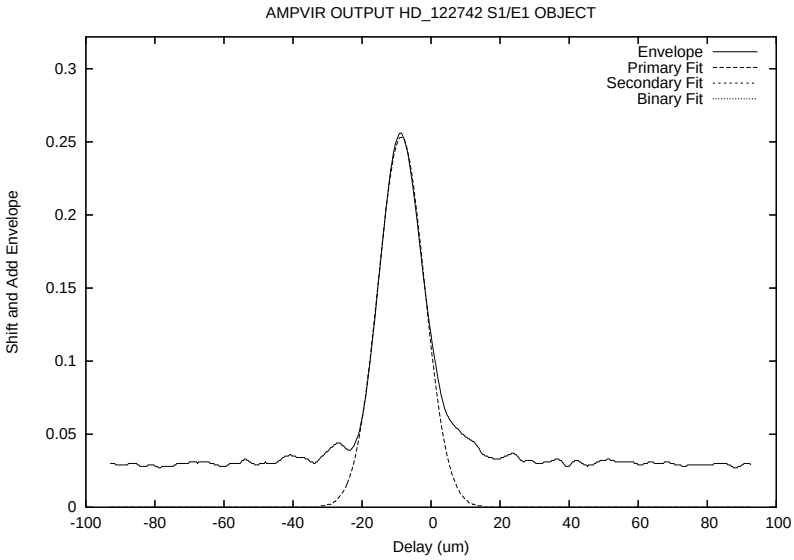


Figure. A.141: HD 122742 Fringe Envelope on 2007 March 12 on the E1/S1 Baseline.

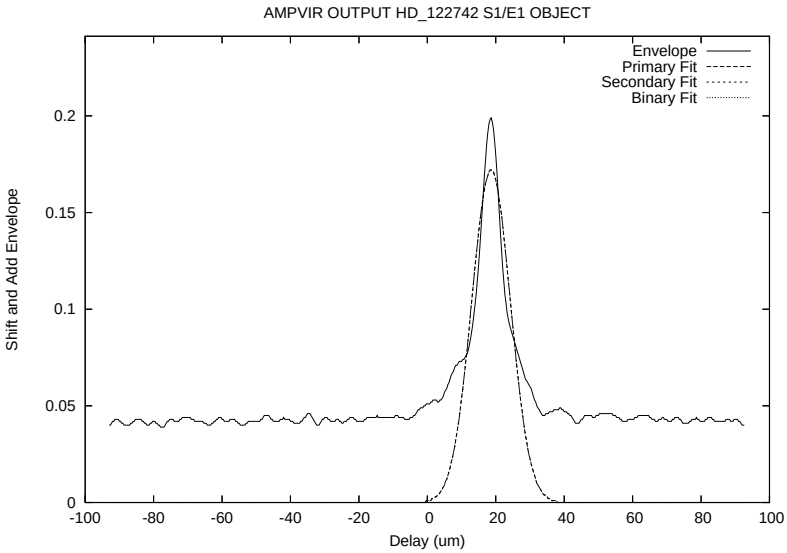


Figure. A.142: HD 122742 Fringe Envelope on 2007 March 30 on the E1/S1 Baseline.

### A.3.9 HD 126053

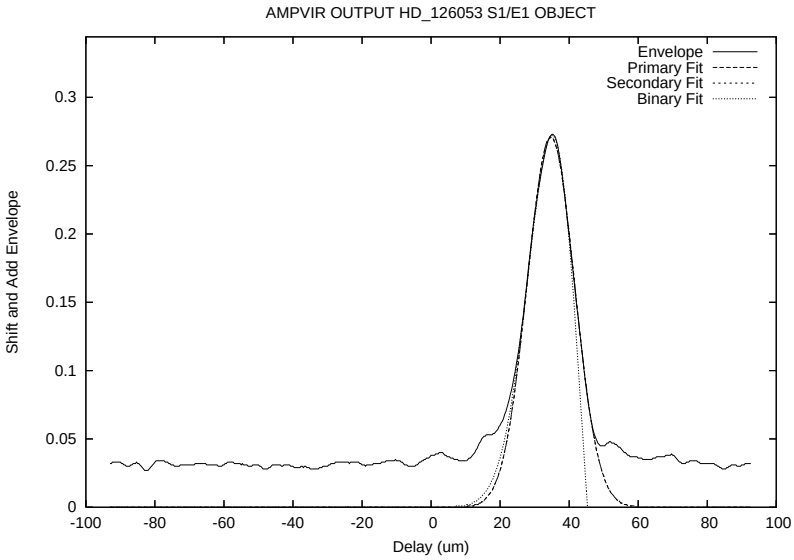


Figure. A.143: HD 126053 Fringe Envelope on 2007 March 12 on the E1/S1 Baseline.

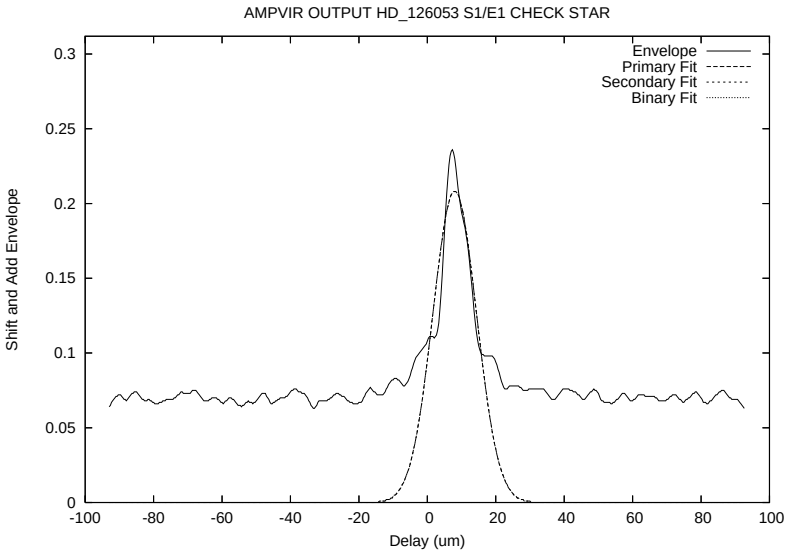


Figure. A.144: HD 126053 Fringe Envelope on 2007 March 30 on the E1/S1 Baseline.

## A.3.10 HD 126660

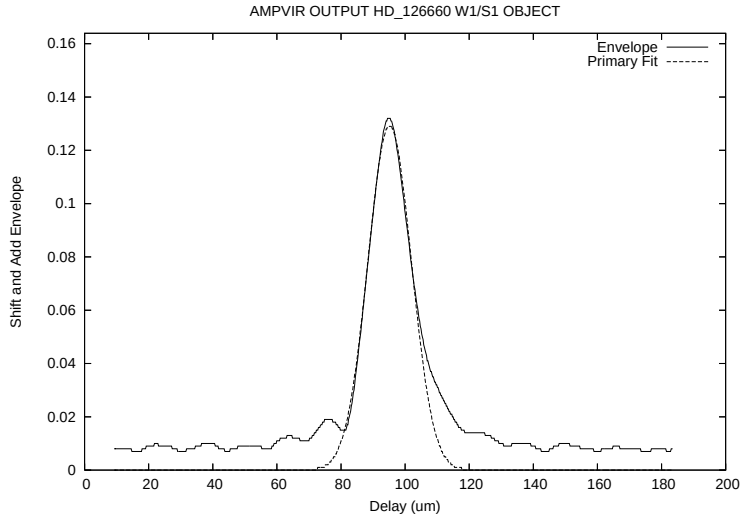


Figure. A.145: HD 126660 Fringe Envelope on 2006 June 5 on the W1/S1 Baseline.

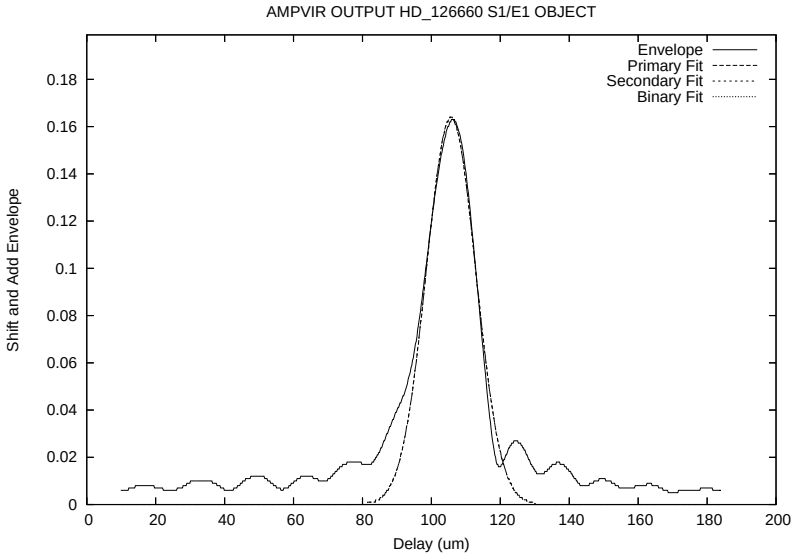


Figure. A.146: HD 126660 Fringe Envelope on 2006 June 6 on the E1/S1 Baseline.

## A.3.11 HD 128167

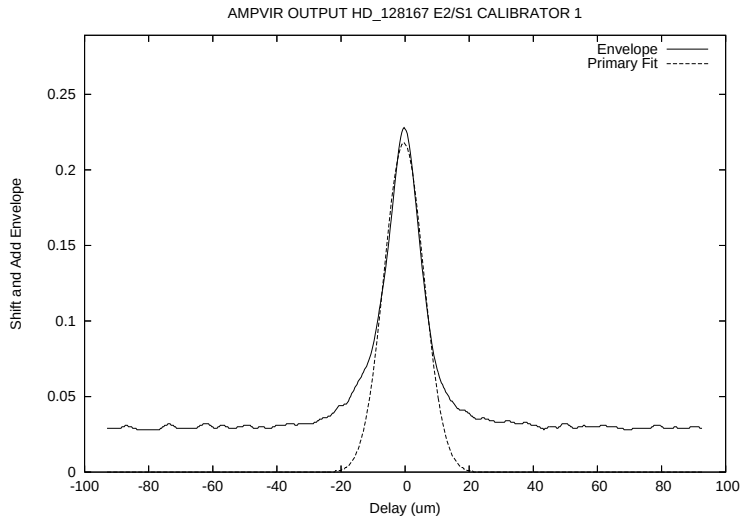


Figure. A.147: HD 128167 Fringe Envelope on 2007 June 1 on the E2/S1 Baseline.

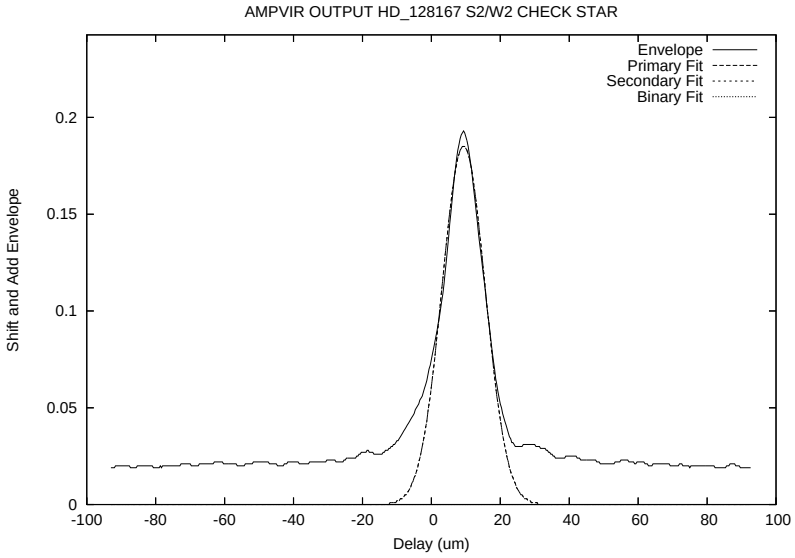


Figure. A.148: HD 128167 Fringe Envelope on 2008 June 4 on the W2/S2 Baseline.

## A.3.12 HD 130948

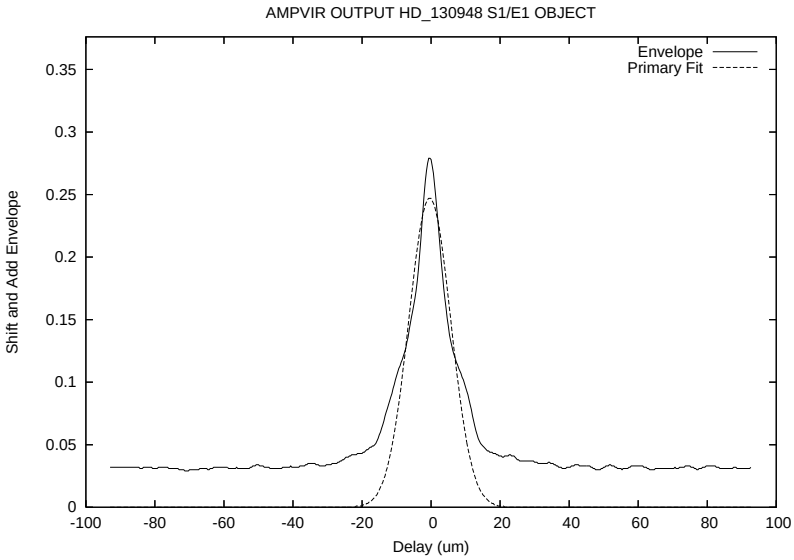


Figure. A.149: HD 130948 Fringe Envelope on 2007 Feburary 4 on the E1/S1 Baseline.

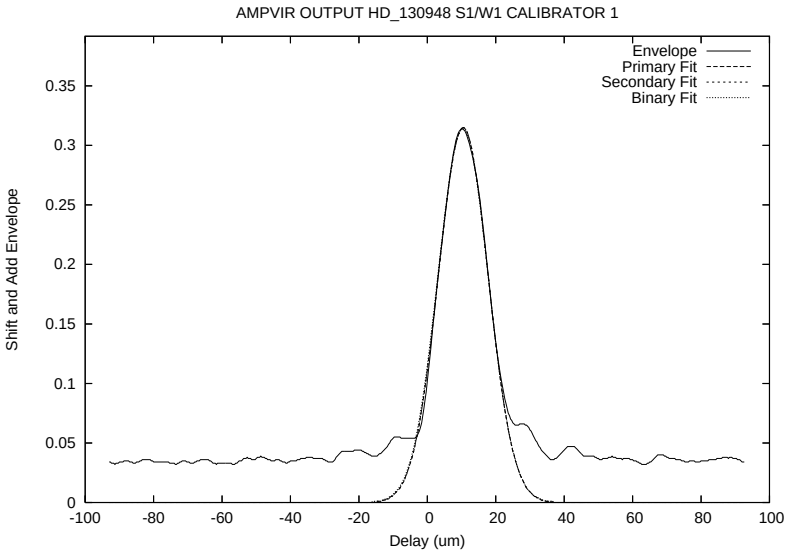


Figure. A.150: HD 130948 Fringe Envelope on 2007 June 23 on the W1/S1 Baseline.

## A.3.13 HD 131156

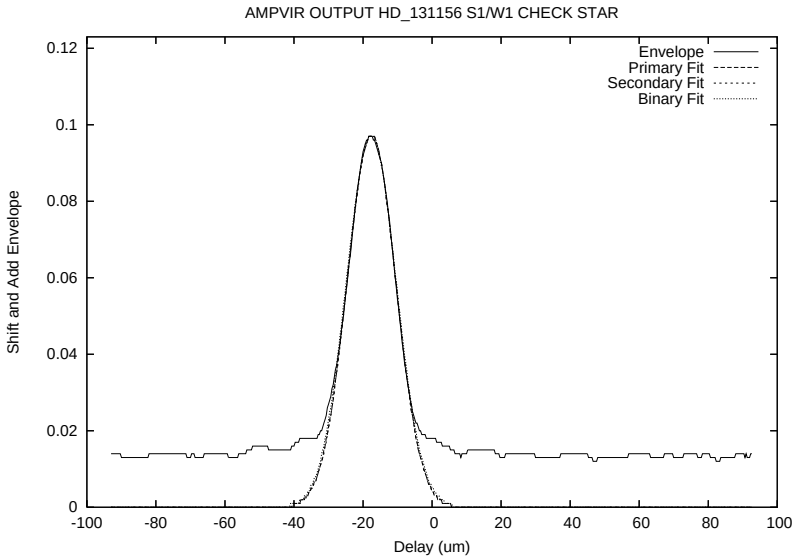


Figure. A.151: HD 131156 Fringe Envelope on 2007 May 28 on the W1/S1 Baseline.

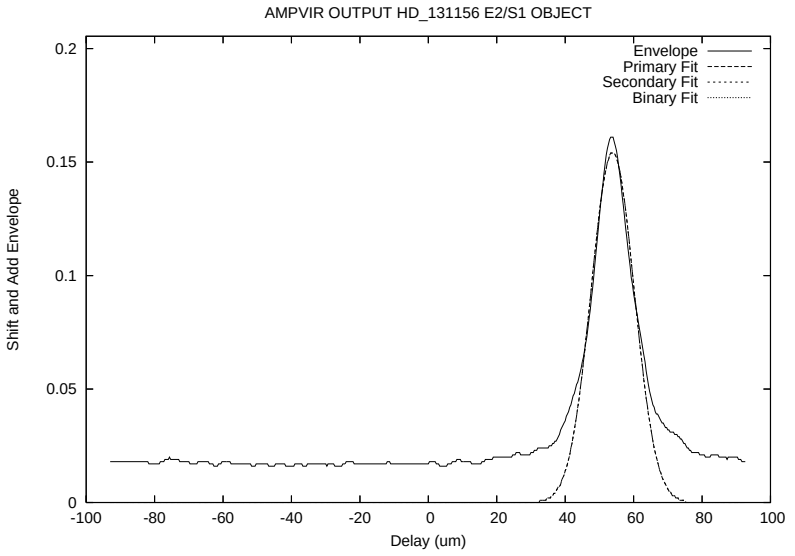


Figure. A.152: HD 131156 Fringe Envelope on 2007 June 1 on the E2/S1 Baseline.

### A.3.14 HD 133640

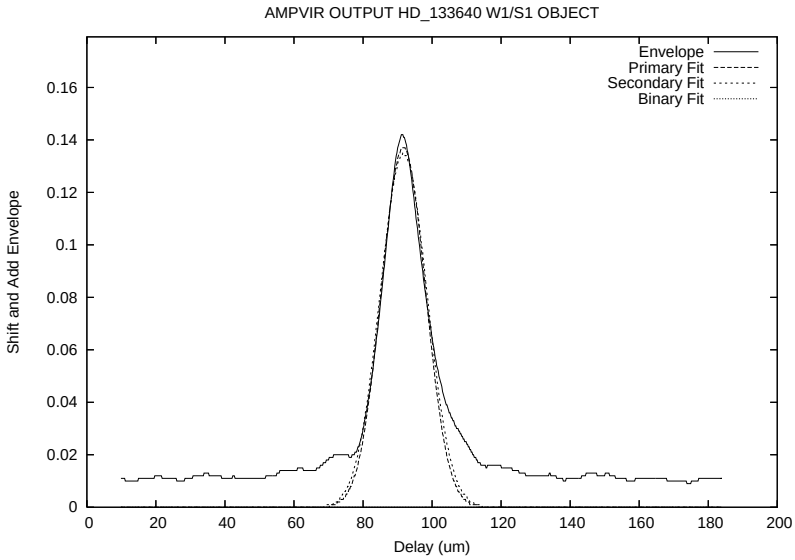


Figure. A.153: HD 133640 Fringe Envelope on 2006 June 5 on the W1/S1 Baseline.

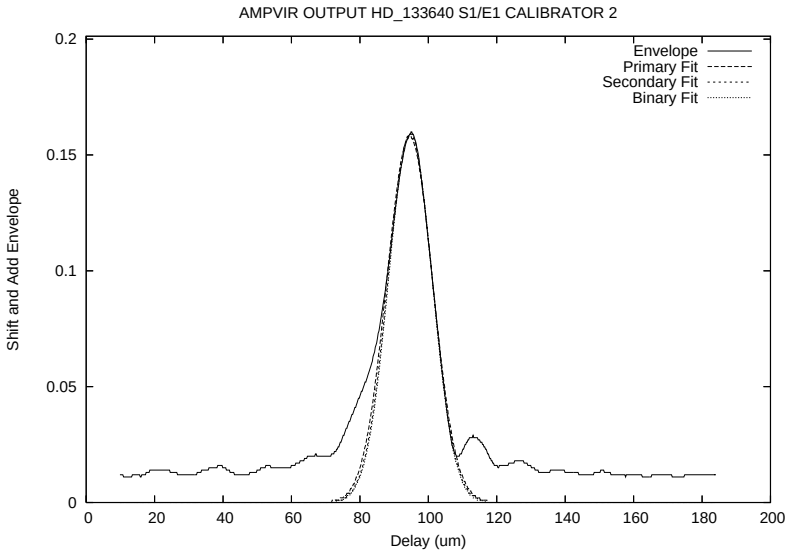


Figure. A.154: HD 133640 Fringe Envelope on 2006 June 6 on the E1/S1 Baseline.

## A.3.15 HD 134083

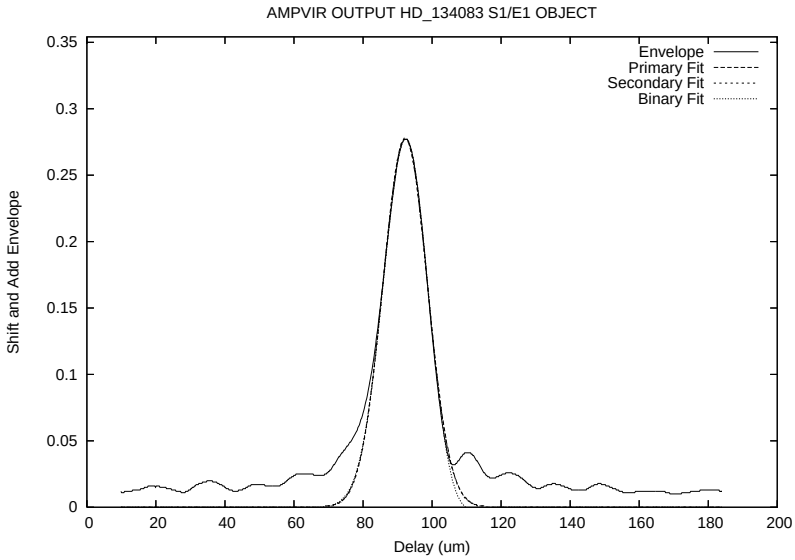


Figure. A.155: HD 134083 Fringe Envelope on 2006 June 9 on the E1/S1 Baseline.

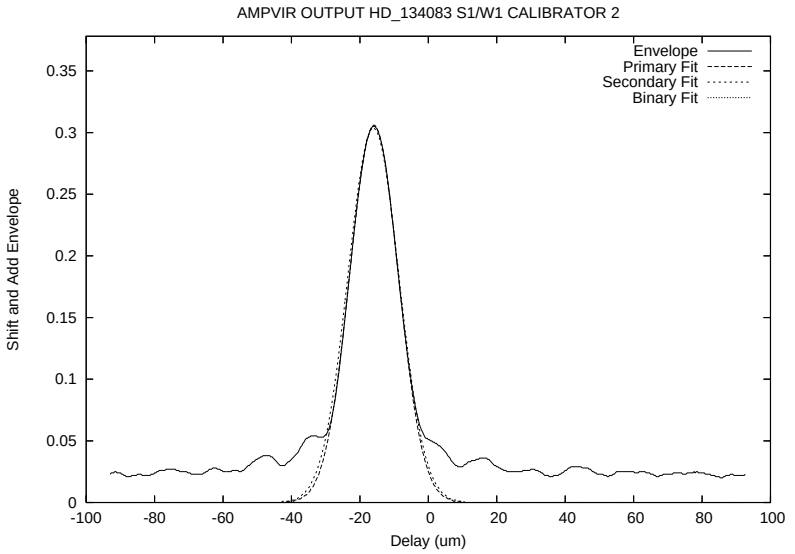


Figure. A.156: HD 134083 Fringe Envelope on 2007 June 23 on the W1/S1 Baseline.

## A.3.16 HD 134323

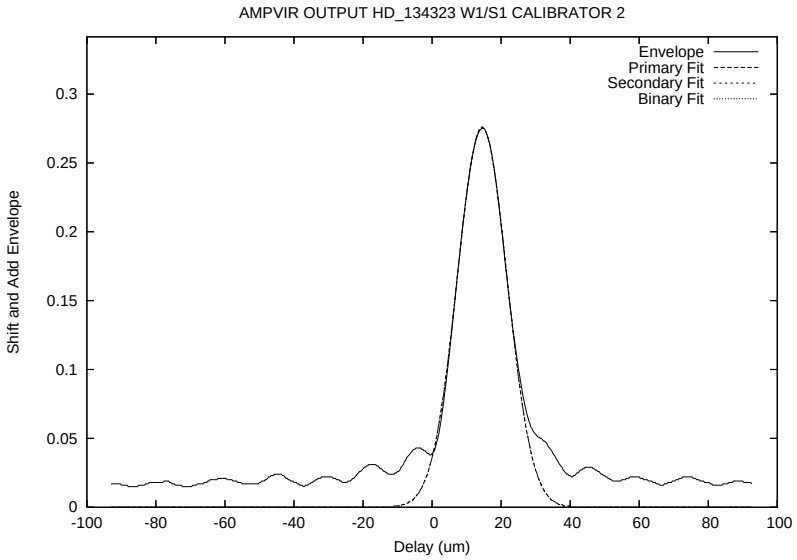


Figure. A.157: HD 134323 Fringe Envelope on 2007 May 30 on the W1/S1 Baseline.

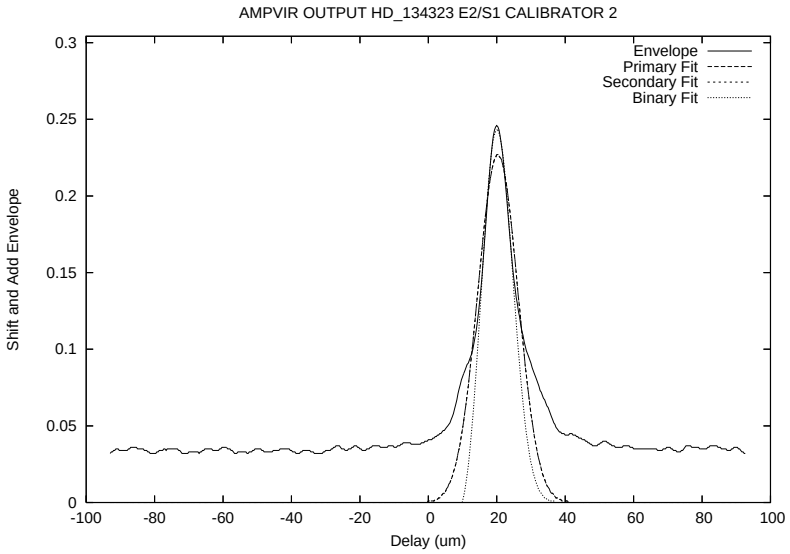


Figure. A.158: HD 134323 Fringe Envelope on 2007 June 1 on the E2/S1 Baseline.

## A.3.17 HD 136064

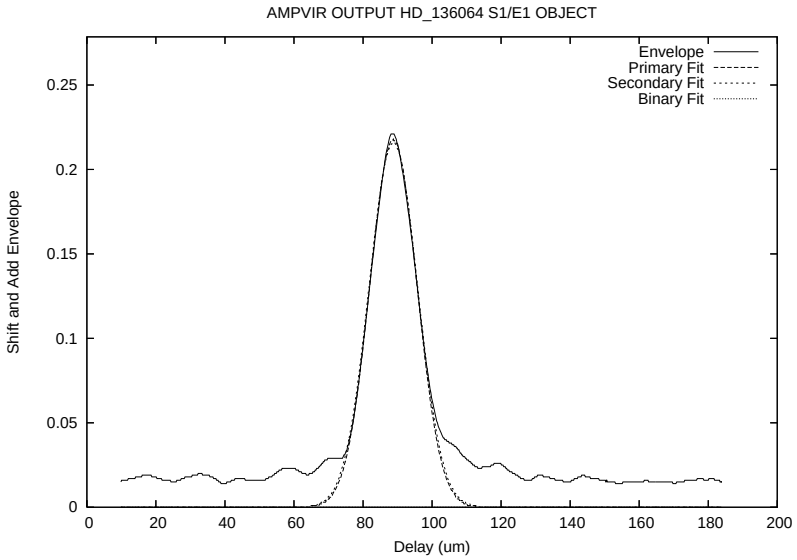


Figure. A.159: HD 136064 Fringe Envelope on 2006 June 3 on the E1/S1 Baseline.

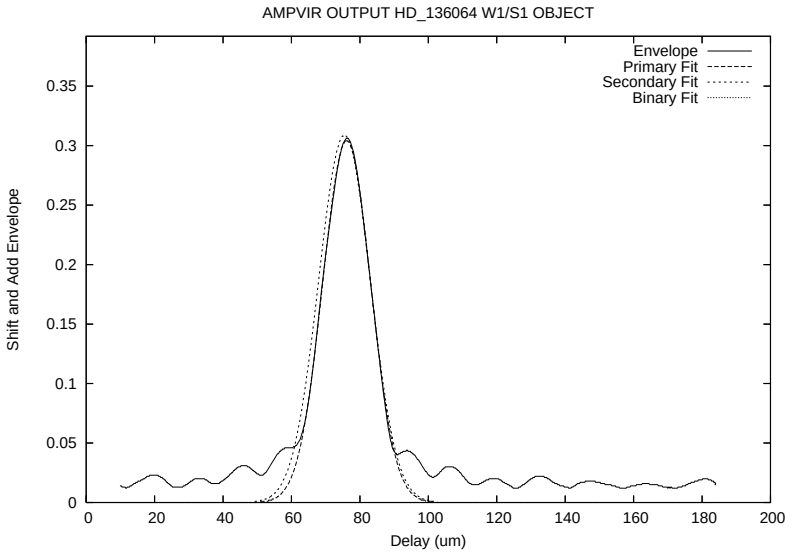


Figure. A.160: HD 136064 Fringe Envelope on 2006 June 5 on the W1/S1 Baseline.

## A.3.18 HD 137107

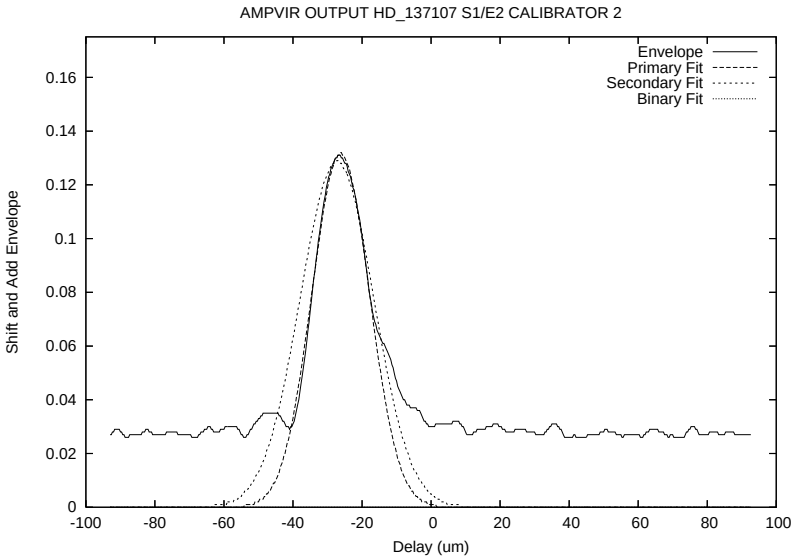


Figure. A.161: HD 137107 Fringe Envelope on 2007 May 27 on the E2/S1 Baseline.

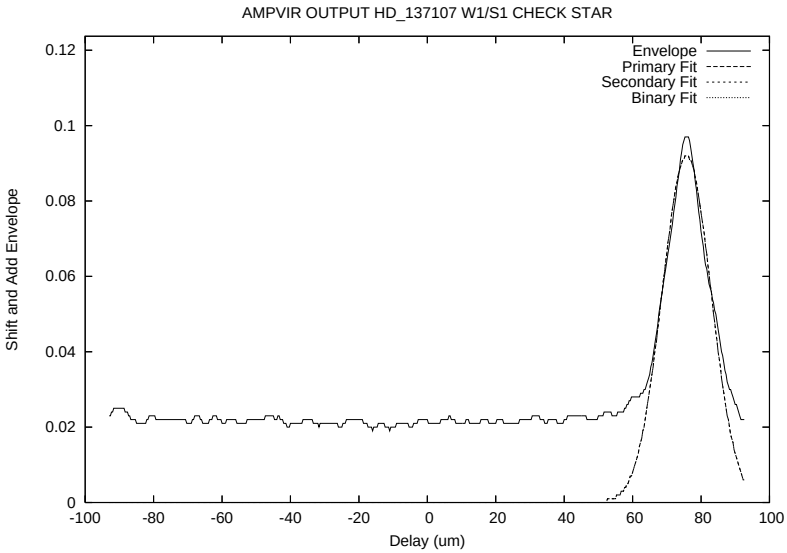


Figure. A.162: HD 137107 Fringe Envelope on 2007 May 30 on the W1/S1 Baseline.

## A.3.19 HD 137108

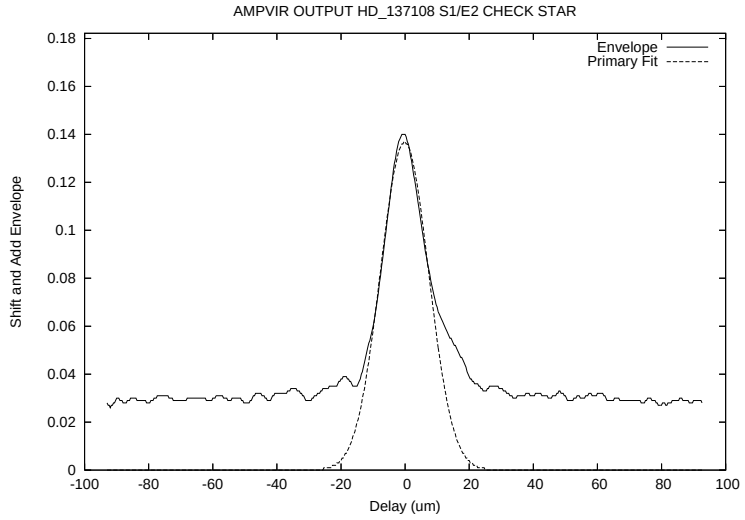


Figure. A.163: HD 137108 Fringe Envelope on 2007 May 27 on the E2/S1 Baseline.

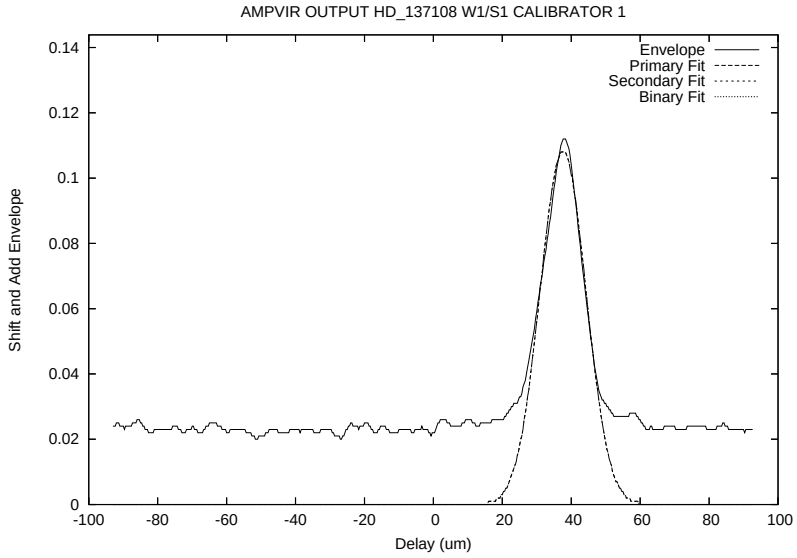


Figure. A.164: HD 137108 Fringe Envelope on 2007 May 30 on the W1/S1 Baseline.

## A.3.20 HD 140538

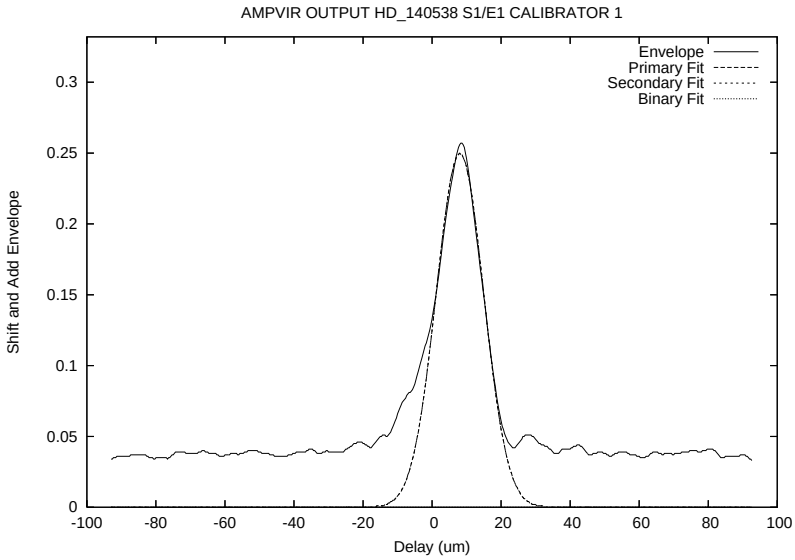


Figure. A.165: HD 140538 Fringe Envelope on 2007 April 2 on the E1/S1 Baseline.

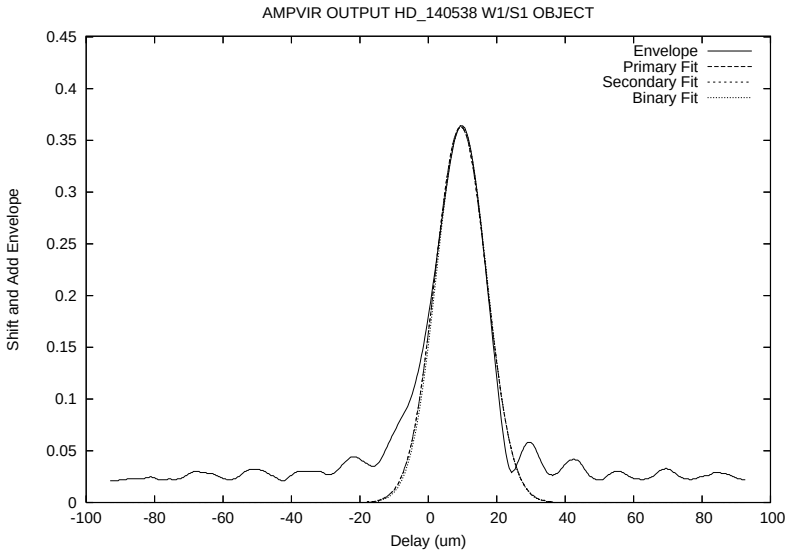


Figure. A.166: HD 140538 Fringe Envelope on 2007 May 30 on the W1/S1 Baseline.

## A.3.21 HD 141004

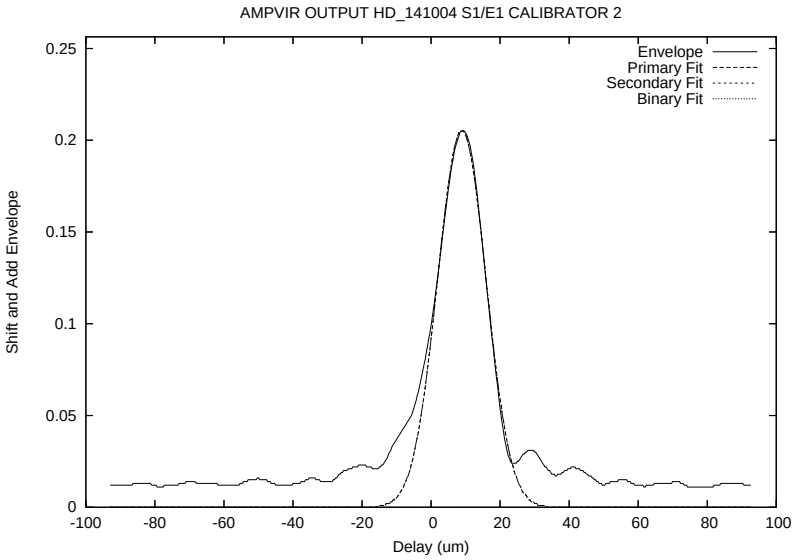


Figure. A.167: HD 141004 Fringe Envelope on 2007 April 2 on the E1/S1 Baseline.

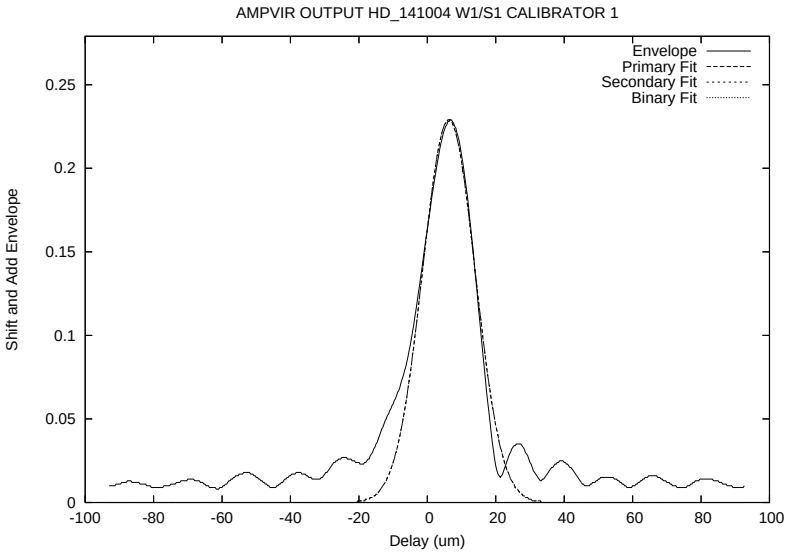


Figure. A.168: HD 141004 Fringe Envelope on 2007 May 30 on the W1/S1 Baseline.

## A.3.22 HD 142373

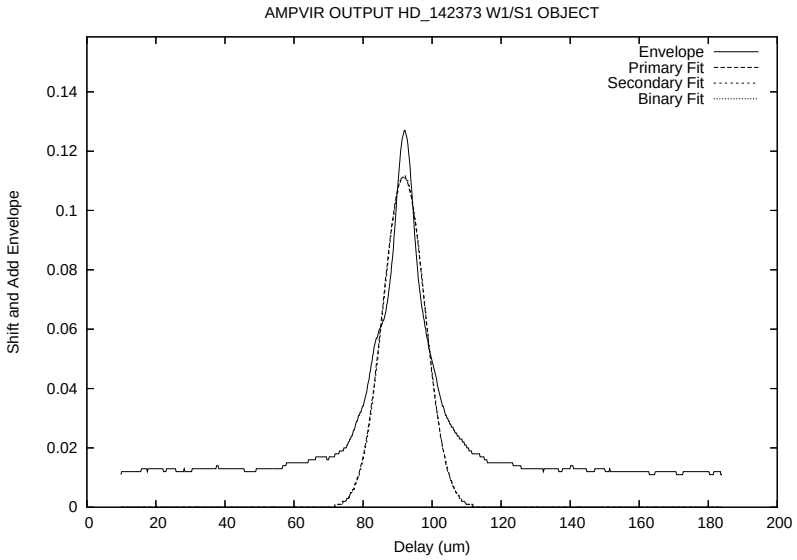


Figure. A.169: HD 142373 Fringe Envelope on 2006 June 5 on the W1/S1 Baseline.

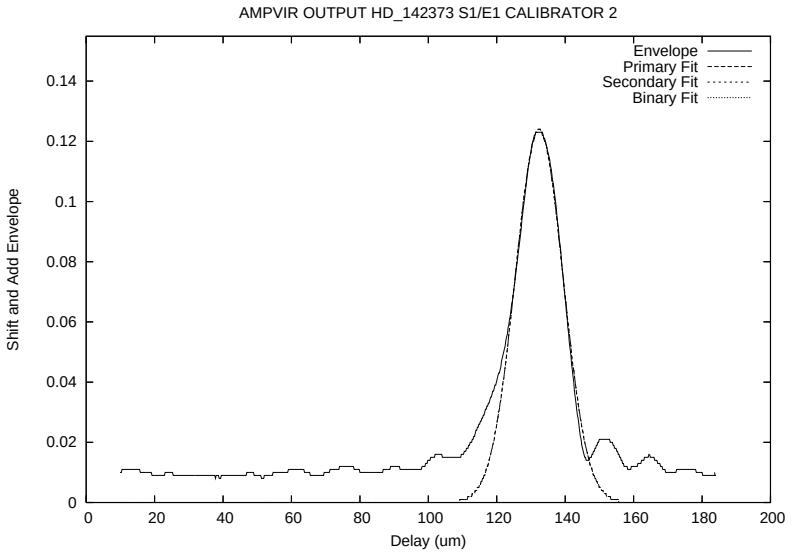


Figure. A.170: HD 142373 Fringe Envelope on 2006 June 6 on the E1/S1 Baseline.

## A.3.23 HD 142860

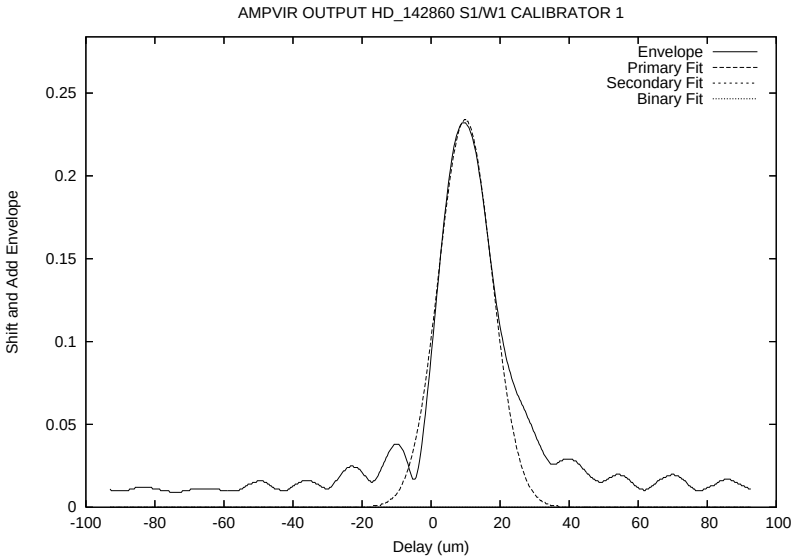


Figure. A.171: HD 142860 Fringe Envelope on 2007 June 23 on the W1/S1 Baseline.

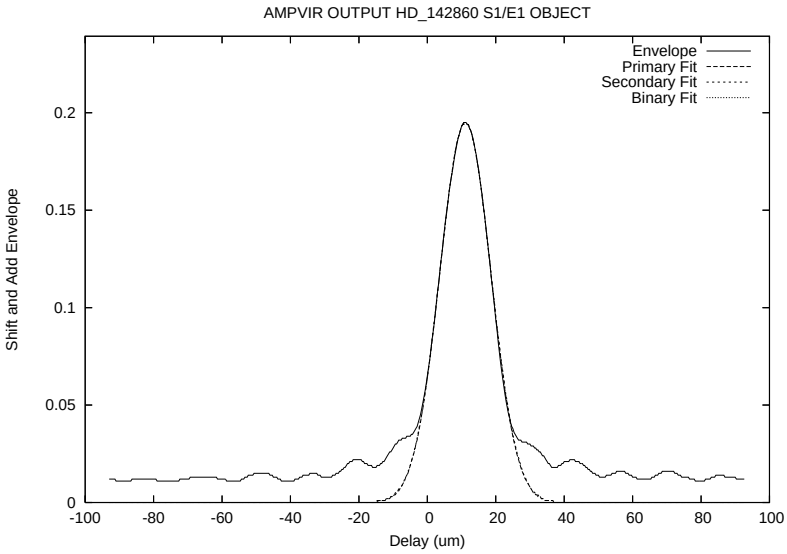


Figure. A.172: HD 142860 Fringe Envelope on 2007 July 20 on the E1/S1 Baseline.

## A.3.24 HD 143761

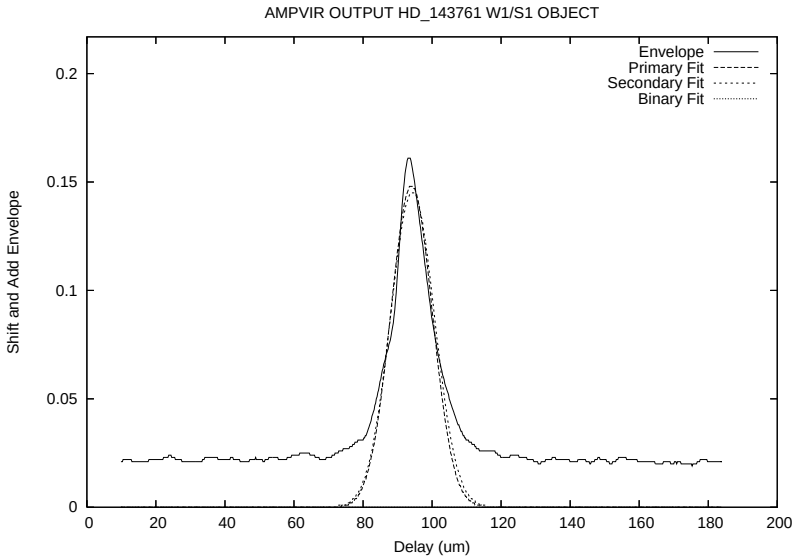


Figure. A.173: HD 143761 Fringe Envelope on 2006 June 5 on the W1/S1 Baseline.

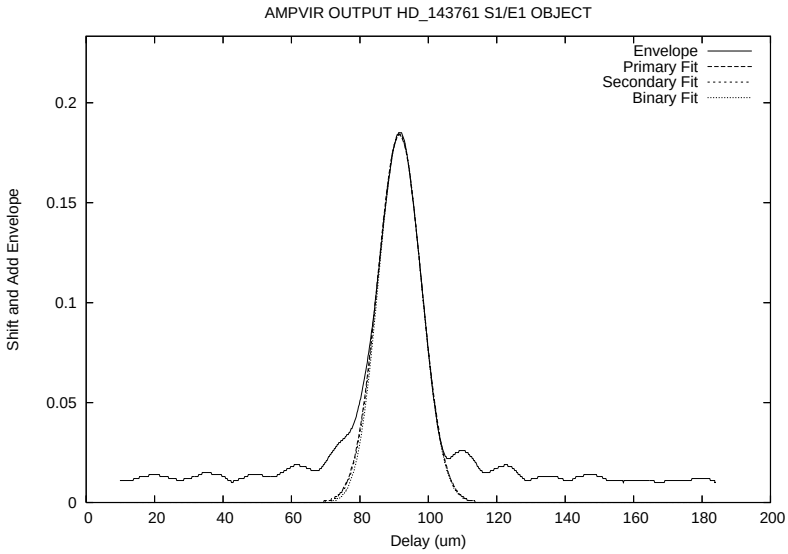


Figure. A.174: HD 143761 Fringe Envelope on 2006 June 6 on the E1/S1 Baseline.

## A.3.25 HD 144284

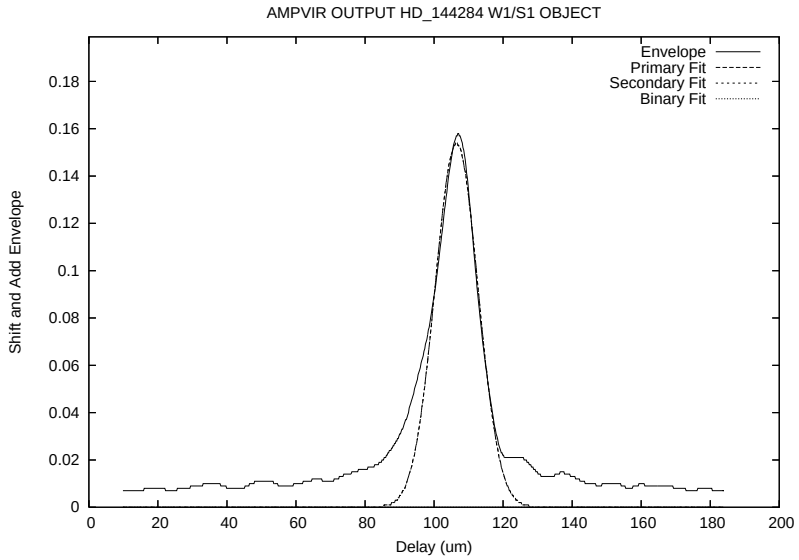


Figure. A.175: HD 144284 Fringe Envelope on 2006 June 5 on the W1/S1 Baseline.

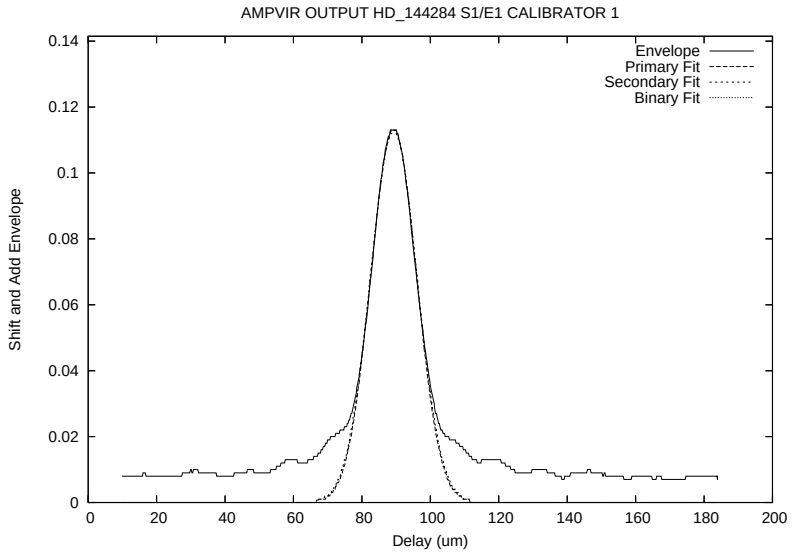


Figure. A.176: HD 144284 Fringe Envelope on 2006 June 6 on the E1/S1 Baseline.

## A.3.26 HD 144579

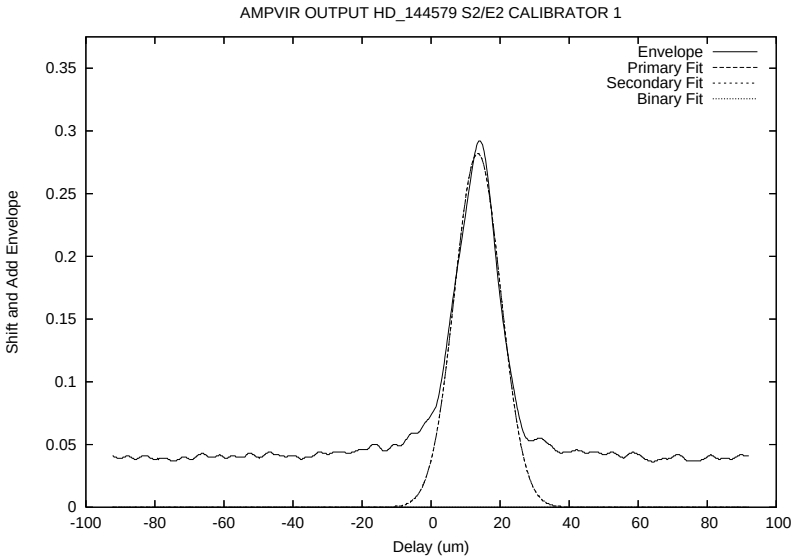


Figure. A.177: HD 144579 Fringe Envelope on 2007 June 23 on the E2/S2 Baseline.

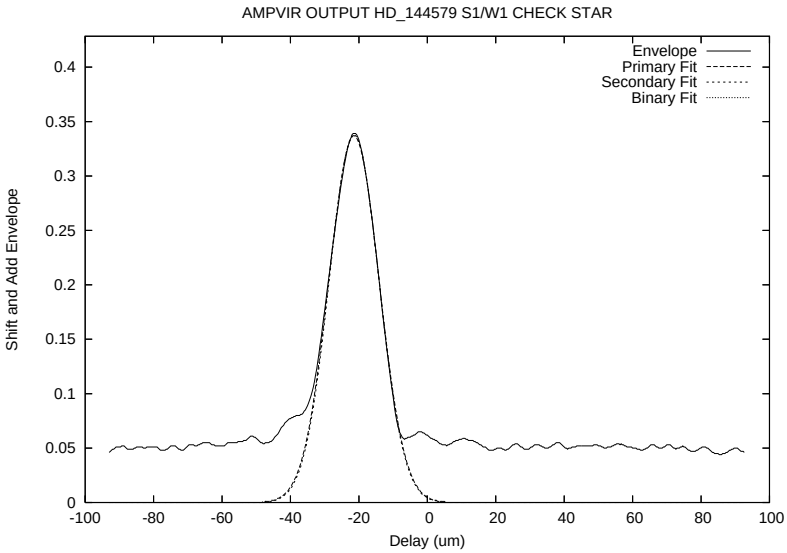


Figure. A.178: HD 144579 Fringe Envelope on 2007 July 8 on the W1/S1 Baseline.

## A.3.27 HD 146362

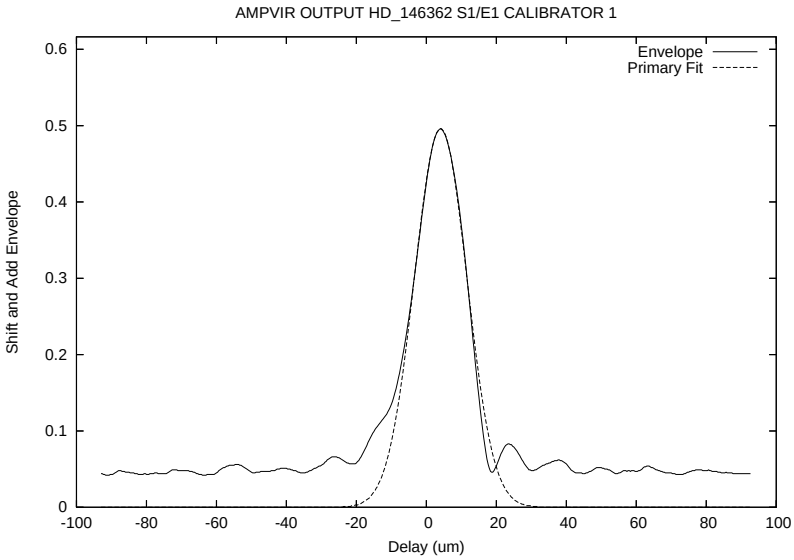


Figure. A.179: HD 146362 Fringe Envelope on 2007 May 16 on the E1/S1 Baseline.

## A.3.28 HD 151623

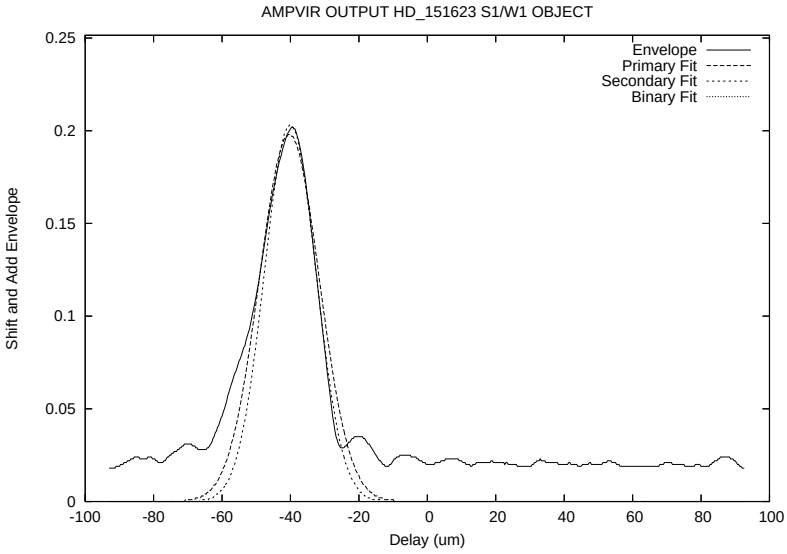


Figure. A.180: HD 151623 Fringe Envelope on 2007 May 28 on the W1/S1 Baseline.

## A.3.29 HD 147266

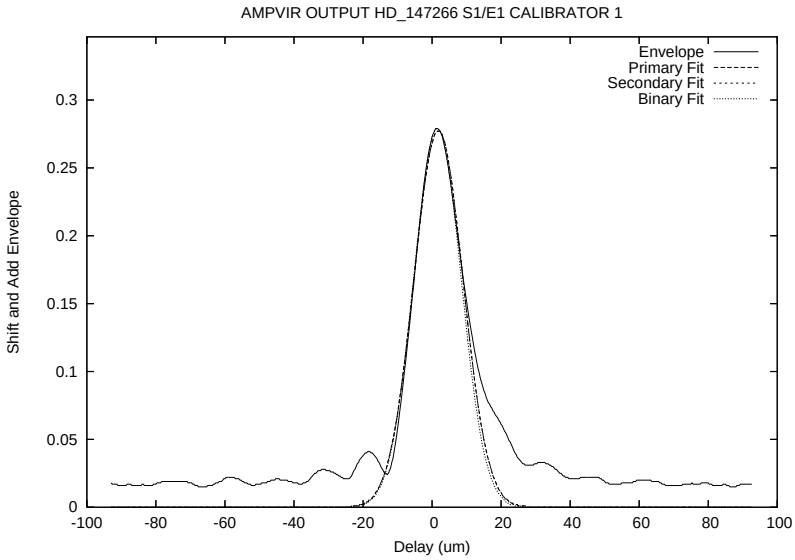


Figure. A.181: HD 147266 Fringe Envelope on 2007 April 2 on the E1/S1 Baseline.

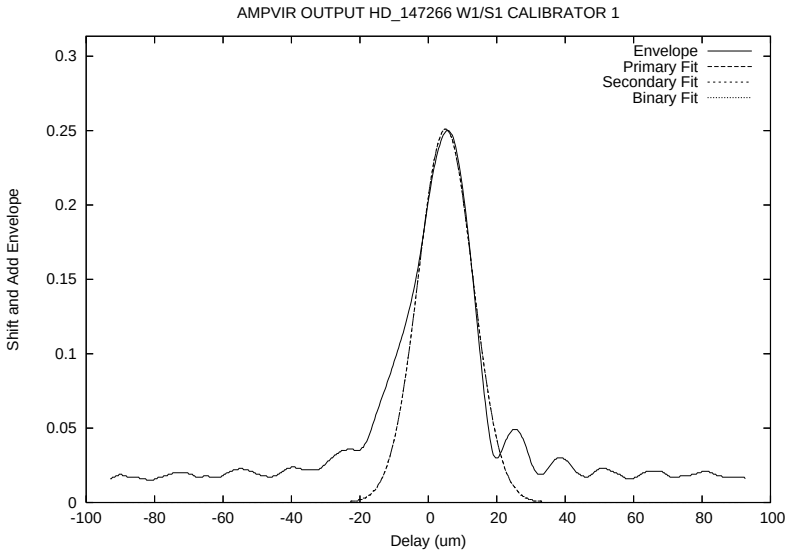


Figure. A.182: HD 147266 Fringe Envelope on 2007 May 30 on the W1/S1 Baseline.

## A.3.30 HD 150680

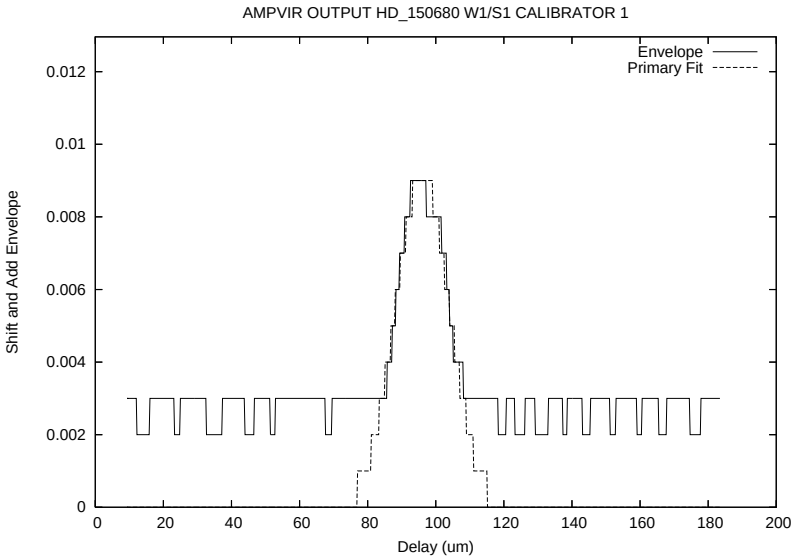


Figure. A.183: HD 150680 Fringe Envelope on 2006 June 4 on the W1/S1 Baseline.

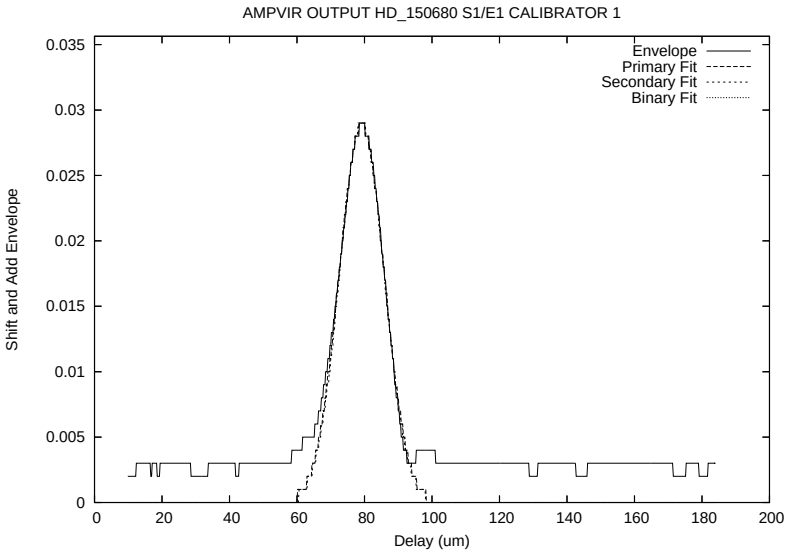


Figure. A.184: HD 150680 Fringe Envelope on 2006 June 6 on the E1/S1 Baseline.

## A.3.31 HD 151613

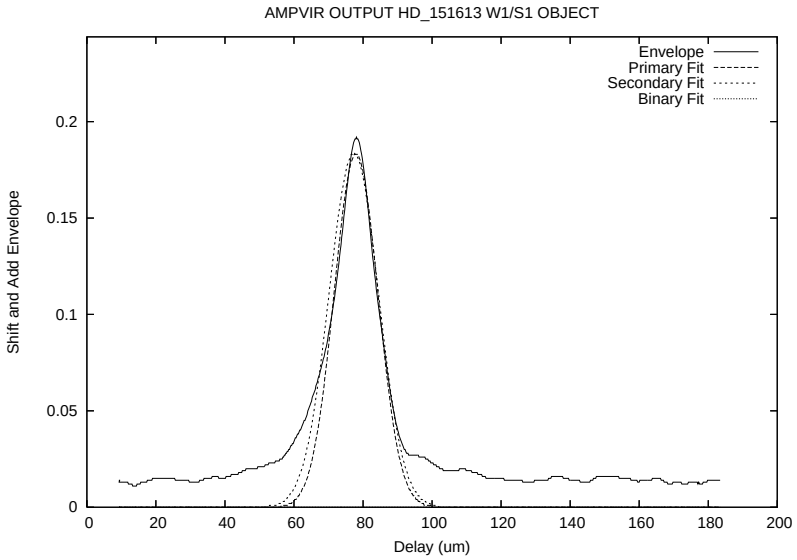


Figure. A.185: HD 151613 Fringe Envelope on 2006 June 5 on the W1/S1 Baseline.

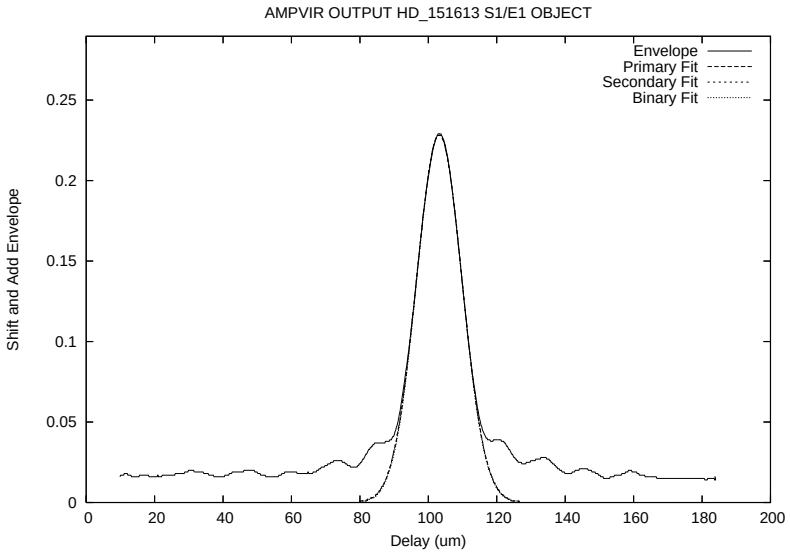


Figure. A.186: HD 151613 Fringe Envelope on 2006 June 6 on the E1/S1 Baseline.

## A.3.32 HD 152391

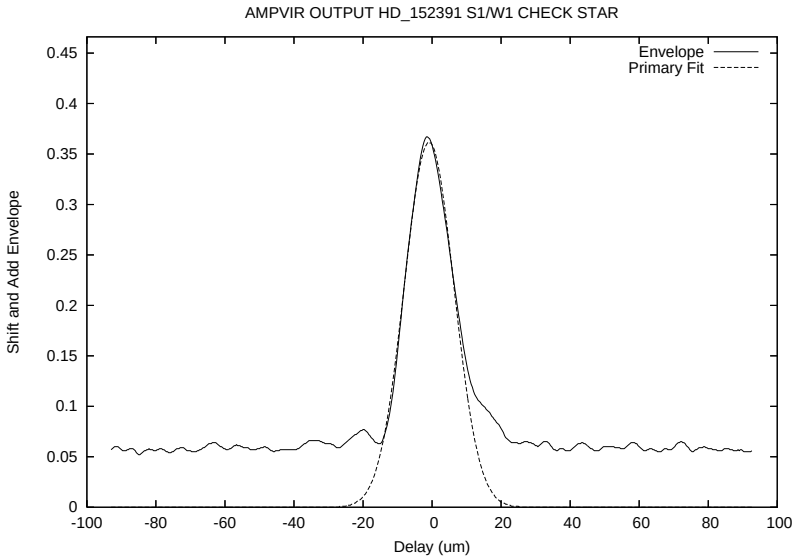


Figure. A.187: HD 152391 Fringe Envelope on 2007 June 23 on the W1/S1 Baseline.

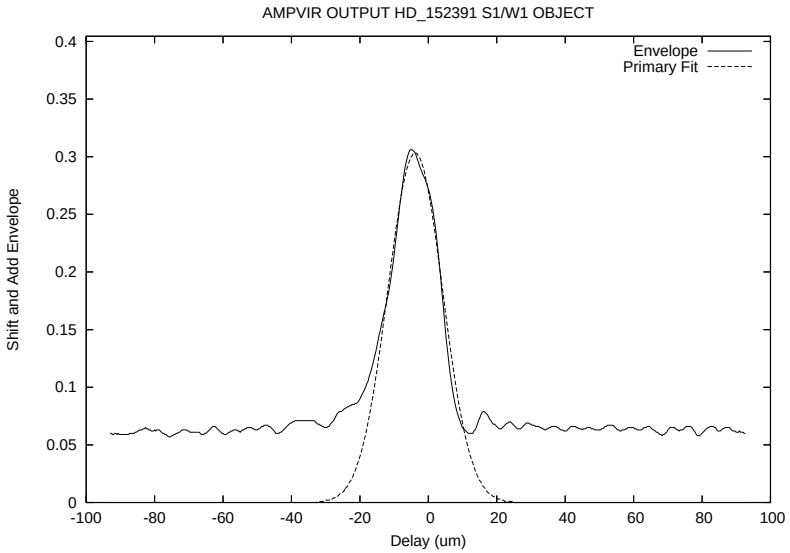


Figure. A.188: HD 152391 Fringe Envelope on 2007 July 22 on the W1/S1 Baseline.

## A.3.33 HD 153597

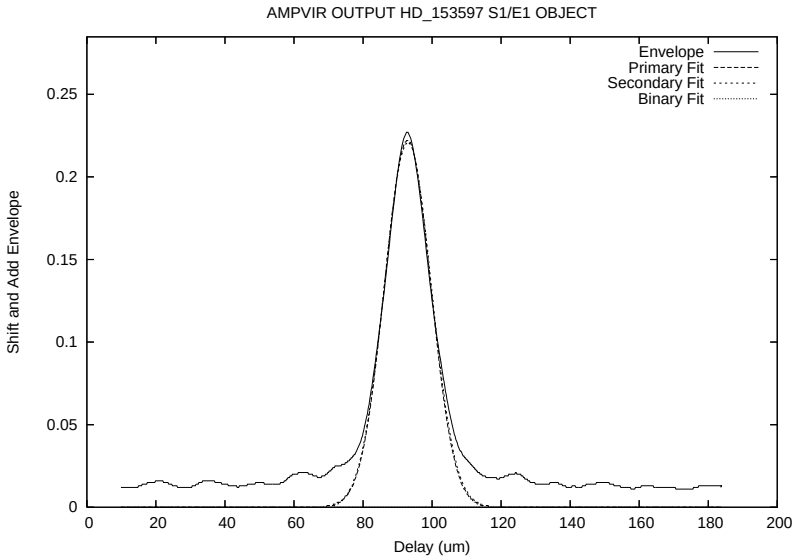


Figure. A.189: HD 153597 Fringe Envelope on 2006 June 3 on the E1/S1 Baseline.

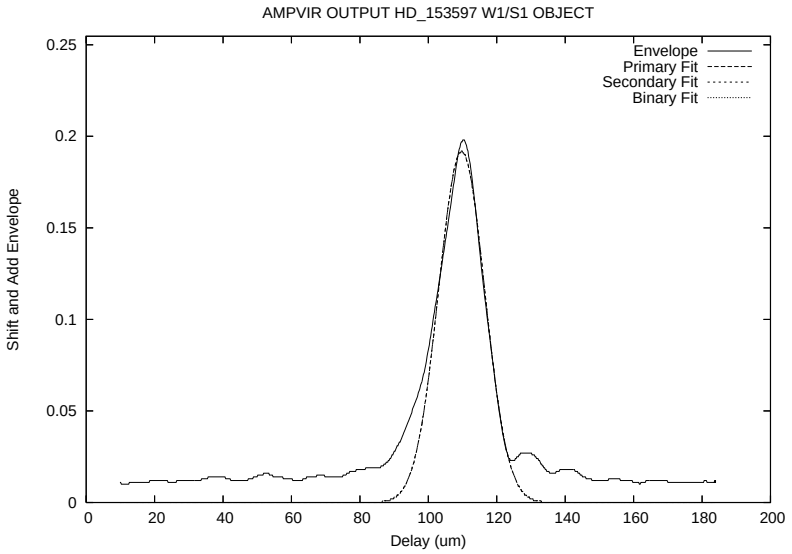


Figure. A.190: HD 153597 Fringe Envelope on 2006 June 5 on the W1/S1 Baseline.

## A.3.34 HD 154417

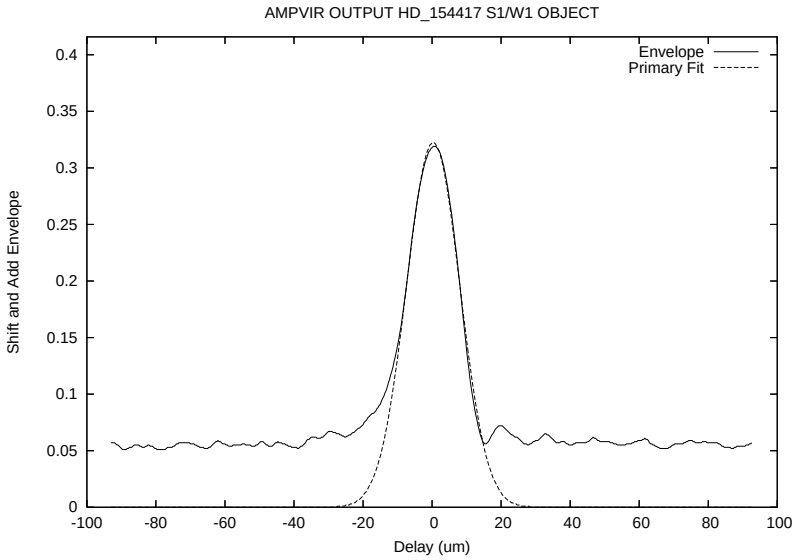


Figure. A.191: HD 154417 Fringe Envelope on 2007 April 2 on the E1/S1 Baseline.

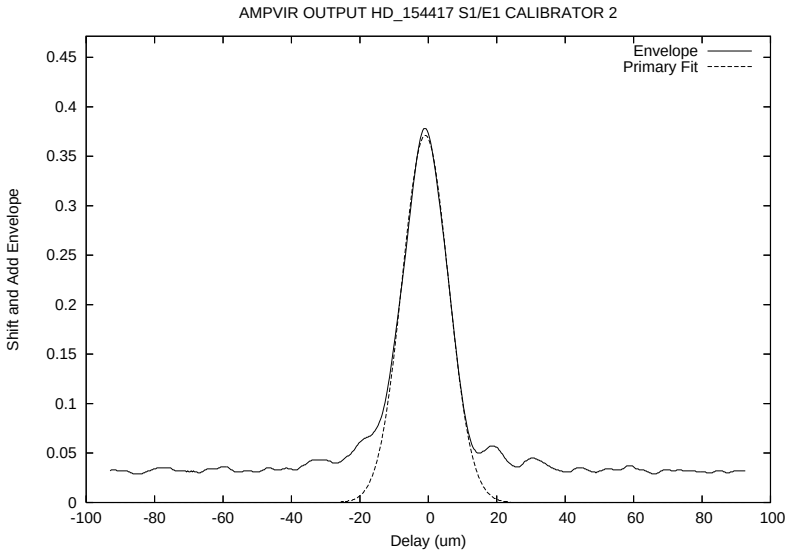


Figure. A.192: HD 154417 Fringe Envelope on 2007 July 22 on the W1/S1 Baseline.

## A.3.35 HD 154633

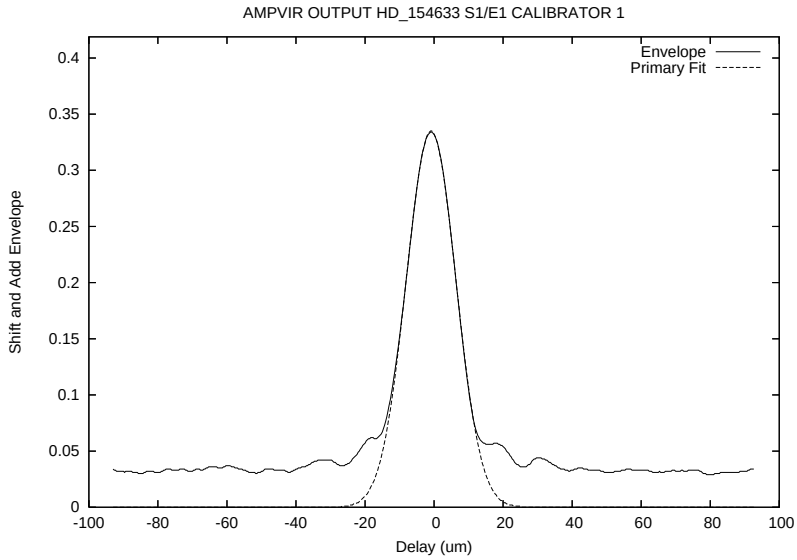


Figure. A.193: HD 154633 Fringe Envelope on 2007 June 21 on the E1/S1 Baseline.

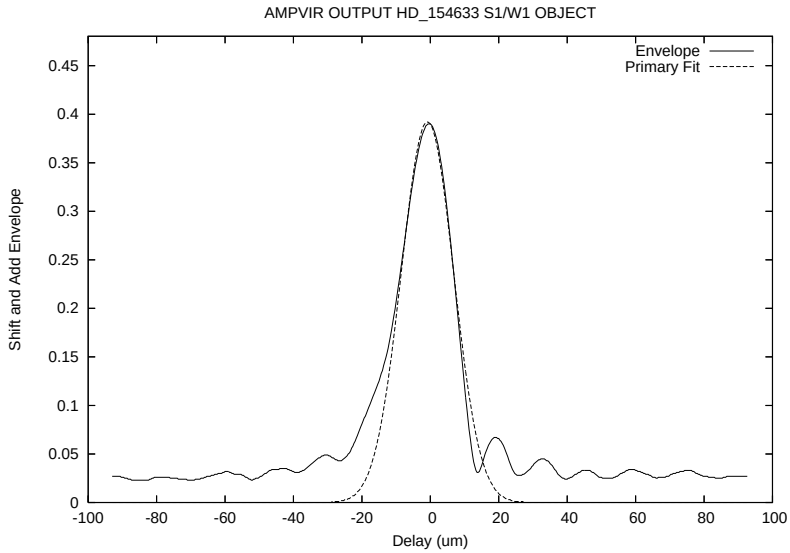


Figure. A.194: HD 154633 Fringe Envelope on 2007 June 22 on the W1/S1 Baseline.

## A.3.36 HD 157214

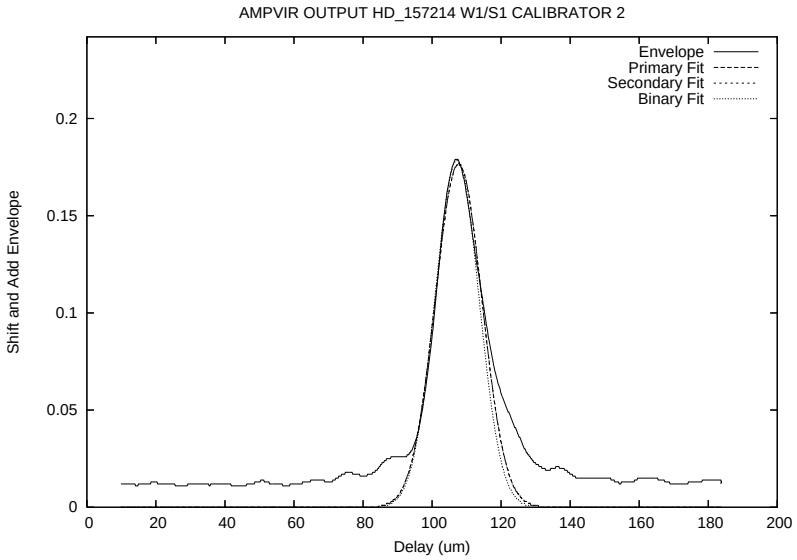


Figure. A.195: HD 157214 Fringe Envelope on 2006 June 4 on the W1/S1 Baseline.

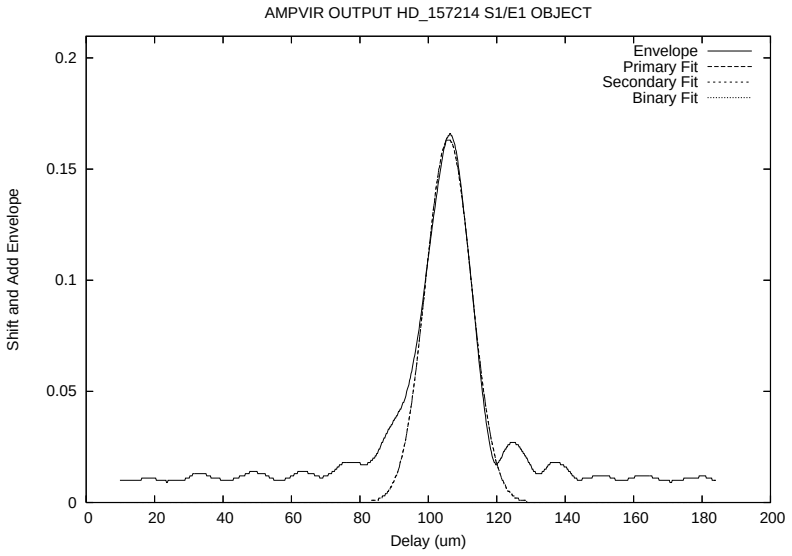


Figure. A.196: HD 157214 Fringe Envelope on 2006 June 6 on the E1/S1 Baseline.

## A.3.37 HD 160269

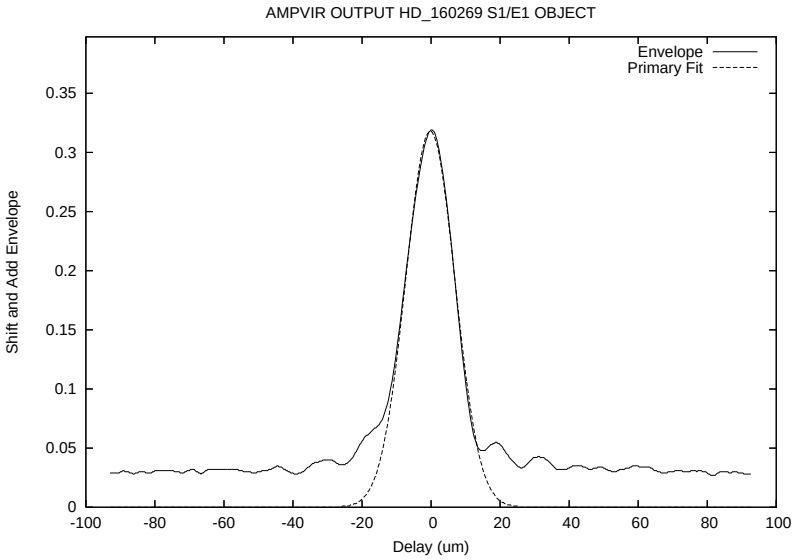


Figure. A.197: HD 160269 Fringe Envelope on 2007 June 21 on the E1/S1 Baseline.

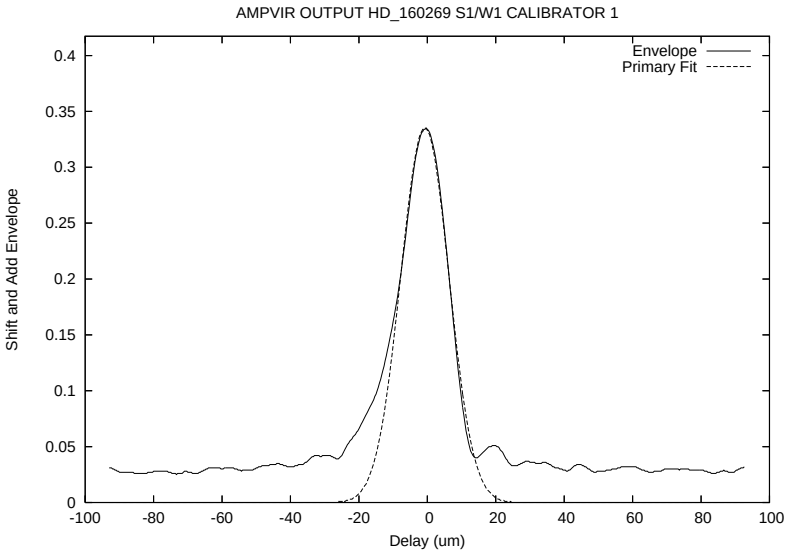


Figure. A.198: HD 160269 Fringe Envelope on 2007 June 22 on the W1/S1 Baseline.

## A.3.38 HD 161797

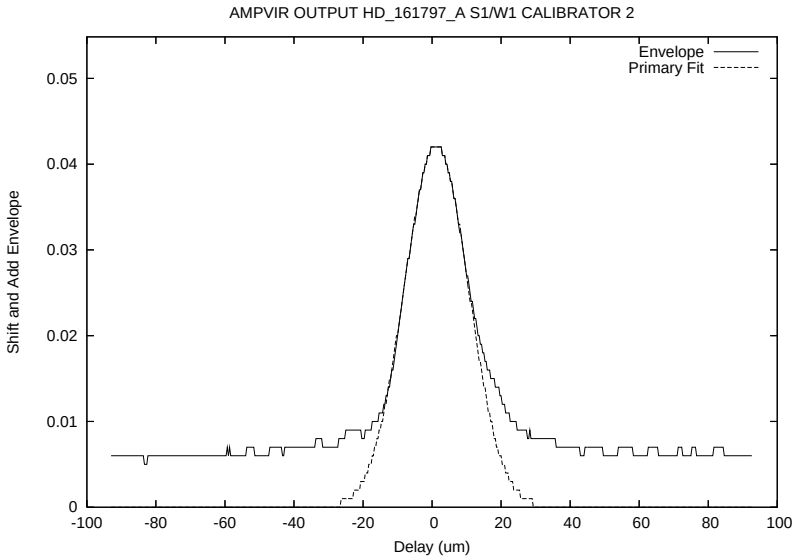


Figure. A.199: HD 161797 Fringe Envelope on 2006 September 13 on the W1/S1 Baseline.

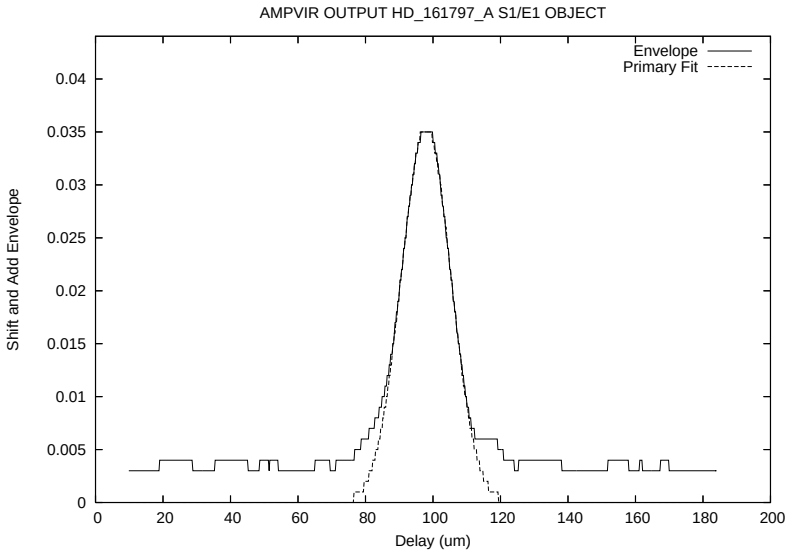


Figure. A.200: HD 161797 Fringe Envelope on 2007 June 23 on the E1/S1 Baseline.

## A.3.39 HD 162003

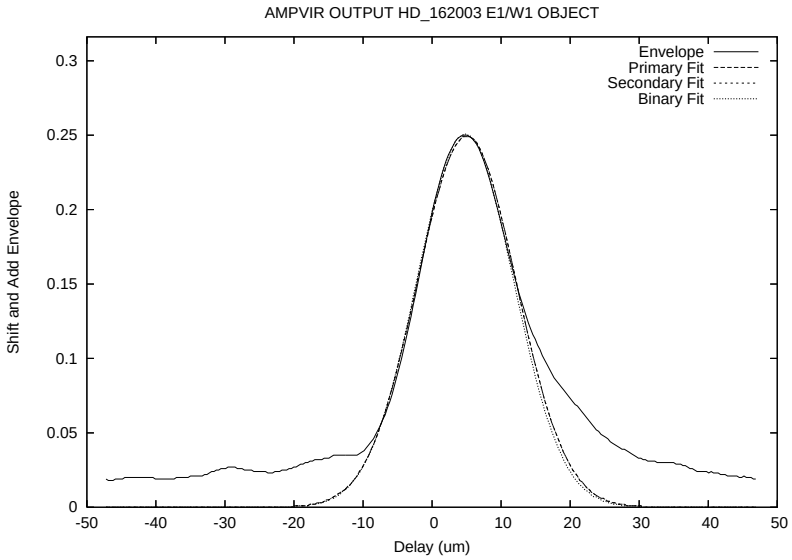


Figure. A.201: HD 162003 Fringe Envelope on 2007 October 10 on the E1/W1 Baseline.

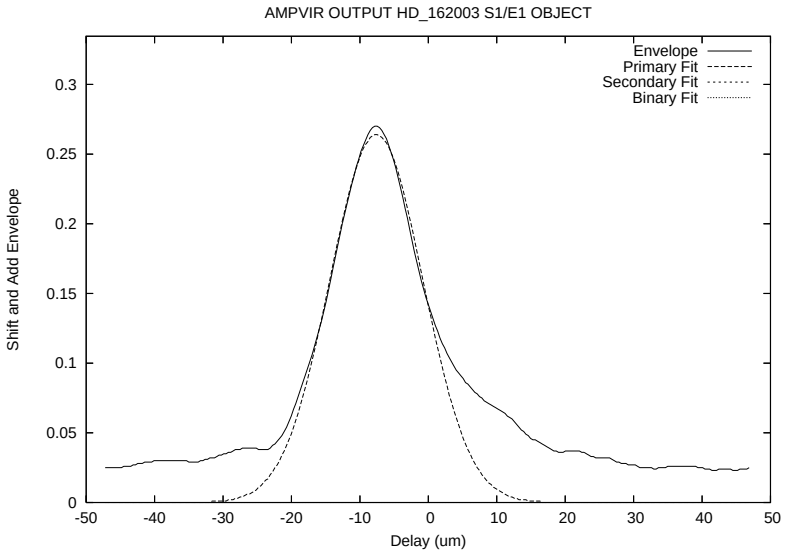


Figure. A.202: HD 162003 Fringe Envelope on 2007 November 17 on the E1/S1 Baseline.

## A.3.40 HD 162004

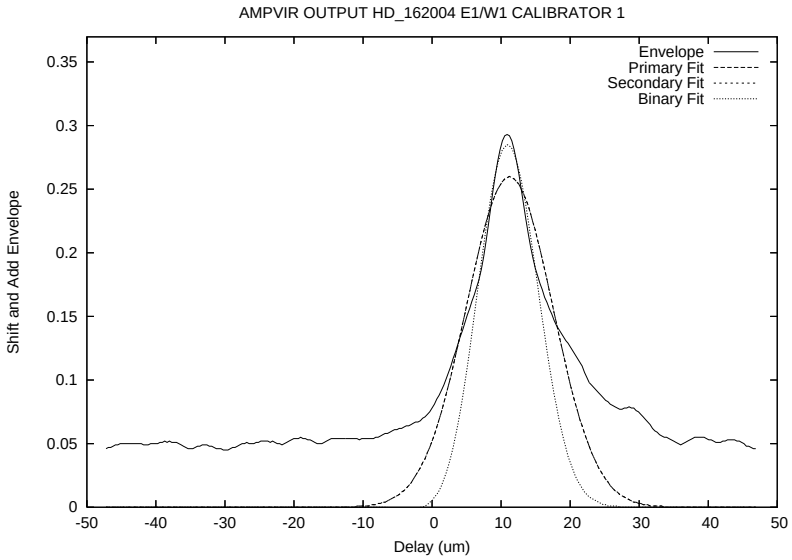


Figure. A.203: HD 162004 Fringe Envelope on 2007 October 10 on the E1/W1 Baseline.

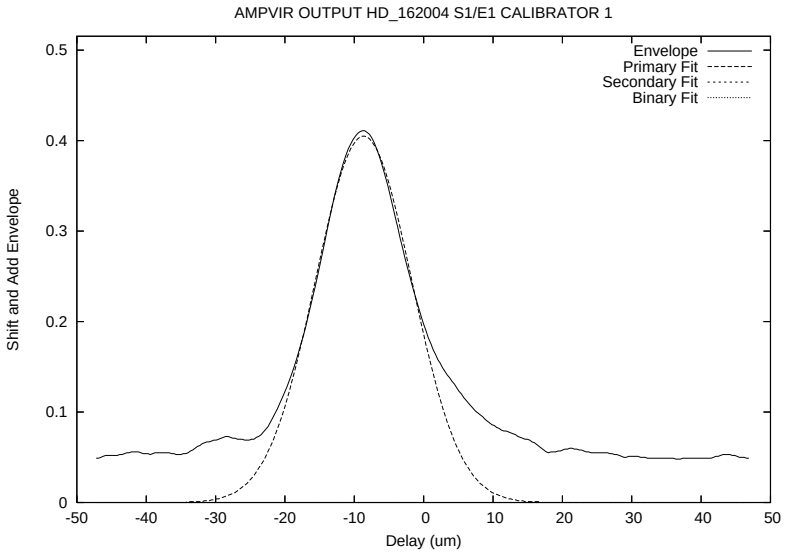


Figure. A.204: HD 162004 Fringe Envelope on 2007 November 17 on the E1/S1 Baseline.

## A.3.41 HD 165341

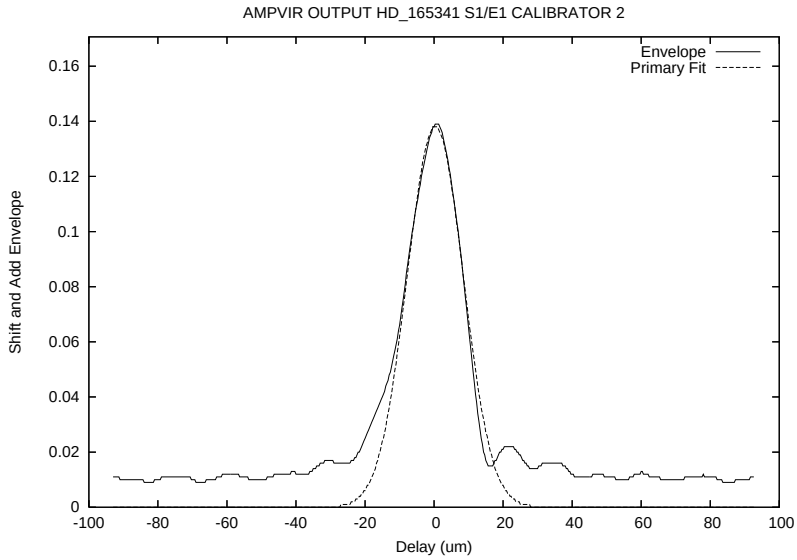


Figure. A.205: HD 165341 Fringe Envelope on 2007 July 22 on the E1/S1 Baseline.

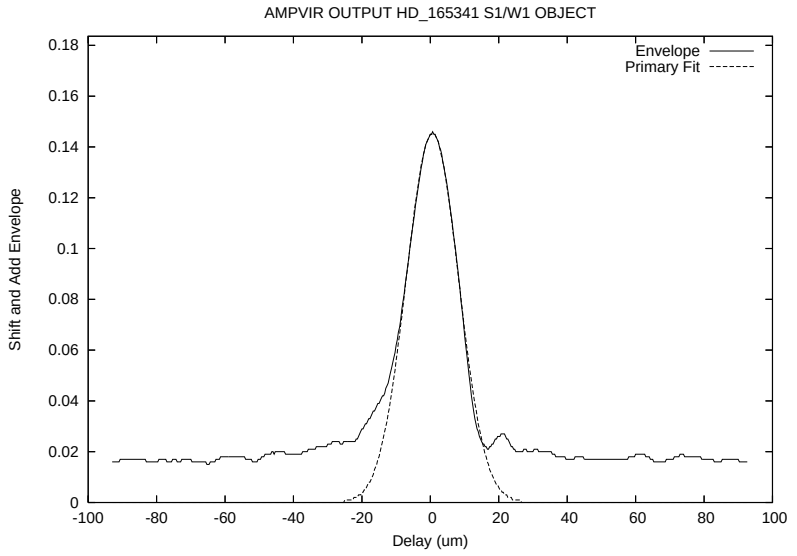


Figure. A.206: HD 165341 Fringe Envelope on 2007 July 22 on the W1/S1 Baseline.

## A.3.42 HD 165908

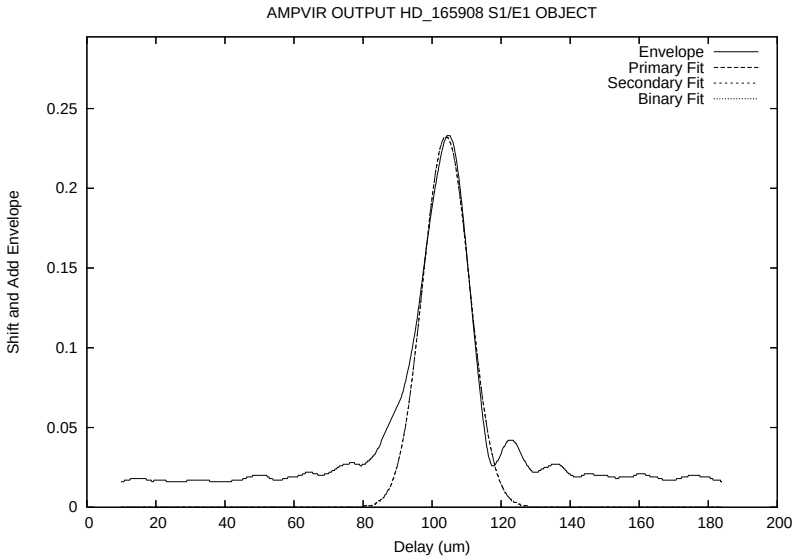


Figure. A.207: HD 165908 Fringe Envelope on 2006 September 9 on the E1/S1 Baseline.

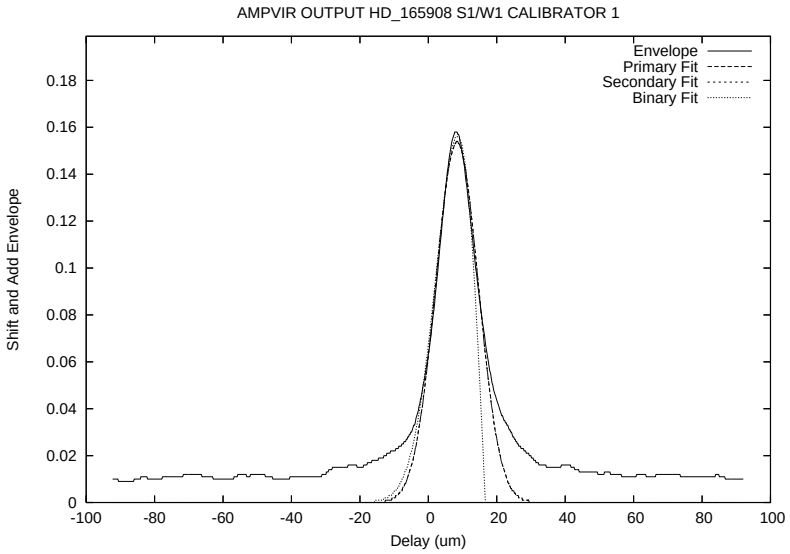


Figure. A.208: HD 165908 Fringe Envelope on 2007 October 2 on the W1/S1 Baseline.

## A.3.43 HD 168009

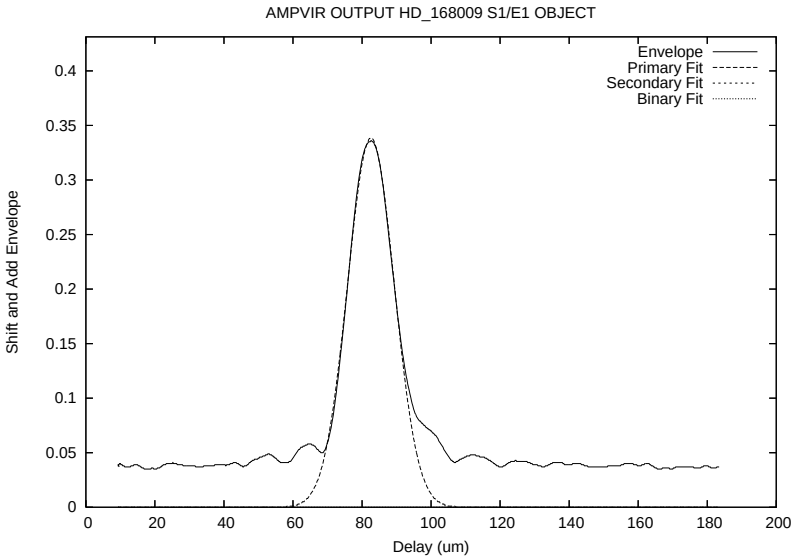


Figure. A.209: HD 168009 Fringe Envelope on 2006 September 9 on the E1/S1 Baseline.

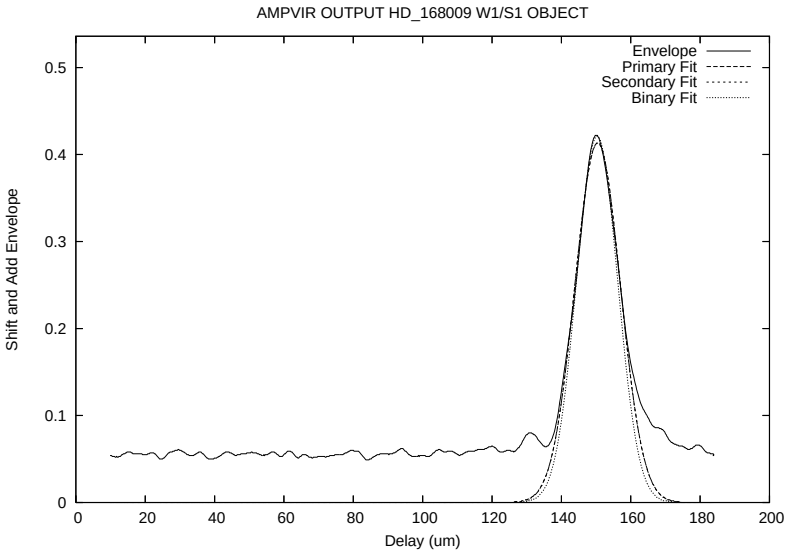


Figure. A.210: HD 168009 Fringe Envelope on 2006 September 11 on the W1/S1 Baseline.

## A.3.44 HD 168151

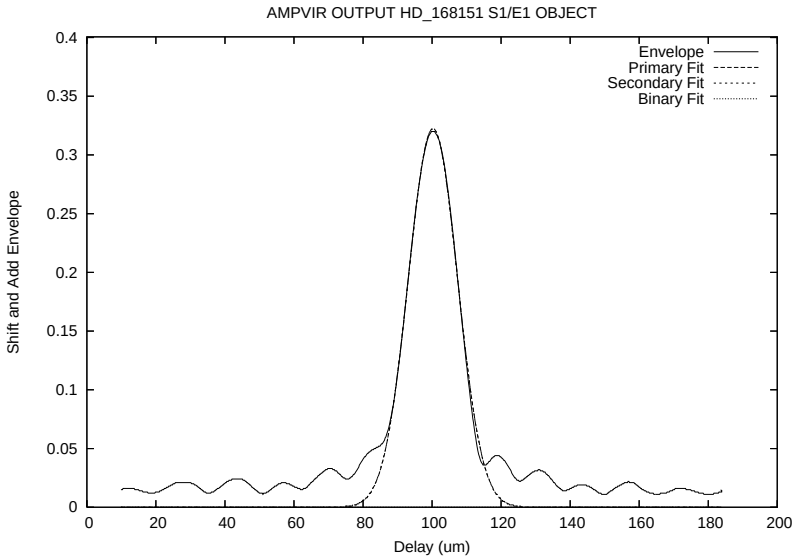


Figure. A.211: HD 168151 Fringe Envelope on 2005 June 3 on the E1/S1 Baseline.

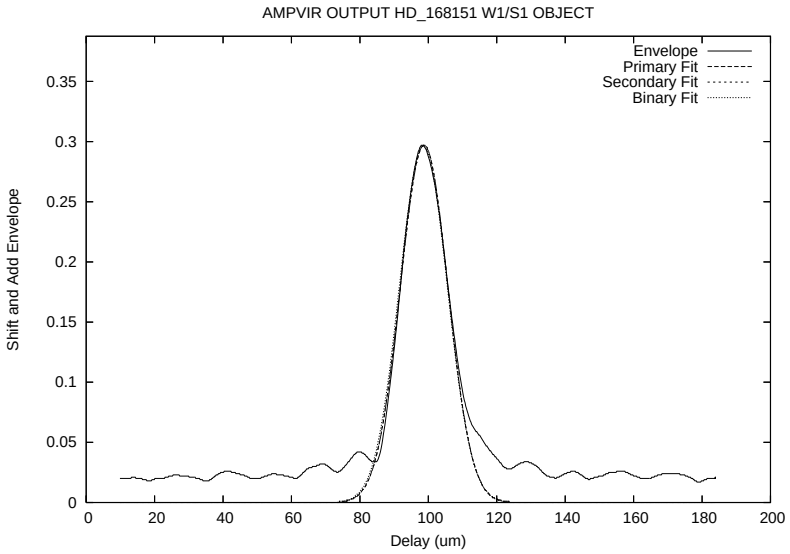


Figure. A.212: HD 168151 Fringe Envelope on 2006 June 5 on the W1/S1 Baseline.

## A.3.45 HD 173667

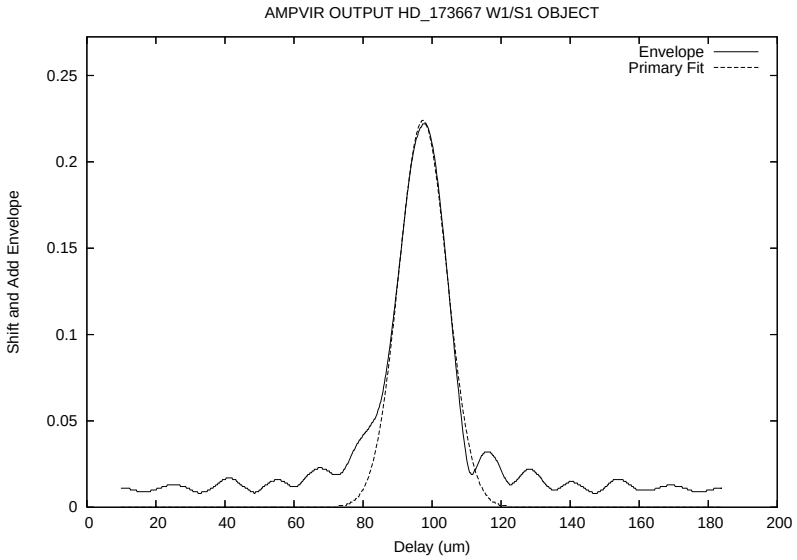


Figure. A.213: HD 173667 Fringe Envelope on 2006 September 19 on the W1/S1 Baseline.

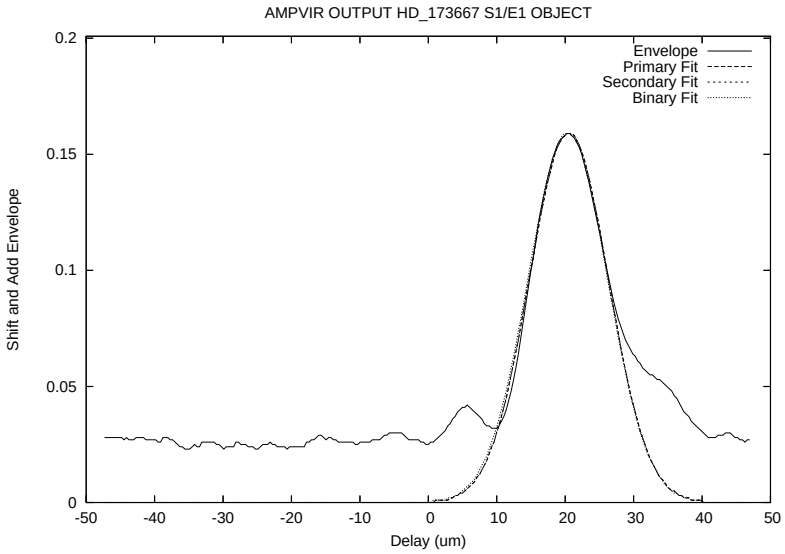


Figure. A.214: HD 173667 Fringe Envelope on 2007 September 10 on the E1/S1 Baseline.

## A.3.46 HD 175225

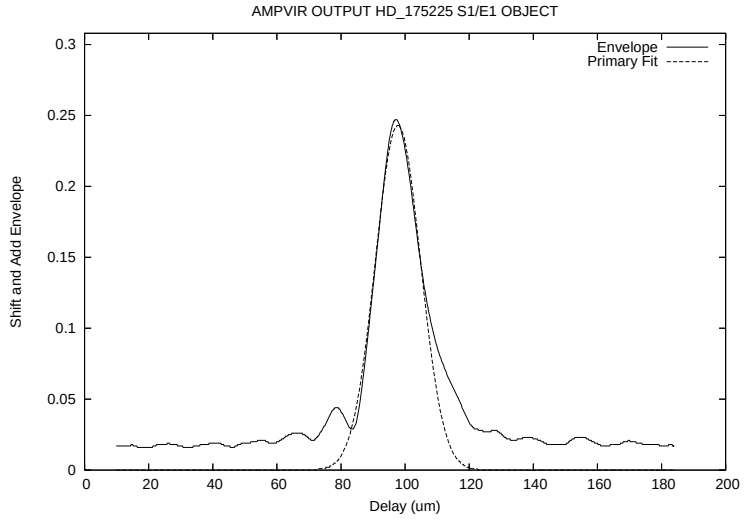


Figure. A.215: HD 175225 Fringe Envelope on 2006 September 9 on the E1/S1 Baseline.

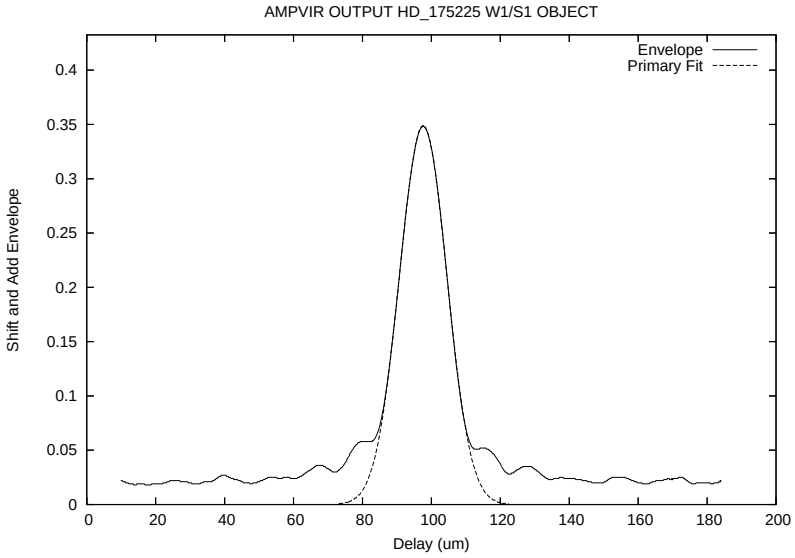


Figure. A.216: HD 175225 Fringe Envelope on 2006 September 11 on the W1/S1 Baseline.

# A.4 Observed Stars Right Ascension 19-23 Hours

## A.4.1 HD 176051

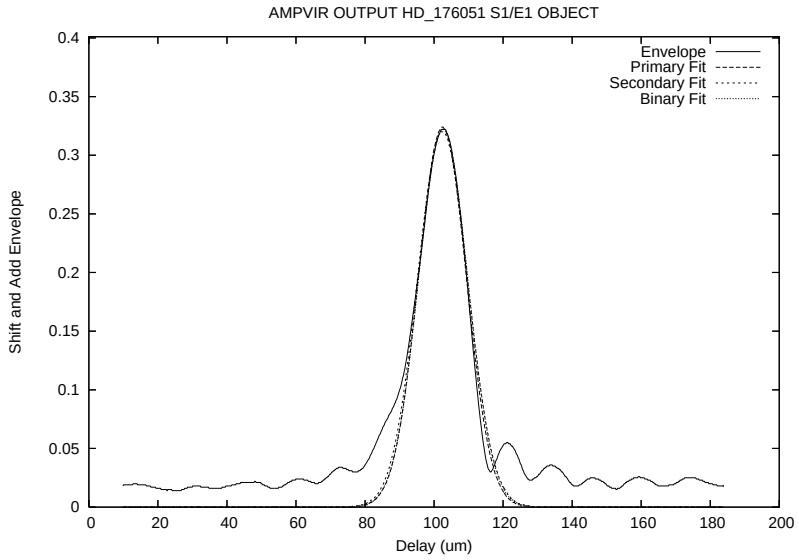


Figure. A.217: HD 176051 Fringe Envelope on 2006 September 9 on the E1/S1 Baseline.

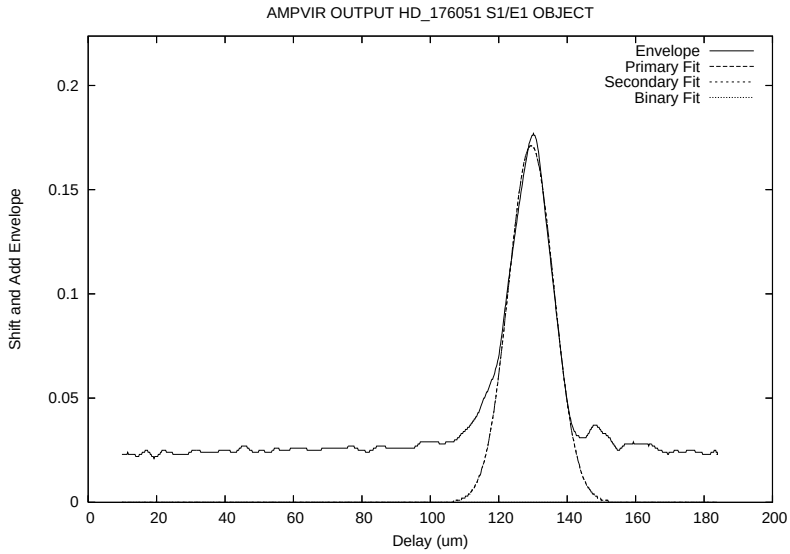


Figure. A.218: HD 176051 Fringe Envelope on 2006 September 10 on the E1/S1 Baseline.

## A.4.2 HD 180777

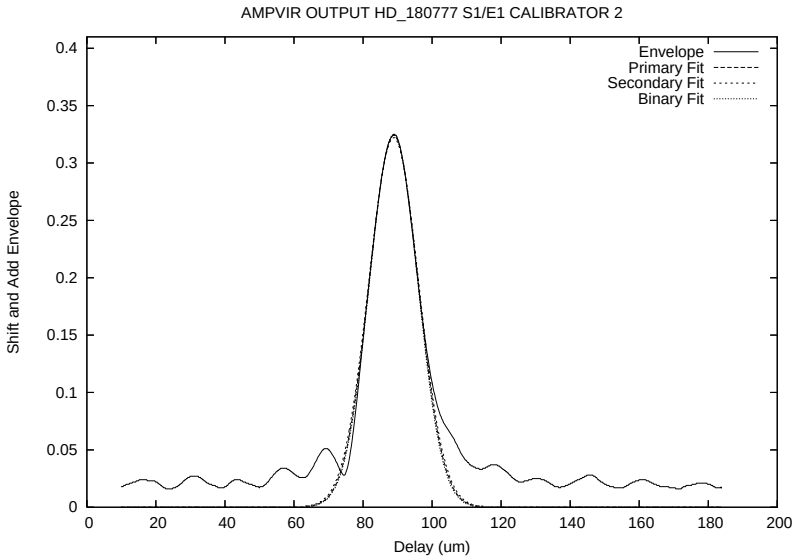


Figure. A.219: HD 180777 Fringe Envelope on 2006 June 3 on the E1/S1 Baseline.

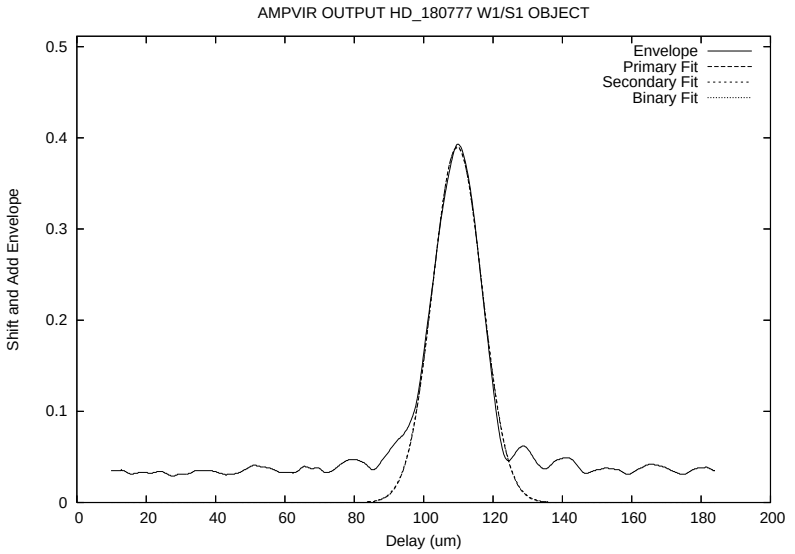


Figure. A.220: HD 180777 Fringe Envelope on 2006 June 5 on the W1/S1 Baseline.

### A.4.3 HD 182572

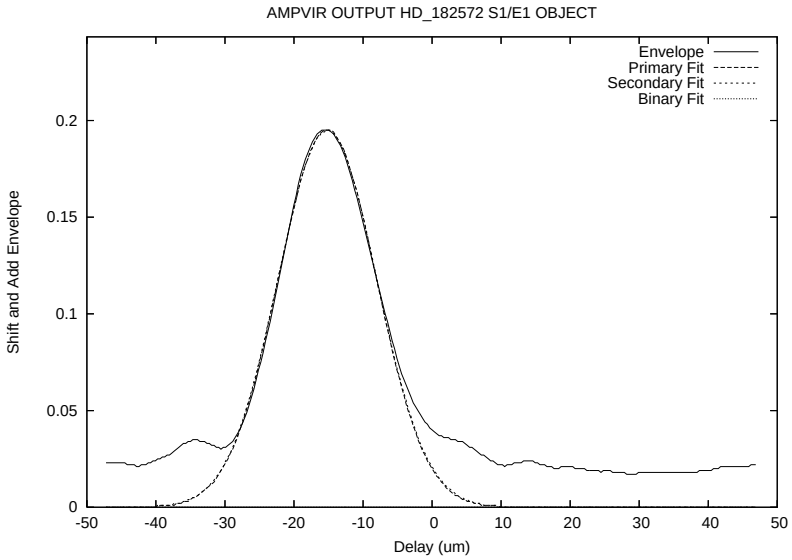


Figure. A.221: HD 182572 Fringe Envelope on 2006 September 19 on the E1/S1 Baseline.

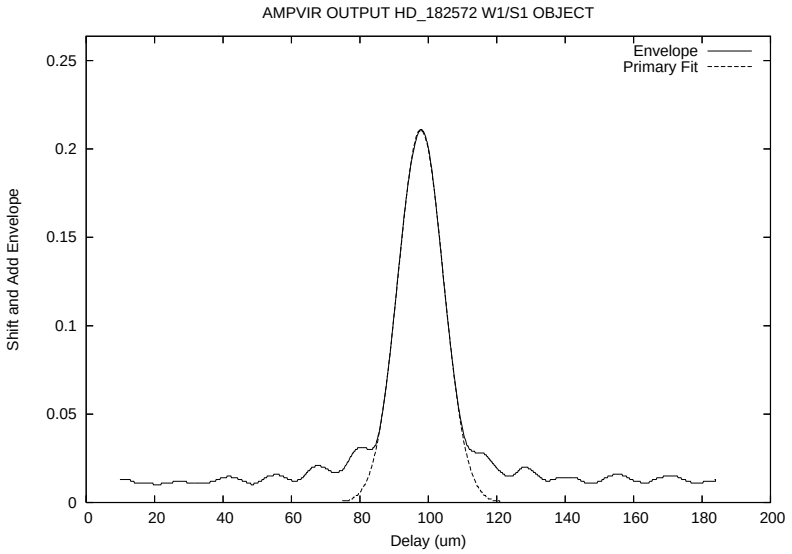


Figure. A.222: HD 182572 Fringe Envelope on 2007 September 9 on the W1/S1 Baseline.

## A.4.4 HD 185395

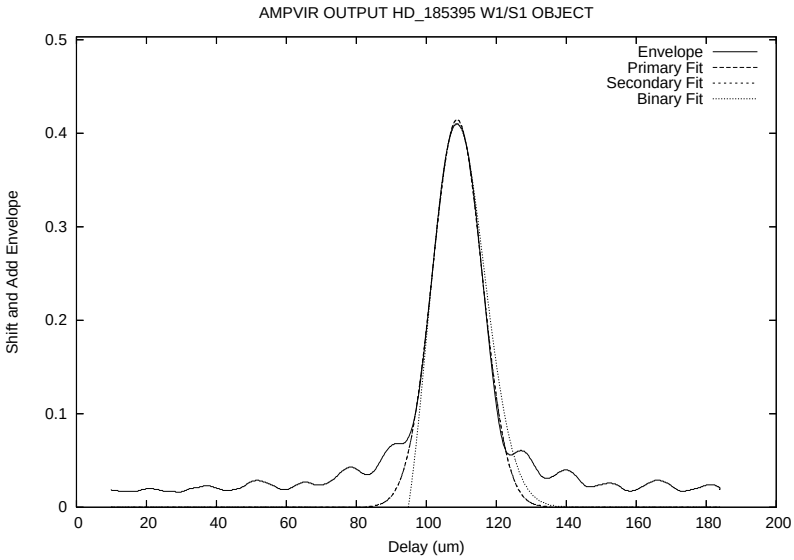


Figure. A.223: HD 185395 Fringe Envelope on 2006 September 11 on the W1/S1 Baseline.

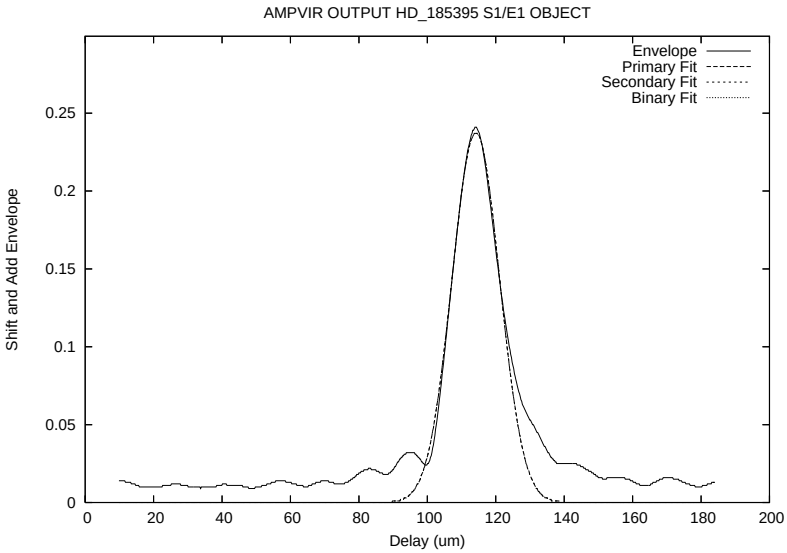


Figure. A.224: HD 185395 Fringe Envelope on 2006 September 13 on the E1/S1 Baseline.

## A.4.5 HD 186408

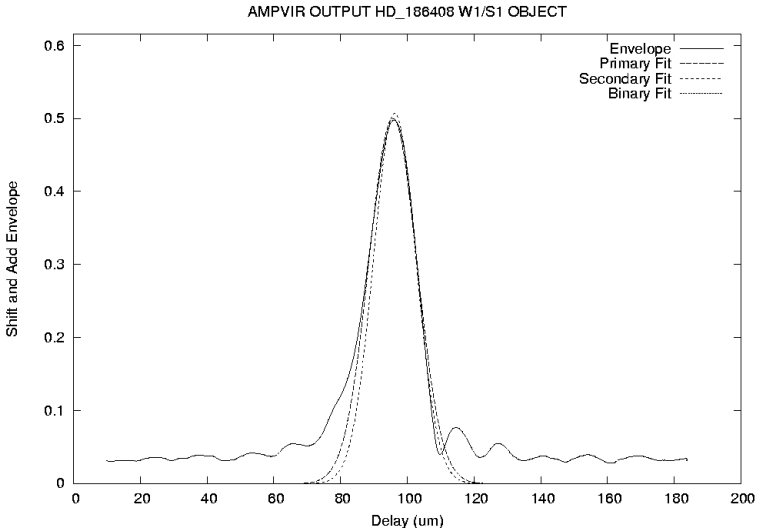


Figure. A.225: HD 186408 Fringe Envelope on 2006 September 11 on the W1/S1 Baseline.

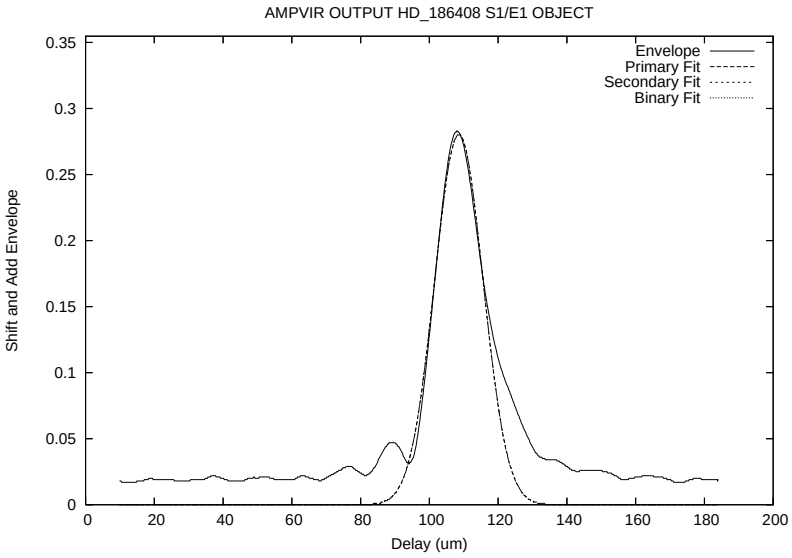


Figure. A.226: HD 186408 Fringe Envelope on 2006 September 13 on the E1/S1 Baseline.

## A.4.6 HD 186427

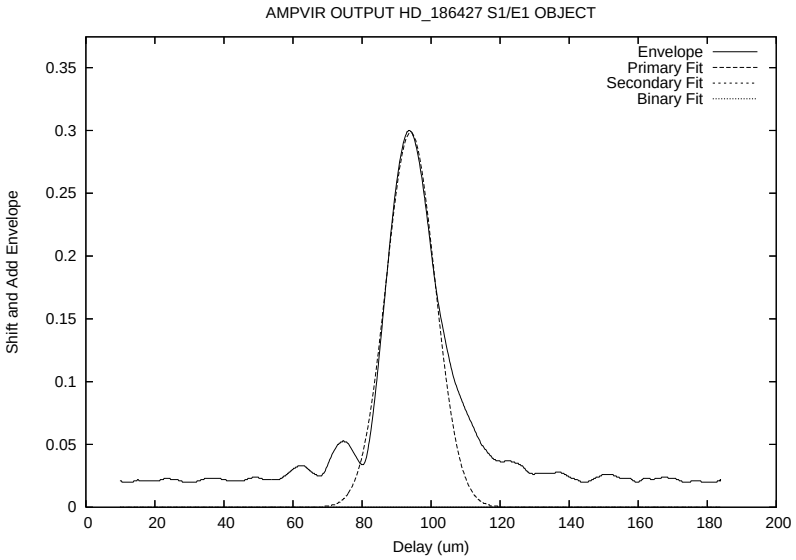


Figure. A.227: HD 186427 Fringe Envelope on 2006 September 11 on the W1/S1 Baseline.

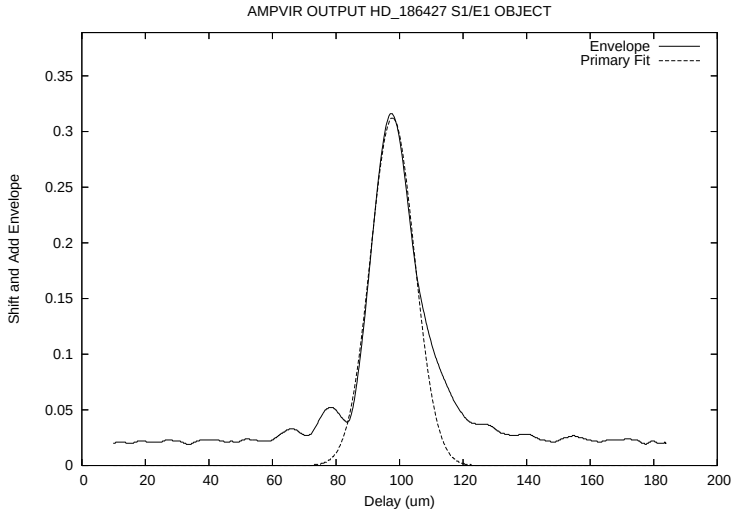


Figure. A.228: HD 186427 Fringe Envelope on 2006 September 13 on the E1/S1 Baseline.

## A.4.7 HD 186760

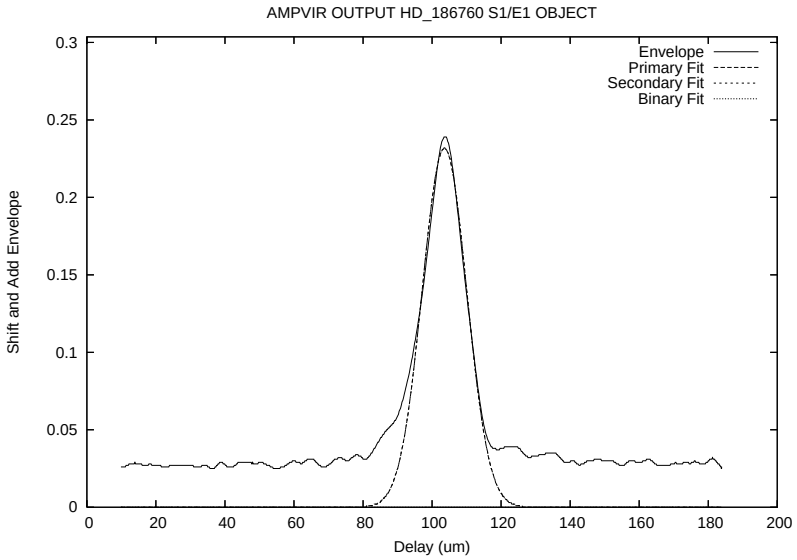


Figure. A.229: HD 186760 Fringe Envelope on 2007 June 21 on the E1/S1 Baseline.

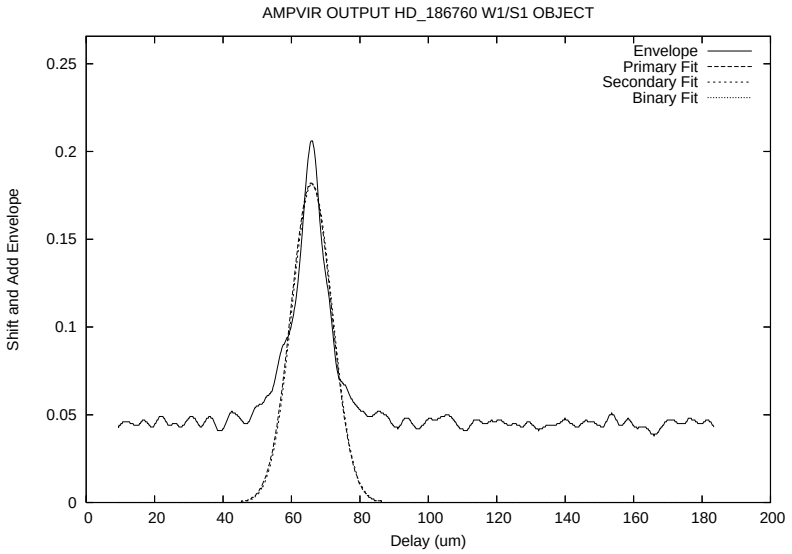


Figure. A.230: HD 186760 Fringe Envelope on 2007 June 22 on the W1/S1 Baseline.

## A.4.8 HD 187013

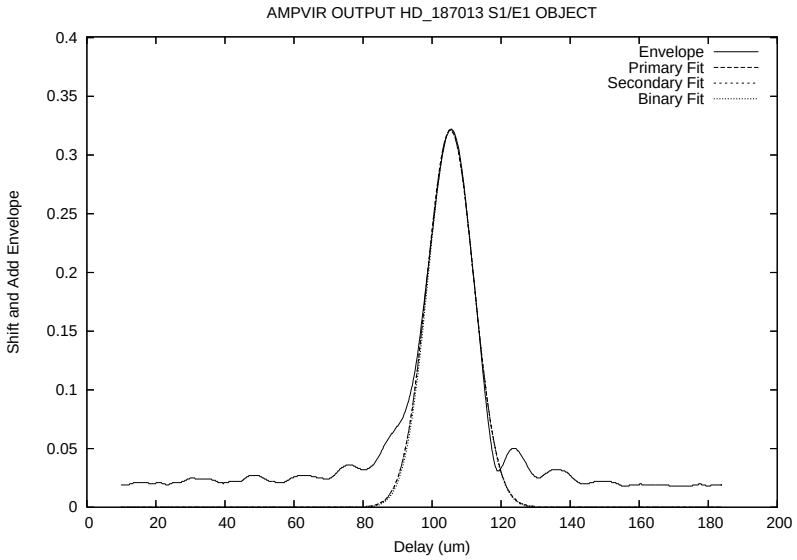


Figure. A.231: HD 187013 Fringe Envelope on 2005 October 6 on the E1/S1 Baseline.

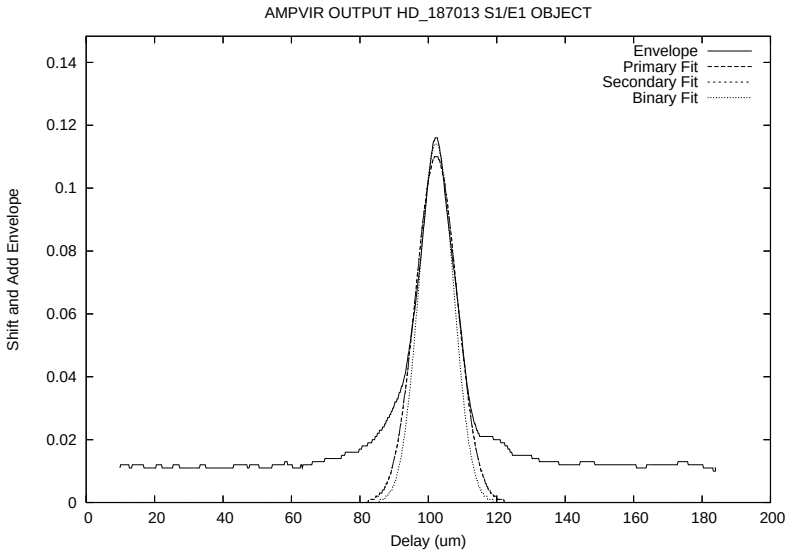


Figure. A.232: HD 187013 Fringe Envelope on 2006 September 10 on the E1/S1 Baseline.

## A.4.9 HD 187691

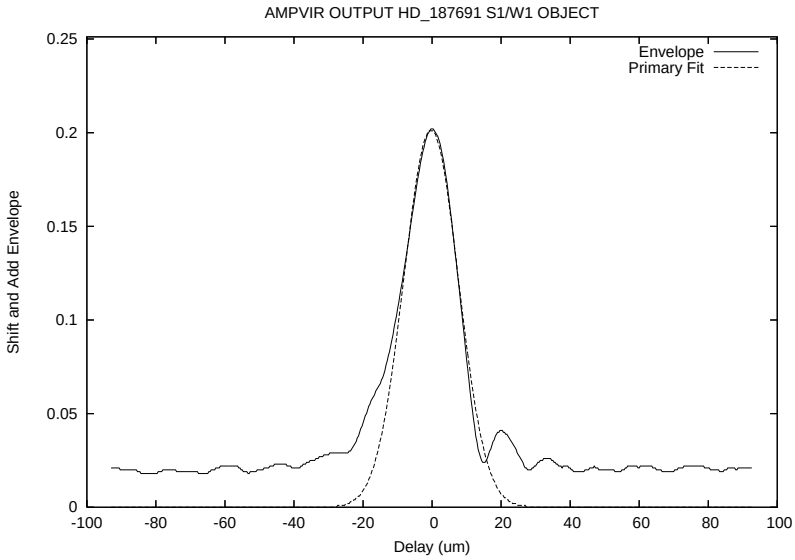


Figure. A.233: HD 187691 Fringe Envelope on 2007 July 22 on the W1/S1 Baseline.

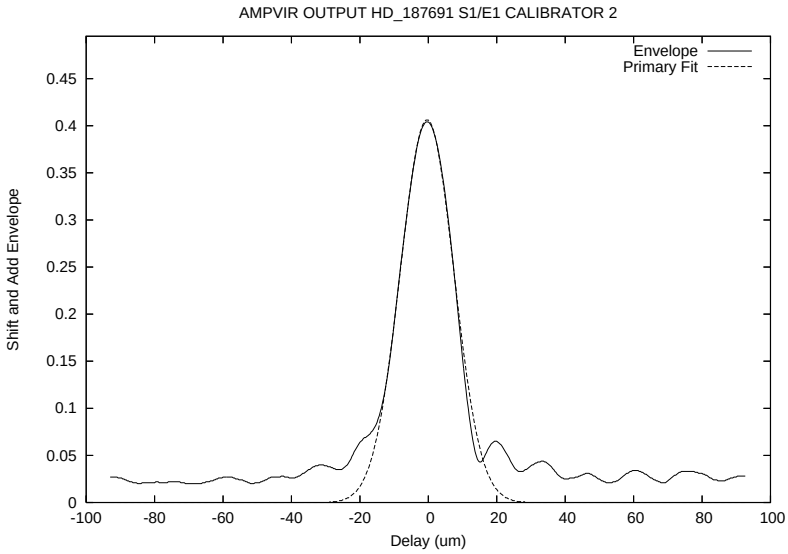


Figure. A.234: HD 187691 Fringe Envelope on 2007 July 22 on the E1/S1 Baseline.

## A.4.10 HD 188512

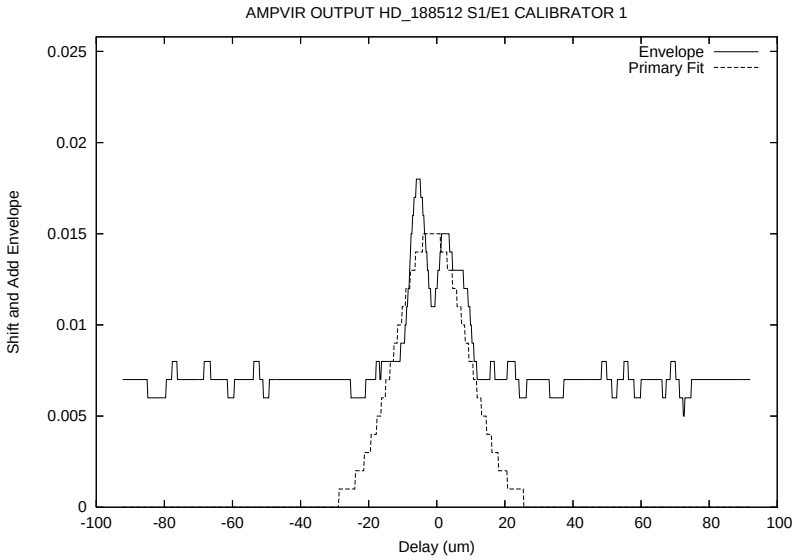


Figure. A.235: HD 188512 Fringe Envelope on 2007 July 22 on the E1/S1 Baseline. Very resolved star on this baseline.

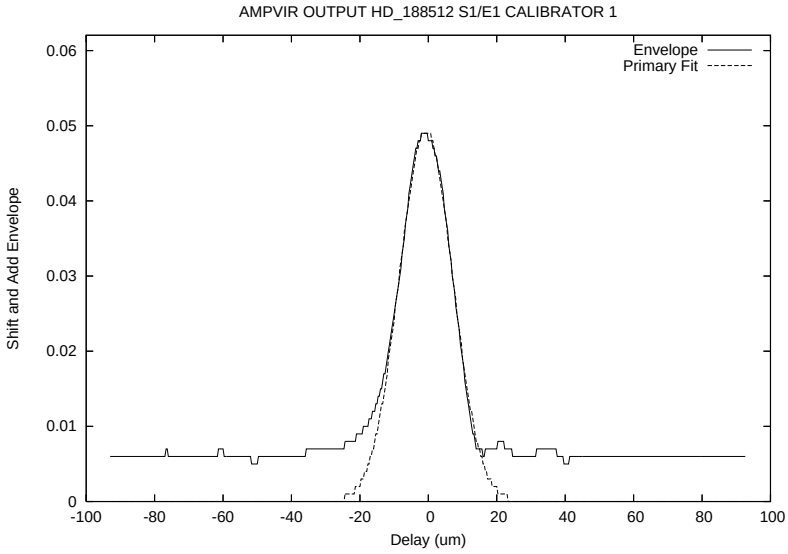


Figure. A.236: HD 188512 Fringe Envelope on 2007 July 24 on the E1/S1 Baseline. Very resolved star on this baseline.

## A.4.11 HD 190360

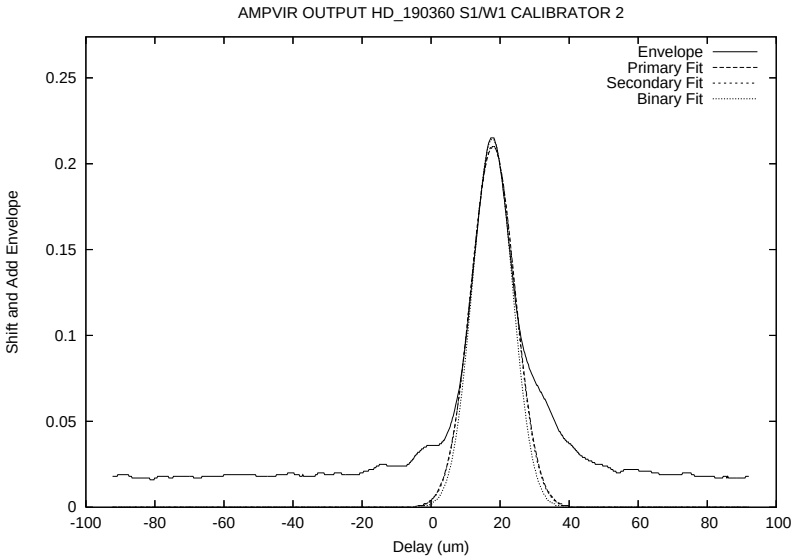


Figure. A.237: HD 190360 Fringe Envelope on 2007 October 19 on the W1/S1 Baseline.

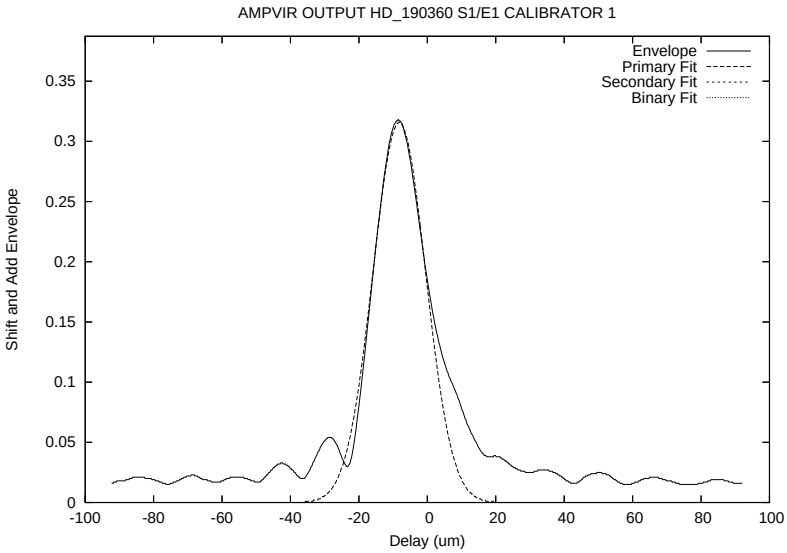


Figure. A.238: HD 190360 Fringe Envelope on 2007 October 19 on the E1/S1 Baseline.

## A.4.12 HD 190406

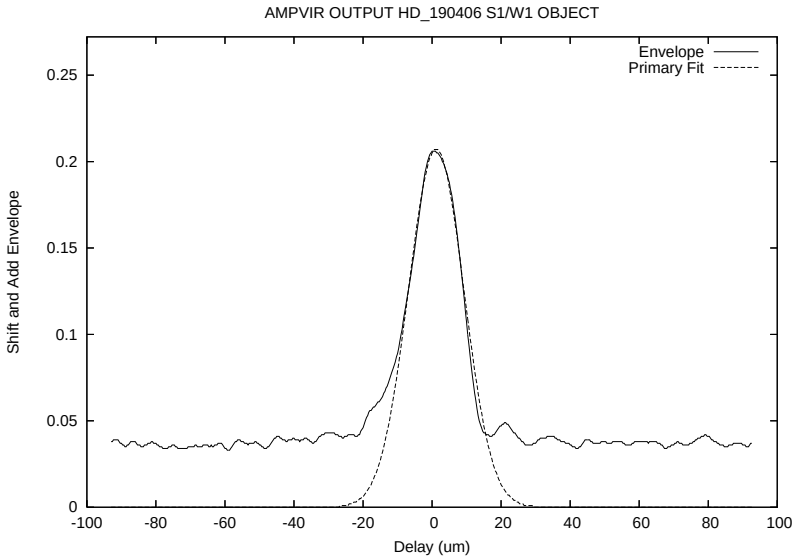


Figure. A.239: HD 190406 Fringe Envelope on 2007 July 22 on the W1/S1 Baseline.

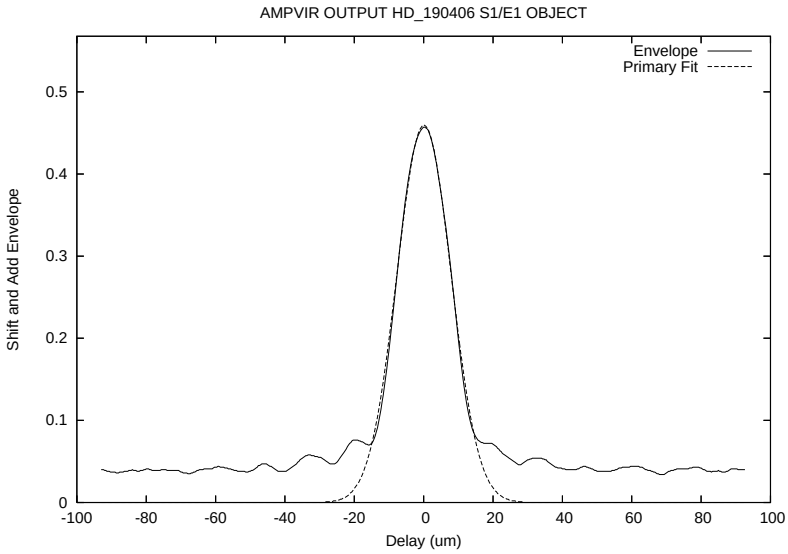


Figure. A.240: HD 190406 Fringe Envelope on 2007 July 22 on the E1/S1 Baseline.

## A.4.13 HD 193664

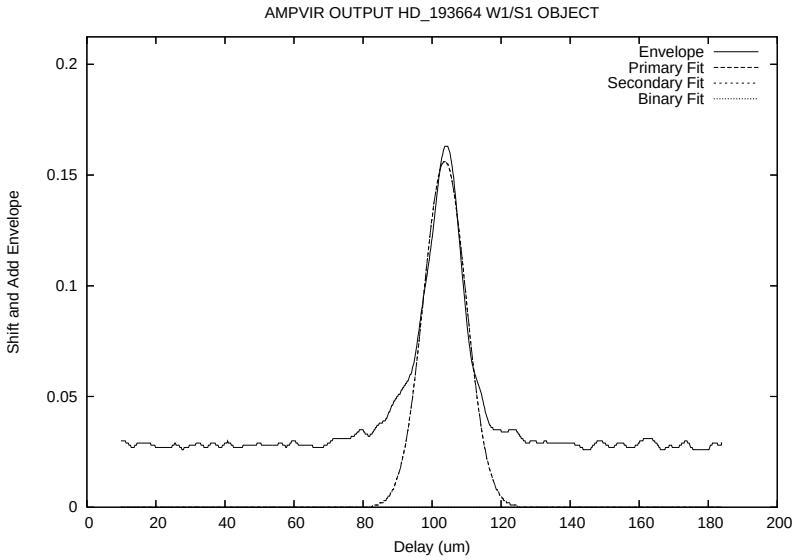


Figure. A.241: HD 193664 Fringe Envelope on 2005 October 5 on the W1/S1 Baseline.

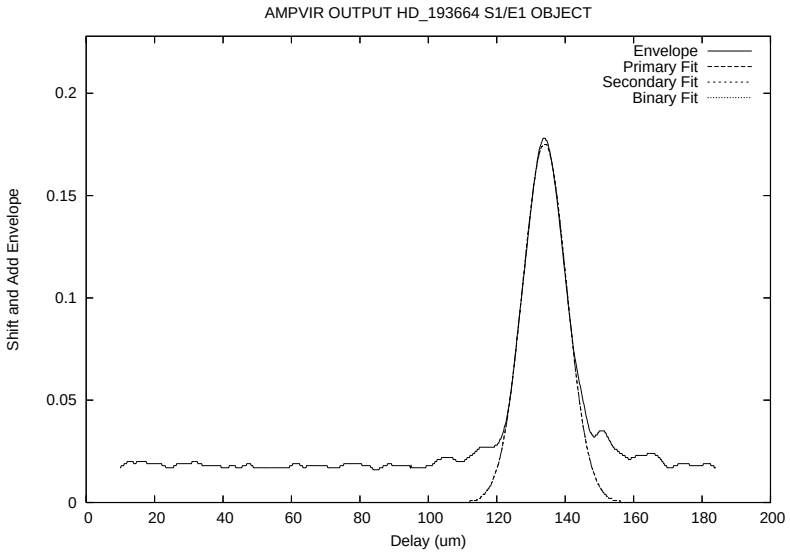


Figure. A.242: HD 193664 Fringe Envelope on 2005 October 11 on the E1/S1 Baseline.

## A.4.14 HD 194012

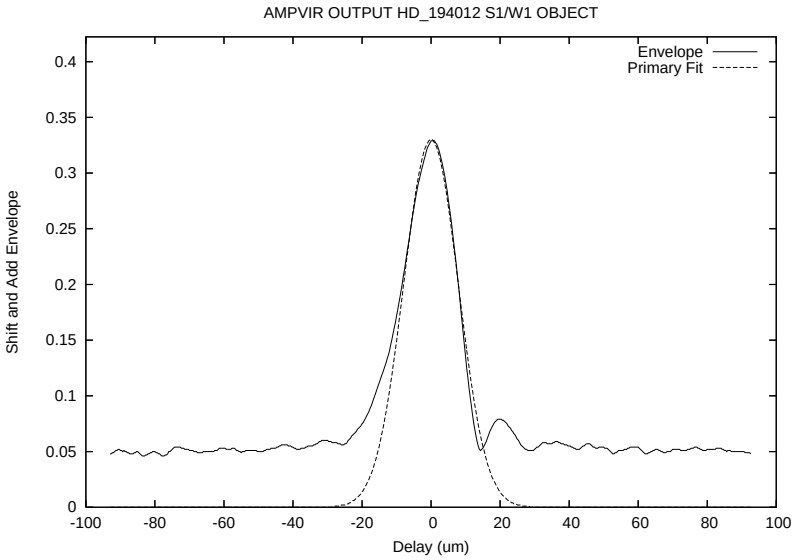


Figure. A.243: HD 194012 Fringe Envelope on 2007 July 22 on the W1/S1 Baseline.

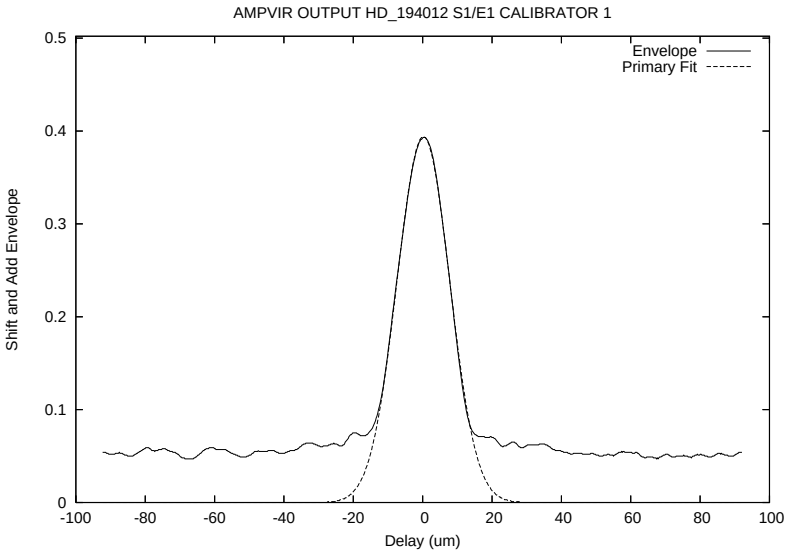


Figure. A.244: HD 194012 Fringe Envelope on 2007 July 22 on the E1/S1 Baseline.

## A.4.15 HD 202444

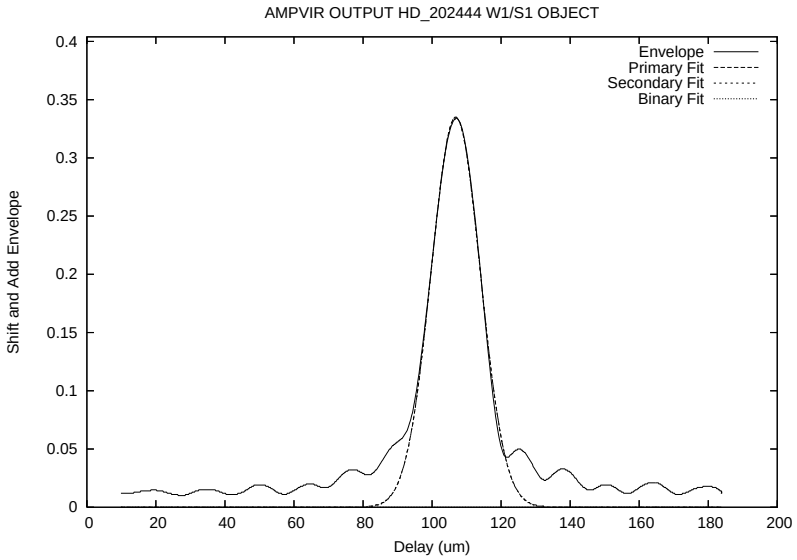


Figure. A.245: HD 202444 Fringe Envelope on 2006 September 11 on the W1/S1 Baseline.

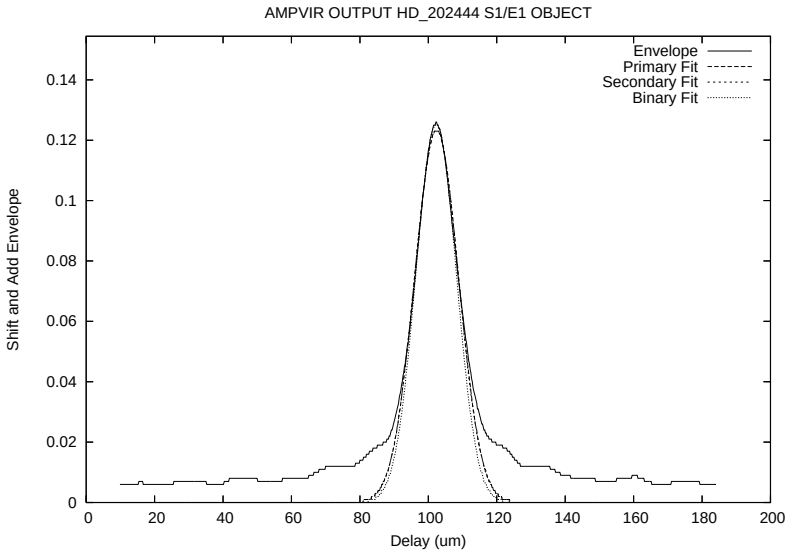


Figure. A.246: HD 202444 Fringe Envelope on 2006 September 13 on the E1/S1 Baseline.

## A.4.16 HD 202573

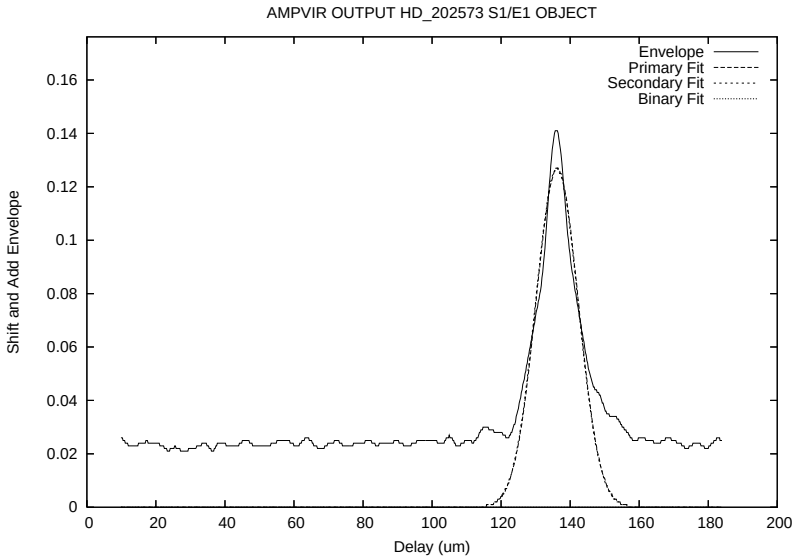


Figure. A.247: HD 202573 Fringe Envelope on 2005 October 7 on the E1/S1 Baseline.

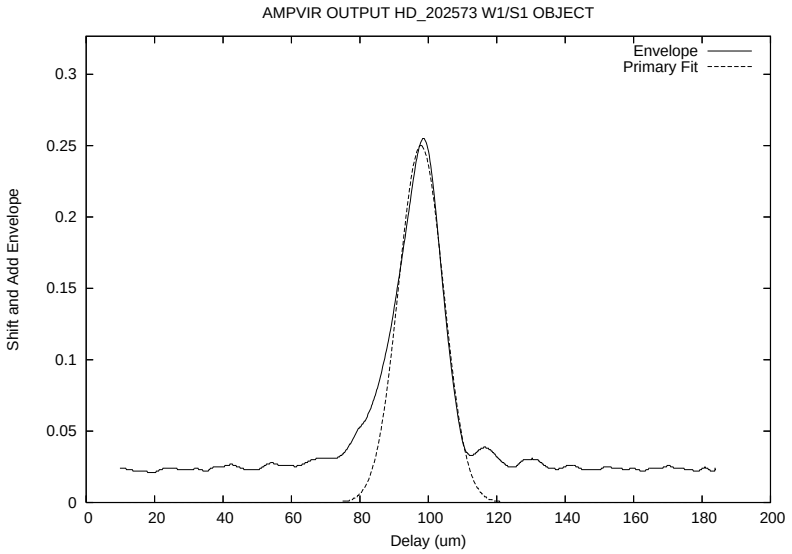


Figure. A.248: HD 202573 Fringe Envelope on 2006 September 19 on the W1/S1 Baseline.

## A.4.17 HD 206826

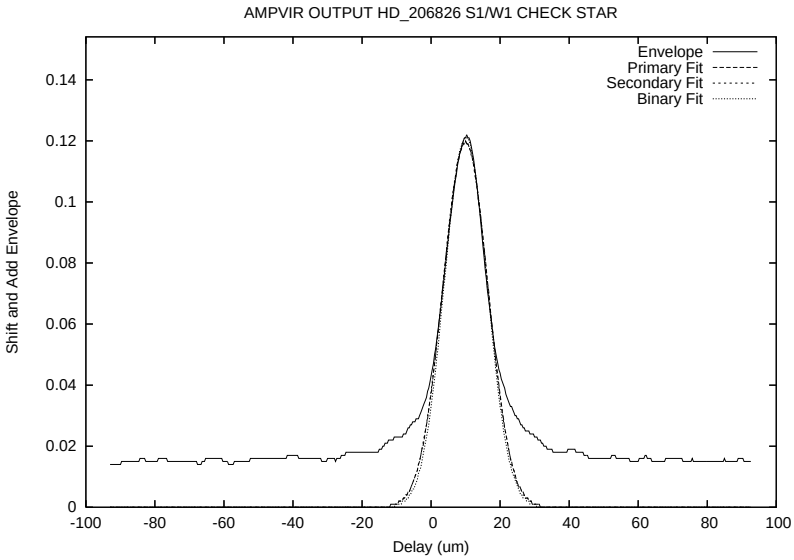


Figure. A.249: HD 206826 Fringe Envelope on 2007 October 19 on the W1/S1 Baseline.

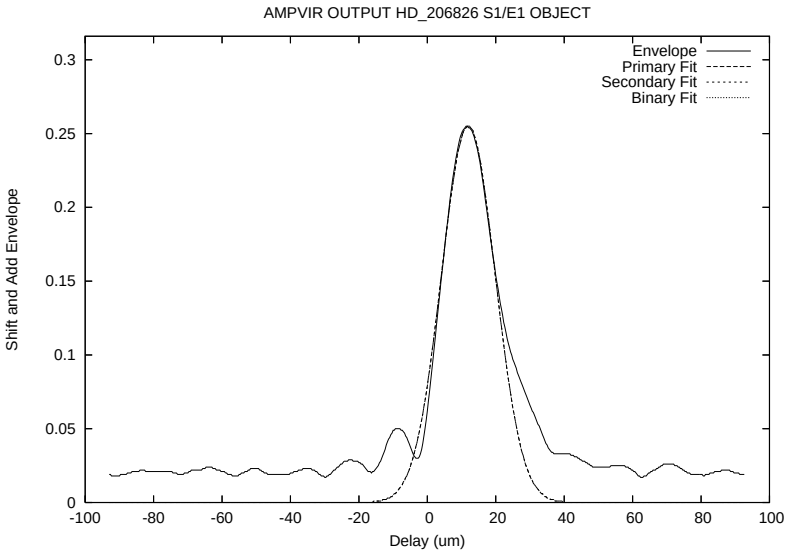


Figure. A.250: HD 206826 Fringe Envelope on 2007 October 19 on the E1/S1 Baseline.

## A.4.18 HD 210027

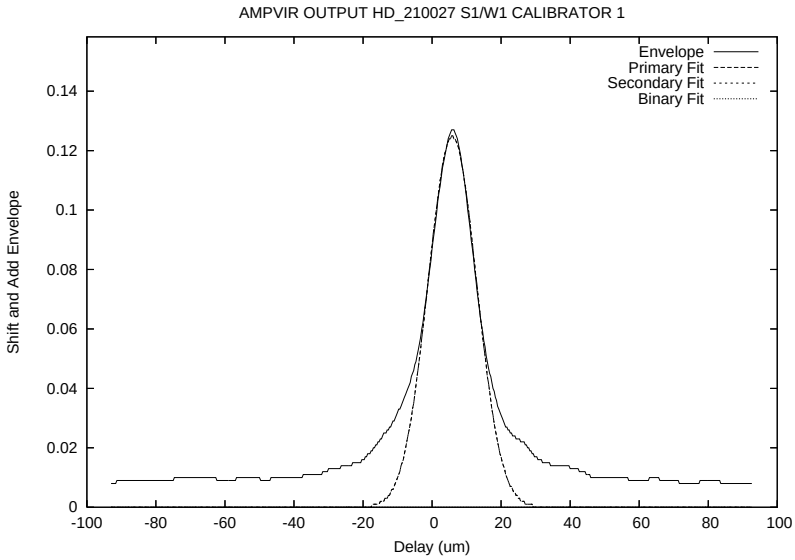


Figure. A.251: HD 210027 Fringe Envelope on 2007 October 19 on the W1/S1 Baseline.

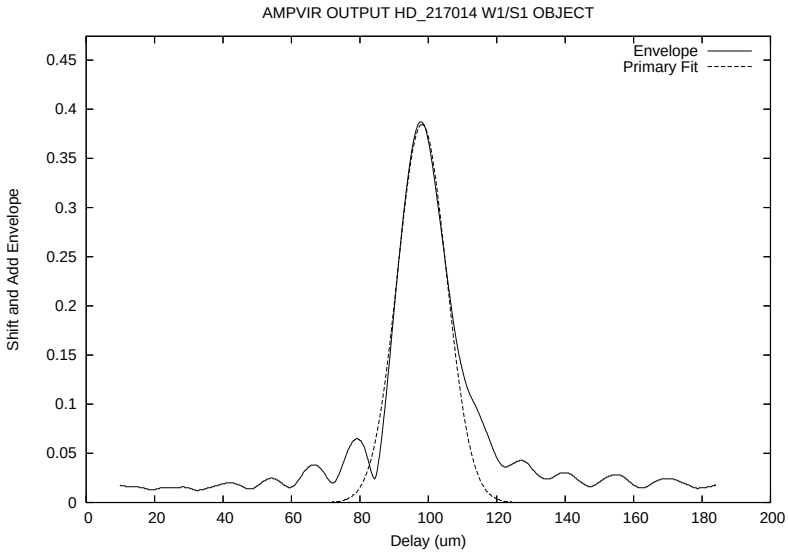


Figure. A.252: HD 210027 Fringe Envelope on 2007 October 19 on the E1/S1 Baseline.

## A.4.19 HD 215648

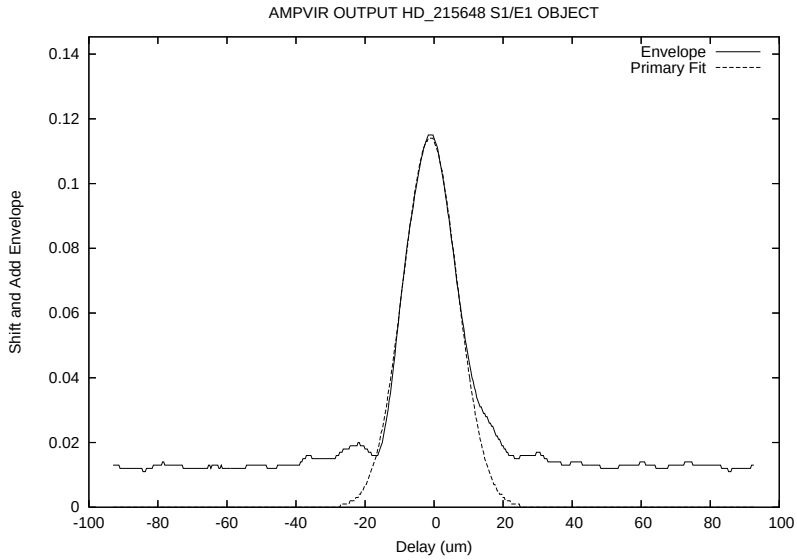


Figure. A.253: HD 215648 Fringe Envelope on 2007 July 16 on the E1/S1 Baseline.

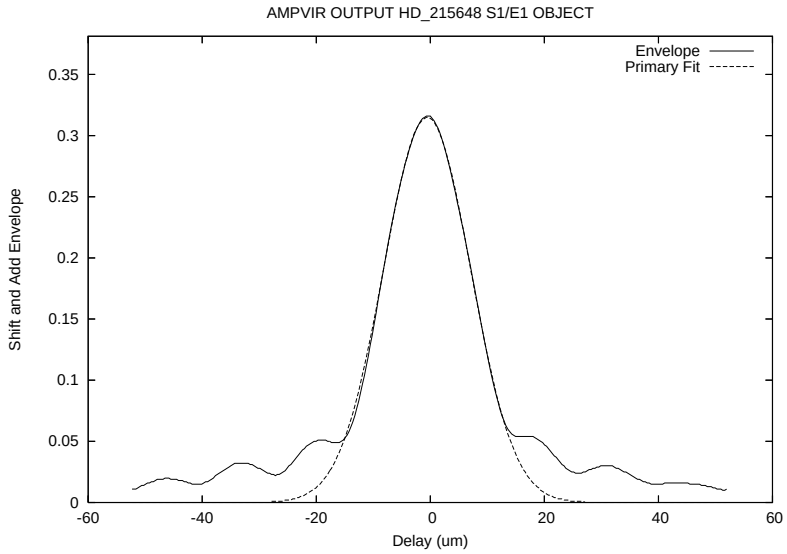


Figure. A.254: HD 215648 Fringe Envelope on 2007 July 21 on the E1/S1 Baseline.

## A.4.20 HD 217014

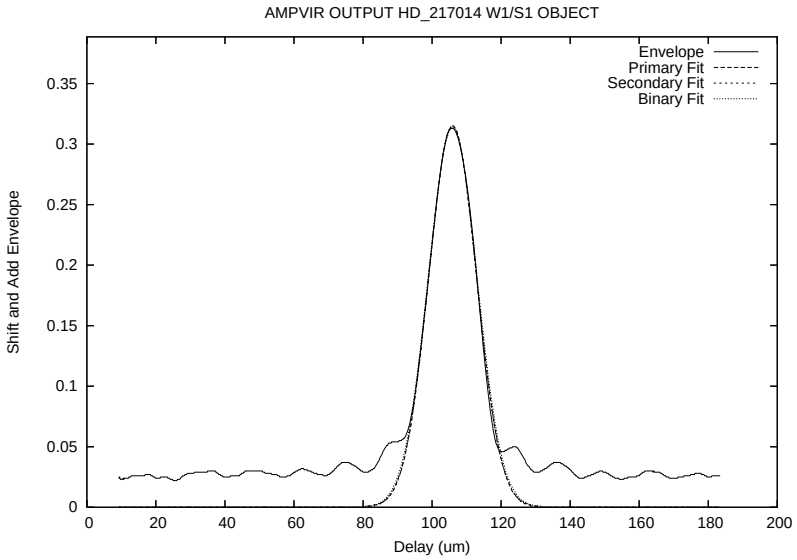


Figure. A.255: HD 217014 Fringe Envelope on 2006 September 10 on the W1/S1 Baseline.

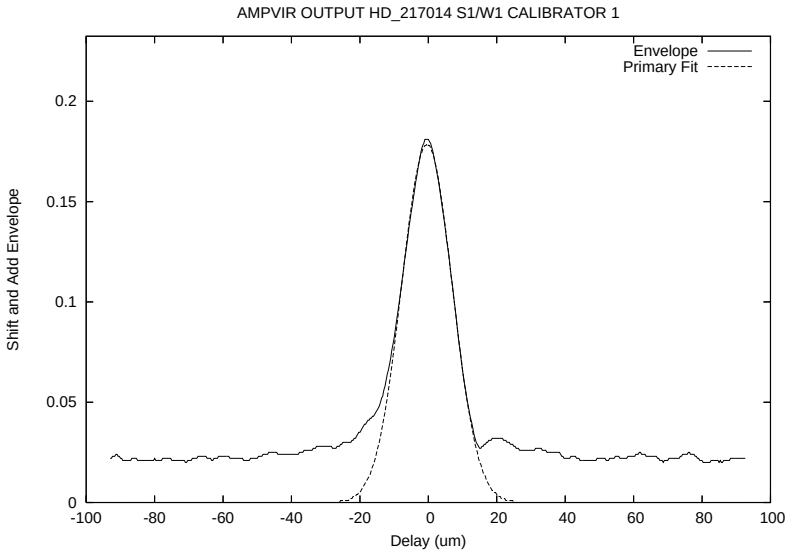


Figure. A.256: HD 217014 Fringe Envelope on 2006 September 19 on the W1/S1 Baseline.

## A.4.21 HD 219080

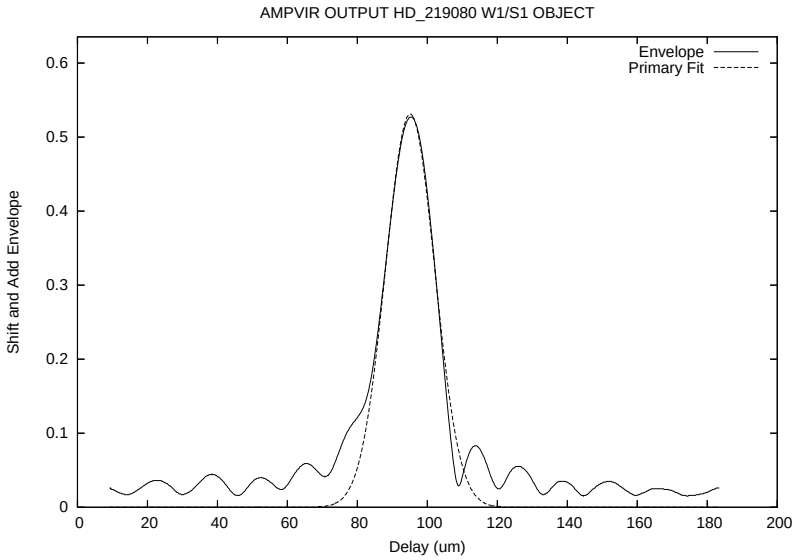


Figure. A.257: HD 219080 Fringe Envelope on 2005 October 2 on the W1/S1 Baseline.

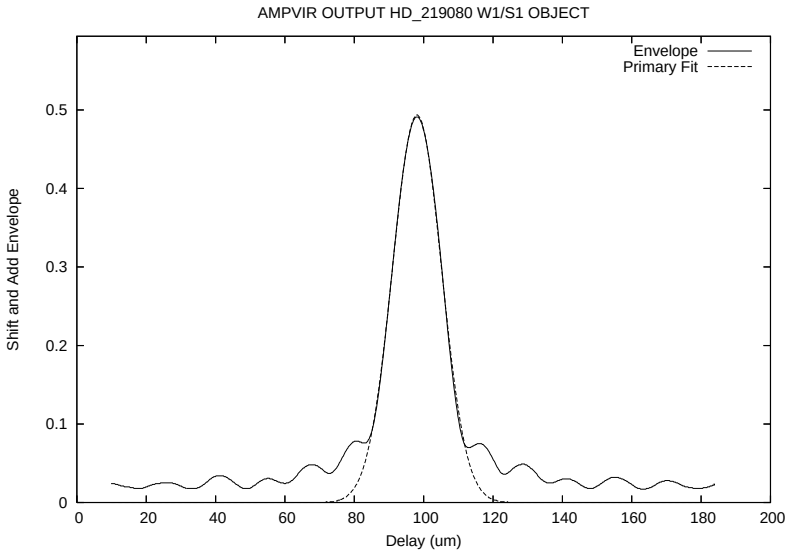


Figure. A.258: HD 219080 Fringe Envelope on 2005 October 7 on the E1/S1 Baseline.

## A.4.22 HD 222368

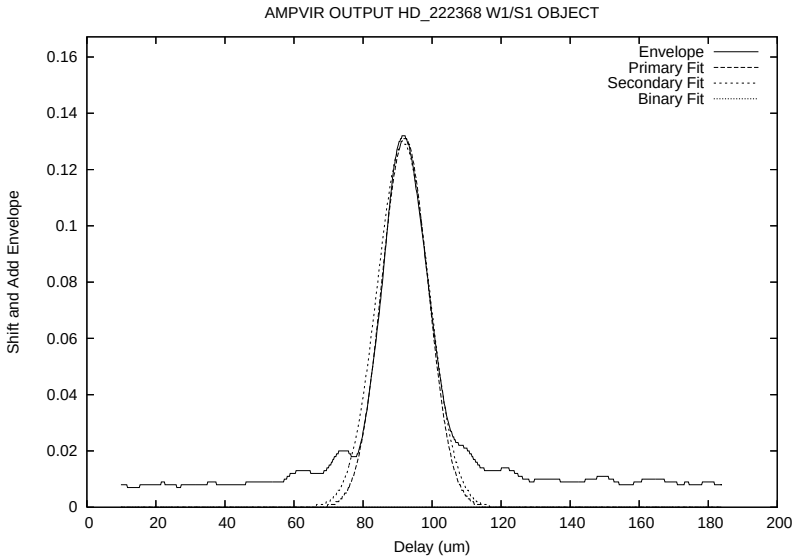


Figure. A.259: HD 222368 Fringe Envelope on 2005 October 2 on the W1/S1 Baseline.

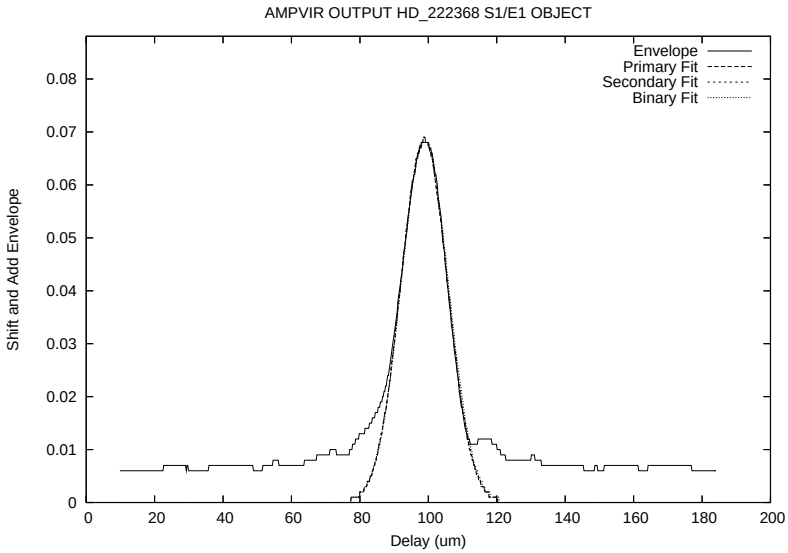


Figure. A.260: HD 222368 Fringe Envelope on 2005 October 7 on the E1/S1 Baseline.

## A.4.23 HD 223778

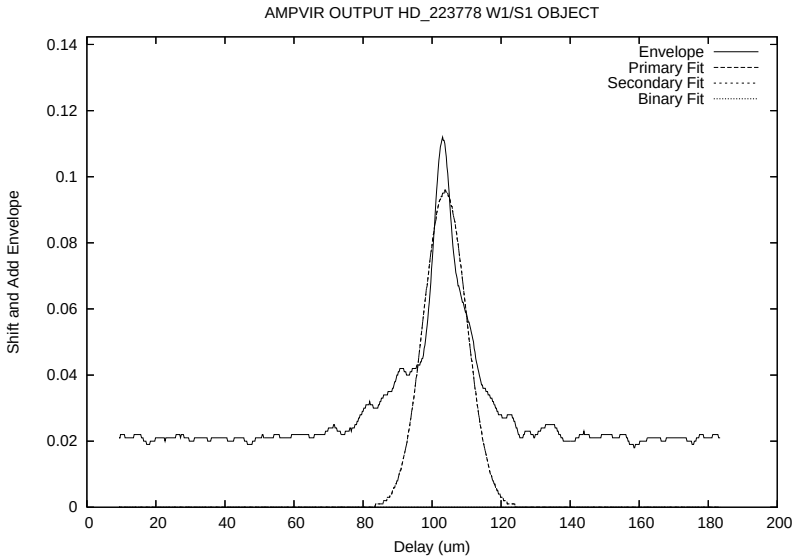


Figure. A.261: HD 223778 Fringe Envelope on 2005 October 5 on the W1/S1 Baseline.

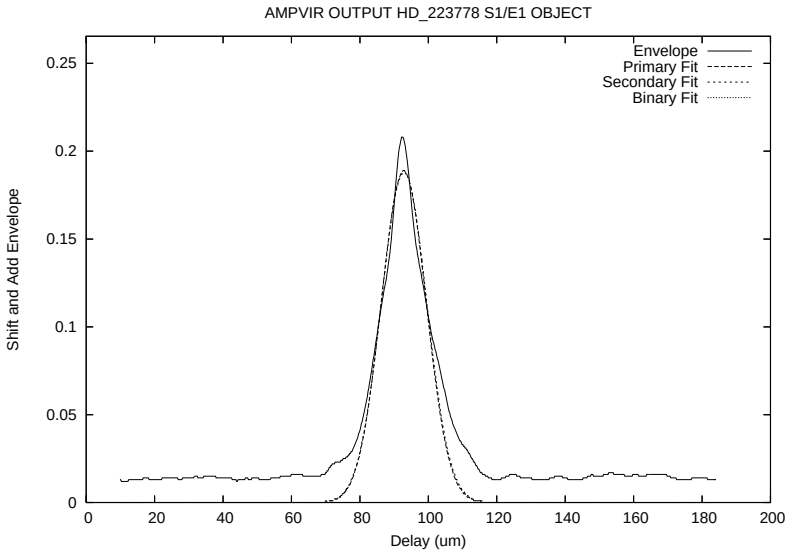


Figure. A.262: HD 223778 Fringe Envelope on 2005 October 11 on the E1/S1 Baseline.

## A.4.24 HD 224930

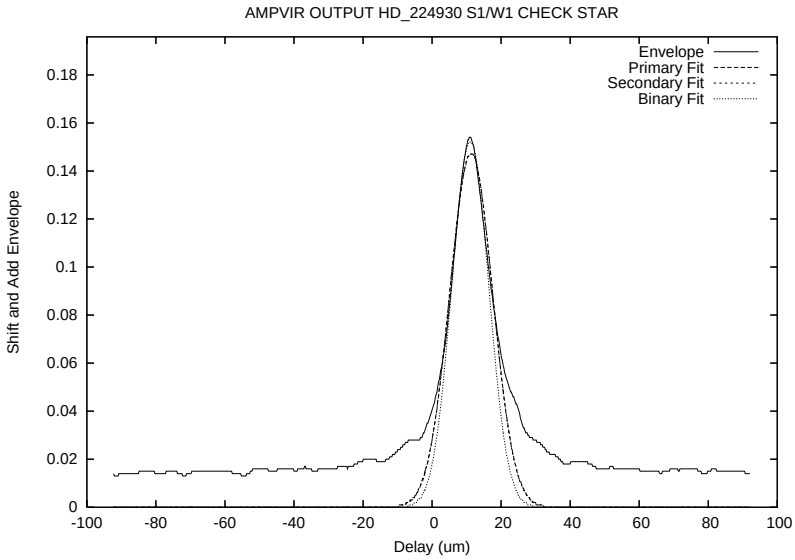


Figure. A.263: HD 224930 Fringe Envelope on 2007 October 19 on the W1/S1 Baseline.

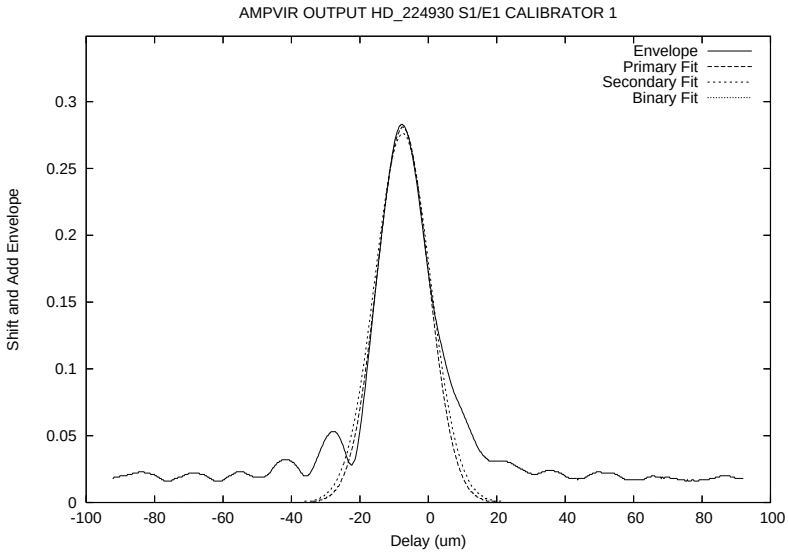


Figure. A.264: HD 224930 Fringe Envelope on 2007 October 19 on the E1/S1 Baseline.

# – B —

# Separated Fringe Packet Systems

Several different types of plots exist in this appendix. Example fringe envelope fits are the same as those in Appendix A including the second fringe envelope Gaussian fits as well as the double fringe fits. Also included here are triangulation plots for each case where multiple observations allow for the calculation of the position of the secondary. For these plots, the two □ icons represent the locations of the two stars at that time with the dashed line between them as the direction vector to the secondary. Each individual solid line represents one data file and is a ⊥ line from the the peak of the secondary fringe. Where these lines meet can be considered the true location of the secondary with the circle as the error in secondary placement. Additionally, if enough data are present, orbit plots are contained herein showing any previous orbits and the data points determined from the SFP analysis.

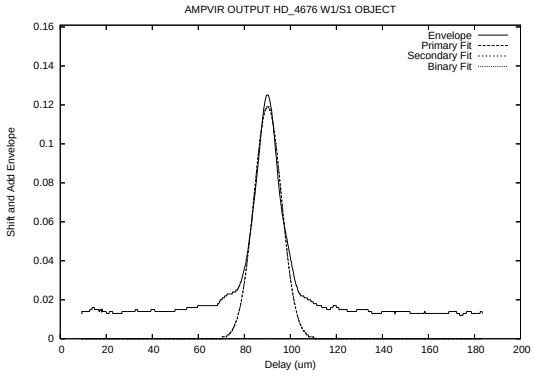


Figure. B.1: HD 4676 SFP Fringe Envelope on 2005 October 2 using the W1/S1 baseline. No secondary fringe on this baseline.

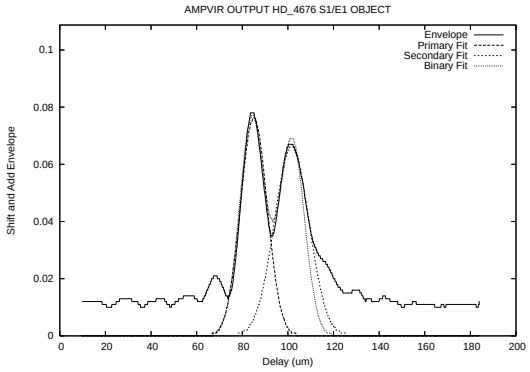


Figure. B.2: HD 4676 SFP Fringe Envelope on 2005 October 7 using the E1/S1 baseline.

# B.1 HD 4676

Due to the short period and small separation, separated fringes were only detected once for HD 4676. This system contains the detection of the closest separated fringes and gives a useful lower limit to the acquisition of a secondary packet. See Chapter 6.2.1.1

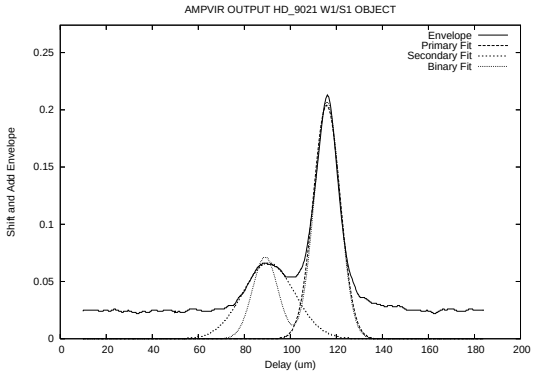


Figure. B.3: HD 9021 SFP Fringe Envelope on 2006 September 17 using the W1/S1 baseline.

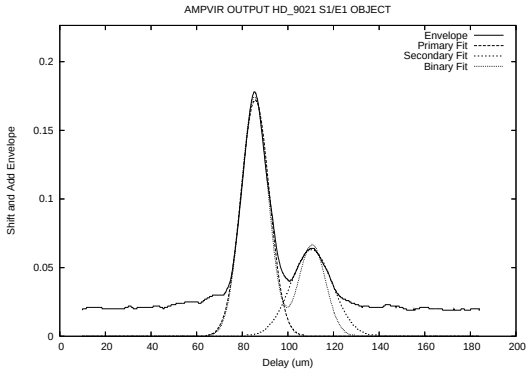


Figure. B.4: HD 9021 SFP Fringe Envelope on 2006 September 18 using the E1/S1 baseline.

## B.2 HD 9021

An F star and its companion resolved for the first time as seperate packets since the spectroscopic orbit was presented Wright & Pugh (1954). The semi-major axis for the astrometric orbit (Jancart et al. 2005) seems too small to fit the current separations. More observations of this system are needed for further analysis. See Chapter 6.2.2.1

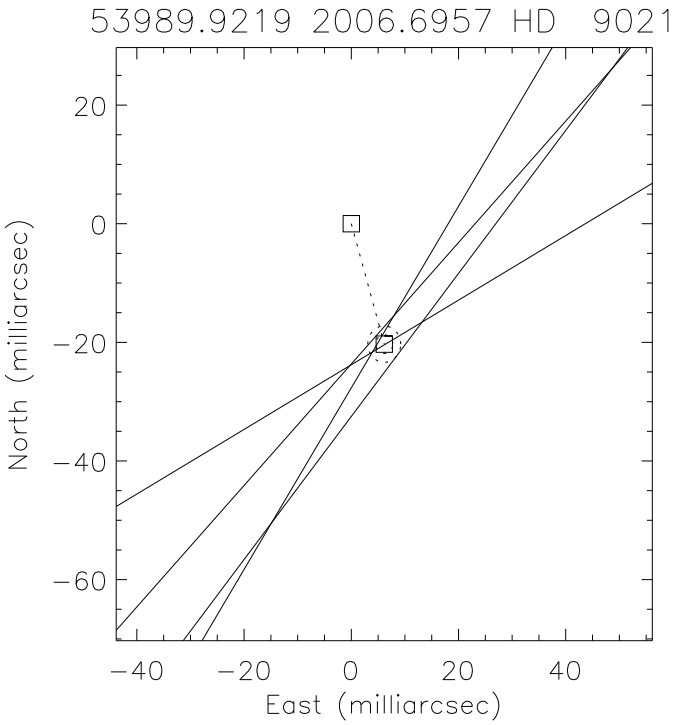


Figure. B.5: Triangulation Plot for HD 9021 on 2006.6957. Calculation from 4 data files from 2006 September 11 to September 12

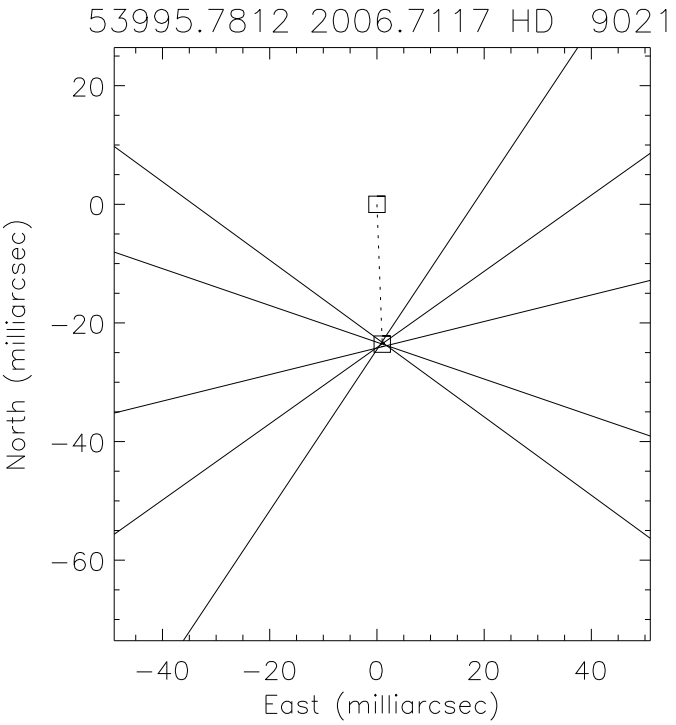


Figure. B.6: Triangulation Plot for HD 9021 on 2006.7117. Calculation from 5 data files from 2006 September 17 to September 18.

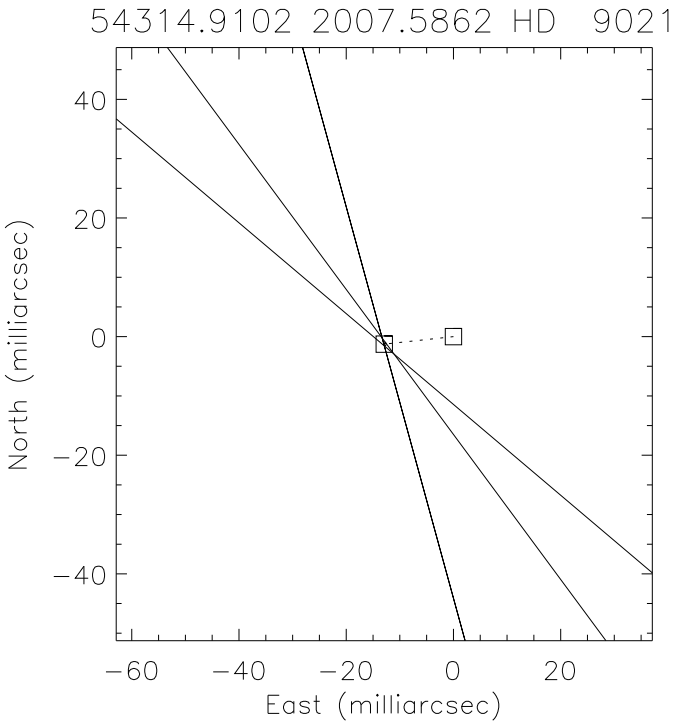


Figure. B.7: Triangulation Plot for HD 9021 on 2007.5862. Calculation from 3 data files from 2007 August 2 to August 3.

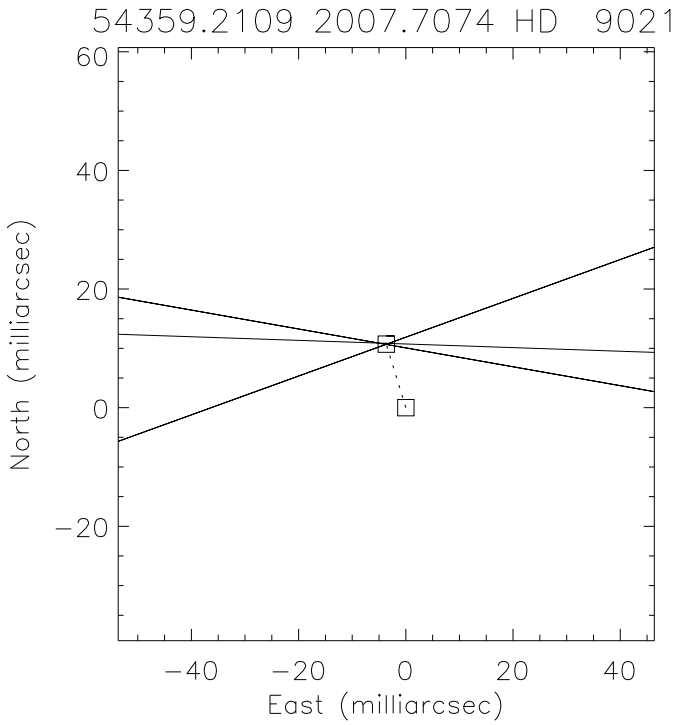


Figure. B.8: Triangulation Plot for HD 9021 on 2007.7070. Calculation from 3 data files from 2007 September 15 to September 17.

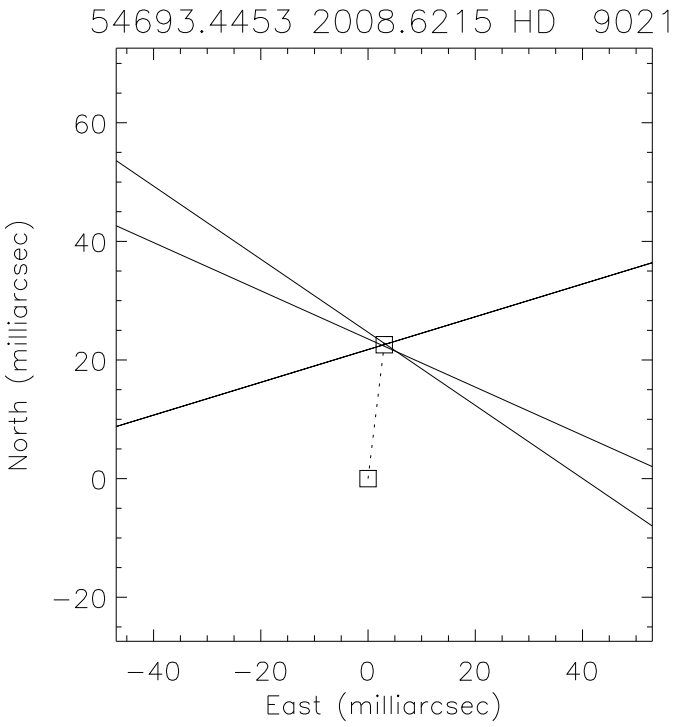


Figure. B.9: Triangulation Plot for HD 9021 on 2008.6215. Calculation from 3 data files from 2008 August 15.

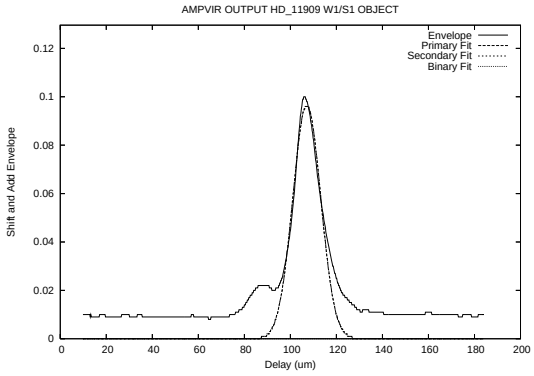


Figure. B.10: HD 11909 SFP Fringe Envelope on 2005 October 2 using the W1/S1 baseline.

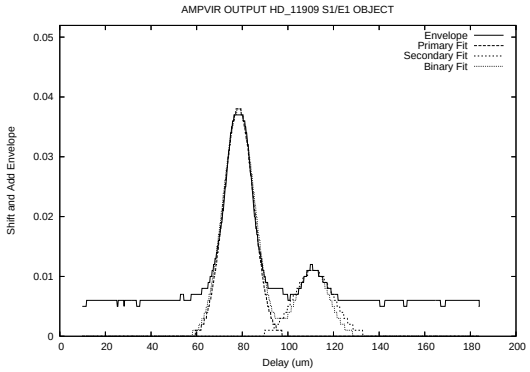


Figure. B.11: HD 11909 SFP Fringe Envelope on 2005 October 7 using the E1/S1 baseline.

## B.3 HD 11909

With a period of a little more than four years, this system was moving slow enough at the time of data collection to permit combination of the two data sets with a five day delay between them. This appears to be the first visual detection of the secondary after almost 15 speckle observations could not detect it. This is not surprising as the separation calculated for the secondary is ∼23 mas and the system is more than 100 parsecs away. See Chapter 6.2.1.2

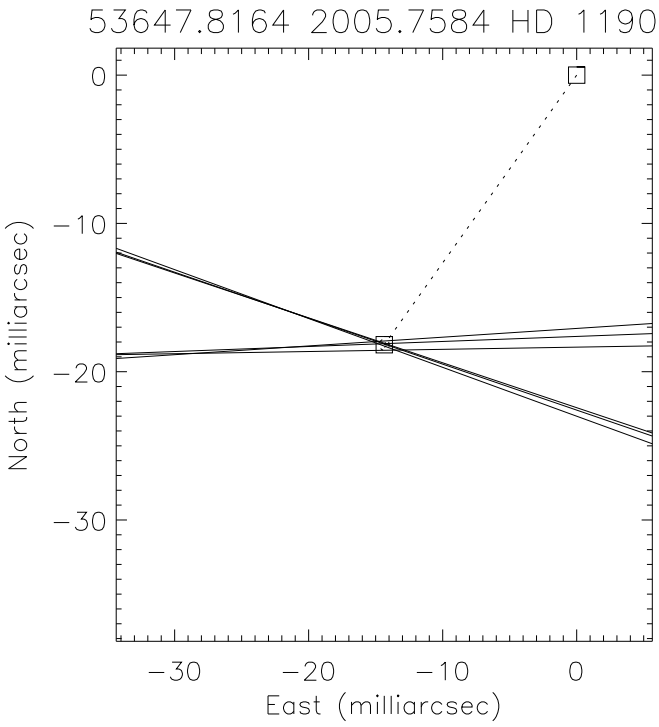


Figure. B.12: Triangulation Plot for HD 11909 on 2005.7584. Calculated from 6 data files from 2005 October 2 to October 7.

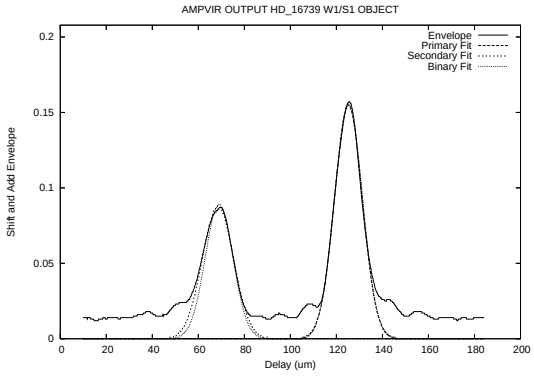


Figure. B.13: HD 16739 SFP Fringe Envelope on 2006 September 17 using the W1/S1 baseline.

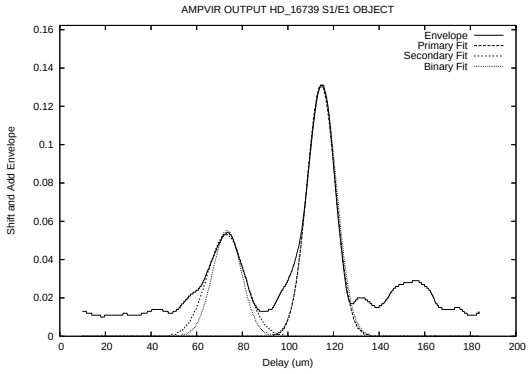


Figure. B.14: HD 16739 SFP Fringe Envelope on 2006 September 18 using the E1/S1 baseline.

## B.4 HD16739

A well studied binary that was instrumental in furthering the SFP process. Sadly, not many observations were taken to add more points to the orbit. Shown here are what little data were taken and the locations of where the observations predict the secondary to be. See Chapter 6.2.2.2

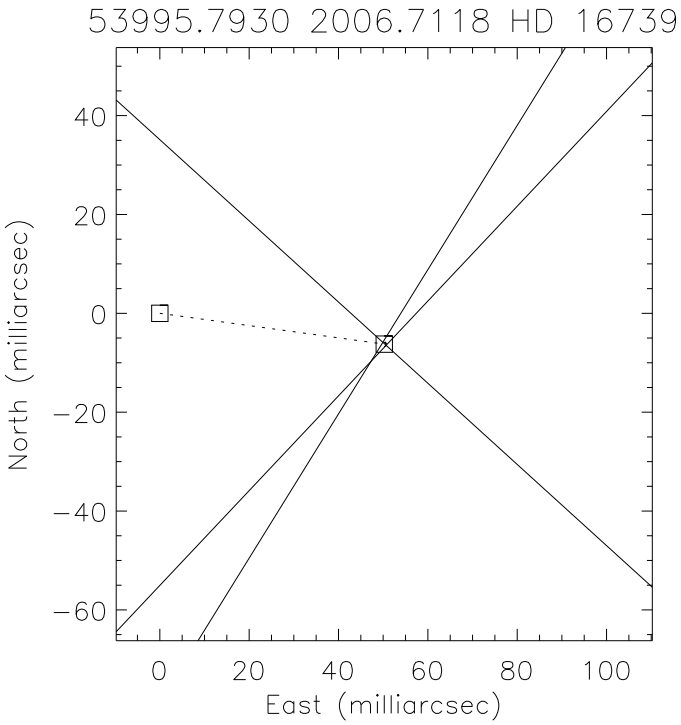


Figure. B.15: Triangulation Plot for HD 16739 on 2006.7118. 3 data files from 2006 September 17 to September 18.

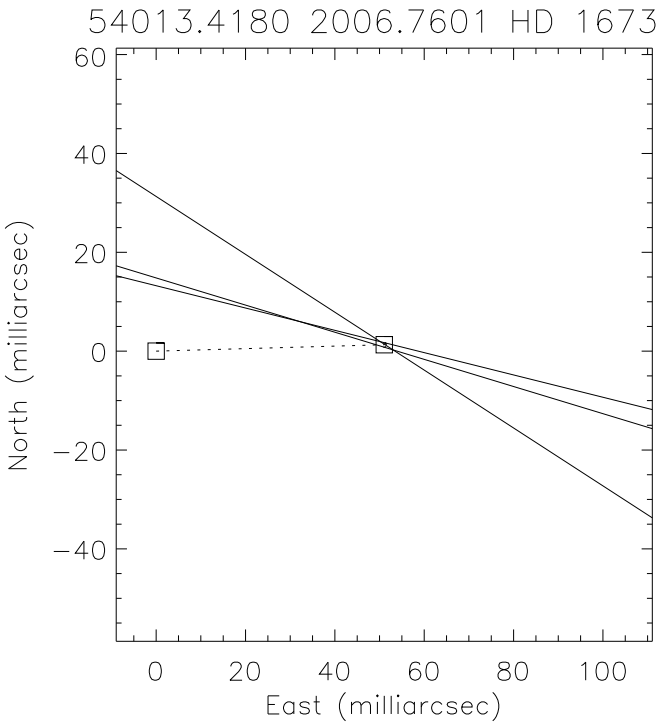


Figure. B.16: Triangulation Plot for HD 16739 on 2006.7601. Calculated from 3 data files from 2006 October 5.

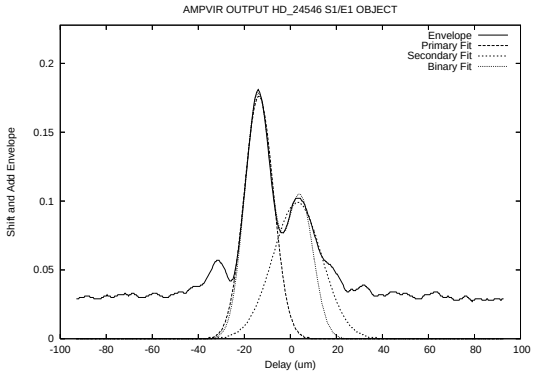


Figure. B.17: HD 24546 SFP Fringe Envelope on 2007 January 26 using the E1/S1 baseline.

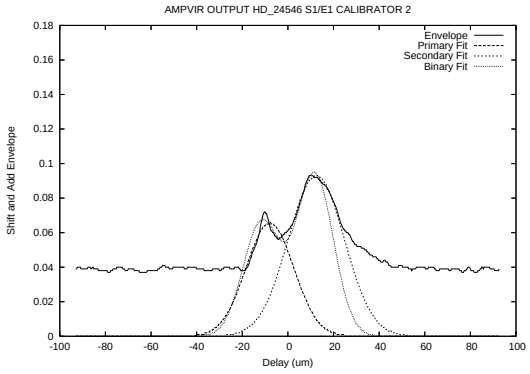


Figure. B.18: HD 24546 SFP Fringe Envelope on 2007 Feburary 4 using the E1/S1 baseline.

## B.5 HD 24546

With a very fast (30 day) orbit, and erratic observations, no real information can be gleaned from the data included here other than the detection of the secondary. See Chapter 6.2.1.3

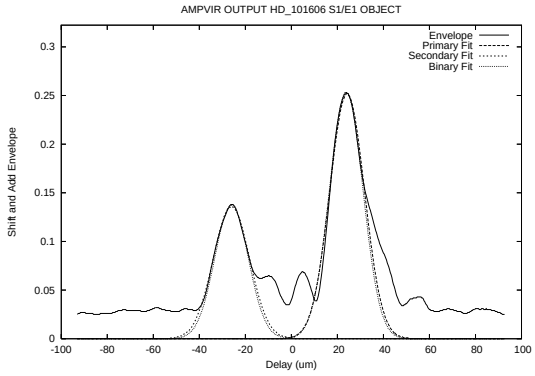


Figure. B.19: HD 101606 SFP Fringe Envelope on 2007 March 9 using the E2/S2 baseline.

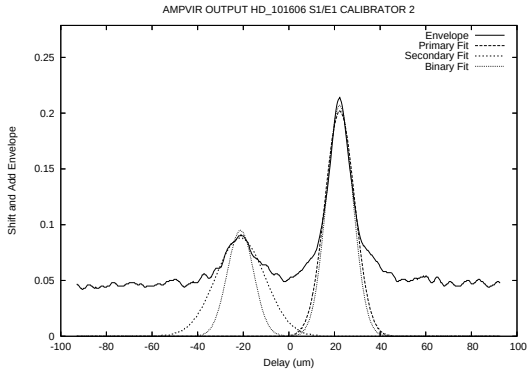


Figure. B.20: HD 101606 SFP Fringe Envelope on 2007 March 11 using the E1/S1 baseline.

## B.6 HD 101606

This system was flagged for more observations when time was available, but due to the season that these stars were up, further data collection was not possible. Although not even enough for a single triangulated data point, we report detection of the secondary with the CHARA Array. See Chapter 6.2.1.4

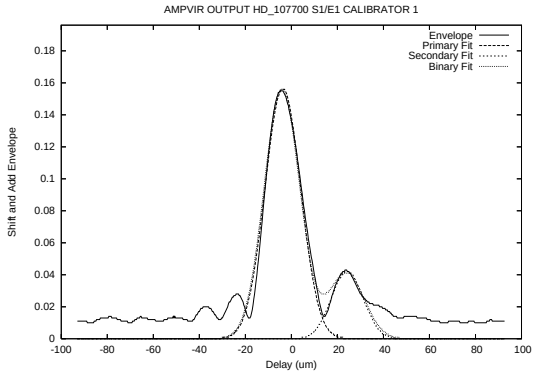


Figure. B.21: HD 107700 SFP Fringe Envelope on 2007 March 10 using the E1/S1 baseline.

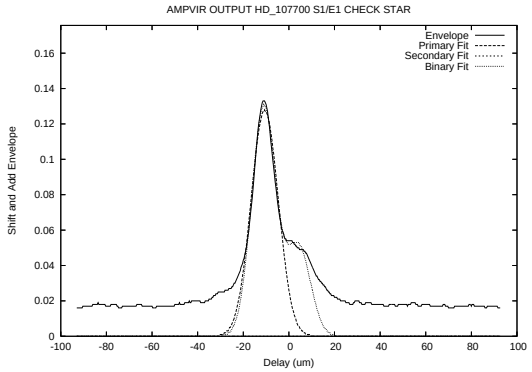


Figure. B.22: HD 107700 SFP Fringe Envelope on 2007 March 11 using the E1/S1 baseline.

## B.7 HD 107700

As with HD 101606, we were unable to get more observations of this system due to bad weather. See Chapter 6.2.1.5

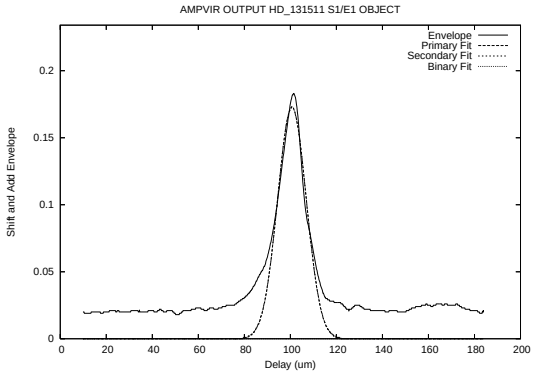


Figure. B.23: HD 131511 SFP Fringe Envelope on 2006 June 08 using the E1/S1 baseline.

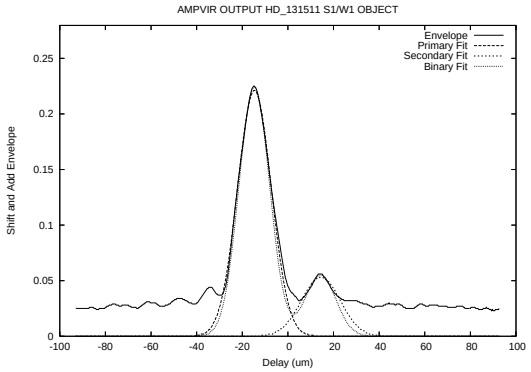


Figure. B.24: HD 131511 SFP Fringe Envelope on 2007 June 23 using the W1/S1 baseline.

## B.8 HD 131511

This would be a fine target for further study as the separation and the relatively short period (125 days) would allow decent phase coverage with not too long a time commitment. See Chapter 6.2.1.6

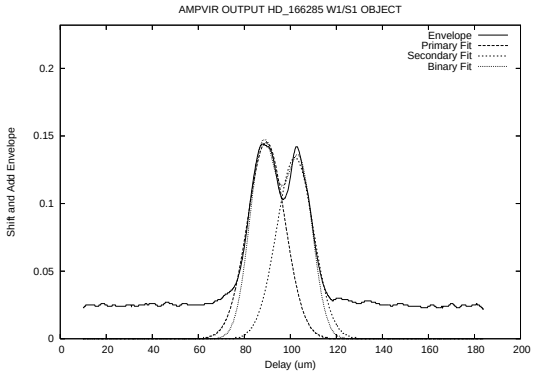


Figure. B.25: HD 166285 SFP Fringe Envelope on 2006 September 19 using the W1/S1 baseline.

## B.9 HD 166285

Only observed once due to scheduling and weather issues, this system is another prime target for follow-up observations with a medium length period, near equal size fringes, and is catagorized as overluminous for its spectral type. See Chapter 6.2.1.7

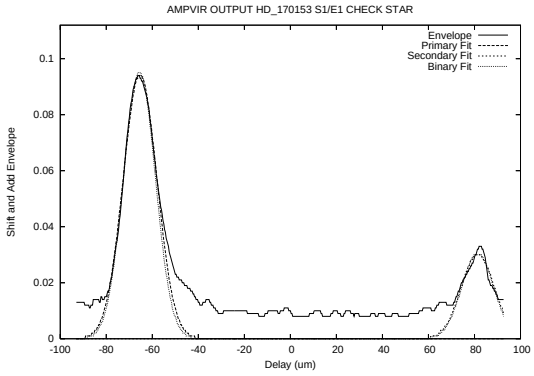


Figure. B.26: HD 170153 SFP Fringe Envelope on 2007 August 2 using the E1/S1 baseline.

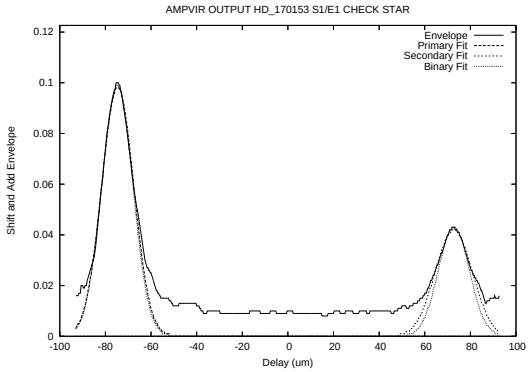


Figure. B.27: HD 170153 SFP Fringe Envelope on 2007 August 2 using the E1/S1 baseline.

## B.10 HD 170153

$\chi$ Draconis: A very well observed system with several orbital improvements over the years that have increased the quality of the orbit. Little is known about the closest visual approaches which are in the perfect range for future SFP work. Due to the very large parallax and size of the primary, this star is a good example of the situation where the primary star has the smaller fringe packet since the primary's estimated diameter is more than 1.5 mas and the star is at least partially resolved on the longest baselines needed to see both fringe packets. See Chapter 6.2.2.3

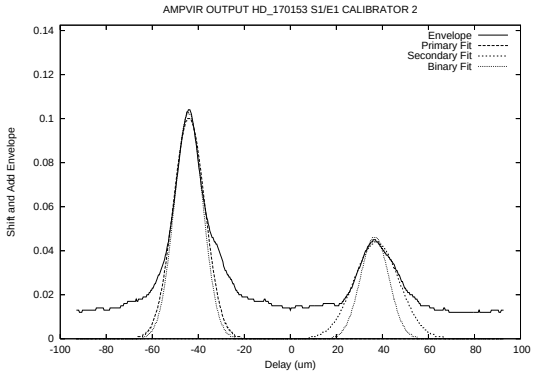


Figure. B.28: HD 170153 SFP Fringe Envelope on 2007 August 2 using the E1/S1 baseline.

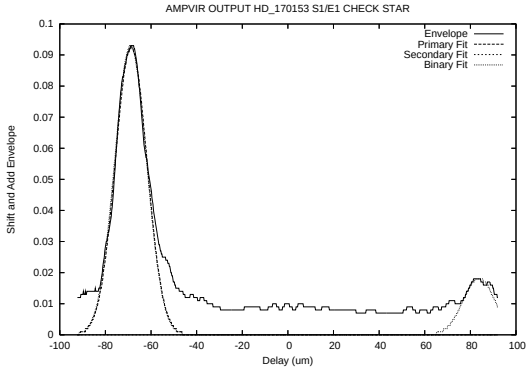


Figure. B.29: HD 170153 SFP Fringe Envelope on 2007 August 3 using the E1/S1 baseline.

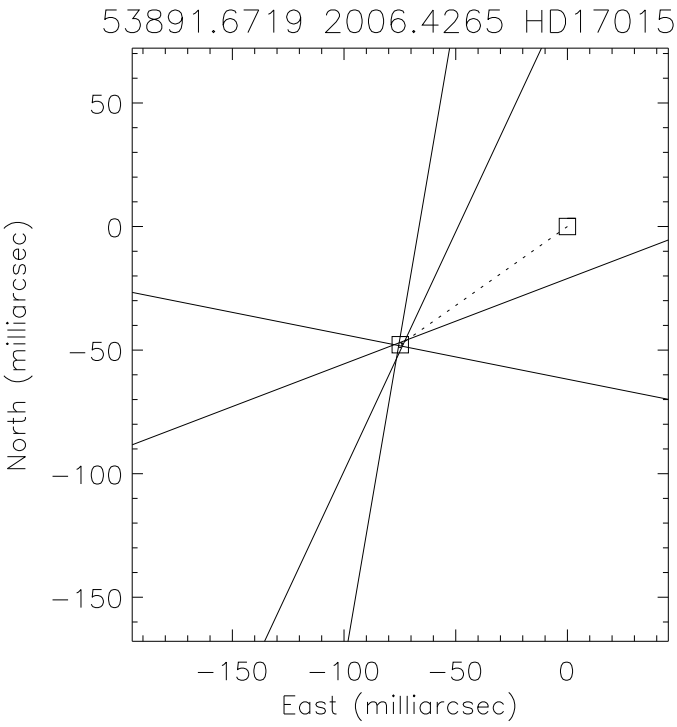


Figure. B.30: Triangulation Plot for HD 170153 on 2006.4265. Calculated from 3 data files from 2006 June 5.

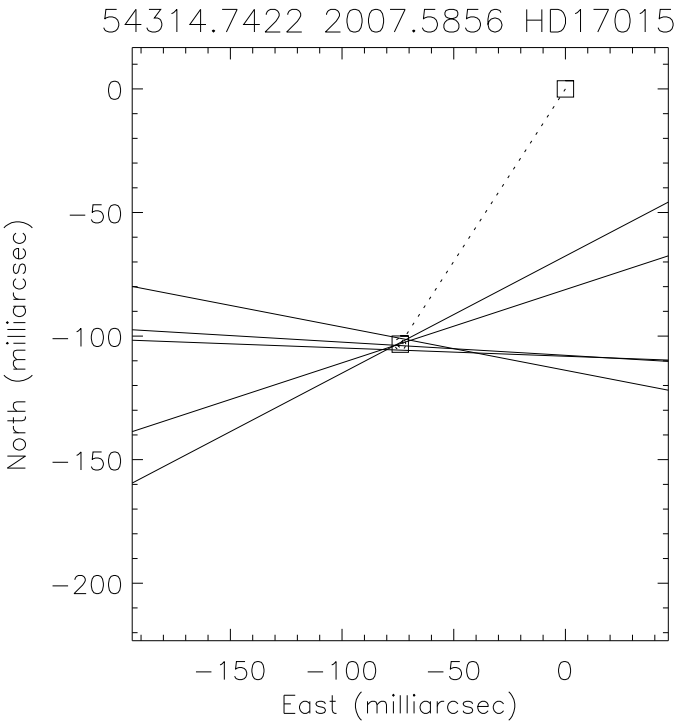


Figure. B.31: Triangulation Plot for HD 170153 on 2007.5856. Calculated from 5 data files from 2007 August 2 to August 3.

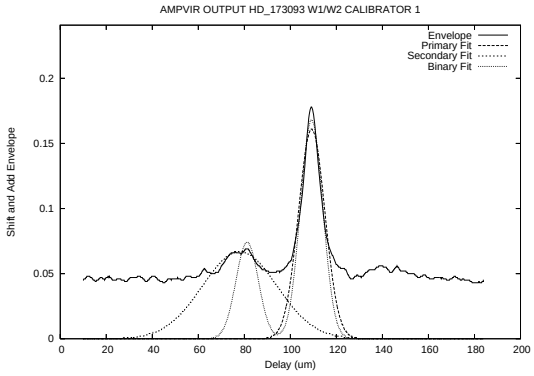


Figure. B.32: HD 173093 SFP Fringe Envelope on 2006 May 14 using the W1/W2 baseline.

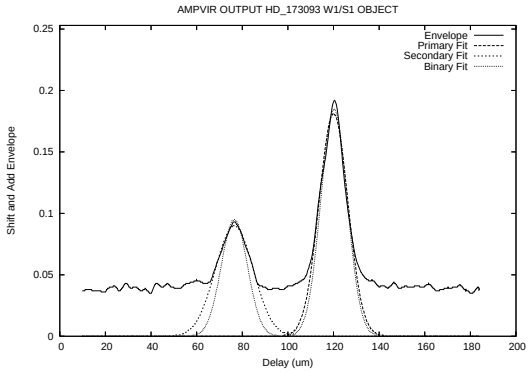


Figure. B.33: HD 173093 SFP Fringe Envelope on 2006 September 19 using the W1/S1 baseline.

## B.11 HD 173093

This system's companion was discovered during visibility work as a bad calibrator when a second fringe was discovered. It was not on either the CHARA Spectroscopic Binary Catalog nor the D&M survey but was adopted anyway for further SFP study. Sadly the baseline used for the triangulation plot did not have much rotation so the tenative position has a rather large error. See Chapter 6.2.2.4

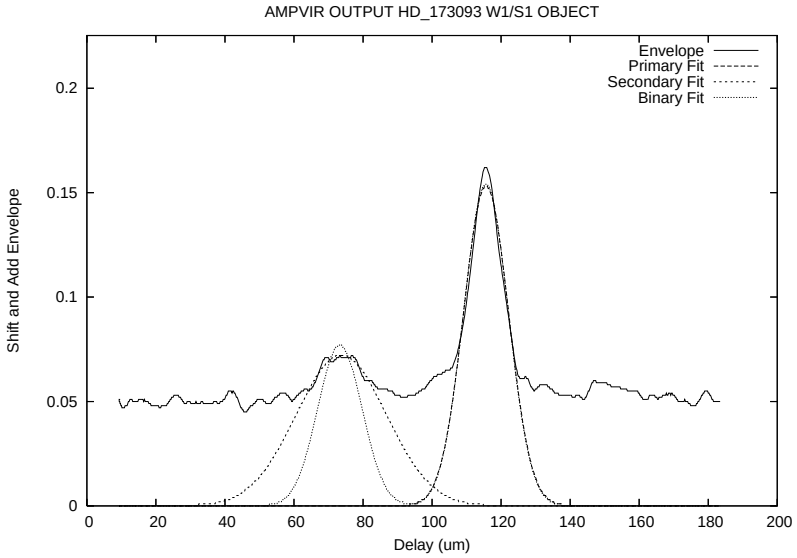


Figure. B.34: HD 173093 SFP Fringe Envelope on 2006 September 19 using the W1/S1 baseline. Not realistic due to lack of baseline rotation.

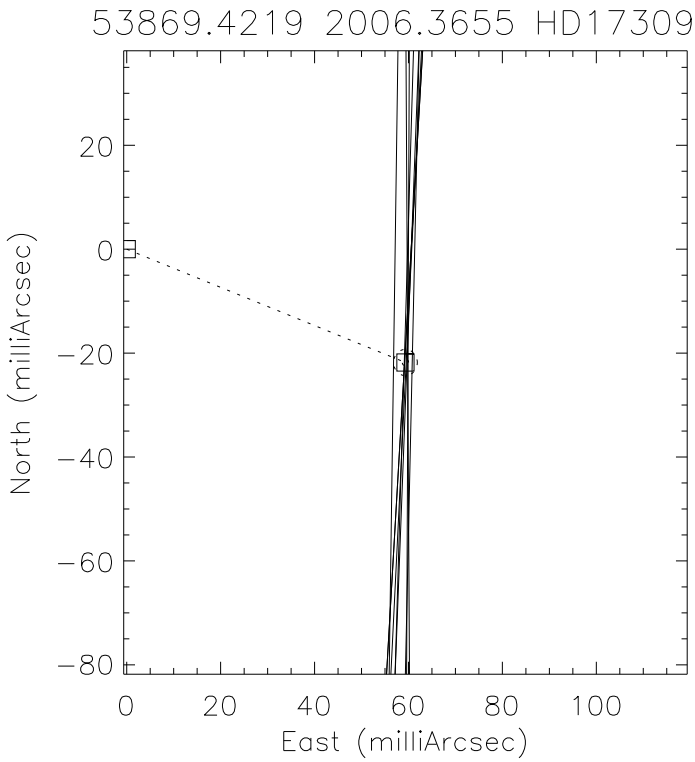


Figure. B.35: Triangulation Plot for HD 173093 2006.3665. Calculated from 8 data files from 2006 May 12.

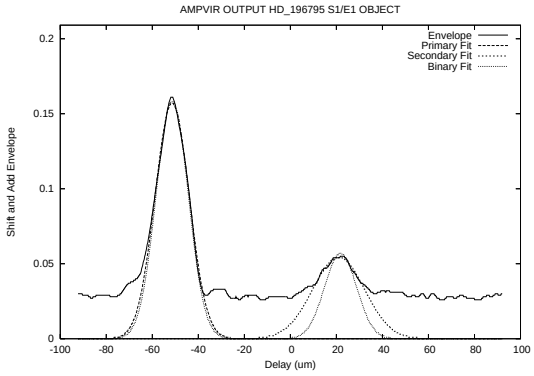


Figure. B.36: HD 196795 SFP Fringe Envelope on 2006 October 19 using the E1/S1 baseline.

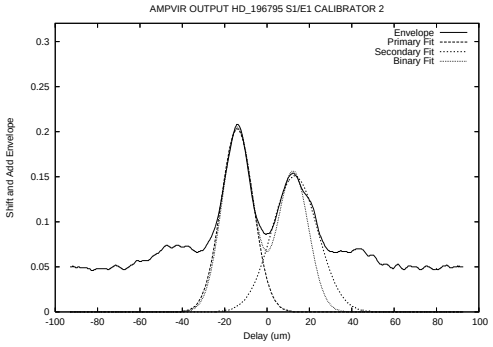


Figure. B.37: HD 196795 SFP Fringe Envelope on 2007 July 24 using the E1/S1 baseline.

## B.12 HD 196795

A very interesting hierarchical triple system, HD 196795 was unable to be observed much during this project due to time constraints. Separated fringe packets were observed for this system on several occasions and it warrants further study as the inner system is a double-lined spectroscopic binary with high eccentricity that is not coplanar with its outer companion. See Chapter 6.2.1.8

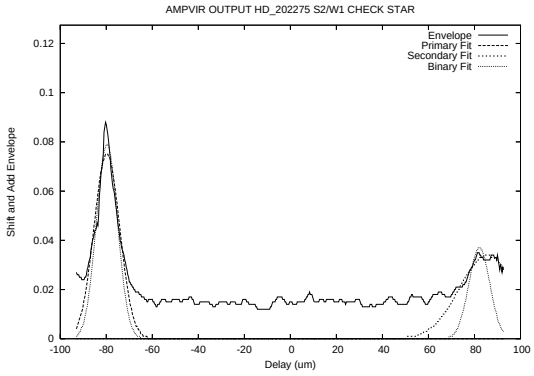


Figure. B.38: HD 202275 SFP Fringe Envelope on 2007 June 16 using the W1/S2 baseline.

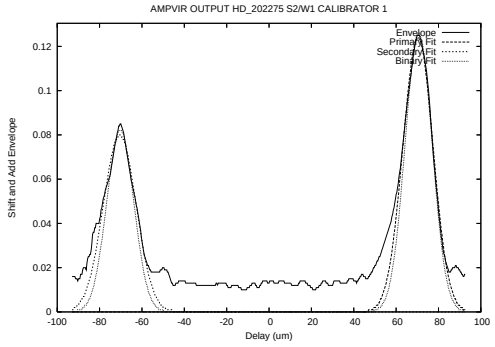


Figure. B.39: HD 202275 SFP Fringe Envelope on 2007 June 16 using the W1/S2 baseline.

## B.13 HD 202275

For the typical baselines being used in this survey, HD 202275 proved to be far too wide ($\geq$ 100 mas or more) to collect data on. The data that have been collected on this system are far too spotty to be useful, but the acquisition of fringe data at shorter baselines would help this greatly. See Chapter 6.2.1.9

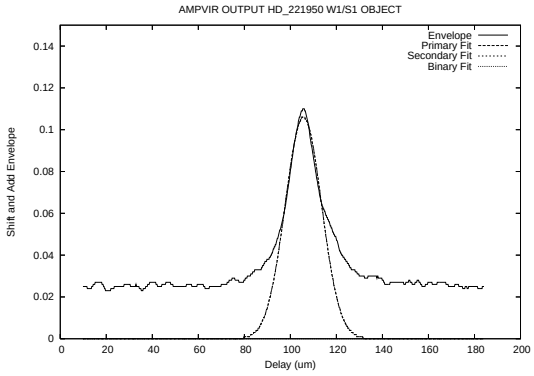


Figure. B.40: HD 221950 SFP Fringe Envelope on 2005 October 2 using the W1/S1 baseline.

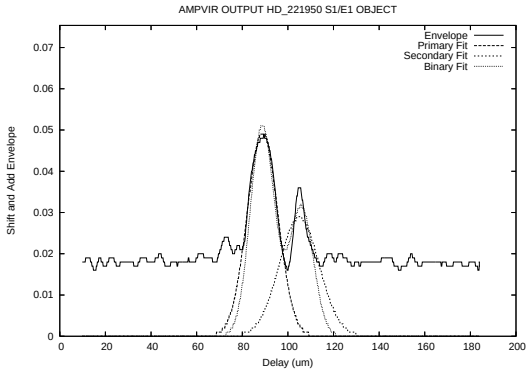


Figure. B.41: HD 221950 SFP Fringe Envelope on 2007 October 7 using the E1/S1 baseline.

## B.14 HD 221950

Another detection of SFP on a system with less than a 50-day orbit. Secondary fringes were only detected on a single baseline and on a night with bad seeing. Follow-up on this system would confirm a secondary packet and possibly lead to very precise masses with the very high precision recent spectroscopic orbit just released. See Chapter 6.2.1.10

# – C —

# SFP Case Studies

This appendix includes envelope, triangulation and orbit plots for the three interesting systems with the most data from the SFP survey. The example fringe envelopes and triangulation plots are the same type and style as those that appear in Appendix A and B. When available, orbit plots are included in each section. For each orbit plot, the star symbol represents data points taken at the CHARA Array, circles denote speckle interferometry measurements, and the *H* represents a HIPPARCOS measurement. For orbits, the black line is the newly calculated orbital path, while the dotted line represents the previous orbit if it exists.

## C.1 HD 181655

A late G dwarf with a newly discovered companion, this system contains the first companion discovered with a SFP search and promises a future orbit when enough data become available. Full information on this system is contained in Chapter 7.1.

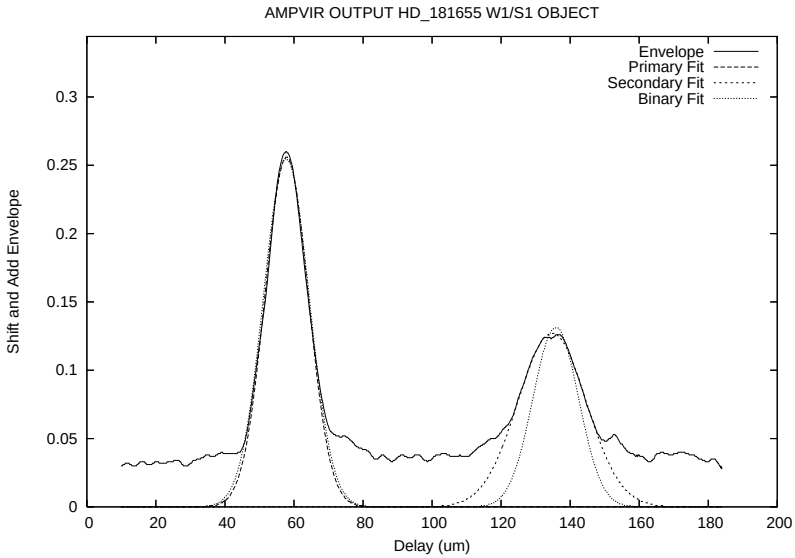


Figure. C.1: HD 181655 SFP Fringe Envelope on 2006 September 12 using the W1/S1 baseline.

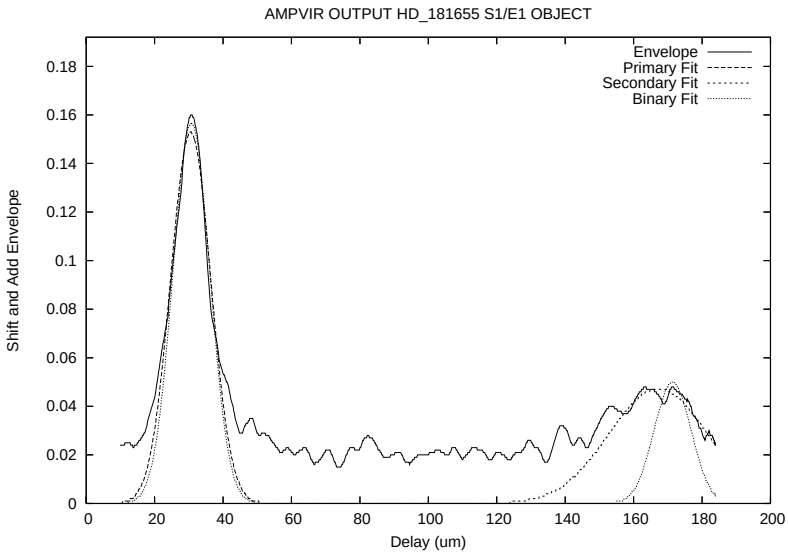


Figure. C.2: HD 181655 SFP Fringe Envelope on 2006 September 13 using the E1/S1 baseline.

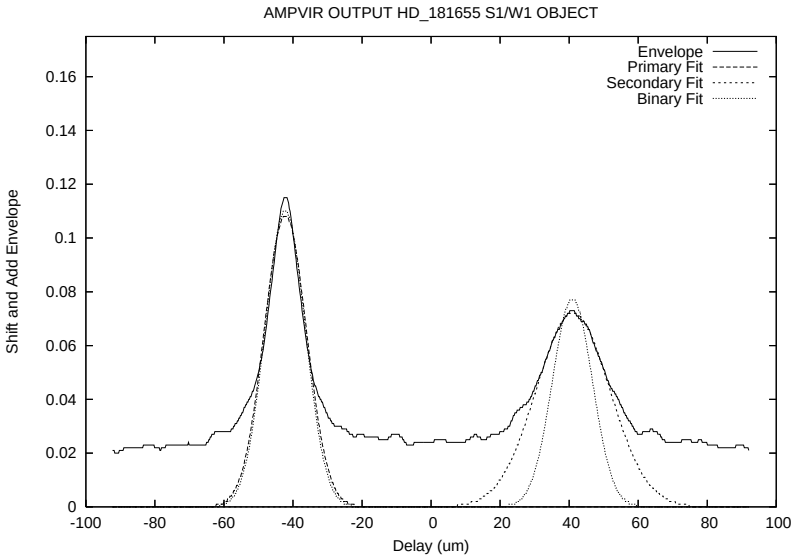


Figure. C.3: HD 181655 SFP Fringe Envelope on 2007 October 2 using the W1/S1 baseline.

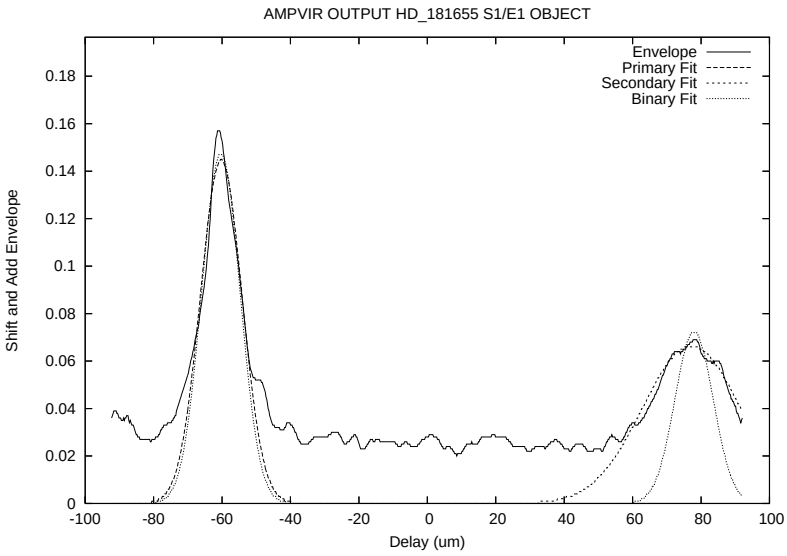


Figure. C.4: HD 181655 SFP Fringe Envelope on 2007 October 2 using the E1/S1 baseline.

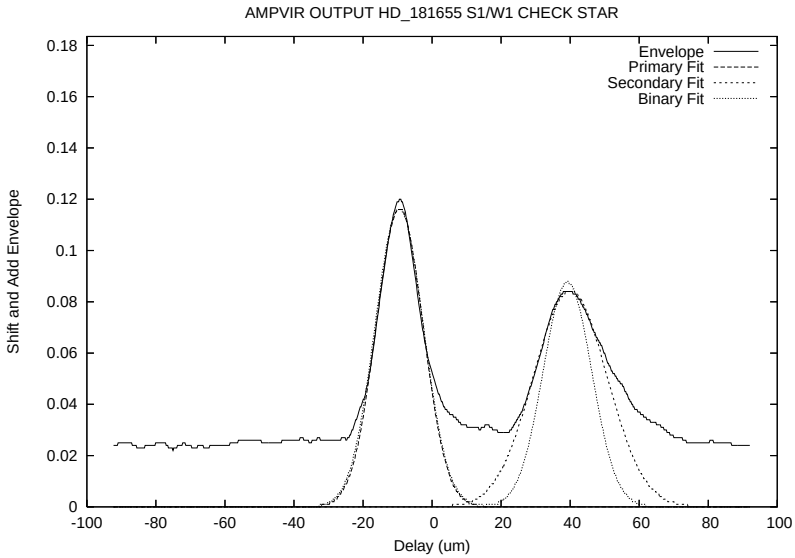


Figure. C.5: HD 181655 SFP Fringe Envelope on 2007 October 20 using the W1/S1 baseline.

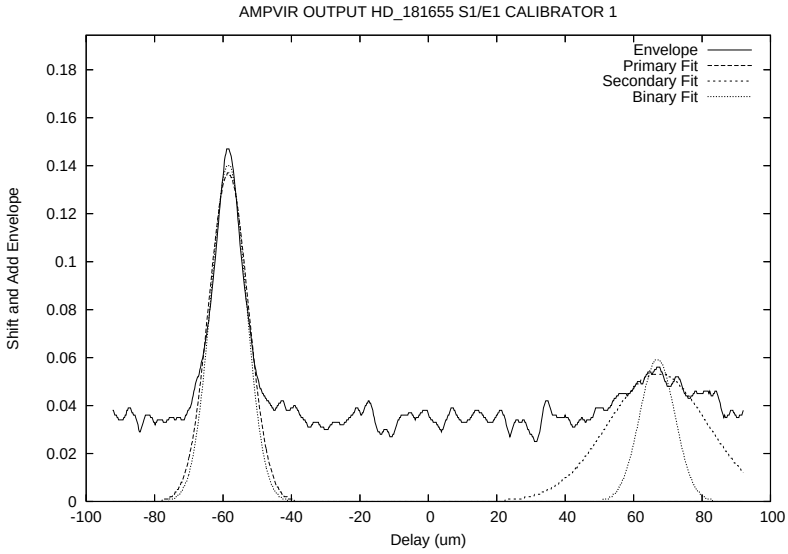


Figure. C.6: HD 181655 SFP Fringe Envelope on 2007 October 20 using the E1/S1 baseline.

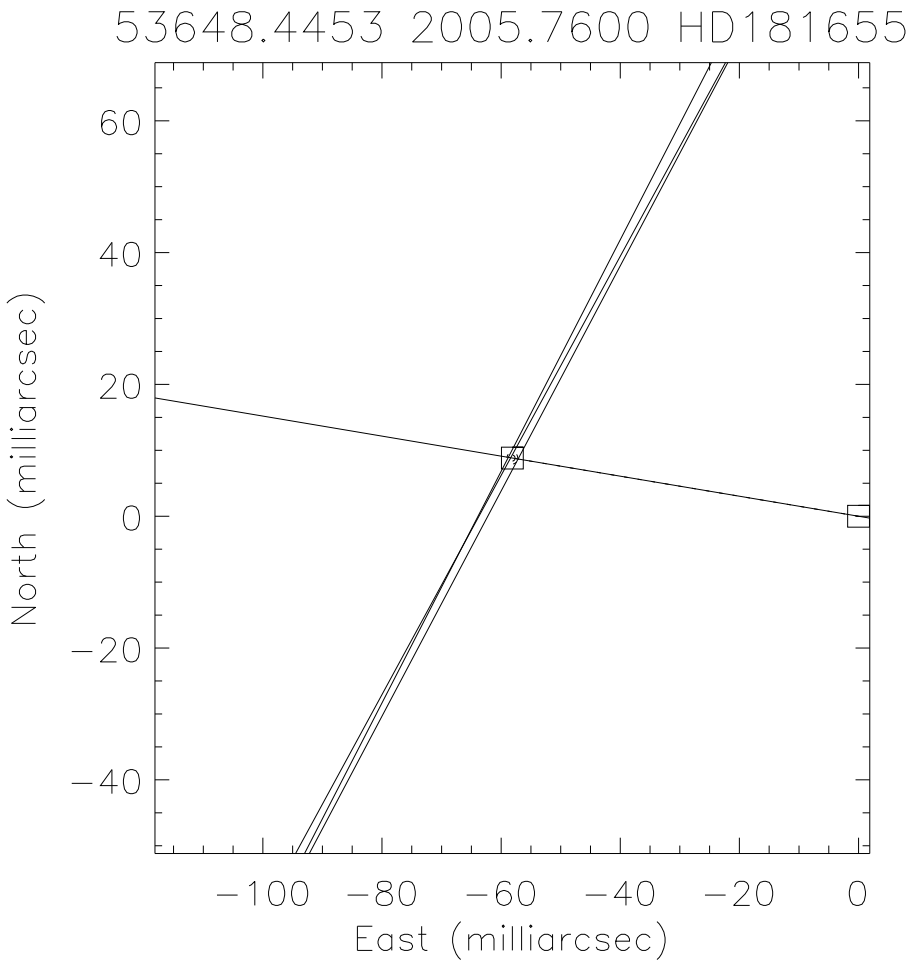


Figure. C.7: Triangulation Plot for HD 181655 on 2005.7600. Calculation from 4 data files from 2005 October 5 to October 6.

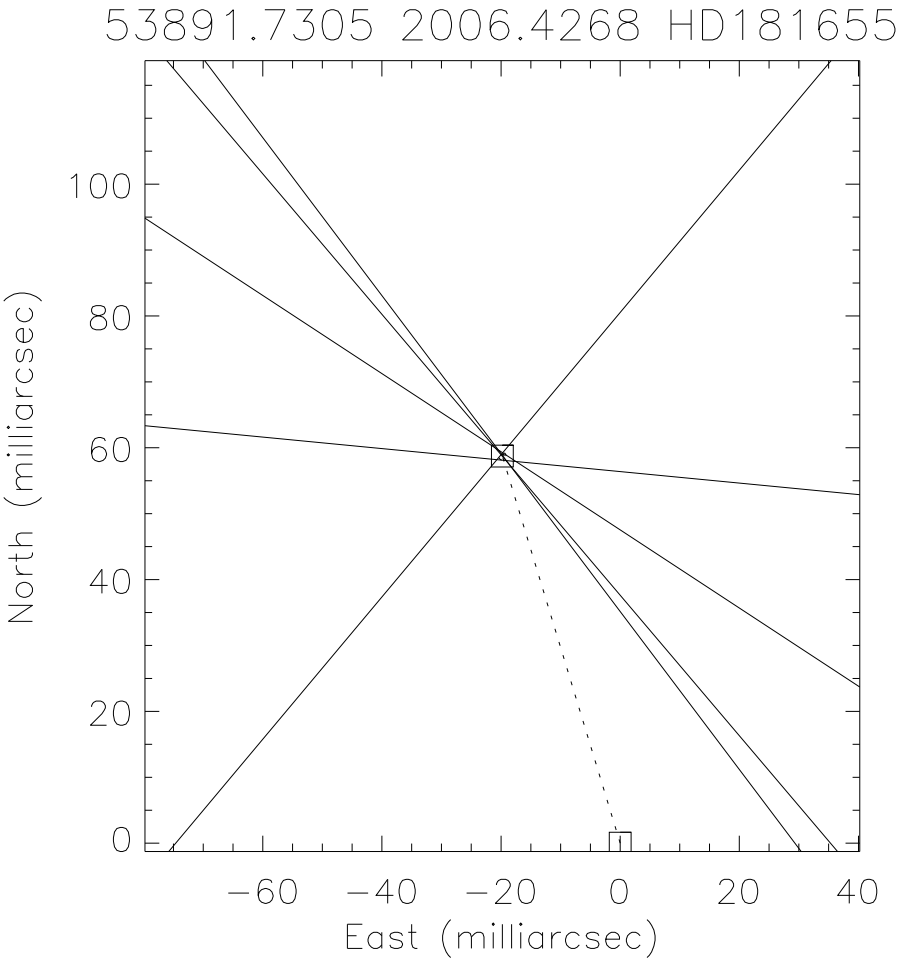


Figure. C.8: Triangulation Plot for HD 181655 on 2006.4268. Calculation from 5 data files from 2006 June 4 to June 6.

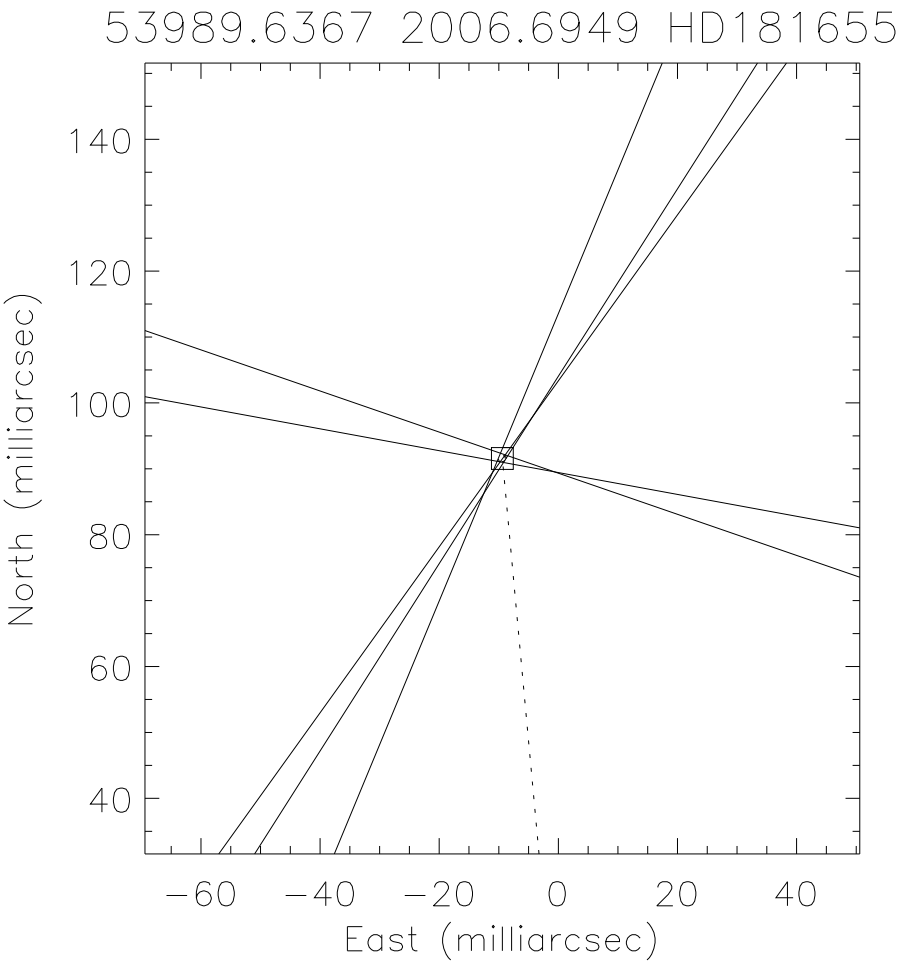


Figure. C.9: Triangulation Plot for HD 181655 on 2006.6938. Calculated from 5 data files from 2006 September 10 to September 13.

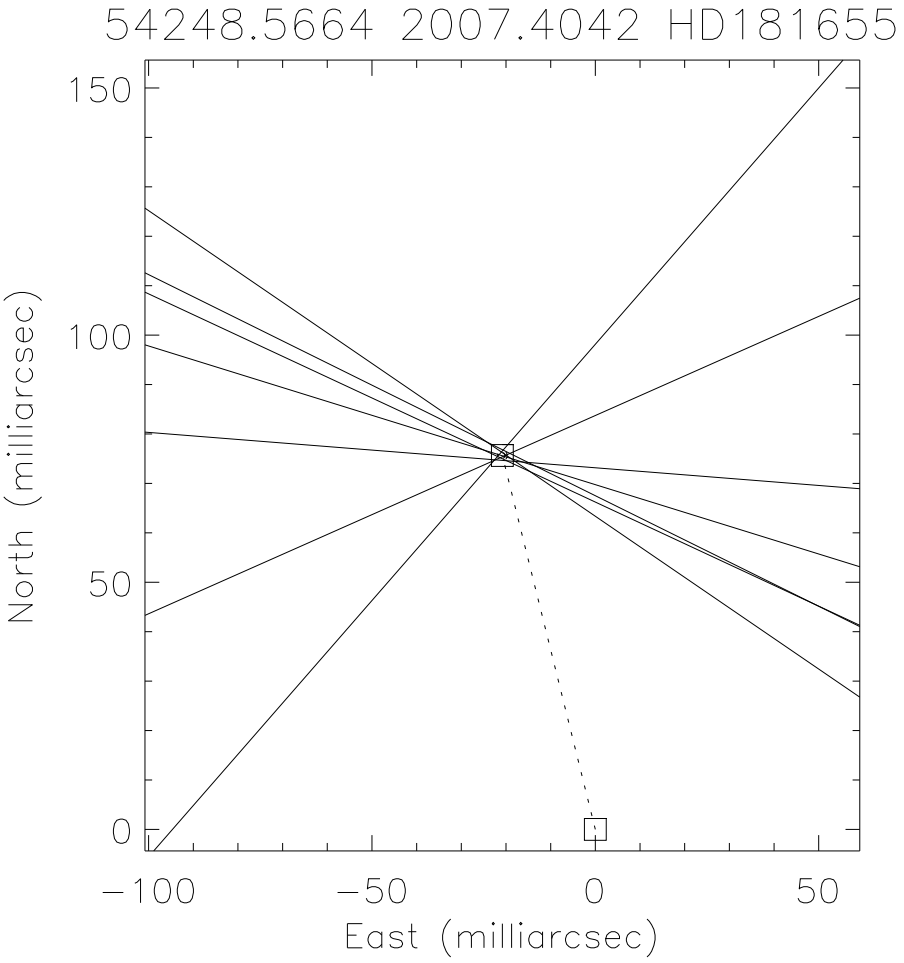


Figure. C.10: Triangulation Plot for HD 181655 on 2007.4099. Calculated from 8 data files from 2007 May 27 to May 30.

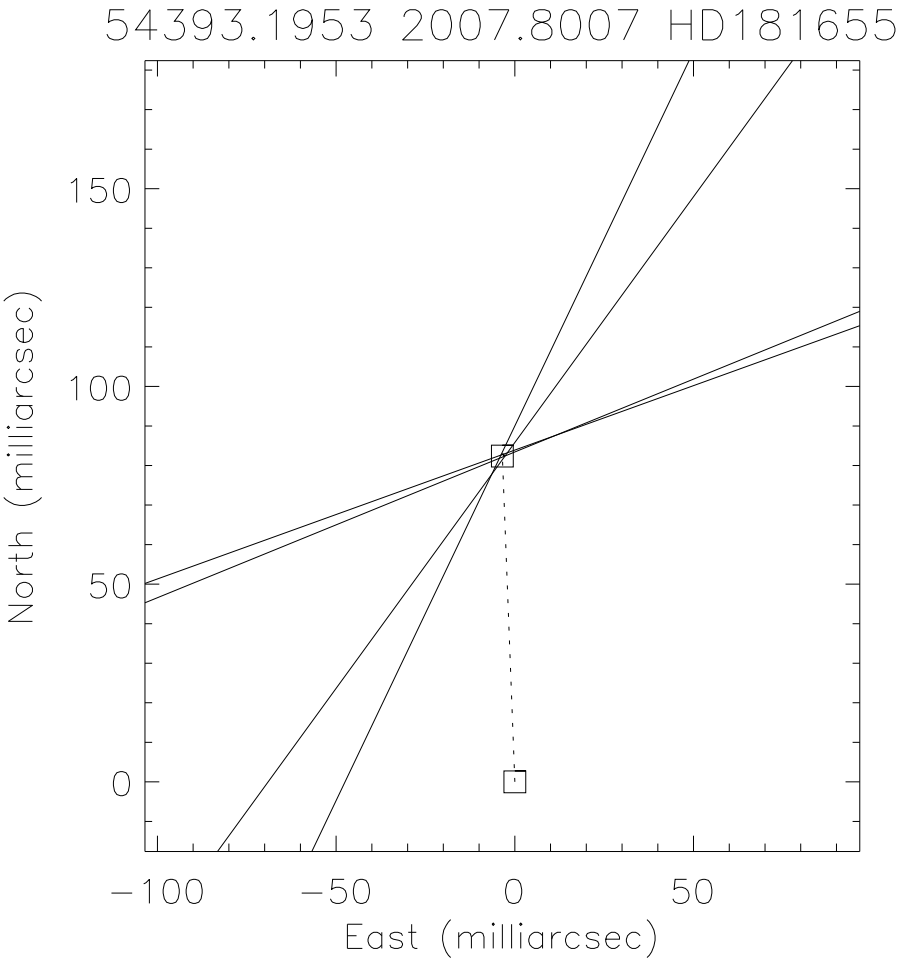


Figure. C.11: Triangulation Plot for HD 181655 on 2007.8007. Calculated from 4 data files from 2007 October 20.

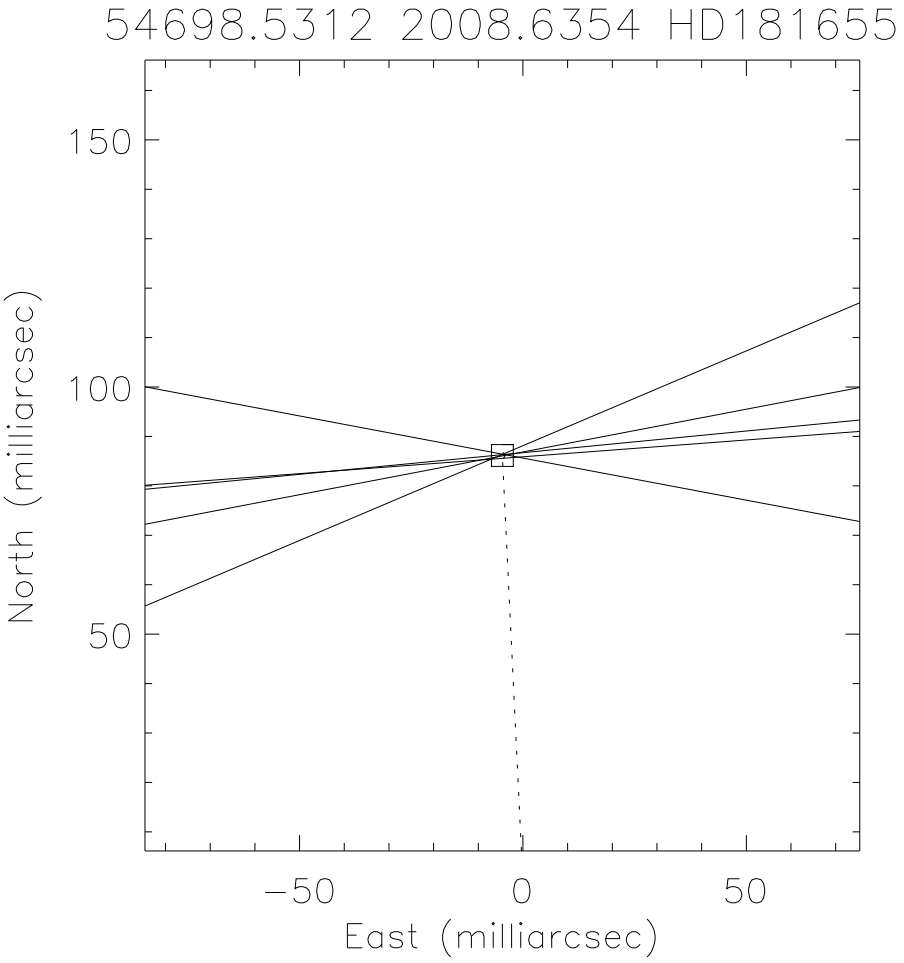


Figure. C.12: Triangulation Plot for HD 181655 on 2008.6354. Calculated from 5 data files from 2008 August 19 to August 21.

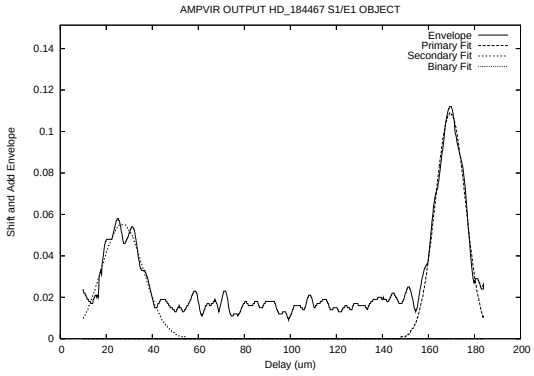


Figure. C.13: HD 184467 SFP Fringe Envelope on 2006 June 3 using the E1/S1 baseline.

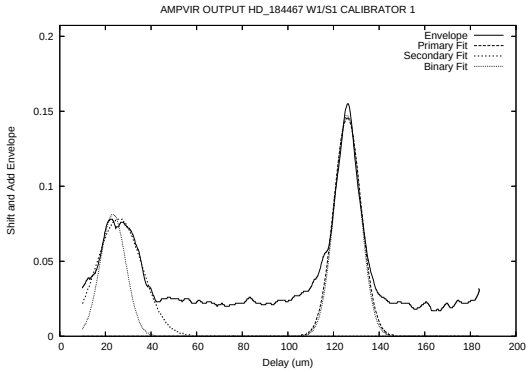


Figure. C.14: HD 184467 SFP Fringe Envelope on 2006 June 4 using the W1/S1 baseline.

## C.2 HD 184467

A previous IAU radial velocity standard star for many years, HD 184467 has since been determined to be a double-lined spectroscopic binary with a visual orbit determined by speckle interferometry. Additional data from the CHARA SFP survey allowed for a refinement of the previous orbit and further validation of the SFP method of secondary location. See Chapter 7.2 for complete details on this system.

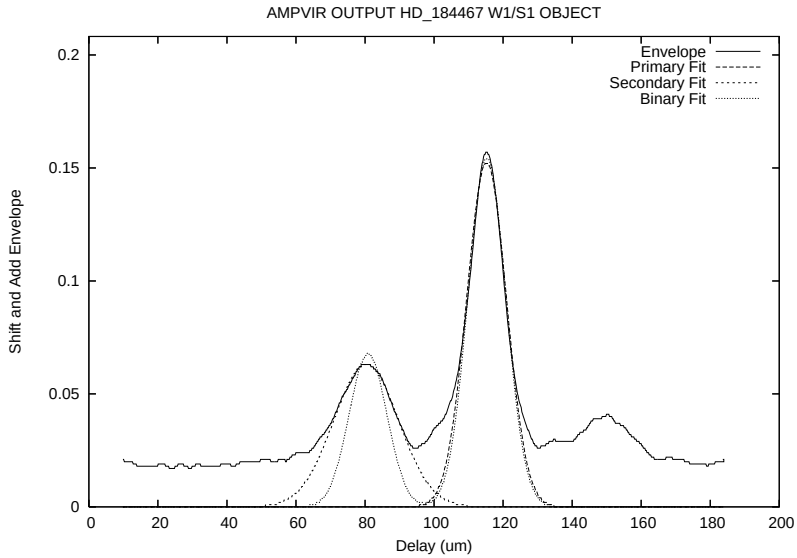


Figure. C.15: HD 184467 SFP Fringe Envelope on 2006 June 5 using the W1/S1 baseline.

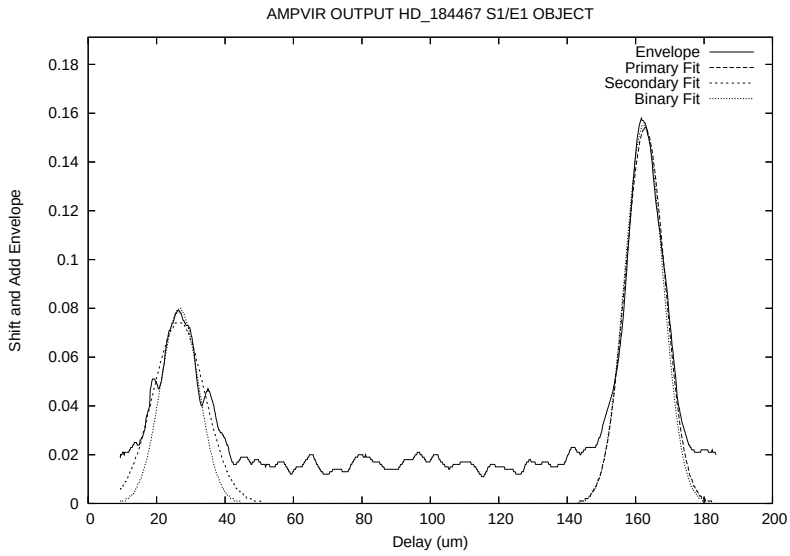


Figure. C.16: HD 184467 SFP Fringe Envelope on 2006 June 6 using the E1/S1 baseline.

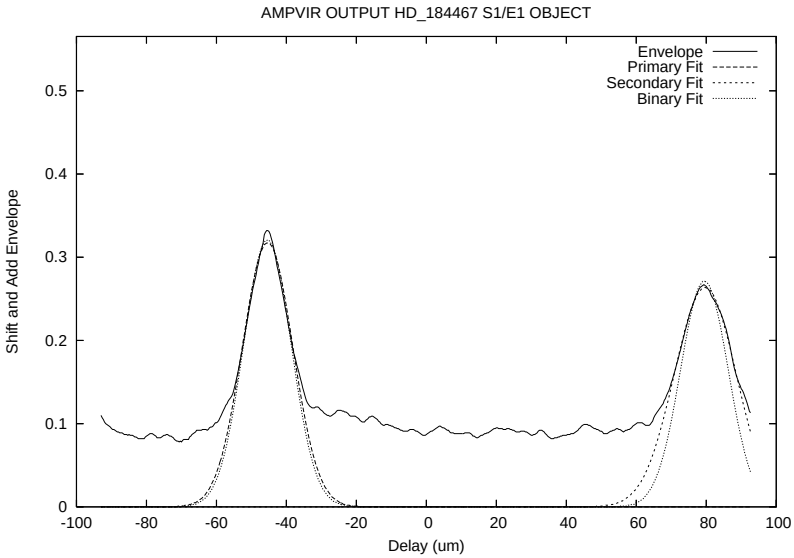


Figure. C.17: HD 184467 SFP Fringe Envelope on 2006 July 26 using the E1/S1 baseline.

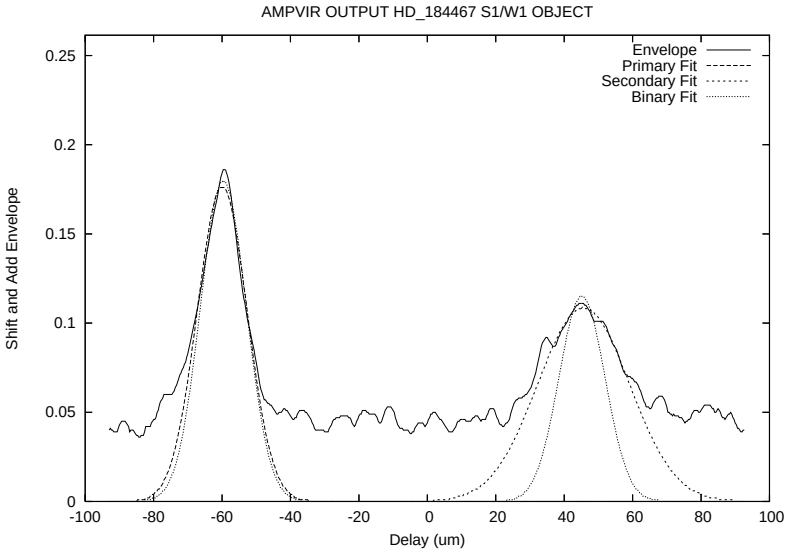


Figure. C.18: HD 184467 SFP Fringe Envelope on 2006 July 26 using the W1/S1 baseline.

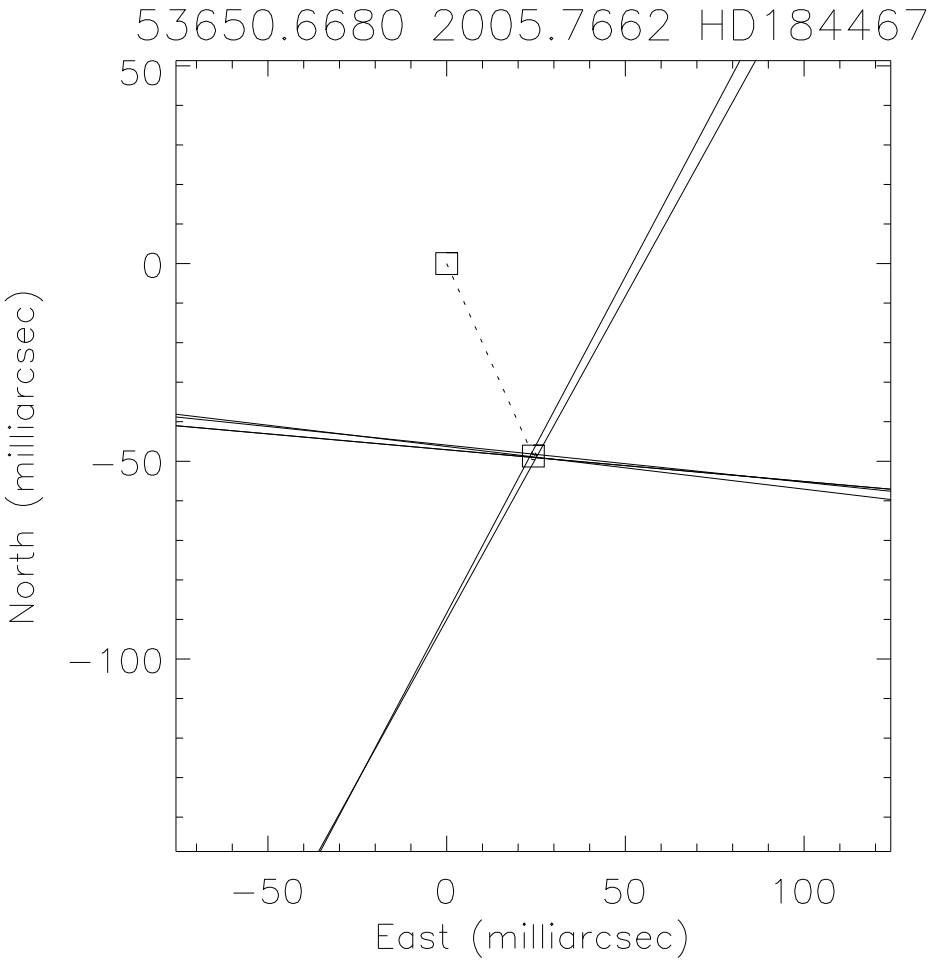


Figure. C.19: Triangulation Plot for HD 184467 on 2005.7662. Calculated from 5 data files from 2005 October 4 to October 11.

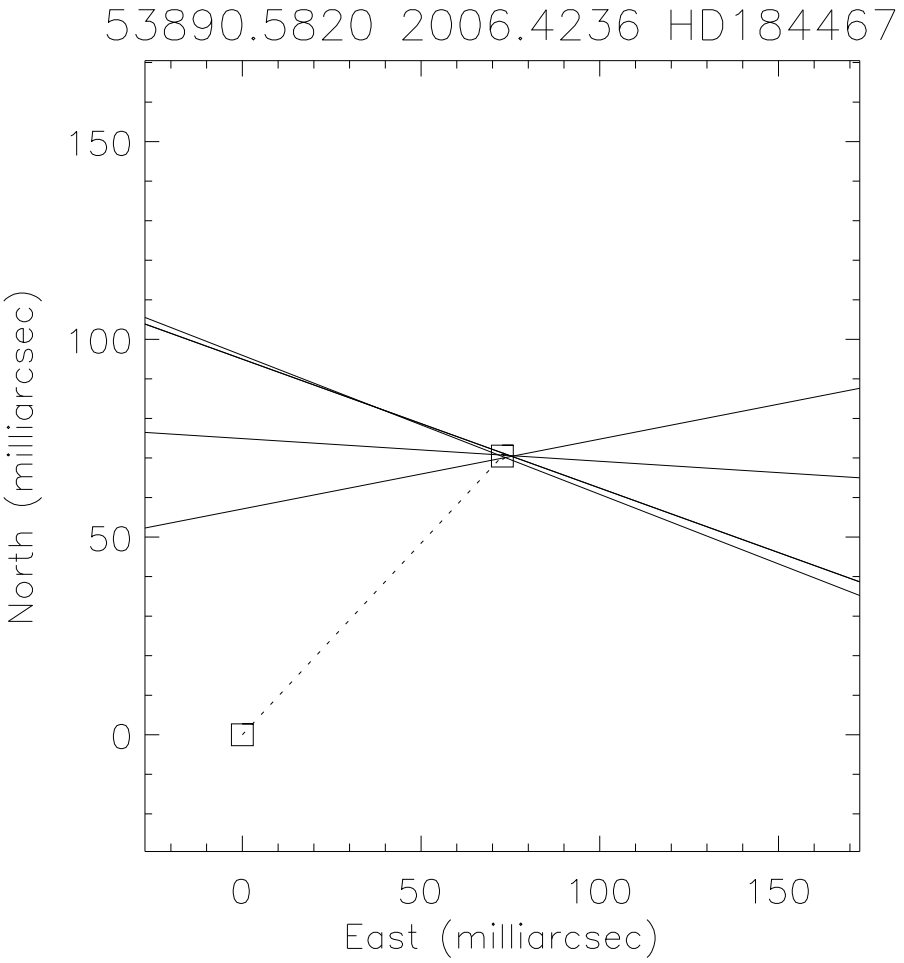


Figure. C.20: Triangulation Plot for HD 184467 on 2006.4236. Calculated from 4 data files from 2006 June 4 to June 5.

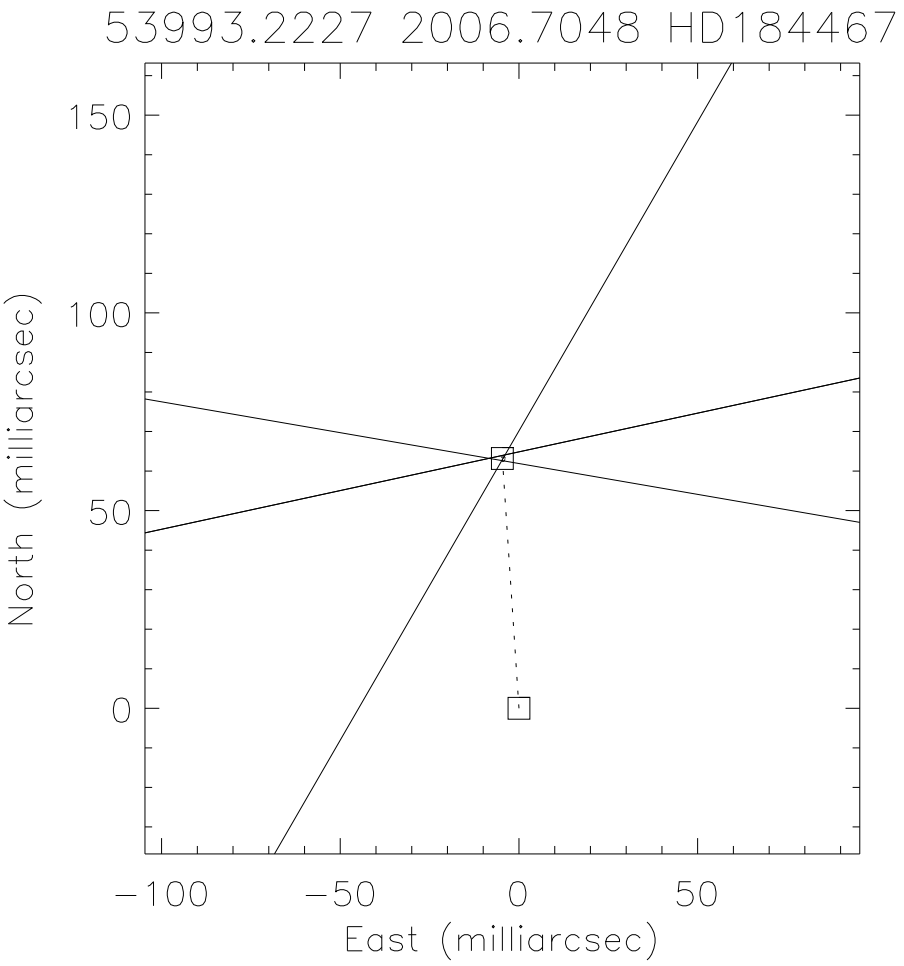


Figure. C.21: Triangulation Plot for HD 184467 on 2006.7048. Calculated from 3 data files from 2006 September 12 to September 18.

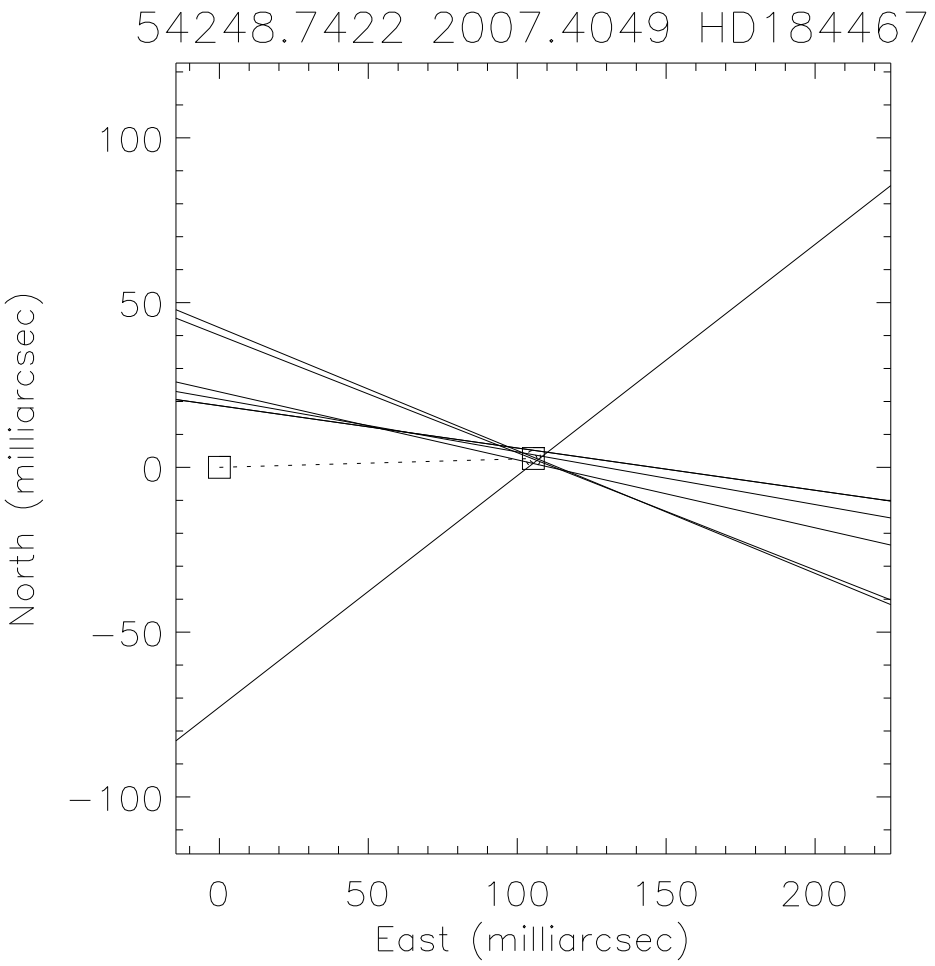


Figure. C.22: Triangulation Plot for HD 184467 on 2007.4049. Calculated from 6 data files from 2007 May 27 to May 29.

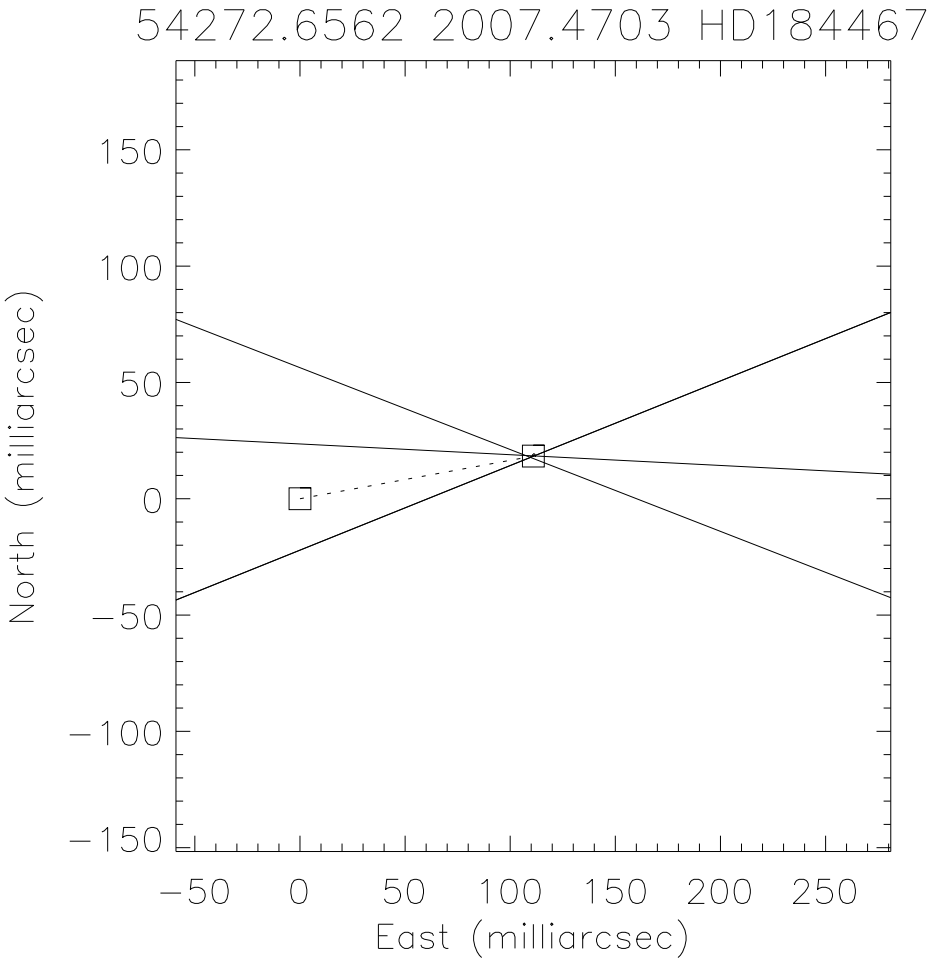


Figure. C.23: Triangulation Plot for HD 184467 on 2007.4703. Calculated from 3 data files from 2007 June 21.

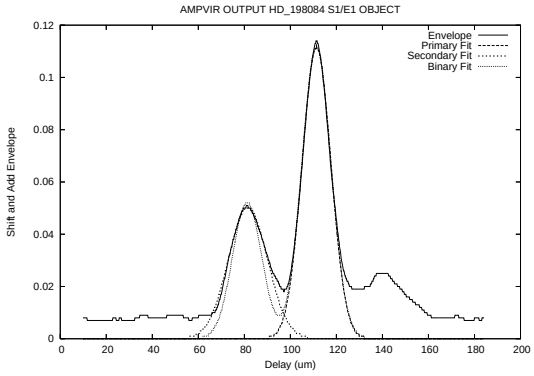


Figure. C.24: HD 198084 SFP Fringe Envelope on 2006 June 3 using the E1/S1 baseline.

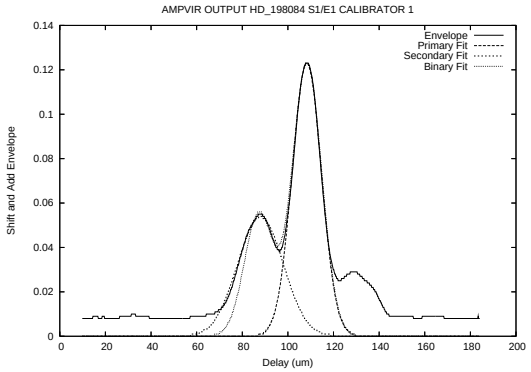


Figure. C.25: HD 198084 SFP Fringe Envelope on 2006 June 3 using the E1/S1 baseline.

## C.3 HD 198084

This nearly equal pair of late F stars provided the largest collection of data and was the most consistant producer of secondary fringes in the project. The monitoring of this system has produced a well defined orbit for a spectroscopic binary with no previous visual detection of the secondary. Future work determining the radii of the individual components will allow the determination of every physical parameter for the system. Chapter 7.3 contains full details of this object.

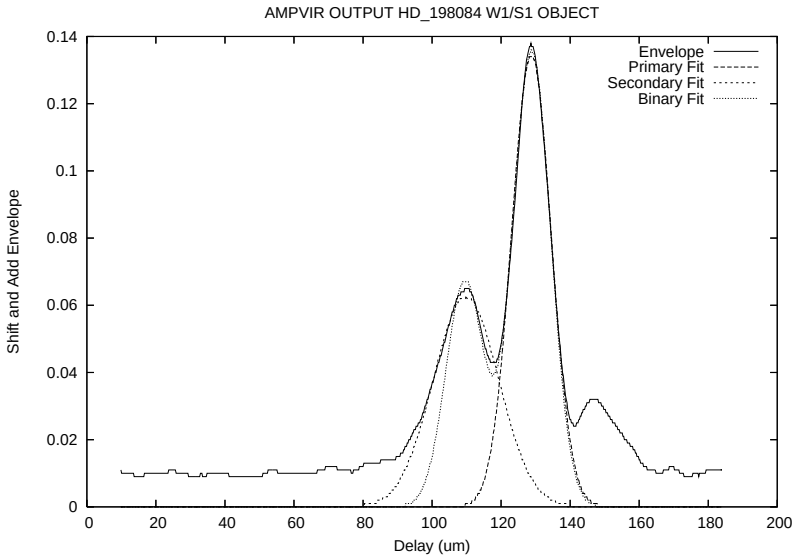


Figure. C.26: HD 198084 SFP Fringe Envelope on 2006 June 4 using the W1/S1 baseline.

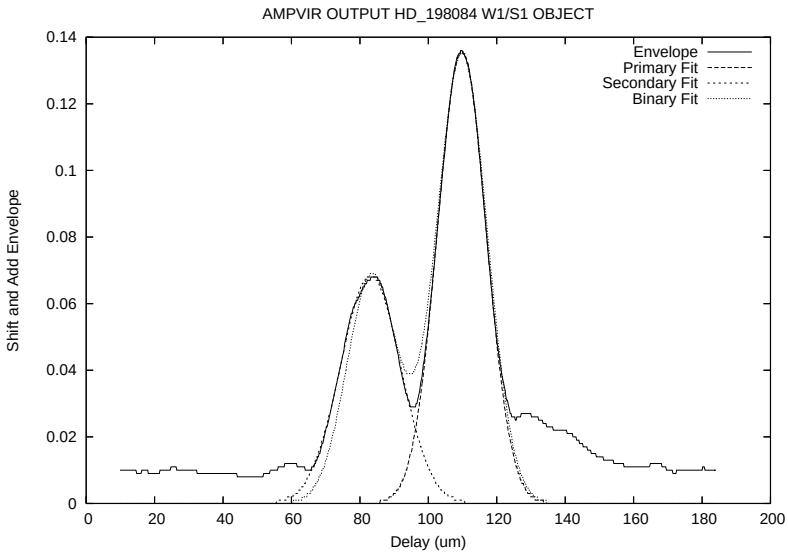


Figure. C.27: HD 198084 SFP Fringe Envelope on 2006 June 5 using the W1/S1 baseline.

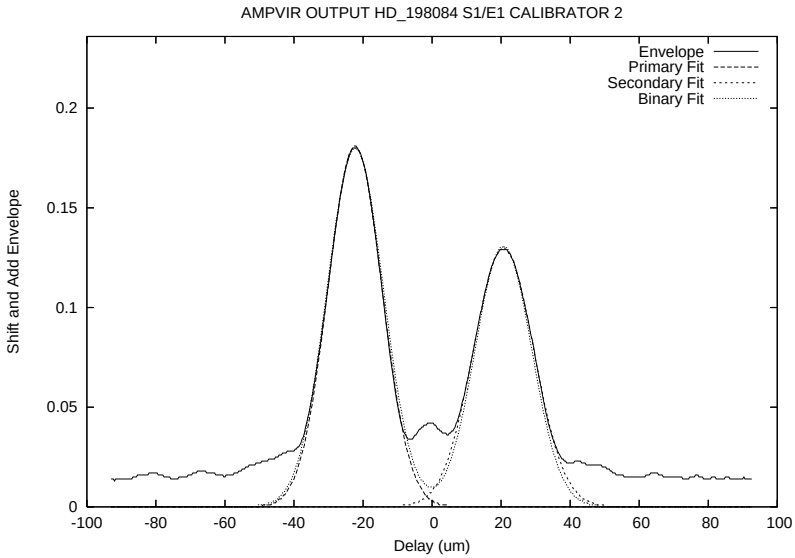


Figure. C.28: HD 198084 SFP Fringe Envelope on 2007 June 26 using the E1/S1 baseline.

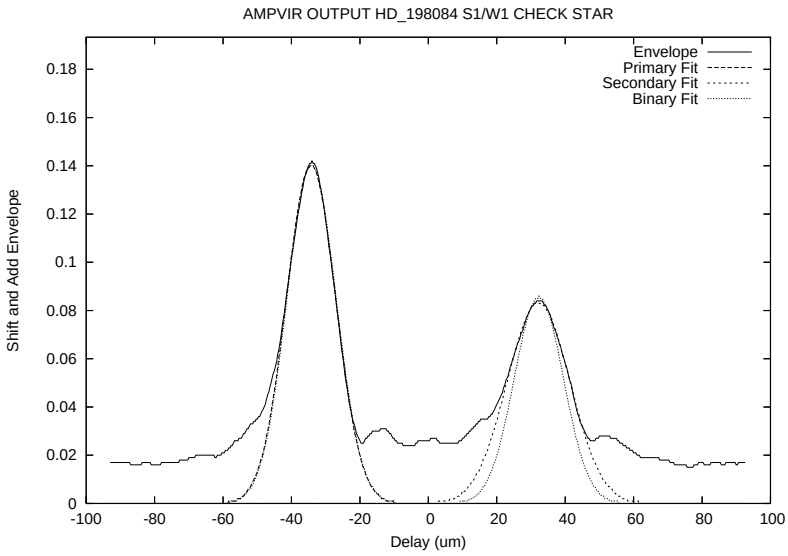


Figure. C.29: HD 198084 SFP Fringe Envelope on 2007 June 26 using the W1/S1 baseline.

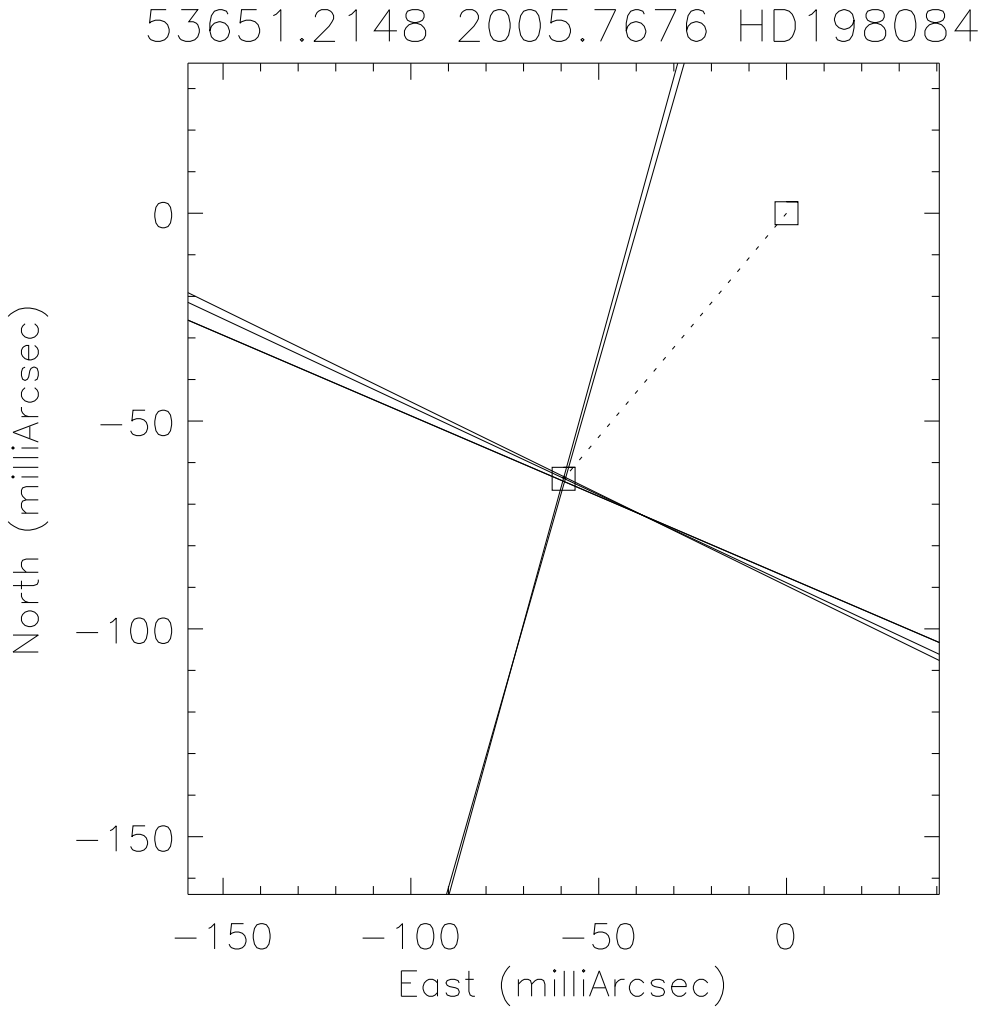


Figure. C.30: Triangulation Plot for HD 198084 on 2005.7676. Calculated from 5 data files from 2005 October 5 to October 11

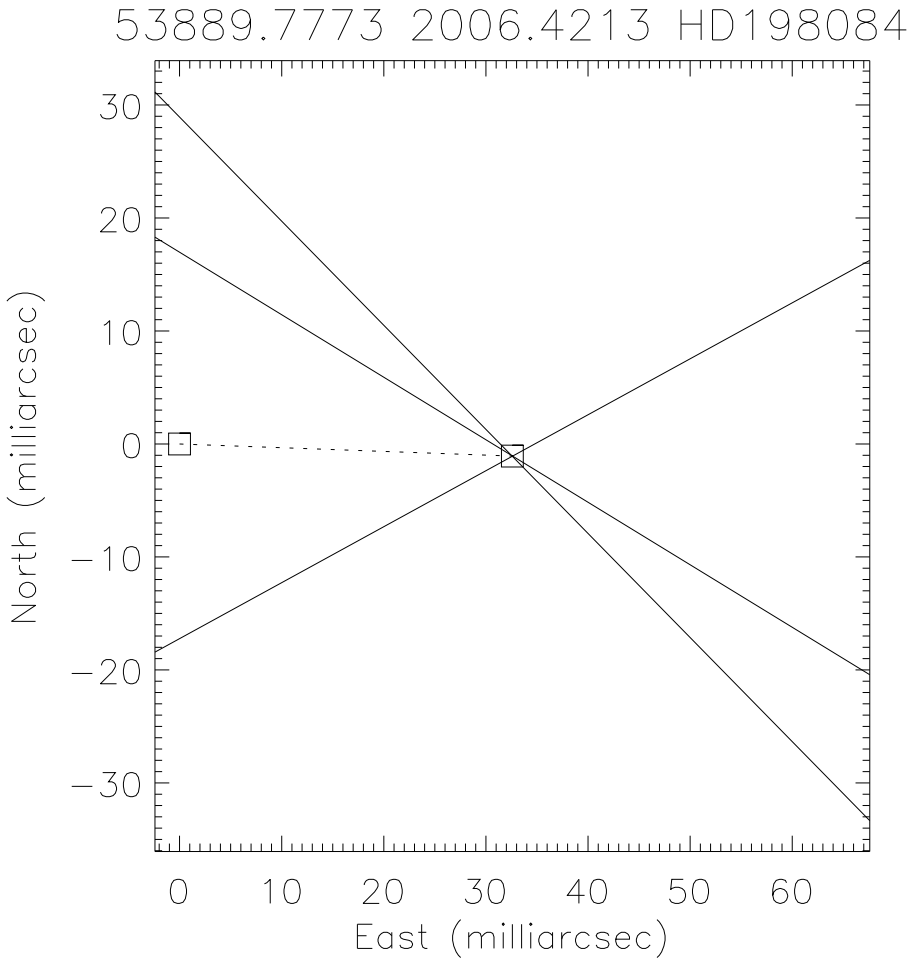


Figure. C.31: Triangulation Plot for HD 198084 on 2006.4213. Calculated from 3 data files from 2006 June 3.

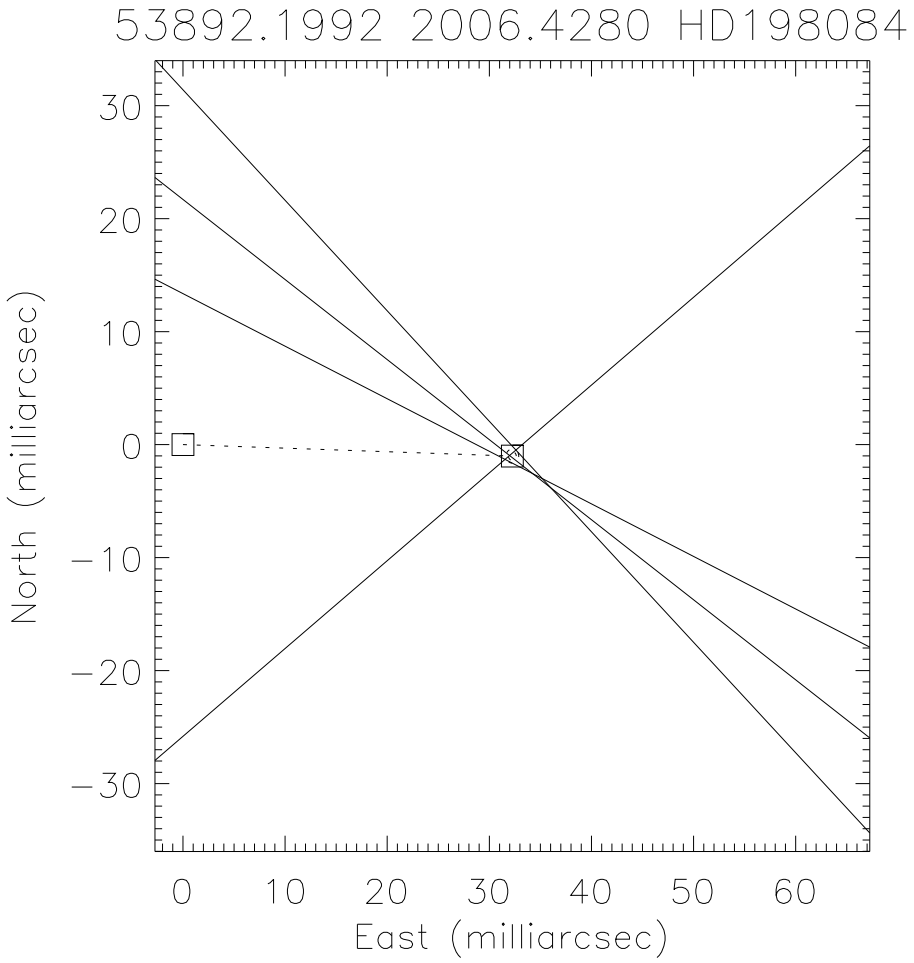


Figure. C.32: Triangulation Plot for HD 198084 on 2006.4286. Calculated from 4 data files from 2006 June 6.

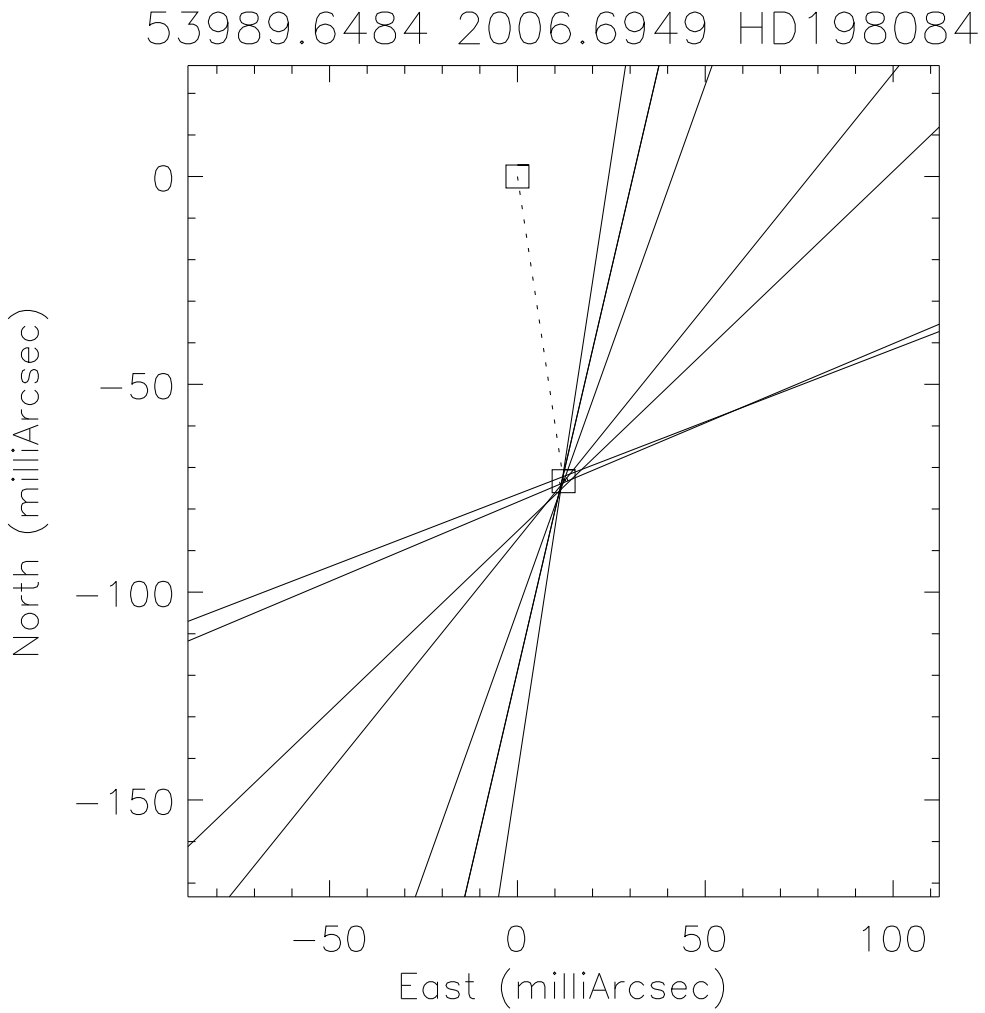


Figure. C.33: Triangulation Plot for HD 198084 on 2006.6949. Calculated from 7 data files from 2006 September 11 to September 12.

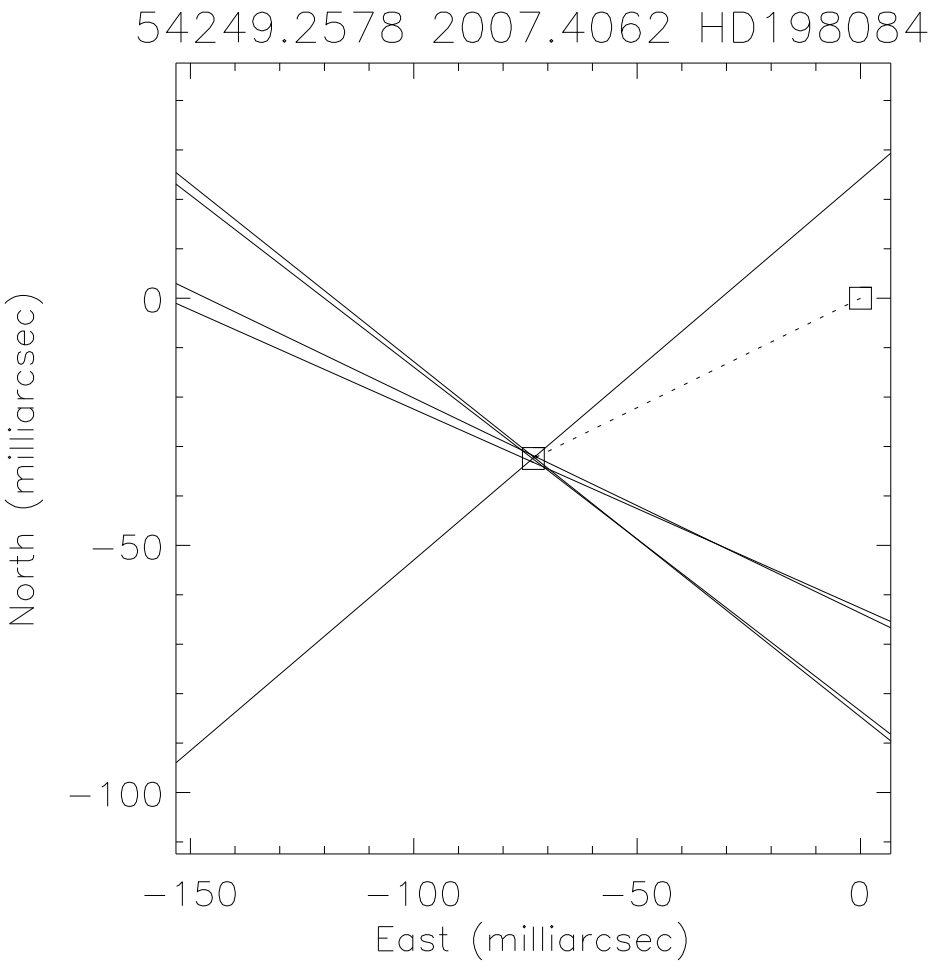


Figure. C.34: Triangulation Plot for HD 198084 on 2007.4062. Calculated from 4 data files from 2007 May 29

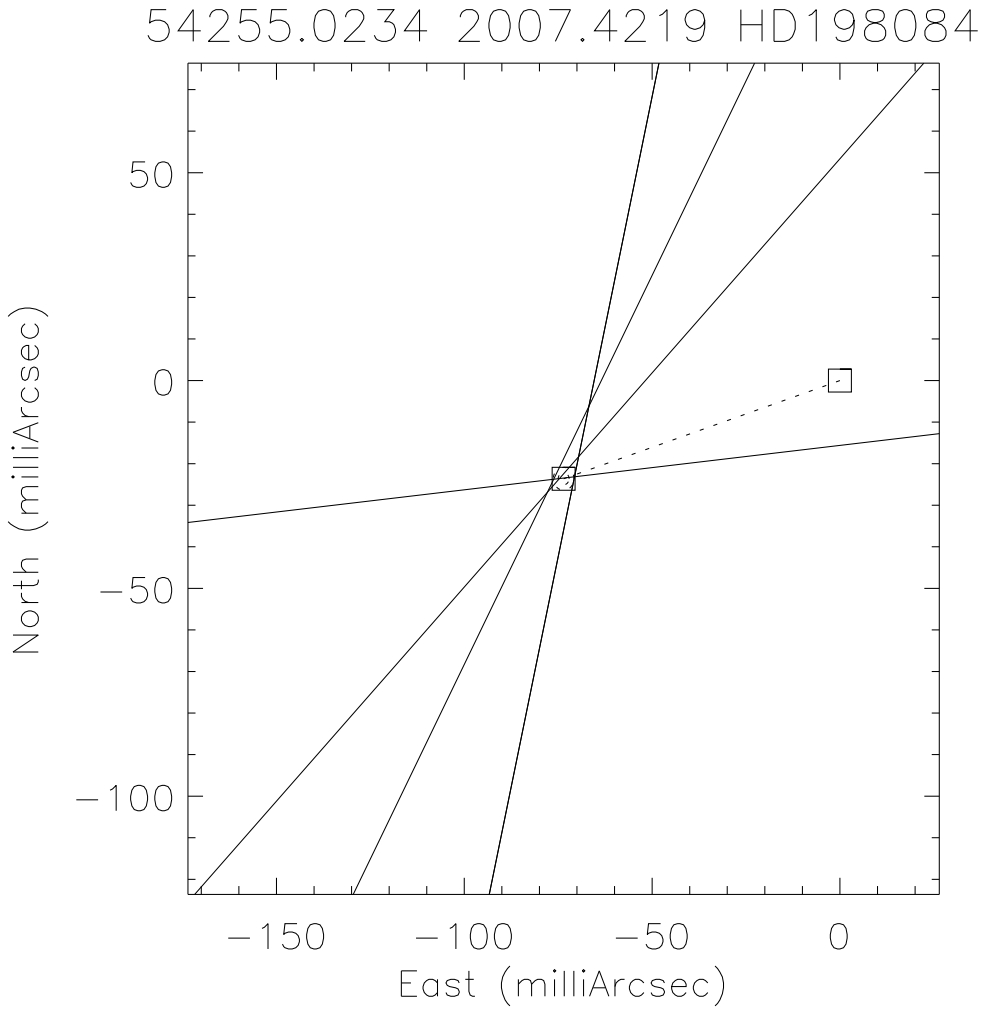


Figure. C.35: Triangulation Plot for HD 198084 on 2007.4219. Calculated from 4 data files from 2007 June 3 to June 4.

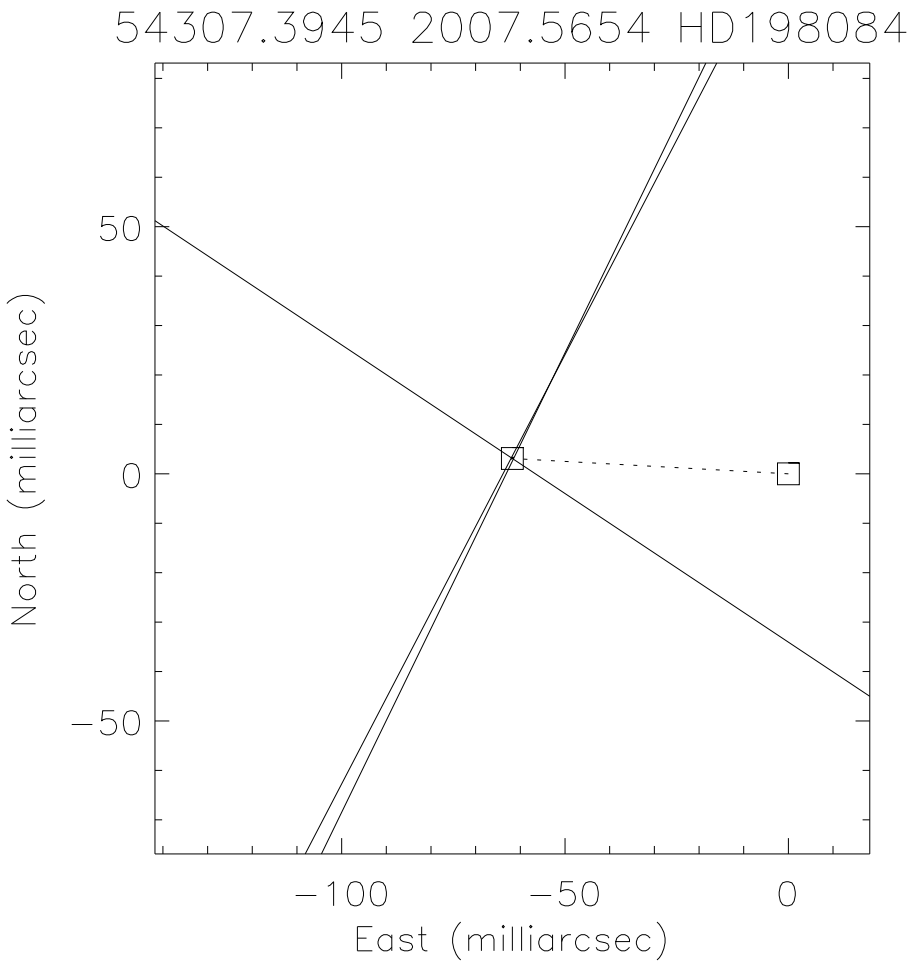


Figure. C.36: Triangulation Plot for HD 198084 on 2007.5654. Calculated from 3 data files from 2007 July 26.

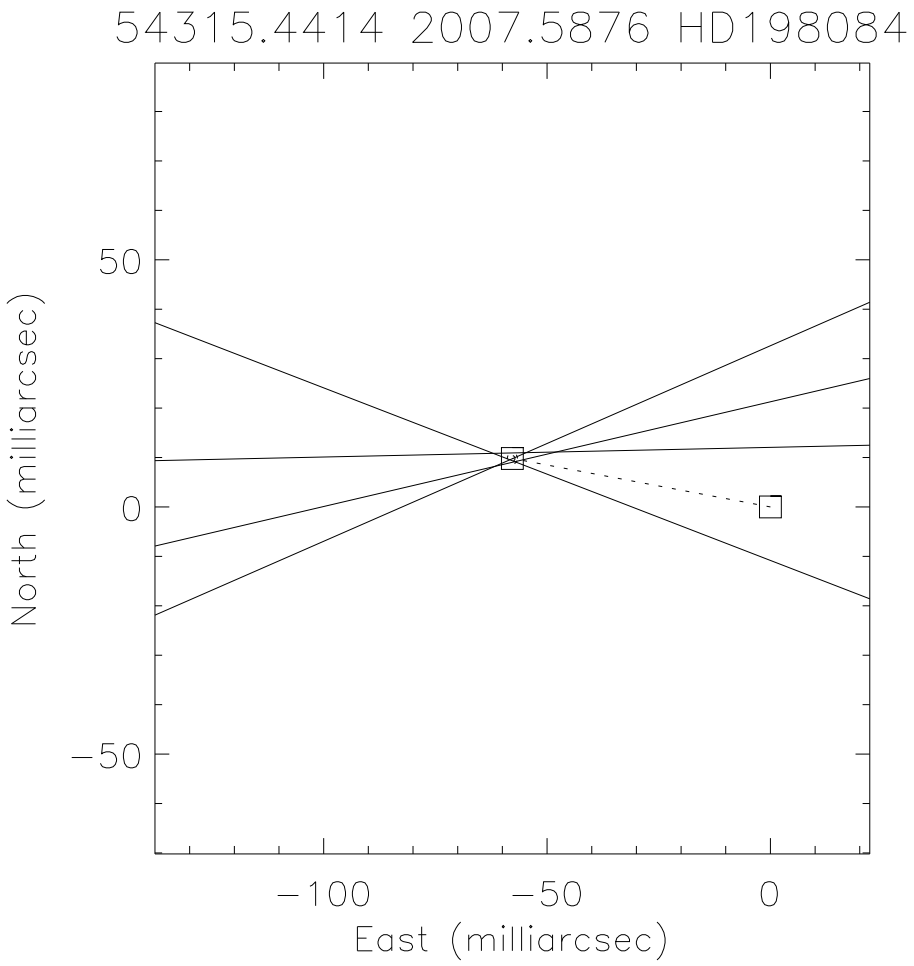


Figure. C.37: Triangulation Plot for HD 198084 on 2007.5876. Calculated from 4 data files from 2007 August 3.

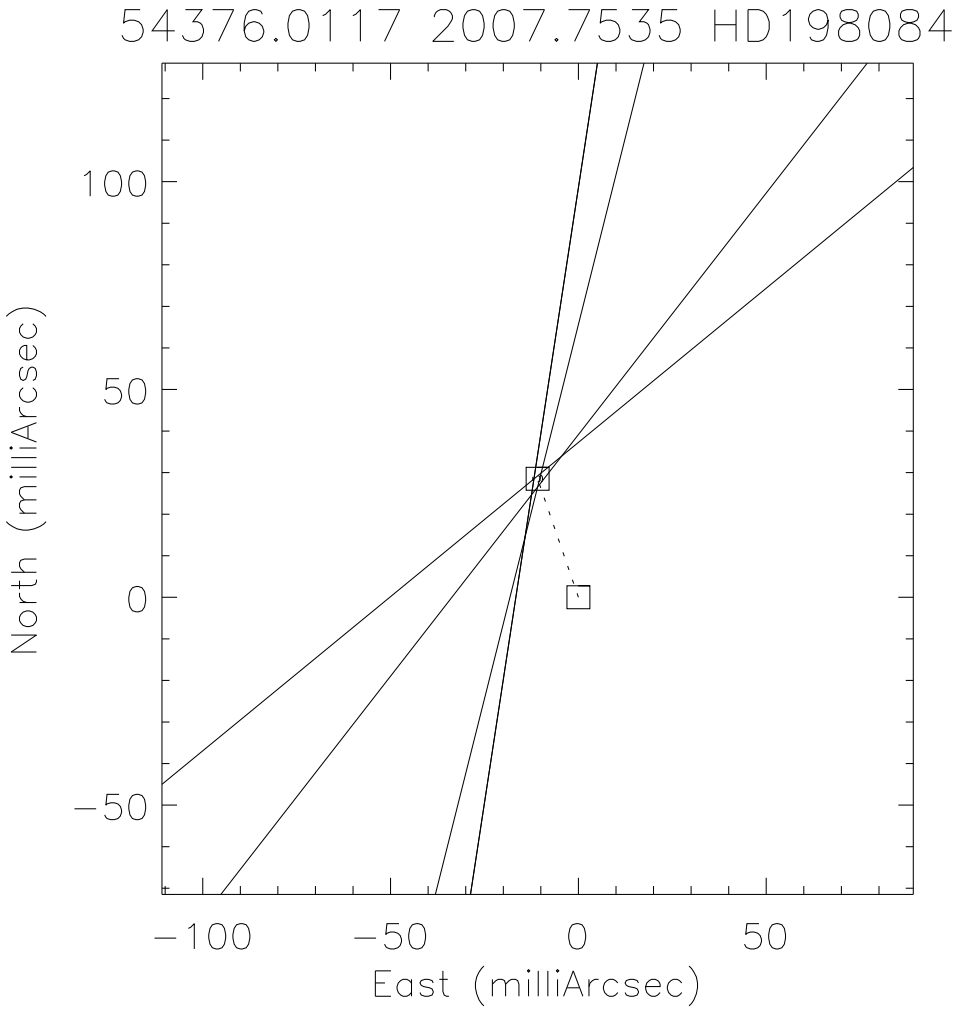


Figure. C.38: Triangulation Plot for HD 198084 on 2007.7535. Calculated from 4 data files from 2007 October 3.

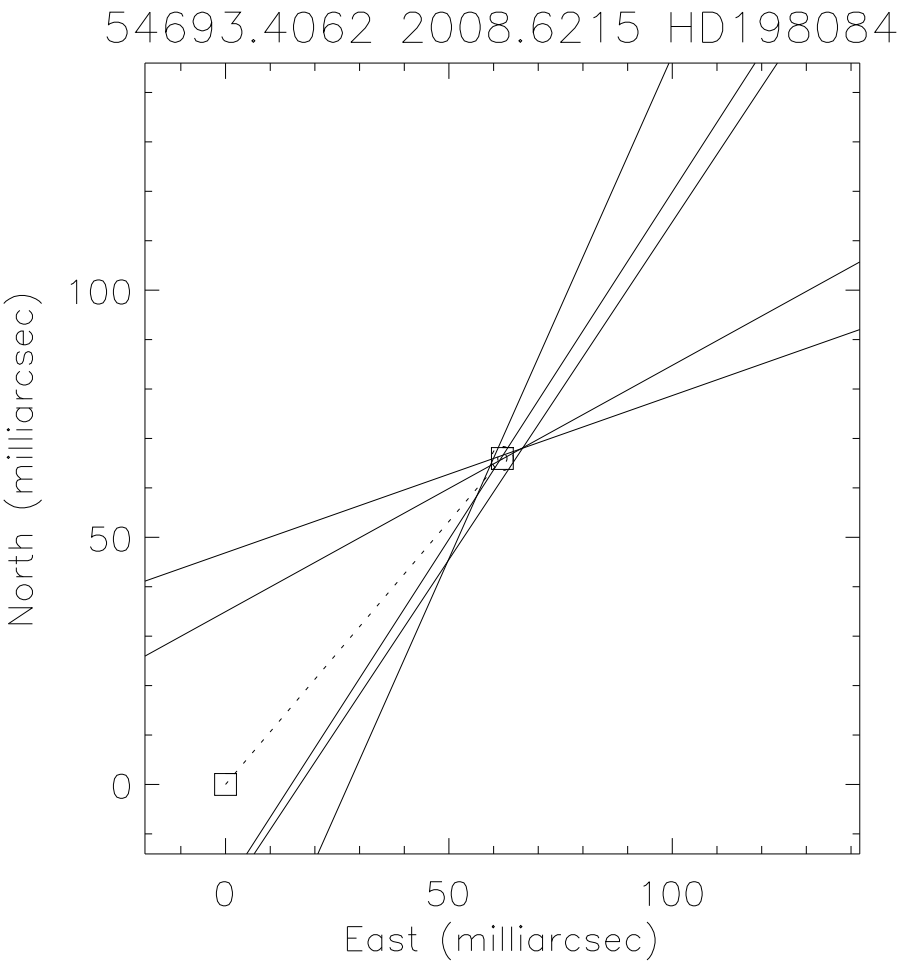


Figure. C.39: Triangulation Plot for HD 198084 on 2008.6215. Calculated from 5 data files from 2008 August 15.

# – D —

# MathCAD Program for Luminosity

This appendix includes the program written in MathCAD for the calculation of component masses, magnitudes, and luminosities for HD 198084. Inputs for this program include orbital elements from the spectroscopic and visual orbits, amplitude ratio from the separated fringes, $V$, $\Delta V$, $K$, $\Delta K$, and parallaxes. Calculations determine the individual masses in two different ways (from $M \sin^3 i$ and Keplers Laws) and an additional mass calculation based on the calculated orbital parallax instead of HIPPARCOS. Also included is the determination of the $K$ magnitude difference from the fringe packet amplitude ratio. As no $V$ magnitude ratio was available, assumptions were made ($\Delta V = \Delta K$ or $\Delta V$ from M-L relation bolometric magnitude difference) and the program calculates the apparent, absolute and bolometric magnitudes for each assumption. Two separate luminosity relation formulae were used on each calculated case. This program also includes error propagation calculations for each appropriate step. The final sections, D.19 and D.20, contain configurable plots for comparison with known main-sequence Mass/Luminosity relations.

## Mass Estimates With Error Bars — HD 198084

**Using Spectroscopic Results and inclination from interferometry:**

Input parameters:

$i \equiv 22.71 \cdot \frac{\pi}{180}$ $\quad \Delta i \equiv 0.11 \cdot \frac{\pi}{180}$ from interferometry

$Msin1 \equiv 0.0786$ $\quad \Delta Msin1 \equiv 0.0057$ from spectroscopic orbit

$Msin2 \equiv 0.0736$ $\quad \Delta Msin2 \equiv 0.0050$ from spectroscopic orbit

Calculations:

$$M(Msin, i) \equiv \frac{Msin}{(\sin(i))^3} \qquad \Delta M(Msin, \Delta Msin, i \Delta i) \equiv \sqrt{\left(\frac{d}{dMsin} M(Msin, i) \cdot \Delta Msin\right)^2 + \left(\frac{d}{di} M(Msin, i) \cdot \Delta i\right)^2}$$

Primary Star

$M(Msin1, i) = 1.366$ Msol $\quad \Delta M(Msin1, \Delta Msin1, i \Delta i) = 0.101$ Msol $\quad MSp \equiv \frac{0.101}{1.366}$

Secondary Star

$M(Msin2, i) = 1.279$ Msol $\quad \Delta M(Msin2, \Delta Msin2, i \Delta i) = 0.089$ Msol $\quad MSp = 0.074$

Checking extreme values of i for 1-sigma variance:

$M1low \equiv \frac{Msin1}{\sin(i + \Delta i)^3}$ $\quad M1low = 1.347$ $\quad M1hgh \equiv \frac{Msin1}{\sin(i - \Delta i)^3}$ $\quad M1hgh = 1.385$

$M(Msin1, i) - M1low = 0.019$ $\quad M1hgh - M(Msin1, i) = 0.019$

$M2low \equiv \frac{Msin2}{\sin(i + \Delta i)^3}$ $\quad M2low = 1.262$ $\quad M2hgh \equiv \frac{Msin2}{\sin(i - \Delta i)^3}$ $\quad M2hgh = 1.297$

$M(Msin2, i) - M2low = 0.017$ $\quad M2hgh - M(Msin2, i) = 0.018$

$Ma \equiv M(Msin1, i)$ $\quad \Delta Ma \equiv \Delta M(Msin1, \Delta Msin1, i \Delta i)$

$Ma = 1.366$ $\quad \Delta Ma = 0.101$

$Mb \equiv M(Msin2, i)$ $\quad \Delta Mb \equiv \Delta M(Msin2, \Delta Msin2, i \Delta i)$

$Mb = 1.279$ $\quad \Delta Mb = 0.089$

Figure. D.1: MathCAD Mass and Luminosity Program Page 1

**Using interferometric-α, spec-P, Kepler's third law and Hipparcos parallax**

Input parameters:

$\alpha \doteq .06448$ arcsec $\quad \Delta\alpha \doteq 0.00119$ arcsec — from interferometry

$plx \doteq 0.03626$ arcsec $\quad \Delta plx \doteq 0.00036$ arcsec — from Hipparcos

$p \doteq 1.434314$ yrs $\quad \Delta p \doteq 0.0041862$ yrs — from spectroscopy

1.4343154

0.0041856

$q \doteq 0.936 \quad \Delta q \doteq 0.032$ — from spectroscopy

1.428367 1.434314

Calculations:

$$a(\alpha, plx) \doteq \frac{\alpha}{plx} \qquad \Delta a(\alpha, \Delta\alpha, plx, \Delta plx) \doteq \sqrt{\left(\frac{d}{d\alpha} a(\alpha, plx)\cdot\Delta\alpha\right)^2 + \left(\frac{d}{dplx} a(\alpha, plx)\cdot\Delta plx\right)^2}$$

$a(\alpha, plx) = 1.7783$ AU $\qquad \Delta a(\alpha, \Delta\alpha, plx, \Delta plx) = 0.0373$ AU

$$MSum(a, p) \doteq \frac{a^3}{p^2} \qquad \Delta MSum(a, \Delta a, p, \Delta p) \doteq \sqrt{\left(\frac{d}{da} MSum(a, p)\cdot\Delta a\right)^2 + \left(\frac{d}{dp} MSum(a, p)\cdot\Delta p\right)^2}$$

$MSum(a(\alpha, plx), p) = 2.7334$ Msol $\qquad \Delta MSum(a(\alpha, plx), \Delta a(\alpha, \Delta\alpha, plx, \Delta plx), p, \Delta p) = 0.1726$ Msol

$$Mp(MSum, q) \doteq \frac{MSum}{1+q} \qquad \Delta Mp(MSum, \Delta MSum, q, \Delta q) \doteq \sqrt{\left(\frac{d}{dMSum} Mp(MSum, q)\cdot\Delta MSum\right)^2 + \left(\frac{d}{dq} Mp(MSum, q)\cdot\Delta q\right)^2}$$

$Mp(MSum(a(\alpha, plx), p), q) = 1.412$ Msol $\qquad \Delta Mp(MSum(a(\alpha, plx), p), \Delta MSum(a(\alpha, plx), \Delta a(\alpha, \Delta\alpha, plx, \Delta plx), p, \Delta p), q, \Delta q) = 0.092$ Msol

$$Ms(MSum, q) \doteq \frac{MSum}{1+q}\cdot q \qquad \Delta Ms(MSum, \Delta MSum, q, \Delta q) \doteq \sqrt{\left(\frac{d}{dMSum} Ms(MSum, q)\cdot\Delta MSum\right)^2 + \left(\frac{d}{dq} Ms(MSum, q)\cdot\Delta q\right)^2}$$

$Ms(MSum(a(\alpha, plx), p), q) = 1.322$ Msol $\qquad \Delta Ms(MSum(a(\alpha, plx), p), \Delta MSum(a(\alpha, plx), \Delta a(\alpha, \Delta\alpha, plx, \Delta plx), p, \Delta p), q, \Delta q) = 0.087$

$$PerMp1 \doteq \frac{0.088}{1.383} \qquad PerMp1 = 0.064 \qquad PerMs1 \doteq \frac{0.086}{1.350} \qquad PerMs1 = 0.064$$

Msol

$Ma\eta \doteq Mp(MSum(a(\alpha, plx), p), q) \qquad Mb\eta \doteq Ms(MSum(a(\alpha, plx), p), q)$

$\Delta Ma\eta \doteq \Delta Mp(MSum(a(\alpha, plx), p), \Delta MSum(a(\alpha, plx), \Delta a(\alpha, \Delta\alpha, plx, \Delta plx), p, \Delta p), q, \Delta q)$

$Ma\eta = 1.412 \qquad \Delta Ma\eta = 0.092$

$\Delta Mb\eta \doteq \Delta Ms(MSum(a(\alpha, plx), p), \Delta MSum(a(\alpha, plx), \Delta a(\alpha, \Delta\alpha, plx, \Delta plx), p, \Delta p), q, \Delta q)$

$Mb\eta = 1.322 \qquad \Delta Mb\eta = 0.087$

Figure. D.2: MathCAD Mass and Luminosity Program Page 2

**Using interferometric-α, spec-P, Kepler's third law and Hipparcos parallax**

Input parameters: Calculated Orbital Parallax

$\alpha\phi := .06448$ arcsec $\Delta\alpha\phi := 0.00119$ arcsec from interferometry

$xplx := 0.035448$ arcsec $\Delta xplx := 0.001239$ arcsec from Hipparcos

$p\phi := 1.434314$ yrs $\Delta p\phi := 0.0041862$ yrs from spectroscopy

$q\phi := 0.9754$ $\Delta q\phi := 0.015$ from spectroscopy

Calculations:

$$a\phi(\alpha\phi, xplx) := \frac{\alpha\phi}{xplx} \qquad \Delta a\phi(\alpha\phi, \Delta\alpha\phi, xplx\Delta\ xplx) := \sqrt{\left(\frac{d}{d\alpha\phi} a\phi(\alpha\phi, xplx)\cdot\Delta\alpha\phi\right)^2 + \left(\frac{d}{dxplx} a\phi(\alpha\phi, xplx)\cdot\Delta xplx\right)^2}$$

$a\phi(\alpha\phi, xplx) = 1.819$ AU

$\Delta a\phi(\alpha\phi, \Delta\alpha\phi, xplx\Delta\ xplx) = 0.0719$ AU

$$MSum\phi(a\phi, p\phi) := \frac{a\phi^3}{p\phi^2} \qquad \Delta MSum\phi(a\phi, \Delta a\phi, p\phi\Delta\ p\phi) := \sqrt{\left(\frac{d}{da\phi} MSum\phi(a\phi, p\phi)\cdot\Delta a\phi\right)^2 + \left(\frac{d}{dp\phi} MSum\phi(a\phi, p\phi)\cdot\Delta p\phi\right)^2}$$

$MSum\phi(a\phi(\alpha\phi, xplx), p\phi) = 2.9256$ Msol $\Delta MSum\phi(a\phi(\alpha\phi, xplx), \Delta a\phi(\alpha\phi, \Delta\alpha\phi, xplx\Delta\ xplx), p\phi\Delta\ p\phi) = 0.3473$ Msol

$$Mp\phi(MSum\phi, q\phi) := \frac{MSum\phi}{1 + q\phi} \qquad \Delta Mp\phi(MSum\phi, \Delta MSum\phi, q\phi\Delta\ q\phi) := \sqrt{\left(\frac{d}{dMSum\phi} Mp\phi(MSum\phi, q\phi)\cdot\Delta MSum\phi\right)^2 + \left(\frac{d}{dq\phi} Mp\phi(MSum\phi, q\phi)\cdot\Delta q\phi\right)^2}$$

$Mp\phi(MSum\phi(a\phi(\alpha\phi, xplx), p\phi), q\phi) = 1.481$ Msol

$\Delta Mp\phi(MSum\phi(a\phi(\alpha\phi, xplx), p\phi), \Delta MSum\phi(a\phi(\alpha\phi, xplx), \Delta a\phi(\alpha\phi, \Delta\alpha\phi, xplx\Delta\ xplx), p\phi\Delta\ p\phi), q\phi\Delta\ q\phi) = 0.176$ Msol

$$Ms\phi(MSum\phi, q\phi) := \frac{MSum\phi}{1 + q\phi}\cdot q\phi \qquad \Delta Ms\phi(MSum\phi, \Delta MSum\phi, q\phi\Delta\ q\phi) := \sqrt{\left(\frac{d}{dMSum\phi} Ms\phi(MSum\phi, q\phi)\cdot\Delta MSum\phi\right)^2 + \left(\frac{d}{dq\phi} Ms\phi(MSum\phi, q\phi)\cdot\Delta q\phi\right)^2}$$

$Ms\phi(MSum\phi(a\phi(\alpha\phi, xplx), p\phi), q\phi) = 1.445$ Msol

$\Delta Ms\phi(MSum\phi(a\phi(\alpha\phi, xplx), p\phi), \Delta MSum\phi(a\phi(\alpha\phi, xplx), \Delta a\phi(\alpha\phi, \Delta\alpha\phi, xplx\Delta\ xplx), p\phi\Delta\ p\phi), q\phi\Delta\ q\phi) = 0.172$ Msol

$PerMp2 := \frac{0.176}{1.481}$ $PerMp2 = 0.119$ $PerMs2 := \frac{0.172}{1.445}$ $PerMs2 = 0.119$

$Ma\phi := Mp\phi(MSum\phi(a\phi(\alpha\phi, xplx), p\phi), q\phi)$

$Ma\phi = 1.481$

$\Delta Ma\phi := \Delta Mp\phi(MSum\phi(a\phi(\alpha\phi, xplx), p\phi), \Delta MSum\phi(a\phi(\alpha\phi, xplx), \Delta a\phi(\alpha\phi, \Delta\alpha\phi, xplx\Delta\ xplx), p\phi\Delta\ p\phi), q\phi\Delta\ q\phi)$

$\Delta Ma\phi = 0.176$

$Mb\phi := Ms\phi(MSum\phi(a\phi(\alpha\phi, xplx), p\phi), q\phi)$

$Mb\phi = 1.445$

$\Delta Mb\phi := \Delta Ms\phi(MSum\phi(a\phi(\alpha\phi, xplx), p\phi), \Delta MSum\phi(a\phi(\alpha\phi, xplx), \Delta a\phi(\alpha\phi, \Delta\alpha\phi, xplx\Delta\ xplx), p\phi\Delta\ p\phi), q\phi\Delta\ q\phi)$

$\Delta Mb\phi = 0.172$

Figure. D.3: MathCAD Mass and Luminosity Program Page 3

**Error for Orbital Parallax**

$e \fallingdotseq 0.547$ $\Delta e \fallingdotseq 0.00741$ $P \fallingdotseq 1.4343154 \cdot 365.242189$

$inc \fallingdotseq 22.71$ $\Delta inc \fallingdotseq 0.11$ $\Delta P \fallingdotseq 0.0041856 \cdot 365.242189$

$sep \fallingdotseq 64.48$ $\Delta sep \fallingdotseq 1.19$ $P = 523.872$

$\Delta P = 1.529$

$Kp \fallingdotseq 8.42$ $\Delta Kp \fallingdotseq 0.34$

$Ks \fallingdotseq 9.00$ $\Delta Ks \fallingdotseq 0.37$

$$aau(e, Kp, Ks, P, inc) \fallingdotseq \left[ \frac{\left[ 13751 \cdot \sqrt{(1 - e^2)} \cdot (Kp + Ks) \cdot P \right]}{\sin(inc \cdot deg) \cdot 1.496 \cdot 10^8} \right]$$

$aau(e, Kp, Ks, P, inc) = 1.819$ AU

$$dde \fallingdotseq \frac{d}{de} aau(e, Kp, Ks, P, inc) \cdot \Delta e$$

$$ddKp \fallingdotseq \frac{d}{dKp} aau(e, Kp, Ks, P, inc) \cdot \Delta Kp$$

$$ddKs \fallingdotseq \frac{d}{dKs} aau(e, Kp, Ks, P, inc) \cdot \Delta Ks$$

$$ddP \fallingdotseq \frac{d}{dP} aau(e, Kp, Ks, P, inc) \cdot \Delta P$$

$$ddinc \fallingdotseq \frac{d}{dinc} aau(e, Kp, Ks, P, inc) \cdot \Delta inc$$

$$\Delta aau(e, \Delta e, Kp \Delta Kp, Ks \Delta Ks, P \Delta P, inc \Delta inc) \fallingdotseq \sqrt{(dde)^2 + (ddKp)^2 + (ddKs)^2 + (ddP)^2 + (ddinc)^2}$$

$\Delta aau(e, \Delta e, Kp \Delta Kp, Ks \Delta Ks, P \Delta P, inc \Delta inc) = 0.054$ AU

$aaux \fallingdotseq aau(e, Kp, Ks, P, inc)$ $aauerr \fallingdotseq \frac{0.054}{1.819}$

$\Delta aaux \fallingdotseq \Delta aau(e, \Delta e, Kp \Delta Kp, Ks \Delta Ks, P \Delta P, inc \Delta inc)$ $aauerr = 0.03$

$$\Pi orb(aaux, sep) \fallingdotseq \frac{sep}{aaux}$$

$$\Delta \Pi orb(aaux, \Delta aaux, sep \Delta sep) \fallingdotseq \sqrt{\left( \frac{d}{daaux} \Pi orb(aaux, sep) \cdot \Delta aaux \right)^2 + \left( \frac{d}{dsep} \Pi orb(aaux, sep) \cdot \Delta sep \right)^2}$$

$\Pi orb(aaux, sep) = 35.45$ $\Delta \Pi orb(aaux, \Delta aaux, sep \Delta sep) = 1.246$

$$d \fallingdotseq \frac{10^3}{\Pi orb(aaux, sep)}$$

$plx = 0.036$ $\Pi \fallingdotseq 0.035448$

$\Delta plx = 3.6 \times 10^{-4}$ $\Delta \Pi \fallingdotseq 0.001239$

$d = 28.209$ pc $\Delta d \fallingdotseq .999$

Figure. D.4: MathCAD Mass and Luminosity Program Page 4

**Calculation of individual apparent K magnitudes**

$mabk \doteq 3.267$ $\Delta mabk \doteq 0.242$ $Ma \doteq 1.366$ $\Delta Ma \doteq 0.101$

$bratio \doteq 1.391$ $\Delta bratio \doteq 0.0475$ $Mb \doteq 1.279$ $\Delta Mb \doteq 0.089$

$\Delta mk(bratio) \doteq 2.5 \cdot (\log(bratio))$ $\delta\Delta mk(bratio, \Delta bratio) \doteq \frac{d}{dbratio} \Delta mk(bratio) \cdot \Delta bratio$

$\Delta mk(bratio) = 0.358$ $\delta\Delta mk(bratio, \Delta bratio) = 0.037$

$\Delta mk1 \doteq \Delta mk(bratio)$ $\delta\Delta mk1 \doteq \delta\Delta mk(bratio, \Delta bratio)$

$magbk(mabk, \Delta mk1) \doteq \left[ mabk + \left[ 2.5 \cdot \left[ \log\left[ 1 + \left( 10^{0.4 \cdot \Delta mk1} \right) \right] \right] \right] \right]$

$magbk(mabk, \Delta mk1) = 4.213$

$\Delta magbk(mabk, \Delta mabk, \Delta mk1, \delta\Delta mk1) \doteq \sqrt{\left( \frac{d}{dmabk} magbk(mabk, \Delta mk1) \cdot \Delta mabk \right)^2 + \left( \frac{d}{d\Delta mk1} magbk(mabk, \Delta mk1) \cdot \delta\Delta mk1 \right)^2}$

$\Delta magbk(mabk, \Delta mabk, \Delta mk1, \delta\Delta mk1) = 0.243$

$magbk1 \doteq magbk(mabk, \Delta mk1)$ $magak1 \doteq magbk1 - \Delta mk1$ $magak1 = 3.855$ individual K magnitudes

$\Delta magk1 \doteq \Delta magbk(mabk, \Delta mabk, \Delta mk1, \delta\Delta mk1)$ $magak1 = 3.855$ $magbk1 = 4.213$

**Calculation of individual apparent V magnitudes**
**Assumption 1: Mag difference from Mass/Lum**

$\Delta mv \doteq 0.273$ $\delta\Delta mv \doteq 0.124$

$mabv \doteq 4.516$ $\Delta mabv \doteq 0.010$

$magbv(mabv, \Delta mv) \doteq \left[ mabv + \left[ 2.5 \cdot \left[ \log\left[ 1 + \left( 10^{0.4 \cdot \Delta mv} \right) \right] \right] \right] \right]$

$magbv(mabv, \Delta mv) = 5.414$

$magav \doteq magbv(mabv, \Delta mv) - \Delta mv$ $magav1 \doteq magav$ Individual V magnitudes (Assumption 1)

$magav = 5.141$ $magbv1 \doteq magbv(mabv, \Delta mv)$ $magav1 = 5.141$ $magbv1 = 5.414$

$\Delta magbv(mabv, \Delta mabv, \Delta mv, \delta\Delta mv) \doteq \sqrt{\left( \frac{d}{dmabv} magbv(mabv, \Delta mv) \cdot \Delta mabv \right)^2 + \left( \frac{d}{d\Delta mv} magbv(mabv, \Delta mv) \cdot \delta\Delta mv \right)^2}$

$\Delta magbv(mabv, \Delta mabv, \Delta mv, \delta\Delta mv) = 0.07$

$\Delta magbv1 \doteq \Delta magbv(mabv, \Delta mabv, \Delta mv, \delta\Delta mv)$ $\Delta magbv1 = 0.07$ $BC \doteq -0.15$

Figure. D.5: MathCAD Mass and Luminosity Program Page 5

**Calculation of individual apparent V magnitudes**
**Assumption 2: ΔK = ΔV**

$\Delta\chi v \doteq 0.349$ $\delta\Delta\chi v \doteq 0.042$

$mabv \doteq 4.516$ $\Delta mabv \doteq 0.010$

$magbv\chi(mabv, \Delta\chi v) \doteq \left[ mabv + \left[ 2.5 \cdot \left[ \log\left[ 1 + \left( 10^{0.4 \cdot \Delta\chi v} \right) \right] \right] \right] \right]$ $magbv\chi(mabv, \Delta\chi v) = 5.457$

$magav\chi \doteq magbv\chi(mabv, \Delta\chi v) - \Delta\chi v$

$magav\chi = 5.108$

Individual V Magnitudes (Assumption 2)

$magav\chi x \doteq magav\chi$ $magav\chi x = 5.108$

$magbv\chi x \doteq magbv\chi(mabv, \Delta\chi v)$ $magbv\chi x = 5.457$

$$\Delta magbv\chi(mabv, \Delta mabv\Delta\chi\ v\ \delta\Delta\chi\ v) \doteq \sqrt{\left( \frac{d}{dmabv} magbv\chi(mabv, \Delta\chi v) \cdot \Delta mabv \right)^2 + \left( \frac{d}{d\Delta\chi v} magbv\chi(mabv, \Delta\chi v) \cdot \delta\Delta\chi v \right)^2}$$

$\Delta magbv\chi(mabv, \Delta mabv\Delta\chi\ v\ \delta\Delta\chi\ v) = 0.026$

$\Delta magbv\chi x \doteq \Delta magbv\chi(mabv, \Delta mabv\Delta\chi\ v\ \delta\Delta\chi\ v)$ $av\chi \doteq magav\chi x$

$\Delta magav\chi \doteq 0.073$ $bv\chi \doteq magbv\chi x$ $\Delta v\chi \doteq 0.073$

**V - K Magnitudes from Both Assumptions**

$VmKp1 \doteq magav - magak1$ $VmKp2 \doteq magav\chi - magak1$

$VmKs1 \doteq magbv1 - magbk1$ $VmKs2 \doteq magbv\chi x - magbk1$

$VmKp1 = 1.286$ $VmKp2 = 1.253$

$\Delta VmK1 \doteq \sqrt{(\Delta magk1)^2 + (\Delta magbv1)^2}$

$VmKs1 = 1.2$ $VmKs2 = 1.244$

$\Delta VmK1 = 0.253$ $\Delta VmK2 \doteq \sqrt{(\Delta magk1)^2 + (\Delta magav\chi)^2}$ $\Delta VmK2 = 0.254$

**Absolute K Magnitude from Hipparcos plx**

$AbsMka(magak1, plx) \doteq [magak1 + 5 \cdot (\log(plx)) + 5]$ $AbsMka(magak1, plx) = 1.652$

$AbsMkb(magbk1, plx) \doteq [magbk1 + 5 \cdot (\log(plx)) + 5]$ $AbsMkb(magbk1, plx) = 2.011$

$$\Delta AbsMka(magak1, \Delta magk1, plx\Delta\ plx) \doteq \sqrt{\left( \frac{d}{dmagak1} AbsMka(magak1, plx) \cdot \Delta magk1 \right)^2 + \left( \frac{d}{dplx} AbsMka(magak1, plx) \cdot \Delta plx \right)^2}$$

$$\Delta AbsMkb(magbk1, \Delta magk1, plx\Delta\ plx) \doteq \sqrt{\left( \frac{d}{dmagbk1} AbsMkb(magbk1, plx) \cdot \Delta magk1 \right)^2 + \left( \frac{d}{dplx} AbsMkb(magbk1, plx) \cdot \Delta plx \right)^2}$$

$\Delta AbsMka(magak1, \Delta magk1, plx\Delta\ plx) = 0.244$ $\Delta AbsMkb(magbk1, \Delta magk1, plx\Delta\ plx) = 0.244$ $\Delta AbsMk \doteq \Delta AbsMkb(magbk1, \Delta magk1, plx\Delta\ plx)$

**Absolute K Magnitude from My Parallax**

$AbsMkax(magak1, \Pi) \doteq [magak1 + 5 \cdot (\log(\Pi)) + 5]$

$AbsMkbx(magbk1, \Pi) \doteq [magbk1 + 5 \cdot (\log(\Pi)) + 5]$

$AbsMkax(magak1, \Pi) = 1.603$ $AbsMkbx(magbk1, \Pi) = 1.961$

$$\Delta AbsMkax(magak1, \Delta magk1\Pi\ \Delta\Pi\ ) \doteq \sqrt{\left( \frac{d}{dmagak1} AbsMkax(magak1, \Pi) \cdot \Delta magk1 \right)^2 + \left( \frac{d}{d\Pi} AbsMkax(magak1, \Pi) \cdot \Delta\Pi \right)^2}$$

$$\Delta AbsMkbx(magbk1, \Delta magk1\Pi\ \Delta\Pi\ ) \doteq \sqrt{\left( \frac{d}{dmagbk1} AbsMkb(magbk1, \Pi) \cdot \Delta magk1 \right)^2 + \left( \frac{d}{d\Pi} AbsMkb(magbk1, \Pi) \cdot \Delta\Pi \right)^2}$$

$\Delta AbsMkax(magak1, \Delta magk1\Pi\ \Delta\Pi\ ) = 0.255$ $\Delta AbsMkbx(magbk1, \Delta magk1\Pi\ \Delta\Pi\ ) = 0.255$ $\Delta AbsMkx \doteq \Delta AbsMkbx(magbk1, \Delta magk1\Pi\ \Delta\Pi\ )$

Figure. D.6: MathCAD Mass and Luminosity Program Page 6


Figure. D.7: MathCAD Mass and Luminosity Program Page 7

**Luminosities from Bolometric Magnitudes (Assumption 1) and parallaxes: apparent Mag, distance BC**

$BC = -0.15$

**Variables**

$map \equiv 0.5$ $\quad mass \equiv map, (0.02 + map) \cdot 3.5 \cdot map$

$Lmx(mass) \equiv 10^{[(3.8 \log(mass))+0.08]}$

$Lm1(mass) \equiv mass^{3.76}$ $\quad Lm2(mass) \equiv mass^{4.0}$

$Lm3(mass) \equiv mass^{3.5}$ $\quad Lm4(mass) \equiv mass^{3.81}$

$\Delta Hip \equiv \Delta plx$

$\Delta Hip = 3.6 \times 10^{-4}$

$\Delta My \equiv \Delta \Pi$

$My \equiv (\Pi)$

$Hip \equiv (plx)$ $\quad Hip = 0.036$ $\quad \Delta My = 1.239 \times 10^{-3}$

$My = 0.035$

**Luminosities from Bolometric Magnitudes**

$$LaHip1(Hip, magav1) \equiv 10^{\left[\frac{(magav1+5\cdot\log(Hip)+0.26+BC)}{-2.5}\right]}$$

$LaHip1(Hip, magav1) = 6.038$

$$LaMy1(My, magav1) \equiv 10^{\left[\frac{(magav1+5\cdot\log(My)+0.26+BC)}{-2.5}\right]}$$

$LaMy1(My, magav1) = 6.318$

$$LbHip1(Hip, magbv1) \equiv 10^{\left[\frac{(magbv1+5\cdot\log(Hip)+0.26+BC)}{-2.5}\right]}$$

$LbHip1(Hip, magbv1) = 4.696$

$$LbMy1(My, BolVs) \equiv 10^{\left[\frac{(magbv1+5\cdot\log(My)+0.26+BC)}{-2.5}\right]}$$

$LbMy1(My, magbv1) = 4.913$

**Errors for Luminosities**

$$\Delta LaHip1(Hip, \Delta Hip, magav1\,\Delta\, magbv1) \equiv \sqrt{\left(\frac{d}{dHip} LaHip1(Hip, magav1)\cdot\Delta Hip\right)^2 + \left(\frac{d}{dmagav1} LaHip1(Hip, magav1)\cdot\Delta magbv1\right)^2}$$

$$\Delta LbHip1(Hip, \Delta Hip, magbv1\,\Delta\, magbv1) \equiv \sqrt{\left(\frac{d}{dHip} LaHip1(Hip, magbv1)\cdot\Delta Hip\right)^2 + \left(\frac{d}{dmagbv1} LaHip1(Hip, magbv1)\cdot\Delta magbv1\right)^2}$$

$$\Delta LaMy1(My, \Delta My, magav1\,\Delta\, magbv1) \equiv \sqrt{\left(\frac{d}{dMy} LaMy1(My, magav1)\cdot\Delta My\right)^2 + \left(\frac{d}{dmagav1} LaMy1(My, magav1)\cdot\Delta magbv1\right)^2}$$

$$\Delta LbMy1(My, \Delta My, magav1\,\Delta\, magbv1) \equiv \sqrt{\left(\frac{d}{dMy} LbMy1(My, magav1)\cdot\Delta My\right)^2 + \left(\frac{d}{dmagav1} LaMy1(My, magav1)\cdot\Delta magbv1\right)^2}$$

$Mp1 \equiv 1.366$ $\quad Mpe1 \equiv \log(LaHip1(Hip, magav1))$ $\quad Mpe1 = 0.781$

$Ms1 \equiv 1.289$ $\quad Mse1 \equiv \log(LbHip1(Hip, magbv1))$ $\quad Mse1 = 0.672$

$Mp2 \equiv 1.54$ $\quad Mpe2 \equiv \log(LaMy1(My, magav1))$ $\quad Mpe2 = 0.801$

$Ms2 \equiv 1.50$ $\quad Mse2 \equiv \log(LbMy1(My, magbv1))$ $\quad Mse2 = 0.691$

$\Delta LaHip1(Hip, \Delta Hip, magav1\,\Delta\, magbv1) = 0.41$

$\Delta LbHip1(Hip, \Delta Hip, magbv1\,\Delta\, magbv1) = 0.319$

$\Delta LaMy1(My, \Delta My, magav1\,\Delta\, magbv1) = 0.603$

$\Delta LbMy1(My, \Delta My, magbv1\,\Delta\, magbv1) = 0.469$

$\Delta LaH1 \equiv \Delta LaHip1(Hip, \Delta Hip, magav1\,\Delta\, magbv1)$

$\Delta LbH1 \equiv \Delta LbHip1(Hip, \Delta Hip, magbv1\,\Delta\, magbv1)$

$\Delta LaM1 \equiv \Delta LaMy1(My, \Delta My, magav1\,\Delta\, magbv1)$

$\Delta LbM1 \equiv \Delta LbMy1(My, \Delta My, magbv1\,\Delta\, magbv1)$

Figure. D.8: MathCAD Mass and Luminosity Program Page 8

**Luminosities from Bolometric Magnitudes (Assumption 2) and parallaxes: apparent Mag, distance BC**

### Luminosities from Bolometric Magnitudes

$$LaHip2(Hip, magav\chi) \doteq 10^{\left[\frac{(magav\chi + 5\cdot\log(plx) + 0.26 + BC)}{-2.5}\right]}$$

$$LaMy2(My, magav\chi) \doteq 10^{\left[\frac{(magav\chi + 5\cdot\log(\Pi) + 0.26 + BC)}{-2.5}\right]}$$

$LaHip2(Hip, magav\chi) = 6.222$

$LaMy2(My, magav\chi) = 6.51$

$$LbHip2(Hip, magbv\chi x) \doteq 10^{\left[\frac{(magbv\chi x + 5\cdot\log(plx) + 0.26 + BC)}{-2.5}\right]}$$

$$LbMy2(My, magbv\chi x) \doteq 10^{\left[\frac{(magbv\chi x + 5\cdot\log(\Pi) + 0.26 + BC)}{-2.5}\right]}$$

$LbHip2(Hip, magbv\chi x) = 4.512$

$LbMy2(My, magbv\chi x) = 4.721$

### Errors for Luminosities

$$\Delta LaHip2(Hip, \Delta Hip, magav\chi \Delta\ magav\chi) \doteq \sqrt{\left(\frac{d}{dHip} LaHip2(Hip, magav\chi)\cdot\Delta Hip\right)^2 + \left(\frac{d}{dmagav\chi} LaHip2(Hip, magav\chi)\cdot\Delta magav\chi\right)^2}$$

$$\Delta LbHip2(Hip, \Delta Hip, magbv\chi x \Delta\ magav\chi) \doteq \sqrt{\left(\frac{d}{dHip} LaHip2(Hip, magbv\chi x)\cdot\Delta Hip\right)^2 + \left(\frac{d}{dmagbv\chi x} LaHip2(Hip, magbv\chi x)\cdot\Delta magav\chi\right)^2}$$

$$\Delta LaMy2(My, \Delta My, magav\chi \Delta\ magav\chi) \doteq \sqrt{\left(\frac{d}{dMy} LaMy2(My, magav\chi)\cdot\Delta My\right)^2 + \left(\frac{d}{dmagav\chi} LaMy2(My, magav\chi)\cdot\Delta magav\chi\right)^2}$$

$$\Delta LbMy2(My, \Delta My, magbv\chi x \Delta\ magav\chi) \doteq \sqrt{\left(\frac{d}{dMy} LbMy2(My, magbv\chi x)\cdot\Delta My\right)^2 + \left(\frac{d}{dmagbv\chi x} LaMy2(My, magbv\chi x)\cdot\Delta magav\chi\right)^2}$$

$Mp1 \doteq 1.366$

$Mpe1\chi \doteq \log(LaHip1(Hip, magav\chi))$

$Mpe1\chi = 0.794$

$Ms1 \doteq 1.289$

$Mse1\chi \doteq \log(LbHip1(Hip, magbv\chi x))$

$Mse1\chi = 0.654$

$Mp2 \doteq 1.54$

$Mpe2\chi \doteq \log(LaMy1(My, magav\chi))$

$Mpe2\chi = 0.814$

$Ms2 \doteq 1.50$

$Mse2\chi \doteq \log(LbMy1(My, magbv\chi x))$

$Mse2\chi = 0.691$

$\Delta LaHip2(Hip, \Delta Hip, magav\chi \Delta\ magav\chi) = 0.418$

$\Delta LaH2 \doteq \Delta LaHip2(Hip, \Delta Hip, magav\chi \Delta\ magav\chi)$

$\Delta LbHip2(Hip, \Delta Hip, magbv\chi x \Delta\ magav\chi) = 0.303$

$\Delta LbH2 \doteq \Delta LbHip2(Hip, \Delta Hip, magbv\chi x \Delta\ magav\chi)$

$\Delta LaMy2(My, \Delta My, magav\chi \Delta\ magav\chi) = 0.438$

$\Delta LaM2 \doteq \Delta LaMy2(My, \Delta My, magav\chi \Delta\ magav\chi)$

$\Delta LbMy2(My, \Delta My, magbv\chi x \Delta\ magav\chi) = 0.317$

$\Delta LbM2 \doteq \Delta LbMy2(My, \Delta My, magbv\chi x \Delta\ magav\chi)$

Figure. D.9: MathCAD Mass and Luminosity Program Page 9

$MassP \equiv 1.366$ $\Delta MassP \equiv 0.101$

$MassS \equiv 1.279$ $\Delta MassS \equiv 0.089$

**From Allen = log M/M* = 0.48 - 0.105Mbol**

**(0.48 - log M)/0.105 = Mbol (Assumption 1)**

**Bolometric Magnitudes from Mass assumptions from Msin^3i**

$$MbolP(MassP) \equiv \frac{[0.48 - (\log(MassP))]}{0.105}$$

$MbolP(MassP) = 3.281$

$MbolPx \equiv MbolP(MassP)$

$$MbolS(MassS) \equiv \frac{[0.48 - (\log(MassS))]}{0.105}$$

$MbolS(MassS) = 3.554$

$MbolSx \equiv MbolS(MassS)$

**Error in Bolometric Magnitude**

$$\Delta MbolP(MassP, \Delta MassP) \equiv \sqrt{\left(\frac{d}{dMassP} MbolP(MassP) \cdot \Delta MassP\right)^2}$$

$\Delta MbolP(MassP, \Delta MassP) = 0.306$

$\Delta MbolPx \equiv \Delta MbolP(MassP, \Delta MassP)$

$$\Delta MbolS(MassS, \Delta MassS) \equiv \sqrt{\left(\frac{d}{dMassS} MbolS(MassS) \cdot \Delta MassS\right)^2}$$

$\Delta MbolS(MassS, \Delta MassS) = 0.288$

$\Delta MbolSx \equiv \Delta MbolS(MassS, \Delta MassS)$

**Luminosities from Standard Formula Mbol= -2.5 (L/Lsun) + 4.74**

$$LxP(MbolPx) \equiv 10^{\left(1.86 + \frac{MbolPx}{-2.5}\right)}$$

$LxP(MbolPx) = 3.527$

$LxPx \equiv LxP(MbolPx)$

$$LxS(MbolSx) \equiv 10^{\left(1.86 + \frac{MbolSx}{-2.5}\right)}$$

$LxS(MbolSx) = 2.745$

**Error in Luminosity**

$LxSx \equiv LxS(MbolSx)$

$$\Delta LxP(MbolPx, \Delta MbolPx) \equiv \sqrt{\left(\frac{d}{dMbolPx} LxP(MbolPx) \cdot \Delta MbolPx\right)^2}$$

$\Delta LxP(MbolPx, \Delta MbolPx) = 0.994$

$\Delta LxPx \equiv \Delta LxP(MbolPx, \Delta MbolPx)$

$$\Delta LxS(MbolSx, \Delta MbolSx) \equiv \sqrt{\left(\frac{d}{dMbolSx} LxS(MbolSx) \cdot \Delta MbolSx\right)^2}$$

$\Delta LxS(MbolSx, \Delta MbolSx) = 0.728$

$\Delta LxSx \equiv \Delta LxS(MbolSx, \Delta MbolSx)$

**Log of Luminosity for comparison with table**

$xp \equiv \log(LxPx)$ $xs \equiv \log(LxSx)$

$xp = 0.547$ $xs = 0.439$

**Used Above ΔV in Assumption 1**

$\omega mV \equiv MbolSx - MbolPx$

$\omega mV = 0.272$

**Error for ΔV**

$$\Delta\Delta MbolPx \equiv \frac{\Delta MbolPx}{MbolPx}$$

$\Delta\Delta MbolPx = 0.093$

$$\Delta\Delta MbolSx \equiv \frac{\Delta MbolSx}{MbolSx}$$

$\Delta\Delta MbolSx = 0.081$

$$\Delta\Delta mV \equiv \sqrt{\left(\Delta\Delta MbolPx^2 + \Delta\Delta MbolSx^2\right)}$$

$\Delta\Delta mV = 0.123$

Figure. D.10: MathCAD Mass and Luminosity Program Page 10

**Bolometric Magnitudes from Mass assumptions from Kepler - Hip**

$$MbolP\eta(Ma\eta) \doteq \frac{[0.48 - (\log(Ma\eta))]}{0.105} \qquad MbolP\eta(Ma\eta) = 3.145$$

$MbolPx\eta \doteq MbolP\eta(Ma\eta)$

$$MbolS\eta(Mb\eta) \doteq \frac{[0.48 - (\log(Mb\eta))]}{0.105} \qquad MbolS\eta(Mb\eta) = 3.418$$

$MbolSx\eta \doteq MbolS\eta(Mb\eta)$

**Error in Bolometric Magnitude**

$$\Delta MbolP\eta(Ma\eta, \Delta Ma\eta) \doteq \sqrt{\left(\frac{d}{dMa\eta} MbolP\eta(Ma\eta)\cdot\Delta Ma\eta\right)^2}$$

$\Delta MbolP\eta(Ma\eta, \Delta Ma\eta) = 0.27$ $\quad \Delta MbolPx\eta \doteq \Delta MbolP\eta(Ma\eta, \Delta Ma\eta)$

$$\Delta MbolS\eta(Mb\eta, \Delta Mb\eta) \doteq \sqrt{\left(\frac{d}{dMb\eta} MbolS\eta(Mb\eta)\cdot\Delta Mb\eta\right)^2}$$

$\Delta MbolS\eta(Mb\eta, \Delta Mb\eta) = 0.271$ $\quad \Delta MbolSx\eta \doteq \Delta MbolS\eta(Mb\eta, \Delta Mb\eta)$

**Used Above ΔV in Assumption 1**

$\eta mV \doteq MbolSx\eta - MbolPx\eta$

$\eta mV = 0.274$

**Luminosities from Standard Formula Mbol= -2.5 (L/Lsun) + 4.74 Kepler - Hip**

$$LxP\eta(MbolPx\eta) \doteq 10^{\left(1.86+\frac{MbolPx\eta}{-2.5}\right)} \qquad LxS\eta(MbolSx\eta) \doteq 10^{\left(1.86+\frac{MbolSx\eta}{-2.5}\right)}$$

$LxP\eta(MbolPx\eta) = 4$ $\quad LxPx\eta \doteq LxP\eta(MbolPx\eta)$ $\qquad LxS\eta(MbolSx\eta) = 3.109$ $\quad LxSx\eta \doteq LxS\eta(MbolSx\eta)$

$$\Delta LxP\eta(MbolPx\eta, \Delta MbolPx\eta) \doteq \sqrt{\left(\frac{d}{dMbolPx\eta} LxP\eta(MbolPx\eta)\cdot\Delta MbolPx\eta\right)^2}$$

$\Delta LxP\eta(MbolPx\eta, \Delta MbolPx\eta) = 0.995$ $\quad \Delta LxPx\eta \doteq \Delta LxP\eta(MbolPx\eta, \Delta MbolPx\eta)$

**Log of Luminosity for comparison with table**

$xp\eta \doteq \log(LxPx\eta)$ $\qquad xs\eta \doteq \log(LxSx\eta)$

$xp\eta = 0.602$ $\qquad xs\eta = 0.493$

$$\Delta LxS\eta(MbolSx\eta, \Delta MbolSx\eta) \doteq \sqrt{\left(\frac{d}{dMbolSx\eta} LxS\eta(MbolSx\eta)\cdot\Delta MbolSx\eta\right)^2}$$

$\Delta LxS\eta(MbolSx\eta, \Delta MbolSx\eta) = 0.777$ $\quad \Delta LxSx\eta \doteq \Delta LxS\eta(MbolSx\eta, \Delta MbolSx\eta)$

Figure. D.11: MathCAD Mass and Luminosity Program Page 11

**Bolometric Magnitudes from Mass assumptions from Kepler - Hip**

$$MbolP\phi(Ma\phi) \doteq \frac{[0.48 - (\log(Ma\phi))]}{0.105}$$

$MbolP\phi(Ma\phi) = 2.947$

$MbolPx\phi \doteq MbolP\phi(Ma\phi)$

$$MbolS\phi(Mb\phi) \doteq \frac{[0.48 - (\log(Mb\phi))]}{0.105}$$

$MbolS\phi(Mb\phi) = 3.05$

**Error in Bolometric Magnitude**

$MbolSx\phi \doteq MbolS\phi(Mb\phi)$

$$\Delta MbolP\phi(Ma\phi,\Delta Ma\phi) \doteq \sqrt{\left(\frac{d}{dMa\phi} MbolP\phi(Ma\phi)\cdot\Delta Ma\phi\right)^2}$$

$\Delta MbolP\phi(Ma\phi,\Delta Ma\phi) = 0.492$

$\Delta MbolPx\phi \doteq \Delta MbolP\phi(Ma\phi,\Delta Ma\phi)$

**Used Above ΔV in Assumption 1**

$\phi mV \doteq MbolSx\phi - MbolPx\phi$

$$\Delta MbolS\phi(Mb\phi,\Delta Mb\phi) \doteq \sqrt{\left(\frac{d}{dMb\phi} MbolS\phi(Mb\phi)\cdot\Delta Mb\phi\right)^2}$$

$\phi mV = 0.103$

$\Delta MbolS\phi(Mb\phi,\Delta Mb\phi) = 0.492$

$\Delta MbolSx\phi \doteq \Delta MbolS\phi(Mb\phi,\Delta Mb\phi)$

**Luminosities from Standard Formula Mbol= -2.5 (L/Lsun) + 4.74 Kepler - Hip**

$$LxP\phi(MbolPx\phi) \doteq 10^{\left(1.86+\frac{MbolPx\phi}{-2.5}\right)}$$

$$LxS\phi(MbolSx\phi) \doteq 10^{\left(1.86+\frac{MbolSx\phi}{-2.5}\right)}$$

$LxP\phi(MbolPx\phi) = 4.799$

$LxS\phi(MbolSx\phi) = 4.365$

$LxPx\phi \doteq LxP\phi(MbolPx\phi)$

$LxSx\phi \doteq LxS\phi(MbolSx\phi)$

$$\Delta LxP\phi(MbolPx\phi,\Delta MbolPx\phi) \doteq \sqrt{\left(\frac{d}{dMbolPx\phi} LxP\phi(MbolPx\phi)\cdot\Delta MbolPx\phi\right)^2}$$

$\Delta LxP\phi(MbolPx\phi,\Delta MbolPx\phi) = 2.175$

$\Delta LxPx\phi \doteq \Delta LxP\phi(MbolPx\phi,\Delta MbolPx\phi)$

$$\Delta LxS\phi(MbolSx\phi,\Delta MbolSx\phi) \doteq \sqrt{\left(\frac{d}{dMbolSx\phi} LxS\phi(MbolSx\phi)\cdot\Delta MbolSx\phi\right)^2}$$

$\Delta LxS\phi(MbolSx\phi,\Delta MbolSx\phi) = 1.978$

$\Delta LxSx\phi \doteq \Delta LxS\phi(MbolSx\phi,\Delta MbolSx\phi)$

**Log of Luminosity for comparison with table**

$xp\phi \doteq \log(LxPx\phi)$

$xs\phi \doteq \log(LxSx\phi)$

$xp\phi = 0.681$

$xs\phi = 0.64$

Figure. D.12: MathCAD Mass and Luminosity Program Page 12

$MassP\omega \doteq 1.366$ $\Delta MassP\omega \doteq 0.101$

$MassS\omega \doteq 1.279$ $\Delta MassS\omega \doteq 0.089$

**From Allen = log M/M* = 0.46 - 0.10Mbol**

**(0.46 - log M)/0.10 = Mbol (different formula)**

**Bolometric Magnitudes from Mass assumptions**

$$MbolP\omega(MassP\omega) \doteq \frac{[0.46 - (\log(MassP\omega))]}{0.10}$$

$MbolP\omega(MassP\omega) = 3.245$

$MbolPx\omega \doteq MbolP\omega(MassP\omega)$

$$MbolS\omega(MassS\omega) \doteq \frac{[0.46 - (\log(MassS\omega))]}{0.10}$$

$MbolS\omega(MassS\omega) = 3.531$

**Error in Bolometric Magnitude**

$MbolSx\omega \doteq MbolS\omega(MassS\omega)$

$$\Delta MbolP\omega(MassP\omega, \Delta MassP\omega) \doteq \sqrt{\left(\frac{d}{dMassP\omega} MbolP\omega(MassP\omega)\cdot\Delta MassP\omega\right)^2}$$

$\Delta MbolP\omega(MassP\omega, \Delta MassP\omega) = 0.321$

$\Delta MbolPx\omega \doteq \Delta MbolP\omega(MassP\omega, \Delta MassP\omega)$

$$\Delta MbolS\omega(MassS\omega, \Delta MassS\omega) \doteq \sqrt{\left(\frac{d}{dMassS\omega} MbolS\omega(MassS\omega)\cdot\Delta MassS\omega\right)^2}$$

$\Delta MbolSx\omega \doteq \Delta MbolS\omega(MassS\omega, \Delta MassS\omega)$

$\Delta MbolS\omega(MassS\omega, \Delta MassS\omega) = 0.302$

**Luminosities from Standard Formula Mbol= -2.5 (L/Lsun) + 4.74**

$$LxP\omega(MbolPx\omega) \doteq 10^{\left(1.86+\frac{MbolPx\omega}{-2.5}\right)}$$

$LxP\omega(MbolPx\omega) = 3.646$

$LxPx\omega \doteq LxP\omega(MbolPx\omega)$

$$LxS\omega(MbolSx\omega) \doteq 10^{\left(1.86+\frac{MbolSx\omega}{-2.5}\right)}$$

$LxS\omega(MbolSx\omega) = 2.802$

$LxSx\omega \doteq LxS\omega(MbolSx\omega)$

**Error in Luminosity**

$$\Delta LxP\omega(MbolPx\omega, \Delta MbolPx\omega) \doteq \sqrt{\left(\frac{d}{dMbolPx\omega} LxP\omega(MbolPx\omega)\cdot\Delta MbolPx\omega\right)^2}$$

$\Delta LxP\omega(MbolPx\omega, \Delta MbolPx\omega) = 1.078$

$\Delta LxPx\omega \doteq \Delta LxP\omega(MbolPx\omega, \Delta MbolPx\omega)$

$$\Delta LxS\omega(MbolSx\omega, \Delta MbolSx\omega) \doteq \sqrt{\left(\frac{d}{dMbolSx\omega} LxS\omega(MbolSx\omega)\cdot\Delta MbolSx\omega\right)^2}$$

$\Delta LxS\omega(MbolSx\omega, \Delta MbolSx\omega) = 0.78$

$\Delta LxSx\omega \doteq \Delta LxS\omega(MbolSx\omega, \Delta MbolSx\omega)$

**Error for ΔV**

$$\Delta\Delta MbolPx\omega \doteq \frac{\Delta MbolPx\omega}{MbolPx\omega}$$

$\Delta\Delta MbolPx\omega = 0.099$

$$\Delta\Delta MbolSx\omega \doteq \frac{\Delta MbolSx\omega}{MbolSx\omega}$$

$\Delta\Delta MbolSx\omega = 0.086$

**Log of Luminosity for comparison with table**

$xp\omega \doteq \log(LxPx\omega)$ $xs\omega \doteq \log(LxSx\omega)$

$xp\omega = 0.562$ $xs\omega = 0.447$

**Used Above ΔV**

$\omega mV\omega \doteq MbolSx\omega - MbolPx\omega$

$\omega mV\omega = 0.286$

$$\Delta\Delta mV\omega \doteq \sqrt{\left(\Delta\Delta MbolPx\omega^2 + \Delta\Delta MbolSx\omega^2\right)}$$

$\Delta\Delta mV\omega = 0.131$

Figure. D.13: MathCAD Mass and Luminosity Program Page 13


Figure. D.14: MathCAD Mass and Luminosity Program Page 14

**Bolometric Magnitudes from Mass assumptions from Kepler - Hip**

$$MbolP\omega\phi(Ma\phi) \doteq \frac{[0.46 - (\log(Ma\phi))]}{0.10} \qquad MbolS\omega\phi(Mb\phi) \doteq \frac{[0.46 - (\log(Mb\phi))]}{0.10}$$

$MbolP\omega\phi(Ma\phi) = 2.894$ $MbolS\omega\phi(Mb\phi) = 3.003$

$MbolPx\omega\phi \doteq MbolP\omega\phi(Ma\phi)$ $MbolSx\omega\phi \doteq MbolS\omega\phi(Mb\phi)$

$Ma\phi = 1.481$

$Mb\phi = 1.445$

$\Delta Ma\phi = 0.176$

$\Delta Mb\phi = 0.172$

**Error in Bolometric Magnitude**

$$\Delta MbolP\omega\phi(Ma\phi, \Delta Ma\phi) \doteq \sqrt{\left(\frac{d}{dMa\phi} MbolP\omega\phi(Ma\phi) \cdot \Delta Ma\phi\right)^2}$$

$\Delta MbolP\omega\phi(Ma\phi, \Delta Ma\phi) = 0.517$ $\Delta MbolPx\omega\phi \doteq \Delta MbolP\omega\phi(Ma\phi, \Delta Ma\phi)$

$$\Delta MbolS\omega\phi(Mb\phi, \Delta Mb\phi) \doteq \sqrt{\left(\frac{d}{dMb\phi} MbolS\omega\phi(Mb\phi) \cdot \Delta Mb\phi\right)^2}$$

$\Delta MbolS\omega\phi(Mb\phi, \Delta Mb\phi) = 0.517$ $\Delta MbolSx\omega\phi \doteq \Delta MbolS\omega\phi(Mb\phi, \Delta Mb\phi)$

**Used Above ΔV in Assumption 1**

$\phi\omega mV \doteq MbolSx\omega\phi - MbolPx\omega\phi$

$\phi\omega mV = 0.108$

**Luminosities from Standard Formula Mbol= -2.5 (L/Lsun) + 4.74 Kepler - Hip**

$$LxP\omega\phi(MbolPx\omega\phi) \doteq 10^{\left(1.86 + \frac{MbolPx\omega\phi}{-2.5}\right)} \qquad LxS\omega\phi(MbolSx\omega\phi) \doteq 10^{\left(1.86 + \frac{MbolSx\omega\phi}{-2.5}\right)}$$

$LxP\omega\phi(MbolPx\omega\phi) = 5.038$ $LxS\omega\phi(MbolSx\omega\phi) = 4.56$

$LxPx\omega\phi \doteq LxP\omega\phi(MbolPx\omega\phi)$

$LxSx\omega\phi \doteq LxS\omega\phi(MbolSx\omega\phi)$

$$\Delta LxP\omega\phi(MbolPx\omega\phi, \Delta MbolPx\omega\phi) \doteq \sqrt{\left(\frac{d}{dMbolPx\omega\phi} LxP\omega\phi(MbolPx\omega\phi) \cdot \Delta MbolPx\omega\phi\right)^2}$$

$\Delta LxP\omega\phi(MbolPx\omega\phi, \Delta MbolPx\omega\phi) = 2.397$ $\Delta LxPx\omega\phi \doteq \Delta LxP\omega\phi(MbolPx\omega\phi, \Delta MbolPx\omega\phi)$

$$\Delta LxS\omega\phi(MbolSx\omega\phi, \Delta MbolSx\omega\phi) \doteq \sqrt{\left(\frac{d}{dMbolSx\omega\phi} LxS\omega\phi(MbolSx\omega\phi) \cdot \Delta MbolSx\omega\phi\right)^2}$$

$\Delta LxS\omega\phi(MbolSx\omega\phi, \Delta MbolSx\omega\phi) = 2.17$ $\Delta LxSx\omega\phi \doteq \Delta LxS\omega\phi(MbolSx\omega\phi, \Delta MbolSx\omega\phi)$

**Log of Luminosity for comparison with table**

$xp\omega\phi \doteq \log(LxPx\omega\phi)$ $xs\omega\phi \doteq \log(LxSx\omega\phi)$

$xp\omega\phi = 0.702$ $xs\omega\phi = 0.659$

Figure. D.15: MathCAD Mass and Luminosity Program Page 15

## Summary of Data

**Masses from i and Msin^3 i**

M(Msin1, i) = 1.366 ΔM(Msin1, ΔMsin1, iΔ i) = 0.101

M(Msin2, i) = 1.279 ΔM(Msin2, ΔMsin2, iΔ i) = 0.089

**Masses from Kepler's Laws with Hipparcos Parallax**

Mp(MSum(a(α, plx), p), q) = 1.412

Ms(MSum(a(α, plx), p), q) = 1.322

ΔMp(MSum(a(α, plx), p), ΔMSum(a(α, plx), Δa(α, Δα, plxΔ plx), pΔ p), qΔ q) = 0.092

ΔMs(MSum(a(α, plx), p), ΔMSum(a(α, plx), Δa(α, Δα, plxΔ plx), pΔ p), qΔ q) = 0.087

**Masses from Kepler's Laws with Orbital Parallax**

Mp(MSum(a(α, xplx), p), q) = 1.511

Ms(MSum(a(α, xplx), p), q) = 1.414

ΔMp(MSum(a(α, xplx), p), ΔMSum(a(α, xplx), Δa(α, Δα, xplxΔ xplx), pΔ p), qΔ q) = 0.181

ΔMs(MSum(a(α, xplx), p), ΔMSum(a(α, xplx), Δa(α, Δα, xplxΔ xplx), pΔ p), qΔ q) = 0.170

**Orbital Parallax**

Πorb(aaux, sep) = 35.45

ΔΠorb(aaux, Δaaux, sepΔ sep) = 1.246

Using: $\frac{L}{Lsun} = C \left(\frac{d}{dsun}\right)^2 \quad 10^{[0.4(msun-m)]}$

**Assumption 1 Mbol with Hip and Orb parallax**

LaHip1(Hip, magav1) = 6.038 ΔLaH1 = 0.41

LbHip1(Hip, magbv1) = 4.696 ΔLbH1 = 0.319

LaMy1(My, magav1) = 6.318 ΔLaM1 = 0.603

LbMy1(My, magbv1) = 4.913 ΔLbM1 = 0.469

**Assumption 2 Mbol with Hip and Orb parallax**

LaHip2(Hip, magavχ) = 6.222 ΔLaH2≒ 0.364

LbHip2(Hip, magbvχx) = 4.512 ΔLbH2≒ 0.264

LaMy2(My, magavχ) = 6.51 ΔLaM2≒ 0.53

LbMy2(My, magbvχx) = 4.721 ΔLbM2≒ 0.279

Figure. D.16: MathCAD Mass and Luminosity Program Page 16

**Individual K Apparent and Absolute Magnitudes from Hipparcos and Orbital Parallax**

magak1 = 3.855 AbsMka(magak1, plx) = 1.652 AbsMkax(magak1 ,Π) = 1.603

magbk1 = 4.213 AbsMkb(magbk1 , plx) = 2.011 AbsMkbx(magbk1 ,Π) = 1.961

Δmagbk(mabk , Δmabk Δ mk1 δΔ mk1) = 0.243 ΔAbsMk = 0.244 ΔAbsMkx = 0.255

**Individual Apparent and Absolute V and Bolometric Magnitudes using ΔV = 0.273**

magav1 = 5.141 BolVp = 2.788 Δmagbv1≒ 0.07 AbsMvp(magav1, plx) = 2.938 ΔAbsMvpx = 0.074

magbv1 = 5.414 BolVs = 3.061 AbsMvs(magbv1, plx) = 3.211 ΔAbsMvsx = 0.074

**Individual Apparent and Absolute V and Bolometric Magnitudes using ΔV = 0.349**

magavχx = 5.108 BolVpχ = 2.755 Δmagavχ = 0.073 Mva(avχ, plx) = 2.905 ΔAbsMvaχ = 0.076

magbvχx = 5.457 BolVsχ = 3.104 Mvb(bvχ, plx) = 3.254 ΔAbsMvbχ = 0.076

**Individual V - K For Assumption 1 and 2 and overall from 2Mass and Johnson UBV**

VmKp1 = 1.286 VmKp2 = 1.253

VmKs1 = 1.2 VmKs2 = 1.244

VmK≒ mabv – mabk

VmK = 1.249

Figure. D.17: MathCAD Mass and Luminosity Program Page 17

**Allen Formula 1**

Using : $\frac{M}{Msun} = 0.48 - 0.105Mbol$

**Bolometric Magnitudes from Hipparcos distance Masses Msin^3i**

MbolPx = 3.281 ΔMbolPx = 0.306

MbolSx = 3.554 ΔMbolSx = 0.288

**Luminosities from:** $Mbol = 2.5\log\left(\frac{L}{Lsun}\right) + 4.74$

LxPx = 3.527 ΔLxPx = 0.994

LxSx = 2.745 ΔLxSx = 0.728

**Log of luminosities for comparison with ZAMS Table**

xp = 0.547 xs = 0.439

**Bolometric Magnitudes from Hipparcos distance Masses Kepler - Hip**

MbolPxη = 3.145 ΔMbolPxη = 0.27

MbolSxη = 3.418 ΔMbolSxη = 0.271

**Luminosities from:** $Mbol = 2.5\log\left(\frac{L}{Lsun}\right) + 4.74$

LxPxη = 4 ΔLxPxη = 0.995

LxSxη = 3.109 ΔLxSxη = 0.777

**Log of luminosities for comparison with ZAMS Table**

xpη = 0.602 xsη = 0.493

**Bolometric Magnitudes from Hipparcos distance Masses Kepler - Orb**

MbolPxϕ = 2.947 ΔMbolPxϕ = 0.492

MbolSxϕ = 3.05 ΔMbolSxϕ = 0.492

**Luminosities from:** $Mbol = 2.5\log\left(\frac{L}{Lsun}\right) + 4.74$

LxPxϕ = 4.799 ΔLxPxϕ = 2.175

LxSxϕ = 4.365 ΔLxSxϕ = 1.978

**Log of luminosities for comparison with ZAMS Table**

xpϕ = 0.681 xsϕ = 0.64

**Allen Formula 2**

Using : $\frac{M}{Msun} = 0.46 - 0.10Mbol$

**Bolometric Magnitudes from Hipparcos distance Masses Msin^3i**

MbolPxω = 3.245 ΔMbolPxω = 0.321

MbolSxω = 3.531 ΔMbolSxω = 0.302

**Luminosities from:** $Mbol = 2.5\log\left(\frac{L}{Lsun}\right) + 4.74$

LxPxω = 3.648 ΔLxPxω = 1.078

LxSxω = 2.802 ΔLxSxω = 0.78

**Log of luminosities for comparison with ZAMS Table**

xpω = 0.562 xsω = 0.447

**Bolometric Magnitudes from Hipparcos distance Masses Kepler - Hip**

MbolPxωη = 3.102 ΔMbolPxωη = 0.283

MbolSxωη = 3.389 ΔMbolSxωη = 0.285

**Luminosities from:** $Mbol = 2.5\log\left(\frac{L}{Lsun}\right) + 4.74$

LxPxωη = 4.161 ΔLxPxωη = 1.086

LxSxωη = 3.194 ΔLxSxωη = 0.838

**Log of luminosities for comparison with ZAMS Table**

xpωη = 0.619 xsωη = 0.504

**Bolometric Magnitudes from Hipparcos distance Masses Kepler - Orb**

MbolPxωϕ = 2.894 ΔMbolPxωϕ = 0.517

MbolSxωϕ = 3.003 ΔMbolSxωϕ = 0.517

**Luminosities from:** $Mbol = 2.5\log\left(\frac{L}{Lsun}\right) + 4.74$

LxPxωϕ = 5.038 ΔLxPxωϕ = 2.397

LxSxωϕ = 4.56 ΔLxSxωϕ = 2.17

**Log of luminosities for comparison with ZAMS Table**

xpωϕ = 0.702 xsωϕ = 0.659

Figure. D.18: MathCAD Mass and Luminosity Program Page 18

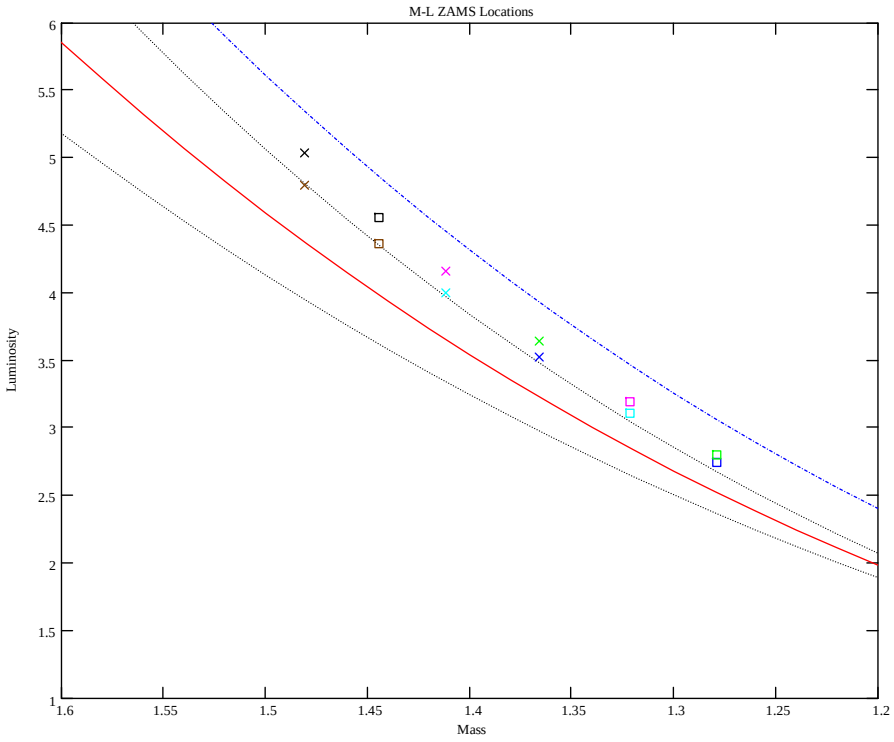


Figure. D.19: MathCAD Mass and Luminosity Program Page 19. Configurable graph with four different Mass/Luminosity main-sequence relations.

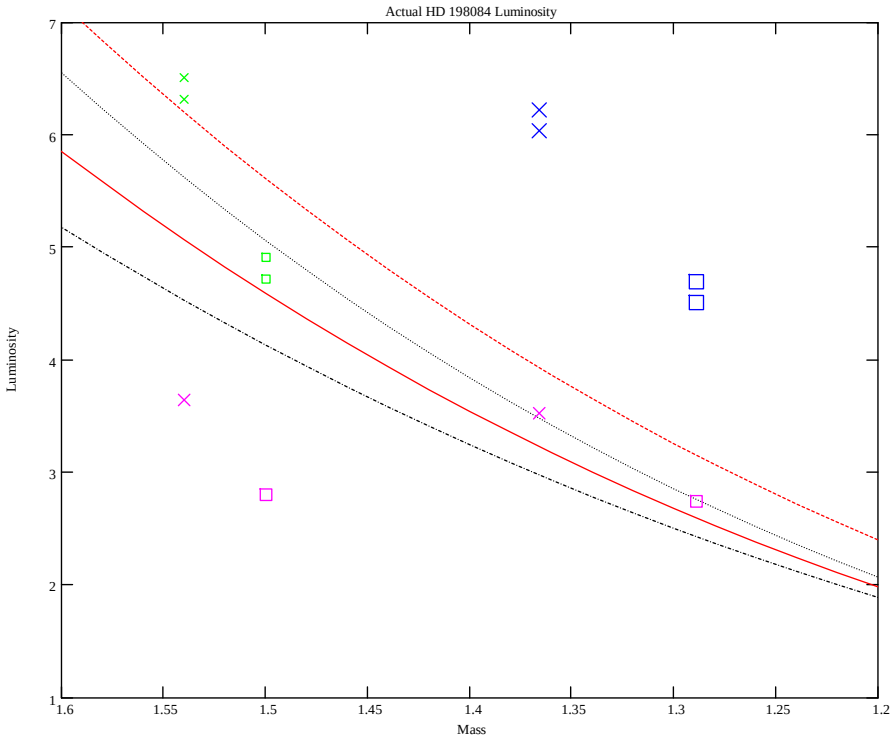


Figure. D.20: MathCAD Mass and Luminosity Program Page 20. Configurable graph with four different Mass/Luminosity main-sequence relations.